

**APPENDIX A**  
**OUTSIDE SOURCES QUALIFIED FOR INTENDED USE**



## A.1 QUALIFICATION OF VEGETATION PARAMETERS FOR USE AS DIRECT INPUT

This section documents the demonstration that data for vegetation parameters are suitable for their intended use as inputs for calculating net infiltration at Yucca Mountain. Appropriate data sources were identified through literature searches for each of vegetation parameter inputs. Because these data were not acquired or developed for the Yucca Mountain Project (YMP), they are qualified for use as input to this report in accordance with SCI-PRO-006, *Models* Section 6.2.1.K. The following vegetation parameter inputs are addressed:

- Plant height (Sections A1.1 to A1.3)
- Timing of phenological events (Section A1.1) and physiological activity (Section A1.2)
- Stomatal conductance (Section A1.4)
- Rooting depth (Sections A1.5 and A1.6).

The attributes of the data considered in the determination of suitability are the extent to which the data demonstrate properties of interest and the reliability of the data source.

### A1.1 PLANT HEIGHT AND TIMING OF PHENOLOGICAL EVENTS

Plant heights were used in the calculation of transpiration coefficients ( $K_{cb}$ ) (Section D.3.2.1), and in the calculation of the fraction of soil surface covered by vegetation ( $f_c$ ) used in soil water balance calculations (Section 6.5.3.3). Plant heights for Present-Day and Monsoon climates are addressed in this section. Plant heights for the Glacial Transition climate are addressed in Section A1.3.

Timing of phenological events for dominant vegetation at Yucca Mountain was used in conjunction with timing of physiological activity (e.g., stomatal conductance, transpiration, and photosynthesis) to establish growth stages for use in development of  $K_{cb}$  profiles (Section D.3.2.1). Timing of phenological events is addressed in this section. Timing of physiological activity is addressed in Section A1.2.

Statistics describing shrub height for Mojave Desert vegetation associations reported by Rundel and Gibson (1996 [DIRS 103614], p. 88, Table 4.1 and p. 89, Table 4.2) were used in the calculation of  $K_{cb}$ s and  $f_c$ , respectively. Timing of phenological stages for drought-deciduous and evergreen species reported by Rundel and Gibson (1996 [DIRS 103614], Figure 4.13, p. 106) were used to establish the initial ranges for growth stages. Timing of phenological stages for *Bromus madritensis* ssp. *rubens* reported by Newman (1992 [DIRS 174673], p. 3) were used to develop growth stages for annual vegetation. Applicable plant height and timing data (i.e., months when stages were documented) from these publications are presented in Table 6.5.3.3-1, Table D-4, Section D3.2.1, and Table D-2.

The following information was used to evaluate whether the plant height and timing data reported by Rundel and Gibson (1996 [DIRS 103614], pp. 88 and p.89, Tables 4.1 and 4.2, respectively) and timing data reported by Newman (1992 [DIRS 174673], p. 3) were suitable for use in  $K_{cb}$  and  $f_c$  development.

- **Extent to Which the Data Demonstrate Properties of Interest**—Plant heights are most applicable to  $K_{cb}$  and  $f_c$  calculations if they are for vegetation associations that are common at Yucca Mountain and are based on data gathered from field studies conducted at the Nevada Test Site (NTS) or within the Mojave Desert region. As described in Sections D3.2.1 and 6.5.3.3, plant heights from Rundel and Gibson (1996 [DIRS 103614], pp. 88 and 89, Tables 4.1 and 4.2, respectively) were for several vegetation associations that occur at Yucca Mountain including those typical of Mojave (low to mid elevations at Yucca Mountain), transition (mid to upper elevations at Yucca Mountain), and Great Basin deserts (upper elevation north slopes). Plant heights in Rundel and Gibson (1996 [DIRS 103614], p. 88, Table 4.1 and p.89, Table 4.2) were based on data gathered during field studies conducted on the NTS.

Timing of phenological stages for desert plants are most applicable to establishing growth stages for this analysis if they are for dominant plant species at Yucca Mountain and if they are based on data gathered from field studies conducted at the NTS or within the Mojave Desert region. As described in Section D3.2.1 the phenological stages from Rundel and Gibson (1996 [DIRS 103614], Figure 4.13, p. 106) were from studies conducted on the NTS for two evergreen species (*Ephedra nevadensis* and *Larrea tridentata*) and four drought deciduous species (*Ambrosia dumosa*, *Grayia spinosa*, *Lycium andersonii*, and *Lycium palladum*), all of which are dominant or co-dominant in Yucca Mountain vegetation associations (see Section D.2.2 for a description of Yucca Mountain vegetation). The phenological stages from Newman (1992 [DIRS 174673], p. 3) were for the dominant annual species in Yucca Mountain vegetation associations and were based on a literature review of *Bromus madritensis* ecology in the Mojave Desert.

- **Reliability of Data Sources**—The data reported by Rundel and Gibson (1996 [DIRS 103614]) were the results of several years of intensive ecological studies collected under prestigious research programs. The research programs were conducted by organizations such as the Desert Biome program of the International Biological Program (IBP) and the Laboratory of Biomedical and Environmental Sciences at the University of California, Los Angeles. The data reported by Newman (1992 [DIRS 174673], p. 3) were compiled by the Nature Conservancy to provide the Nature Conservancy's Stewardship staff and other land managers with current information on those species that are most important to protect or control. It was concluded that these data sources were reliable for use as input to this model.
- **Availability of Corroborating Data**—Plant heights reported by Rundel and Gibson (1996 [DIRS 103614], p. 88, Table 4.1 and p. 89, Table 4.2) reflect the short stature of plants in Mojave Desert vegetation associations and are corroborated by general descriptions of true desert vegetation which is dominated by shrubs and dwarf shrubs (Smith et al. 1997 [103636], p. 21). Phenological stages for desert plants are variable among species and across years of differing precipitation. Those reported by Rundel and Gibson (1996 [DIRS 103614], Figure 4.13, p. 106) reflected this variability and were generally corroborated by the physiological data used to help develop growth stages. The timing of phenological stages for *Bromus madritensis* reported by Newman (1992 [DIRS 174673], p. 3) was typical of that described for winter annuals. In general, winter

annuals are known to germinate in the fall, over winter they remain in a semi-dormant condition, resume rapid growth in late winter or early spring, and have seed set and senescence in late spring to early summer (Hulbert 1955 [DIRS 177129], p. 191).

Because the data considered here were for appropriate vegetation associations and dominant species found at Yucca Mountain, were from studies conducted on the NTS and Mojave Desert region, and were from reliable data sources, it was concluded that the data were suitable for the specific applications in this analysis. Confidence in the reliability of the data was increased by corroborative information. Thus, the data were considered qualified for the intended uses.

## **A1.2 TIMING OF PHYSIOLOGICAL ACTIVITY FOR MOJAVE DESERT VEGETATION**

Measured periods of physiological activity (e.g., photosynthesis, stomatal conductance, and transpiration) for Mojave Desert shrub species reported by Hamerlynck et al. (2000 [DIRS 177022], p. 602, Figure 6), Hamerlynck et al. (2002 [DIRS 177128], Figure 7, p. 103) Hamerlynck et al. (2002 [DIRS 177046], p 774), and Smith et al. (1995 [DIRS 103628], Figure 2, pp. 342, 343, and 349) were used, along with the timing of phenological stages, to establish growth stages used in development of  $K_{cb}$  profiles (Section D.3.2.1). Applicable timing information (i.e., start/end and type of activity) from these publications are presented in Section D.3.2.1.

The following information was considered to evaluate whether the timing of physiological activity data in the listed publications were suitable for use in establishment of growth stages for  $K_{cb}$  development.

- **Extent to Which the Data Demonstrate Properties of Interest**—Timing of physiological activity for desert plants is most applicable to establishing growth stages for this analysis if they are for dominant plant species at Yucca Mountain and if they are based on data gathered from field studies conducted on the NTS or within the Mojave Desert region. As described in Section D3.2.1, physiological studies used in this analysis were conducted on two evergreen species (*L. tridentata* and *E. nevadensis*) and two drought deciduous species (*L. andersonii* and *A. dumosa*) that are dominant in Yucca Mountain vegetation associations. The studies were conducted on the NTS (Hamerlynck et al. 2000 [DIRS 177022], p. 602, Figure 6; Hamerlynck et al. 2002 [DIRS 177128], Figure 7, p. 103; Smith et al. 1995 [DIRS 103628], Figure 2, pp. 342 to 343) and on the East Mojave National Preserve (Hamerlynck et al. 2002 [DIRS 177046], p 774).
- **Reliability of Data Sources**—The data from Hamerlynck et al. (2000 [DIRS 177022], p. 602, Figure 6), Hamerlynck et al. (2002 [DIRS 177128], Figure 7, p. 103), Hamerlynck et al. (2002 [DIRS 177046], p. 774), and Smith et al. (1995 [DIRS 103628], Figure 2, pp. 342 to 343) came from peer-reviewed publications and were thus judged to be appropriate for publication by experts in the field of vegetation science specific to the Mojave Desert. In addition, the methods of data collection were described in sufficient detail to determine whether the data were applicable for determining growth stages. It was concluded that these data sources were reliable for use in this analysis.

Because the data considered here were for dominant species relevant to Yucca Mountain, were from studies conducted at the NTS and Mojave Desert region, and were from reliable data sources, it was concluded that the data are suitable for the specific application in this model. Thus, the data are considered qualified for the intended use.

### A1.3 PLANT HEIGHT FOR THE GLACIAL TRANSITION CLIMATE

Plant heights from the sources in Table A-1 were used in Section 6.5.3.3 to develop the nominal value and distribution for plants heights used to calculate  $f_c$  for the Glacial Transition climate. Because the vegetation of the Glacial Transition climate will likely differ from that of the Present-Day and Monsoon climates, a different dataset was required to establish plant height. Plant heights from these sources are presented in Table 6.5.3.3-2.

Table A-1. Sources for Plant Heights for the Glacial Transition Climate

Source
Stewart and Hull 1949 [DIRS177146], pp. 58 to 59
Schultz and McAdoo 2002 [DIRS 178065], p. 2
Weber et al. 1993 [DIRS 177931], p. 1
Utah State University, Cooperative Extension 2004 [DIRS 177643], p. 1
Utah State University, Cooperative Extension 2002 [DIRS 177644], p. 2
Utah State University, Cooperative Extension 2002 [DIRS 177646], p. 2
Utah State University, Cooperative Extension 2002 [DIRS 177647], p. 1
Utah State University, Cooperative Extension 2002 [DIRS 177648], p. 2
Utah State University, Cooperative Extension 2002 [DIRS 177649], p. 2
Utah State University, Cooperative Extension 2002 [DIRS 177650], p. 2

- Extent to Which the Data Demonstrate Properties of Interest**—Plant heights are most applicable to this model if they are for common plant species of the Great Basin desert that could occur at Yucca Mountain under Glacial Transition conditions (see Section 6.5.3.1 for analysis of potential future vegetation). Data should be collected from Great Basin desert environments. As described in Section 6.5.3.2, all plant heights in the listed sources were for common Great Basin plant species. All data from the listed sources were collected in the Great Basin desert in Nevada and Utah.
- Reliability of Data Sources**—Stewart and Hull (1949 [DIRS 177146], pp. 58 to 59) and Weber et al. (1993 [DIRS 177931]) were peer-reviewed publications and were thus judged to be appropriate for publication by experts in the field of vegetation science.

Because of the paucity of peer-reviewed literature that actually reported plant height for Great Basin plants, the literature search was extended to include United States Department of Agriculture (USDA) divisions and University Cooperative extensions that provided fact sheets on Great Basin plant species in Nevada and Utah (Table 6.5.3.3-2).

The USDA Natural Resources Conservation Service (NRCS) PLANTS Database provides standardized information about vascular plants of the United States (U.S.). The database includes names, plant symbols, checklists, distributional data, species abstracts, characteristics

(including plant height), images, crop information, automated tools, onward Web links, and references. PLANTS is a collaborative effort of the USDA NRCS National Plant Data Center (NPDC), the USDA NRCS Information Technology Center (ITC), the USDA National Information Technology Center (NITC), and many other partners. This data is considered to be Established Fact.

The USDA Forest Service sponsors a Fire Effects Information System (FEIS) that is available online. The FEIS database contains literature reviews, taken from current English-language literature, for about 900 plant species, 7 lichen species, about 100 wildlife species and 10 research project summaries, and 16 Kuchler plant communities of North America. Background information on taxonomy, distribution, basic biology, and ecology of each species is included. Reviews are thoroughly documented, and each contains a complete bibliography. Managers from several land management agencies (United States Department of Agriculture, Forest Service and United States Department of Interior, Bureau of Indian Affairs, Bureau of Land Management, Fish and Wildlife Service, and National Park Service) identified the species to be included in the database. Those agencies funded the original work and continue to support maintenance and updating of the database. Data from these sources are considered to be Established Fact.

The Utah State University (USU) Cooperative Extension web page “Range Plants of Utah” was established through collaboration of range conservationists, botanists, and other experts from the USU Cooperative Extension. The University of Nevada Reno (UNR) Cooperative Extension sponsors publication of a variety of topics on natural resources including management and ecology of common sagebrush in Nevada. The sources listed in Table A-1 were prepared by professionals in the field of natural resources. Cooperative Extension Services are partnerships between state land-grant colleges and the U.S. Department of Agriculture Cooperative State Research, Education, and Extension Service. They serve as the outreach branches of state universities and the Department of Agriculture. The mission of the Cooperative Extension Services is to develop and disseminate information on agriculture, horticulture, health, environment, economics, and other topics of importance developed by the USDA and universities. Personnel working for Cooperative Extension Services are recognized experts in botany, range conservation, agriculture, and horticulture.

Because the plant height data considered here were for common species of the Great Basin desert of Nevada and Utah and were from reliable data sources, it was concluded that the data are suitable for the specific application in this analysis. Thus, the data are considered qualified for the intended use.

#### **A1.4 STOMATAL CONDUCTANCE**

Stomatal conductance values from published literature sources in Table A-2 were used in Section D3.2.3 to calculate stomatal resistance ( $r_l$ ) for dominant plant species in Yucca Mountain vegetation associations. These data were needed to calculate the stomatal resistance correction factor ( $F_r$ ) for use in development of  $K_{cbs}$  (Equation D-6). Applicable stomatal conductance information (i.e., rates, temperatures, plant species) from these publications are presented in Table D-17.

Table A-2. Sources of Published Measurements of Stomatal Conductance for Mojave Desert Vegetation

Sources
Hamerlynck et al. 2000 [DIRS 177130], p. 188
Hamerlynck et al. 2000 [DIRS 177022], p. 602
Hamerlynck et al. 2002 [DIRS 177128], p. 101
Hamerlynck et al. 2004 [DIRS 176045], p. 213
Huxman et al. 1999 [DIRS 177133], p. 774
Huxman and Smith 2001 [DIRS 177132], p. 197
Naumburg et al. 2003 [DIRS 177143], p. 280, Figure 3
Pataki et al. 2000 [DIRS 177161], p. 893
Smith et al. 1995 [DIRS 103628], pp. 343 and 344

The following information was considered to evaluate whether the stomatal conductance data in the listed publications were suitable for calculating stomatal resistance for use in  $K_{cb}$  calculations.

- Extent to Which the Data Demonstrate Properties of Interest**—Rates of stomatal conductance are most applicable to calculating stomatal resistance for this analysis if they are for dominant plant species at Yucca Mountain, are measured during periods of peak activity for mid-season growth stages and during periods of reduced activity for initial and end-of-late season growth stages, and if they are based on data gathered from field studies conducted on the NTS or within the Mojave Desert region. As described in Section D3.2.3 and Table D-17, rates of stomatal conductance in the listed sources were measured for the dominant annual (*Bromus madritensis*), three dominant drought-deciduous species (*L. andersonii*, *A. dumosa*, and *Krameria erecta*), and three dominant evergreens (*L. tridentata*, *E. nevadensis*, and *Ericameria cooperi*) in Yucca Mountain vegetation associations. Conductances were measured under a variety of conditions during several time periods allowing identification of low and high physiological activity. All but two of the studies were conducted in the field on the NTS or within the Mojave Desert region. Two of the studies (Hamerlynck et al. (2000 [DIRS 177130], p. 188 and Huxman et al. (1999 [DIRS 177133], p. 774) were conducted in a glasshouse at the University of Nevada, Las Vegas. Treatments were evaluated and data from those that induced stress and resulted in low conductance were not used. Data from control treatments and treatments that created optimum growing conditions were compared to field measured values and deemed appropriate for initial/end and mid-season stages, respectively.
- Reliability of Data Sources**—The data from the listed sources (Table A-2) came from peer-reviewed publications and were thus judged to be appropriate for publication by experts in the field of vegetation science specific to the Mojave Desert. In addition, the methods of data collection were described in sufficient detail to determine whether the data were applicable for calculating stomatal resistance. It was concluded that these data sources were reliable for use in this analysis.



Because the data considered here were for dominant species relevant to Yucca Mountain, were from studies conducted at the NTS, Mojave Desert region, or from appropriate glasshouse studies, and were from reliable data sources, it was concluded that the data were suitable for the specific application in this analysis. Additionally, study methods were described in sufficient detail to determine that the data were suitable for use as input to this model. Thus, the data were considered qualified for the intended use.

### A1.5 ROOTING DEPTHS FOR PRESENT-DAY AND MONSOON CLIMATES

Rooting depths from published literature sources in Table A-3 were used in Section 6.5.3.2 to develop mean maximum effective rooting depth ( $Z_r$ ) for present-day and monsoon climate states.  $Z_r$  is used in the MASSIF model to calculate water content in the root zone and root zone water depletion (Section 6.4). Rooting depths from these publications are presented in Table 6.5.3.2-1.

Table A-3. Sources of Published Measurements of Rooting Depths for Desert Plants

Sources
Canadell et al. 1996 [DIRS 177626], p. 588, Appendix 1
Hansen and Ostler 2003 [DIRS 177619], p. 85, Table 7-1
Jackson et al. 2002 [DIRS 177171], p. 624, Table 1
Rundel and Gibson 1996 [DIRS 103614], p. 99, Figure 4-10
Rundel and Nobel 1991 [DIRS 128001], p. 355 – 357
Schenk and Jackson 2002 [DIRS 177638], p. 491, Figure 9
Yoder and Nowak 1999 [DIRS 177167], p. 91, Figure 6
Harris 1967 [DIRS 177630], p.97, Figure 6
Hulbert (1955 [DIRS 177129] p.191
Link et al. 1990 [DIRS 177142], p. 512
Rickard 1985 [DIRS 177635], p.170
Foxx et al. 1984 [DIRS 177628], p. 5, Table 3

The following information was considered to evaluate whether rooting depths in the listed publications were suitable for use in development of  $Z_r$  for Present-Day and Monsoon climates.

- Extent to Which the Data Demonstrate Properties of Interest**—Rooting depths are most applicable to this analysis if they are for common plant species at Yucca Mountain that have the potential for deep root growth. Study locations should be in desert environments and can be outside of the Mojave Desert in order to include maximum rooting depth potentials for xeric shrubs. As described in Section 6.5.3.2, all rooting depths in the listed publications were for common deep rooting species at Yucca Mountain, for shrubs in xeric environments in western and southwestern United States receiving the same range of precipitation as Yucca Mountain, or for a common exotic grass with the potential for forming monocultures. Sources with rooting depths for the exotic grass were included because of its presence at Yucca Mountain and its potential for forming monocultures at the expense of deeper-rooted shrubs. All of the studies were conducted in appropriate desert environments, including the NTS, Chihuahuan, and Great Basin deserts. For the reasons listed above, the data provided in these sources demonstrate the property of interest (maximum rooting depth).

- Reliability of Data Sources** – The data from all but two of the listed sources (Table A-3) came from peer-reviewed publications and were thus judged to be appropriate for publication by experts in the field of plant root science specific to desert environments. In addition, the methods of data collection were described in sufficient detail to determine whether the data were applicable for calculating  $Z_r$ . The two, non peer-reviewed sources, Hansen and Ostler (2003 [DIRS 177619], p. 85, Table 7-1) and Foxx et al. (1984 [DIRS 177628]), p. 6, Table 3) were publications by Bechtel Nevada Ecological Services and Los Alamos National Laboratory, respectively. Hansen and Ostler (2003 [DIRS 177619]) included a comprehensive literature search and a limited field study on rooting depths for several plant species on the NTS. Both authors have advanced degrees in vegetation science fields and have several years of experience studying Mojave Desert plant ecology. Foxx et al. (1984 [DIRS 177628]) obtained means and ranges of rooting depths for several species (including several from the Great Basin and Mojave deserts) from an extensive bibliographic study that contained 1,034 different rooting citations. The authors are professionals employed by national laboratory. Based on these factors, it was concluded that these data sources were reliable for use in this analysis.

Because the data considered here were for xeric shrubs and an exotic grass relevant to Yucca Mountain, were from studies conducted at the NTS and other appropriate desert habitats, and were from reliable data sources, it was concluded that the data were suitable for the specific application in this analysis. Additionally, study methods were described in sufficient detail to determine whether the data were applicable for this analysis. Thus, the data were considered qualified for the intended use.

## A1.6 ROOTING DEPTHS FOR THE GLACIAL TRANSITION CLIMATE

Rooting depths from sources in Table A-4 were used in Section 6.5.3.2 to develop mean maximum effective rooting depth ( $Z_r$ ) for the Glacial Transition climate. Rooting depths from these sources are presented in Table 6.5.3.2-2.

Table A-4. Sources of Rooting Depths for Potential Glacial Transition Vegetation

Sources
Canadell et al. 1996 [DIRS 177626], p. 588, Appendix 1
Foxx et al. 1984 [DIRS 177628], p. 5 and 6, Table 3
Harris 1967 [DIRS 177630], p. 97, Figure 6
Hulbert 1955 [DIRS 177129], p. 191
Leffler et al. 2004 [DIRS 177926], p. 10, Figure 1
Link et al. 1990 [DIRS 177142], p. 512
Richards and Caldwell 1987 [DIRS 177927], p. 488
Rickard 1985 [DIRS 177635], p. 170
Ryel et al. 2003 [DIRS 177632], p. 760
Sturges and Trlica 1978 [DIRS 177928], pp. 1282 to 1285
Seyfried et al. 2005 [DIRS 178060], pp. 282 to 283

The following information was considered to evaluate whether rooting depths in the listed sources were suitable for use in development of  $Z_r$  for the Glacial Transition climate.

- **Extent to Which the Data Demonstrate Properties of Interest**—Rooting depths are most applicable to this analysis if they are for common plant species of the Great Basin desert that could occur at Yucca Mountain under Glacial Transition conditions (see Section 6.5.3.1 for analysis of potential future vegetation). The plant species considered should have the potential for deep root growth. Data should be collected from Great Basin desert environments. As described in Section 6.5.3.2, all rooting depths in the listed sources were for common Great Basin species. With one exception, all of the species had potential for growing roots deep into the soil profile. Sources with rooting depths for *Bromus tectorum*, an exotic annual grass, were included because of the potential for this species to form monocultures at the expense of deeper rooting shrubs and grasses. All data from the listed sources were collected in the Great Basin desert.
- **Reliability of Data Sources**—The data from all but one of the listed sources (Table A-4) came from peer-reviewed publications and were thus judged to be appropriate for publication by experts in the field of plant root science specific to desert environments. The use of the source that is not peer reviewed, Foxx et al. 1984 [DIRS 177628] is justified in Section A1.5.

Because the data considered here were for common Great Basin plants, were from studies conducted in Great basin desert habitats, and were from reliable data sources, it was concluded that the data were suitable for the specific application in this analysis. Additionally, study methods were described in sufficient detail to determine whether the data were applicable for developing  $Z_r$ . Thus, the data were considered qualified for the intended use.

## **A2. QUALIFICATION OF EVAPOTRANSPIRATION DATA AND CALCULATION METHODS FOR USE AS DIRECT INPUT**

This Section documents the demonstration that data and calculation methods are suitable for their intended use as inputs for calculating evapotranspiration at Yucca Mountain. Because these data were not acquired or developed for the Yucca Mountain Project (YMP), they are qualified for use as input to this report in accordance with SCI-PRO-006, *Models*, Section 6.2.1.K. The following inputs are addressed:

- Surface Albedo (Section A2.1)
- Solar Radiation on Inclined Surfaces (Section A2.2)
- Evaporation Layer Depth (Section A2.3)
- Solar Constant (Section A2.4)
- Dew point temperature offset (Section A2.5).

The attributes of the data considered in the determination of suitability are the extent to which the data demonstrate properties of interest and the reliability of the data source.

## A2.1 SURFACE ALBEDO VALUES

The following information was used to evaluate whether the surface albedo values presented by Brutsaert (1982 [DIRS 176615], p 136, Table 6.4) were suitable for use in development of input parameters for simulating evapotranspiration.

**Extent to Which the Data Demonstrate Properties of Interest**—Terrain albedo is used to calculate reflected radiation from areas surrounding model grid cells, which affects the energy balance of these grid cells.

**Reliability of Data Source**—The referenced source by W. Brutsaert, *Evaporation into the Atmosphere*, was published in 1982 and has been in print ever since. The book, even though it is dated, is still current in its theory and is regarded as a foremost authority on evapotranspiration theory and boundary layer meteorology. The text is widely cited and the information contained therein is considered reliable and qualified for the intended use. The author W. Brutsaert is a professional and highly regarded expert in the technical field of environmental physics and engineering. Dr. W. Brutsaert, a professor at Cornell University since 1962, is a member of the national Academy of Engineering, and was awarded the 1999 Horton Medal by the American Geophysical Union for outstanding contributions to geophysical aspects of hydrology and the 2003 Jule G. Charney Award from the American Meteorological Society for research achievement in the atmospheric and hydrologic sciences. He has published extensively on the topic of environmental biophysics and has received many awards and honors. Therefore, the information from the source by W. Brutsaert is considered to be reliable and qualified for the intended use.

## A2.2 SOLAR RADIATION ON INCLINED SURFACES

The following information was used to evaluate whether the values and equations in studies by Duffie and Beckman (1980 [DIRS 176264]; 1991 [DIRS 176616]) were suitable for use in calculation solar radiation on inclined surfaces.

**Extent to Which the Data Demonstrate Properties of Interest**—The equations and parameters taken from these sources are intended for, and are sufficient for, the calculation of available solar radiation on inclined surfaces. Therefore they are appropriate for calculation of potential evapotranspiration.

**Reliability of Data Source**—The referenced sources by Duffie and Beckman, *Solar Engineering of Thermal Processes*, were published in 1980 ([DIRS 176264], First Edition) and 1991 ([DIRS 176616], Second Edition). The third Edition of *Solar Engineering of Thermal Processes* was recently published in August, 2006; therefore, the information from this book is considered to be reliable and qualified for the intended use and has been in publication for approximately 26 years. The book provides a complete coverage on the basic theory of solar radiation and its calculation. The authors are recognized authorities on the topic of solar radiation and they hold several professional awards. John A. Duffie (deceased) was Professor Emeritus of Chemical Engineering and past Director of the Solar Energy Laboratory at the University of Wisconsin–Madison. William A. Beckman is the Ouweneel-Bascom Professor Emeritus of Mechanical Engineering and Director of the Solar Energy Laboratory at the University of

Wisconsin–Madison. Therefore, the equations for solar energy input to inclined surfaces are considered to be reliable and qualified for the intended use.

### A2.3 EVAPORATION LAYER DEPTH

The following information was used to evaluate whether the recommendations on assigning evaporation layer depth presented by Allen et al. (2005 [DIRS 176009], p. 4) were suitable for use in developing net infiltration estimates for Yucca Mountain.

**Extent to Which the Data Demonstrate Properties of Interest**—Due to the differences between soil characteristics at Yucca Mountain and those more typical of agricultural areas, it was considered appropriate to expand the range in evaporation layer depth suggested by Allen et al. (1998 [DIRS 157311], p. 144). This paper provides guidance to consider the length of drying periods in the assignment of this parameter, which would tend to increase the evaporation layer thickness for a relatively dry site such as Yucca Mountain.

**Reliability of Data Source**—The referenced source by Allen et al., *FAO-56 Dual Crop Coefficient Method for Estimating Evaporation from Soil and Application Extensions*, was published in 2005 in the *Journal of Irrigation and Drainage Engineering*. The author, Dr. Richard G. Allen, is a professor of water resources engineering at the University of Idaho. Allen has published extensively on subject topics specifically relating to the calculation of reference evapotranspiration and holds many professional awards, including three best paper awards from ASCE Journals. Allen is regarded as an international authority on the calculation of evapotranspiration and supporting components. Allen is also the main author of *Crop evapotranspiration* (Allen et al. 1998 [DIRS 157311]) and a principal editor of *The ASCE Standardized Reference Evapotranspiration Equation* (Allen et al. 2005 [DIRS 176207]), two widely used publications on the subject of reference evapotranspiration considered here as Established Fact. Therefore, the guidance provided in this paper is considered to be reliable and qualified for its intended use.

### A2.4 SOLAR CONSTANT

The following information was used to evaluate whether the data summary of measurements of the solar constant as a function of time presented by Dewitte et al. (2004 [DIRS 178528], p. 214) were suitable for use in developing net infiltration estimates for Yucca Mountain.

**Extent to Which the Data Demonstrate Properties of Interest**—Dewitte et al. (2004 [DIRS 178528]) presents a time history of available solar irradiance measurements and estimates the uncertainty in any long term estimates of this quantity. The solar constant is used as direct input to calculations of evapotranspiration and therefore a good understanding of possible changes in this value with time is potentially important.

**Reliability of Data Source**—The referenced source by Dewitte et al., *Measurement and Uncertainty of the Long Term Total Solar Irradiance Trend*, was published in 2004 in the journal *Solar Physics*. The first author, Steven Dewitte is a Professor in the department of Electronics and Information Processing at the Royal Meteorological Institute Belgium. The second author, Dominique Crommelynck is the honorary head of the Royal Meteorological Institute Belgium

and is a noted expert in the field of solar measurements. Therefore, the data and analysis provided in this paper is considered reliable and qualified for its intended use.

## **A2.5 DEW POINT TEMPERATURE OFFSET**

The following information was used to evaluate whether the data obtained from a peer-reviewed journal article by Temesgen et al. (1999 [DIRS 178312], pp. 29 to 30) were suitable for use in developing net infiltration estimates for Yucca Mountain. The specific data used from this source is the upper bound on the dew point temperature offset used in the calculation of reference evapotranspiration in Section 6.5.4.1.

**Extent to Which the Data Demonstrate Properties of Interest**—Temesgen et al. (1999 [DIRS 178312], p. 29 to 30) paper presents a study that compared predicted and measured evapotranspiration at a number of international sites that differed in their atmospheric aridity. In relatively humid environments, the minimum daily temperature is typically very near the dew point temperature due to latent heating that occurs when water vapor condenses at or below the dew point temperature. However, in arid climates, minimum daily temperature frequently falls significantly lower than the dew point temperature because there is little water available to condense. Because the calculation of reference evapotranspiration requires that the meteorological data be collected over “an extensive surface of green grass, shading the ground and not short of water” (Allen et al. 1998 [DIRS 157311], p. 25), a dew point temperature offset is generally applied in the calculation of reference evapotranspiration in order to adjust temperature data collected over nonideal surfaces so it is more representative of these reference conditions (e.g., Allen et al. 1998 [DIRS 157311], pp. 58 to 59). Temesgen et al. (1999 [DIRS 178312], pp. 29 to 30, Table 4) lists a range of dew point temperature offsets for various arid and humid sites around the world. The highest dew point temperature offset (shown as “TD”) value listed on Table 4 is 10°C for several of the arid locations for both summer and winter seasons. This value is used as direct input for the upper bound on the uncertainty distribution for the dew point offset parameter discussed in Section 6.5.4.1. The source contains the exact type of information needed to constrain this parameter and is appropriate for its intended use.

**Reliability of Data Source**—The referenced source by Temesgen et al., *Adjusting Temperature Parameters to Reflect Well-Watered Conditions*, was published in 1999 in the *Journal of Irrigation and Drainage Engineering*. The first author, B. Temesgen was a graduate student of Dr. Richard G. Allen, the second author and now a professor of water resources engineering at the University of Idaho. Allen has published extensively on subject topics specifically relating to the calculation of reference evapotranspiration and holds many professional awards, including three best paper awards from ASCE Journals. Allen is regarded as an international authority on the calculation of evapotranspiration and supporting components. Allen is also the main author of *Crop evapotranspiration* (Allen et al. 1998 [DIRS 157311]) and a principal editor of *The ASCE Standardized Reference Evapotranspiration Equation* (Allen et al. 2005 [DIRS 176207]), two widely used publications on the subject of reference evapotranspiration considered here as Established Fact. Finally, the third author, Dr. Donald T. Jensen is currently the Utah state climatologist. The qualifications of these authors and the reliability of the peer-reviewed journal both justify the qualification of this data for use in this report.

### **A3. QUALIFICATION OF SUBLIMATION COEFFICIENT FOR USE AS DIRECT INPUT**

The following information was used to evaluate whether the measurements of fraction of snowpack lost to sublimation reported by Hood et al. (1999 [DIRS 177996]) were suitable for use in development of the sublimation parameter (SUB). This source is used as direct input in Section 6.5.1.7.

**Extent to Which the Data Demonstrate Properties of Interest**—Hood et al., (1999 [DIRS 177996]) report measured sublimation over a nine-month period and is therefore more reliable than previous studies which were based on data only from the snowmelt season.

**Reliability of Data Source**—The median value of 10% snow sublimation used in the infiltration model originates from studies cited by Hood et al. (1999 [DIRS 177996]). These studies include the author's own study in which they found snow sublimation to be about 15% of the total seasonal snow accumulation at Niwot Ridge in the Colorado Front Range. They also cite seasonal sublimation estimates of 18% and 20% for the Sierra Nevada, California, reported in two other studies. Seasonal snow sublimation is extremely difficult to measure, and there is large inherent uncertainty in this parameter. Hood et al. (1999 [DIRS 177996]) can be considered to be experts in the field given their organizations and publication records. Their organizations include the Institute of Arctic and Alpine Research (INSTAAR) at University of Colorado, Boulder, and the National Operational Hydrologic Remote Sensing Center, which provides comprehensive snow observations, analyses, data sets and map products for the Nation. Eran Hood, Mark Williams, and Don Cline have all published numerous articles related to snow. Therefore, the information from this journal article is considered to be reliable and qualified for the intended use.

### **A4. ESTABLISHED FACT INPUTS**

A number of references cited as direct input are Established Fact as defined in SCI-PRO-004 Rev 2, p. 7 and Attachment 1. These are listed below with an explanation. These do not include DTNs designated as established fact.

1. Allen et al., 1998 [DIRS 157311] *FAO Irrigation and Drainage Paper No. 56 Crop Evapotranspiration*. This is a United Nations report that is a set of guidelines used by international scientists and engineers in their work practices.
2. Allen et al. 2005 [DIRS 176207] *The ASCE Standardized Reference Evapotranspiration Equation*. This is an ASCE publication that is considered the standard handbook and reference on calculating reference evapotranspiration.
3. Maidment 1993 [DIRS 125317] *Handbook of Hydrology*. This is a scientific handbook and a standard reference utilized by civil engineers and hydrologists.
4. IEEE/ASTM SI 10-1997 Standard for Use of the International System of Units (SI): The Modern Metric System. This is the standard by which all scientists apply units.

5. U.S. Department of Agriculture government publications including “fact sheets” by Anderson (2002 [DIRS 177625]), Tirmenstein (1999 [DIRS 177641]; 1999 [DIRS 177642]), USDA (2002 [DIRS 178073]), and Zlatnik (1999 [DIRS 177639]). The USDA intended these for scientists to use as sources of information regarding specific plant species.



**APPENDIX B**  
**GEOSPATIAL DATABASE**



## B1. INTRODUCTION

This appendix describes the technical processes within a Geographic Information System (GIS) to develop spatial inputs for the Mass Accounting System for Soil Infiltration and Flow (MASSIF) model. A GIS is the combined hardware and software used for storage, retrieval, mapping and analysis of geographic data. Using a GIS, data were collated from a range of sources, processed into a usable format, and combined into a single spatial database containing input values and their associated spatial coordinates for the MASSIF model. A complementary set of calibration data was produced in conjunction with the overall model inputs. These calibration files provided model inputs for areas with existing stream gage data to serve as a check of model accuracy.

A spatial database is a table with fields (columns) of variables that include real world coordinates. In a GIS, these coordinates can be used to visually display the tabular data as points, lines, or for the MASSIF model, rectangular map grids that form the individual model cells. Each record (row) in the table represents a single 30-m<sup>2</sup> grid cell within the MASSIF model. A spatial database is constructed by combining individual data layers based on shared coordinates or data within a field. A GIS also allows queries of the spatial relationship between the various data fields. For the purpose of the MASSIF model, for each record in the database, the GIS stores a unique grid cell number, universal transverse mercator (UTM) coordinates, latitude and longitude, elevation, a downstream grid cell identifier, slope, azimuth, soil depth, soil type, bedrock type, and a measure of vegetation called “potential vegetation response” (PVR; see Appendix E). The GIS can be queried to give data values at a given point or the full range of variables contained in an area. The visual display capability together with the measurement of spatial relationships makes GIS an ideal tool for preparing and examining data inputs for the MASSIF model.

Building the infiltration model spatial database was a multistage process involving importing some data layers and using the GIS to generate others within the spatial database. The database contains nine data layers supplying inputs to the MASSIF model and four spatial values that supply geographic coordinates within a 30- × 30-m grid framework. The project grid measures 367 columns by 691 rows resulting in 253,597 grid cells. The project area boundary is defined by UTM NAD 27 Zone 11 coordinates with a southwest corner at 544,646-m east/4,067,118-m north and a northwest corner at 555,656-m east/4,087,848-m north.

During the process of building the spatial database, several important tasks were completed. Defining the watershed subset boundaries within the larger project area boundary was the first task (Section B2). This delineation in turn defined the model boundary, a 139,092-grid-cell subset of the project area. The initial data layer, elevation, was selected and the processing steps developed (Section B2.1). Next, the elevation data needed to undergo a three-stage watershed characterization process that defined the actual watershed boundaries and created ancillary data layers required by the spatial database (Section B2.2). Then, these files required formatting to prepare them for the spatial database (Section B2.3).

Not all the necessary data were created during the watershed delineation process. Additional spatial database information consisted of bedrock and soil characteristics that required formatting and editing to prepare the layers for the spatial database (Section B3.1). The PVR was a data

layer calculated using Normalized Differentiated Vegetation Index (NDVI) measurements as detailed in Appendix E. The last required data layer was the field with the downstream cell identification number. This field was determined using a grid cell identification number and the direction of surface water flow leaving that grid cell (Section B3.2).

The assembly of the spatial database required conjoining the separate data layers into a single more comprehensive format (Section B4). The database covers the entire model area, but it was necessary to subdivide it into the individual watersheds delineated earlier (Section B4.1).

Concurrent with the modeled watersheds, a study using actual surface flow data required the delineation of six streamflow watersheds (Section B5). This process used imported stream gage locations (Section B5.1) to constrain the watershed delineation process. The streamflow watershed boundaries were used to divide the spatial database into small study areas that can be used to compare model results to real world observations (Section B5.2).

The final result from this process was a spatial database split into eleven project watersheds and subdivided into six, smaller representative drainages that sample select portions of the project area. These final files are formatted into comma-delimited text files that serve as direct input into the MASSIF model.

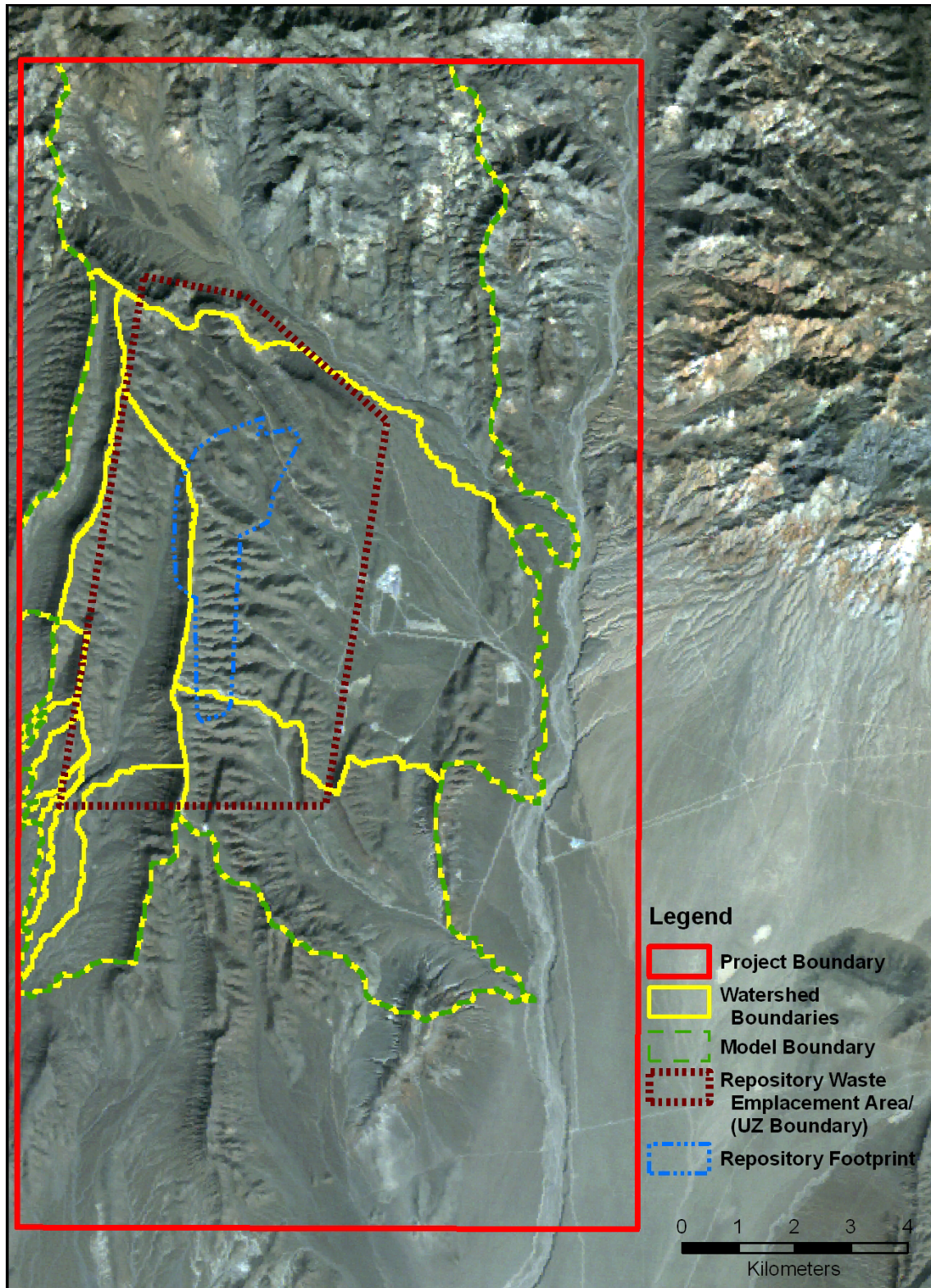
## **B2. GIS WATERSHED CHARACTERIZATION**

The MASSIF infiltration model addresses the area that drains Yucca Mountain above the proposed repository waste emplacement area. Eleven separate drainages (or watersheds) were identified; three larger watersheds drain the east face of the ridge and eight smaller watersheds drain the west face. Each watershed formed a component of the MASSIF model.

The watersheds were delimited using elevation and slope to define surface water flow direction to a single outlet (pour point). Defining the eleven watersheds also delineated the overall infiltration model boundary within the larger project boundary. The larger rectangular project boundary encompassed 226.34 km<sup>2</sup>. The mix of eleven larger (up to 41.16 km<sup>2</sup>) and smaller (down to 0.11 km<sup>2</sup>) watersheds made up the individual model components that were used to calculate net infiltration. The infiltration model boundary, comprised of the combination of these eleven watersheds, encompassed 125.18 km<sup>2</sup>. Figure B-1 shows the relationship between these three sets of boundaries. The following discussion details the tools and source data used to create these watershed delineations.

### **B2.1 SOFTWARE AND DATA CONSIDERATIONS**

In a GIS, spatial attributes are stored in conjunction with descriptive attributes allowing tabular data to be displayed in reference to their position on the earth. Data can consist of points, lines, and polygon shapes with multiple attributes connected to each of these features, allowing a layering of data values. With the layered features, spatial relationships can be measured and complex models can be constructed. The capacity to combine separate data layers and run a model to extract additional data layers from existing layers is extremely important for the infiltration model database; therefore, GIS is the perfect tool for the tasks required.



Source: Output DTNs: SN0608DRAINDYM.001, SN0612FTPRNUZB.002, and SN0608NDVILSTM.001.

Figure B-1. Boundaries within Project Area

The GIS used for these tasks is ArcGIS (ArcGIS Desktop Version 9.1 STN: 11205-9.1-00 [DIRS 76015]), from Environmental Systems Research Institute (ESRI), the market leader in off-the-shelf GIS software. In addition, the Spatial Analyst extension increases the flexibility of ArcGIS to work with raster-based data. Using the Model Builder functionality of the ArcGIS ArcToolbox, a fully automated routine was established where base data and parameters can be loaded into the model to then have a series of watershed characterization tasks applied iteratively to derive a final watershed catchment grid. In addition, nearly all the data processing functions required to prepare the spatial inputs for MASSIF were conducted within the GIS database. The spatial database format also allowed data queries to be conducted prior to running MASSIF.

The most accurate topographic data available were chosen from a field of three data sets. Spatial data supply the measures of elevation, azimuth, and slope that play important roles for accessing parameters, including vegetation cover, runoff, and evapotranspiration (ET) that are active in the calculation of net infiltration in each model grid. Therefore, spatial accuracy is crucial for model accuracy.

The three candidate data sets for topographic data were U.S. Geological Service (USGS) digital elevation model (DEM), the USGS National Elevation Dataset (NED) and the Shuttle Radar Topography Mission (SRTM) data. All elevation data sets are created through a sampling technique using different methods and resolution. A set of single elevation values can never truly represent all the variability found in all represented grid cells no matter the data resolution be it 10 m or 30 m. With this knowledge, there is an understanding that the data may need some modification to effectively model certain aspects of the landscape.

DEM, and as a result NED, data is created from using existing contour maps and augmented with aerial photography. Much of this data consists of passively collected data, so even though the resolution may be quite high (up to 10-m square) actual measurements used to create the data are limited and most data values were created through interpolation.

USGS DEM data often are used to supply the topological information necessary to run basic watershed characterization models. A DEM is constructed as a 10-m or 30-m grid where the centroid of each grid cell is assigned an elevation based on its corresponding location on a topographic map. Because they are digitized from maps that represent earlier interpretation of topography, these data incorporate inherent flaws, especially in areas that experience significant elevation change over a short distance.

NED was compiled by the USGS to assemble the best available topographic data into a continuous elevation model for the entire country. This dataset typically employs the USGS 10-m DEM data, when available, that is nine times more detailed than the coarser 30-m data. For the YMP, the NED metadata indicated that 10-m data were available and incorporated into the dataset; however, these data still contain inherent limitations of accuracy because they were formulated by extrapolating elevation data from topographic maps.

SRTM is a more recent dataset that was collected through an interferometric synthetic-aperture radar system carried aboard a U.S. space shuttle mission during February 2000. These data are highly accurate because the active sensor collected a data value for each 30-m target, meaning no extrapolation was necessary. The data will still be limited by having a single value in a 30-m<sup>2</sup>

grid cell represent all the possible variation in that cell, but this is the case with all three of the data sets spacing. One drawback with SRTM datasets are occasional problematic gaps due to radar shadow at low angles of incidence or signal interference from numerous vertical surfaces (i.e., signal bounces between tall buildings or forest tree trunks). These influences are not problematic for the remote treeless Yucca Mountain region, and the dataset showed none of these characteristics.

The availability of three adequate data sets raised the issue of which would best serve the model's needs. The 30-m DEM was eliminated because, with its 10-m resolution, the NED superseded the coarser DEM; however, the question remained whether to use NED or SRTM data. A raster subtraction method was employed to observe the differences between these datasets. The resulting grid showed a misalignment between the two data sets. Smith and Sandwell (2003 [DIRS 177358]) faced this question on a project in the Amazon and devised a selection method that compared SRTM, NED, and high-resolution aerial laser datasets. Their results showed the NED possessed an 11.87-m longitudinal and 10.58-m latitudinal shift versus the spatially accurate, high-resolution laser imagery. The laser data were used as the benchmark because a Laser Imaging Detection and Range (LIDAR) system is an active sensor, typically flown from an aircraft that has very fine resolution and can easily incorporate ground control points for accuracy. A comparable shift was not detected with the SRTM. On the basis of the Smith and Sandwell (2003 [DIRS 177358]) results, SRTM data were selected as the superior choice for the infiltration model. In addition, the SRTM data has been subjected an independent assessment of accuracy that is detailed below (Rodriguez et al. 2005 [DIRS 177738]). A similar investigation for the NED data set is planned, but has not been completed and users have to compile the errors present in each contributing DEM to access overall accuracy.

The SRTM data were obtained from the USGS Earth Resources Observation and Science (EROS) Data Center (DTN: SN0601SRTMDTED.001 [DIRS 177242]).

### Assessment of SRTM Accuracy

The NASA Shuttle Radar Topography Mission (SRTM) collected interferometric radar data that was used to generate a near global topography data product. This data underwent a ground-truth analysis to provide a detail measure of the different components of the error, their magnitudes, and spatial structure (Rodriguez et al. 2005 [DIRS 177738]).

The data was collected to meet the following performance requirements:

1. The linear vertical absolute height error shall be less than 16 m for 90% of the data
2. The linear vertical relative height error shall be less than 10 m for 90% of the data
3. The circular absolute geolocation error shall be less than 20 m for 90% of the data
4. The circular relative geolocation error shall be less than 15 m for 90% of the data.

The table shown below summarizes the SRTM performance observed by comparison against the available ground-truth data. The displayed measurements represent 90% errors in meters. It has been modified here to display just the North America results.

	<b>N. America – Observed</b>	<b>Required</b>
Absolute Geolocation Error	12.6	<16
Absolute Height Error	9.0	<10
Relative Height Error	7.0	<15

The study's authors found, "the analysis had shown that the SRTM error could be divided into very long wavelength (continental scale or larger) errors and short wavelength random errors. The ground-truth data were not appropriate for validating relative geolocation errors. It is expected that the main sources of geolocation errors are also long wavelength, so that the relative geolocation error will in general be smaller than the absolute geolocation error, since common errors will cancel. The absolute geolocation performance is better than that required for the relative geolocation, which provides indirect evidence that the relative geolocation requirement was also met" (Rodriguez et al. 2005 [DIRS 177738], page 9).

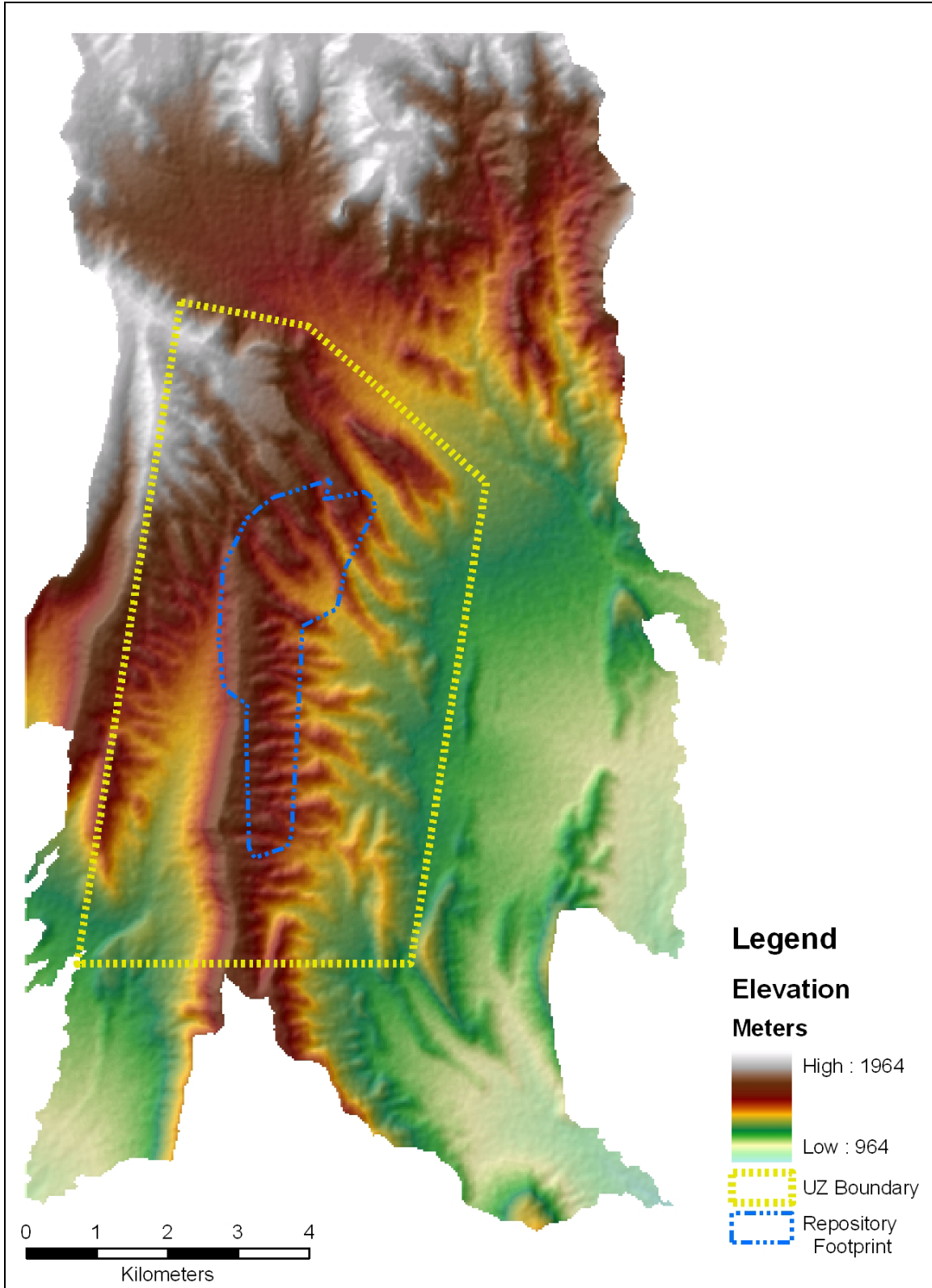
Smith and Sandwell (2003 [DIRS 177358]) further showed the small error involved in the geolocation measurements in the SRTM data. In all, the error falls within the breadth of a single model pixel. As to the height error, for this infiltration model a small flux in actual measured height could potentially interfere in the delineation of a watershed by creating a pixel surrounded with higher elevation values, creating a 'sink' with no access for flowing water to exit the cell. A GIS step of filling such sinks and thus removing the error impact is discussed in Section B2.2, Processing the Elevation Data.



## **B2.2 PROCESSING THE ELEVATION DATA**

The raw form of the SRTM data required processing for use in the spatial database, as the SRTM file format and map coordinate projection do not correspond to those needed for the infiltration model. Once format and projection were revised, the elevation data could then serve as the base data layer from which multiple derivative data layers could be created. These additional layers provided information, such as slope direction and steepness that is required by the MASSIF infiltration model.

The raw form of the SRTM data layer was processed using Research Systems, Inc. (RSI) Environment for Visualizing Images (ENVI; ENVI + IDL, Version 4.2: STN: 11204-4.2-00) image processing software. ENVI offers more options in choosing how to process raster data than ArcGIS software. All the data processing represented in Sections B2.2 and B2.3 are archived in 'Drainage Delineation at Yucca Mountain' (Output DTN: SN0608DRAIN DY M.001). The SRTM data were divided as a subset within the project boundary, set to 30-m pixels and reprojected to UTM NAD 83 Zone 11. This conflicted with the MASSIF model requirement of UTM NAD 27 Zone 11 but would be reprojected in Section B-4, *Assembling the Spatial Database*, after concurrent image processing tasks detailed in Appendix E were completed. With the data resized and reprojected, the elevation data were saved as an ESRI grid file ready for watershed delineation. Figure B-2 highlights the elevation range from 964 m to 1,964 m across the YMP area.



Source: Output DTNs: SN0701SPALAYER.002 and SN0612FTPRNUZB.002.

Figure B-2. Elevation across Project Area

A three-stage watershed delineation process was required to generate the fewest number of watersheds that would cover the Repository Waste Emplacement Area. Each stage set a different water flow accumulation value (15,000, 1,000, and 200) which controlled the size of the resulting model watersheds. The MASSIF model runs each watershed separately, so a fewer number of drainages results in fewer modeling steps. Moreover, all watersheds must drain to single points on the edge of the YMP area, otherwise intermediate runoff values would need to be passed between drainages during the computation. Therefore, the size of the drainages was dictated by two factors: the topography of the region and the placement of the YMP boundary. The surface area of each watershed varied widely, a result of the three nearly identical delineation stages needed to generate the eleven drainage basins that cover Yucca Mountain: three large, three moderate, and five small basins. During each stage, a specific threshold variable was set that would determine the size of the resulting drainages. Thus each stage was responsible for generating either the large, medium, or small drainage basins. Variable basin sizes were necessary because the MASSIF model needed to trace potential infiltration from all locations directly over the repository footprint down the mountain slopes to each basin's pour point (the bottom-most part of the basin). The further the drainage travels, the greater is the size of the watershed; i.e., the more distant a pour point is from the headwaters, more space is provided for numerous smaller drainages to combine together and form larger, wider basin delineations. The YMP boundary, as defined, allowed the less steep eastern slopes to be followed out to distant pour points resulting in three large watersheds, but the steeper western basins were truncated by the close proximity of the YMP boundary. This limited the distance the drainages traveled before a pour point was assigned. Thus several small- and medium-sized watersheds were generated, as opposed to a few larger units had the YMP boundary allowed the drainages to travel further downslope. The results would be the same no matter how many watersheds were defined, as long as each grid unit within the Repository Waste Emplacement Area was assigned to a watershed within MASSIF.

The required size of the watersheds in each stage also limited how much of the Repository Waste Emplacement Area was covered. The first stage created a few large watersheds but did not cover areas where only smaller drainages could fit. Stage two created many more watersheds, but only three added additional coverage in areas previously missed in stage one. Stage three created many, very small drainages, but only five were required to fill the remaining coverage gap over the Repository Waste Emplacement Area. The final step was the process of fitting the eleven watersheds from the three-stage delineation process back together to create a single file representing the MASSIF model project area. Below are the details that completed this process.

The full Terrain Processing toolbox that ArcGIS utilized was a series of nine separate computations. The accompanying schematic, recreated (for legibility) from a screen-captured image while using the 'Full Terrain Processing' ArcToolbox, graphically displays the steps detailed here (Figure B-3). The figure shows the GIS tasks used and output files created during watershed delineation. All the tasks contained in the Full Terrain Processing toolbox are available individually within the ArcGIS Spatial Analyst.

The *fill* function was the first process applied to the SRTM data. *Fill* located low points or 'sinks' in the data set where all the surrounding pixels were of higher values. These sinks were accurate elevation values at the center of a data collection grid. However, elevation variation within a specific 30-m grid cell might be high enough that the elevation at the center might not

represent an elevation suitable to allow a small potential drainage to pass through the grid cell from an upstream grid cell or into a downstream cell. These sinks are probably artifacts of the sampling technique used to create the elevation dataset, where 900 potential  $1\text{m}^2$  elevation values are represented by a single value. Thus, these sinks are a consequence of simplifying the YMP area elevation to a specific set of grid-cell elevations, which neglect smaller scale features. There is really no geomorphic reason to expect significant sinks in the model domain because spillover from these sinks during heavy precipitation events would lead to erosion and the elimination of the sinks over time. Such features are more characteristic of karst terrain. If a pixel was identified as a sink, the *fill* function raised the elevation value in the pixel until a surrounding pixel is identified as having an equal or lower value, thus capable of accepting any potential accumulated surface flow that would have collected within the sink with no identified outlet cell in which to flow. The output ‘filled SRTM’ grid mirrored the original SRTM data with only small adjustments made to certain ‘sink’ pixels. Simple spatial subtraction between these two grids showed that most of the sinks occurred along drainage bottoms. Table B-1 shows how many pixels’ elevation was modified by the *Fill* function over the YMP area, within the smaller delineated watersheds model area, and over the repository footprint, stressing just how slightly (1.06 %, 0.44%, and 0.11%) this vital step affected the data. *Fill* is a required process to convert the current elevation dataset into a usable form for hydrology modeling within ArcGIS, because an uninterrupted flow is critical as opposed to slightly modifying a representative grid cell elevation value.

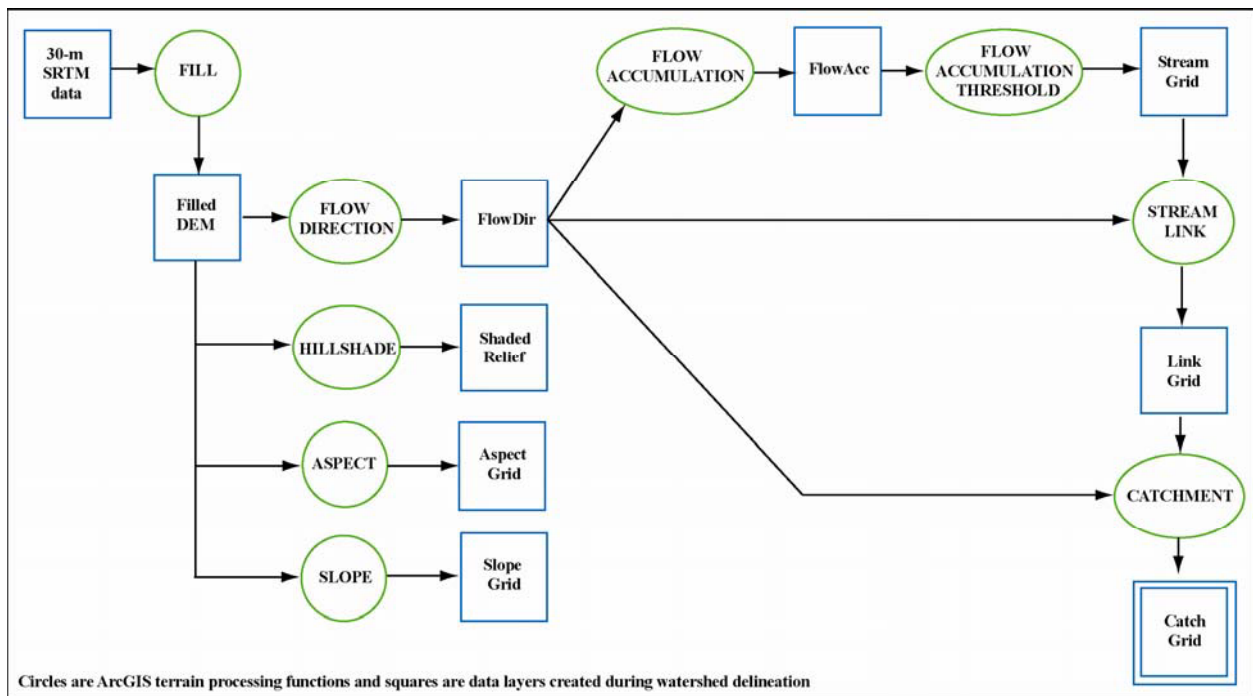


Figure B-3. Full Terrain Processing ArcToolbox Steps

Table B-1. Elevation Change Documented as a Result of the *Fill* Process

Elevation Change	Number of Pixels in Project Area	Percentage of Project Area	Number of Pixels in Model Area	Percentage of Model Area	Number of Pixels in Footprint Area	Percentage of Footprint Area
0	250,916	98.94	138,483	99.56	6,350	99.89
1	2,248	0.89	502	0.36	5	0.07
2	376	0.15	90	0.06	2	0.03
3	50	< 0.01	13	< 0.01	1	0.01
4	5	< 0.01	2	< 0.01	0	0
9	1	< 0.01	1	< 0.01	0	0
16	1	< 0.01	1	< 0.01	0	0

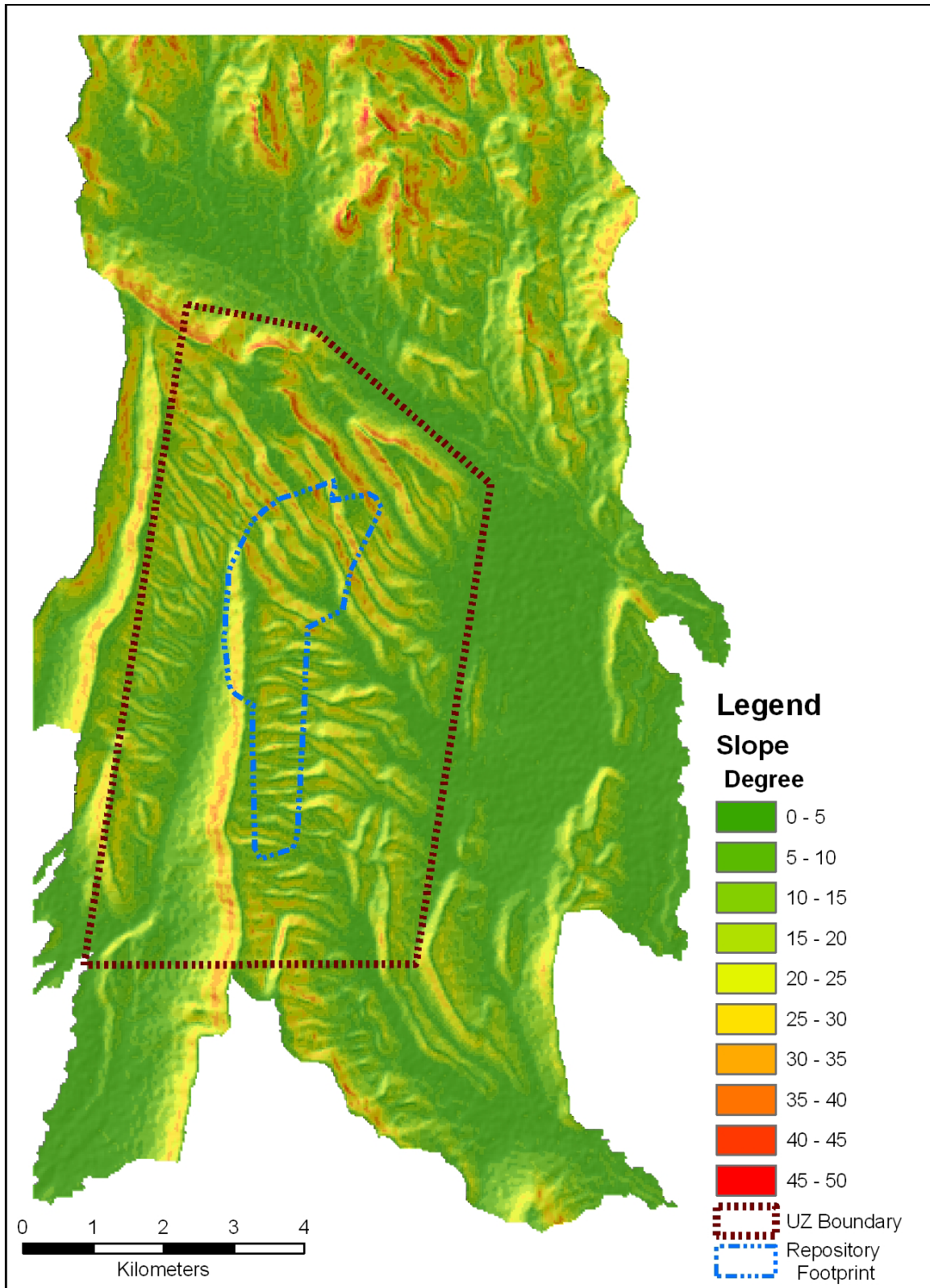
Source: DTN: SN0601SRTMDTED.001 [DIRS 177242]; Output DTN: SN0608DRAINDYM.001.

The resulting ‘filled SRTM’ layer provided the elevation data layer for the MASSIF model, but this layer was also used to create five additional datasets equally important to the model. Two of these extra layers, slope and azimuth, were stand-alone products; two more, catchment and flow accumulation, were used to organize the database but were not included in the final database; and the fifth, flow direction, required additional processing to convert it into a layer providing the downslope cell ID number. The filled elevation data, and all subsequent generated data layers used to create the MASSIF spatial database, are assembled together in Output DTN: SN0606T0502206.011.

The full suite of output created in the Full Terrain Processing ArcToolbox (Figure B-3) was as follows. The *hillshade* function created a raster layer that resembled a three-dimensional representation of the YMP area by calculating light and shadow effects based on topography and a default sun angle of 315° and a 45° incident angle. The hillshade layer was only a visual aid in presenting the data layers and did not provide a direct input to the MASSIF model.

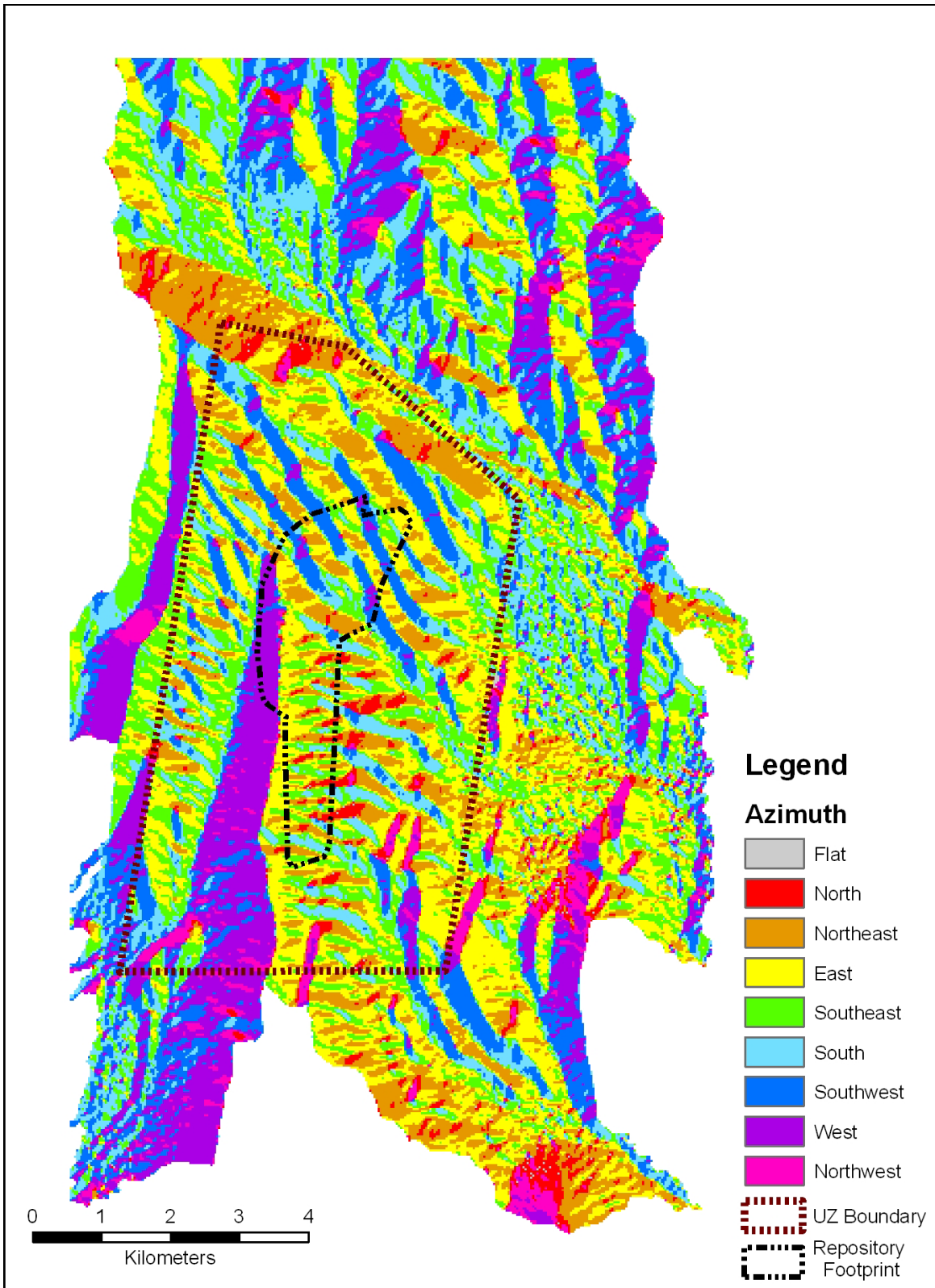
The elevation data were also used to create additional layers within the GIS including the slope and azimuth over the model area. The surface slope of each grid cell was calculated using the *slope* function in ArcGIS, which uses the elevations at eight neighboring cells. Slope is defined from 0° (horizontal) to 90° (vertical). Slopes over the infiltration modeling domain ranged between 0° and 49° (rounded to the nearest degree). A map of slopes over the modeling area is presented in Figure B-4.

The azimuth layer was created using the *azimuth* function in ArcGIS, which estimates the compass direction of a vector normal to the surface of each grid cell. This parameter is used for calculations involving the direction of incoming solar radiation. Azimuths were defined between 0° and 360° (rounded to the nearest degree) and proceeding clockwise, with 90° representing east. A map of azimuths over the modeling area is presented in Figure B-5.



Source: Output DTNs: SN0701SPALAYER.002 and SN0612FTPRNUZB.002.

Figure B-4. Slope across Project Area



Source: Output DTNs: SN0701SPALAYER.002 and SN0612FTPRNUZB.002.

Figure B-5. Azimuth across Project Area

The *flow direction* function is similar to azimuth, but instead of a compass direction, the function created a numeric code for each cell that represented which neighboring cell water would flow into when leaving the current cell. The resulting layer had values 1, 2, 4, 8, 16, 32, 64, and 128 representing east, southeast, south, southwest, west, northwest, north, and northeast, respectively. This need to determine a direction of flow was why all ‘sinks’ in the SRTM data set needed to be filled in the previous step. The Full Terrain Processing ArcToolbox used the resultant ‘flow direction’ data layer to create three additional data sets.

By examination of the flow direction relationships, the *flow accumulation* function calculated the number of upstream pixels for every pixel. The ‘flow direction’ layer was employed to trace paths of flow with accumulation counts increasing with each new pixel entered or when joining two or more convergent flow paths. A *Flow Accumulation Threshold* was applied to this function to limit the number of drainages represented to only those representing significant accumulation, in this initial case 15,000 upstream grid cells. The resulting ‘stream grid’ highlighted just these larger streams that possessed a total accumulation of 15,000 upstream cells. The *Stream Link* function assigned unique identifiers to each stream identified as having overcome the flow accumulation threshold.

The last model layer prepared from the topographic data was ‘catchment’ delineation, the definition of each basin boundary. This delineation process used the concept of pour point, the lowest point along a drainage representing the downslope edge of a drainage basin before it joins another stream from an adjoining basin. Using these pour point locations and the ‘flow direction’ raster as input, the *Catchment* function mapped all basin boundaries. This function observed where flow direction diverged in opposing directions and assigned that as a basin boundary with all sub-basin boundaries dissolved within the larger basin defined by the pour point at the catchment’s outlet.

The resulting catchment raster layer formed seven watersheds. Only three of these watersheds covered a portion of the Repository Waste Emplacement Area and were retained for use in the MASSIF model. This completed the first stage of the project area watershed delineation process. With the Flow Threshold set at 15,000, the resulting basin catchments were all large, but more of the Repository Waste Emplacement Area still fell outside these initial large watersheds. Therefore, the process had to be repeated to generate smaller watersheds to fit into gaps left by the large watersheds. The second and third stages followed the same delineation process using the Full Terrain Processing ArcToolbox, but the flow accumulation value was set to 1,000 and 200 to produce medium and small catchment basins, respectively. The end result of this delineation process was three nearly identical sets of output files, with only the size of the basins in the catchment layer the significant difference, as set by the flow accumulation threshold.

### **B2.3    FORMATTING THE TERRAIN DATA**

During the drainage delineation process, several GIS layers were calculated from the SRTM data. These data files required additional processing to convert them to a format for import into the spatial database. All the GIS layers prepared to this point were raster files, square grid cells with single data values attached. To build a single output file, the data were converted into vector files, a series of rectilinear shapes bounding areas of equal value, whose data values could be combined into multiple-field tables. This process of data formatting is discussed below.



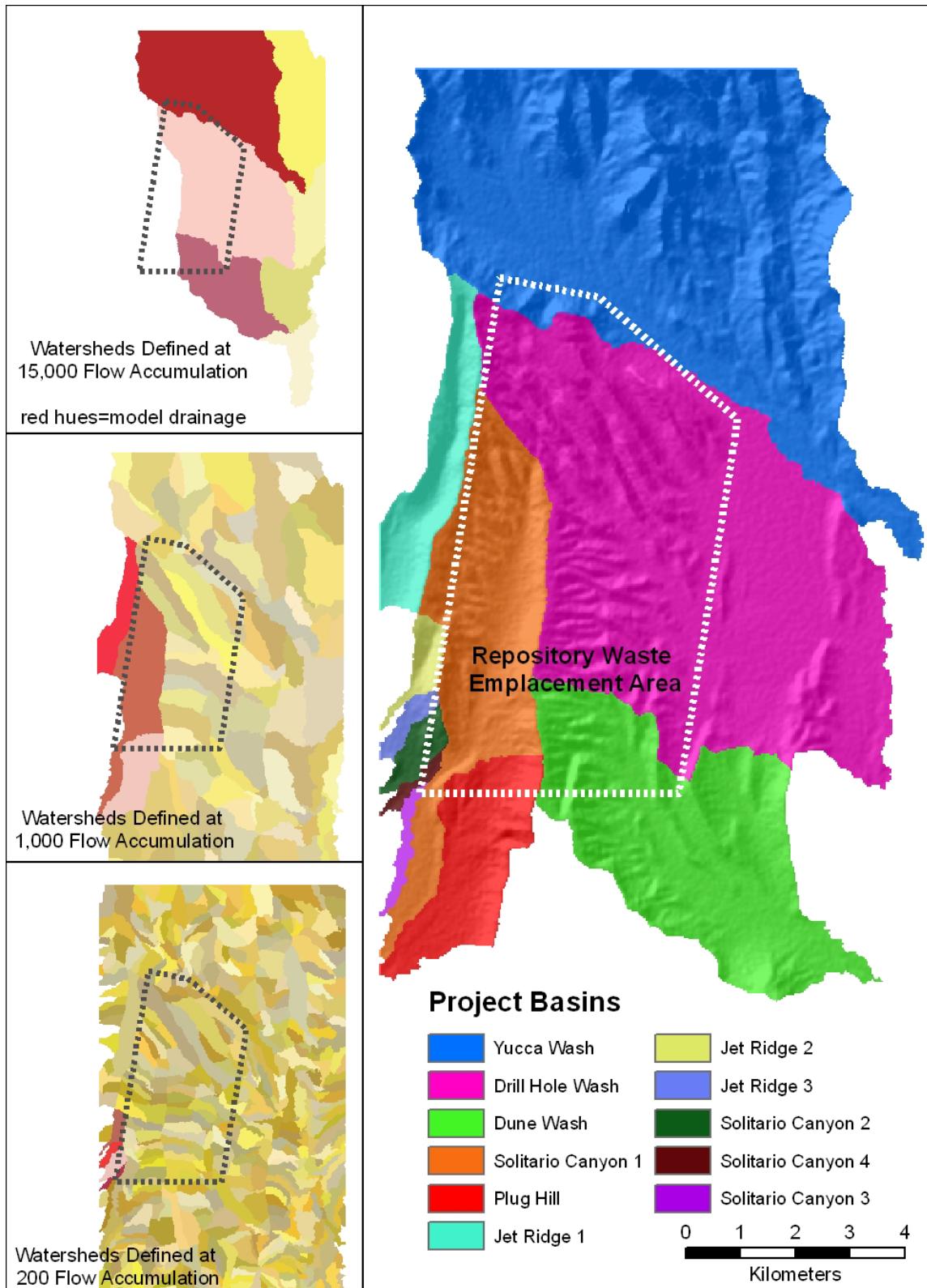
The catchment delineation process used three similar processing streams to produce the necessary outputs. Most of the steps in each delineation produced identical output, except for the catchment size layer, which was dependent on the flow accumulation setting. Therefore, elevation, slope, azimuth and other files were consistent throughout the processing and were not affected by the variable flow accumulation settings between the separate processing streams. With three sets of identical data, only one set needed to be prepared for inclusion in MASSIF. For consistency in description, unless otherwise specified, all terrain data extractions used data prepared during the processing run with flow accumulation set to 200 instead of the identical data sets from the 1,000 and 15,000 flow accumulation model runs.

Four of the raster layers, 'Filldem200', 'Azimuth200', 'Slope200' and 'Flowaccum200' comprised continuous data (floating point grids) that would not transfer into vector format without an additional process. To accomplish this, the decimal range of the values for each raster layer needed to be rounded up or down to create integer values.

The *Raster Calculator* ArcGIS Spatial Analyst performed this with the following formula that analyzes the portion of the continuous value right of the decimal and rounds up or down accordingly:

```
Int(con([grid1] > 0,con(Abs([grid1] - Int([grid1])) >= 0.5,Ceil([grid1]), Floor([grid1])),con(Abs([grid1] - Int([grid1])) <= 0.5,Floor([grid1]),Ceil([grid1])))
```

The delineated catchment files required a different approach to prepare them for the spatial database. The goal of the watershed delineation was to generate as few watersheds as possible that intersect with the Repository Waste Emplacement Area. Experimentation with threshold settings came upon the combination of three settings that would effectively accomplish this goal. Each of the terrain processing stages created a unique catchment file based on the value of flow accumulation threshold (15,000; 1,000; and 200). Each file contained certain watersheds that needed to be included in the final model (those covering a portion of the Repository Waste Emplacement Area and not already covered by a larger watershed) while the others were discarded. The watersheds identified for inclusion were each given a unique sequential number and the remaining watersheds (those that fall completely outside of the Repository Waste Emplacement Area) were set as 'No Data' using the *Reclass* function on each file. The flow accumulation set at 15,000 produced seven basins, three of which were saved. The second stage with a 1,000 flow accumulation produced 105 watersheds. Five of the watersheds covered portions of the Repository Waste Emplacement Area not already covered by the 15,000 flow accumulation settings. Three of the watersheds drain to the same pour point on the edge of the project boundary, so they were combined. Therefore of the five saved watersheds, three were ready to be used in MASSIF. The final stage produced 600 watersheds with the flow accumulation value set at 200. Six of these watersheds covered the last unaccounted for parts of the Repository Waste Emplacement Area. Two of these basins shared a pour point and were combined into a single watershed, thus resulting in five final watersheds. The sets of three, three, and five basins were merged into a final collection of 11 project watersheds. Figure B-6 shows this three-stage process and the final 11 drainages. This file was converted to a vector file producing a set of shapes that outlined the project grid cell that belonged in each surface drainage.



Source: Output DTNs: SN0701SPALAYER.002 and SN0612FTPRNUZB.002.

Figure B-6. Results of Three-Stage Watershed Delineation and Final Basin Combination

### **B3. ADDITIONAL SPATIAL DATABASE PREPARATION**

The final form of the spatial database for the MASSIF infiltration model contained 13 data fields compiled from different data layers. Some layers were created in the steps detailed above and others had been prepared as stand alone data products. Three such products, soil type, soil depth, and bedrock geology, were prepared from geology and soil data outside of the current GIS and were provided in a spatial database for inclusion in MASSIF. The potential vegetative response (PVR) data were created concurrently with the spatial database and imported upon its completion. From the SRTM data and the watershed delineation process, elevation, downstream grid cell identification (ID), slope, azimuth, catchment, and flow accumulation were made available. Two other layers created during the delineation process, catchment and flow accumulation, did not actually go into the final version of the database but were necessary to divide and sort the final data. The grid cell identification number and the spatial coordinates in UTM and latitude and longitude are generic data layers based on the location and dimensions of the YMP area.

#### **B3.1 IMPORTING PREPARED DATA LAYERS**

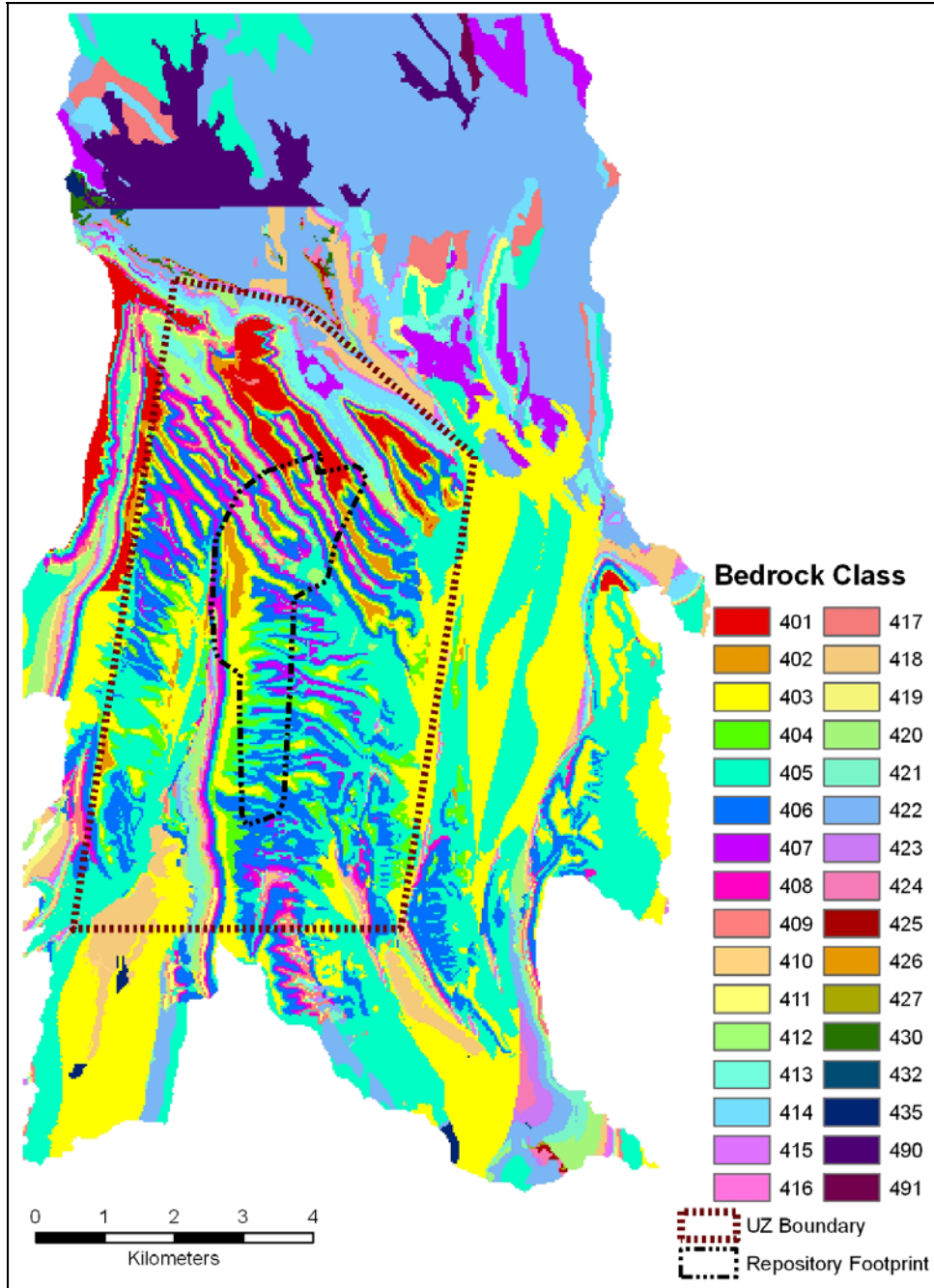
Soil type, soil depth, and bedrock geology were model inputs independently prepared by project specialists. Each input layer was prepared from existing geologic and pedologic data for Yucca Mountain. It was necessary to update each of these three inputs to format them to MASSIF requirements. Details of their preparations and a discussion of the significances of individual classes are in Section 6.5.2. Their DTNs are MO0608SPASDFIM.006 [DIRS 178082] (containing soil type and soil depth) and MO0603SPAGRIDD.003 [DIRS 177121] (containing Bedrock geology), respectively. These data were large ASCII files supplied as tables detailing the data values for each 30-m cell in the MASSIF project boundary. The tables also included latitude, longitude, and UTM coordinates to allow the data to be displayed in a spatial database. All data processing tasks represented in Sections B3.1 and B3.2 are archived in ‘Spatial Data Layers at Yucca Mountain’ (Output DTN: SN0701SPALAYER.002).

The range of bedrock values and soil depth across the project area from these files are displayed in Figures B-7 and B-8, respectively. During the course of the project, questions arose about the third downloaded data sets, soil type. A decision, documented in Section 6.5.2.1, was made to edit these data prior to entering them into MASSIF due to an unusable data field.

Soil type data required changes from its downloaded form (DTN: MO0608SPASDFIM.006 [DIRS 178082]). The following change was conducted in ArcGIS, and the edited version is preserved in the spatial database (Output DTN: SN0606T0502206.011). Ten values were represented in this layer, but two of the values did not represent an actual soil class. Soil class ‘8’ represented exposed bedrock, and everywhere it is present, it is paired with the accompanying soil depth class ‘5,’ that represents no soil depth. Soil Class ‘10’ had a similar problem as it was originally assigned to areas that had been disturbed by dirt roads or ground clearing. This designation was not consistent across the project area, as most grid cells containing a road were not designated as such. This designation also represented the surface condition and not the actual soil properties, so the accompanying data tables possessed no soil characteristic information for grid cells with this ‘10’ value. Therefore, each ‘10’ value was subjected to a nearest neighbor correction. Cell values of ‘10’ were on-screen edited to the soil

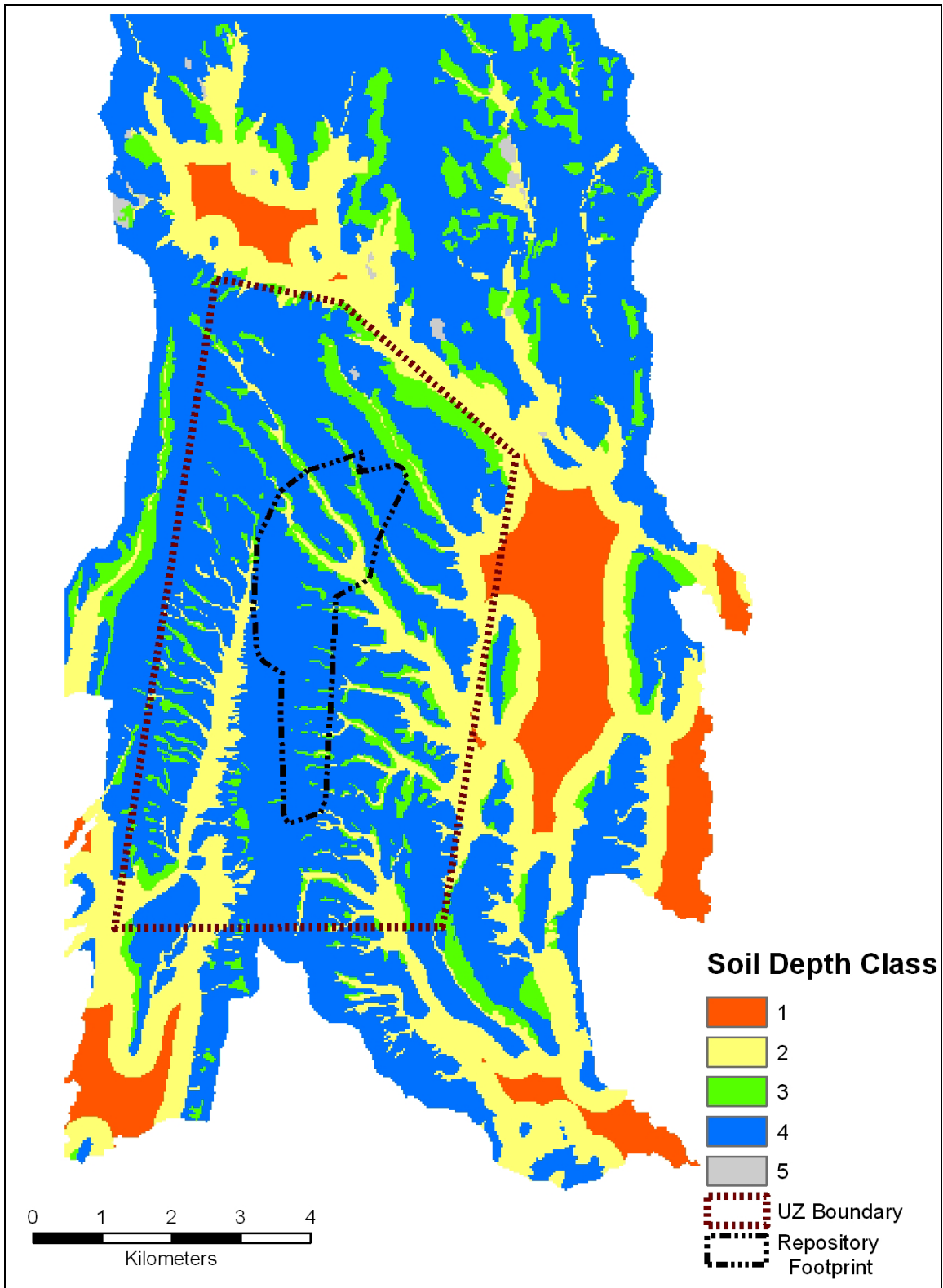
value most prevalent of those surrounding it while taking topographic factors (slope breaks and drainages) into consideration. Figure B-9 displays the inconsistent road classification and the 'fix' that was applied. In this figure, seventeen red pixels are overlaying roads and bladed surfaces in the left-hand frame, but are replaced with the model soil classes in the right-hand frame. Nine classes were now present in the final soil class input layer instead of the original ten. This edit occurred in grid cells with surface disturbances across the entire project area and is displayed in Figure B-10.

After completing these changes, the soil and bedrock datasets were imported into the spatial database. The soil type layer contained fields for grid cell ID and UTM coordinates, and latitude/longitude coordinates, providing a means of adding this information to the model.



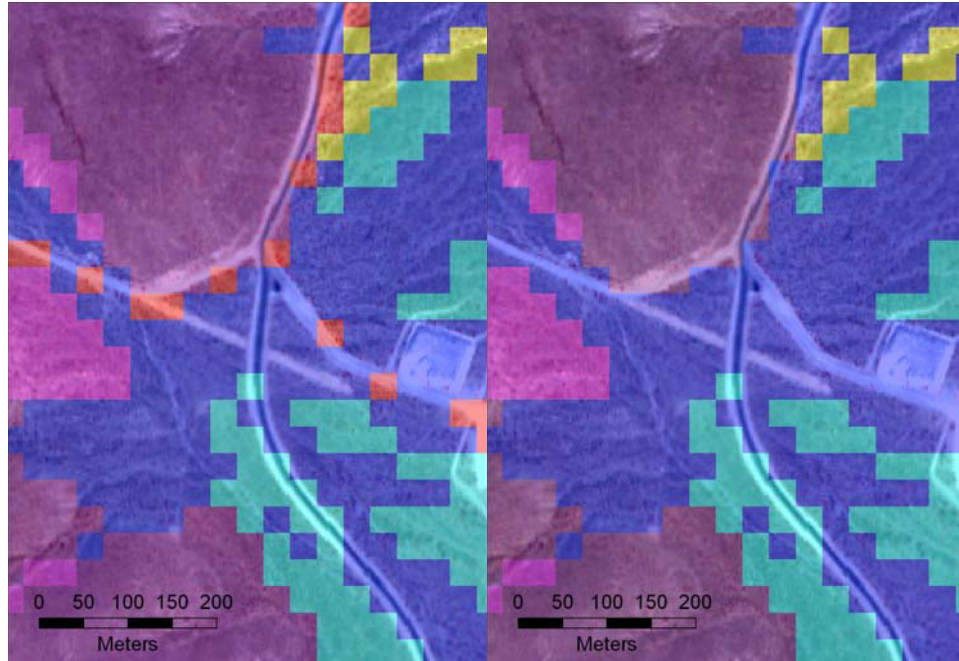
Source: Output DTNs: SN0701SPALAYER.002 and SN0612FTPRNUZB.002. DTN: MO0603SPAGRIDD.003 [DIRS 177121].

Figure B-7. Bedrock Zones across Project Area as described in Section 6.5.2



Source: Output DTNs: SN0701SPALAYER.002 and SN0612FTPRNUZB.002.

Figure B-8. Soil Depth Zones across Project Area as described in Section 6.5.2



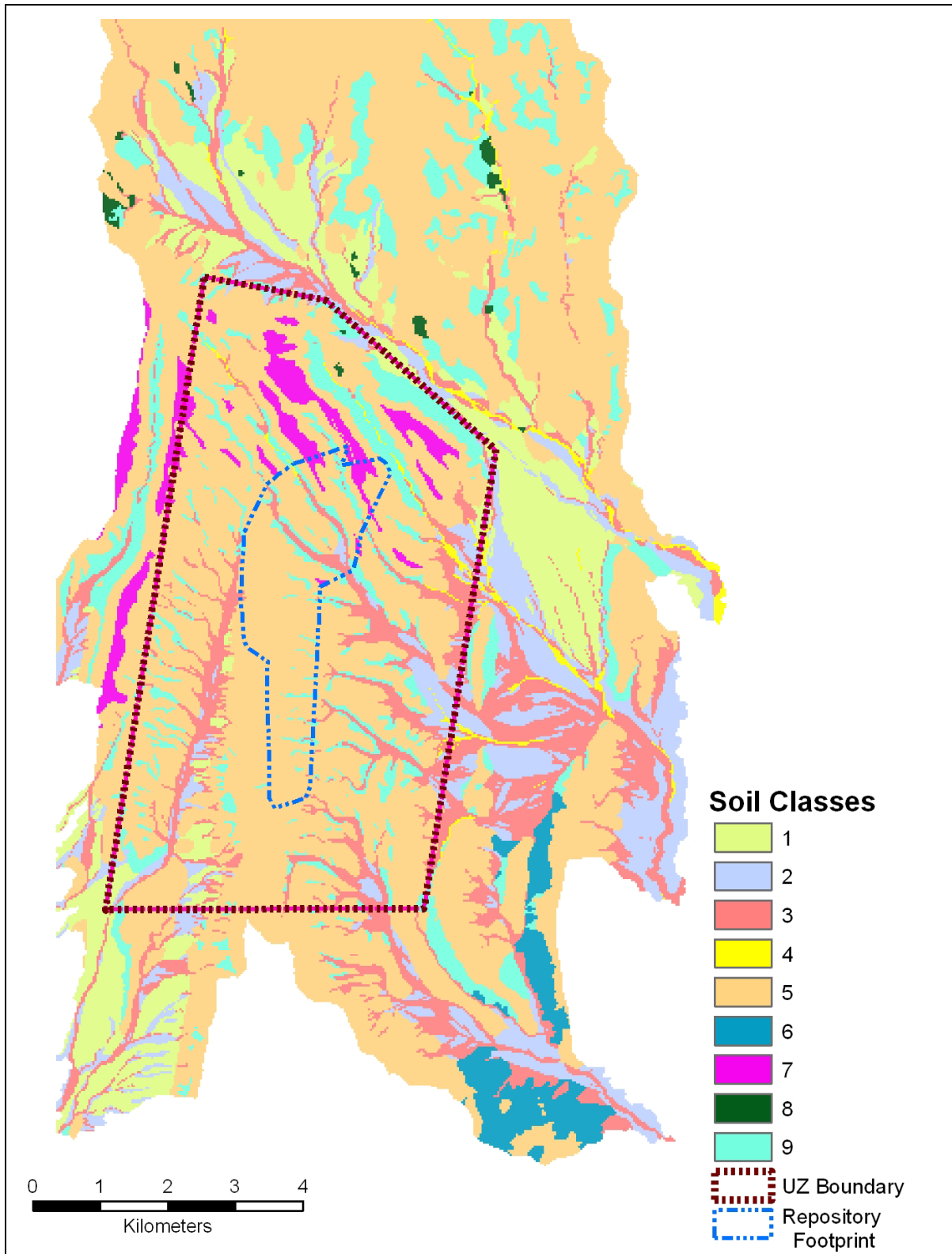
Source: Output DTN: SN0701SPALAYER.002.

Figure B-9. Road Soil Class (Red pixels in left frame) Removed within Project Area and Replaced with Appropriate Soil Class (right frame)

One other data layer was imported from outside the GIS, the PVR, prepared concurrently from Normalized Difference Vegetation Index (NDVI) calculations conducted in ENVI 4.2. Construction of the PVR layer is performed in Output DTN: SN0608PVRATYMT.001 and described in Appendix E with the final result displayed in Figure B-11. The PVR data layer comes out of the image processing ready for inclusion into the spatial database and no further processing was required.

### B3.2 DOWNSTREAM CELL CALCULATIONS

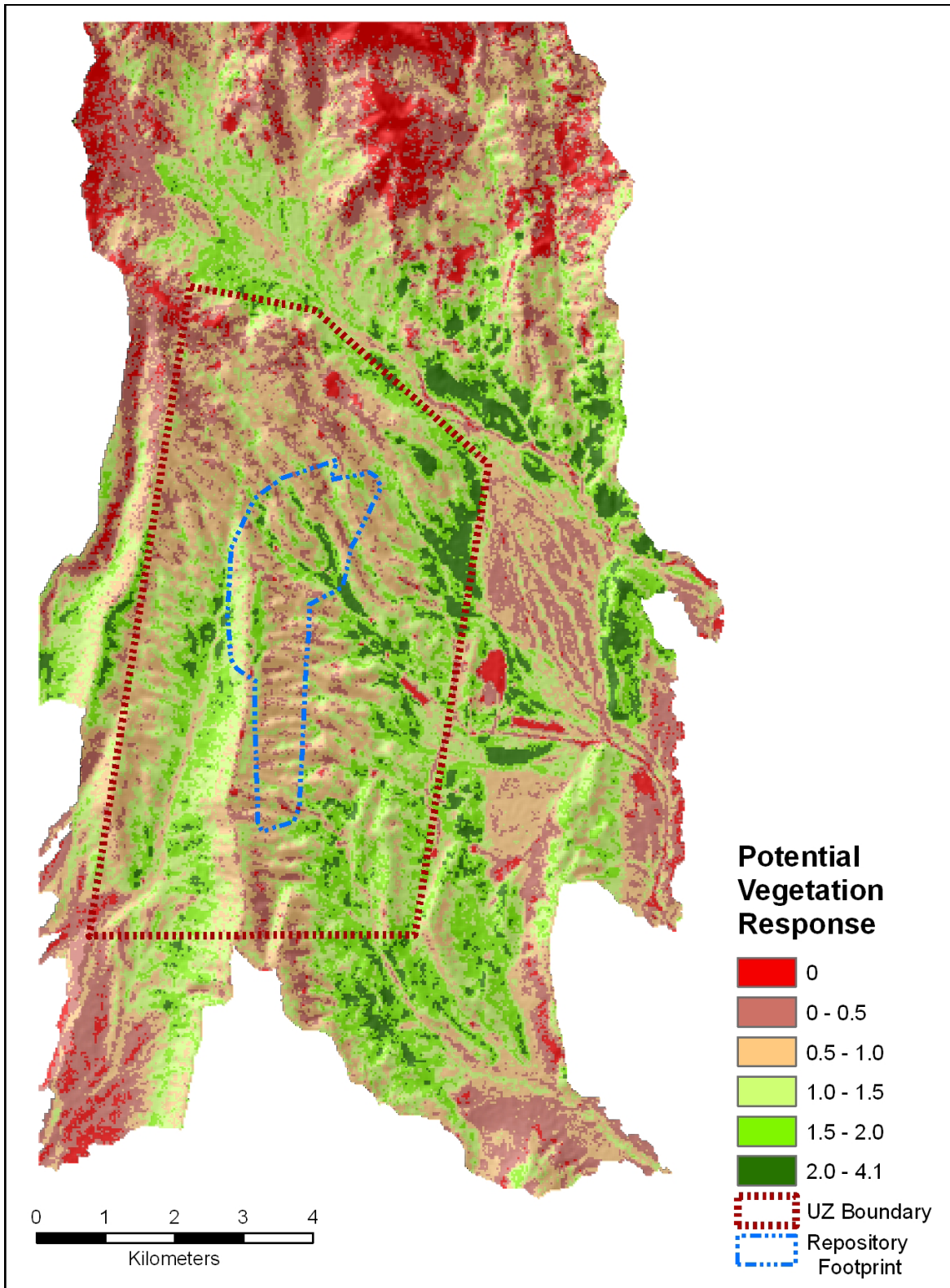
The MASSIF model required each model grid cell to know which model cell its surface water flows into. This was important to model correctly the overland flow within the model. ArcGIS did not have a direct means for calculating this value, so additional steps were required to create this data layer. To generate the downstream cell number from each cell, the Flow Direction grid from the Flow200 processing was required. As detailed earlier, Flow Direction provides a grid of eight numbers (1, 2, 4, 8, 16, 32, 64, 132) that represent the downslope direction into the eight surrounding grid cells. Using this information, together with the width of the model boundary grid (367 cells), it was possible to reclassify the flow direction grid into a template for use in Spatial Analyst's Raster Calculator. The Figure B-12 diagram below details the spatial relationships involved during the reclassification.



Source: Output DTNs: SN0701SPALAYER.002 and SN0612FTPRNUZB.002.

Figure B-10. Soil Type Zones across Project Area as described in Section 6.5.2





Source: Output DTNs: SN0701SPALAYER.002 and SN0612FTPRNUZB.002.

Figure B-11. PVR Values across Project Area as described in Appendix E

Each cell's ID number was added to the downslope reclassified layer (right grid in Figure B-12) to provide the cell ID of the downslope cell. For an example, if the overland flow from cell ID number 1,000 moved into the cell to the southeast, its downslope ID number would be 1,368 (1,000 + 368). The output of this calculation served as the final input layer. With the exception of the downloaded data, all the remaining data layers were extracted from data projected in UTM NAD 83. ArcGIS 9 can integrate data that are in different reference projections, but as a service for future users without this version of ESRI GIS software, each data layer was reprojected to UTM NAD 27 as the last step. All the necessary data now resided in the spatial database, but the spatial relationships among these layers still needed to be developed.

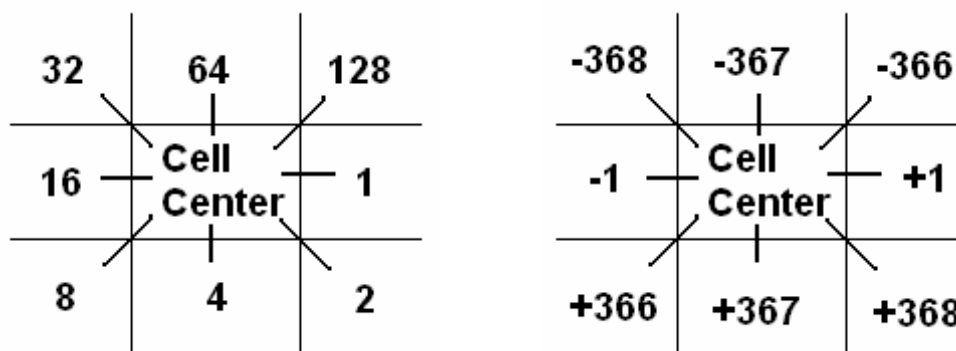


Figure B-12. Downstream Cell ID Adjustment Values

#### B4. ASSEMBLING THE SPATIAL DATABASE

To assemble the files into a single output, a series of tabular joins were performed on the previously prepared layers (soil type, soil depth, and bedrock) using the cell ID number as the field shared between layers. A tabular join combines two data sets that share a common field of unique values in their attribute tables. These joins brought the data fields, Cell ID, UTM coordinates, Lat/Long, Soil Depth, Soil Type, and Bedrock Type together in a single file projected to UTM NAD 27 Zone 11. All data processing tasks represented in Sections B4 and B4.1 are archived in Output DTN: SN0608ASSEMBLY.001, 'Assembly data for geospatial inputs to MASSIF Model of Yucca Mountain.'

The terrain data layers (elevation, slope, and azimuth) were spatially joined due to their lack of the model cell ID field. A spatial join is a method of combining data layers that share an identical location, in this case a grid cell location. The spatial join started by examining terrain layers that were grids of polygons, each of which covered the center of one or more model grid cell centers. The grid cells in the joined file gained the table attributes of the data layers polygons that overlaid its center. The intersect tool was used in ArcMap to perform these spatial joins. Since the intersect tool was limited to working with two files at a time, a series of intermediate files were created and further combined to create a final file that brought together model inputs Elevation, Slope, Azimuth, and PVR along with accessory files Downslope Adjustment, Catchment, and Flow Accumulation, all projected to UTM 83 Zone 11. Before continuing, this combined file was reprojected to UTM NAD 27 Zone 11 to bring it into agreement with the other earlier joined file of soil and bedrock information.

A final spatial join brought these two files together in a single database. Since the Cell ID and Downslope Adjustment fields were together in the same table, it was possible to perform a calculation that created the last required model input, Downslope Cell ID. The Downslope Adjustment column was created to factor the difference between a current Cell ID and the Cell ID of its downslope neighbor. Within the attribute table, a new column was created, named Downstream, and its values were calculated as Cell ID + Downslope Adjustment.

As a result of the tabular and spatial joins, all necessary data were assembled into a single file. The required data fields were present, but duplicate information was joined as well. It was therefore necessary to delete unneeded or repeated fields until only those fields shown in Table B-2 were present. Some of these fields (FID, Catchment, FlowAcc) were not needed for the MASSIF model but were necessary for the organization of the final spatial database preparation, as detailed below. This shapefile was preserved as Output DTN: SN0606T0502206.011, to better review the individual layers prior to the watershed division in the next step.

Table B-2. Preliminary Spatial Database Attributes

Field	Name	Description
1	FID	Feature ID, an ArcGIS identifier
2	Shape	A field placeholder for the feature polygon geometry
3	Cellid	Unique grid cell ID number for the MASSIF model
4	Utm_E	UTM NAD 27 Zone 11 easting coordinate in meters
5	Utm-N	UTM NAD 27 Zone 11 northing coordinate in meters
6	Lat	Latitude coordinate in decimal degrees
7	Long	Longitude coordinate in decimal degrees
8	Elevation	Grid cell elevation in meters
9	Downstream	Unique grid cell ID number of downstream grid cell
10	Catchment	ID number of one of eleven project watersheds
11	Slope	Grid cell slope in degrees
12	Azimuth	Grid cell slope orientation in compass bearing degrees
13	SoildepthC	Grid cell soil depth class
14	Soil_type	Grid cell soil type class
15	IHU	Grid cell bedrock type class
16	PVR	Grid cell potential vegetation response
17	FlowAcc	Grid cell total flow accumulation count

Source: Output DTN: SN0606T0502206.011.

#### B4.1 WATERSHED BASIN SUBDIVISION

The data now resided in one data file representing every 30-m pixel in the project area with a set of geographic data attached to each in an attribute table. Combined, the data from these pixels represented all surface water flow across the project area toward eleven separate catchment outlets. The MASSIF model could not process these different flow patterns concurrently; therefore, it was necessary to divide the model into separate drainages, each processed in turn. Total net infiltration across the model area was the combined sum from each of eleven basins.

The subdivision of the spatial database was accomplished using the ‘catchment’ field in the data table. The catchment column represented spatial boundaries defined during the watershed delineation. The catchment layer contains a number from one to eleven for each grid cell that represents the basin where the grid cell was located. Each set of cells, defined by a unique catchment number, was saved separately and named for their representative drainage. Table B-3 shows the eleven values representing the drainages in the project area.

Table B-3. Project Area Watershed Catchments

Catchment ID	Catchment Name
1	yucca_wash
2	drill_hole_wash
3	dune_wash
4	solitario_canyon1
5	plug_hill
6	jet_ridge1
7	jet_ridge2
8	jet_ridge3
9	solitario_canyon2
10	solitario_canyon4
11	solitario_canyon3

Source: Output DTN: SN0701SPALAYER.002.

The result of the database subdivision was eleven spatial database files comprising ArcGIS shapefiles each consisting of a set of files that detailed the graphic representation, the map coordinate system and a Dbase 4 spreadsheet (.dbf) containing the associated tabular attribute information. The MASSIF model required that the data be entered in a particular order. The data needed to have the columns in a particular order, labeled consistently, and the records needed to be sorted in order from highest elevation to lowest. This generic .dbf spreadsheet was opened in Microsoft Excel 2003 where the columns and records were sorted.

Elevation was the primary column (Table B-2) that constrained the data sort, but it was possible for more than one cell (in each drainage) to share an elevation value. Excel could not know which value was actually upstream and would default to the first listed in the file, which might not actually be upstream, especially on a slight north facing slope where upstream cell ID numbers are greater than their corresponding downstream neighboring cells. For this very reason, the flow accumulation layer was prepared. Using the ‘flow accumulation’ column as the secondary sort constraint, the computer differentiated downslope cells by knowing a greater water accumulation value would occur in downstream cells that shared the same elevation on a gentle slope. Each of the eleven files was subjected to the same process of sorting with ‘elevation’ descending and ‘flow accumulation’ ascending.

A few last edits rendered each file ready for input into the MASSIF model. The last record in each file represented the pour point, the basin outlet, or the model cell where all the accumulated water exited the drainage. Since the downstream cell from this grid cell resided in a different drainage, the MASSIF model needed to know that this record represented the last cell in the respective drainage. For the model’s purposes, a ‘-3’ was entered as the downstream cell

identifier to signify that this value represented the final record. In addition, all extraneous columns were eliminated, specifically, Catchment, Flow Accumulation, Shape, and FID (Table B-2) as these data values were not required for the infiltration model. The remaining data in the following order formed the spatial inputs for the MASSIF model, as shown in Table B-4. New column headings were added to each table to format each to MASSIF specifications. As a last step, each drainage was saved as a comma-separated value (.csv) text file, a format easily imported into the MASSIF model. For the purpose of simplicity within MASSIF, the drainage output files were renumbered into a sequential order based on the grid cell count within each drainage as shown in Table B-5 (Output DTN: SN0606T0502206.011).

Table B-4. Final Spatial Database Specifications

Field #	Database Name	MASSIF Name
1	Cellid	Cell_ID
2	Utm_E	UTM_E(m)
3	Utm-N	UTM_N(m)
4	Lat	Latitude(deg)
5	Long	Longitude(deg)
6	Elevation	Elevation(m)
7	Downstream	Dnstream_ID
8	Slope	Slope(deg)
9	Azimuth	Azimuth(deg)
10	SoildepthC	Soil_Depth_Zone
11	Soil_type	Soil_Type_Zone
12	IHU	Bedrock_Type_Zone
13	PVR	PVR

Source: Output DTN: SN0606T0502206.011.

Table B-5. Final Spatial Database Filenames

Catchment #	Final File Name	Order Change	Grid Count
1	01_yucca_wash.csv		45,981
2	02_drill_hole_wash.csv		45,103
3	03_dune_wash.csv		19,423
4	04_solitario_canyon1.csv		13,944
5	05_plug_hill.csv		6,272
6	06_jet_ridge1.csv		5,074
9	07_solitario_canyon2.csv	x	943
7	08_jet_ridge2.csv	x	917
8	09_jet_ridge3.csv	x	567
11	10_solitario_canyon3.csv	x	545
10	11_solitario_canyon4.csv	x	334

Source: Output DTN: SN0606T0502206.011.

## B5. DELINEATING GAUGED WATERSHEDS

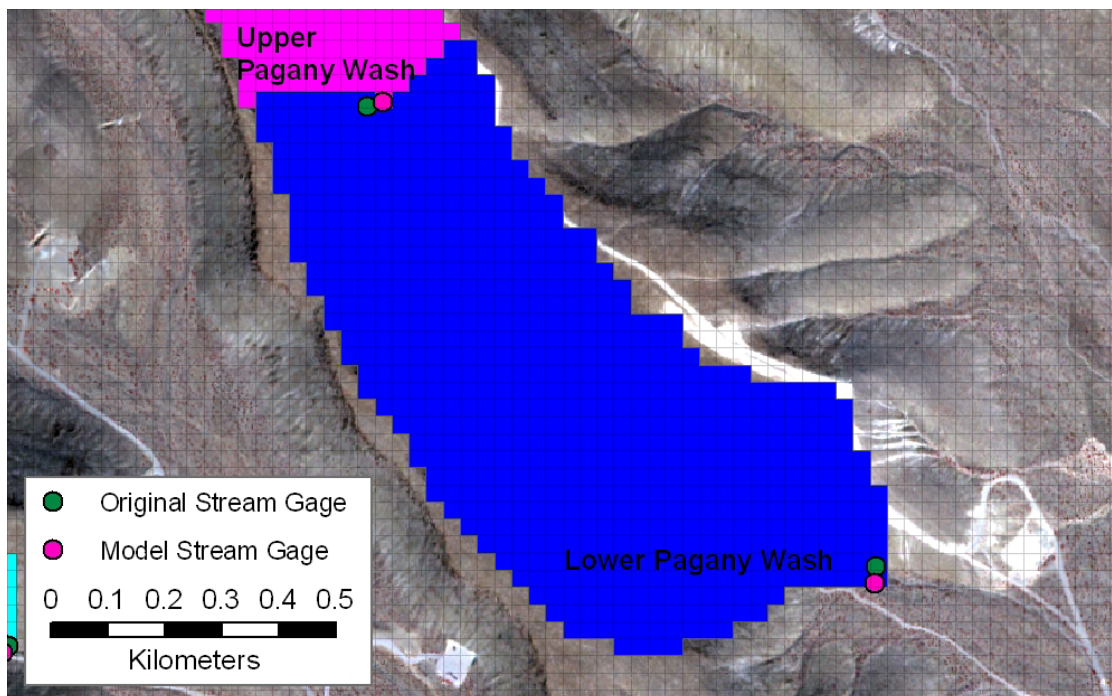
In addition to the eleven drainage basins that make up the model area, a subset of six drainages were needed to calculate model results that could be compared directly against actual runoff values collected at six surface stream gages located in the project area. This comparison was

used to validate the model. Principles similar to those used to create the project area catchments were used to create these gauged watersheds. Previously during the watershed delineation (Section B2.2), the amount of flow accumulation was used to define the project area drainages. In the case of the gauged watersheds, specific locations (stream gages) defined the lower end of each drainage (pour points). All data processing tasks represented in Sections B5.1 and B5.2 are archived in Output DTN: SN0608ASSEMBLY.001, ‘Assembly data for geospatial inputs to MASSIF Model of Yucca Mountain.’

### B5.1 IMPORTING THE GAUGE LOCATIONS

The stream gage locations were provided as sets of coordinates DTN: MO0601GSCSPINF.000 [DIRS 177236]. These spatial tabular data were input into the GIS to incorporate them into the spatial database. The gage locations were compared to the created elevation model of the project area.

Due to slight variations in the original elevation data set and the subsequent *Filled* data layer, the model stream network did not always follow actual stream channels. The differences between the two did not overly affect the delineation process, as all that was needed was a slight lateral shift in the pour point location, while the upstream dimensions (number of model grid cells) remained the same (Figure B-13).



Source: Output DTN: SN0608CWATSHED.001.

Figure B-13. Stream Gages: Original and Spatial Database Locations

This is a common situation when hydrologic modeling uses cell based elevation data. The elevation data is represented by a sample value that does not always reflect the lowest potential

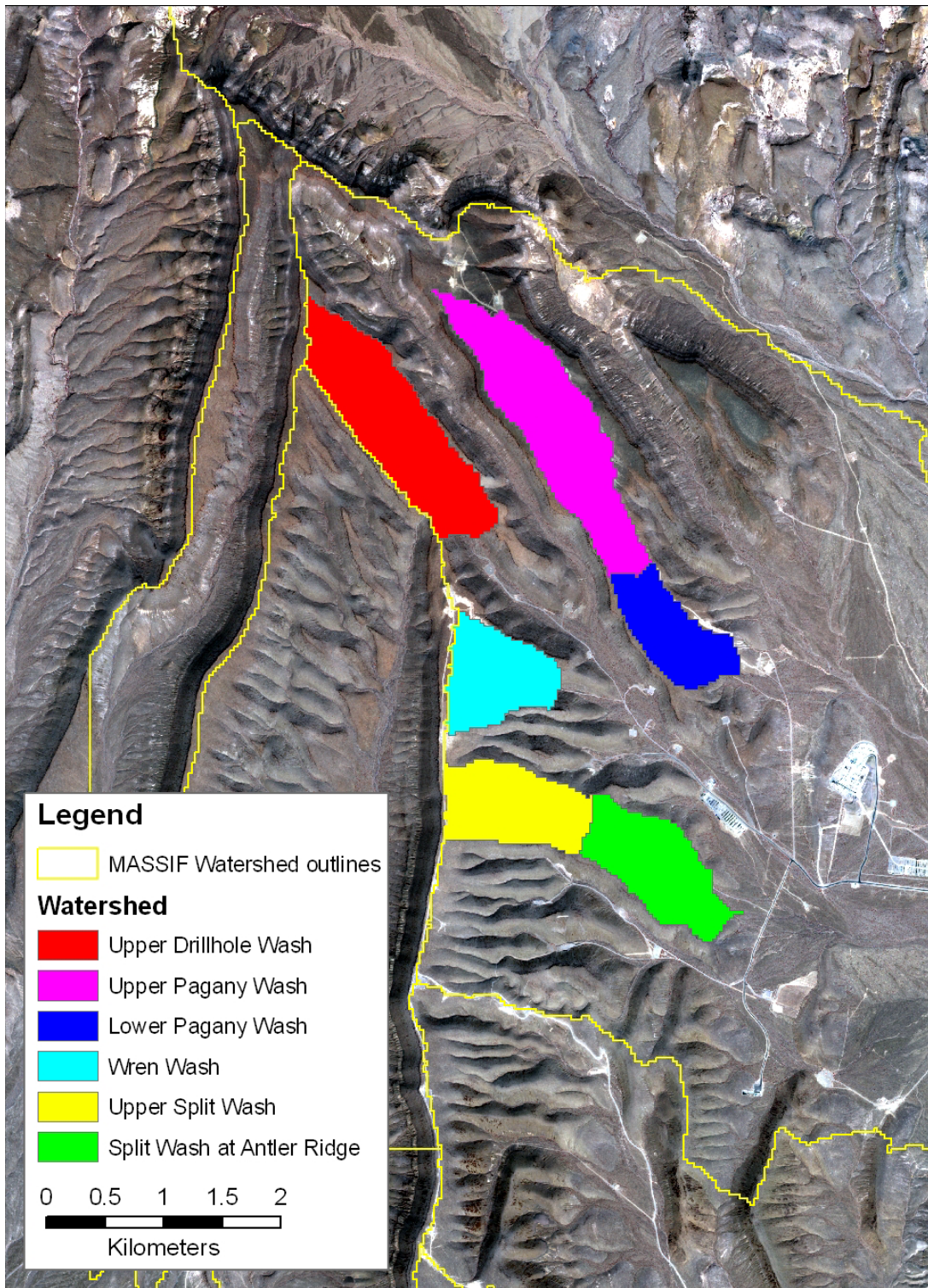
elevation in that cell, which is required for watershed delineation. For the MASSIF model, a single elevation value was being used to represent all variations within a 30-m by 30-m square grid cell, so often a small, narrow drainage was not captured as the dominate trait of that grid cell. However, the general trend of the landscape was incorporated, and the drainage was defined to follow this trend. In steep narrow valleys the model easily follows the natural terrain, but in wide flat valleys with little relief, the model might struggle to follow a small braided stream. In these cases, the model would instead create a representative drainage that followed the general slope and azimuth trend with the understanding that this was the highest probability for the drainage location. The model would follow this slope/azimuth trend until a difference in elevation would once again create a break in the slope to help redefine where the drainage actually has to run.

The *Snap Pour Point* function in ArcGIS hydrology tools was developed to compensate for this drainage discrepancy. *Snap Pour Point* takes point features, such as gages, and assigns it an exact location on the modeled drainage system so that it can be used for direct future output from the model. The *Snap Pour Point* function is an automated task that is most helpful in manipulating large datasets. For the small number of gages in this model, the same function was replicated manually with on-screen digitizing with a higher degree of accuracy, as pour point/gage could be snapped to the drainage to ensure the shift is minimized to as small a lateral shift as possible in order to maintain the watershed dimension.

As a result of this process, the watershed surface area upstream from a particular model pour point was a close match to actual upstream dimensions from stream gage. Two of the actual stream gages fell within a cell designated as a model stream. In three of the six examples, the necessary shift was only into the adjacent cell. Only one example needed a two-pixel shift due to low elevation variability and filled DEM characteristics associated with the drainage passing through a culvert under an elevated road. The shifts are not that important in construction of the gauged watersheds, as the size of any watershed is based on the topography of the land to provide width and the overall distance of the drainage to provide length. Shifting the pour point perpendicular to the drainage does not change the length of the watershed and has minimal effect on the resulting grid cell count (surface area).

## **B5.2 DELINEATION AND GAUGED AREA CLIP**

This delineation process used the two original and four adjusted gage locations to generate the gauged watersheds. This step used the same filled DEM generated during project area watershed delineation processing with flow accumulation set to 200. The delineation was performed by the GIS identifying all upstream grid cells from each gage location based on flow direction and slope characteristics. The output was six small watersheds, two of which were located immediately below their upstream neighbors (Figure B-14). These files were used to create the boundary file that will clip the previous project area data file. Using the same spatial database for the project area that was assembled previously (Output DTN: SN0606T0502206.011) and instead of splitting it into the eleven project drainages, it was divided into the six much smaller gauged basins. This clip confined the input cells to just those that feed the streams that pass each gage. This allows a direct comparison between actual stream gage measurements and the modeled expected results.



Source: DTN: MO0601GSCSPINF.000 [DIRS 177236]; Output DTN: SN0608CWATSHED.001.

Figure B-14. Gauged Watersheds within the Drill Hole Wash Watershed



As was the case with the other input files prepared, the MASSIF model required that the data be entered in a particular order. The data needed to have the columns in a particular order and the records needed to be sorted in order from highest elevation to lowest and the secondary sort variable set as flow accumulation. Again, the final record in each file needed a ‘-3’ entered as the downstream cell value. In the two cases where there were adjacent upper and lower delineated drainages, the lower drainages output table was a combination of both the upper and lower catchments representing the total surface flow passing the lower pour point.

These six files supplied all the spatial information needed to run the MASSIF infiltration model on just these six gauged watersheds. The required resorted and relabeled columns resembled the details earlier provided in Table B-4.

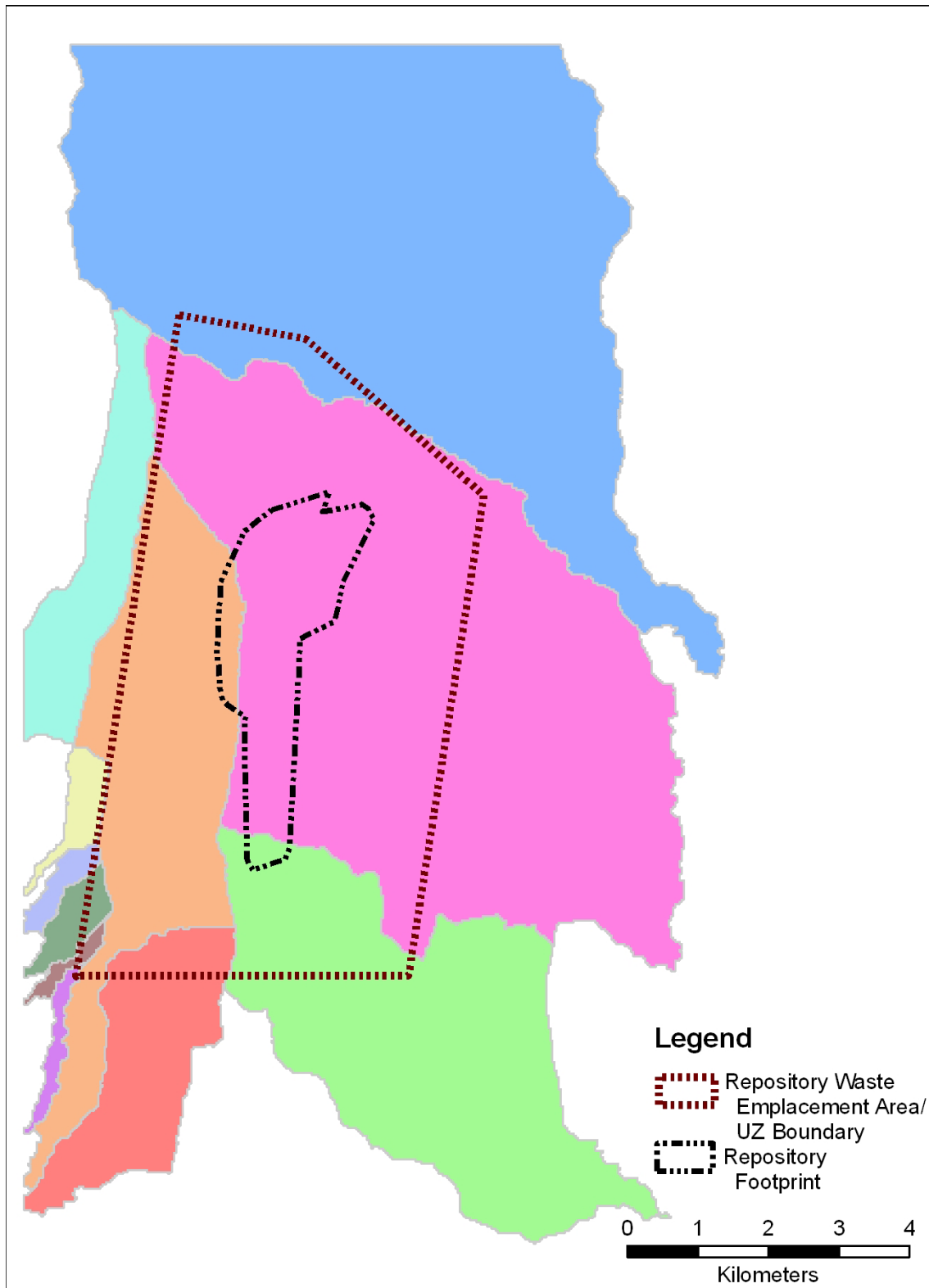
## **B6. ADDING BOUNDARY IDENTIFIERS TO THE SPATIAL DATA**

After the completion of the spatial database for the MASSIF model (Output DTN: SN0606T052206.011), an ancillary database was created that would include model cell identifiers keyed to the location of the repository footprint and the larger area of impact, the Repository Waste Emplacement Area, also referred to as the unsaturated zone (UZ) area. The knowledge of whether a model grid cell was located within the UZ or repository footprint boundaries was not required to run the MASSIF model properly, but it was useful for explanatory purposes when examining MASSIF results. The file was structured to be easily incorporated into MASSIF model calculations when desired. All data processing tasks represented in Sections B6.1 and B6.2 are archived in ‘Assembly data for geospatial inputs to MASSIF Model of Yucca Mountain’ (Output DTN: SN0608ASSEMBLY.001).

### **B6.1 ANCILLARY BOUNDARY FILES CREATION**

Boundary coordinates for the repository footprint and the UZ area were both imported from DTN: LB0208HYDSTRAT.001 [DIRS 174491]. *Repository02\_Table.xls* contained the 30 vertices of the irregular-shaped footprint. These coordinates were provided in the form of State Plane 27 meters. This was converted to State Plane 27 feet (the traditional unit of measurement for State Plane projections) and saved as *repository\_footprint.txt*. This text file was opened in ArcView where the coordinates were displayed as points and saved as an ESRI shapefile. This point shapefile was converted to UTM NAD 27 Zone 11 and saved once again. Using these points as guides, a polygon shapefile was constructed using each vertex in order. This resulted in *Repository\_Footprint\_update.shp*.

The same steps were used for the UZ boundary coordinates as found *UZ02\_Model\_Domain.txt*. It was also in the form of State Plane meters, and converted to State Plane feet in *UZ\_boundary2.txt*. Once entered into ArcView, the coordinates were displayed as points, saved, and reprojected to UTM NAD 27 Zone 11. This resulting file was saved as *UZ\_Boundary\_UTM\_NAD27.shp*. Figure B-15 displays these two boundaries and their relationship to the MASSIF model watersheds.



Source: Output DTNs: SN0608DRAINDYM.001 and SN0612FTPRNUZB.002.

Figure B-15. Repository Waste Emplacement Area/UZ Boundary and the Repository Footprint

In order to make these data compatible to the existing spatial database, it was necessary to modify one of the interim data files that led to the creation of the final spatial database. *All\_Layers\_Joined\_nad27.shp* points file from folder *E2\_All\_Join* in Output DTN: SN0608ASSEMBLY.001. This file is a point shapefile for the entire project area where each point contains all the MASSIF inputs for a specific model grid cell and is the version of the spatial database prior to the final step of subdivision in the eleven model drainages. Two fields were added to the shapefile's attribute table, one titled 'footprint' and another labeled 'UZ'. A subset of points within *All\_Layers\_Joined\_nad27.shp* was then selected using the UZ boundary file as the selection criterion. All points selected were assigned a '1' value in the attribute table, leaving the unselected points as '0' under the UZ heading. The selection was cleared and second selection of points was conducted using the repository footprint shapefile. These selected points were assigned a '1', leaving the remainder as '0' in the footprint column. The final was saved as *All\_Layers\_plus\_footprint\_and\_UZ.shp*.

## **B6.2 BOUNDARY FILES SUBDIVISION**

The following preparation methods were nearly identical to the steps taken in Section B4.1 except only three data columns were required and the output was condensed into a single output file, *All\_Layers\_plus\_footprint\_and\_UZ.shp*. It was then saved into eleven separate shapefiles, once again based on using catchment in the selection process, but this time incorporating the file renaming scheme by size in a single step.

As was the case with the other input files prepared, the MASSIF model required that the data be entered in a particular order. The data needed to be sorted in order from highest elevation to lowest. The renumbering of the final elevation record in each file to a '-3' was not necessary at this step since this column will not be part of the final output.

A few last edits rendered each file ready for input as an ancillary input into the MASSIF model. All columns were deleted with the exception of Cell\_ID, Footprint, and UZ and saved as .csv files. The contents in each file were combined into a single file based on order of watershed size that is evident in each file name (order shown in Table B-6). This final combined file is saved as *Updated\_UZ\_and\_Footprint\_with\_MASSIF\_ID\_Number.csv* and is made available to the MASSIF model as Output DTN: SN0612FTPRNUZB.002.

Table B-6. Boundary Files Watershed Catchments

Catchment ID	Catchment Name
1	01_yucca_wash
2	02_drill_hole_wash
3	03_dune_wash
4	04_solitario_canyon1
5	05_plug_hill
6	06_jet_ridge1
7	08_jet_ridge2
8	09_jet_ridge3
9	07_solitario_canyon2
10	11_solitario_canyon4
11	10_solitario_canyon3

Source: Output DTN: SN0612FTPRNUZB.002.

**APPENDIX C**  
**CALCULATION OF  $ET_0$  (REFERENCE EVAPOTRANSPIRATION) AS A FUNCTION**  
**OF SLOPE AND AZIMUTH**



## C1. CALCULATIONS

This appendix contains step-by-step procedures for calculating grass reference evapotranspiration ( $ET_0$ ) for surfaces having a variety of combinations of slope and aspect. Procedures include the calculation of solar radiation ( $R_s$ ) for sloping surfaces by translating measurements or estimates of solar radiation made on a horizontal plane. The translation procedures follow those used by Reindl et al. (1990 [DIRS 176480]) and by Duffie and Beckman (1980 [DIRS 176264] and 1991 [DIRS 176616]). The procedure assumes that each surface has an extensive uniform slope at each point of calculation (grid cell). Effects of protruding surrounding terrain that cast shadows on the grid cell are not considered (see Section 5). This simplification of terrain provides the ability to utilize daily integrations, of direct and diffuse solar radiation over the mountain, that have an analytical basis. The calculated solar radiation is used to compute  $ET_0$  and is applied to discrete classes of azimuth and slope for infiltration modeling. The procedure applies to present-day climatic conditions and to future expected climates.

The  $ET_0$  calculations follow the standardized FAO-56 Penman-Monteith method (Allen et al. 1998 [DIRS 157311]). The  $ET_0$  procedure by Allen et al. (1998 [DIRS 157311]) uses weather inputs of daily maximum and minimum air temperature from a representative reference weather station. Weather parameters of solar radiation, humidity, and wind speed, commonly used in calculating  $ET_0$ , are estimated using air temperature as input or, in the case of wind speed, as a general value that varies with the time of year. The techniques for estimating solar radiation, humidity, and wind speed are described in this section.

The base estimated solar radiation on the horizontal surface, and its translation to solar radiation for each grid cell, uses a single value for latitude representing the study area associated with a particular reference weather station. A single value for latitude is used because solar calculations change less than 2% on any given day over the range in latitude of the study area, which is less than 40 km in length in a north-south direction. The small change in solar radiation was determined by comparing theoretical daily extraterrestrial radiation listed in Allen et al. (1998 [DIRS 157311], Table 2.6), over the latitude range of the study area.

### C1.1 INITIAL CALCULATIONS

Steps 1 through 18 are calculations required in solar radiation computations or in  $ET_0$  computations. These calculations are general to all grid cells on Yucca Mountain.

**INPUTS:** Daily maximum and minimum air temperature,  $T_{max\ reference}$  and  $T_{min\ reference}$  respectively, associated with the reference weather station along with the latitude and elevation of the weather station.

Step 1. Estimate mean daily dew-point temperature,  $T_{dew\ general}$  using  $T_{min\ reference}$  measured at or simulated for the reference weather station, as described by Allen et al. (2005 [DIRS 176207], Equation E.1):

$$T_{dew\ general} = T_{min\ reference} - K_o \quad (\text{Eq. C-1})$$

where

$K_o$  is an empirically derived offset. For the southern Nevada climate present-day conditions,  $K_o$  was set to 4.5°C, which is an average of 4°C to 5°C recommended in Allen et al. (2005 [DIRS 176207], p. D-29) for spring, summer, and fall periods when the climate is arid to semiarid.  $K_o$  was set to 2°C for winter when the climate is somewhat more humid. The values used for  $K_o$  will create dew-point temperature–humidity data sets that reflect weather conditions over an ET reference setting of well-watered clipped grass cover that is part of the standard  $ET_0$  calculation definition. It is important, in applying the  $ET = K_c ET_0$  approach (where ET is actual ET and  $K_c$  is a transpiration or ‘crop’ coefficient and  $ET_0$  is the reference ET), that the  $ET_0$  calculation represents the reference evapotranspiration that occurs from the standardized reference ET surface. This standardized reference surface, by definition, is an extensive surface of transpiring grass that conditions the atmospheric boundary layer by evaporative cooling and by the addition of water vapor. The conditioning of the boundary layer constitutes an important feedback process to the  $ET_0$  rate and moderates it. The  $K_c$  coefficient, which represents the ratio of actual ET to  $ET_0$ , and the soil water stress reduction function, which reduces the ET value when soil water content is insufficient to support ET fully, are designed to function in concert with the standardized  $ET_0$  value (Allen et al. 1998 [DIRS 157311], pp. 58, 91, and 161). The  $ET_0$  calculation represents a near upper limit on ET that is experienced under full vegetation cover and adequate soil moisture supply. Under conditions of less than full vegetation cover or less than adequate soil moisture supply, the actual ET rate will be reduced below the standardized  $ET_0$  rate, even though the actual air temperature may increase and humidity may decrease due to the reduced ET (Brutsaert 1982 [DIRS 176615], pp. 224, 225 and Figure 10.5). Therefore, even though the ambient potential ET rate computed from ambient temperature and humidity conditions for the dry environment increases under these conditions, by definition, the standardized  $ET_0$  rate remains constant, as it should, due to the adherence to humidity (i.e., dew-point temperature) conditions defined for the reference ET condition. Therefore, it is important that the  $ET_0$  calculation be made using  $T_{dew\ general}$  estimated using  $K_o$  values that represent the reference ET condition.

The value simulated for  $T_{dew\ general}$  will change daily as the value for  $T_{min\ reference}$  changes. The  $T_{dew\ general}$  from Equation C-1 is applied for a single reference weather location, or locations within the study area, with the value derived for  $T_{dew\ general}$  used to represent  $T_{dew}$  and humidity conditions at all locations within the study area. Section 6.5.4.1 discusses exactly what values of  $K_o$  were used and when they were applied for the Mass Accounting System for Soil Infiltration and Flow (MASSIF) analysis of net infiltration. The value  $K_o = 4.5^\circ\text{C}$  recommended by Allen et al. (2005 [DIRS 176207], p. D-29) for use in a range of climates spanning arid and semiarid is expected to hold for future climate regimes.



- Step 2. Calculate actual vapor pressure  $e_a$  for use in the FAO Penman-Monteith equation and for estimating precipitable water ( $W$ ) over the study area (Allen et al. 1998 [DIRS 157311], Equation 14):

$$e_{a\ general} = e^o(T_{dew\ general}) = 0.6108 \exp\left[\frac{17.27 T_{dew\ general}}{T_{dew\ general} + 237.3}\right] \quad (\text{Eq. C-2})$$

where

$$\begin{aligned} e_{a\ general} &= \text{actual vapor pressure (kPa)} \\ T_{dew\ general} &= \text{dew point temperature (}^\circ\text{C), from Step 1.} \end{aligned}$$

The entire air mass that passes across Yucca Mountain is assumed to have actual vapor pressure as represented by  $e_{a\ general}$ .

- Step 3. Calculate the inverse square relative distance between earth and sun,  $d_r$ , for use in the extraterrestrial radiation ( $R_a$ ) calculation (Allen et al. 1998 [DIRS 157311], Equation 23):

$$d_r = 1 + 0.033 \cos\left(\frac{2\pi}{365} J\right) \quad (\text{Eq. C-3})$$

where

$$J = \text{number of the day in the year between 1 (1 January) and 365 or 366 (31 December).}$$

- Step 4. Calculate declination of the earth,  $\delta$  (Allen et al. 1998 [DIRS 157311], Equation 24):

$$\delta = 0.409 \sin\left(\frac{2\pi}{365} J - 1.39\right) \quad (\text{Eq. C-4})$$

Steps 5 through 18 can be computed outside of the grid cell calculation loop when all grid cells are assumed to have the same latitude. This is a valid assumption provided that the entire study area is less than about 40 mi north to south, because extraterrestrial radiation,  $R_a$ , varies only slightly with small changes in latitude.

- Step 5. Calculate the sunset hour angle,  $\omega_s$ , for a horizontal surface (Allen et al. 1998 [DIRS 157311], Equation 25):

$$\omega_s = \arccos\left[-\tan(\varphi_{reference}) \tan(\delta)\right] \quad (\text{Eq. C-5})$$

where

$$\begin{aligned}\omega_s &= \text{sunset hour angle (rad)} \\ \varphi_{reference} &= \text{latitude of the reference weather station (rad) (input)} \\ \delta &= \text{solar declination, from Step 4.}\end{aligned}$$

- Step 6. Calculate extraterrestrial radiation on a horizontal surface for one 24-hr period,  $R_{a\ hor}$  (Allen et al. 1998 [DIRS 157311], Equation 21):

$$R_{a\ hor} = \frac{24(60)}{\pi} G_{sc} d_r \left[ \omega_s \sin(\varphi_{reference}) \sin(\delta) + \cos(\varphi_{reference}) \cos(\delta) \sin(\omega_s) \right] \quad (\text{Eq. C-6})$$

where

$$\begin{aligned}R_{a\ hor} &= \text{24-hr extraterrestrial radiation for a horizontal surface (MJ m}^{-2} \text{ d}^{-1}) \\ G_{sc} &= \text{solar constant (0.0820 MJ m}^{-2} \text{ min}^{-1}) \\ d_r &= \text{squared inverse relative distance factor for the earth-sun, dimensionless, from Step 3} \\ \omega_s &= \text{sunset hour angle (radians), from Step 5} \\ \varphi_{reference} &= \text{latitude of the reference weather station (rad) (input)} \\ \delta &= \text{solar declination (radians), from Step 4.}\end{aligned}$$

- Step 7. Calculate sine of mean solar elevation over 24-hr period,  $\sin\beta_{24}$ , weighted by extraterrestrial radiation (Allen et al. 2005 [DIRS 176207], Equation D.5):

$$\sin\beta_{24} = \sin \left[ 0.85 + 0.3 \varphi_{reference} \sin \left( \frac{2\pi}{365} J - 1.39 \right) - 0.42 (\varphi_{reference})^2 \right] \quad (\text{Eq. C-7})$$

where

$$\begin{aligned}\sin\beta_{24} &= \text{sine of the average } \beta \text{ (radians) during the daylight period, weighted according to } R_a \\ \varphi_{reference} &= \text{latitude of the reference weather station (rad) (input)} \\ J &= \text{day of the year.}\end{aligned}$$

Values for  $\sin\beta_{24}$  from Equation C-7 should be limited to greater than or equal to 0.01 for numerical stability in Step 10 (Allen et al. 2005 [DIRS 176207], p. D-9).

- Step 8. Calculate mean atmospheric pressure for the reference weather station,  $P_{reference}$  using the elevation of the reference weather station (Allen et al. 1998 [DIRS 157311], Equation 7):

$$P_{reference} = 101.3 \left( \frac{293 - 0.0065 Z_{reference}}{293} \right)^{5.26} \quad (\text{Eq. C-8})$$

where

$P_{reference}$  = atmospheric pressure at the reference weather station (kPa)  
 $z_{reference}$  = elevation of reference weather station, relative to mean sea level (m).

The 293 parameter in Eq. C-8 results from the definition of the standard atmosphere for reference  $ET_0$  calculation where standard air temperature equals 20°C (Allen et al. 1998 [DIRS 157311], p. 31).

Step 9. Calculate precipitable water,  $W$ , at the reference weather station (Allen et al. 2005 [DIRS 176207], Equation D.3):

$$W = 0.14 e_{a\ general} P_{reference} + 2.1 \quad (\text{Eq. C-9})$$

where

$W$  = precipitable water in the atmosphere passing over the study area (mm)  
 $P_{reference}$  = atmospheric pressure at reference weather station (kPa), from Step 8  
 $e_{a\ general}$  = general, actual vapor pressure of the air, at approximately 2 m (kPa), from Step 2.

Step 10. Calculate 24-hr transmissivity for beam radiation,  $K_{Bo\ hor}$  (Allen et al. 2005 [DIRS 176207], Equation D.2):

$$K_{Bo\ hor} = 0.98 \exp \left[ \frac{-0.00146 P_{reference}}{K_{cIn} \sin \beta_{24}} - 0.075 \left( \frac{W}{\sin \beta_{24}} \right)^{0.4} \right] \quad (\text{Eq. C-10})$$

where

$K_{Bo\ hor}$  = 24-hr transmissivity for clear-sky beam radiation (dimensionless)  
 $K_{cIn}$  = atmospheric cleanliness-turbidity coefficient (dimensionless),  $0 < K_{cIn} \leq 1.0$  where  $K_{cIn} = 1.0$  for clean air and  $K_{cIn} \leq 0.5$  for extremely turbid, dusty or polluted air.  $K_{cIn} = 1.0$  was used for Yucca Mountain for present day conditions, because the air in the area is unpolluted. The  $K_{cIn} = 1.0$  was used in determining  $K_{Rs}$  in Eq. C-13 for estimating  $R_{sm\ hor}$  from daily maximum and minimum air temperature and is therefore set to 1.0 here to be congruent with the  $R_{sm\ hor}$  estimate.  
 $P_{reference}$  = atmospheric pressure at reference weather station (kPa), from Step 8

$W$  = precipitable water in the atmosphere (mm), from Step 9

$\sin\beta_{24}$  = sine of average  $\beta$  during the daylight period (radians), from Step 7. Values for  $\sin\beta_{24}$  must be limited to greater than or equal to 0.01 for numerical stability (Allen et al. 2005 [DIRS 176207], p. D-8).

Equation C-10 was developed by Allen et al. (2005 [DIRS 176207], Equation D.2) for specific application to clear sky conditions.

Step 11. Calculate 24-hr transmissivity for diffuse radiation,  $K_{Do\ hor}$  using the ASCE EWRI function (Allen et al. 2005 [DIRS 176207], Equation D.4):

$$\begin{aligned} K_{Do\ hor} &= 0.35 - 0.36 K_{Bo\ hor} \text{ for } K_{Bo\ hor} \geq 0.15 \\ K_{Do\ hor} &= 0.18 + 0.82 K_{Bo\ hor} \text{ for } K_{Bo\ hor} < 0.15 \end{aligned} \quad (\text{Eq. C-11})$$

where

$K_{Do\ hor}$  = 24-hr transmissivity for clear-sky diffuse radiation (dimensionless)

$K_{Bo\ hor}$  = 24-hr transmissivity for direct radiation (dimensionless), from Step 10.

Step 12. Calculate clear sky solar radiation over the 24-hr period,  $R_{so\ hor}$  (Allen et al. 2005 [DIRS 176207], Equation D.1):

$$R_{so\ hor} = (K_{Bo\ hor} + K_{Do\ hor}) R_{a\ hor} \quad (\text{Eq. C-12})$$

where

$R_{so\ hor}$  = clear sky solar radiation over the 24-hr period ( $\text{MJ m}^{-2} \text{d}^{-1}$ )

$K_{Do\ hor}$  = transmissivity for clear-sky diffuse radiation (dimensionless), from Step 11

$K_{Bo\ hor}$  = transmissivity for direct radiation (dimensionless), from Step 10

$R_{a\ hor}$  = extraterrestrial radiation, horizontal surface ( $\text{MJ m}^{-2} \text{d}^{-1}$ ), from Step 6.

The  $R_{so\ hor}$  is calculated using humidity data from the reference station. It applies, however, to the entire study area, because  $R_{so\ hor}$  is only weakly sensitive to elevation, changing less than 1% to 2% over the range in elevations experienced in the study area (Appendix C3).

- Step 13. Estimate solar radiation on a horizontal surface,  $R_{sm\ hor}$ , using  $T_{max}$  and  $T_{min}$  at reference weather station (Allen et al. 1998 [DIRS 157311], Equation 50; Allen 1997 [DIRS 176568], Equation 1):

$$R_{sm\ hor} = K_{Rs} \sqrt{(T_{max\ reference} - T_{min\ reference})} R_{a\ hor} \quad (\text{Eq. C-13})$$

where

$R_{sm\ hor}$  =estimated solar radiation for horizontal surface ( $\text{MJ m}^{-2} \text{d}^{-1}$ )

$R_{a\ hor}$  =extraterrestrial radiation for horizontal surface ( $\text{MJ m}^{-2} \text{d}^{-1}$ ), from Step 6

$T_{max\ reference}$  =maximum air temperature measured at the reference weather station ( $^{\circ}\text{C}$ )

$T_{min\ reference}$  =minimum air temperature measured at the reference weather station ( $^{\circ}\text{C}$ )

$K_{Rs}$  =adjustment coefficient ( $^{\circ}\text{C}^{-0.5}$ ).

The  $R_{sm\ hor}$  from Equation C-13 must be limited to less than or equal to  $R_{so\ hor}$  from Equation C-12, since it is theoretically impossible for  $R_s$  on a horizontal surface (i.e., the estimate from Eq. C-13) to exceed  $R_s$  for a horizontal surface under cloud-free conditions (i.e., the estimate from Eq. C-12).

The  $R_{sm\ hor}$  is calculated for use at all grid cells, provided, a single latitude is used to represent the mountain for purposes of computing extraterrestrial radiation on a horizontal surface in Step 6. For present-day (and future climate) conditions,  $K_{Rs} = 0.19$  is used for Yucca Mountain, rather than the general value of 0.16 recommended in FAO-56 (Allen et al. 2005 [DIRS 176207]), based on an analysis of diffuse solar radiation measurements from Yucca Mountain (Appendix C3) and on findings by Allen (1997 [DIRS 176568]) for high elevation locations.  $R_{sm\ hor}$  is applied to the entire Yucca Mountain study area because clear sky solar radiation,  $R_{so\ hor}$ , and consequently  $R_{sm\ hor}$ , is only weakly sensitive to elevation, changing less than 1% to 2% over the range in elevations experienced in the study area, based on a sensitivity analysis conducted in Appendix C3.

## **C1.2 SETUP FOR TRANSLATION OF HORIZONTAL SOLAR RADIATION TO ANY SLOPE AS REPRESENTED BY FIXED COMBINATIONS OF SLOPE AND ASPECT**

These calculations are general to all grid cells associated with the reference weather station. The horizontal solar radiation is calculated for the reference weather station using a single latitude and reference elevation for the study area. This value is then modified at each grid cell to account for effects of slope and azimuth.

- Step 14. Calculate total short-wave transmissivity,  $\tau_{sw\ hor}$ , also referred to in literature as a ‘clearness index,  $K_t$ ’, associated with the measured  $R_s$  value (Duffie and Beckman 1991 [DIRS 176616], Equation 2.9.2):

$$\tau_{sw\ hor} = \frac{R_{sm\ hor}}{R_{a\ hor}} \quad (\text{Eq. C-14})$$

where

$\tau_{sw\ hor}$  = total short-wave transmissivity (dimensionless)

$R_{sm\ hor}$  = solar radiation for horizontal surface ( $\text{MJ m}^{-2} \text{d}^{-1}$ ), from Step 13,

$R_{a\ hor}$  = extraterrestrial radiation for horizontal surface ( $\text{MJ m}^{-2} \text{d}^{-1}$ ), from Step 6.

Because  $R_{sm\ hor}$  is estimated using Eq. C-13, Eq. C-14 reduces to  $\tau_{sw\ hor} = K_{Rs} (T_{max\ reference} - T_{min\ reference})^{0.5}$ , which defines  $\tau_{sw\ hor}$  as a function of the difference between daily extremes in air temperature.

- Step 15. Partition the atmospheric transmissivity from Step 14 into its diffusive and direct beam components. Calculate apparent  $K_{B\ hor}$  associated with the actual total short-wave transmissivity using the procedure by Vignola and McDaniels (1986 [DIRS 176481]). The partitioning of atmospheric transmissivity is applied to all days, including those having cloud cover. Therefore, the clear sky-oriented equations of Equations C-10 and C-11 (Allen et al. 2005 [DIRS 176207]) do not apply here. A form of the equation by Vignola and McDaniels (1986 [DIRS 176481], p. 411) from Equation C-51 is used:

$$K_{D\ hor} = 0.984 \tau_{sw\ hor} \quad \text{for } \tau_{sw\ hor} < 0.175$$

$$K_{D\ hor} = -0.022 + 1.280 \tau_{sw\ hor} - 0.828(\tau_{sw\ hor})^2 - 0.765(\tau_{sw\ hor})^3 \quad \text{for } 0.175 \leq \tau_{sw\ hor} \leq 0.8$$

$$K_{D\ hor} = 0.08 \quad \text{for } \tau_{sw\ hor} > 0.8 \quad (\text{Eq. C-15})$$

where

$K_{D\ hor}$  = 24-hour transmissivity for diffuse radiation (dimensionless)

$\tau_{sw\ hor}$  = total short-wave transmissivity (dimensionless), from Step 14.

Equation C-15 has been rearranged from the equation by Vignola and McDaniels (1986 [DIRS 176481], p. 411), so that the left-hand side of the equation contains only  $K_{D\ hor}$ , rather than  $K_{B\ hor}$ . Equation C-15 has been found to agree closely with diffuse versus transmissivity data collected near Yucca Mountain (Section C4). The last line of Equation C-15 is required to limit the original polynomial expression by Vignola and McDaniels (1986 [DIRS 176481], p. 411) to the domain of their regression data set ( $\tau_{sw\ hor} \leq 0.8$ ) where  $K_{D\ hor}$  is set to 0.08.

Equation C-15 is used to adjust  $R_{sm\ hor}$  to all slopes, and it describes the atmospheric transmissivity component representing diffuse radiation well under both clear and cloudy conditions as compared to Equation C-11 (Allen et al. 2005 [DIRS 176207]), which is intended primarily for clear sky conditions only. Equations C-10 and C-11 are used in calculating  $R_{so\ hor}$ , because they explicitly consider the effects of humidity and elevation. Appendix C4 includes the analysis performed to develop Equation C-15.

- Step 16. Calculate actual direct beam transmissivity or index,  $K_{B\ hor}$ , as the difference between total transmissivity and diffuse transmissivity (Allen 1996 [DIRS 176485], Equation 7):

$$K_{B\ hor} = \tau_{sw\ hor} - K_{D\ hor} \quad (\text{Eq. C-16})$$

where

$K_{B\ hor}$  = 24-hr transmissivity for direct radiation (dimensionless)

$K_{D\ hor}$  = 24-hr transmissivity for diffuse radiation (dimensionless), from Step 15

$\tau_{sw\ hor}$  = total short-wave transmissivity (dimensionless), from Step 14.

- Step 17. Calculate direct beam radiation on the horizontal surface,  $I_{b\ hor}$ , based on the measured  $R_{sm\ hor}$ :

$$I_{b\ hor} = K_{B\ hor} * R_{a\ hor} \quad (\text{Eq. C-17})$$

where

$I_{b\ hor}$  = direct beam radiation on the horizontal surface ( $\text{MJ m}^{-2} \text{d}^{-1}$ )

$R_{a\ hor}$  = extraterrestrial radiation for horizontal surface ( $\text{MJ m}^{-2} \text{d}^{-1}$ ), from Step 6

$K_{B\ hor}$  = 24-hr transmissivity for direct radiation (dimensionless), from Step 16.

- Step 18. Calculate the diffuse component,  $I_{d\ hor}$ , of  $R_{sm\ hor}$  for a horizontal surface:

$$I_{d\ hor} = K_{D\ hor} * R_{a\ hor} \quad (\text{Eq. C-18})$$

where

$I_{d\ hor}$  = diffuse radiation on the horizontal surface ( $\text{MJ m}^{-2} \text{d}^{-1}$ )

$K_{D\ hor}$  = 24-hr transmissivity for diffuse radiation (dimensionless), from Step 15

$R_{a\ hor}$  = extraterrestrial radiation for horizontal surface ( $\text{MJ m}^{-2} \text{d}^{-1}$ ), from Step 6.

### C1.3 CELL-SPECIFIC CALCULATIONS

The following steps are unique to each grid cell because of the requirement of specific values for slope or aspect (azimuth) affecting solar radiation and elevation affecting air temperature and  $ET_0$ .

Step 19. Define terrain albedo  $\alpha_T$  for the valley areas adjacent to the study area. A value  $\alpha = 0.15$  (Brutsaert 1982 [DIRS 176615], p. 136, Table 6.4) is recommended for darker soils or significant vegetation and  $\alpha = 0.35$  for light soils having little vegetation.

$$\alpha_T = [\text{Input Value}] \text{ (dimensionless)} \quad (\text{Eq. C-19})$$

The terrain albedo is used in Step 24 for calculating reflected radiation from areas below a sloped grid cell that reaches the specified grid cell. Therefore, the terrain albedo does not represent the albedo of the grid cell itself; it represents a spatially averaged value of the albedo of the surrounding valley areas that can reflect solar radiation toward grid cells. This value can be affected by seasonality and climatic regimes that can also affect ground cover of surrounding areas. The value for terrain albedo has only a small effect on the solar radiation estimate and  $ET_0$ , changing  $ET_0$  by less than  $0.3 \text{ mm d}^{-1}$  for all slope–aspect combinations in the study area when terrain albedo is varied from 0.1 to 0.4. The  $0.3 \text{ mm d}^{-1}$  value is less than the  $1.0 \text{ mm d}^{-1}$  uncertainty noted for  $ET$  using precision weighing lysimeters by Allen et al. (2005 [DIRS 176009], p. 12). Therefore, a single value  $\alpha_T = 0.22$  is used for the study area.

The following steps must be computed for each specific grid cell using the  $R_b$  adjustment factor from the  $R_b$  look-up table that is created in Appendix C2. This  $R_b$  look-up table is not printed here; it is read into the MASSIF infiltration model.

Step 20. Calculate  $I_b$ , the direct beam on the inclined surface having a specific slope–aspect combination, using the  $R_b$  adjustment factor determined from the look-up table, computed in Step 44 (Duffie and Beckman 1980 [DIRS 176264], Equations 2.15.2):

$$I_b = I_{b\ hor} * R_b \quad (\text{Eq. C-20})$$

where

$I_b$  = direct beam radiation on the inclined surface ( $\text{MJ m}^{-2} \text{d}^{-1}$ )  
 $I_{b\ hor}$  = direct beam radiation on the horizontal surface ( $\text{MJ m}^{-2} \text{d}^{-1}$ ), from Step 17



$R_b$  = direct radiation ratio (dimensionless), from  $R_b$  look-up table, Output DTN: SN0602T0502206.003 (Appendix C2).

$R_b$  is defined as the ratio of beam radiation on an incline to the beam radiation on a horizontal plane.  $R_b$  is a function of latitude, slope, azimuth, and day of year. The  $R_b$  look-up table (Appendix C2) includes values for  $R_b$  for specific values of slope and azimuth for every day of the year.

The following calculations in Steps 21 to 27 are based on the anisotropic diffuse model by Reindl et al. (1990 [DIRS 176480], Equation 5).

Step 21. By definition, the anisotropic index  $A_t$  for simulating circumsolar brightening is (Reindl et al. 1990 [DIRS 176480], p. 11; Duffie and Beckman (1991 [DIRS 176616], Equation 2.16.3):

$$A_t = K_{B\ hor} \quad (\text{Eq. C-21})$$

where

$A_t$  = anisotropic index (dimensionless)

$K_{B\ hor}$  =24-hr transmissivity for direct radiation (dimensionless), from Step 16.

Step 22. Calculate the modulating function ( $f$ ) for horizontal brightness (Reindl et al. 1990 [DIRS 176480], p. 11; Duffie and Beckman 1991 [DIRS 176616], Equation 2.16.6):

$$f = \sqrt{\frac{I_{b\ hor}}{R_{sm\ hor}}} \quad (\text{Eq. C-22})$$

where

$f$  =modulating function for diffuse brightening near the horizon (dimensionless)

$I_{b\ hor}$  =direct beam radiation on the inclined surface ( $\text{MJ m}^{-2} \text{d}^{-1}$ ), from Step 17

$R_{sm\ hor}$  =solar radiation for horizontal surface ( $\text{MJ m}^{-2} \text{d}^{-1}$ ), from Step 13.

Step 23. Calculate the diffuse component for the inclined surface (Reindl et al. 1990 [DIRS 176480], Equation 5; Duffie and Beckman 1991 [DIRS 176616], Equation 2.16.5):

$$I_d = I_{d\ hor} \left[ (1 - A_t) \left( \frac{1 + \cos(s)}{2} \right) (1 + f \sin^3(s/2)) + A_t R_b \right] \quad (\text{Eq. C-23})$$

where

$I_d$  = diffuse radiation on the inclined surface ( $\text{MJ m}^{-2} \text{d}^{-1}$ )

$I_{d\text{ hor}}$  = diffuse radiation on the horizontal surface ( $\text{MJ m}^{-2} \text{d}^{-1}$ ), from Step 18

$A_t$  = anisotropic index for circumsolar brightening (dimensionless), from Step 21

$f$  = modulating function for diffuse brightening near the horizon (dimensionless), from Step 22

$R_b$  = direct radiation ratio (dimensionless), from the look-up table (Output DTN: SN0602T0502206.003) (Appendix C2)

$s$  = slope (radians).

Step 24. Calculate the reflected radiation from lower lying terrain to the inclined surface (Reindl et al. 1990 [DIRS 176480], Equation 1):

$$I_r = R_{sm\text{ hor}} * \alpha_T * \left( \frac{1 - \text{Cos}(s)}{2} \right) \quad (\text{Eq. C-24})$$

where

$I_r$  = reflected radiation that reach the inclined surface ( $\text{MJ m}^{-2} \text{d}^{-1}$ )

$R_{sm\text{ hor}}$  = solar radiation for horizontal surface ( $\text{MJ m}^{-2} \text{d}^{-1}$ ), from Step 13

$s$  = cell slope (radians)

$\alpha_T$  = albedo of the surrounding terrain (dimensionless), from Step 19.

Step 25. Calculate the total radiation received by the inclined surface (Hay 1979 [DIRS 176151], Equation 21):

$$R_{sm\text{ inc}} = I_b + I_d + I_r \quad (\text{Eq. C-25})$$

where

$R_{sm\text{ inc}}$  = solar radiation for the inclined surface ( $\text{MJ m}^{-2} \text{d}^{-1}$ )

$I_b$  = direct beam radiation on the inclined surface ( $\text{MJ m}^{-2} \text{d}^{-1}$ ), from Step 20

$I_d$  = diffuse radiation on the inclined surface ( $\text{MJ m}^{-2} \text{d}^{-1}$ ), from Step 23

$I_r$  = reflected radiation that reaches the inclined surface ( $\text{MJ m}^{-2} \text{d}^{-1}$ ), from Step 24.

The  $I_r$  is reflected radiation from lower lying terrain. This equation is used implicitly by Reindl et al. (1990 [DIRS 176480]) and Duffie and Beckman (1980 [DIRS 176264]; 1991 [DIRS 176616]), but is used in equation form by Hay (1979 [DIRS 176151]). Equation C-25 is equivalent to the equation by Duffie and Beckman (1991 [DIRS 76616], Equation 2.16.7) when all equation substitutions are made for  $I_b$ ,  $I_d$  and  $I_r$ , as in Equations C-20, C-23, and C-24.

Step 26. Reproject  $R_{sm\ inc}$  to a horizontal projection (equivalent):

$$R_{s(equiv)hor} = \frac{R_{sm\ inc}}{\cos(s)} \quad (\text{Eq. C-26})$$

where

$R_{s(equiv)hor}$  = solar radiation for the inclined surface, reprojected to a horizontal plane ( $\text{MJ m}^{-2} \text{d}^{-1}$ )

$R_{sm\ inc}$  = solar radiation for the inclined surface ( $\text{MJ m}^{-2} \text{d}^{-1}$ ), from Step 25

$s$  = cell slope (radians).

The  $R_{s(equiv)hor}$  is the  $R_s$  that occurs on the inclined slope, but it is expressed in terms of energy per horizontal grid area to be consistent with precipitation and other water balance terms.

#### C1.4. $ET_0$ CALCULATION

Step 27. Using  $T_{max\ reference}$  and  $T_{min\ reference}$  from the reference weather station, calculate  $T_{max\ lapse}$  and  $T_{min\ lapse}$  for each cell in the grid using a terrestrial temperature lapse rate. The terrestrial temperature lapse rate is set equal to the standard dry, adiabatic lapse rate of  $10^\circ\text{C}$  per 1,000 m (Maidment 1993 [DIRS 125317], p. 3.3). This adiabatic lapse rate is a reasonable approximation to the terrestrial lapse rate in areas, like Yucca Mountain, where the terrain is not steep and conditions are generally windy enough to cause airflow over (rather than around) the terrain and dry enough that condensation is insignificant. Under conditions of condensation, a saturated adiabatic lapse rate can be used, where that rate ranges from  $6.9^\circ\text{C}$  per 1,000 m at  $0^\circ\text{C}$  to  $3.6^\circ\text{C}$  per 1,000 m at  $30^\circ\text{C}$  at sea level (Rosenberg et al. 1983 [DIRS 177526], p. 120). The rate averages  $5.4^\circ\text{C}$  per 1,000 m at  $0^\circ\text{C}$  at 50 kPa air pressure (Rosenberg et al. 1983 [DIRS 177526], p. 120), which corresponds to about 5,700 m elevation. For the elevation range of the study area (approximately 970 to 1,970 m), the saturated adiabatic lapse rate would be expected to range from

approximately 6.4°C per 1,000 m at 0°C to approximately 3.3°C per 1,000 m at 30°C. However, because conditions of water vapor condensation occur only during precipitation events, which are relatively rare to the study area, the terrestrial lapse rate will follow the adiabatic lapse rate a majority of the time. The sensitivity of infiltration to the value for the lapse rate has been shown to be small (Section 71.4). Therefore, the dry adiabatic lapse rate has been used as the environmental lapse rate for all conditions. The correction to air temperature for lapse is made as:

$$T_{\max} = T_{\max \text{ reference}} - \frac{LR}{1000}(z_{\text{cell}} - z_{\text{reference}}) \quad (\text{Eq. C-27a})$$

$$T_{\min} = T_{\min \text{ reference}} - \frac{LR}{1000}(z_{\text{cell}} - z_{\text{reference}}) \quad (\text{Eq. C-27b})$$

where

$T_{\max}$  = maximum temperature during the 24-hr period corrected for elevation (°C)

$T_{\min}$  = minimum temperature during the 24-hr period corrected for elevation (°C)

$T_{\max \text{ reference}}$  = maximum air temperature measured at the reference weather station (°C)

$T_{\min \text{ reference}}$  = minimum air temperature measured at the reference weather station (°C)  $LR$  = environmental lapse rate (°C per 1,000 m)

$z_{\text{cell}}$  = elevation of the grid cell (m)

$z_{\text{reference}}$  = elevation of the reference weather station (m).

The corrected  $T_{\max}$  and  $T_{\min}$  are used in the  $ET_0$  calculations.

Step 28. Wind speed at 2-m height. For the study area application, daily wind speed has been approximated by linearly interpolating between mean monthly values for wind speed developed from measured data (Output DTN: SN0610T0502206.030). This approach accounts for seasonal differences. The monthly wind speed set was used for the total study area and for future climates (assumption in Section 5). Wind speed parameter development is discussed in Section 6.5.1, Appendix F, and in detail in Output DTN: SN0610T0502206.030 and follows the following form:

$$u_2(\text{day}) = u_2(\text{month}_i) + \frac{u_2(\text{month}_i) - u_2(\text{month}_{i+1})}{\text{midday}(\text{month}_i) - \text{midday}(\text{month}_{i+1})} * (\text{day} - \text{midday}(\text{month}_i)) \quad (\text{Eq. C-28})$$

where

$$\begin{aligned} u_2(day) &= \text{wind speed at 2-m height (m s}^{-1}\text{) on Julian day = } day \\ u_2(month_i) &= \text{mean monthly wind speed for month, } i \\ midday(month_i) &= \text{Julian day that is the middle of month, } i \end{aligned}$$

In this calculation, the months bounding the each day of the linear interpolation are determined manually in Output DTN: SN0610T0502206.030.

Step 29. Calculate daily mean saturation vapor pressure,  $e_s$ , associated with the daily extreme temperatures corrected for elevation (Allen et al. 1998 [DIRS 157311], Equation 12):

$$e_s = \frac{e^o(T_{max}) + e^o(T_{min})}{2} \quad (\text{Eq. C-29a})$$

where

$$e^o(T_{max}) = 0.6108 \exp\left[\frac{17.27 T_{max}}{T_{max} + 237.3}\right] \quad (\text{Eq. C-29b})$$

$$e^o(T_{min}) = 0.6108 \exp\left[\frac{17.27 T_{min}}{T_{min} + 237.3}\right] \quad (\text{Eq. C-29c})$$

and

$e_s$  =daily mean saturation vapor pressure (kPa)

$T_{max}$  =maximum temperature during the 24-hr period ( °C) corrected for elevation, from Step 27

$T_{min}$  =minimum temperature during the 24-hr period ( °C) corrected for elevation, from Step 27.

$e^o(T)$  =saturation vapor pressure function calculated at temperature  $T$ .

Step 30. Calculate mean air temperature corrected for elevation (Allen et al. 1998 [DIRS 157311], Equation 9):

$$T = \frac{T_{max} + T_{min}}{2} \quad (\text{Eq. C-30})$$

where

$T$  = mean air temperature, °C, corrected for elevation

$T_{max}$  = maximum temperature during the 24-hr period (°C), from Step 27, corrected for elevation

$T_{min}$  = minimum temperature during the 24-hr period (°C), from Step 27, corrected for elevation

Step 31. Limit actual vapor pressure,  $e_a$ , of the grid cell to less than or equal to  $e_s$  to keep the vapor pressure deficit ( $e_s - e_a$ ) in the  $ET_0$  equation (Step 37), nonnegative:

$$e_a = \min[e_{a \text{ general}}, e_s] \quad (\text{Eq. C-31})$$

where

$e_a$  = actual vapor pressure at the grid cell (kPa)

$e_{a \text{ general}}$  = general actual vapor pressure of the general air mass (kPa), from Step 2

$e_s$  = saturation vapor pressure (kPa), from Step 29.

The occurrence of  $e_s = e_a$  indicates that air is saturated at the mean condition for the day and the potential for cloud formation exists. In these situations, the amount of solar radiation estimated by Equation C-13 will generally produce  $R_{sm \text{ hor}}$  less than or equal to  $R_{so \text{ hor}}$  due to relatively small difference between  $T_{max}$  and  $T_{min}$  responsible for producing this condition ( $e_s = e_a$ ) as compared to clear sky conditions when  $T_{max}$  and  $T_{min}$  tend to be larger. Under clear sky conditions,  $e_s$  will tend to exceed  $e_a$  and C-31 will not be implemented. Implementation of Equation C-31 will therefore tend to be synchronized with estimated cloudy conditions implicit to the  $R_{sm \text{ hor}}$  estimate.

Step 32. Calculate slope of saturation vapor pressure curve at air temperature  $T$  ( $\Delta$ ) (Allen et al. 1998 [DIRS 157311], Equation 13):

$$\Delta = \frac{4098 \left[ 0.6108 \exp\left(\frac{17.27 T}{T + 237.3}\right) \right]}{(T + 237.3)^2} \quad (\text{Eq. C-32})$$

where

$\Delta$  = slope of saturation vapor pressure curve (kPa °C<sup>-1</sup>)

$T$  = lapsed air temperature (°C), from Step 30.

Step 33a. Calculate atmospheric pressure,  $P$ , at each grid cell for calculating the psychrometric constant. Use the elevation of each grid cell (Allen et al. 1998 [DIRS 157311], Equation 7):

$$P_{cell} = 101.3 \left( \frac{293 - 0.0065 z_{cell}}{293} \right)^{5.26} \quad (\text{Eq. C-33a})$$

where

$$\begin{aligned} P_{cell} &= \text{atmospheric pressure at the grid cell (kPa)} \\ z_{cell} &= \text{elevation of grid cell above sea level (m)}. \end{aligned}$$

The calculation of  $P_{cell}$  changes with cell elevation.

Step 33b. Calculate psychrometric constant Gamma (Allen et al. 1998 [DIRS 157311], Equation 8):

$$\gamma_c = \frac{c_p P_{cell}}{\varepsilon \lambda} = 0.665 \times 10^{-3} P_{cell} \quad (\text{Eq. C-33b})$$

where

$$\begin{aligned} \gamma_c &= \text{psychrometric constant (kPa } ^\circ\text{C}^{-1}\text{)} \\ P_{cell} &= \text{atmospheric pressure (kPa), from Step 33a} \\ \lambda &= \text{latent heat of vaporization} = 2.45 \text{ (MJ kg}^{-1}\text{)} \\ c_p &= \text{specific heat at constant pressure, } 1.013 \times 10^{-3} \text{ (MJ kg}^{-1} \text{ } ^\circ\text{C}^{-1}\text{)} \\ \varepsilon &= \text{ratio molecular weight of water vapor/dry air} = 0.622. \end{aligned}$$

Step 34. Calculate the horizontal equivalent for net short wave radiation on the incline  $R_{ns}$  (Allen et al. 1998 [DIRS 157311], Equation 38):

$$R_{ns} = (1 - \alpha) R_{s(equiv)hor} \quad (\text{Eq. C-34})$$

where

$$\begin{aligned} R_{ns} &= \text{net solar or shortwave radiation (MJ m}^{-2} \text{ day}^{-1}\text{)} \\ \alpha &= \text{albedo of the standard grass reference, which is 0.23 (dimensionless)} \\ R_{s(equiv)hor} &= \text{incoming solar radiation on the incline, reprojected to a horizontal equivalent (MJ m}^{-2} \text{ day}^{-1}\text{), from Step 26.} \end{aligned}$$

Step 35. Calculate the net outgoing long wave radiation (Allen et al. 1998 [DIRS 157311], Equation 39):

$$R_{nl} = \sigma \left[ \frac{T_{max,K}^4 + T_{min,K}^4}{2} \right] \left( 0.34 - 0.14 \sqrt{e_a} \right) \left( 1.35 \frac{R_{sm\ hor}}{R_{so\ hor}} - 0.35 \right) \quad (\text{Eq. C-35})$$

where

$R_{nl}$  = net outgoing longwave radiation ( $\text{MJ m}^{-2} \text{ day}^{-1}$ ) (on a horizontal equivalent projection)

$\sigma$  = Stefan-Boltzmann constant,  $4.903 \times 10^{-9}$  ( $\text{MJ K}^{-4} \text{ m}^{-2} \text{ day}^{-1}$ )

$T_{max,K}$  = daily maximum absolute temperature,  $\text{K} = ^\circ\text{C} + 273.16$ , from Step 27

$T_{min,K}$  = daily minimum absolute temperature,  $\text{K} = ^\circ\text{C} + 273.16$ , from Step 27

$e_a$  = actual vapor pressure for the grid cell (kPa), from Step 31

$R_{sm\ hor}$  = calculated solar radiation on horizontal surface ( $\text{MJ m}^{-2} \text{ day}^{-1}$ ), from Step 13

$R_{so\ hor}$  = calculated clear-sky radiation on a horizontal surface ( $\text{MJ m}^{-2} \text{ day}^{-1}$ ), from Step 12.

The  $R_{sm\ hor}/R_{so\ hor}$  is an indicator of overall cloudiness for the area and must be limited to less than or equal to 1.0. The value represents conditions at the reference weather station and is applied to all grid cells.

Step 36. Calculate net radiation on the inclined surface,  $R_n$  (Allen et al. 1998 [DIRS 157311], Equation 40), projected to a horizontal projection:

$$R_n = R_{ns} - R_{nl} \quad (\text{Eq. C-36})$$

where

$R_n$  = net radiation ( $\text{MJ m}^{-2} \text{ day}^{-1}$ ) (on a horizontal equivalent projection)

$R_{ns}$  = net solar or shortwave radiation ( $\text{MJ m}^{-2} \text{ day}^{-1}$ ), from Step 34

$R_{nl}$  = net outgoing long-wave radiation ( $\text{MJ m}^{-2} \text{ day}^{-1}$ ), from Step 35.



Step 37. Calculate  $ET_0$  using Penman-Monteith equation (Allen et al. 1998 [DIRS 157311], Equation 6):

$$ET_0 = \frac{0.408 \Delta(R_n - G) + \gamma_c \frac{900}{T + 273} u_2 (e_s - e_a)}{\Delta + \gamma_c (1 + 0.34 u_2)} \quad (\text{Eq. C-37})$$

where

- $ET_0$  = reference evapotranspiration ( $\text{mm day}^{-1}$ )
- $R_n$  = net radiation on the inclined slope (but with horizontal reprojection) ( $\text{MJ m}^{-2} \text{day}^{-1}$ ), from Step 36
- $G$  = soil heat flux density ( $\text{MJ m}^{-2} \text{day}^{-1}$ ), use  $G=0$  for daily time step (Allen et al. 1998 [DIRS 157311], Equation 42)
- $T$  = lapsed mean daily air temperature at 2- m height ( $^{\circ}\text{C}$ ), from Step 30
- $u_2$  = wind speed at 2-m height ( $\text{m s}^{-1}$ ), from Step 28
- $e_s$  = saturation vapor pressure (kPa), from Step 29
- $e_a$  = actual vapor pressure (kPa), from Step 31
- $e_s - e_a$  = saturation vapor pressure deficit (kPa), ( $e_s - e_a \geq 0$ )
- $\Delta$  = slope vapor pressure curve ( $\text{kPa } ^{\circ}\text{C}^{-1}$ ), from Step 32
- $\gamma_c$  = psychrometric constant ( $\text{kPa } ^{\circ}\text{C}^{-1}$ ), from Step 33.

The  $ET_0$  from Step 37 represents the reference ET in  $\text{mm d}^{-1}$  for an inclined surface but is expressed on a horizontal basis.

## C2. CREATION OF LOOK-UP TABLE (LUT) FOR PARAMETER $R_b$

The  $R_b$  is defined as the ratio of beam radiation on an incline to the beam radiation on a horizontal plane. The  $R_b$  parameter is used by Duffie and Beckman (1980 [DIRS 176264], Equation 2.15.2) to translate direct beam radiation from horizontal to tilted surfaces. The  $R_b$  parameter is used in Step 20 of the  $ET_0$  calculation procedure. The Duffie and Beckman (1980 [DIRS 176264]) equation in Step 44 stems from work by Klein (1977 [DIRS 176152]).

The product of Steps 38 to 44 is the  $R_b$  look-up table that includes values for  $R_b$  that are unique for each slope–aspect day-of-year combination associated with a reference latitude. It is produced by applying Steps 38 to 44 for a series of specific slope–aspect day-of-year combinations.

Steps 38 to 44 (Duffie and Beckman 1980 [DIRS 176264] and 1991 [DIRS 176616]; Klein 1977 [DIRS 176152]; Revfeim 1976 [DIRS 176482]) are used to compute integration limits for beam radiation during the 24-hr period. These equations are generally valid for all slope–aspect combinations except those where the sun may appear twice during the day. Twice-per-day solar appearance may occur for steep north facing slopes whenever the slope is greater than the solar angle above the horizon at solar noon; that is, when:

$$\sin s > \sin \varphi \cos \delta + \cos \varphi \sin \delta$$

where  $s$  is the slope in radians,  $\varphi$  = latitude (radians), and  $\delta$  = solar declination (radians), from Step 4. This condition does not occur within the defined latitude, slope, and azimuth classifications utilized in the MASSIF infiltration model.

Nomenclature of slope and aspect used in all steps:

$s$  is surface slope where, by definition here and by Duffie and Beckman (1980 [DIRS 176264] and 1991 [DIRS 176616]):

$s = 0$  for horizontal, and

$s = \pi/2$  radians for vertical slope ( $s$  is always positive and represents the slope in any direction).

$\gamma$  is the surface aspect angle where, as defined by Duffie and Beckman (1980 [DIRS 176264] and 1991 [DIRS 176616]):

$\gamma = 0$  for slopes oriented due south

$\gamma = -\pi/2$  radians for slopes oriented due east

$\gamma = +\pi/2$  radians for slopes oriented due west

$\gamma = \pm \pi$  radians for slopes oriented due north.

Step 38. Calculate the effective latitude ( $\varphi_{\text{eff}}$ ) for a given slope and aspect as described by Revfeim (1976 [DIRS 176482], Equation 2):

$$\varphi_{\text{eff}} = \arcsin[\cos(s) * \sin(\varphi) - \sin(s) * \cos(\varphi) * \cos(\gamma)] \quad (\text{Eq. C-38})$$

where

$s$  = slope (radians)

$\varphi$  = latitude (radians)

$\gamma$  = surface aspect angle (radians).

The  $\varphi_{\text{eff}}$  is used in subsequent calculation steps to determine limits for beginning and ending of beam (direct) radiation during a day. The  $\varphi_{\text{eff}}$  is effective latitude that incorporates the effect of slope and aspect angle on the solar angle relative to the slope.

Step 39. Check whether the inclined surface receives any direct beam radiation during the day:

- a. Calculate  $\varphi_{eff} - \delta$ , where  $\varphi_{eff}$  is from Step 38, and  $\delta$  is the declination from Step 4.
- b. If  $\varphi_{eff} - \delta \geq \pi/2$ , then the surface does not receive any direct beam radiation during the day, so that  $R_b = 0$ . Therefore, if this conditional is true, no additional calculations are made for  $R_b$ .

In equation form:

$$\text{if } \varphi_{eff} - \delta \geq \pi / 2 \quad \text{then } R_b = 0 \quad (\text{Eq. C-39})$$

and Steps 40 to 44 are skipped.

Otherwise, if  $\varphi_{eff} - \delta < \pi/2$ :

Step 40. Set up for the solution of daily integration limits for beam (direct) radiation using Duffie and Beckman (1991 [DIRS 176616]). Calculate parameter  $A$  for each slope-aspect combination (Duffie and Beckman 1991 [DIRS 176616], Equation 2.20.5g):

$$A = \cos(s) + \tan(\varphi) \cos(\gamma) \sin(s) \quad (\text{Eq. C-40})$$

where

- $s$  = slope (radians)
- $\varphi$  = latitude (radians)
- $\gamma$  = surface aspect angle (radians).

Step 41. Calculate parameter  $B$  for each slope-aspect combination and day of the year (Duffie and Beckman 1991 [DIRS 176616], Equation 2.20.5h):

$$B = \cos(\omega_s) \cos(s) + \tan(\delta) \sin(s) \cos(\gamma) \quad (\text{Eq. C-41})$$

where

- $s$  = slope (radians)
- $\delta$  = solar declination (radians), from Step 4
- $\gamma$  = surface aspect angle (radians)
- $\omega_s$  = sunset hour angle (radians), from Step 5.

- Step 42. Calculate parameter  $C$  for each slope–aspect combination (Duffie and Beckman 1991 [DIRS 176616], Equation 2.20.5i):

$$C = \frac{\sin(s)\sin(\gamma)}{\cos(\varphi)} \quad (\text{Eq. C-42})$$

where

- $s$  = slope (radians)
- $\gamma$  = surface aspect angle (radians)
- $\varphi$  = latitude (radians).

- Step 43. Calculate the 24-hr integration limits  $\omega_{sr}$  (sunrise hour angle for inclined surface) and  $\omega_{ss}$  (sunset hour angle for inclined surface) (Duffie and Beckman 1991 [DIRS 176616], Equations 2.20.5e and 2.20.5f) for the  $R_b$  equation. The required steps are presented in sequential order of computation.

Steps 43.1, 43.2a, 43.3a, and 43.4 are not listed by Duffie and Beckman (1991 [DIRS 176616]) but are necessary to eliminate numerical errors caused by taking the square root of a nonpositive number (Step 43.1), or taking the arccosine of a value outside the  $-1$  to  $1$  domain (Steps 43.2a, 43.2b, 43.3a, and 43.3b). The steps also eliminate negative values calculated for  $R_b$ . If any of the conditionals of Steps 43.1, 43.2a, or 43.3a are true, then the parameter listed as the second listed item of the “min” function of Equation 43.2b (sunrise) and/or Equation 43.3b (sunset) is disqualified, and the min function defaults to the first item ( $\omega_{sr}$  and/or  $\omega_{ss}$ ). This conditional check is carried out in Step 43.1.

- Step 43.1. Check for negative values in the square root argument used in Steps 43.3a and 43.3b.

According to Klein and Theilacker (1981 [DIRS 176484]), the quantity within the square root (Steps 43.2b and 43.3b) will be negative if the surface orientation is such that the solar incidence angle is less or greater than 90 degrees at all times;  $\omega_{sr}$  and  $\omega_{ss}$  should be set to  $-\omega_s$  and  $\omega_s$ , respectively, under these circumstances (Klein and Theilacker 1981 [DIRS 176484, p.31]).

Therefore,

$$\text{if } (A^2 - B^2 + C^2 < 0) \text{ then } \omega_{sr} = -\omega_s \text{ and } \omega_{ss} = \omega_s \quad (\text{Eq. C-43.1})$$

where  $\omega_{sr} = -\omega_s$  and  $\omega_{ss} = \omega_s$  are the normal sunrise and sunset angles on horizontal slopes; proceed to Step 44.

Otherwise:

Step 43.2a. Check for out-of-domain values in the arccosine function in Step 43.2b:

$$\text{if } \left( \frac{AB + C\sqrt{A^2 - B^2 + C^2}}{A^2 + C^2} < -1 \right) \text{ or } \left( \frac{AB + C\sqrt{A^2 - B^2 + C^2}}{A^2 + C^2} > 1 \right) \text{ then } \omega_{sr} = -\omega_s \text{ (Eq. C-43.2a)}$$

where  $\omega_{sr} = -\omega_s$  is the normal sunrise angle on horizontal slopes; proceed to Step 43.3a.

Otherwise:

Step 43.2b. Apply the equation by Duffie and Beckman (1991 [DIRS 176616], Equation 2.20.5e):

$$|\omega_{sr}| = \min \left[ \omega_s, \arccos \left( \frac{AB + C\sqrt{A^2 - B^2 + C^2}}{A^2 + C^2} \right) \right] \quad (\text{Eq. C-43.2b})$$

and

$$\omega_{sr} = \begin{cases} -|\omega_{sr}| & \text{if } (A > 0 \text{ and } B > 0) \text{ or } (A \geq B) \\ |\omega_{sr}| & \text{otherwise} \end{cases} \quad (\text{Eq. C-43.2c})$$

where  $\omega_{sr} = -|\omega_{sr}|$  is the normal limit.

Step 43.3a. Check for out-of-domain values for the arccosine function in Step 43.3b.

$$\text{if } \left( \frac{AB - C\sqrt{A^2 - B^2 + C^2}}{A^2 + C^2} < -1 \right) \text{ or } \left( \frac{AB - C\sqrt{A^2 - B^2 + C^2}}{A^2 + C^2} > 1 \right) \text{ then } \omega_{ss} = \omega_s \text{ (Eq. C-43.3a)}$$

where  $\omega_{ss} = \omega_s$  is the normal sunset angle on horizontal slopes; proceed to Step 44.

Otherwise:

Step 43.3b. Apply the equation by Duffie and Beckman (1991 [DIRS 176616], Equation 2.205f):

$$|\omega_{ss}| = \min \left[ \omega_s, \arccos \left( \frac{AB - C\sqrt{A^2 - B^2 + C^2}}{A^2 + C^2} \right) \right] \quad (\text{Eq. C-43.3b})$$

and

$$\omega_{ss} = \begin{cases} |\omega_{ss}| & \text{if } (A > 0 \text{ and } B > 0) \text{ or } (A \geq B) \\ -|\omega_{ss}| & \text{otherwise} \end{cases} \quad (\text{Eq. C-43.3c})$$

where  $\omega_{ss} = |\omega_{ss}|$  is the normal limit.

Step 43.4. Prevent negative values for  $R_b$ . As a last step, prior to calculation of  $R_b$ , a check should be performed to prevent negative values for  $R_b$  from being calculated in Step 44. Negative values for  $R_b$  may occur under conditions of very low sun angles during all of the day; for example, during winter on northerly facing slopes. This is prevented by reversing the signs computed for the integration limits.

$$\text{if } (A < B) \text{ and } \gamma > 0 \text{ then } \omega_{sr} = -\omega_{sr} \quad (\text{Eq. C-43.4a})$$

$$\text{if } (A < B) \text{ and } \gamma < 0 \text{ then } \omega_{ss} = -\omega_{ss} \quad (\text{Eq. C-43.4b})$$

Step 44. Calculate the beam adjustment ratio  $R_b$  (Duffie and Beckman 1980 [DIRS 176264], Equation 2.16.5; Klein 1977 [DIRS 176152], Equation 11):

$$R_b = \frac{\begin{aligned} &\cos(s) \sin(\delta) \sin(\varphi) (\omega_{ss} - \omega_{sr}) \\ &- \sin(\delta) \cos(\varphi) \sin(s) \cos(\gamma) (\omega_{ss} - \omega_{sr}) \\ &+ \cos(\varphi) \cos(\delta) \cos(s) (\sin(\omega_{ss}) - \sin(\omega_{sr})) \\ &+ \cos(\delta) \cos(\gamma) \sin(\varphi) \sin(s) (\sin(\omega_{ss}) - \sin(\omega_{sr})) \\ &- \cos(\delta) \sin(s) \sin(\gamma) (\cos(\omega_{ss}) - \cos(\omega_{sr})) \end{aligned}}{2(\cos(\varphi) \cos(\delta) \sin(\omega_s) + \omega_s \sin(\varphi) \sin(\delta))} \quad (\text{Eq. C-44})$$

Variable ‘s’ (slope) in the equation for  $R_b$  is expressed as ‘ $\beta$ ’ by Duffie and Beckman (1980 [DIRS 176264]). All angles are in radians. Parameter  $\omega_s$  in the denominator of Equation 44 is from Step 5 and is not the same as the parameter  $\omega_{ss}$  that appears in the numerator.

As described by Duffie and Beckman (1980 [DIRS 176264], p. 95): “This equation is not valid for surfaces that receive beam radiation more than once during the day; that is, for surfaces on which the sun sets and then rises between normal sunrise and sunset.” No such surfaces exist within the Yucca Mountain net infiltration modeling domain.

### Definition of Classes for the $R_b$ Look-up Table

A look-up table of  $R_b$  values was developed based on latitude, slope, and azimuth classes defined in Table C-1. A total of 78 classes were specified with each class representing a unique slope and azimuth combination. The specified azimuth values were 0 degrees (surface facing north), 30, 60, 90 (east), 120, 150, 180 (south), 210, 240, 270 (west), 300, 330, and 360 (north). The

specified slope values were 0 degrees (horizontal surface), 2.5, 7.5, 15, 25, and 40 degrees. Steps 38 to 44 were applied to each of these 78 classes and for each day of the year resulting in 28,548  $R_b$  values in the look-up table (Output DTN: SN0602T0502206.003,  $R_b\_Ver1.2.03.xls$ ).

In Table C-1, north azimuth is represented by both 0 and 360 to facilitate the use of the look-up table. For the same reason, there is a zero slope combination for each azimuth class, despite the fact that azimuth is undefined for a horizontal (zero slope) surface and  $R_b$  is unity (1).

Table C-1. Azimuth and Slope Combinations for Each Class Used to Construct the  $R_b$  Look-up Table

Class	Azimuth (deg)	Slope (deg)	Class	Azimuth (deg)	Slope (deg)	Class	Azimuth (deg)	Slope (deg)
1	0	0.0	31	150	0.0	61	300	0.0
2	0	2.5	32	150	2.5	62	300	2.5
3	0	7.5	33	150	7.5	63	300	7.5
4	0	15.0	34	150	15.0	64	300	15.0
5	0	25.0	35	150	25.0	65	300	25.0
6	0	40.0	36	150	40.0	66	300	40.0
7	30	0.0	37	180	0.0	67	330	0.0
8	30	2.5	37	180	2.5	68	330	2.5
9	30	7.5	39	180	7.5	69	330	7.5
10	30	15.0	40	180	15.0	70	330	15.0
11	30	25.0	41	180	25.0	71	330	25.0
12	30	40.0	42	210	40.0	72	330	40.0
13	60	0.0	43	210	0.0	73	360	0.0
14	60	2.5	44	210	2.5	74	360	2.5
15	60	7.5	45	210	7.5	75	360	7.5
16	60	15.0	46	210	15.0	76	360	15.0
17	60	25.0	47	210	25.0	77	360	25.0
18	60	40.0	48	210	40.0	78	360	40.0
19	90	0.0	49	240	0.0	—	—	—
20	90	2.5	50	240	2.5	—	—	—
21	90	7.5	51	240	7.5	—	—	—
22	90	15.0	52	240	15.0	—	—	—
23	90	25.0	53	240	25.0	—	—	—
24	90	40.0	54	240	40.0	—	—	—
25	120	0.0	55	270	0.0	—	—	—
26	120	2.5	56	270	2.5	—	—	—
27	120	7.5	57	270	7.5	—	—	—
28	120	15.0	58	270	15.0	—	—	—
29	120	25.0	59	270	25.0	—	—	—
30	120	40.0	60	270	40.0	—	—	—

Source: Output DTN: SN0602T0502206.003,  $R_b\_Ver1.2.03.xls$ .

### **C3. PARAMETERIZATION OF SOLAR RADIATION EQUATIONS FOR YUCCA MOUNTAIN**

Calibration of the solar radiation estimation procedure was performed using data collected at the Yucca Mountain meteorological monitoring site (Output DTN: MO0602SPAWEATH.000). The analysis consisted of the following:

- Analysis of measured daily solar radiation ( $R_s$ ) data to evaluate the appropriate coefficient  $K_{R_s}$  (Step 13) to be used for the estimation of solar radiation from daily maximum and minimum air temperature ( $T_{max}$  and  $T_{min}$ ) at the Yucca Mountain site.
- Analysis of the variation in estimated clear sky solar radiation over the elevation range of the Yucca Mountain study area.

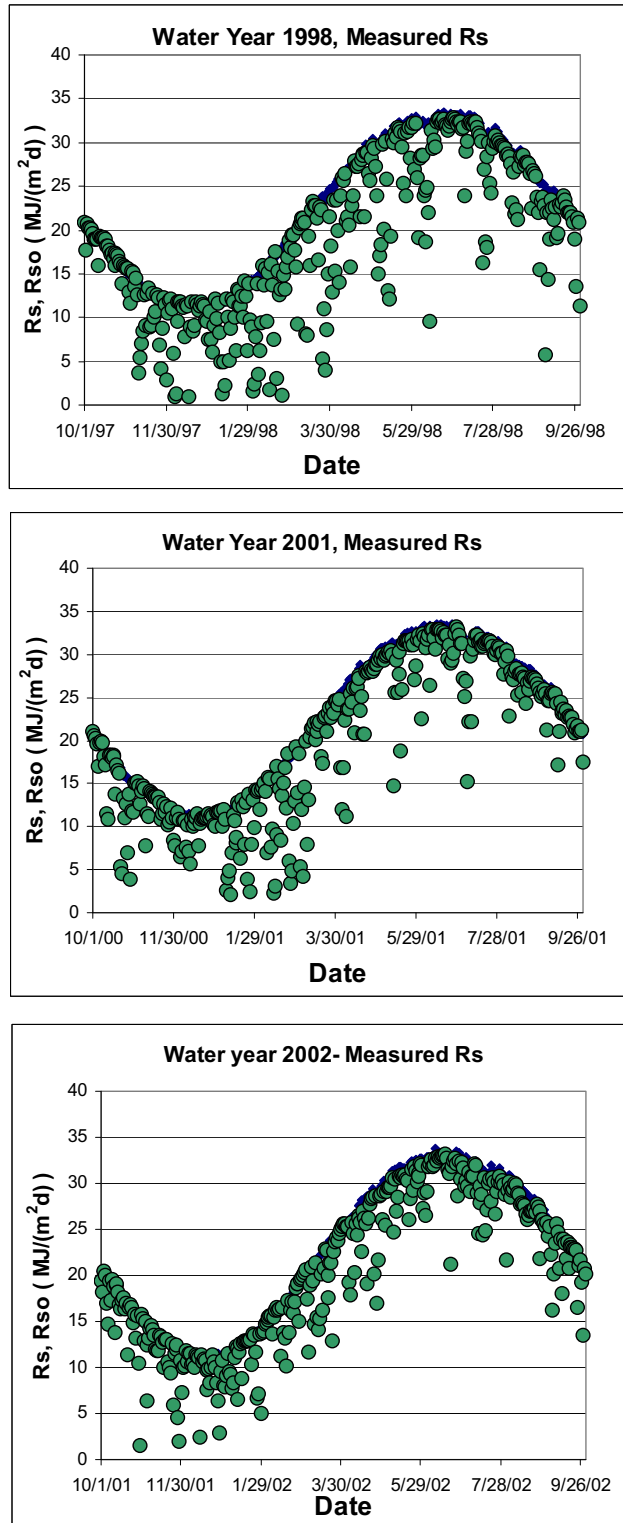
Three years of daily  $R_s$  and  $T_{max}$  and  $T_{min}$  measurements from the Yucca Mountain meteorological monitoring site (Output DTN: MO0602SPAWEATH.000) were evaluated to determine the appropriate value of  $K_{R_s}$  in Equation C-13 and the estimation consistency from year to year. The three years evaluated, 1998, 2001 and 2002, were the same years used in the transpiration coefficient section (Appendix D), and represent relatively wet, average and dry years.

The analysis was performed in an Excel® worksheet named *Hargreaves\_KRS\_YM\_xls*, included in Output DTN: SN0602T0602206.005.

#### **C3.1 INTEGRITY ASSESSMENT OF SOLAR RADIATION DATA**

Solar radiation data were visually examined by plotting 24-hr measurements of global solar radiation overlaid by clear sky ( $R_{so}$ ) curves versus day of year (Allen et al. 2005 [DIRS 176207], p. D-5; Allen 1996 [DIRS 176485], p. 97). Figure C-1 shows  $R_{so}$  envelopes and measured values of daily global solar radiation  $R_s$  for the three years.





Source: Output DTN: SN0602T0502206.005.

Figure C-1. Comparison of Measured Total Solar Radiation (  $R_s$  ) (points) with a Theoretical Clear Sky (  $R_{so}$  ) Curve (solid line) for Yucca Mountain for Water Years 1998, 2001, and 2002

In general, upper values for  $R_s$  that typically occur on cloudless days were in close agreement with the estimated  $R_{so}$ , indicating good calibration of the sensor and good management of the sensor operation and data collection. The  $R_{so}$  curve was calculated using Equation C-12 with  $K_{Bo\ hor}$  based on Equation C-10, and using  $W$  based on  $e_a$  from Equation C-46 of the following section, rather than using  $T_{dew}$  from Equation C-1. The  $e_a$  based on Equation C-46 used measured daily minimum relative humidity data, which is preferable during the assessment of data quality, rather than using the  $T_{dew}$  from Equation C-1, which is an estimated value.

### C3.2 EVALUATION OF THE $K_{Rs}$ COEFFICIENT OF HARGREAVES SOLAR RADIATION EQUATION

The Hargreaves equation (C-13) was used to estimate solar radiation from maximum and minimum daily air temperature (Allen et al. 1998 [DIRS 157311], Equation 50). Equation C-13 is repeated here as Equation C-45:

$$R_s = K_{Rs} \sqrt{(T_{max} - T_{min})} R_a \quad (\text{Eq. C-45})$$

where

- $R_a$  = extraterrestrial solar radiation ( $\text{MJ m}^{-2} \text{d}^{-1}$ )
- $T_{max}$  = maximum air temperature ( $^{\circ}\text{C}$ )
- $T_{min}$  = minimum air temperature ( $^{\circ}\text{C}$ )
- $K_{Rs}$  = Hargreaves adjustment coefficient ( $^{\circ}\text{C}^{-0.5}$ ).

Equation C-45 is the same equation as Equation C-13.

Four values for the  $K_{Rs}$  coefficient were evaluated: 0.16, 0.18, 0.19, and 0.20. These values were found by Allen (1997 [DIRS 176568]) to be representative of locations in the western United States.

### C3.3 CALCULATION OF ACTUAL VAPOR PRESSURE

The measurement parameter in the reviewed weather data set that represented humidity was minimum relative humidity. This parameter was used in calculations of  $W$ , the amount of precipitable water in the atmosphere. Actual vapor pressure was calculated from  $RH_{min}$  using the following equation (Allen et al. 2005 [DIRS 176207], Equation 13):

$$e_a = e^{\circ}(T_{max}) \frac{RH_{min}}{100} \quad (\text{Eq. C-46})$$

where

- $e_a$  = actual vapor pressure (kPa)
- $T_{max}$  = maximum air temperature ( $^{\circ}\text{C}$ )
- $RH_{min}$  = minimum relative humidity (%)
- $e^{\circ}(T_{max})$  = saturation vapor pressure corresponding to  $T_{max}$  (kPa).

The  $e^o(T_{max})$  is calculated as (Allen et al. 2005 [DIRS 176207], Equation 7):

$$e^o(T_{max}) = 0.6108 \exp \left[ \frac{17.27 T_{max}}{T_{max} + 237.3} \right] \quad (\text{Eq. C-47})$$

Precipitable water ( $W$ ) used in the  $R_{so}$  equation was calculated from  $e_a$  using Equation C-9.

### C3.4 RESULTS

Comparisons between measured and estimated solar radiation are shown in Figures C-2, C-4, and C-6 for the three water years evaluated. In all three years, solar radiation estimates were consistent with measurements and relatively little scatter was observed. A value for  $K_{R_s}$  between  $0.19 \text{ }^\circ\text{C}^{-0.5}$  and  $0.20 \text{ }^\circ\text{C}^{-0.5}$  tended to best estimate the daily  $R_s$ , based on the ratio of summed estimated  $R_s$  over each year to observed  $R_s$  equal to 1.0 and based on minimization of the root mean square error (RMSE).

Figures C-3, C-5 and C-7 show estimated values of  $R_s$  using Equation C-45 (Hargreaves equation) with specific values for  $K_{R_s}$  and clear-sky solar radiation envelopes for the water years 1998, 2001, and 2002. In these graphs and in the statistical analyses, estimated values for  $R_s$  were constrained to less than or equal to  $R_{so}$  because  $R_{so}$  represents a physical upper limit on  $R_s$ .

Table C-2 shows ratios between the sum of measured daily solar radiation and the sum of estimated daily solar radiation for four candidate values of  $K_{R_s}$ . A ratio = 1 means that the sum of measured daily solar radiation for the water year is equal to the sum of estimated solar radiation; a ratio < 1 means that total estimated solar radiation is less than total measured solar radiation (underestimation). Table C-3 summarizes RMSE for the three years and candidate values for  $K_{R_s}$ .

In general, the use of the standard value  $K_{R_s} = 0.16 \text{ }^\circ\text{C}^{-0.5}$  from FAO-56 (Allen et al. 1998 [DIRS 157311], Equation 50) produced a significant underestimation of total solar radiation of around 15%. For year 1998, the best result, a ratio = 0.995, was obtained using  $K_{R_s} = 0.19 \text{ }^\circ\text{C}^{-0.5}$  and the RMSE was minimized with this value. For water years 2001 and 2002, an annual ratio of 1.0 was obtained for a value for  $K_{R_s}$  between  $0.19 \text{ }^\circ\text{C}^{-0.5}$  and  $0.20 \text{ }^\circ\text{C}^{-0.5}$ . RMSE was lowest in 2001 for  $K_{R_s} = 0.19 \text{ }^\circ\text{C}^{-0.5}$  and in 2002 for  $K_{R_s} = 0.20 \text{ }^\circ\text{C}^{-0.5}$ . The value for  $K_{R_s} = 0.192 \text{ }^\circ\text{C}^{-0.5}$  over the three year period to obtain a mean annual ratio of 1.0. This value was rounded to  $0.19 \text{ }^\circ\text{C}^{-0.5}$  and was used to estimate daily solar radiation in the model.

### C3.5 CONCLUSIONS

Based on the three year record, a value of  $K_{R_s} = 0.19 \text{ }^\circ\text{C}^{-0.5}$  was determined to be the most appropriate value for estimating  $R_s$  from daily maximum and minimum air temperature for the Yucca Mountain site for Present-Day conditions. It is assumed that this value is adequate to use for future climate conditions at Yucca Mountain (Section 5.6, #9).

Table C-2. Ratio Between the Yearly Sum of Estimated Daily Solar Radiation (using Hargreaves Equation) and Yearly Sum of Measured Daily Solar Radiation for Water Years 1998, 2001, and 2002, Yucca Mountain Site

Water Year	$K_{Rs}$	Annual Ratio <sup>a</sup>
1998	0.16	0.839
	0.18	0.943
	0.19	0.995
	0.20	1.043
2001	0.16	0.832
	0.18	0.936
	0.19	0.987
	0.20	1.031
2002	0.16	0.825
	0.18	0.928
	0.19	0.979
	0.20	1.023

Source: Output DTN: SN0602T0502206.005.

<sup>a</sup> The annual ratio was calculated as:

$$Ratio = \frac{\sum_i^n R_{s(Hargreaves)}}{\sum_i^n R_{s(measured)}}$$

In this equation, the subscripts "i" and "n" represent the first and last days of the water year.

Table C-3. Root Mean Square Error (RMSE) for Daily Solar Radiation Estimated Using the Hargreaves Equation and Measured Daily Solar Radiation for Water Years 1998, 2001, and 2002, Yucca Mountain Site, for Four Values for Parameter  $K_{Rs}$ 

Water Year	$K_{Rs}$	n	RMSE <sup>a</sup> MJ m <sup>-2</sup> d <sup>-1</sup>	RMSE % of Annual Daily Mean
1998	0.16	365	4.53	23.5
	0.18	365	3.24	16.8
	0.19	365	3.00	15.5
	0.20	365	3.10	16.1
2001	0.16	366	4.47	22.2
	0.18	366	2.92	14.5
	0.19	366	2.58	12.8
	0.20	366	2.62	13.0

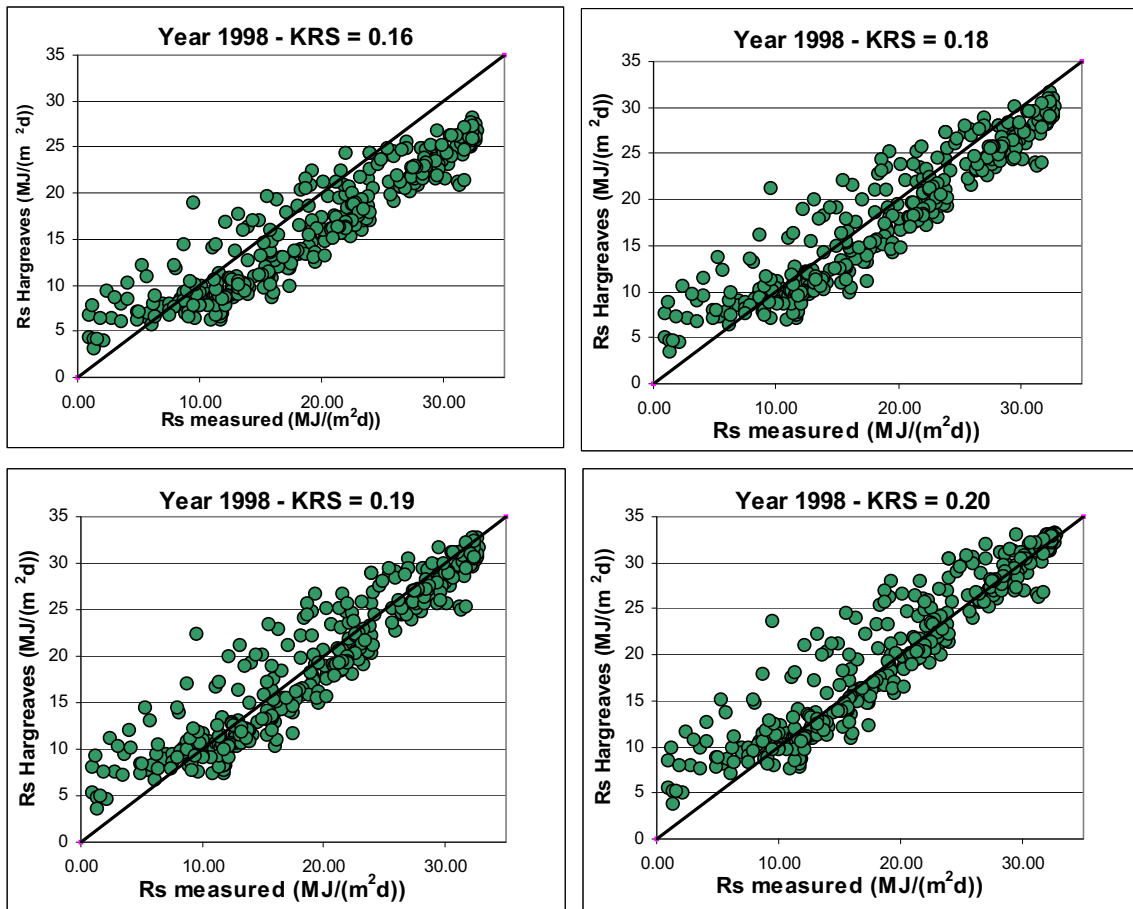
Table C-3. Root Mean Square Error (RMSE) for Daily Solar Radiation Estimated Using the Hargreaves Equation and Measured Daily Solar Radiation for Water Years 1998, 2001, and 2002, Yucca Mountain Site, for Four Values for Parameter  $K_{Rs}$  (Continued)

Water Year	$K_{Rs}$	n	RMSE <sup>a</sup> MJ m <sup>-2</sup> d <sup>-1</sup>	RMSE % of Annual Daily Mean
2002	0.16	365	4.39	21.2
	0.18	365	2.66	12.9
	0.19	365	2.20	10.6
	0.20	365	2.19	10.6

<sup>a</sup> The RMSE was calculated as:

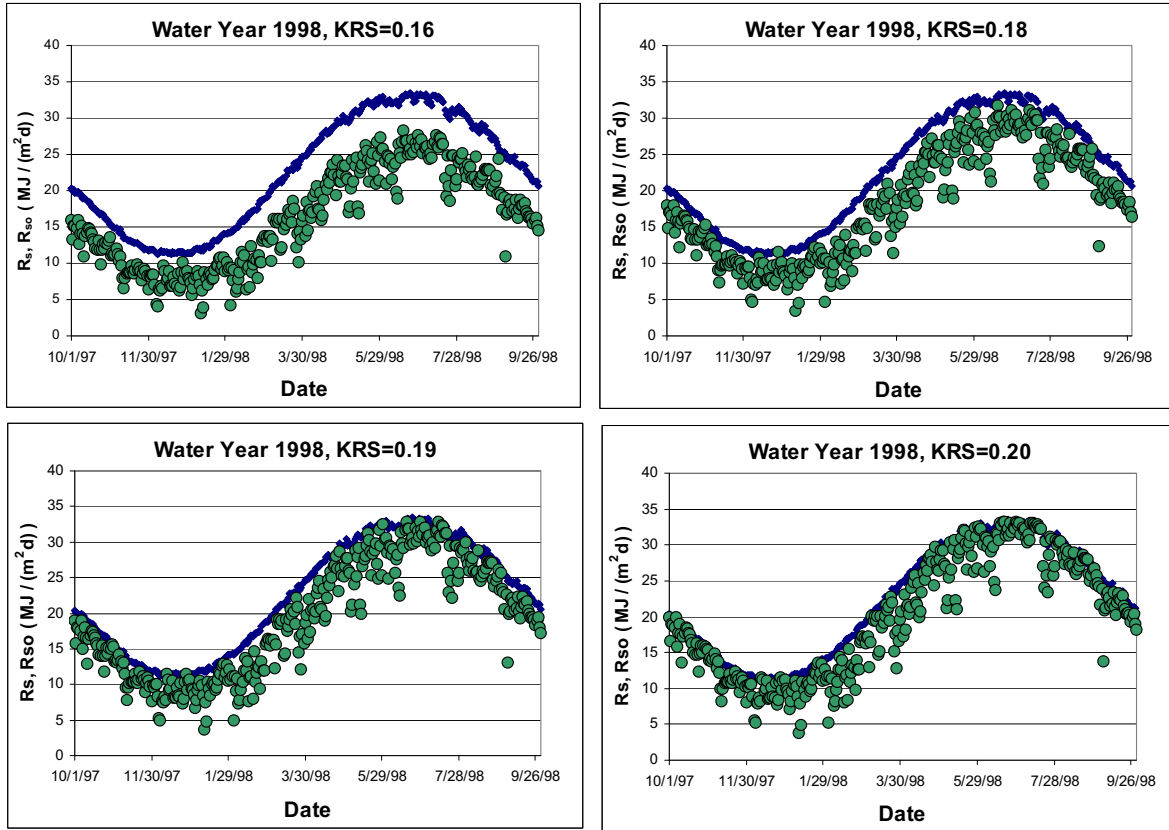
$$RMSE = \left[ \frac{\sum_i^n (R_{s(Hargreaves)} - R_{s(measured)})^2}{n} \right]^{0.5}$$

In this equation, the subscripts "i" and "n" represent the first and last days of the water year.



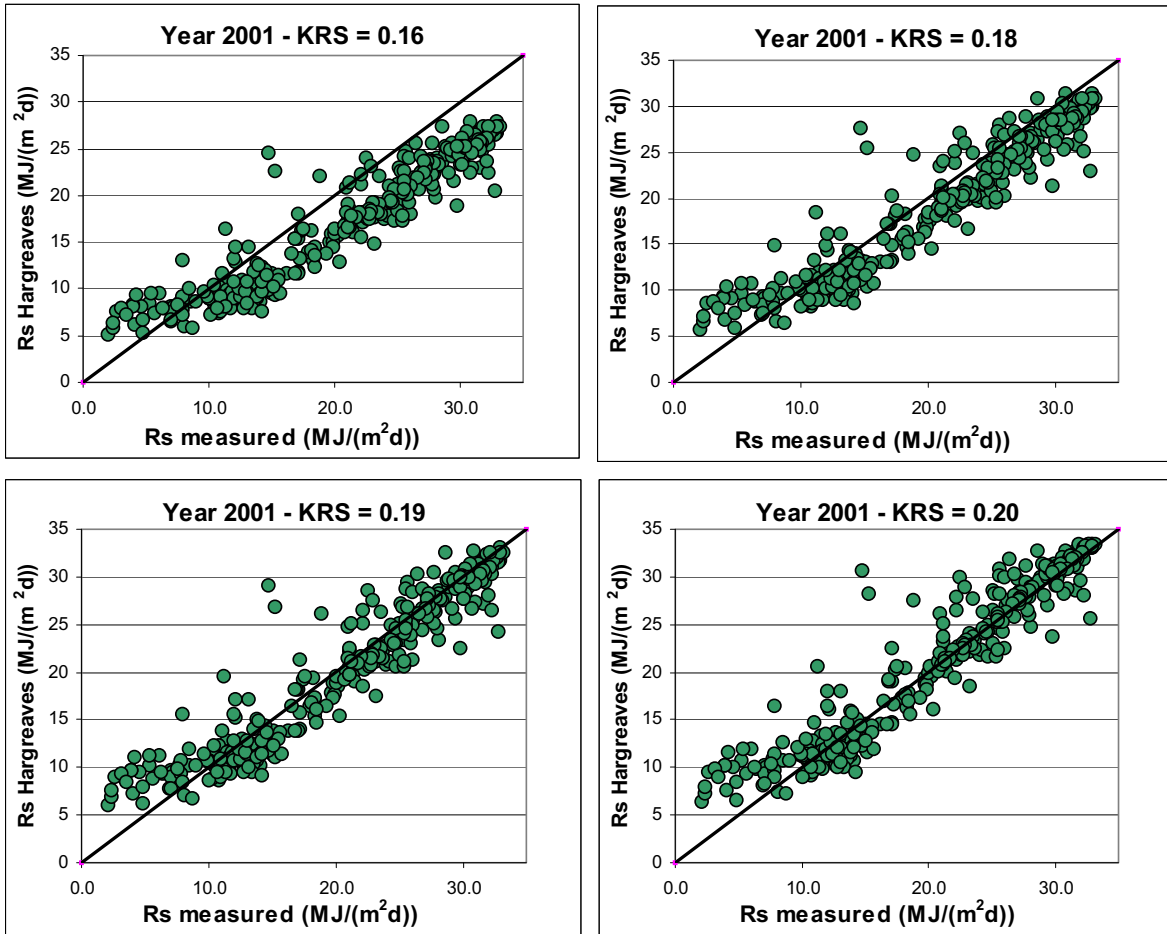
Source: Output DTN: SN0602T0502206.005.

Figure C-2.  $R_s$  Estimated Using the Hargreaves Equation with Four Values for  $K_{R_s}$  versus  $R_s$  Measured for Water Year 1998, Yucca Mountain Monitoring Site



Source: Output DTN: SN0602T0502206.005.

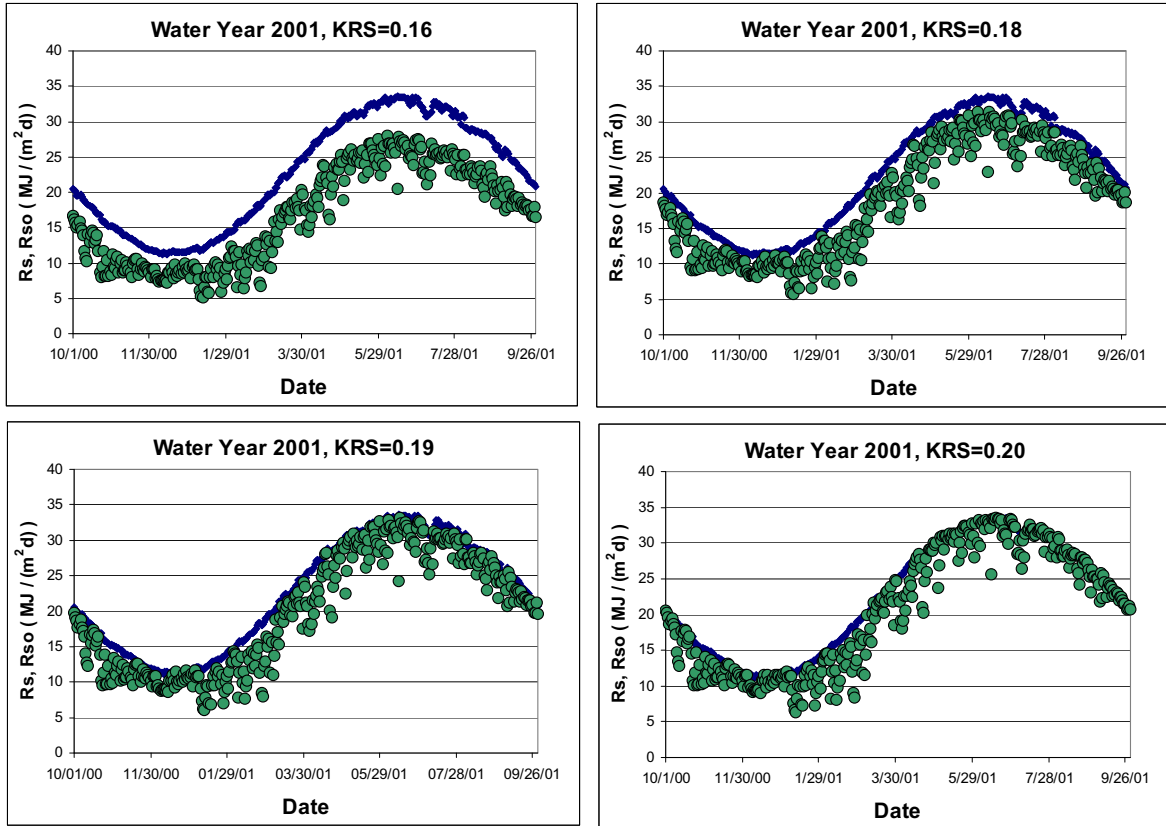
Figure C-3.  $R_s$  Estimated Using the Hargreaves Equation with Four Values for  $K_{R_s}$  and Clear-sky Solar Radiation Envelopes for Water Year 1998, Yucca Mountain Monitoring Site



Source: Output DTN: SN0602T0502206.005.

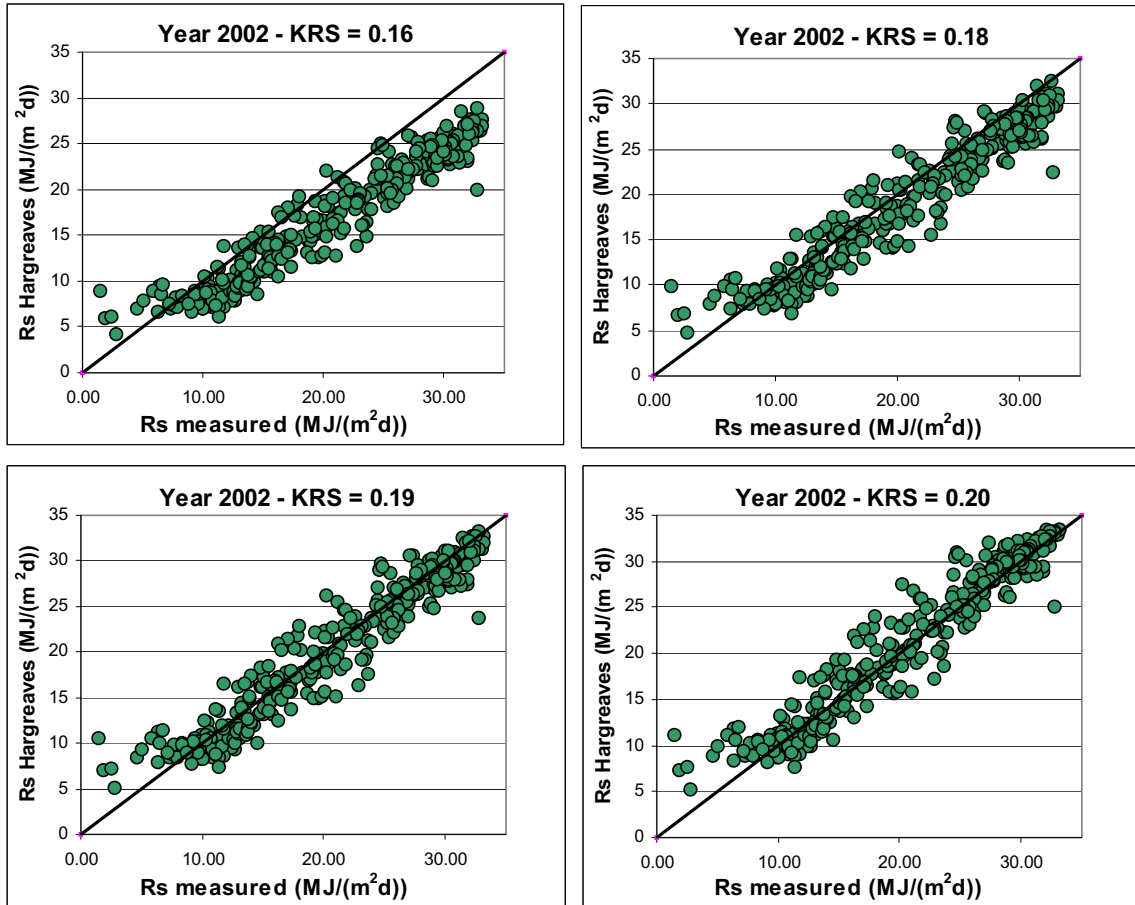
Figure C-4.  $R_s$  Estimated Using the Hargreaves Equation with Four Values for  $K_{RS}$  versus  $R_s$  Measured for Water Year 2001, Yucca Mountain Monitoring Site





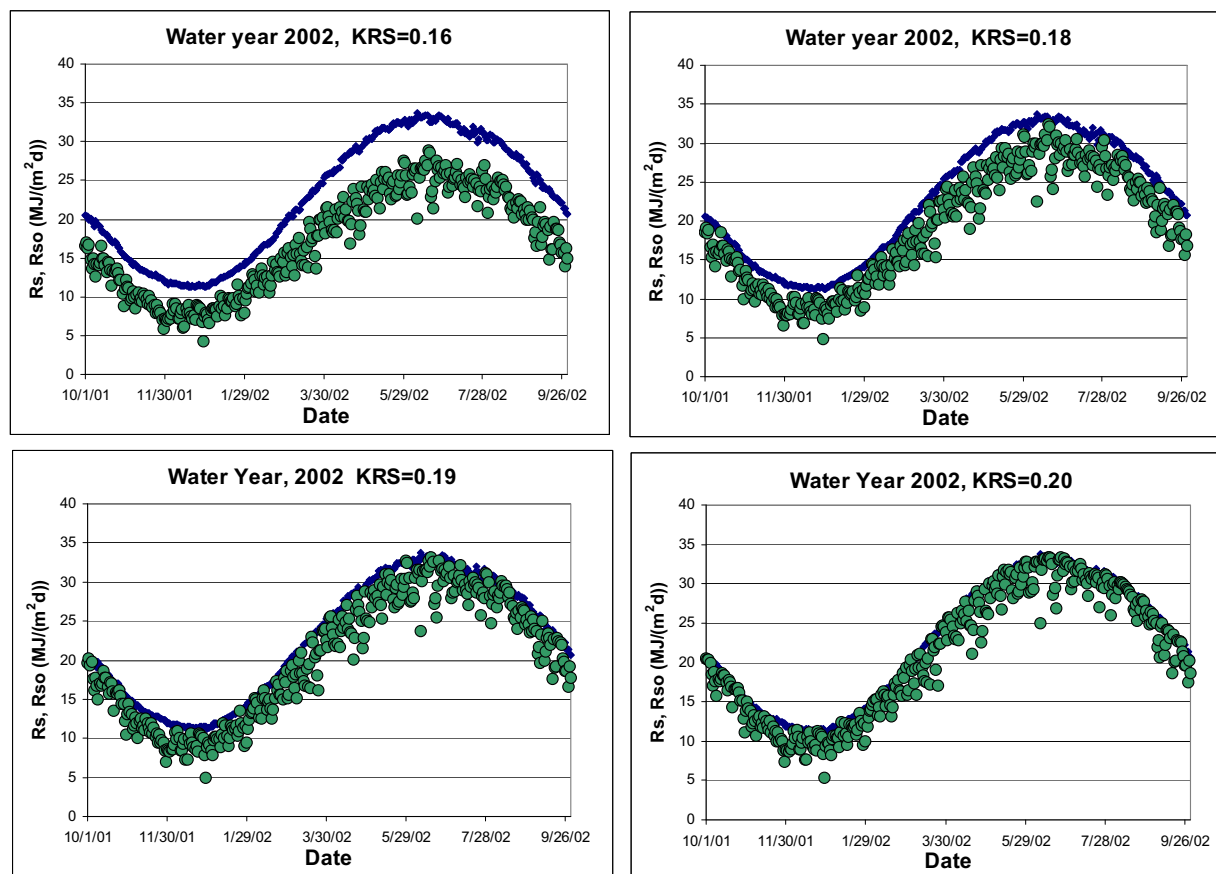
Source: Output DTN: SN0602T0502206.005.

Figure C-5.  $R_s$  Estimated Using the Hargreaves Equation with 4 Values for  $K_{RS}$  and Clear-sky Solar Radiation Envelopes for Water Year 2001, Yucca Mountain Monitoring Site



Source: Output DTN: SN0602T0502206.005.

Figure C-6.  $R_s$  Estimated Using the Hargreaves Equation with Four Values for  $K_{R_s}$  versus  $R_s$  Measured for Water Year 2002, Yucca Mountain Monitoring Site



Source: Output DTN: SN0602T0502206.005.

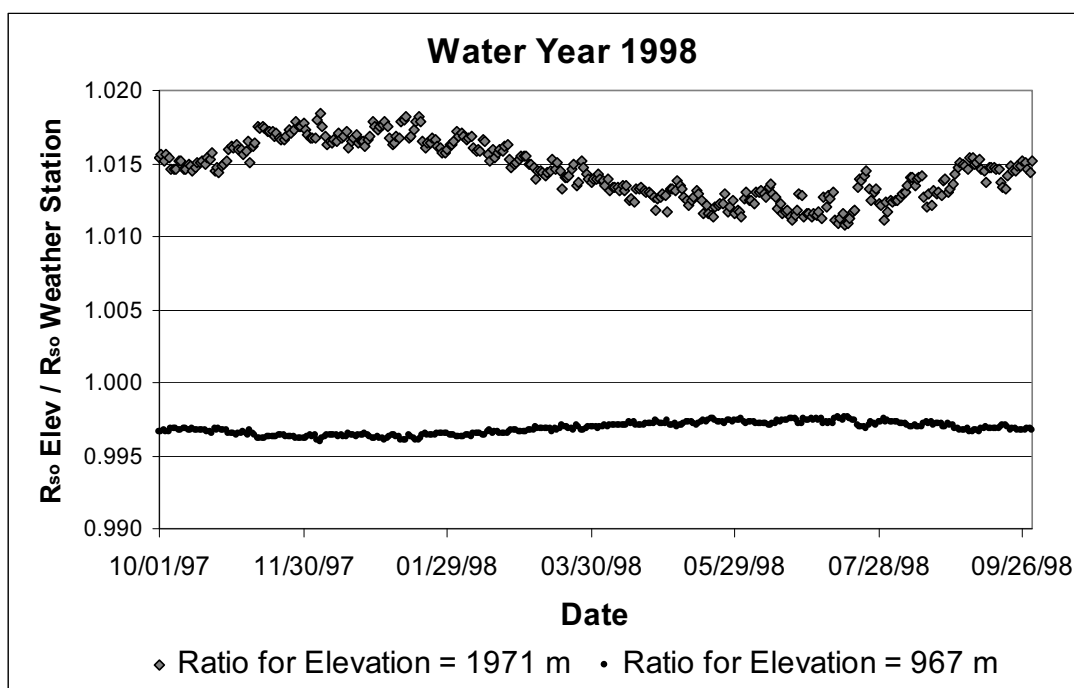
Figure C-7.  $R_s$  Estimated Using the Hargreaves Equation with Four Values for  $K_{R_s}$  and Clear-sky Solar Radiation Envelopes for Water Year 2002, Yucca Mountain Monitoring Site

### C3.6 ANALYSIS OF THE VARIATION OF CLEAR-SKY SOLAR RADIATION WITH ALTITUDE AT THE YUCCA MOUNTAIN SITE

The intensity of clear sky solar radiation increases with elevation due to smaller optical depth of the overlying atmosphere. An analysis was performed to determine the sensitivity of the estimation of  $R_{so\ hor}$  and  $R_s$  from Equation C-45 over the elevation range for Yucca Mountain. The elevation range evaluated was from 967 to 1,971 m. This range included the elevation of the reference weather station used to determine  $K_{R_s}$  (1,143 m).

Figure C-8 shows the variation of the ratio between  $R_{so\ hor}$  calculated at the two extreme altitudes and  $R_{so\ hor}$  calculated at the elevation of the reference weather station based on measured relative humidity data (Output DTN: MO0602SPAWEATH.000) for water year 1998.  $R_{so\ hor}$  was calculated using Equation C-12. The results were nearly identical for years 2001 and 2002. The ratio between  $R_{so\ hor}$  calculated at 967 m over  $R_{so\ hor}$  calculated at 1,143 m varied from 0.996 to 0.998 during each of the three water years 1998, 2001 and 2002 (data shown for year 1998 in Figure C-8); therefore, expected maximum variation in estimated  $R_{so}$  and  $R_s$  is about 0.4% between these elevations. The ratio of  $R_{so\ hor}$  calculated at 1,971 m over  $R_{so\ hor}$  calculated at 1,143 m ranged from 1.010 to 1.018 for all three water years; therefore, the maximum variation

in estimated  $R_{so}$  and  $R_s$  is less than 1.8% between these elevations. These differences are much smaller than the mean estimation error in daily  $R_{so\ hor}$ , which averaged about 13% over the annual periods. Therefore, the use of constant elevation during computation of  $R_{so}$  and estimation of  $R_s$  from temperature data is justified over the elevation range of the study area.



Source: Output DTN: SN0602T0502206.005.

Figure C-8. Variation of the Ratio between  $R_{so\ hor}$  Calculated at Two Extreme Elevations (967 m and 1,971 m) near or on Yucca Mountain over  $R_{so\ hor}$  Calculated at a Reference Weather Station (elevation = 1,143 m) during Water Year 1998

#### C4. EVALUATION OF DIFFUSE AND TOTAL RADIATION MEASUREMENTS FROM NEAR YUCCA MOUNTAIN

##### C4.1 INTRODUCTION

The following summarizes an analysis of diffuse radiation data collected near Yucca Mountain, Nevada, by the National Oceanic and Atmospheric Administration (NOAA) SURFRAD network. The purpose of the analysis was to demonstrate the ability for published equations, including those by Vignola and McDaniels (1986 [DIRS 176481]), to estimate diffuse solar radiation for the study area with relatively high accuracy. Daily totals of diffuse and direct solar radiation measured at the Desert Rock weather station in Nevada (DTN: SN0511NOAADATA.001 [DIRS 177238]) were used in the analysis (Output DTN: SN0602T0502206.004).

A station latitude of  $36.6^\circ$  and an elevation of 1,007 m for the Desert Rock station were used in calculations reported herein. The elevation parameter was used to estimate theoretical clear sky solar radiation, and latitude was used to determine sun angles.

Quality control of the data has been performed routinely by NOAA. The NOAA quality control process flagged records that were suspected to contain errors. Flagged records were not included in this analysis.

#### C4.2 COMPARISON OF DIFFUSE COMPONENT TO SIMPLE MODELS FOR AVERAGE DIFFUSE INDICES

Total shortwave transmissivity is the sum of direct and diffuse transmissivity (Allen 1996 [DIRS 176485], Equation 7):

$$\tau_{sw\ hor} = K_{B\ hor} + K_{D\ hor} \quad (\text{Eq. C-48})$$

where

- $K_{B\ hor}$  = 24-hr transmissivity for direct radiation (dimensionless)
- $K_{D\ hor}$  = 24-hr transmissivity for diffuse radiation (dimensionless), from Step 15
- $\tau_{sw\ hor}$  = total short-wave transmissivity (dimensionless), from Step 14.

The  $K_{D\ hor}$  value is solved by rearranging Equation C-48 for  $K_{D\ hor}$ . The value for  $\tau_{sw\ hor}$  was determined from the ratio of measured daily solar radiation ( $R_s$ ) to estimated clear sky solar radiation ( $R_{so}$ ) using Equation C-14.

Several models, as follows, were evaluated for estimating the diffuse solar component, based on the Desert Rock solar radiation data:

1. The ASCE-EWRI function (Allen et al. 2005 [DIRS 176207]) previously described for Equation C-11 is also used for Equation C-49 to estimate diffuse transmissivity for any sky conditions:

$$\begin{aligned} K_{D\ hor} &= 0.35 - 0.36 K_{B\ hor} \quad \text{for } K_{B\ hor} \geq 0.15 \\ K_{D\ hor} &= 0.18 + 0.82 K_{B\ hor} \quad \text{for } K_{B\ hor} < 0.15 \end{aligned} \quad (\text{Eq. C-49})$$

where

- $K_{D\ hor}$  = 24-hr transmissivity for diffuse radiation (dimensionless)
- $K_{B\ hor}$  = 24-hr transmissivity for direct radiation (dimensionless).

2. Vignola and McDaniels (1986 [DIRS 176481], p. 411):

$$\begin{aligned} K_{B\ hor} &= 0.016 \tau_{sw\ hor} \quad \text{for } \tau_{sw\ hor} < 0.175 \\ K_{B\ hor} &= 0.022 - 0.280 \tau_{sw\ hor} + 0.828 (\tau_{sw\ hor})^2 + 0.765 (\tau_{sw\ hor})^3 \quad \text{for } \tau_{sw\ hor} \geq 0.175 \end{aligned} \quad (\text{Eq. C-50})$$

where

$$\begin{aligned} K_{Bo\ hor} &= 24\text{-hr transmissivity for diffuse radiation (dimensionless)} \\ \tau_{sw\ hor} &= \text{total short-wave transmissivity (dimensionless).} \end{aligned}$$

Equation C-50 was transformed to estimate  $K_{D\ hor}$  by rearranging Equation C-48,  $K_{B\ hor} = \tau_{sw\ hor} - K_{D\ hor}$ , and limits were provided to the polynomial equation when beyond its development range of  $\tau_{sw\ hor} \leq 0.8$ .

$$K_{D\ hor} = 0.984\tau_{sw\ hor} \quad \text{for } \tau_{sw\ hor} < 0.175$$

$$K_{D\ hor} = -0.022 + 1.280\tau_{sw\ hor} - 0.828(\tau_{sw\ hor})^2 - 0.765(\tau_{sw\ hor})^3 \quad \text{for } 0.175 \leq \tau_{sw\ hor} \leq 0.8 \quad (\text{Eq. C-51})$$

$$K_{D\ hor} = 0.08 \quad \text{for } \tau_{sw\ hor} > 0.8$$

3. Collares (Collares-Pereira and Rabl 1979 [DIRS 176487]; Duffie and Beckman 1980 [DIRS 176264], Equation 2.11.1):

$$K_{D\ hor}/\tau_{sw\ hor} = 0.99 \quad \text{for } \tau_{sw\ hor} \leq 0.17$$

$$K_{D\ hor}/\tau_{sw\ hor} = -0.54\tau_{sw\ hor} + 0.632 \quad \text{for } 0.75 < \tau_{sw\ hor} < 0.80$$

$$K_{D\ hor}/\tau_{sw\ hor} = 1.188 - 2.272\tau_{sw\ hor} + 9.473(\tau_{sw\ hor})^2 - 21.865(\tau_{sw\ hor})^3 + 14.648(\tau_{sw\ hor})^4 \quad \text{for } 0.17 < \tau_{sw\ hor} < 0.75 \quad (\text{Eq. C-52})$$

$$K_{D\ hor}/\tau_{sw\ hor} = 0.2 \quad \text{for } \tau_{sw\ hor} \geq 0.8$$

4. Erbs (Erbs et al. 1982 [DIRS 176486]; Duffie and Beckman (1991) [DIRS 176151], Equation 2.10.1):

$$K_{D\ hor}/\tau_{sw\ hor} = 1.0 - 0.09\tau_{sw\ hor} \quad \text{for } \tau_{sw\ hor} \leq 0.22$$

$$K_{D\ hor}/\tau_{sw\ hor} = 0.9511 - 0.1604\tau_{sw\ hor} + 4.388(\tau_{sw\ hor})^2 - 16.638(\tau_{sw\ hor})^3 + 12.336(\tau_{sw\ hor})^4 \quad \text{for } 0.22 < \tau_{sw\ hor} \leq 0.80 \quad (\text{Eq. C-53})$$

$$K_{D\ hor}/\tau_{sw\ hor} = 0.165 \quad \text{for } \tau_{sw\ hor} > 0.8$$

5. Orgill and Hollands (1977 [DIRS 176483]; Duffie and Beckman 1980 [DIRS 176264], Equation 2.10.1):

$$K_{D\ hor}/\tau_{sw\ hor} = 1.0 - 0.249\tau_{sw\ hor} \quad \text{for } \tau_{sw\ hor} < 0.35$$

$$K_{D\ hor}/\tau_{sw\ hor} = 1.557 - 1.84\tau_{sw\ hor} \quad \text{for } 0.35 < \tau_{sw\ hor} < 0.75 \quad (\text{Eq. C-54})$$

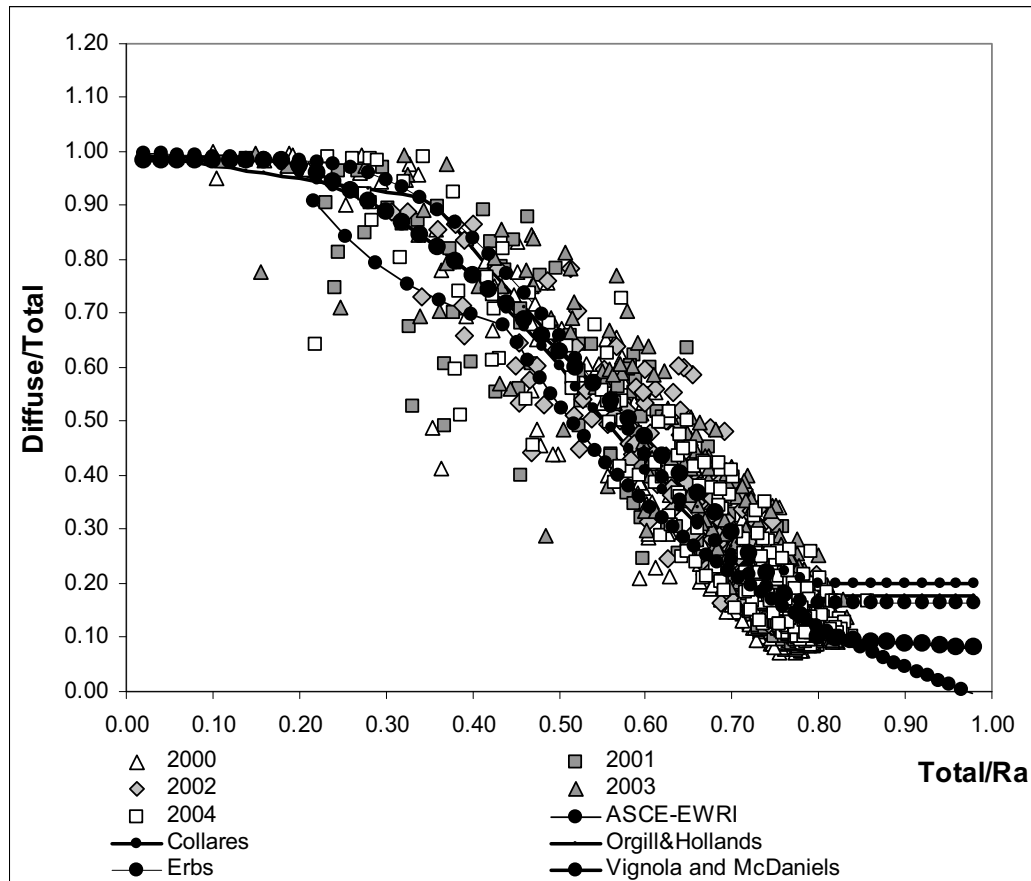
$$K_{D\ hor}/\tau_{sw\ hor} = 0.177 \quad \text{for } \tau_{sw\ hor} > 0.75$$

Figure C-9 shows plots of the measured diffusive component of daily solar radiation ( $I_d$ ) divided by the total measured radiation ( $R_s$ ) versus  $R_s$  divided by extraterrestrial radiation ( $R_a$ ). The  $I_d$  was calculated as  $K_{D\ hor}$  times  $R_a$ . Data from years 2000–2004 are plotted in the same figure along with estimated ratios from five different diffuse–transmissivity functions. The ASCE-EWRI function (Allen et al. 2005 [DIRS 176207]) models the relationship between

diffuse and direct beam radiation (Equation C-11), which is intended primarily for clear sky conditions. The function by Vignola and McDaniels (1986 [DIRS 176481]) is in the form of a relationship between beam radiation coefficients; the regression coefficients of Vignola and McDaniels, representing the average calibration over all sites in the Pacific Northwest study, were applied (Equation C-51). The Collares function is by Collares-Pereira and Rabl (1979 [DIRS 176487]) (Equation C-52), and the Erbs function is by Erbs et al. (1982 [DIRS 176486]) (Equation C-53). The Orgill and Hollands (1977 [DIRS 176483]) function is a close linearized approximation of the curvilinear Erbs function (Erbs et al. 1982 [DIRS 176486]) (Equation C-54).

The ASCE-EWRI function (Allen et al. 2005 [DIRS 176207]) fits the  $K_{D\ hor}/\tau_{D\ hor}$  data relatively well in the  $\tau_{D\ hor} > 0.5$  domain ( $\tau_{D\ hor} = R_{s\ hor}/R_{a\ hor}$  where  $R_{s\ hor}$  is ‘total’ radiation) (Figure C-9). This domain is where the ASCE-EWRI function has greatest focus; it was created primarily for predicting behavior under clear sky conditions. The Collares (Collares-Pereira and Rabl 1979 [DIRS 176487]), Orgill and Hollands (1977 [DIRS 176483]), and Erbs (Erbs et al. 1982 [DIRS 176486]) functions all represent the measured data set relatively well. All three of these methods, however, suffer from the establishment of too high a lower limit for estimated  $K_{D\ hor}/\tau_{sw\ hor}$  (ranging from 0.165 to 0.2) at high values for  $\tau_{sw\ hor}$ . The relatively high elevation of Yucca Mountain coupled with its relatively clean air apparently reduce the ratio of diffuse to total radiation under clear sky conditions and produces higher values for  $\tau_{sw\ hor}$  under the clear sky conditions.

The Vignola-McDaniels (1986 [DIRS 176481]) curve lies within the domain of the measured data and agrees well with the other published functions just discussed. The Vignola-McDaniels (1986 [DIRS 176481]) curve extends toward  $K_{D\ hor} = 0.08$  in the domain of clear sky conditions.



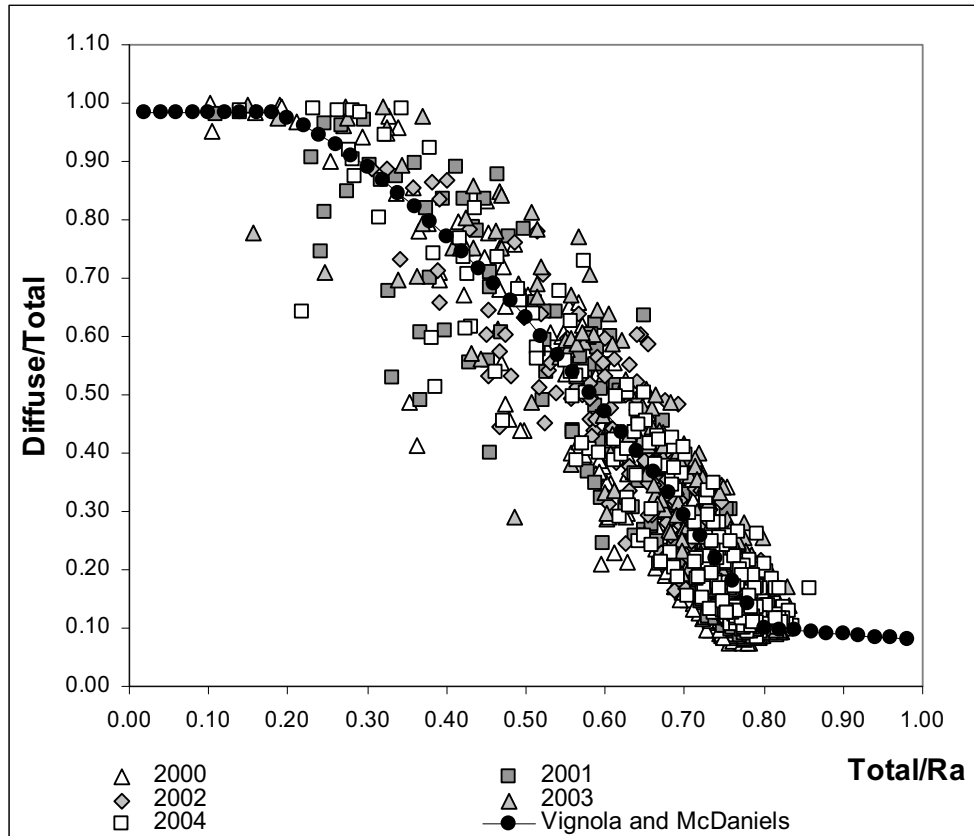
Source: Output DTN: SN0603T0502206.006.

Figure C-9. Comparison of Measured Diffusive Component of Daily Solar Radiation ( $I_d$ ) Divided by the Total Measured Radiation ( $R_s$ ) versus  $R_s$  Divided by Extraterrestrial Radiation ( $R_a$ ) for Daily Measurements near Yucca Mountain with Some Established Functions for Estimating the Mean Relationship

### C4.3 SELECTION AND ESTABLISHMENT OF A METHOD TO ESTIMATE THE DIFFUSE INDEX

Based on its simple shape, the relatively large scatter in the  $K_{D\ hor}/\tau_{sw\ hor}$  data, its close agreement with data by Collares-Pereira and Rabl (1979 [DIRS 176487]), and its relatively good approximation of the mean behavior of the data, the Vignola and McDaniels (1986 [DIRS 176481]) curve was used to translate solar radiation from the horizontal surface to inclined surfaces on Yucca Mountain. Figure C-10 shows a plot of measured data versus estimated data using the Vignola and McDaniels (1986 [DIRS 176481]) function.





Source: Vignola and McDaniel 1986 [DIRS 176481]; Output DTN: SN0603T0502206.006.

Figure C-10. Comparison of Measured Diffusive Component of Daily Solar Radiation ( $I_d$ ) Divided by the Total Measured Radiation ( $R_s$ ) versus  $R_s$  Divided by Extraterrestrial Radiation ( $R_a$ ) for Daily Measurements near Yucca Mountain with the Vignola and McDaniel Function

Table C-4. List of Symbols and Descriptions

Symbol	Description	Units
$A$	Duffie and Beckman 1991 parameter	(unitless)
$A_t$	anisotropic index	(unitless)
$B$	Duffie and Beckman 1991 parameter	(unitless)
$C$	Duffie and Beckman 1991 parameter	(unitless)
$DOY$	day of the year (1 – 365 or 366) J = 1 = January 1	(unitless)
$ET_0$	reference crop evapotranspiration	mm day <sup>-1</sup>
$G_{day}$	daily soil heat flux density	MJ m <sup>-2</sup> d <sup>-1</sup>
$HR_{min}$	minimum relative humidity	%
$I_{b\ hor}$	direct beam radiation on the horizontal surface	MJ m <sup>-2</sup> d <sup>-1</sup>
$I_b$	direct beam radiation on the inclined surface	MJ m <sup>-2</sup> d <sup>-1</sup>
$I_{d\ hor}$	diffuse radiation on the horizontal surface	MJ m <sup>-2</sup> d <sup>-1</sup>
$I_d$	diffuse radiation on the inclined surface	MJ m <sup>-2</sup> d <sup>-1</sup>

Table C-4. List of Symbols and Descriptions (Continued)

Symbol	Description	Units
$I_r$	reflected radiation received by the inclined surface	$\text{MJ m}^{-2} \text{d}^{-1}$
$J$	day of the year (1 – 365 or 366) $J = 1 = \text{January 1}$	(unitless)
$K_B$	the clearness index for direct beam radiation (dimensionless)	(unitless)
$K_{B_{o\ hor}}$	the transmissivity index for clear-sky direct beam radiation, horizontal surface (dimensionless)	(unitless)
$K_{B\ hor}$	the transmissivity index for direct beam radiation, horizontal surface (dimensionless)	(unitless)
$K_D$	the transmissivity index for diffuse radiation (dimensionless)	(unitless)
$K_{D_{o\ hor}}$	the transmissivity index for clear-sky diffuse radiation, horizontal surface (dimensionless)	(unitless)
$K_{D\ hor}$	the transmissivity index for diffuse radiation, horizontal surface (dimensionless)	(unitless)
$K_{cIn}$	atmospheric turbidity coefficient (dimensionless)	(unitless)
$K_o$	average difference between $T_{min}$ and mean daily $T_{dew}$	$^{\circ}\text{C}$
$K_{R_s}$	adjustment coefficient for predicting $R_s$ from air temperature	$^{\circ}\text{C}^{-0.5}$
$LR$	adiabatic lapse rate	$^{\circ}\text{C}/1000 \text{ m}$
$P_{reference}$	atmospheric pressure at the reference weather station	kPa
$P_{cell}$	atmospheric pressure at grid cell	kPa
$R_{a\ hor}$	extraterrestrial radiation, horizontal surface	$\text{MJ m}^{-2} \text{d}^{-1}$
$R_b$	ratio between inclined and horizontal direct beam solar radiation	(unitless)
$R_n$	net radiation at the surface	$\text{MJ m}^{-2} \text{d}^{-1}$
$R_{ns}$	net short-wave radiation, defined as being positive downwards and negative upwards	$\text{MJ m}^{-2} \text{d}^{-1}$
$R_s$	measured or calculated solar radiation	$\text{MJ m}^{-2} \text{d}^{-1}$
$R_{sm\ hor}$	measured or calculated solar radiation, horizontal surface	$\text{MJ m}^{-2} \text{d}^{-1}$
$R_{sm\ inc}$	calculated solar radiation, inclined surface	$\text{MJ m}^{-2} \text{d}^{-1}$
$R_{sequiv\ hor}$	horizontally projected solar radiation for inclined surface	$\text{MJ m}^{-2} \text{d}^{-1}$
$R_{so\ hor}$	clear-sky radiation for horizontal surface	$\text{MJ m}^{-2} \text{d}^{-1}$
$s$	surface slope	radians
$T$	mean daily air temperature at 1.5-m to 2.5-m height	$^{\circ}\text{C}$
$T_{dew\ general}$	dew point temperature representative of the air mass that passes across the <i>application area</i>	$^{\circ}\text{C}$
$T_{max\ reference}$	daily maximum air temperature measured at reference weather station	$^{\circ}\text{C}$
$T_{max\ lapse}$	lapse corrected daily maximum air temperature	$^{\circ}\text{C}$
$T_{max\ lapse,K}$	lapse corrected daily maximum air temperature	K
$T_{min\ reference}$	daily minimum air temperature measured at reference weather station	$^{\circ}\text{C}$
$T_{min\ lapse}$	lapse corrected daily minimum air temperature	$^{\circ}\text{C}$
$T_{min\ lapse,K}$	lapse corrected daily minimum air temperature	K
$W$	precipitable water in the atmosphere	mm

Table C-4. List of Symbols and Descriptions (Continued)

Symbol	Description	Units
$d_r$	inverse relative distance earth-sun (dimensionless)	(unitless)
$f$	modulating function	(unitless)
$e_a$	mean actual vapor pressure at 1.5-m to 2.5-m height	kPa
$e_{a\ general}$	mean actual vapor pressure at 1.5-m to 2.5-m height kPa representative of the air mass that passes across the application area derived from a reference location	kPa
$e^{\circ T}$	saturation vapor pressure function	kPa
$e_s$	saturation vapor pressure at 1.5-m to 2.5-m height	kPa
$u_2$	mean daily or hourly wind speed at 2-m height	$m\ s^{-1}$
$z$	site elevation above mean sea level	m
$z_{reference}$	elevation of the reference weather station above sea level	m
$z_{cell}$	elevation of cell above sea level	m
$\alpha_T$	"alpha" = albedo or canopy reflection coefficient for a given grid cell (dimensionless)	(unitless)
$\beta$	"beta" = angle of the sun above the horizon	radians
$\gamma$	"gamma" = grid cell aspect	(unitless)
$\gamma_c$	"gamma" = psychrometric constant	$kPa\ ^{\circ}C^{-1}$
$\Delta$	"delta" = slope of the saturation vapor pressure-temperature curve	$kPa\ ^{\circ}C^{-1}$
$\delta$	"delta" = solar declination	radians
$\varphi_{eff}$	"phi" = effective latitude for a given cell slope and aspect	radians
$\varphi_{reference}$	"phi" = latitude of the reference weather station	radians
$\sigma$	"sigma" = Stefan-Boltzmann constant	$4.901\ 10^{-9}\ MJ\ K^{-4}\ m^{-2}\ d^{-1}$
$\tau_{sw\ hor}$	total shortwave transmissivity, associated with $R_{sm\ hor}$	(unitless)
$\omega$	"omega" solar time angle, solar noon = 0	radians
$\omega_s$	sunset hour angle for horizontal surface	radians
$\omega_{ss}$	sunset hour angle for inclined surface	radians
$\omega_{sr}$	sunrise hour angle for inclined surface	radians

INTENTIONALLY LEFT BLANK

**APPENDIX D**  
**METHODS FOR DERIVING TRANSPIRATION COEFFICIENTS FOR VEGETATION**  
**AT YUCCA MOUNTAIN**



## D1. INTRODUCTION

Plant water use is an important component of the water balance for vegetated natural systems and is the primary mechanism controlling water loss from the soil during periods when plants are active (i.e., during the growing season when soil moisture is available). Because of the inevitable loss of water through stomates during the acquisition of carbon for photosynthesis, 95% to 99% of the water that passes through a plant is lost through transpiration (Nobel 1983 [DIRS 160500], p. 506). Thus, transpiration is an accurate estimate of water uptake by plant roots (Nobel 1983 [DIRS 160500], p. 506). Estimates of evapotranspiration ( $ET$ ) from vegetated surfaces are commonly used to evaluate water loss through the combined processes of evaporation and transpiration.

The arid climate at Yucca Mountain is characterized by low and unpredictable rainfall, extreme temperatures, and high evaporative demand. Vegetation cover in the Yucca Mountain area is limited by both timing and amount of precipitation that is received over the course of a water year (WY [October 1 through September 30]). Characterizing the timing and magnitude of vegetation response to precipitation and converting that response to values that can be used in the MASSIF model are crucial for representation of infiltration at the Yucca Mountain site.

Two methods of characterizing vegetation at Yucca Mountain were used, normalized difference vegetation index (NDVI) derived from satellite imagery (Appendix E) and basal transpiration coefficients ( $K_{cb}$ ) derived from ground measurements of vegetation characteristics. The linear relationship between  $K_{cb}$  and NDVI makes it possible to estimate  $K_{cb}$  from NDVI (Bausch and Neale 1987 [DIRS 177652]; Duchemin et al. 2005 [DIRS 178498]). This linear relationship is described for the vegetation at Yucca Mountain in Section 6.5.3.7 and used in the MASSIF model to estimate  $K_{cb}$  from NDVI for each grid cell in the infiltration model domain (Sections 6.5.3.4 through 6.5.3.7).

Normalized difference vegetation index is an indicator of vegetation vigor often used for measurement of environmental response to landscape-scale hydrology, including global climate change (e.g., Justice et al. 1998 [DIRS 176742]; Stow 1995 [DIRS 176887]; Running and Nemani 1991 [DIRS 176819]), rainfall (e.g., Wang et al. 2003 [DIRS 176761]; Ji and Peters 2003 [DIRS 176743]), and  $ET$  (e.g., Kerr et al. 1989 [DIRS 176823]; Chong et al. 1993 [DIRS 176821]; Kustas et al. 1994 [DIRS 176757]; Seevers and Ottman 1994 [DIRS 176764]; Szilagyi et al. 1998 [DIRS 176839]; Szilagyi 2000 [DIRS 176735]; Szilagyi 2002 [DIRS 176840]). It is used in the MASSIF model to characterize timing and magnitude of vegetation response to precipitation and to capture spatial dynamics in  $ET$  related to slope, elevation, soil characteristics, and aspect for each of the grid cells in the model domain (Appendix E).

Transpiration coefficients ( $K_c$ ) are widely used in conjunction with reference evapotranspiration ( $ET_0$ ) to estimate actual crop evapotranspiration ( $ET_c$ ) in agricultural systems. The methods for estimating crop water use were standardized in the Food and Agricultural Organization of the United Nations [FAO] Irrigation and Drainage Paper 56 (Allen et al. 1998 [DIRS 157311]). The FAO-56 methods were extended to natural vegetation using measured values of leaf area index ([LAI] a unitless measure of leaf area per ground area) or effective ground cover (percent of ground covered by vegetation) and adjustments for stomatal control (Allen et al. 1998

[DIRS 157311], pp. 187 to 193). To account for the effects of soil evaporation, the FAO-56 methods included a dual transpiration coefficient ( $K_c = K_{cb} + K_e$ ), which was selected for use in the MASSIF model (Section 6.4.4). This dual coefficient consists of a basal transpiration component ( $K_{cb}$ ), representing plant transpiration under nonlimiting water conditions, and an evaporation component ( $K_e$ ).  $K_{cb}$  profiles (or curves) are time based and are calculated in this appendix for the growing seasons of three representative wet, dry, and average precipitation years. The  $K_{cb}$  profiles are used to:

- Evaluate NDVI processing methods and algorithms in Sections E2.5, E3.3, and E7
- Confirm a linear relationship between  $K_{cb}$ s and NDVI developed for desert vegetation at Yucca Mountain (Section E7.2)
- Develop a least squares regression between  $K_{cb}$  and NDVI for use in the MASSIF model to predict  $K_{cb}$  from NDVI for each grid cell in the model domain (Section 6.5.3.7).

This appendix describes the development of  $K_{cb}$  profiles using FAO-56 methods and development of the  $K_{cb}$  input parameters that describe the characteristics of the vegetation that is expected to be present at Yucca Mountain. The input parameters include vegetation growth stages, vegetation height, vegetation cover and species composition, stomatal resistance, and weather parameters (e.g., wind speed and relative humidity). The output of these calculations is included in Output DTN: MO0606SPABASAL.001.

- Section D2 includes a brief discussion on plant water use, followed by a description of the vegetation at Yucca Mountain and how vegetation types and associations are used in the development of  $K_{cb}$ s.
- Section D3.1 describes equations from FAO-56 and how those equations are used to calculate  $K_{cb}$ s for desert vegetation.
- Section D3.2 describes the development of input parameters for  $K_{cb}$  calculations.
- Section D4 includes example calculations and  $K_{cb}$  profiles. Development of uncertainty for  $K_{cb}$  profiles is also described.
- Section D5 describes development of a potential Glacial Transition  $K_{cb}$  profile defined by an invasive annual grass.
- Section D6 describes development of  $ET_0$  for a generic area at Yucca Mountain. This  $ET_0$  is used with  $K_{cb}$ s to estimate potential transpiration (PT). The resulting PTs are used to evaluate the appropriateness of the magnitude of  $K_{cb}$ s for desert vegetation. Criticisms of the use of  $K_{cb}$ s to predict  $ET$  for desert vegetation are also addressed in this section.



## D2. BACKGROUND INFORMATION

### D2.1 PLANT WATER USE

A discussion of the processes that result in transpiration is included here to show how transpiration can be used as a reliable measure of plant water use. Photosynthesis is the process by which light energy is used to drive the synthesis of organic compounds in plants. The photosynthetic process requires atmospheric carbon dioxide ( $\text{CO}_2$ ). To gain  $\text{CO}_2$  for photosynthesis, plants must lose water to the atmosphere. Carbon dioxide diffuses through small pores in the leaf surface (stomata) to intercellular spaces of the leaf and photosynthetic cells (Figure D-1). Concurrently, water moves in the opposite direction, from wet cell membranes inside the leaf through open stomata to the atmosphere, a process called transpiration (Figure D-1). Because water and  $\text{CO}_2$  share the same diffusional pathway through the stomata, there is an inevitable cost of water for  $\text{CO}_2$  gain.

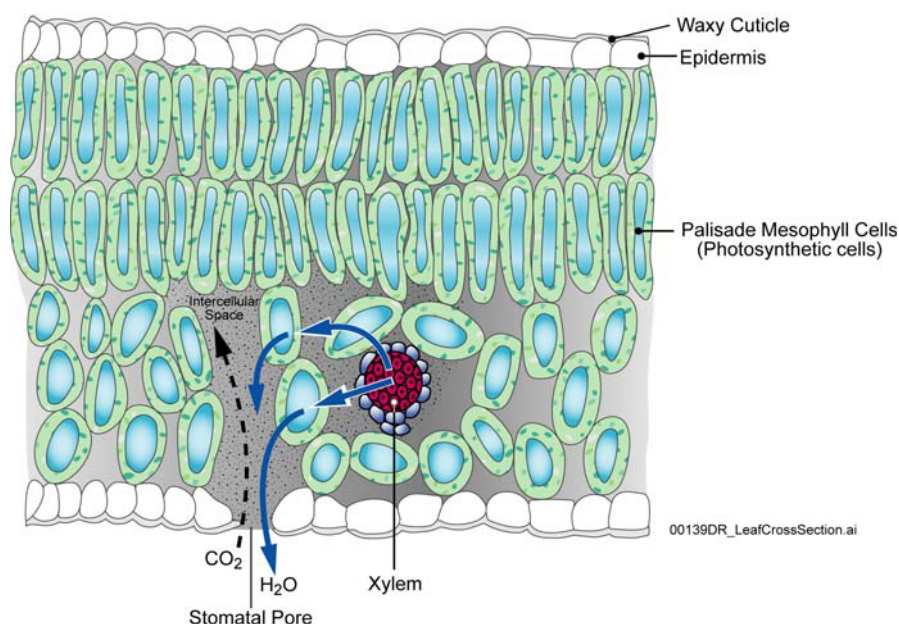
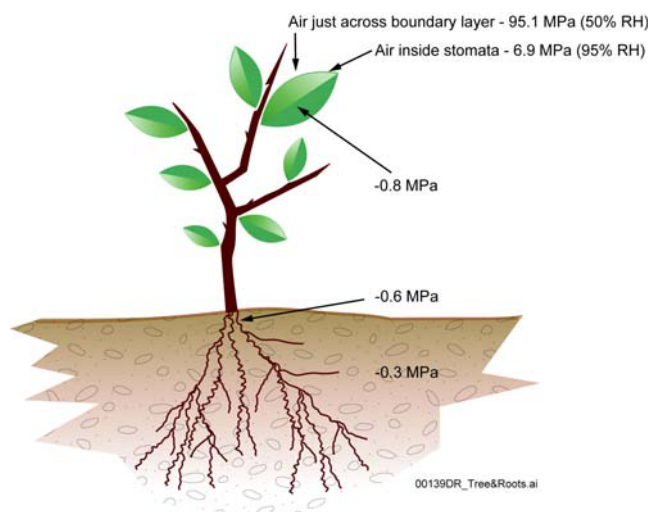


Figure D-1. Leaf Cross Section Showing Diffusional Pathway for Carbon Dioxide ( $\text{CO}_2$ ) and Water ( $\text{H}_2\text{O}$ )

Water moves from the soil, through the plant, to the atmosphere down an increasingly negative water potential gradient (Figure D-2). Water potential is a thermodynamic parameter that describes the energy status of water in the soil-plant-atmosphere system (Brady and Weil 1999 [DIRS 160019], pp. 178 and 179). The soil acts as a water reservoir, with texture (percent of sand, silt, and clay) determining the water holding capacity. Soils with high clay and silt content hold water more tightly than sandy soils. Water enters the plant through the roots and moves in a column of high tensile water through specialized cells, called xylem, and into the atmosphere through open stomata. Water flow through the soil-plant-atmosphere system represents important processes in the overall hydrologic cycle.

When soil moisture is limiting, plants can reduce water loss through stomatal closure. However, stomatal closure also results in reducing the supply of CO<sub>2</sub>, which ultimately reduces plant productivity. In arid regions, approximately 400 to 700 units of water are lost for every unit of dry matter produced by a plant (Brady and Weil 1999 [DIRS 160019], pp. 227 and 228). This is because the diffusion gradient for water from inside the leaf to the atmosphere is orders of magnitude steeper than that for CO<sub>2</sub> diffusion into the leaf. Water is required for photosynthesis and other metabolic processes; however, 95% to 99% of the water that passes through a plant is lost through transpiration (Nobel 1983 [DIRS 160500], p. 506). Thus, transpiration is an accurate estimate of water uptake by plant roots (Nobel 1983 [DIRS 160500], p. 506). Water is also lost from the soil and other surfaces (plant litter) through the process of direct evaporation. Direct evaporation from the soil generally occurs in the upper 0.15 m of the soil profile (Allen et al. 1998 [DIRS 157311], p. 144). Evapotranspiration (*ET*) is the combined water loss through plant transpiration and direct evaporation.



NOTE: Water moves through the system along a gradient of increasingly negative water potentials.

Figure D-2. Water Potential (MPa) in Various Components of the Soil-Plant-Atmosphere System

## D2.2 YUCCA MOUNTAIN VEGETATION

The flora and climate of Yucca Mountain have been described as characteristically Mojavean (Beatley 1975 [DIRS 103356] and 1976 [DIRS 102221]), with vegetation on the crest and upper slopes that is transitional to Great Basin Desert flora (Beatley 1976 [DIRS 102221]). Lower elevations and midslopes up to about 1,300 m are dominated by Mojave Desert shrub species including *Larrea tridentata*, *Ambrosia dumosa*, *Grayia spinosa*, *Lycium andersonii*, *Lycium pallidum*, *Krameria erecta*, and *Ephedra nevadensis*. Dominance of these species and plant community composition is dependent on a variety of environmental factors including slope, aspect, soils, and elevation. The transition between the two deserts occurs above ~1,300 m at Yucca Mountain in a zone that varies between *Artemisia*-dominated shrub communities of the Great Basin (steep hill slopes facing northeast to northwest) and *Larrea*-dominated communities of the Mojave (lower elevations). Other important species at Yucca Mountain that inter-grade

into both desert types include *Coleogyne ramosissima*, *Atriplex confertifolia*, *Eriogonum fasciculatum*, *Lycium* spp., *Ephedra* spp., and *Ericameria* spp.

Vegetation communities at Yucca Mountain have been characterized by a number of authors (e.g., Beatley 1976 [DIRS 102221]; O’Farrell and Collins 1984 [DIRS 102160]; CRWMS M&O 1996 [DIRS 102235]) and have often been described in terms of associations. A vegetation association is defined as an assemblage of species with distinctive physiognomy and dominance hierarchy (Barbour et al. 1980 [DIRS 127394], p. 5). However, discrepancies among authors exist with respect to classification of vegetation associations at Yucca Mountain (e.g., classifications by Beatley 1976 [DIRS 102221]), and it is recognized that not all vegetation can be unambiguously classified. This is largely due to the complexity and variability of vegetation assemblages across the landscape, with plant species distributed according to individual tolerance limits and competitive ability. Regardless of such discrepancies, the concept can be useful for identifying dominant species and vegetation types for different areas of the infiltration model domain.

Based on Beatley (1976 [DIRS 102221]) and O’Farrell and Collins (1984 [DIRS 102160]), four vegetation associations were identified for use in ecological studies that were initiated in the late 1980s to address specific questions about the effects of the site characterization process on biological resources at Yucca Mountain (CRWMS M&O 1996 [DIRS 102235]). The four associations (*Coleogyne* [COL], *Larrea–Ambrosia* [LA], *Lycium–Grayia* [LG], and *Larrea–Lycium–Grayia* [LLG]) were described after the dominant plant species (Table D-1).

Table D-1. Classification of Vegetation Associations Sampled at Yucca Mountain

Vegetation Association <sup>1</sup>				
	<i>Coleogyne</i>	<i>Larrea–Ambrosia</i>	<i>Lycium–Grayia</i>	<i>Larrea–Lycium–Grayia</i>
Abbreviation	COL	LA	LG	LLG
Desert	Transition	Mojave	Transition	Mojave
Soil and Topography	Shallow, gravelly soils of upper bajadas and ridge tops with flat to gradually sloping terrain	Deep, loose sandy soil lacking surface pavement on low elevation bajadas and basins	Sandy soil, from volcanic parent material on bajadas and ridges; higher elevations	Sandy loam soil of volcanic origin on bajadas and valleys; mid elevations
Physiognomy	<i>Coleogyne</i> dominant	<i>Larrea</i> and <i>Ambrosia</i> dominant	No dominant	<i>Larrea</i> dominant
Dominant Species <sup>2</sup>	<i>Coleogyne ramosissima</i> (blackbrush), <i>Ambrosia dumosa</i> (burrobush), <i>Ephedra nevadensis</i> (Nevada jointfir), <i>Lycium pallidum</i> (pale wolfberry)	<i>Ambrosia dumosa</i> , <i>Larrea tridentata</i> (creosotebush), <i>Menodora spinescens</i> (spiny menodora), <i>Lycium pallidum</i>	<i>Ephedra nevadensis</i> , <i>Grayia spinosa</i> (spiny hopsage), <i>Eriogonum fasciculatum</i> (Eastern Mojave buckwheat), <i>Lycium andersonii</i> (Anderson’s wolfberry)	<i>Larrea tridentata</i> , <i>Ephedra nevadensis</i> , <i>Ambrosia dumosa</i> , <i>Krameria erecta</i> (littleleaf ratany)

<sup>1</sup> Classification is based on Beatley 1976 [DIRS 102221] and O’Farrell and Collins 1984 [DIRS 102160].

<sup>2</sup> Dominant species are the perennials with the greatest mean cover. The common name is included in parentheses following the first use of the scientific name.

In 1989, twelve Ecological Study Plots (ESPs) were established in each of the four vegetation associations (total of 48 plots) at various locations in the Yucca Mountain area. The ESPs were 4 ha (200 × 200 m) in size and randomly located within each association (CRWMS M&O 1996

[DIRS 102235], p. 10, Figure 3-1; and DTN: MO9901ESPYMNYE.000 [DIRS 177247], for ESP locations). The ESPs were established to describe the vegetation and ecology of Yucca Mountain and to study the effects of site characterization on the Yucca Mountain environment. Biotic (e.g., vegetation cover, species composition, and primary production) and abiotic measurements (e.g., precipitation and soil characteristics) were made on the ESPs from 1989 through 1994.

Percent ground cover per plant species was measured on ESPs each spring following peak growth from 1989 through 1994 (CRWMS M&O 1996 [DIRS 102235] for complete description of data collection methods and results). Over the years of study, the COL association generally had intermediate cover of vegetation or cover equal to one or more of the remaining three associations (CRWMS M&O 1996 [DIRS 102235], p. 31, Figure 4-10). One of the main input parameters that distinguish  $K_{cb}$ s among vegetation associations is percent vegetation cover. Because vegetation cover for the COL association was similar to that of the LG and LLG associations, the  $K_{cb}$  profile would also be similar. Therefore, COL was not used as a separate association for  $K_{cb}$  calculations.

The LA, LG, and LLG vegetation associations are the most common in the infiltration model domain and  $K_{cb}$  calculations were based on cover data for these three associations. The LA association is representative of low elevation vegetation (940 to 1,150 m, DTN: MO9907SADESYM.000 [DIRS 177169]). The low elevations of LA associations make them unimportant to infiltration that might occur above the proposed repository but were included because they occur within the infiltration modeling domain. The LG association is representative of the vegetation that overlies the proposed repository on the upper slopes and crest of Yucca Mountain (elevation = 1,300 to 1,600 m, DTN: MO9907SADESYM.000 [DIRS 177169]). The LG association is considered critically important to the infiltration modeling effort because the vegetation is representative of that overlying the proposed repository. The LLG association is representative of the vegetation of midelevation (1,150 to 1,266 m, DTN: MO9907SADESYM.000 [DIRS 177169]) intermountain valleys within the infiltration modeling domain. The  $K_{cb}$ s calculated for the LG association are used to develop the  $K_{cb}$ -NDVI<sup>1</sup> relationship for desert vegetation at Yucca Mountain as described in Section 6.5.3.7. The slope and intercept of this relationship are used in the MASSIF model to estimate  $K_{cb}$  from NDVI' for each grid cell for each day of the year as described in Sections 6.5.3.4 through 6.5.3.7. The  $K_{cb}$ s estimated for the LA, LLG, and LG associations are used to evaluate the appropriateness of NDVI and associated processing parameters (Sections E2 and E7), potential contribution of vegetation types to association water use (Section D5), and whether use of FAO-56 methods results in  $K_{cb}$ s that are of an appropriate magnitude for desert vegetation (Section D6).

NDVI' was determined for WY1998 (wet), WY2001 (average), and WY2000 (dry), with precipitation totals of 358 mm, 186 mm, and 38 mm, respectively (Table D-2).

---

<sup>1</sup> NDVI' is NDVI corrected for differing atmospheric conditions between satellite overpasses and for specific ground conditions characterizing the Yucca Mountain environment, including the presence of rock varnish. This correction is described in Section 6.5.3.5 and Appendix E, Section E2.

Table D-2. Paired Wet, Average, and Dry Water Years used for NDVI' and  $K_{cb}$  Estimations

NDVI' Precipitation Totals <sup>a</sup>		$K_{cb}$ Precipitation Totals <sup>b</sup>		Difference in WY Totals
Water Year	PCP (mm)	Water Year	PCP (mm)	PCP (mm)
1998 (wet)	358	1993 (wet)	240	118
2001 (average)	186	1991 (average)	150	36
2002 (dry)	38	1990 (dry)	60	22

<sup>a</sup> Output DTN: MO0602SPAWEATH.000.

<sup>b</sup> Approximate average annual precipitation for the different vegetation associations from CRWMS M&O 1996 [DIRS 102235], p. 21, Figure 4-3.

WY1998 and WY2000 were selected because they represented very wet and dry years and were needed to establish timing of plant responses and a baseline of minimum plant activity for the Yucca Mountain area (Section E1.4). Satellite images of the model domain (which included the ESPs) were obtained for selected days during the growing season for these three years for development of NDVI' (Section E1.4). Vegetation cover and species composition, needed for  $K_{cb}$  calculations, were measured on the ESPs during peak growth periods from 1989 to 1994. Vegetation cover at Yucca Mountain is largely dependent on precipitation, therefore, precipitation records for the ESPs from 1989 to 1994 were evaluated to determine wet, normal, and dry years that could be paired with the years that NDVI' were determined for. Based on precipitation records, vegetation cover data were used from the following three years in  $K_{cb}$  calculations:

- WY1991 (average), an average precipitation year for the Yucca Mountain area (about 150 mm [Table D-2])
- WY1993 (wet), the highest precipitation year on record for the years that cover data were collected (about 240 mm [Table D-2])
- WY1990 (dry), the lowest precipitation year on record for the years that cover data were collected (about 60 mm [Table D-2]).

To evaluate NDVI' processing parameters, the wet, dry, and average precipitation years (Table Dx) from the two data sets (NDVI' and  $K_{cb}$ ) were paired by normalizing and scaling NDVI' using annual precipitation (Appendix E). For the  $K_{cb}$  – NDVI' regression, wet and average years (Table D-2) from the two data sets were paired. The dry year was not used in the  $K_{cb}$  – NDVI' regression because the vegetation signal for 2002 was essentially zero throughout the year for the LG association (Section E7.1).

The differences in precipitation between the paired dry years (1990 and 2002) and the paired average precipitation years (1991 and 2001) were small: 22 mm for the dry years and 36 mm for the average years (Table D-2). The differences were within the range of variation in precipitation observed within years among vegetation associations at Yucca Mountain (CRWMS M&O 1996 [DIRS 102235], p. 21, Figure 4-3). Therefore, it is reasonable to assume that vegetation cover would be similar for the two below average and the two average precipitation years. The difference in precipitation of 118 mm between the paired wet years (1993 and 1998, Table D-2) could have translated into differences in vegetation cover. However, there are limits

to the amount of vegetation that can be supported by the Yucca Mountain system that are imposed by factors other than total precipitation that is received during a water year. These factors include nutrient availability, inter- and intra-specific competition among plants, timing of precipitation, and precipitation runoff. To account for potential differences in cover that might have occurred between the paired water years, NDVI' was adjusted to account for differences in precipitation totals (and therefore potential vegetation) between cover data and satellite data collection years (Section 6.5.3.7 and Appendix E). The ratios of water year precipitation for paired wet years and paired average years were used to adjust NDVI' (Section 6.5.3.7 and Appendix E).

Plant species were divided into three types for  $K_{cb}$  calculations: annuals, drought deciduous shrubs, and evergreen to semi-evergreen shrubs. Annual plants complete their life cycle (germination, through flowering and seed production, through senescence) within a single growing season. Common annuals at Yucca Mountain include grasses such as *Bromus madritensis* ssp. *rubens* and *vulpia octoflora*, and forbs such as *Amsinckia tridentate*, *Cryptantha* spp., and *Chaenactis* spp. Drought deciduous shrubs shed their leaves in the summer, when soil moisture becomes limiting, and initiate leaf growth when temperature and soil moisture are favorable. Common drought deciduous shrubs at Yucca Mountain include *Ambrosia dumosa*, *Lycium* spp., and *Grayia spinosa*. Because perennial grasses (e.g., *Achnatherum hymenoides*) and forbs (e.g., *Sphaeralcea ambigua*) made up a small percentage of total cover on ESPs (Tables D-7 to D-15), and the length and timing of their development are similar to that of drought deciduous species, these growth forms were included in the drought deciduous vegetation type for the analysis. Evergreen to semi-evergreen shrubs are drought resistant plants that maintain a canopy throughout the year. These include leafless shrubs with green stems (i.e., *Ephedra* spp.), green stemmed shrubs with ephemeral leaves (i.e., *Ericameria* spp.), and shrubs that maintain leaves throughout the year (i.e., *Larrea tridentate*). For simplicity, the evergreen to semi-evergreen shrub type will be referred to as evergreen through the rest of this analysis.

Basal transpiration coefficient profiles for the LA, LG, and LLG vegetation associations were developed by calculating separate profiles for the three vegetation types (annuals, drought deciduous, and evergreen species), then summing those  $K_{cb}$ s to get one profile for each association. See Section D3.1 for further discussion on summing vegetation type profiles.

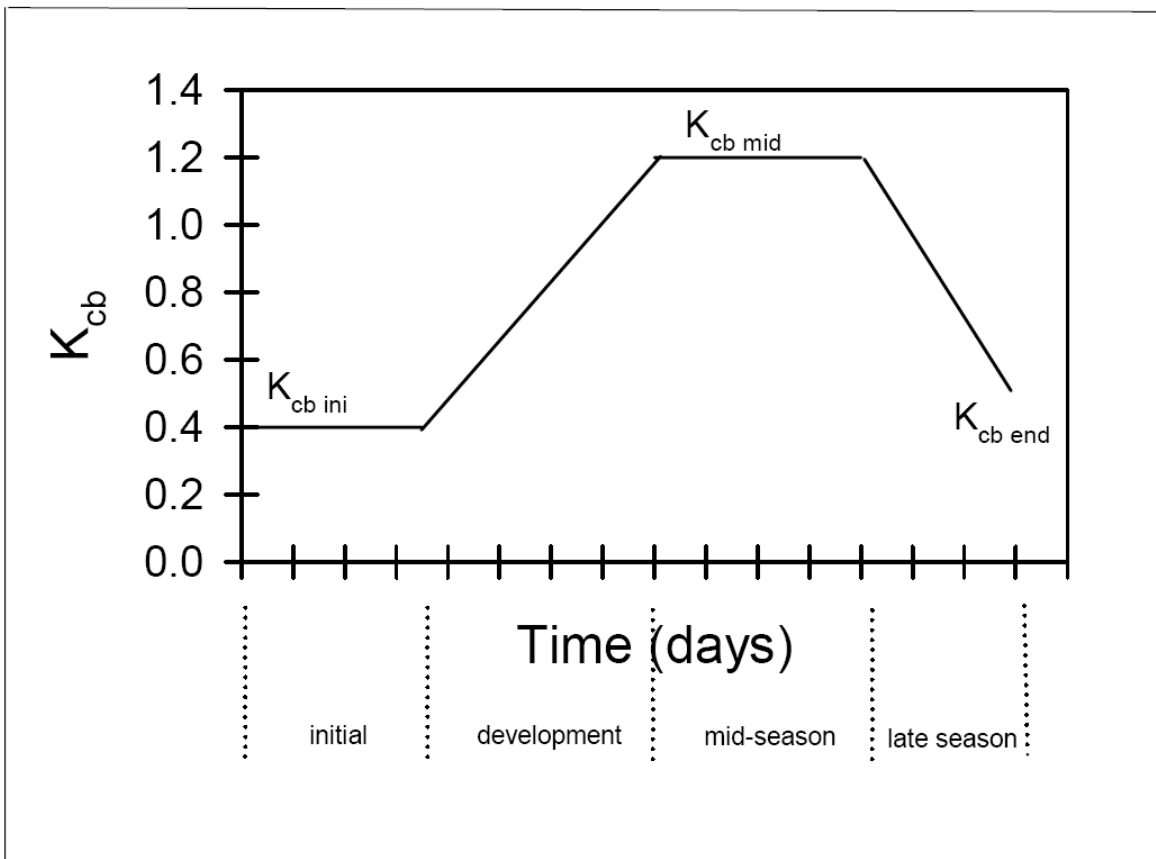
### D3. METHODS

#### D3.1 BASAL TRANSPIRATION COEFFICIENT EQUATIONS

The equations used to develop  $K_{cb}$  profiles for desert vegetation are presented in this section.

The FAO-56  $K_{cb}$  profile for agricultural crops reflects transpiration under optimal growth and nonlimiting water conditions. The generalized  $K_{cb}$  profile (Figure D-3) includes four growth stages (Allen et al. 1998 [DIRS 157311], pp. 95 and 96): an initial growth stage (planting date to approximately 10% ground cover), a development stage (10% ground cover to effective full cover), a midseason stage (effective full cover to start of maturity), and a late season stage (maturity to harvest or senescence). Effective full cover for agricultural crops is defined as the

time when soil shading is nearly complete or 100% covered (Allen et al. 1998 [DIRS 157311], p. 95).



Source: Allen et al. 1998 [DIRS 157311], p. 100, Figure 26.

Figure D-3. Generalized Crop Coefficient Curve

Characteristics of desert vegetation at Yucca Mountain differ from agricultural crops in several ways, including low effective ground cover that rarely exceeds 30% during peak growth periods, little morphological change in mature perennial vegetation across growth stages compared to agricultural crops (e.g., little change in vegetation height and maintenance of a percentage of green canopy throughout the year), and greater degree of stomatal control resulting in lower rates of water loss compared to agricultural crops. Additionally, climatic conditions at Yucca Mountain differ from standard FAO-56 conditions with lower minimum relative humidity ( $RH_{min}$ ) and higher wind speeds ( $u_2$ ). To account for these differences, FAO-56 methods for calculating  $K_{cb}$  for natural vegetation using effective ground cover, adjustments for stomatal control over water loss, and adjustments for local  $RH_{min}$  and  $u_2$  were used Allen et al. (1998 [DIRS 157311], pp. 187 to 193).

Transpiration coefficients for initial ( $K_{cb\ ini}$ ), midseason ( $K_{cb\ mid}$ ), and end of the late season ( $K_{cb\ end}$ ) growth stages were calculated for vegetation types using Equation D-1 (Allen et al. 1998 [DIRS 157311], p. 187, Equation 98):

$$K_{cb} = K_{c\ min} + (K_{cb\ full} - K_{c\ min}) \left( \min(1, 2f_c, (f_{c\ eff})^{\left(\frac{1}{1+h}\right)}) \right) \quad (\text{Eq. D-1})$$

where

- $K_{cb}$  = basal  $K_{cb}$  when plant density and/or leaf areas are lower than for full cover conditions
- $K_{c\ min}$  = minimum  $K_c$  for bare soil in the presence of vegetation ( $K_{c\ min} \approx 0$ )
- $K_{cb\ full}$  = estimated basal  $K_{cb}$  during the midseason, at peak plant size or height, and full ground cover (Equation D-4)
- $f_c$  = observed fraction of soil surface that is covered by vegetation type (0.01 to 1)
- $f_{c\ eff}$  = effective fraction of soil surface covered or shaded by vegetation type (0.01 to 1)
- $h$  = plant height (m).

Equation D-1 was recommended for calculating  $K_{cb\ mid}$  and  $K_{cb\ end}$  (Allen et al. 1998 [DIRS 157311], pp. 187 to 193). Methods for calculating  $K_{cb\ ini}$  under standard FAO-56 conditions were suggested for natural, nontypical vegetation (Allen et al. 1998 [DIRS 157311], p. 183). However, those methods were specifically suggested for newly planted annual crops with the magnitude of  $K_{cb\ ini}$  primarily determined by soil wetting frequency during irrigation and natural precipitation events. Established perennial vegetation at Yucca Mountain maintains height and some percentage of leaf area during the initial growth stage. Therefore, to account for effects of perennial plant height and cover during the initial growth stage, Equation D-1 was used with plant height and reduced cover (compared to that measured at peak growth; Sections D3.2.1 and D3.2.2) to calculate  $K_{cb\ ini}$ . Because height of annual vegetation varies over the course of the growing season with shorter vegetation during the initial growth stage, both height and cover were reduced (from peak values) to calculate  $K_{cb\ ini}$  for annuals using Equation D-1. Daily  $K_{cb}$  values for the initial, mid, and end of late season stages were estimated by using daily weather data inputs to calculate  $K_{cb\ full}$  (Equation D-6) and the stomatal resistance correction factor ( $F_r$ , Equation D-7). According to Allen et al. (2005 [DIRS 176009], p. 4), the equation for  $K_{cb\ full}$  can be used for daily estimates when daily measurements of  $u_2$  and  $RH_{min}$  are available. To be consistent and to keep the equations on a daily time step, daily weather data inputs were also used for  $F_r$  calculations (Equation D-7).

The FAO-56 equation for area- and height-weighting where different fractions of ground are covered by different crops (Allen et al. 2005 [DIRS 176009], p. 199, Equation 104) was not used because of differences in growing season length and stomatal resistance for vegetation types (Section D.3.2). Using Equation 98 to calculate separate profiles for vegetation types and then summing to get one profile for each association (and water year) accounts for this variation, which is important with respect to seasonal  $ET$ . The vegetation types are independent of one another, with growth stage lengths, cover, and height developed for each type. Because each profile is essentially weighted by cover for the vegetation type, the relative importance of each type is accounted for in the summed profile for each association. Summing the vegetation type profiles resulted in use of total cover that was measured for each association. Setting  $K_{c\ min}$  to



zero in Equation D-1 (as recommended for deserts [see below]) eliminates overestimation of residual evaporation from bare soil in the summed profiles.

Under arid conditions at Yucca Mountain, the upper soil layer dries to very low water content during periods between precipitation events (CRWMS M&O 1999 [DIRS 105031], p. 14, Table 3). Under dry soil conditions and sparse rainfall, Allen et al. (1998 [DIRS 157311], pp. 207 and 209) recommended setting  $K_{c\ min}$  to zero to provide for conditions when transpiration is equal to zero. Under these conditions, the soil water balance is controlled by the evaporation term ( $K_e$ ) of the dual transpiration coefficient. Evaporation following precipitation events is accounted for in the infiltration model by  $K_e$ .

In Equation D-1, the last term designates use of the minimum of 1,  $2f_c$ , and  $(f_{c\ eff})^{(1/1+h)}$ . Cover measurements showed that the total  $2f_c$  summed across vegetation types for an association never exceeded a value of 1. Values for  $f_{c\ eff}$  were determined for round or spherical shaped canopies using cover data from Yucca Mountain vegetation associations according to Equation D-2 (Allen et al. 1998 [DIRS 157311], p. 188):

$$f_{c\ eff} = \frac{f_c}{\sin(\eta)} \leq 1 \quad (\text{Eq. D-2})$$

where  $\sin(\eta)$  is the sine of the mean angle of the sun,  $\eta$ , above the horizon during midday hours when maximum evapotranspiration is likely to occur. Allen et al. (1998 [DIRS 157311], p. 188) suggest calculating  $f_{c\ eff}$  for solar noon using Equation D-3 to calculate  $\sin(\eta)$ :

$$\sin(\eta) = \sin(\psi) \sin(\delta) + \cos(\psi) \cos(\delta) \quad (\text{Eq. D-3})$$

where

$$\begin{aligned} \psi &= \text{latitude (radians),} \\ \delta &= \text{solar declination (radians).} \end{aligned}$$

Solar declination ( $\delta$ ) is calculated daily (Allen et al. 1998 [DIRS 157311], p. 46, Equation 24):

$$\delta = 0.409 \sin\left(\frac{2\pi}{365} J - 1.39\right) \quad (\text{Eq. D-4})$$

where

$$J = \text{day of year}$$

To help minimize water loss in arid environments, desert plants are capable of a higher degree of stomatal control than agricultural species (Allen et al. 1998 [DIRS 157311], p. 191). Therefore, it was necessary to apply a stomatal resistance correction factor ( $F_r$ , Equation D-7) to Equation D-1 when stomatal resistance was estimated to be greater than  $100 \text{ s m}^{-1}$  (Allen et al. 1998 [DIRS 157311], p. 191). The  $F_r$  accounts for increases in stomatal resistance during periods of low physiological activity (i.e., initiating or senescing leaves). The  $F_r$  does not account for effects of water stress on stomatal resistance. The impact of water stress is

implemented by the stress factor ( $K_s$ ) of the FAO-56 procedure that is used in the daily soil water balance model (Section 6.4).

Transpiration coefficients for development and late growth stages were calculated by linear interpolation between  $K_{cb\ ini}$  and  $K_{cb\ mid}$  and between  $K_{cb\ mid}$  and  $K_{cb\ end}$ , respectively (Allen et al. 1998 [DIRS 157311], p. 132, Equation 66):

$$K_{cb\ i} = K_{cb\ prev} + \left( \frac{i - \sum L_{prev}}{L_{stage}} \right) (K_{cb\ next} - K_{cb\ prev}) \quad (\text{Eq. D-5})$$

where

- $i$  = day number within the growing season (1...length of the growing season),
- $K_{cb, i}$  = transpiration coefficient on day  $i$ ,
- $K_{cb\ prev}$  =  $K_{cb}$  at the end of the previous stage,
- $K_{cb\ next}$  =  $K_{cb}$  at the beginning of the next stage,
- $L_{stage}$  = length of the stage under consideration (days),
- $\sum L_{prev}$  = sum of the length of all previous stages (days).

The following six steps were used to calculate daily  $K_{cbs}$  using Equation D-1 and adjusting for stomatal control:

1. Calculate adjustment for the influence of vegetation height for  $K_{cb}$  for full cover condition under standard climate ( $K_{cb, h}$ ) (Allen et al. 1998 [DIRS 157311], p. 189, Equation 101):

$$K_{cb, h} = 1.0 + 0.1h \quad (\text{Eq. D-6})$$

$K_{cb, h}$  is limited to 1.2 for when  $h > 2$  (Allen et al. 1998 [DIRS 157311], p. 189).

2. Calculate  $K_{cb\ full}$  (Allen et al. 1998 [DIRS 157311], p. 189, Equation 100):

$$K_{cb\ full} = K_{cb, h} + [0.04(u_2 - 2) - 0.004(RH_{min} - 45)] \left( \frac{h}{3} \right)^{0.3} \quad (\text{Eq. D-7})$$

where

- $K_{cb, h}$  =  $K_{cb}$  for full cover vegetation under a standard climate (Eq. D-6),
- $u_2$  = mean wind speed at 2-m height ( $\text{m s}^{-1}$ ),
- $RH_{min}$  = minimum daily relative humidity (%),
- $h$  = mean maximum plant height (m).

Equation D-7 adjusts for regional climatic differences from the standard climate of FAO-56 ( $u_2 = 2 \text{ m s}^{-1}$  and  $RH_{min} = 45\%$ ). This equation can be used for daily estimates when daily measurements of  $u_2$  and  $RH_{min}$  are available (Allen et al. 2005 [DIRS 176009], p. 4).

3. Calculate adjustment for stomatal control (Allen et al. 1998 [DIRS 157311], p. 191, Equation 102):

$$F_r \approx \frac{\Delta + \gamma(1 + 0.34u_2)}{\Delta + \gamma\left(1 + 0.34u_2 \frac{r_l}{100}\right)} \quad (\text{Eq. D-8})$$

where

- $F_r$  = stomatal resistance correction factor,
- $\Delta$  = slope of the saturation vapor pressure curve ( $\text{kPa } ^\circ\text{C}^{-1}$ ),
- $\gamma$  = Psychrometric constant ( $\text{kPa } ^\circ\text{C}^{-1}$ ),
- $r_l$  = mean leaf resistance for the vegetation in question ( $\text{s m}^{-1}$ ).

4. Determine the minimum of  $(1, 2f_c,$  and  $f_c \text{ eff}^{(1/1+h)})$ .
5. Use values from Steps 1 through 4 in Equation D-1 to calculate daily  $K_{cbs}$  for each vegetation type per association and water year.
6. Adjust daily  $K_{cbs}$  (from Step 5) for stomatal control:

$$(K_{cb} \times F_r) \quad (\text{Eq. D-9})$$

The final step in generating the  $K_{cb}$  profiles was to calculate  $K_{cb}$  for development and late stages using Equation D-5.

Example calculations using Equations D-1 through D-9 and  $K_{cb}$  profiles are in Section D4.

## D3.2 INPUT DATA

Inputs required to develop  $K_{cb}$  profiles are developed in this section. Inputs include growth stage lengths, vegetation height (h), vegetation cover ( $f_c$ ), stomatal resistance ( $r_l$ ), minimum relative humidity ( $RH_{min}$ ), wind speed ( $u_2$ ), slope of the saturation vapor pressure curve ( $\Delta$ ), and the psychrometric constant ( $\gamma$ ).

### D3.2.1 Growth Stages and Vegetation Height

Growth stages for the three vegetation types and vegetation height for the three associations were developed from data collected from Rock Valley and the Nevada Test Site (NTS) under several research programs, including the Desert Biome program of the International Biological Program (IBP). Several years of intensive ecological studies were conducted under the IBP and were continued through research funded by the U.S. Department of Energy (DOE) and the University of California, Los Angeles. These studies and the ecological communities and processes at Rock

Valley and other locations on the NTS are described by Rundel and Gibson (1996 [DIRS 103614]).

For agricultural species, Allen et al. (1998 [DIRS 157311], pp. 103 to 108) divided vegetation development into four growth stages (initial, development, midseason, and late season) that are related to leaf area index (ground area covered by plant canopy) and developmental stages. The initial stage begins at the planting date, for annuals, or at the onset of leaf growth, for perennials, and ends when the vegetation has reached approximately 10% ground cover. The development stage runs from 10% cover to effective full cover, which for many agricultural species occurs when flowering is initiated. The midseason stage begins when effective full cover is reached and ends at the start of maturity. The late season stage runs from maturity to harvest or senescence. The stages are crop specific and the stage lengths are affected by local climatic factors.

For desert vegetation, the length of the growing season is constrained by species-specific developmental processes, adaptations to desert conditions, and local climatic factors. Significant variation in timing and period of phenological stages occurs in response to monthly and yearly climatic conditions. For Yucca Mountain, growth stages were developed for annual, drought deciduous, and evergreen vegetation types based on information for dominant species within each type. The timing of initiation of leaf buds, leaves, flowers, fruits, leaf fall, and dormancy reported for Mojave Desert shrubs in Rundel and Gibson (1996 [DIRS 103614], Figure 4.13, p. 106) was used to define initial, development, mid- and late season growth stages for drought deciduous and evergreen vegetation (Table D-3).

Table D-3. Phenological Stages for Drought Deciduous and Evergreen Species

Species <sup>a</sup>	Bud Initiation <sup>a</sup>	Leaf Initiation <sup>a</sup>	Flower Initiation <sup>a</sup>	Fruit Initiation <sup>a</sup>	Leaf Fall <sup>a</sup>	Dormancy <sup>a</sup>
<i>Ephedra nevadensis</i>	February to April	March to April	May	May to June	—	—
<i>Larrea tridentata</i>	April to May	March to July	May	June	July to March	—
<i>Ambrosia dumosa</i>	February to April	March to May	May	June	May to August	July to February
<i>Grayia spinosa</i>	February to March	March to May	April	April to May	May to July	July to February
<i>Lycium andersonii</i>	February to March	March to May	April	April to June	May to July	July to February
<i>Lycium pallidum</i>	February to April	March to May	April	May to June	May to August	July to February

<sup>a</sup>Dates are from Rundel and Gibson 1996 [DIRS 103614], Figure 4.13, p. 106; ranges were established from the 1969 and 1970 data.

The bud initiation period was considered for the initial growth stage (period of low physiological activity or leaf area index), the early period of leaf initiation was considered for the development stage (period of increasing physiological activity or leaf area index), the remaining period of leaf initiation through flower initiation and the beginning of fruit initiation was considered for the midstage (period of highest seasonal physiological activity or leaf area index), and fruit initiation through leaf fall was considered for the late stage (period of declining physiological activity or leaf area index) (Table D-3).

When available, measured periods of physiological activity (i.e., photosynthesis, stomatal conductance, or transpiration) for dominant shrub species were used along with the timing of phenological stages in Rundel and Gibson (1996 [DIRS 103614], p. 106, Figure 4.13) to develop growth stages. For annual vegetation, reported growing season lengths and timing of phenological stages for *Bromus madritensis* were used to develop growth stages.

Stage lengths were developed for average precipitation years. Appropriate stage lengths were reduced to represent below average precipitation years and were increased to represent above average precipitation years.

For evergreen species, *Ephedra nevadensis* exhibited bud initiation February through April, while *L. tridentata* initiated bud growth later in April and May (Table D-3). However, positive stomatal conductance was measured on evergreen leaves of *L. tridentata* as early as January (Hamerlynck et al. 2000 [DIRS 177022], p. 602, Figure 6), indicating physiological activity and transpiration. Leaf initiation occurred March through April for *E. nevadensis* and March through July for *L. tridentata*, with flower initiation in May for both species (Table D-3). Stomatal conductance measurements were shown to be relatively high in March and April for *E. nevadensis* plants growing in Crater Flat (13 km north-west of Yucca Mountain) and increased in May at two of three sites studied by Smith et al. (1995 [DIRS 103628], Figure 2, p. 343), indicating increased transpiration in May. Fruit initiation occurred from May to June for *E. nevadensis* and in June for *L. tridentata*, with leaf fall starting in July for *L. tridentata*. Low but positive stomatal conductance rates were reported for *E. nevadensis* and *L. tridentata* through the end of September and first of October, respectively (Smith et al. 1995 [DIRS 103628], Figure 2, p. 343; Hamerlynck et al. 2000 [DIRS 177022], p. 602, Figure 6).

Based on this information, February 1 through 28, March 1 through 31, April 1 through May 15, and May 16 through September 30 were assigned to the initial, development, mid, and late growth stages, respectively, for evergreen species (Table D-4). Summer rainfall is uncommon in the northern Mojave Desert with approximately 70% falling between November and March (Rundel and Gibson 1996 [DIRS 103614], p. 53). Once soil dries down from winter recharge, it generally stays dry (Rundel and Gibson 1996 [DIRS 103614], p. 53). This is especially true of drought years. Because of the slow growth habit and moderate water use efficiency of evergreen vegetation, it was assumed that, on average, the length of the late season growth stage would be most affected by drought. Additionally, for some evergreen species, leaf emergence may be triggered by photoperiod rather than precipitation (Smith et al. 1997 [DIRS 103636], p. 61). With high temperatures and little precipitation after March or April, it is reasonable to suggest that physiological activity of evergreen vegetation would slow, and stomata would close to prevent water loss around June or July in a drought year. This is supported by observations of leaf fall for *L. tridentata* in July and subsequent summer months (Table D-3), and low precipitation during summer months in the drought year of 2002 (Figure E-4). Therefore, to represent dry years for evergreen species, the late stage period was changed to May 16 through June 30 (Table D-4). During above average precipitation years, growth by evergreen vegetation can be maintained over longer time periods when water is available (Smith et al. 1997 [DIRS 103636], pp. 59 and 60). For evergreen vegetation it was assumed that the length of the mid stage would be most affected due to favorable temperatures and moisture availability later in the spring during an above average precipitation year. In 1998, precipitation that fell through April, May, and June (Figure E-4) may have been sufficient to prolong growth expected of evergreens during

the mid stage. Therefore, to represent above average precipitation years, the length of the mid stage for evergreen vegetation was increased by 30 days to April 1 through June 15 (Table D-4). The length of the late stage was changed to June 16 through September 30. The length of the late stage was not extended into October because it is likely that air temperature and depleted soil moisture would limit physiological activity in the fall and winter months (Smith et al. 1995 [DIRS 103628], pp. 342 and 349).

Drought deciduous species *A. dumosa*, *G. spinosa*, *L. andersonii*, and *L. pallidum* exhibited bud initiation from February through April, leaf initiation from March through July, and flower initiation in April or May (Table D-3). Leaves were present on *L. andersonii* in March at the onset of a study on the NTS by Hamerlynck et al. (2002 [DIRS 177128], Figure 7, p. 103) indicating that leaf initiation had occurred prior to March. Leaf area of *L. andersonii* increased and peaked between April 27 and May 11. Both leaf area and leaf number decreased substantially between May 11 and May 25 (Hamerlynck et al. 2002 [DIRS 177128], Figure 7, p. 103). Additionally, net photosynthesis in *A. dumosa* declined to the photosynthetic compensation point by May 4 in a study at the East Mojave National Preserve (Hamerlynck et al. 2002 [DIRS 177046], p 774).

Table D-4. Growth Stage Lengths for Three Vegetation Types at Yucca Mountain

<b>Below-Average Precipitation Year</b>			
<b>Growth Stage</b>	<b>Annual</b>	<b>Drought Deciduous</b>	<b>Evergreen</b>
Initial	N/A	Feb. 15 to 28 DOY 46 to 59	Feb. 1 to 28 DOY 32 to 59
Development	N/A	Mar. 1 to 15 DOY 60 to 74	Mar. 1 to 31 DOY 60 to 90
Mid	N/A	Mar. 16 to Apr. 15 DOY 75 to 105	Apr. 1 to May 15 DOY 91 to 135
Late	N/A	Apr. 16 to 30 DOY 106 to 120	May 16 to Jun. 30 DOY 136 to 181
<b>Average Precipitation Year</b>			
<b>Growth Stage</b>	<b>Annual<sup>1</sup></b>	<b>Drought Deciduous<sup>2</sup></b>	<b>Evergreen<sup>3</sup></b>
Initial	Jan. 1 to 31 DOY 1 to 31	Feb. 1 to 28 DOY 32 to 59	Feb. 1 to 28 DOY 32 to 59
Development	Feb. 1 to 28 DOY 32 to 59	Mar. 1 to 15 DOY 60 to 74	Mar. 1 to 31 DOY 60 to 90
Mid	Mar. 1 to 31 DOY 60 to 90	Mar. 16 to Apr. 30 DOY 75 to 120	Apr. 1 to May 15 DOY 91 to 135
Late	Apr. 1 to 15 DOY 91 to 105	May 1 to 15 DOY 121 to 135	May 16 to Sept. 30 DOY 136 to 273

Table D-4. Growth Stage Lengths for Three Vegetation Types at Yucca Mountain (Continued)

Above-Average Precipitation Year (Continued)			
Growth Stage	Annual	Drought Deciduous	Evergreen
Initial	Oct. 1 to Jan. 31 DOY 274 to 31	Feb. 1 to 28 DOY 32 to 59	Feb. 1 to 28 DOY 32 to 59
Development	Feb. 1 to 28 DOY 32 to 59	Mar. 1 to 15 DOY 60 to 74	Mar. 1 to 31 DOY 60 to 90
Mid	Mar. 1 to May 1 DOY 60 to 121	Mar. 16 to May 31 DOY 75 to 151	Apr. 1 to Jun. 15 DOY 91 to 166
Late	May 2 to 16 DOY 122 to 136	Jun. 1 to Jun. 15 DOY 152 to 166	Jun. 16 to Sept. 30 DOY 167 to 273

Source: Newman 1992 [DIRS 174673], p. 3; Hulbert 1955 [DIRS 177129], p. 1. Rundel and Gibson 1996 [DIRS 103614], Figure 4.13, p. 106; Hamerlynck et al. 2002 [DIRS 177128], Figure 7, p. 103; Hamerlynck et al. 2002 [DIRS 177046], p. 774. Rundel and Gibson 1996 [DIRS 103614], Figure 4.13, p. 106; Hamerlynck et al. 2000 [DIRS 177022], p. 602, Figure 6; Smith et al. 1995 [DIRS 103628], pp. 342 to 343, Figure 2, and 349.

Thus, for the drought deciduous species during an average precipitation year, February 1 through 28, March 1 through 15, March 16 through April 30, and May 1 through 15 were assigned to the initial, development, mid, and late growth stages, respectively (Table D-4). Timing of precipitation for drought years is variable and unpredictable (CRWMS M&O 1996 [DIRS 102235], p. 3) and likely has a greater effect on lengths of different growth stages for drought deciduous than for evergreen vegetation. This is because timing of phenological events for drought deciduous vegetation, such as leaf or flower initiation, are dependent on precipitation (Smith et al. 1997 [DIRS 103636], p. 61). Additionally, drought deciduous vegetation is more sensitive to the onset of dry soil conditions than evergreen vegetation (e.g., leaf drop occurs more readily). It was assumed that, on average, during a drought year the phenological stages that would be most affected would be bud and leaf initiation, and flower development. Based on Rundel and Gibson (1996 [DIRS 103614], Table 4.14, p. 109), first dates of leafing for four drought deciduous species (*A. dumosa*, *G. spinosa*, *L. andersonii*, and *L. pallidum*) varied on average by about 15 days from one consecutive year to the next over nine years. Based on this, the initial, mid, and late growth stages were reduced by 15 days for a below-average precipitation year. This resulted in growth stage lengths of February 15 through 28, March 1 through 15, March 16 through April 15, and April 16 through 30 for the initial, development, mid, and late growth stages, respectively (Table D-4). As with evergreen vegetation, it was assumed that the length of the mid stage would be most affected by above-average precipitation years through extension of the time period of favorable temperatures and soil moisture for growth. Therefore, the length of the mid stage was increased by 15 days to March 16 through May 31 (Table D-4). This moved the late season stage to June 1 through June 15. The length of the late season stage was not increased because high temperatures and evaporative demands that are common in June generally result in rapid dry down of soils and subsequent leaf fall for drought deciduous species.

*Bromus madritensis* spp. *rubens* was the dominant annual species on vegetation associations and, in most cases, was the only annual species that exhibited significant cover (Tables D-7 through D-15). *Bromus madritensis* spp. *rubens* is an invasive winter annual grass that germinates in the fall (September through December) and remains a vegetative rosette or tuft until growth resumes in late winter or early spring (Newman 1992 [DIRS 174673], p. 3; Hulbert

1955 [DIRS 177129], p. 1). This grass grows quickly when temperatures allow, then generally sets seed and senesces in late spring to early summer months (Hulbert 1955 [DIRS 177129], p. 1; Newman 1992 [DIRS 174673], p. 3). Based on this information, the time periods of January 1 through 31, February 1 through 28, March 1 through 31, and April 1 through 15 were assigned to the initial, development, mid, and late stages, respectively (Table D-4). No annual cover was recorded for the representative dry year (Tables D-8, D-9, and D-10); therefore, growth stages were not developed. In above average precipitation years, fall rains could result in germination of *Bromus madritensis*, followed by slow growth to semi dormant conditions under cool winter temperatures (Newman 1992 [DIRS 174673], p. 3). Additionally, if moisture is available, *Bromus madritensis* can germinate in winter and spring months (Newman 1992 [DIRS 174673], p. 3). To account for fall germination in above-average precipitation years, the initial stage was changed to October 1 through January 31 (Table D-4). The midstage was extended by 30 days (March 1 through May 1) to account for growth of spring germinating cohorts and extension of the time period of available moisture with above average precipitation. This resulted in moving the late season to May 2 through May 16 (Table D-4). The length of the late season stage was not increased for the same reasons discussed for drought deciduous species.

Rundel and Gibson (1996 [DIRS 103614], pp. 87 to 89) describe vegetation characteristics for Great Basin, transition, and Mojave Desert associations that were based on 10 years of data. The range of mean vegetation heights for the *Larrea–Ambrosia* association (0.27 to 0.32 m) (Table D-5), *Larrea–Grayia–Lycium* association (0.34 to 0.48 m) (Table D-5), and *Grayia–Lycium* association (0.38 m) (Table D-5) were most appropriate for use in this analysis because the association descriptions based on Beatley's work (Rundel and Gibson 1996 [DIRS 103614], pp. 87 to 89) correspond to the LA, LLG, and LG associations for Yucca Mountain. Ranges for vegetation heights were reported for four additional associations (Table D-5) but were not selected for the following reasons:

1. Cover data for this analysis (Tables D-8, D-10, D-11, D-13, D-14, and D-16) show that for the LA and LLG vegetation associations, *L. tridentata*, a shrub that can grow to relatively large stature, is either codominant with shorter shrubs, such as *E. nevadensis*, or comprises much less cover than shorter shrubs, such as *A. dumosa*, making the reported maximum height of the range (0.82 m) for *Larrea–Ambrosia–Grayia–Lycium* too high.
2. *Coleogyne ramosissima* was not dominant in the vegetation associations that were chosen for this analysis. Therefore, associations with *C. ramosissima* as a dominant species were not selected.



Table D-5. Mean Vegetation Heights for Seven Vegetation Associations

Vegetation Association <sup>a</sup>	Corresponding Yucca Mountain Vegetation Association	Mean Height of Vegetation (m)
<i>Larrea–Ambrosia</i>	LA	0.27 to 0.32
<i>Larrea–Ambrosia–Grayia–Lycium</i>	NA <sup>b</sup>	0.41 to 0.82
<i>Larrea–Grayia–Lycium</i>	LLG	0.34 to 0.48
<i>Grayia–Lycium</i> <sup>c</sup>	LG	0.38
<i>Coleogyne–Larrea–Grayia–Lycium</i>	NA	0.42 to 0.51
<i>Coleogyne–Grayia–Lycium</i>	NA	0.31 to 0.39
<i>Coleogyne</i>	COL	0.37 to 0.41

Source: <sup>a</sup> Rundel and Gibson 1996 [DIRS 103614], Table 4.1, p. 88.

<sup>b</sup> Not applicable.

<sup>c</sup> Rundel and Gibson 1996 [DIRS 103614], Table 4.2, p. 89.

According to Equation D-4, mean maximum plant height is recommended for  $K_{cb}$  calculations; therefore, the maximum values for the range of heights in Table D-5 were selected for drought deciduous and evergreen species (Table D-6). Because established perennial vegetation was considered for  $K_{cb}$  calculations, one height value was used for all growth stages for drought deciduous and evergreen species.

Mean maximum plant height for annual vegetation was based on published literature values for *Bromus madritensis* and on vegetation heights from Table D-5. Plant height reported for *Bromus madritensis* ranged from 0.20 to 0.50 m (Newman 1992 [DIRS 174673], p. 2). Based on mean heights for perennial shrubs (Table D-5), it is not likely that the dry conditions at Yucca Mountain would normally support annuals with a mean maximum height of 0.50 m. Height ranges for perennial vegetation were lower for the LA association than for the LG and LLG associations, indicating a lower value for annuals would also be appropriate. Therefore, for the LA association, 0.27 m was selected as the mean maximum height for annuals, which is at the low end of the height range for the LA association (Table D-5). For the LG and LLG associations, 0.34 m was selected as the mean maximum height for annuals, which is at the low end of the height range for the LLG association (Table D-5).

Annual species germinate, grow, and complete their life cycle within a year, and so differences in height between the initial and midseason growth stages were considered. *Bromus madritensis* is a winter annual and generally germinates in late fall or winter, rapidly establishes a root system, then overwinters as a small basal rosette ranging from 0.01 to 0.05 m in height (height measured for *Bromus tectorum* in February; Hulbert 1955 [DIRS 177129], Table 6, p. 186). Ten percent of the midseason stage height (about 0.03 m) was about midrange of the height values in Hulbert (1955 [DIRS 177129], Table 6, p. 186). Therefore, 10% of the midseason stage height (about 0.03 m) was used for the initial growth stage for annual vegetation (Table D-6).

Vegetation height was not varied for low-, average, and high-precipitation years. Stress imposed by dryer years was accounted for with measured cover data and growing season length.

Table D-6. Mean Maximum Vegetation Heights

Vegetation Association	Mean Maximum Plant Height (m)		
	Annuals <sup>a</sup>	Drought Deciduous <sup>b</sup>	Evergreen <sup>c</sup>
LA	Initial growth stage = 0.027; midseason growth stage = 0.27	0.32	0.32
LG	Initial growth stage = 0.034; midseason growth stage = 0.34	0.38 <sup>3</sup>	0.38 <sup>3</sup>
LLG	Initial growth stage = 0.034; midseason growth stage = 0.34	0.48	0.48

Sources: <sup>a</sup>Newman 1992 [DIRS 174673], p. 2; Hulbert 1955 [DIRS 177129], Table 6, p. 186; Rundel and Gibson 1996 [DIRS 103614], Table 4.1, p. 88, and Table 4.2, p. 89.

<sup>b</sup>Rundel and Gibson 1996 [DIRS 103614], Table 4.1, p. 88.

<sup>c</sup>Rundel and Gibson 1996 [DIRS 103614], Table 4.2, p. 89.

### D3.2.2 Vegetation Cover Data

Cover data collected during below average (1990), average (1991), and above average (1993) precipitation years from 11 to 12 plots (depending on the year) in the LA, LG, and LLG vegetation associations at Yucca Mountain were used to calculate cover means per species and vegetation type for each association (Tables D-7 through D-15). This was done by extracting the ESP cover data for the LA, LG, and LLG associations from the source file (DTN: MO9907GCESPYMN.000 [DIRS 157659]) for 1990, 1991, and 1993. The data were placed in an Excel® file (Output DTN: MO0606SPAVEGAS.001). Data were sorted by species and ground cover classification (bare ground, litter, gravel, rock, and cobble) within ESPs. For each ESP mean cover per species and ground cover classification was calculated by summing cover per species (or ground cover classification) and dividing the sum by the number of transects that were sampled (8 to 12 transects depending on the site). Association means per species were calculated from the ESP means by summing cover per species and dividing by the number of ESPs measured within an association (Tables D-7 through D-15). Total mean cover per vegetation type and association was determined by summing mean cover per species within a vegetation type and then summing mean cover for the three vegetation types to get the association total (Tables D-7 through D-15). Calculations were done in Excel® spreadsheets using the SUM and AVERAGE commands (Output DTN: MO0606SPAVEGAS.001).

Cover data means were sorted to identify dominant and important species within associations for each year. Species comprising 70% to 90% of the cover data means were considered dominant. Cover data means per species, vegetation type, and association are in Tables D-7 through D-15.

Vegetation cover is not static throughout the year. It changes with phenological stages and in response to environmental conditions. Evergreens such as *A. tridentata* and *L. tridentata* develop ephemeral leaves that are shed as soil moisture becomes limiting (Smith et al. 1997 [DIRS 103636], pp. 79 and 108), and drought deciduous shrubs experience complete defoliation during extended dry periods. Vegetation cover data were collected during peak growth periods for the three years used in this study and represent maximum cover for an average, above average, and below average water year. During the initial growth stage cover is lower than that measured at peak growth. During the initial stage, annuals are emerging and drought deciduous and evergreen species are initiating new leaf growth. However, there were no vegetation cover

data available from Yucca Mountain or in the literature to develop a percent reduction of cover from peak growth to use for the initial growth stage. Therefore, to avoid overestimation of plant water use during the initial stage, it was assumed that drought deciduous and evergreen vegetation cover was 50% of that measured at peak growth. Fifty percent was selected because drought deciduous vegetation puts on leaf area rapidly when soil moisture becomes available (Smith et al. 1997 [DIRS 103636], p. 62), and evergreen vegetation maintains a percentage of leaf area throughout the year (Smith et al. 1997 [DIRS 103636], p. 73). It was assumed for annual vegetation that cover was 10% of that measured at peak growth for normal precipitation years and 30% of that measured at peak growth for above average precipitation years. Ten percent of full cover was selected for normal precipitation years because of the small stature of annual seedlings. Thirty percent of full cover was selected for above average precipitation years because of the potential for initial crowding of *Bromus madritensis* seedlings in response to favorable germination conditions (Newman 1992 [DIRS 174673], p. 3).

Table D-7. Mean Cover from LA Vegetation Associations at Yucca Mountain for a Dry Year (1990)

LA 1990					
Vegetation Type/Species	Life Form <sup>1</sup>	Cover (%)	Vegetation Type/Species	Life Form <sup>1</sup>	Cover (%)
<b>Annuals</b>		0.00	<b>Evergreen</b>		
No annuals recorded			<i>Larrea tridentata</i>	S	1.02
<b>Drought Deciduous</b>			<i>Ephedra nevadensis</i>	S	0.70
<i>Ambrosia dumosa</i>	S	5.82	<i>Ericameria cooperi</i> <sup>6</sup>	S	0.45
<i>Acamptopappus shockleyi</i>	S	2.03	<i>Coleogyne ramosissima</i>	S	0.23
<i>Menodora spinescens</i>	S	1.74	<i>Hymenoclea salsola</i>	S	0.05
<i>Krameria erecta</i> <sup>2</sup>	S	0.90	<b>Total</b>		<b>2.45</b>
<i>Lycium pallidum</i>	S	0.53	<b>Association Total</b>		<b>14.55</b>
<i>Atriplex confertifolia</i>	S	0.35			
<i>Grayia spinosa</i>	S	0.23			
<i>Achnatherum hymenoides</i> <sup>3</sup>	G	0.15			
<i>Krascheninnikovia lanata</i> <sup>4</sup>	S	0.14			
<i>Lycium andersonii</i>	S	0.10			
<i>Salazaria mexicana</i>	S	0.03			
<i>Machaeranthera tortifolia</i>	F	0.03			
<i>Psoralea fremontii</i>	S	0.02			
<i>Eriogonum fasciculatum</i>	S	0.02			
<i>Achnatherum speciosum</i> <sup>5</sup>	G	0.01			
<b>Total</b>		<b>12.10</b>			

Source: Output DTN: MO0606SPAVEGAS.001.

NOTE: Means are based on data collected from twelve 200 × 200 m plots in 1990. Species are arranged in order of dominance within a vegetation type.

<sup>1</sup> G = grass, F = forb, S = shrub.

<sup>2</sup> Previous nomenclature: *Krameria parvifolia*.

<sup>3</sup> Previous nomenclature: *Oryzopsis hymenoides*.

<sup>4</sup> Previous nomenclature: *Ceretooides lanata*.

<sup>5</sup> Previous nomenclature: *Stipa speciosa*.

<sup>6</sup> Previous nomenclature: *Happlopappus cooperi*.

Table D-8. Mean Cover from LG Vegetation Associations at Yucca Mountain for a Dry Year (1990)

LG 1990					
Vegetation Type/Species	Life Form <sup>1</sup>	Cover (%)	Vegetation Type/Species	Life Form <sup>1</sup>	Cover (%)
<b>Annuals</b>			<b>Evergreen</b>		
No annuals recorded		0.00	<i>Ephedra nevadensis</i>	S	2.13
<b>Drought Deciduous</b>			<i>Ericameria cooperi</i> <sup>6</sup>	S	1.28
<i>Eriogonum fasciculatum</i>	S	2.11	<i>Hymenoclea salsola</i>	S	0.67
<i>Lycium andersonii</i>	S	2.05	<i>Ericameria teretifolia</i> <sup>7</sup>	S	0.58
<i>Grayia spinosa</i>	S	1.82	<i>Chrysothamnus viscidiflorus</i>	S	0.32
<i>Achnatherum speciosum</i> <sup>2</sup>	G	0.85	<i>Gutierrezia sarothrae</i>	S	0.23
<i>Atriplex confertifolia</i>	S	0.78	<i>Ephedra viridis</i>	S	0.22
<i>Pleuraphis jamesii</i> <sup>3</sup>	G	0.50	<i>Artemisia tridentata</i>	S	0.18
<i>Ambrosia dumosa</i>	S	0.38	<i>Ericameria linearifolia</i> <sup>8</sup>	S	0.12
<i>Krascheninnikovia lanata</i> <sup>4</sup>	S	0.29	<i>Larrea tridentata</i>	S	0.09
<i>Menodora spinescens</i>	S	0.24	<i>Ericameria nauseosa</i> <sup>9</sup>	S	0.08
<i>Salazaria mexicana</i>	S	0.23	<b>Total</b>		5.90
<i>Lycium pallidum</i>	S	0.08	<b>Association</b>		<b>Total</b>
<i>Atriplex canescens</i>	S	0.07	<b>15.62</b>		
<i>Tetradymia axillaris</i>	S	0.07			
<i>Elymus elymoides</i> <sup>5</sup>	G	0.06			
Others		0.19			
<b>Total</b>		9.72			

Source: Output DTN: MO0606SPAVEGAS.001.

NOTE: Means are based on data collected from twelve 200 × 200 m plots in 1990. Species are arranged in order of dominance within a vegetation type.

<sup>1</sup> G = grass, F = forb, S = shrub.

<sup>2</sup> Previous nomenclature: *Stipa speciosa*.

<sup>3</sup> Previous nomenclature: *Hilaria jamesii*.

<sup>4</sup> Previous nomenclature: *Ceretooides lanata*.

<sup>5</sup> Previous nomenclature: *Sitanion histere*.

<sup>6</sup> Previous nomenclature: *Happlopapus cooperi*.

<sup>7</sup> Previous nomenclature: *Chrysothamnus teretifolius*.

<sup>8</sup> Previous nomenclature: *Happlopapus linearifolius*.

<sup>9</sup> Previous nomenclature: *Crysothamnus nauseosus*.

Table D-9. Mean Cover from LLG Vegetation Associations at Yucca Mountain for a Dry Year (1990)

LLG 1990				
Vegetation Type/Species	Life Form <sup>1</sup>	Cover (%)	Vegetation Type/Species	Life Form <sup>1</sup> Cover (%)
<b>Annuals</b>			<b>Evergreen</b>	
No annuals recorded		0.00	<i>Larrea tridentata</i>	S 2.79
<b>Drought Deciduous</b>			<i>Ephedra nevadensis</i>	S 2.69
<i>Krameria erecta</i> <sup>2</sup>	S	2.00	<i>Ericameria cooperi</i> <sup>5</sup>	S 0.69
<i>Ambrosia dumosa</i>	S	1.56	<i>Hymenoclea salsola</i>	S 0.52
<i>Lycium andersonii</i>	S	0.96	<i>Coleogyne ramosissima</i>	S 0.04
<i>Grayia spinosa</i>	S	0.70	<i>Ephedra viridis</i>	S 0.02
<i>Salazaria mexicana</i>	S	0.36	<b>Total</b>	<b>6.75</b>
<i>Menodora spinescens</i>	S	0.28	<b>Association Total 13.56</b>	
<i>Eriogonum fasciculatum</i>	S	0.23		
<i>Krascheninnikovia lanata</i> <sup>3</sup>	S	0.20		
<i>Achnatherum speciosum</i> <sup>4</sup>	G	0.19		
<i>Lycium pallidum</i>	S	0.16		
<i>Atriplex confertifolia</i>	S	0.04		
Others		0.13		
	<b>Total</b>	<b>6.81</b>		

Source: Output DTN: MO0606SPAVEGAS.001.

NOTE: Means are based on data collected from eleven 200 × 200 m plots in 1990. Species are arranged in order of dominance within a vegetation type.

<sup>1</sup> G = grass, F = forb, S = shrub.

<sup>2</sup> Previous nomenclature: *Krameria parvifolia*.

<sup>3</sup> Previous nomenclature: *Ceretooides lanata*.

<sup>4</sup> Previous nomenclature: *Stipa speciosa*.

<sup>5</sup> Previous nomenclature: *Happlopapus cooperi*.

Table D-10. Mean Cover from LA Vegetation Associations at Yucca Mountain for an Average Precipitation Year (1991)

LA 1991					
Vegetation Type/Species	Life Form <sup>1</sup>	Cover (%)	Vegetation Type/Species	Life Form <sup>1</sup>	Cover (%)
<b>Annuals</b>			<b>Drought Deciduous</b>		
<i>Chaenactis stevioides</i>	F	0.66	<i>Ambrosia dumosa</i>	S	3.38
<i>Vulpia octoflora</i>	G	0.56	<i>Menodora spinescens</i>	S	1.25
<i>Sisymbrium altissimum</i>	F	0.14	<i>Lycium pallidum</i>	S	0.60
<i>Unknown</i>	G	0.11	<i>Acamptopappus shockleyi</i>	S	0.57
<i>Bromus madritensis ssp. rubens</i>	F	0.09	<i>Krameria erecta</i> <sup>2</sup>	S	0.40
<i>Pectocarya platycarpa</i>	F	0.08	<i>Atriplex confertifolia</i>	S	0.15
<i>Eriogonum maculatum</i>	F	0.05	<i>Lycium andersonii</i>	S	0.11
<i>Mentzelia obscura</i>	F	0.05	<i>Psoralea fremontii</i>	S	0.05
Others		0.32	Others		0.13
	<b>Total</b>	<b>2.06</b>		<b>Total</b>	<b>6.64</b>
			<i>Evergreen</i>		
			<i>Larrea tridentata</i>	S	1.06
			<i>Ephedra nevadensis</i>	S	0.46
			<i>Coleogyne ramosissima</i>	S	0.27
			<i>Ericameria cooperi</i> <sup>3</sup>	S	0.03
				<b>Total</b>	<b>1.82</b>
			<b>Association Total</b>		<b>10.52</b>

Source: Output DTN: MO0606SPAVEGAS.001.

NOTE: Means are based on data collected from twelve 200 × 200 m plots in 1991. Species are arranged in order of dominance within a vegetation type.

<sup>1</sup> G = grass, F = forb, S = shrub.

<sup>2</sup> Previous nomenclature: *Krameria parviflora*.

<sup>3</sup> Previous nomenclature: *Happlopappus cooperi*.

Table D-11. Mean Cover from LG Vegetation Associations at Yucca Mountain for an Average Precipitation Year (1991)

LG 1991					
Vegetation Type/Species	Life Form <sup>1</sup>	Cover (%)	Vegetation Type/Species	Life Form <sup>1</sup>	Cover (%)
<b>Annuals</b>			<b>Drought Deciduous</b>		
<i>Bromus madritensis ssp. rubens</i>	G	3.24	<i>Lycium andersonii</i>	S	1.16
<i>Unknown</i>	F	0.45	<i>Grayia spinosa</i>	S	1.04
<i>Amsinckia tessellata</i>	F	0.38	<i>Eriogonum fasciculatum</i>	S	1.04
<i>Salsola iberica</i> <sup>2</sup>	F	0.23	<i>Atriplex confertifolia</i>	S	0.69
<i>Sisymbrium altissimum</i>	F	0.13	<i>Ambrosia dumosa</i>	S	0.53
<i>Mentzelia obscura</i>	F	0.09	<i>Pleuraphis jamesii</i> <sup>3</sup>	S	0.41
<i>Oxytheca perfoliata</i>	F	0.09	<i>Achnatherum speciosum</i> <sup>4</sup>	S	0.40
<i>Descurainia pinnata</i>	F	0.07	<i>Krascheninnikovia lanata</i> <sup>5</sup>	S	0.27
<i>Linanthus demissus</i>	F	0.06	<i>Menodora spinescens</i>	S	0.27
<i>Cryptantha nevadensis</i>	F	0.05	<i>Lycium pallidum</i>	S	0.24
<i>Cryptantha micrantha</i>	F	0.05	<i>Salazaria mexicana</i>	S	0.18
Others		0.22	<i>Sphaeralcea ambigua</i>	S	0.12
	<b>Total</b>	<b>5.06</b>	<i>Atriplex canescens</i>	S	0.08
			<i>Erioneuron pulchellum</i>	G	0.06
			<i>Encelia virginensis</i>	S	0.05
			<i>Eriastrum eremicum</i>	F	0.05
			Others		0.18
			<b>Total</b>		<b>6.77</b>
			<b>Evergreen</b>		
			<i>Ephedra nevadensis</i>	S	2.00
			<i>Ericameria cooperi</i> <sup>6</sup>	S	0.79
			<i>Hymenoclea salsola</i>	S	0.55
			<i>Ericameria teretifolia</i> <sup>7</sup>	S	0.38
			<i>Gutierrezia sarothrae</i>	S	0.38
			<i>Ephedra viridis</i>	S	0.18
			<i>Chrysothamnus viscidiflorus</i>	S	0.13
			<i>Artemisia tridentata</i>	S	0.11
			<i>Ericameria nauseosa</i> <sup>8</sup>	S	0.09
			<i>Ericameria linearifolia</i> <sup>9</sup>	S	0.08
			<i>Larrea tridentata</i>	S	0.08
			<i>Coleogyne ramosissima</i>	S	0.01
			<b>Total</b>		<b>4.78</b>
			<b>Association Total</b>		<b>16.61</b>

Source: Output DTN: MO0606SPAVEGAS.001.

NOTE: Means are based on data collected from twelve 200 m × 200 m plots in 1991. Species are arranged in order of dominance within a vegetation type.

<sup>1</sup> G = grass, F = forb, S = shrub.

<sup>2</sup> Previous nomenclature: *Salsola kali*.

<sup>3</sup> Previous nomenclature: *Hilaria jamesii*.

<sup>4</sup> Previous nomenclature: *Stipa speciosa*.

<sup>5</sup> Previous nomenclature: *Ceratoides lanata*.

<sup>6</sup> Previous nomenclature: *Happlopappus cooperi*.

<sup>7</sup> Previous nomenclature: *Chrysothamnus teretifolius*.

<sup>8</sup> Previous nomenclature: *Chrysothamnus nauseosus*.

<sup>9</sup> Previous nomenclature: *Happlopappus linearifolius*.

Table D-12. Mean Cover from LLG Vegetation Associations at Yucca Mountain for an Average Precipitation Year (1991)

LLG 1991					
Vegetation Type/Species	Life Form <sup>1</sup>	Cover (%)	Vegetation Type/Species	Life Form <sup>1</sup>	Cover (%)
<b>Annuals</b>			<b>Drought Deciduous</b>		
<i>Bromus madritensis ssp. rubens</i>	G	4.55	<i>Krameria erecta</i> <sup>2</sup>	S	0.96
<i>Amsinckia tessellata</i>	F	1.89	<i>Ambrosia dumosa</i>	S	0.49
<i>Mentzelia obscura</i>	F	0.88	<i>Lycium andersonii</i>	S	0.31
<i>Descurainia pinnata</i>	F	0.85	<i>Menodora spinescens</i>	S	0.21
<i>Lotus humistratus</i>	F	0.32	<i>Lycium pallidum</i>	S	0.18
<i>Linanthus demissus</i>	F	0.31	<i>Grayia spinosa</i>	S	0.09
<i>Unknown</i>	F	0.27	<i>Salazaria mexicana</i>	S	0.08
<i>Chorizanthe brevicornu</i>	F	0.18	<i>Eriogonum inflatum</i>	F	0.07
<i>Sisymbrium altissimum</i>	F	0.14	<i>Eriastrum eremicum</i>	F	0.06
<i>Chaenactis stevioides</i>	F	0.12	Others		0.16
<i>Eschescholzia minutiflora</i>	F	0.11		<b>Total</b>	<b>2.61</b>
<i>Phacelia fremontii</i>	F	0.06	<b>Evergreen</b>		
<i>Oxytheca perfoliata</i>	F	0.05	<i>Larrea tridentata</i>	S	1.92
<i>Malacothrix glabrata</i>	F	0.05	<i>Ephedra nevadensis</i>	S	1.78
<i>Cryptantha nevadensis</i>	F	0.05	<i>Hymenoclea salsola</i>	S	0.26
Others		0.26	<i>Coleogyne ramosissima</i>	S	0.11
	<b>Total</b>	<b>10.09</b>	<i>Ericameria cooperi</i> <sup>3</sup>	S	0.08
			<i>Chrysothamnus viscidiflorus</i>	S	0.01
				<b>Total</b>	<b>4.16</b>
			<b>Association Total 16.86</b>		

Source: Output DTN: MO0606SPAVEGAS.001.

NOTE: Means are based on data collected from twelve 200 × 200 m plots in 1991. Species are arranged in order of dominance within a vegetation type.

<sup>1</sup>G = grass, F = forb, S = shrub.

<sup>2</sup>Previous nomenclature: *Krameria parvifolia*.

<sup>3</sup>Previous nomenclature: *Happlopapus cooperi*.



Table D-13. Mean Cover from LA Vegetation Associations at Yucca Mountain for a Wet Year (1993)

LA 1993					
Vegetation Type/Species	Life Form <sup>1</sup>	Cover (%)	Vegetation Type/Species	Life Form <sup>1</sup>	Cover (%)
<b>Annuals</b>			<b>Drought Deciduous</b>		
<i>Chaenactis stevioides</i>	F	1.90	<i>Ambrosia dumosa</i>	S	6.03
<i>Bromus madritensis ssp rubens</i>	G	1.89	<i>Menodora spinescens</i>	S	1.61
<i>Pectocarya platycarpa</i>	F	0.69	<i>Lycium pallidum</i>	S	1.36
<i>Vulpia octoflora</i>	G	0.48	<i>Acamptopappus shockleyi</i>	S	1.06
<i>Cryptantha pterocarya</i>	F	0.41	<i>Krascheninnikovia lanata</i> <sup>2</sup>	S	0.19
Unknown		0.34	<i>Lycium andersonii</i>	S	0.16
<i>Eriophyllum pringlei</i>	F	0.24	<i>Atriplex confertifolia</i>	S	0.15
<i>Cryptantha spp</i>	F	0.21	<i>Achnatherum hymenoides</i> <sup>3</sup>	G	0.14
<i>Cryptantha micrantha</i>	F	0.14	<i>Krameria erecta</i> <sup>4</sup>	S	0.11
<i>Cryptantha circumscissa</i>	F	0.10	<i>Grayia spinosa</i>	S	0.10
<i>Cryptantha nevadensis</i>	F	0.09	<i>Psoralea fremontii</i>	S	0.07
<i>Malacothrix glabrata</i>	F	0.07	Others		0.14
<i>Amsinckia tessellata</i>	F	0.06		<b>Total</b>	<b>11.12</b>
<i>Rafinesquia neomexicana</i>	F	0.05	<b>Evergreen</b>		
Others		0.37	<i>Larrea tridentata</i>	S	1.86
<b>Total</b>		<b>7.04</b>	<i>Ephedra nevadensis</i>	S	0.50
			<i>Coleogyne ramosissima</i>	S	0.30
			<i>Ericameria cooperi</i> <sup>5</sup>	S	0.03
				<b>Total</b>	<b>2.69</b>
			<b>Association Total</b>		<b>20.85</b>

Source: Output DTN: MO0606SPAVEGAS.001.

NOTE: Means are based on data collected from twelve 200 × 200 m plots in 1993. Species are arranged in order of dominance within a vegetation type.

<sup>1</sup> G = grass, F = forb, S = shrub.

<sup>2</sup> Previous nomenclature: *Ceretoidea lanata*.

<sup>3</sup> Previous nomenclature: *Oryzopsis hymenoides*.

<sup>4</sup> Previous nomenclature: *Krameria parvifolia*.

<sup>5</sup> Previous nomenclature: *Happlopappus cooperi*.

Table D-14. Mean Cover from LG Vegetation Associations at Yucca Mountain for a Wet Year (1993)

LG 1993					
Vegetation Type/Species	Life Form <sup>1</sup>	Cover (%)	Vegetation Type/Species	Life Form <sup>1</sup>	Cover (%)
<b>Annuals</b>			<b>Drought Deciduous</b>		
<i>Bromus madritensis ssp rubens</i>	G	11.13	<i>Lycium andersonii</i>	S	2.07
<i>Cryptantha pterocarya</i>	F	0.69	<i>Grayia spinosa</i>	S	1.90
Unknown		0.50	<i>Eriogonum fasciculatum</i>	S	1.34
<i>Cryptantha spp</i>	F	0.48	<i>Ambrosia dumosa</i>	S	0.82
<i>Amsinckia tessellata</i>	F	0.35	<i>Atriplex confertifolia</i>	S	0.56
<i>Lotus humistratus</i>	F	0.15	<i>Pleuraphis jamesii</i> <sup>2</sup>	G	0.42
<i>Syntrichopappus fremontii</i>	F	0.11	<i>Salazaria mexicana</i>	S	0.41
<i>Cryptantha nevadensis</i>	F	0.11	<i>Krascheninnikovia lanata</i> <sup>3</sup>	S	0.40
<i>Cryptantha circumscissa</i>	F	0.09	<i>Menodora spinescens</i>	S	0.32
<i>Phacelia fremontii</i>	F	0.08	<i>Eriogonum inflatum</i>	F	0.19
<i>Pectocarya platycarpa</i>	F	0.07	<i>Sphaeralcea ambigua</i>	F	0.18
<i>Pectocarya setosa</i>	F	0.07	<i>Achnatherum speciosum</i> <sup>4</sup>	G	0.17
<i>Lupinus flavoculatus</i>	F	0.06	<i>Encelia virginensis</i>	S	0.12
<i>Bromus tectorum</i>	G	0.05	<i>Stephanomeria pauciflora</i>	F	0.11
<i>Chaenactis stevioides</i>	F	0.05	<i>Atriplex canescens</i>	S	0.11
Others		0.26	<i>Lycium pallidum</i>	S	0.07
	<b>Total</b>	<b>14.25</b>	<i>Mirabilis bigelovii</i>	F	0.06
			<i>Chamaesyce albomarginata</i> <sup>5</sup>	F	0.05
			Others		0.22
			<b>Total</b>		<b>9.52</b>
			<b>Evergreen</b>		
			<i>Ephedra nevadensis</i>	S	2.61
			<i>Ericameria cooperi</i> <sup>6</sup>	S	1.22
			<i>Hymenoclea salsola</i>	S	0.99
			<i>Ericameria teretifolia</i> <sup>7</sup>	S	0.39
			<i>Ephedra viridis</i>	S	0.30
			<i>Gutierrezia sarothrae</i>	S	0.23
			<i>Ericameria linearifolia</i> <sup>8</sup>	S	0.19
			<i>Chrysothamnus viscidiflorus</i>	S	0.14
			<i>Artemisia tridentata</i>	S	0.12
			<i>Ericameria nauseosa</i> <sup>9</sup>	S	0.11
			<i>Larrea tridentata</i>	S	0.10
			<i>Coleogyne ramosissima</i>	S	0.04
			<b>Total</b>		<b>6.44</b>
			<b>Association Total</b>		<b>30.21</b>

Source: Output DTN: MO0606SPAVEGAS.001.

NOTE: Means are based on data collected from twelve 200 × 200 m plots in 1993. Species are arranged in order of dominance within a vegetation type.

<sup>1</sup> G = grass, F = forb, S = shrub.

<sup>2</sup> Previous nomenclature: *Hilaria jamesii*.

<sup>3</sup> Previous nomenclature: *Ceretooides lanata*.

<sup>4</sup> Previous nomenclature: *Stipa speciosa*.

<sup>5</sup> Previous nomenclature: *Euphorbia albomarginata*.

<sup>6</sup> Previous nomenclature: *Happlopappus cooperi*.

<sup>7</sup> Previous nomenclature: *Chrysothamnus teretifolius*.

<sup>8</sup> Previous nomenclature: *Happlopappus linearifolius*.

<sup>9</sup> Previous nomenclature: *Chrysothamnus nauseosus*.

Table D-15. Mean Cover from LLG Vegetation Associations at Yucca Mountain for a Wet Year (1993)

LLG 1993					
Vegetation Type/Species	Life Form <sup>1</sup>	Cover (%)	Vegetation Type/Species	Life Form <sup>1</sup>	Cover (%)
<b>Annuals</b>			<b>Drought Deciduous</b>		
<i>Bromus madritensis ssp rubens</i>	G	16.17	<i>Ambrosia dumosa</i>	S	1.23
<i>Amsinckia tessellata</i>	F	3.59	<i>Lycium andersonii</i>	S	0.53
<i>Lotus humistratus</i>	F	0.53	<i>Krameria erecta</i> <sup>2</sup>	S	0.47
<i>Cryptantha pterocarya</i>	F	0.44	<i>Lycium pallidum</i>	S	0.44
<i>Vulpia octoflora</i>	G	0.24	<i>Menodora spinescens</i>	S	0.31
Unknown		0.11	<i>Salazaria mexicana</i>	S	0.27
<i>Pectocarya platycarpa</i>	F	0.10	<i>Eriogonum inflatum</i>	F	0.16
<i>Chaenactis stevioides</i>	F	0.09	<i>Chamaesyce albomarginata</i> <sup>3</sup>	F	0.11
<i>Cryptantha spp</i>	F	0.07	<i>Grayia spinosa</i>	S	0.10
<i>Erodium cicutarium</i>	F	0.05	<i>Krascheninnikovia lanata</i> <sup>4</sup>	S	0.08
<i>Pectocarya setosa</i>	F	0.05	<i>Eriogonum fasciculatum</i>	S	0.05
<i>Phacelia fremontii</i>	F	0.04	<i>Encelia virginensis</i>	S	0.05
Others		0.26	<i>Achnatherum speciosum</i> <sup>5</sup>	G	0.05
	<b>Total</b>	21.74	Others		0.24
			<b>Total</b>		4.09
			<b>Evergreen</b>		
			<i>Larrea tridentata</i>	S	3.05
			<i>Ephedra nevadensis</i>	S	2.17
			<i>Hymenoclea salsola</i>	S	0.66
			<i>Coleogyne ramosissima</i>	S	0.14
			<i>Ericameria cooperi</i> <sup>6</sup>	S	0.14
			<b>Total</b>		6.16
			<b>Association Total</b>		<b>31.99</b>

Source: Output DTN: MO0606SPAVEGAS.001.

NOTE: Means are based on data collected from twelve 200 × 200 m plots in 1993. Species are arranged in order of dominance within a vegetation type.

<sup>1</sup> G = grass, F = forb, S = shrub.

<sup>2</sup> Previous nomenclature: *Krameria parvifolia*.

<sup>3</sup> Previous nomenclature: *Euphorbia albomarginata*.

<sup>4</sup> Previous nomenclature: *Ceretooides lanata*.

<sup>5</sup> Previous nomenclature: *Stipa speciosa*.

<sup>6</sup> Previous nomenclature: *Happlopappus cooperi*.

To assess variability among ESPs within each association, and for the NDVI' analysis in Appendix E, association means, standard deviations, standard errors, 90% confidence intervals, and sample size requirements for percent cover were calculated (Table D-16). Total mean cover for the ESPs was placed in a separate Excel® worksheet in Output DTN: MO0606SPAVEGAS.001. Association means and standard deviations (Table D-16) were calculated using the AVERAGE and STDEV commands. Standard errors (Table D-16) were calculated according to Bohnam (1989 [DIRS 127406], p. 64, Equation 3.30) as the standard deviation divided by the square root of n (n = number of ESPs included in the mean calculation). Ninety percent confidence intervals (Table D-16) were calculated according to the following equation (Bohnam 1989 [DIRS 127406], p. 64, Equation 3.33):

$$CI = \frac{t s_c}{\sqrt{n}} \quad (\text{Eq. D-10})$$

where

- $CI$  = Confidence interval
- $t$  = t-table value for single tailed test, with  $\alpha = 0.10$ , and  $n-1$  degrees of freedom
- $s_c$  = Standard deviation of cover data
- $n$  = Number of ESPs in mean calculation.

The following equation was used to determine if an adequate number of ESPs had been sampled to represent cover for the associations at Yucca Mountain (Bonham 1989 [DIRS 127406], p. 67, Equation 3.43):

$$n_c = \frac{t^2 s_c^2}{(d\bar{x}_c)^2} \quad (\text{Eq. D-11})$$

where

- $n_c$  = Number of ESPs required to sample cover of an association to within 10% of the true population mean,
- $t$  = t-table value for single tailed test, with  $\alpha = 0.10$ , and  $n-1$  degrees of freedom,
- $s_c$  = Standard deviation of cover data for ESPs,
- $d$  = Precision that the true difference of the sample mean occurs from the population (= 0.10),
- $\bar{x}_c$  = Mean of cover data for ESPs.

Twelve ESPs were adequate to sample within 10% of the true cover mean for the three vegetation associations (Table D-16). In all cases, more ESPs were sampled than required to meet the designated precision (Table D-16).

Table D-16. Vegetation Cover for Ecological Study Plots Representing the LA, LG, and LLG Vegetation Associations

Cover (%) for LA ESPs				Cover (%) for LG ESPs				Cover (%) for LLG ESPs			
ESP <sup>1</sup>	1990	1991	1993	ESP <sup>2</sup>	1990	1991	1993	ESP <sup>3</sup>	1990	1991	1993
LA2C	12.38	12.50	21.12	LG1C	13.12	15.50	30.87	LLG3C	16.75	16.12	31.72
LA3C	15.25	11.25	22.28	LG2C	15.62	16.88	31.87	LLG4C	12.62	15.50	30.38
LA4C	14.62	14.50	19.12	LG3C	17.38	20.38	36.76	LLG5C	12.87	19.94	32.54
LA5C	15.00	8.75	15.00	LG4C	15.25	14.38	30.38	LLG7C	13.50	16.88	28.88
LA6C	16.25	10.63	23.28	LG5C	13.88	17.62	23.15	LLG8C	14.75	17.12	39.25
LA7C	18.75	13.88	15.75	LG6C	17.38	13.37	25.12	LLG9C	14.25	17.39	25.38
LA1T	12.70	8.12	17.98	LG2T	20.10	22.80	37.00	LLG1T	13.30	19.30	36.76
LA2T	15.80	7.50	18.42	LG3T	14.30	20.40	31.00	LLG2T	8.40	16.90	38.67
LA3T	10.50	8.31	27.20	LG4T	16.60	15.00	28.51	LLG4T	17.40	18.20	29.83
LA4T	13.90	7.50	23.20	LG5T	13.90	11.89	24.09	LLG5T	12.60	18.00	35.62
LA5T	13.60	9.79	22.49	LG6T	14.60	16.80	34.23	LLG6T	12.70	14.67	27.17
LA7T	16.00	13.68	24.28	LG7T	16.00	15.00	29.46	LLG7T	n.d. <sup>4</sup>	12.70	27.42
Mean	14.56	10.53	20.84		15.68	16.67	30.20		13.56	16.89	31.97
SD <sup>5</sup>	2.15	2.60	3.64		1.97	3.19	4.53		2.38	1.99	4.66
SE <sup>6</sup>	0.62	0.75	1.05		0.57	0.92	1.31		0.72	0.57	1.34
90% CI <sup>7</sup>	0.85	1.02	1.43		0.77	1.26	1.78		0.98	0.78	1.83
Samples required <sup>8</sup>	4	11	6		3	7	4		6	3	4

Source: Output DTN: MO0606SPAPEGAS.001.

<sup>1</sup> Name of individual ecological study plots (ESP) representing the *Larrea–Ambrosia* (LA) vegetation association.

<sup>2</sup> Name of individual ESPs representing the *Lycium–Grayia* (LG) vegetation association.

<sup>3</sup> Name of individual ESPs representing the *Larrea–Lycium–Grayia* (LLG) vegetation association.

<sup>4</sup> No data collected from LLG7T in 1990.

<sup>5</sup> Standard deviation.

<sup>6</sup> Standard error.

<sup>7</sup> Confidence interval for vegetation cover mean calculated using Equation D-10.

<sup>8</sup> Number of ESPs required to adequately represent cover of vegetation associations. Samples required were calculated using Equation D-11.

### D3.2.3 Stomatal Resistance

Several studies were identified for Mojave Desert plant species that included measurements of stomatal conductance (Table D-17). Only studies that were conducted in the vicinity of Yucca Mountain or nearby Mojave Desert regions were considered. Many of the studies reviewed were conducted at the Nevada Desert Free-Air CO<sub>2</sub> Enrichment (FACE) Facility located on the NTS (Naumburg et al. 2003 [DIRS 177143], p. 277 for description of site). These studies included conductance measurements made under elevated and ambient CO<sub>2</sub> conditions (e.g., Naumburg et al. 2003 [DIRS 177143]). Only plants in these studies that were measured under ambient CO<sub>2</sub> conditions were considered for this analysis. Conductance values measured under a variety of Mojave Desert conditions during several time periods were selected for dominant species in the three vegetation types so that representative mean values could be calculated for periods of low (initial growth stage and end of the late growth stage) and high (midseason) physiological activity. Relatively lower conductance values reported in the literature were used to represent

leaves at initiation of growth (initial growth stage) and old leaves near senescence (end of late growth stage). Higher conductance values were used to represent young fully expanded leaves expected during the midseason growth stage. Low conductance values indicating stomatal closure or dormancy (equal to or less than  $0.01 \text{ mol m}^{-2} \text{ s}^{-1}$ ) that were reported in some of the studies were not used in this analysis or reported in Table D-17. These low values were ignored because they reflect conditions when the plants were not active (nongrowing season or under other stress) and are thus not representative for estimating stomatal resistance.

Table D-17. Stomatal Conductance References and Values for Mojave Desert Plant Species

Reference	Species	Stomatal Conductance	Temperature	Comments
Huxman et al. 1999 [DIRS 177133], p. 770 [ambient temperature] and 774 [stomatal conductance]	<i>Bromus madritensis ssp rubens</i>	750 ( $\text{mmol m}^{-2} \text{ s}^{-1}$ )	Approximate average of ambient air temperature during the measurement period = $25.0^\circ\text{C}$	Prereproductive measurement. Glasshouse at UNLV <sup>1</sup> . Ambient outdoor conditions were tracked inside glasshouse.
		500 ( $\text{mmol m}^{-2} \text{ s}^{-1}$ )	$25.0^\circ\text{C}$	Measurement made during seed fill.
Huxman and Smith 2001 [DIRS 177132], p. 197	<i>Bromus madritensis ssp rubens</i>	180 ( $\text{mmol m}^{-2} \text{ s}^{-1}$ )	Leaf temperature = $15.0^\circ\text{C}$	Measurements made in the field at the FACE <sup>2</sup> site. Measurements were midday maximum values and were made over course of growing season (DOY 69 to 103).
		300 ( $\text{mmol m}^{-2} \text{ s}^{-1}$ )	$18.0^\circ\text{C}$	
		100 ( $\text{mmol m}^{-2} \text{ s}^{-1}$ )	$21.0^\circ\text{C}$	
		200 ( $\text{mmol m}^{-2} \text{ s}^{-1}$ )	$24.0^\circ\text{C}$	
		100 ( $\text{mmol m}^{-2} \text{ s}^{-1}$ )	$27.0^\circ\text{C}$	
Hamerlynck et al. 2002 [DIRS 177128], p. 101	<i>Lycium andersonii</i>	0.225 ( $\text{mol m}^{-2} \text{ s}^{-1}$ )	Average high air temperature during study period = $20.8^\circ\text{C}$	Measurements made in the field at the FACE site over course of growing season (DOY 90 to 146). Conductances are the average midday maximum values of long shoots and short shoots measured during the same time period.
		0.39 ( $\text{mol m}^{-2} \text{ s}^{-1}$ )	$20.8^\circ\text{C}$	
		0.25 ( $\text{mol m}^{-2} \text{ s}^{-1}$ )	$20.8^\circ\text{C}$	
		0.525 ( $\text{mol m}^{-2} \text{ s}^{-1}$ )	$20.8^\circ\text{C}$	
		0.375 ( $\text{mol m}^{-2} \text{ s}^{-1}$ )	$20.8^\circ\text{C}$	
Naumburg et al. 2003 [DIRS 177143], p. 280, Figure 3	<i>Ambrosia dumosa</i>	300 ( $\text{mmol m}^{-2} \text{ s}^{-1}$ )	Mean air temperature = $19.0^\circ\text{C}$	Daily average stomatal conductance measurements made in the field at the FACE site during various months. Due to paucity of data for drought deciduous species, high conductance values measured in October and November (beyond the late season growth stage) were used.
		200 ( $\text{mmol m}^{-2} \text{ s}^{-1}$ )	$19.0^\circ\text{C}$	
		50 ( $\text{mmol m}^{-2} \text{ s}^{-1}$ )	$28.5^\circ\text{C}$	
		50 ( $\text{mmol m}^{-2} \text{ s}^{-1}$ )	$28.5^\circ\text{C}$	
		200 ( $\text{mmol m}^{-2} \text{ s}^{-1}$ )	$28.5^\circ\text{C}$	
		90 ( $\text{mmol m}^{-2} \text{ s}^{-1}$ )	$28.5^\circ\text{C}$	
		50 ( $\text{mmol m}^{-2} \text{ s}^{-1}$ )	$28.5^\circ\text{C}$	
Naumburg et al. 2003 [DIRS 177143], p. 280	<i>Krameria erecta</i>	100 ( $\text{mmol m}^{-2} \text{ s}^{-1}$ )	Mean chamber air temperature = $28.5^\circ\text{C}$	Average daily stomatal conductance measurements made in the field at the FACE site during various months. Three low values indicating stomatal closure were omitted.
		90 ( $\text{mmol m}^{-2} \text{ s}^{-1}$ )	$28.5^\circ\text{C}$	
		90 ( $\text{mmol m}^{-2} \text{ s}^{-1}$ )	$28.5^\circ\text{C}$	
		140 ( $\text{mmol m}^{-2} \text{ s}^{-1}$ )	$19.0^\circ\text{C}$	
		50 ( $\text{mmol m}^{-2} \text{ s}^{-1}$ )	$28.5^\circ\text{C}$	

Table D-17. Stomatal Conductance References and Values for Mojave Desert Plant Species (Continued)

Reference	Species	Stomatal Conductance	Temperature	Comments
		30 (mmol m <sup>-2</sup> s <sup>-1</sup> )	28.5°C	
		75 (mmol m <sup>-2</sup> s <sup>-1</sup> )	28.5°C	
		75 (mmol m <sup>-2</sup> s <sup>-1</sup> )	28.5°C	
		50 (mmol m <sup>-2</sup> s <sup>-1</sup> )	28.5°C	
		50 (mmol m <sup>-2</sup> s <sup>-1</sup> )	28.5°C	
		75 (mmol m <sup>-2</sup> s <sup>-1</sup> )	28.5°C	
		40 (mmol m <sup>-2</sup> s <sup>-1</sup> )	28.5°C	
Hamerlynck et al. 2000 [DIRS 177130], p. 188	<i>Larrea tridentata</i>	400 (mmol m <sup>-2</sup> s <sup>-1</sup> )	Chamber air temperature = 30.0°C	Glasshouse study at UNLV <sup>2</sup> . Pre- and post-heat treatments under well watered and drought conditions. Measurements made during high heat treatment were not used. Measurements made under drought conditions were used to represent low values expected of older leaves near senescence.
		500 (mmol m <sup>-2</sup> s <sup>-1</sup> )	30.0°C	
		750 (mmol m <sup>-2</sup> s <sup>-1</sup> )	30.0°C	
		200 (mmol m <sup>-2</sup> s <sup>-1</sup> )	30.0°C	
		150 (mmol m <sup>-2</sup> s <sup>-1</sup> )	30.0°C	
		25 (mmol m <sup>-2</sup> s <sup>-1</sup> )	30.0°C	
		100 (mmol m <sup>-2</sup> s <sup>-1</sup> )	30.0°C	
		25 (mmol m <sup>-2</sup> s <sup>-1</sup> )	30.0°C	
Hamerlynck et al. 2004 [DIRS 176045], p. 213	<i>Larrea tridentata</i>	120 (mmol m <sup>-2</sup> s <sup>-1</sup> )	Air temperature = 27.0°C	Measurements made in field in the Mojave National Preserve, CA, during peak growth and dry period. Plants grown on dune soils.
		85 (mmol m <sup>-2</sup> s <sup>-1</sup> )	35.0°C	Measurement made during dry period used to represent low values expected of older leaves near senescence.
Hamerlynck et al. 2000 [DIRS 177022], p. 602	<i>Larrea tridentata</i>	110 (mmol m <sup>-2</sup> s <sup>-1</sup> )	Chamber temperature = 20.0°C	Measurements made in field in the Mojave National Preserve, CA, at various times throughout growing season. Plants grown on dune soils. Measurements made during dry periods were used to represent low values expected of older leaves near senescence.
		70 (mmol m <sup>-2</sup> s <sup>-1</sup> )	12.0°C	
		120 (mmol m <sup>-2</sup> s <sup>-1</sup> )	25.0°C	
		85 (mmol m <sup>-2</sup> s <sup>-1</sup> )	35.0°C	
		80 (mmol m <sup>-2</sup> s <sup>-1</sup> )	40.0°C	
		80 (mmol m <sup>-2</sup> s <sup>-1</sup> )	30.0°C	
		65 (mmol m <sup>-2</sup> s <sup>-1</sup> )	40.0°C	
		65 (mmol m <sup>-2</sup> s <sup>-1</sup> )	40.0°C	
		70 (mmol m <sup>-2</sup> s <sup>-1</sup> )	30.0°C	
Naumburg et al. 2003 [DIRS 177143], p. 280, Figure 3)	<i>Larrea tridentata</i>	125 (mmol m <sup>-2</sup> s <sup>-1</sup> )	Mean prevailing air temperature during measurements = 28.5°C	Measurements made in field at FACE facility over the course of four years. One value measured in December was omitted. Five low values indicating stomatal closure were omitted.
		50 (mmol m <sup>-2</sup> s <sup>-1</sup> )	28.5°C	
		125 (mmol m <sup>-2</sup> s <sup>-1</sup> )	28.5°C	
		100 (mmol m <sup>-2</sup> s <sup>-1</sup> )	28.5°C	
		50 (mmol m <sup>-2</sup> s <sup>-1</sup> )	28.5°C	
		30 (mmol m <sup>-2</sup> s <sup>-1</sup> )	28.5°C	
		125 (mmol m <sup>-2</sup> s <sup>-1</sup> )	19.0°C	
		30 (mmol m <sup>-2</sup> s <sup>-1</sup> )	28.5°C	
		40 (mmol m <sup>-2</sup> s <sup>-1</sup> )	28.5°C	

Table D-17. Stomatal Conductance References and Values for Mojave Desert Plant Species (Continued)

Reference	Species	Stomatal Conductance	Temperature	Comments
		100 (mmol m <sup>-2</sup> s <sup>-1</sup> )	28.5°C	
		50 (mmol m <sup>-2</sup> s <sup>-1</sup> )	28.5°C	
		40 (mmol m <sup>-2</sup> s <sup>-1</sup> )	28.5°C	
		30 (mmol m <sup>-2</sup> s <sup>-1</sup> )	28.5°C	
		30 (mmol m <sup>-2</sup> s <sup>-1</sup> )	28.5°C	
Pataki et al. (2000 [DIRS 177161], p. 893)	<i>Larrea tridentata</i>	90 (mmol m <sup>-2</sup> s <sup>-1</sup> )	Average air temperature during measurement period = 24.0°C	Measurements made in field at FACE facility midJune through midJuly.
		90 (mmol m <sup>-2</sup> s <sup>-1</sup> )	24.0°C	
		80 (mmol m <sup>-2</sup> s <sup>-1</sup> )	24.0°C	
		80 (mmol m <sup>-2</sup> s <sup>-1</sup> )	24.0°C	
		80 (mmol m <sup>-2</sup> s <sup>-1</sup> )	24.0°C	
		80 (mmol m <sup>-2</sup> s <sup>-1</sup> )	24.0°C	
		90 (mmol m <sup>-2</sup> s <sup>-1</sup> )	24.0°C	
		90 (mmol m <sup>-2</sup> s <sup>-1</sup> )	24.0°C	
		90 (mmol m <sup>-2</sup> s <sup>-1</sup> )	24.0°C	
		90 (mmol m <sup>-2</sup> s <sup>-1</sup> )	24.0°C	
		90 (mmol m <sup>-2</sup> s <sup>-1</sup> )	24.0°C	
		70 (mmol m <sup>-2</sup> s <sup>-1</sup> )	24.0°C	
		80 (mmol m <sup>-2</sup> s <sup>-1</sup> )	24.0°C	
		70 (mmol m <sup>-2</sup> s <sup>-1</sup> )	24.0°C	
		80 (mmol m <sup>-2</sup> s <sup>-1</sup> )	24.0°C	
		70 (mmol m <sup>-2</sup> s <sup>-1</sup> )	24.0°C	
		70 (mmol m <sup>-2</sup> s <sup>-1</sup> )	24.0°C	
		70 (mmol m <sup>-2</sup> s <sup>-1</sup> )	24.0°C	
		70 (mmol m <sup>-2</sup> s <sup>-1</sup> )	24.0°C	
		70 (mmol m <sup>-2</sup> s <sup>-1</sup> )	24.0°C	
		70 (mmol m <sup>-2</sup> s <sup>-1</sup> )	24.0°C	
		70 (mmol m <sup>-2</sup> s <sup>-1</sup> )	24.0°C	
		60 (mmol m <sup>-2</sup> s <sup>-1</sup> )	24.0°C	
		60 (mmol m <sup>-2</sup> s <sup>-1</sup> )	24.0°C	
		60 (mmol m <sup>-2</sup> s <sup>-1</sup> )	24.0°C	
		60 (mmol m <sup>-2</sup> s <sup>-1</sup> )	24.0°C	
		50 (mmol m <sup>-2</sup> s <sup>-1</sup> )	24.0°C	
		60 (mmol m <sup>-2</sup> s <sup>-1</sup> )	24.0°C	
		50 (mmol m <sup>-2</sup> s <sup>-1</sup> )	24.0°C	
		50 (mmol m <sup>-2</sup> s <sup>-1</sup> )	24.0°C	
		50 (mmol m <sup>-2</sup> s <sup>-1</sup> )	24.0°C	
		50 (mmol m <sup>-2</sup> s <sup>-1</sup> )	24.0°C	
		50 (mmol m <sup>-2</sup> s <sup>-1</sup> )	24.0°C	
		90 (mmol m <sup>-2</sup> s <sup>-1</sup> )	24.0°C	
		60 (mmol m <sup>-2</sup> s <sup>-1</sup> )	24.0°C	
		160 (mmol m <sup>-2</sup> s <sup>-1</sup> )	24.0°C	Maximum diurnal value



Table D-17. Stomatal Conductance References and Values for Mojave Desert Plant Species (Continued)

Reference	Species	Stomatal Conductance	Temperature	Comments
		160 (mmol m <sup>-2</sup> s <sup>-1</sup> )	24.0°C	Maximum diurnal value
		100 (mmol m <sup>-2</sup> s <sup>-1</sup> )	24.0°C	Maximum diurnal value
Pataki et al. (2000 [DIRS 177161], p. 893)	<i>Ephedra nevadensis</i>	190 (mmol m <sup>-2</sup> s <sup>-1</sup> )	Average air temperature during measurement period = 24.0°C	Measurements made in field at FACE site mid-June through mid-July
		190 (mmol m <sup>-2</sup> s <sup>-1</sup> )	24.0°C	
		170 (mmol m <sup>-2</sup> s <sup>-1</sup> )	24.0°C	
		170 (mmol m <sup>-2</sup> s <sup>-1</sup> )	24.0°C	
		160 (mmol m <sup>-2</sup> s <sup>-1</sup> )	24.0°C	
		150 (mmol m <sup>-2</sup> s <sup>-1</sup> )	24.0°C	
		170 (mmol m <sup>-2</sup> s <sup>-1</sup> )	24.0°C	
		160 (mmol m <sup>-2</sup> s <sup>-1</sup> )	24.0°C	
		150 (mmol m <sup>-2</sup> s <sup>-1</sup> )	24.0°C	
		160 (mmol m <sup>-2</sup> s <sup>-1</sup> )	24.0°C	
		160 (mmol m <sup>-2</sup> s <sup>-1</sup> )	24.0°C	
		120 (mmol m <sup>-2</sup> s <sup>-1</sup> )	24.0°C	
		130 (mmol m <sup>-2</sup> s <sup>-1</sup> )	24.0°C	
		130 (mmol m <sup>-2</sup> s <sup>-1</sup> )	24.0°C	
		130 (mmol m <sup>-2</sup> s <sup>-1</sup> )	24.0°C	
		120 (mmol m <sup>-2</sup> s <sup>-1</sup> )	24.0°C	
		130 (mmol m <sup>-2</sup> s <sup>-1</sup> )	24.0°C	
		130 (mmol m <sup>-2</sup> s <sup>-1</sup> )	24.0°C	
		130 (mmol m <sup>-2</sup> s <sup>-1</sup> )	24.0°C	
		120 (mmol m <sup>-2</sup> s <sup>-1</sup> )	24.0°C	
		130 (mmol m <sup>-2</sup> s <sup>-1</sup> )	24.0°C	
		120 (mmol m <sup>-2</sup> s <sup>-1</sup> )	24.0°C	
		110 (mmol m <sup>-2</sup> s <sup>-1</sup> )	24.0°C	
		90 (mmol m <sup>-2</sup> s <sup>-1</sup> )	24.0°C	
		110 (mmol m <sup>-2</sup> s <sup>-1</sup> )	24.0°C	
		110 (mmol m <sup>-2</sup> s <sup>-1</sup> )	24.0°C	
		70 (mmol m <sup>-2</sup> s <sup>-1</sup> )	24.0°C	
		60 (mmol m <sup>-2</sup> s <sup>-1</sup> )	24.0°C	
		60 (mmol m <sup>-2</sup> s <sup>-1</sup> )	24.0°C	
		50 (mmol m <sup>-2</sup> s <sup>-1</sup> )	24.0°C	
80 (mmol m <sup>-2</sup> s <sup>-1</sup> )	24.0°C			
60 (mmol m <sup>-2</sup> s <sup>-1</sup> )	24.0°C			
Smith et al. (1995 [DIRS 103628], p. 343)	<i>Ephedra nevadensis</i>	0.078 (mol m <sup>-2</sup> s <sup>-1</sup> )	Temperature = 25°C	Maximum daily stomatal conductance measurements made at field sites in Crater Flat March through September. Conductance values are means for three locations (slope, bench, and wash). Two
		0.075 (mol m <sup>-2</sup> s <sup>-1</sup> )	25°C	
		0.093 (mol m <sup>-2</sup> s <sup>-1</sup> )	25°C	
		0.060 (mol m <sup>-2</sup> s <sup>-1</sup> )	25°C	
		0.033 (mol m <sup>-2</sup> s <sup>-1</sup> )	25°C	

Table D–17. Stomatal Conductance References and Values for Mojave Desert Plant Species (Continued)

Reference	Species	Stomatal Conductance	Temperature	Comments
		0.015 (mol m <sup>-2</sup> s <sup>-1</sup> )	25°C	measurements made in mid-October and mid-December were omitted. Temperature was not reported in study.
		0.025 (mol m <sup>-2</sup> s <sup>-1</sup> )	25°C	
Smith et al. (1995 [DIRS 103628], p. 344)	<i>Ericameria cooperi</i> <sup>3</sup>	0.18 (mol m <sup>-2</sup> s <sup>-1</sup> )	Temperature = 25°C	Maximum daily stomatal conductance measurements made at field sites in Crater Flat March through September. Values are means for two locations (slope and bench). Two measurements made in mid-October and mid-December were omitted. One low measurement in August indicating stomatal closure was omitted.
		0.15 (mol m <sup>-2</sup> s <sup>-1</sup> )	25°C	
		0.2 (mol m <sup>-2</sup> s <sup>-1</sup> )	25°C	
		0.085 (mol m <sup>-2</sup> s <sup>-1</sup> )	25°C	
		0.09 (mol m <sup>-2</sup> s <sup>-1</sup> )	25°C	
		0.04 (mol m <sup>-2</sup> s <sup>-1</sup> )	25°C	

<sup>1</sup> University of Nevada Las Vegas.

<sup>2</sup> Nevada Desert Free-Air CO<sub>2</sub> Enrichment (FACE) facility.

<sup>3</sup> Reported in Smith et al. 1995 [DIRS 103628] as *Happlopapus cooperi*.

Equation D-6 requires stomatal resistance ( $r_s$ , the inverse of stomatal conductance) to diffusion of water vapor in units of s m<sup>-1</sup>. Therefore, published stomatal conductance values were converted from units of mol m<sup>-2</sup> s<sup>-1</sup> to velocity units in m s<sup>-1</sup> according to the following conversion factor (LI-COR 1989 [DIRS 177166], p. 3-5):

$$g_v = \frac{(g_m \times R \times T_l)}{P} \quad (\text{Eq. D-12})$$

where

- $g_v$  = stomatal conductance in velocity units (m s<sup>-1</sup>),
- $g_m$  = stomatal conductance in molar units (mol m<sup>-2</sup> s<sup>-1</sup>),
- $R$  = universal gas constant (8.314 Pa m<sup>3</sup> mol<sup>-1</sup> K<sup>-1</sup>),
- $T_l$  = leaf temperature (K),
- $P$  = atmospheric pressure (Pa).

Atmospheric pressure is dependent on elevation. The FACE facility, where most of the conductance data were measured, is at an elevation of 970 m (Naumburg et al. 2003 [DIRS 177143], p. 277), and the study in Crater Flat by Smith et al. (1995 [DIRS 103628], p. 340) was conducted at 1,300 m. To generate resistance values that would be representative of dominant vegetation types at Yucca Mountain, atmospheric pressure was determined for the elevations at which most of the conductance measurements were made and for two additional elevations at Yucca Mountain. Atmospheric pressure for the four elevations were determined from Allen et al. (1998 [DIRS 157311], Table 2.1, pp. 213 and 214). The mean of these pressures (Table D-18) was used in the conductance conversion calculations for all species except *L. tridentata*. Because *L. tridentata* is generally absent above 1,350 m (Rundel and Gibson 1996 [DIRS 103614], p. 84), mean atmospheric pressures for 970 m and 1,300 m were used in the conversion calculations for this species (Table D-18).

Table D-18. Elevation and Atmospheric Pressure

Elevation (m)	Atmospheric Pressure <sup>a</sup> (Pa)	Mean Atmospheric Pressure (Pa)
970 <sup>b</sup>	90,300	<i>L. tridentata</i> = 88,550
1,300 <sup>c</sup>	86,800	
1,400	85,800	86,925
1,500	84,800	

Sources: <sup>a</sup> From Allen et al. 1998 [DIRS 157311], Table 2.1, pp. 213 and 214.

<sup>b</sup> Naumburg et al. 2003 [DIRS 177143], p. 277.

<sup>c</sup> Smith et al. (1995 [DIRS 103628], p. 340.

The leaf temperature at which conductance measurements were made was reported for some of the studies (Table D-17). In cases where leaf temperature was not reported, the ambient air temperature at which the study was conducted was used. Smith et al. (1995 [DIRS 103628]) did not report leaf or air temperatures at which conductance measurements were made. In this case, a temperature of 25°C was used to represent the temperature at which plants generally operate at full stomatal opening.

Temperatures were converted from °C to K:

$$K = ^\circ C + 273.15 \quad (\text{Eq. D-13})$$

Conversions of stomatal conductance from molar units to velocity units and temperature from Celsius to kelvin are in Table D-19. Prior to conversions (Table D-19, column 3), conductance data were sorted for each species and assigned to initial, mid, and end of late season stages. Maximum stomatal conductance rates are species specific and vary across vegetation types. In general, annual species exhibit higher conductances, followed by drought deciduous, then evergreen species. To determine high and low values, conductances were examined for each species within a vegetation type. High values measured on nonstressed plants were assigned to the midseason stage for each species. Low conductance values, generally 0.10 mol m<sup>-2</sup> s<sup>-1</sup> or less and 0.08 mol m<sup>-2</sup> s<sup>-1</sup> or less (depending on the species), were assigned to the initial stage and end of late stages, respectively, to represent the lower values expected of emerging or senescing leaves. In cases where only one low conductance value was available (e.g., *Bromus madritensis*), it was used for both the initial and end of late season stages. For some species (e.g., *L. andersonii*) only high values appropriate for the midseason stage were reported in the reviewed literature.

Table D-19. Stomatal Conductance Values Converted From Molar Units to Velocity Units

Species	Growth Stage	$g^1$ (mol m <sup>-2</sup> s <sup>-1</sup> )	T <sup>2</sup> (°C)	T <sup>3</sup> (K)	$g^4$ (m s <sup>-1</sup> )
<b>Annual Species</b>					
<i>Bromus madritensis</i> ssp. <i>rubens</i>	Initial/End	0.1	21	294.15	0.0028
		0.1	27	300.15	0.0029
	Mid	0.75	25	298.15	0.0214
		0.50	25	298.15	0.0143
		0.18	15	288.15	0.0050

Table D-19. Stomatal Conductance Values Converted From Molar Units to Velocity Units (Continued)

Species	Growth Stage	$g^1$ ( $\text{mol m}^{-2} \text{s}^{-1}$ )	$T^2$ ( $^{\circ}\text{C}$ )	$T^3$ (K)	$g^4$ ( $\text{m s}^{-1}$ )
<i>Bromus madritensis</i> ssp. <i>rubens</i>	Mid	0.3	18	291.15	0.0084
		0.2	24	297.15	0.0057
<b>Drought Deciduous Species</b>					
<i>Ambrosia dumosa</i>	Initial	0.09	28.5	301.65	0.0026
	Mid	0.3	19	292.15	0.0084
		0.2	19	292.15	0.0056
		0.2	28.5	301.65	0.0058
	End	0.05	28.5	301.65	0.0014
		0.05	28.5	301.65	0.0014
		0.05	28.5	292.15	0.0014
<i>Krameria erecta</i>	Initial	0.1	28.5	301.65	0.0029
		0.09	28.5	301.65	0.0026
		0.09	28.5	301.65	0.0026
		0.075	28.5	301.65	0.0022
		0.075	28.5	301.65	0.0022
		0.075	28.5	301.65	0.0022
	Mid	0.14	19	292.15	0.0039
	End	0.05	28.5	301.65	0.0014
		0.05	28.5	301.65	0.0014
		0.04	28.5	301.65	0.0012
		0.03	28.5	301.65	0.0009
		0.05	28.5	301.65	0.0014
	<i>Lycium andersonii</i>	Mid	0.225	20.8	293.95
0.39			20.8	293.95	0.0110
0.25			20.8	293.95	0.0070
0.525			20.8	293.95	0.0148
0.375			20.8	293.95	0.0105
<b>Evergreen Species</b>					
<i>Ephedra nevadensis</i>	Initial	0.1100	24	297.15	0.0031
		0.1100	24	297.15	0.0031
		0.1100	24	297.15	0.0031
		0.0933	25	298.15	0.0027
		0.0900	24	297.15	0.0026
	Mid	0.1900	24	297.15	0.0054
		0.1900	24	297.15	0.0054
		0.1700	24	297.15	0.0048
		0.1700	24	297.15	0.0048
		0.1700	24	297.15	0.0048
		0.1600	24	297.15	0.0045
		0.1600	24	297.15	0.0045
		0.1500	24	297.15	0.0043
		0.1600	24	297.15	0.0045
		0.1600	24	297.15	0.0045

Table D-19. Stomatal Conductance Values Converted From Molar Units to Velocity Units (Continued)

Species	Growth Stage	$g^1$ ( $\text{mol m}^{-2} \text{s}^{-1}$ )	$T^2$ ( $^{\circ}\text{C}$ )	$T^3$ (K)	$g^4$ ( $\text{m s}^{-1}$ )
<i>Ephedra nevadensis</i>	Mid	0.1300	24	297.15	0.0037
		0.1300	24	297.15	0.0037
		0.1300	24	297.15	0.0037
		0.1300	24	297.15	0.0037
		0.1300	24	297.15	0.0037
		0.1300	24	297.15	0.0037
		0.1300	24	297.15	0.0037
		0.1200	24	297.15	0.0034
		0.1200	24	297.15	0.0034
		0.1200	24	297.15	0.0034
		0.1200	24	297.15	0.0034
		0.1200	24	297.15	0.0034
		0.1200	24	297.15	0.0034
	End	0.0800	24	297.15	0.0023
		0.0783	25	298.15	0.0022
		0.0750	25	298.15	0.0021
		0.0700	24	297.15	0.0020
		0.0600	25	298.15	0.0017
		0.0600	24	297.15	0.0017
		0.0600	24	297.15	0.0017
0.0600		24	297.15	0.0017	
0.0500		24	297.15	0.0014	
0.0330		25	298.15	0.0009	
0.0250	25	298.15	0.0007		
0.0150	25	298.15	0.0004		
<i>Ericameria cooperi</i> <sup>1</sup>	Initial	0.0900	25	298.15	0.0026
	Mid	0.0850	25	298.15	0.0024
		0.2000	25	298.15	0.0057
		0.1800	25	298.15	0.0051
		0.1500	25	298.15	0.0043
		0.0400	25	298.15	0.0011
<i>Larrea tridentata</i>	Initial	0.090	24	297.15	0.0025
		0.090	24	297.15	0.0025
		0.090	24	297.15	0.0025
		0.090	24	297.15	0.0025
		0.090	24	297.15	0.0025
		0.090	24	297.15	0.0025
		0.090	24	297.15	0.0025
		0.090	24	297.15	0.0025
	0.085	35	308.15	0.0025	
	Mid	0.750	30	303.15	0.0213
		0.500	30	303.15	0.0142
		0.400	30	303.15	0.0114
		0.200	30	303.15	0.0057

Table D-19. Stomatal Conductance Values Converted From Molar Units to Velocity Units (Continued)

Species	Growth Stage	$g^1$ ( $\text{mol m}^{-2} \text{s}^{-1}$ )	$T^2$ ( $^{\circ}\text{C}$ )	$T^3$ (K)	$g^4$ ( $\text{m s}^{-1}$ )
<i>Larrea tridentata</i>	Mid	0.160	24	297.15	0.0045
		0.160	24	297.15	0.0045
		0.150	30	303.15	0.0043
		0.125	28.5	301.65	0.0035
		0.125	28.5	301.65	0.0035
		0.125	19	292.15	0.0034
		0.120	27	300.15	0.0034
		0.120	25	298.15	0.0034
		0.110	20	293.15	0.0030
		0.100	30	303.15	0.0028
		0.100	28.5	301.65	0.0028
		0.100	28.5	301.65	0.0028
		0.100	24	297.15	0.0028
	End	0.085	35	308.15	0.0025
		0.080	40	313.15	0.0024
		0.080	30	303.15	0.0023
		0.080	24	297.15	0.0022
		0.080	24	297.15	0.0022
		0.080	24	297.15	0.0022
		0.080	24	297.15	0.0022
		0.080	24	297.15	0.0022
		0.080	24	297.15	0.0022
		0.080	24	297.15	0.0022
		0.070	30	303.15	0.0020
		0.070	24	297.15	0.0020
		0.070	24	297.15	0.0020
		0.070	24	297.15	0.0020
		0.070	24	297.15	0.0020
		0.070	24	297.15	0.0020
		0.070	24	297.15	0.0020
		0.070	24	297.15	0.0020
		0.070	24	297.15	0.0020
		0.065	40	313.15	0.0019
		0.065	40	313.15	0.0019
0.070	12	285.15	0.0019		
0.060	24	297.15	0.0017		
0.060	24	297.15	0.0017		
0.060	24	297.15	0.0017		
0.060	24	297.15	0.0017		
0.060	24	297.15	0.0017		
0.060	24	297.15	0.0017		
0.050	28.5	301.65	0.0014		
0.050	28.5	301.65	0.0014		
0.050	28.5	301.65	0.0014		
0.050	24	297.15	0.0014		

Table D-19. Stomatal Conductance Values Converted From Molar Units to Velocity Units (Continued)

Species	Growth Stage	$g^1$ ( $\text{mol m}^{-2} \text{s}^{-1}$ )	$T^2$ ( $^{\circ}\text{C}$ )	$T^3$ (K)	$g^4$ ( $\text{m s}^{-1}$ )
<i>Larrea tridentata</i>	End	0.050	24	297.15	0.0014
		0.050	24	297.15	0.0014
		0.050	24	297.15	0.0014
		0.050	24	297.15	0.0014
		0.050	24	297.15	0.0014
		0.040	28.5	301.65	0.0011
		0.040	28.5	301.65	0.0011
		0.030	28.5	301.65	0.0008
		0.030	28.5	301.65	0.0008
		0.030	28.5	301.65	0.0008
		0.030	28.5	301.65	0.0008
		0.025	30	303.15	0.0007
0.025	30	303.15	0.0007		

<sup>1</sup> Stomatal conductance in molar units. Sources are listed in Table D-17.

<sup>2</sup> Air or leaf temperature for stomatal conductance measurements. Sources are listed in Table D-17.

<sup>3</sup> Air or leaf temperature for stomatal conductance measurements converted from Celsius to kelvin (Equation D-13).

<sup>4</sup> Stomatal conductance converted from molar units to velocity units (Equation D-12).

Weighted mean  $g_v$  for growth stages for the drought deciduous and evergreen vegetation within each association, and for the three years under consideration, were determined. Means were weighted according to relative cover values for each species included in the calculation of mean conductance. Relative cover was determined from Tables D-7 through D-15 by dividing cover per species by the total cover for species that were included in the calculation of mean conductance. Weighting factors and weighted mean conductances are in Table D-20. Because *Bromus madritensis* was the only species used for annual vegetation, it was not necessary to weight those means.

Table D-20. Weighting Factors and Weighted Conductance Means

Vegetation Type/Species	Growth Stage	Weighting Factor <sup>1</sup>			Weighted Mean $g^2$ (m/s)		
		1990	1991	1993	1990	1991	1993
<b>LA Vegetation Association</b>							
<b>Drought Deciduous</b>							
<i>Ambrosia dumosa</i>	Initial	0.866	0.894	0.982	0.0026	0.0026	0.0026
<i>Krameria erecta</i>	Initial	0.134	0.106	0.018			
<i>Ambrosia dumosa</i>	Mid	0.853	0.869	0.957	0.0063	0.0064	0.0067
<i>Krameria erecta</i>	Mid	0.132	0.103	0.018			
<i>Lycium andersonii</i>	Mid	0.015	0.028	0.025			
<i>Ambrosia dumosa</i>	End	0.866	0.894	0.982	0.0014	0.0014	0.0014
<i>Krameria erecta</i>	End	0.134	0.106	0.018			

Table D-20. Weighting Factors and Weighted Conductance Means (Continued)

Vegetation Type/Species	Growth Stage	Weighting Factor <sup>1</sup>			Weighted Mean $g^2$ (m/s)		
		1990	1991	1993	1990	1991	1993
<b>Evergreen</b>							
<i>Ephedra nevadensis</i>	Initial	0.323	0.297	0.209	0.0026	0.0026	0.0026
<i>Ericameria cooperi</i>	Initial	0.207	0.019	0.013			
<i>Larrea tridentata</i>	Initial	0.470	0.684	0.778			
<i>Ephedra nevadensis</i>	Mid	0.323	0.297	0.209	0.0048	0.0052	0.0054
<i>Ericameria cooperi</i>	Mid	0.207	0.019	0.013			
<i>Larrea tridentata</i>	Mid	0.470	0.684	0.778			
<i>Ephedra nevadensis</i>	End	0.407	0.303	0.212	0.0016	0.0016	0.0017
<i>Larrea tridentata</i>	End	0.593	0.697	0.788			
<b>LG Vegetation Association</b>							
<b>Drought Deciduous</b>							
<i>Ambrosia dumosa</i>	Initial	1.0	1.0	1.0	0.0026	0.0026	0.0026
<i>Krameria erecta</i>	Initial	0	0	0			
<i>Ambrosia dumosa</i>	Mid	0.156	0.314	0.284	0.0094	0.0089	0.0090
<i>Krameria erecta</i>	Mid	0	0	0			
<i>Lycium andersonii</i>	Mid	0.844	0.686	0.716			
<i>Ambrosia dumosa</i>	End	1	1	1	0.0014	0.0014	0.0014
<i>Krameria erecta</i>	End	0	0	0			
<b>Evergreen</b>							
<i>Ephedra nevadensis</i>	Initial	0.609	0.697	0.664	0.0028	0.0028	0.0028
<i>Ericameria cooperi</i>	Initial	0.366	0.275	0.310			
<i>Larrea tridentata</i>	Initial	0.026	0.028	0.025			
<i>Ephedra nevadensis</i>	Mid	0.609	0.697	0.664	0.0041	0.0041	0.0041
<i>Ericameria cooperi</i>	Mid	0.366	0.275	0.310			
<i>Larrea tridentata</i>	Mid	0.026	0.028	0.025			
<i>Ephedra nevadensis</i>	End	0.960	0.962	0.963	0.0016	0.0016	0.0016
<i>Larrea tridentata</i>	End	0.041	0.039	0.037			
<b>LLG Vegetation Association</b>							
<b>Drought Deciduous</b>							
<i>Ambrosia dumosa</i>	Initial	0.438	0.338	0.724	0.0025	0.0025	0.0026
<i>Krameria erecta</i>	Initial	0.562	0.662	0.276			
<i>Ambrosia dumosa</i>	Mid	0.345	0.278	0.552	0.0061	0.0057	0.0068
<i>Krameria erecta</i>	Mid	0.442	0.546	0.211			
<i>Lycium andersonii</i>	Mid	0.212	0.176	0.238			
<i>Ambrosia dumosa</i>	End	0.438	0.338	0.724	0.0013	0.0013	0.0014
<i>Krameria erecta</i>	End	0.562	0.662	0.276			



Table D-20. Weighting Factors and Weighted Conductance Means (Continued)

Vegetation Type/Species	Growth Stage	Weighting Factor <sup>1</sup>			Weighted Mean $g^2$ (m/s)		
		1990	1991	1993	1990	1991	1993
<b>Evergreen</b>							
<i>Ephedra nevadensis</i>	Initial	0.436	0.471	0.405	0.0027	0.0027	0.0027
<i>Ericameria cooperi</i>	Initial	0.112	0.021	0.026			
<i>Larrea tridentata</i>	Initial	0.452	0.508	0.569			
<i>Ephedra nevadensis</i>	Mid	0.436	0.471	0.405	0.0048	0.0049	0.0050
<i>Ericameria cooperi</i>	Mid	0.112	0.021	0.026			
<i>Larrea tridentata</i>	Mid	0.452	0.508	0.569			
<i>Ephedra nevadensis</i>	End	0.491	0.481	0.416	0.0016	0.0016	0.0016
<i>Larrea tridentata</i>	End	0.509	0.519	0.584			

<sup>1</sup>Weighting factor was determined from cover per species divided by the sum of cover for all species included in the mean stomatal conductance calculation. Cover values used to calculate weighting factors are in Tables D-7 through D-15.

<sup>2</sup>Mean stomatal conductance per vegetation type for growth stages. Mean conductance per species were calculated from Table D-18. The mean conductances were multiplied by species specific weighting factors then summed to get an average per vegetation type for each vegetation association.

The weighted mean conductances were converted to  $r_l$  according to Equation D-14 (Table D-21).

$$r_l = \frac{1}{g_v} \quad (\text{Eq. D-14})$$

where:  $r_l$  = stomatal resistance ( $\text{s m}^{-1}$ )

Mean  $r_l$  values for growth stages and vegetation types (Table D-21) were used in Equation D-6 to calculate  $F_r$  (see Section D4 for example calculation).

Table D-21. Mean Stomatal Resistance Values Used in Transpiration Coefficient Calculations

Vegetation Association	Vegetation Type	Growth Stage	Mean $r_l$ ( $\text{s/m}$ ) <sup>1</sup>			
			1990	1991	1993	
All Associations <sup>2</sup>	Annual	Initial/End	345			
		Mid	91			
			1990	1991	1993	
LA	Drought Deciduous	Initial	385	385	385	
		Mid	159	156	149	
		End	714	714	714	
	Evergreen	Initial	385	385	385	
		Mid	208	192	185	
		End	625	625	588	
	LG	Drought Deciduous	Initial	385	385	385
			Mid	106	112	111
			End	714	714	714
Evergreen		Initial	357	357	357	
		Mid	244	244	244	
		End	625	625	625	

Table D–21. Mean Stomatal Resistance Values Used in Transpiration Coefficient Calculations (Continued)

Vegetation Association	Vegetation Type	Growth Stage	Mean $r_l$ (s/m) <sup>1</sup>		
LLG	Drought Deciduous	Initial	400	400	385
		Mid	164	175	147
		End	769	769	714
	Evergreen	Initial	370	370	370
		Mid	208	204	200
		End	625	625	625

<sup>1</sup> Mean stomatal resistance ( $r_l$ ) of plant species in each vegetation type. Inputs are weighted mean stomatal conductances from Table D-20. Stomatal resistance was calculated using Equation D-14. Resistance values were rounded to the nearest whole number.

<sup>2</sup> Annuals were represented by *Bromus madritensis* in all associations.

### D3.2.4 Meteorological Parameters

Precipitation data used in Appendices E and F, and meteorological parameters required to calculate  $K_{cb}$  and generic  $ET_0$ , are developed in this section. Meteorological parameters were either measured directly or derived from measured values (e.g., solar radiation).

Atmospheric humidity is an important driver of transpiration from plant leaves and affects stomatal behavior. The air in the intercellular spaces of a leaf is nearly saturated with water vapor (Section D2.1). As the air outside the leaf dries, the leaf-to-air water vapor gradient increases, increasing the rate of water loss through the stomata (Section D2.1). With increasing evaporative demands the plant will begin to close stomata to prevent water loss. However, stomatal closure also results in reduced concentrations of  $CO_2$  for use in photosynthesis. Similarly, when atmospheric humidity is high, the leaf-to-air water vapor gradient decreases. This results in lower evaporative demand, allowing stomates to remain open without high rates of water loss. One humidity parameter (minimum daily relative humidity [ $RH_{min}$ ]) was required for the calculation of  $K_{cb, full}$ , and two (slope of the saturation vapor pressure curve [ $\Delta$ ] and the psychrometric constant [ $\gamma$ ]) were required for the calculation of  $F_r$  (Equations D-4 and D-6, respectively). Mean daily air temperature ( $T$ ) and wind speed at a height of 2 m ( $u_2$ ) were also required for  $K_{cb}$  calculations. In addition to these parameters, the calculation of  $ET_0$  (Section D5) required minimum and maximum daily air temperature and solar radiation ( $R_s$ ). Precipitation data for the 1990, 1991, 1993, 1998, 2001, and 2002 water years were required for analyses in Appendices E and F.

**Data from Yucca Mountain Meteorological Monitoring Sites**—The Yucca Mountain Project has been collecting meteorological data from a network of nine sites since 1985. Meteorological data for calculations of  $K_{cb}$  and  $ET_0$  for a generic location were taken from Yucca Mountain Meteorological Sites 1 and 4. Site 1 is the main meteorological tower located in western Midway Valley at an elevation of 1,143 m. Midway Valley is bounded on the west by Yucca Mountain. Site 4 is located on Alice Hill in the northeastern portion of Midway Valley at an elevation of 1,234 m (CRWMS M&O 1999 [DIRS 115672], pp. 1-1 to 1-6). Site 4 was selected because it was closest in elevation to Site 1 and it was used mainly for data substitutions when Site 1 data were missing.

Weather data collected at the Yucca Mountain monitoring sites during the years that vegetation cover was measured on ESPs (1990, 1991, and 1993) may be less reliable than data collected in later years. With the exception of precipitation, the weather data for 1990 and 1991 were not qualified for use at the time of this analysis, and possible errors were identified in 1993 precipitation data for Site 1. As described in Section D2.2, the years for cover data use were selected to correspond with the average, above average, and below average precipitation years that were selected for NDVI' analysis. For the NDVI' analysis, 2001 (average precipitation), 1998 (above average precipitation), and 2002 (below average precipitation) were used. The  $RH_{min}$  and  $u_2$  corrections to  $K_{cbs}$  used in Equation D-4 represent regional differences in arid climates compared to the representative subhumid climate with calm wind conditions in FAO-56 methods (Allen et al. 1998 [DIRS 157311]). While it is important to capture regional differences in  $RH_{min}$  and  $u_2$  to increase the accuracy of  $K_{cbs}$  for arid climates, variation between years with similar precipitation within an arid climate have little effect on  $K_{cbs}$  (see below). Therefore, it was determined that use of weather data from 1998, 2001, and 2002 paired with cover data from 1993, 1991, and 1990, respectively, would be adequate for calculating  $K_{cbs}$  for above average, average, and below average precipitation years and would avoid use of unqualified weather data.

Hourly wind speed measured at a height of 10 m ( $u_{10}$ ),  $T$ , and  $R_s$  data for 1997, 1998, 2000, 2001, and 2002 were taken from Site 1, which provided the most data for those years. Hourly relative humidity data for 1997 and 1998 were not collected at Site 1, and so data from Site 4 were used. Hourly relative humidity (RH) data for 2000, 2001, and 2002 were taken from Site 1. Source data were taken from DTNs: MO0312SEPQ1997.001 [DIRS 167116], MO0206SEPQ1998.001 [DIRS 166731], MO0209SEPQ2000.001 [DIRS 166730], MO0305SEP01MET.002 [DIRS 166164], and MO0305SEP02MET.002 [DIRS 166163].

Precipitation data were taken from Sites 1, 2 (located on the Yucca Mountain crest at an elevation of 1,478 m), 3 (located in Coyote Wash at an elevation of 1,279 m), and 4. This was done to evaluate precipitation at different elevations on the mountain in Appendix E (1997 to 2002) and to scale NDVI' by precipitation that fell during water years that cover data were collected for (1989 to 1993). The source data for 1997, 1998, 2000, 2001, and 2002 were from DTNs: MO0312SEPQ1997.001 [DIRS 167116], MO0206SEPQ1998.001 [DIRS 166731], MO0209SEPQ2000.001 [DIRS 166730], MO0305SEP01MET.002 [DIRS 166164], and MO0305SEP02MET.002 [DIRS 166163], respectively. The source data for 1989 to 1992 were from DTN: MO0606SEPPRECIP.001 [DIRS 177136]<sup>2</sup>. The source data for 1993 were from DTN: MO0312SEPQ1993.001 [DIRS 176092].

For 1997 to 2002, hourly temperature, wind speed, relative humidity, precipitation and solar radiation data were extracted from the source files and placed in Excel® files (Output DTN: MO0602SPAWEATH.000, “metadata” files for each year). Data that were not needed for this analysis were omitted from the files, resulting in spreadsheets with hourly wind speed, air temperature, relative humidity, precipitation and solar radiation for Site 1 (Output DTN: MO0602SPAWEATH.000), and precipitation for Sites 2, 3, and 4 (Output

---

<sup>2</sup>When the calculations were done, the source data was obtained from DTN: MO0604SEPPRECIP.000, which was later superseded by the above DTN. The source data used from the original DTN was not altered in the superseding DTNs as determined by a comparison check.

DTN: MO0602SPAPRECP.000). The new files were sorted according to Julian Day and time of day and formatted into water years (October 1 to September 30).

Missing data in the source files were identified in cells by 9999. These values were located in the Excel® files and removed using the Find/Replace command. For Site 1, missing temperature, wind speed, relative humidity, and precipitation data were omitted if only 1 or 2 hours out of a day were affected. If more than 2 hours were affected, the data were replaced with data from YMP meteorological monitoring Site 4. All missing solar radiation data were replaced with data from YMP meteorological monitoring Site 4. A record of data replacement was created and placed in a worksheet titled data corrections in each of the Excel® files (Output DTN: MO0602SPAWEATH.000, “metadata” files for each year). Missing precipitation data for Sites 2, 3, and 4 (water years 1998, 2001, and 2002) were identified in a notes column in the Excel® file (Output DTN: MO0602SPAPRECP.000). With one exception, all missing precipitation data for water years 1998, 2001, and 2002 occurred during time periods when no precipitation occurred at the site, and so were not replaced. For water year 1998, day 54, at monitoring Site 3, two hours of data were missing when precipitation might have occurred. However, because of the short time period, the missing data were not replaced.

Hourly precipitation data for 1989 to 1993 (Sites 2, 3, and 4) were extracted from the source files and placed in an Excel® file with separate worksheets for each year (Output DTN: MO0605SEPTOTAL.002). The data were formatted into water years 1990, 1991, and 1993. Missing data in the source files were identified by 9999. Missing data were replaced in the Excel files with data from remaining stations. This was necessary because the gauge for Site 4 was not installed until February 5, 1990, resulting in six missed precipitation events for the water year, and several additional storms were missed at Sites 2, 3, and 4 over the course of the three water years due to gauge malfunctions. For data replacement, the inverse-distance-squared method of interpolating between sites using the following equation was considered for use:

Weighting Factor<sub>*i*</sub> =  $(1/(d_i^2))/S_i(1/(d_i^2))$  where  $d_i$  is the distance of station  $i$  from the indicated coordinates.

However, because the three sites are situated in close proximity and only two were used at any one time to average, this method produced negligible differences compared to taking a simple average of the two sites. Therefore, the mean of two sites was used when a value was missing at one site during a precipitation event. If precipitation was recorded at only one site, and gauges malfunctioned at the other two, the recorded amount was used to replace the missing data at the two malfunctioning sites.

To develop daily totals for solar radiation from hourly values, negative values and values less than one that were recorded for night-time hours were deleted from the dataset (Output DTN: MO0602SPAWEATH.000, “metadata” files). The hourly data were then summed for each day and converted from watts per square meter to megajoules per square meter per day by multiplying the daily sums by the conversion factor 0.0036 (IEEE/ASTM 1997 [DIRS 151762]). These calculations and results are contained in the Excel® files in Output DTN: MO0602SPAWEATH.000.

Daily average wind speed and air temperature were determined from the hourly data using the Excel® command AVERAGE (Output DTN: MO0602SPAWEATH.000, “metadata” files). Daily minimum relative humidity ( $RH_{min}$ ), minimum air temperature, and maximum air temperature were determined from the hourly data using the Excel® commands MINIMUM and MAXIMUM (Output DTN: MO0602SPAWEATH.000, “metadata” files). Daily precipitation totals for the 1998, 2000, and 2001 water years were determined from the hourly data, and yearly totals were determined from the daily totals using the Excel® command SUM (Output DTN: MO0602SPAPRECP.000). Yearly precipitation totals for the 1990, 1991, and 1993 water years were determined from hourly data using the Excel® command SUM (Output DTN: MO0605SEPTOTAL.002). These calculations and results are contained in the Excel® files in Output DTNs: MO0602SPAWEATH.000, MO0602SPAPRECP.000, and MO0605SEPTOTAL.002.

FAO-56 methodology (Allen et al. 1998 [DIRS 157311]) requires wind speed measurements at 2 m above the ground. This is the standard anemometer height required in agrometeorology (Allen et al. 1998 [DIRS 157311], p. 55). Anemometer height at the weather station used in this analysis was 10 m. Because wind speed increases with height above the soil surface, a logarithmic wind profile function is required to adjust wind speeds placed at heights other than the standard 2 m. Therefore, the following correction was made for wind speed (Allen et al. 1998 [DIRS 157311], Equation 47, p. 56):

$$u_2 = u_z \frac{4.87}{\ln(67.8z - 5.24)} \quad (\text{Eq. D-15})$$

where

$u_z$  = wind speed measured at  $z$  m aboveground surface ( $\text{m s}^{-1}$ ),

$z$  = height of measurement aboveground surface (m).

Example: On day 60 of 1998,  $u_{10} = 2.3 \text{ m s}^{-1}$  (Output DTN: MO0602SPAWEATH.000).

$$u_2 = 2.3 \frac{4.87}{\ln(67.8 * 10 - 5.42)} = 1.7 \text{ m s}^{-1} \quad (\text{from Eq. D-15})$$

Mean daily  $u_2$  calculations and values are in Output DTN: MO0603SPAREFET.000.

To assess potential impacts of using cover data and weather data from paired average, above average, and below average precipitation years, monthly mean  $RH_{min}$  and  $u_2$  calculated for growing season months (January to September) of representative years were substituted into  $K_{cb}$  calculations. Water years 1998 and 1993 were selected as representative wet years. Water years 2002 and 1990 were selected as representative dry years. For 1998 and 2002, monthly mean  $RH_{min}$  and  $u_2$  were calculated from data in Output DTN: MO0602SPAWEATH.000 by summing daily values for each month and dividing by the number of days in the month (Table D-22). For 1993, monthly averages were taken from DOE (1995 [DIRS 147785], p. B-2, Table B-1 [ $u_2$ ] and p. B-9, Table B-8 [ $RH_{min}$ ]). For 1990, monthly mean  $RH_{min}$  and  $u_2$  were calculated from data in DTNs: MO9905VMMDJM90.000 [DIRS 150056], MO9905VMMDAJ90.000 [DIRS 150118],

MO9905VMMDJS90.000 [DIRS 150119], and MO9905VMMDOD90.000 [DIRS 150120] by combining the quarterly data files, then summing daily values for each month and dividing by the number of days in the month (Table D-22). For 1998 and 2002, data were taken from Site 1. Relative humidity was not measured at Site 1 in 1993, and errors were identified in precipitation measurements; therefore,  $RH_{min}$  and precipitation were taken from Site 8, which is close to Site 1 and at a similar elevation and exposure (CRWMS M&O 1997 [DIRS 103155], pp. 1-4 and 1-5). For 1990, data were taken from Site 4.

Table D-22. Mean Monthly Wind Speed and Minimum Relative Humidity for Representative Wet and Dry Years

	$RH_{min}$ (%)				Wind Speed (m/s)			
	Below Average Precipitation		Above Average Precipitation		Below Average Precipitation		Above Average Precipitation	
	1990 <sup>1</sup>	2002 <sup>2</sup>	1993 <sup>3</sup>	1998 <sup>2</sup>	1990 <sup>1</sup>	2002 <sup>2</sup>	1993 <sup>4</sup>	1998 <sup>2</sup>
January	NA <sup>5</sup>	20.0	53.1	37.0	NA <sup>5</sup>	3.1	3.1	2.6
February	25.4	13.4	47.3	51.4	5.1	3.3	2.9	3.4
March	18.9	12.7	30.8	34.5	4.6	4.1	2.9	3.4
April	20.9	12.6	15.9	27.6	4.9	4.5	4.3	3.6
May	19.6	8.4	14.5	21.7	5.4	4.1	4.1	4.4
June	16.4	6.6	13.2	17.6	4.4	4.0	3.7	3.4
July	21.2	10.1	9.2	10.3	4.1	3.7	3.7	3.4
August	21.6	6.4	9.9	11.6	4.1	3.8	3.7	3.4
September	26.0	11.3	9.4	22.4	4.1	3.8	3.1	3.1

Source: <sup>1</sup> DTNs: MO9905VMMDJM90.000 [DIRS 150056], MO9905VMMDAJ90.000 [DIRS 150118], MO9905VMMDJS90.000 [DIRS 150119], and MO9905VMMDOD90.000. [DIRS 150120].

<sup>2</sup> Output DTN: MO0602SPAWEATH.000.

<sup>3</sup> DOE 1995 [DIRS 147785], Table B-8.

<sup>4</sup> DOE 1995 [DIRS 147785], Table B-1.

<sup>5</sup> No data were available for January 1990.

### Slope of Saturation Vapor Pressure Curve ( $\Delta$ )

The  $\Delta$  is the slope of the relationship between the saturation vapor pressure of the air and air temperature. Vapor pressure is the component of total atmospheric pressure exerted by the motion of water vapor molecules. Saturation vapor pressure is the vapor pressure the air would have if it were saturated with water vapor molecules at a given temperature. As temperature increases, the saturation vapor pressure also increases.  $\Delta$  is calculated from mean daily air temperature ( $^{\circ}\text{C}$ ) according to the following equation (Allen et al. 1998 [DIRS 157311], Equation 13, p. 37):

$$\Delta = 4098 \left[ \frac{0.6108 \exp\left(\frac{17.27T}{T + 237.3}\right)}{(T + 237.3)^2} \right] \quad (\text{Eq. D-16})$$

where

$\exp(x)$  = 2.7183 (base of natural logarithm) raised to the power (x),

T = mean daily air temperature (°C).

Example:

On day 60, 1998,  $T = 7.8^\circ\text{C}$  (Output DTN: MO0602SPAWEATH.000).

$$\Delta = 4098 \left[ \frac{0.6108 \exp\left(\frac{17.27 \times 7.8}{7.8 + 237.3}\right)}{(7.8 + 237.3)^2} \right] = 4098 \left[ \frac{0.6108 \times 1.7326}{60,074} \right] = 0.072 \text{ kPa } ^\circ\text{C}^{-1} \text{ (from Eq. D-16)}$$

Daily  $\Delta$  values were used in Eq. D-6 to calculate daily  $F_r$ . Daily  $\Delta$  values for the 1998, 2001, and 2002 water years are in Output DTN: MO0603SPAREFET.000.

Psychrometric Constant ( $\gamma$ )

The psychrometric constant represents a balance between the heat required to evaporate water into an air stream from the wick of a wet bulb thermometer (wet wick with thermometer beneath it) and the air's potential to absorb the water and carry it away. The constant is dependent on atmospheric pressure, latent heat of vaporization (energy required for evaporation), the specific heat of air at a constant pressure (quantity of energy required to raise the temperature of a given amount of air by one degree at constant pressure), and the ratio of molecular weight of water vapor to dry air. Values for  $\gamma$  at different altitudes are provided by Allen et al. (1998 [DIRS 157311], Table 2.2, p. 214). The weather station altitude of 1,143 m for the Yucca Mountain meteorological monitoring Site 1 corresponds to a table value for  $\gamma$  of  $0.059 \text{ kPa } ^\circ\text{C}^{-1}$ . This value was used in Equation D-6 to calculate  $F_r$ .

#### D4. EXAMPLE CALCULATIONS AND $K_{CB}$ PROFILES

Transpiration coefficients were calculated daily for the initial, mid, and end of late season growth stages for annuals, drought deciduous, and evergreen species for each of the vegetation associations using Equations D-1 through D-8. The output of these calculations is included in Output DTN: MO0606SPABASAL.001. The following example is for drought deciduous vegetation on the first day of the midseason stage in an LG association using 1993 water year data (Table D-23).

Table D-23. Parameter Values for Example  $K_{cb}$  Calculations Using Annual Vegetation from an LG Vegetation Association

Parameter	Value	Source
First day of midseason stage	March 16, Julian Day 75	Table D-4
Cover for midseason stage	9.52% = 0.0952	Table D-14
Plant height	0.38 m	Table D-6
$r_l$	111 s m <sup>-1</sup>	Table D-20
$u_2$	1.84 m s <sup>-1</sup>	Output DTN: MO0603SPAREFET.000
$RH_{min}$	37.16%	Output DTN: MO0602SPAWEATH.000
$\Delta$	0.093 kPa °C <sup>-1</sup>	Output DTN: MO0603SPAREFET.000
$\gamma$	0.059 kPa °C <sup>-1</sup>	Section D3.2.4

Step 1. Calculate  $K_{cb, h}$  using Equation D-5:

$$K_{cb, h} = 1.0 + 0.1 \times 0.38 = 1.038$$

Step 2. Calculate  $K_{cb, full}$  using Equation D-4:

$$K_{cb, full} = 1.038 + [0.04(1.84 - 2) - 0.004(37.16 - 45)] \left( \frac{0.38}{3} \right)^{0.3} = 1.05$$

Step 3. Calculate  $F_r$  using Equation D-6:

$$F_r \approx \frac{0.093 + 0.059(1 + 0.34 \times 1.84)}{0.093 + 0.059 \left( 1 + 0.34 \times 1.8 \times \frac{111}{100} \right)} = 0.983$$

Step 4. Determine the minimum of (1,  $2f_c$ , and  $f_{c, eff}^{(1/1+h)}$ ):

$$2f_c = 2 \times 0.0952 = 0.1904$$

$$f_{c, eff} \left( \frac{1}{1+h} \right) = \left( \frac{0.0952}{0.7773} \right)^{(0.7246)} = 0.2184$$

The minimum of (1,  $2f_c$ , and  $f_{c, eff}(1/1+h)$ ) is  $2f_c = 0.1904$

Step 5. Calculate  $K_{cb}$  using Equation D-1:

$$K_{cb} = 1.05 \times 0.1904 = 0.200$$

Step 6. Adjust  $K_{cb}$  with the stomatal resistance correction factor ( $K_{cb} \times F_r$ ):

$$0.200 \times 0.983 = 0.197$$



Step 7. Calculate  $K_{cb}$  for development and late stages using Equation D-8. For the development stage,  $K_{cb\ prev}$  was the  $K_{cb}$  for the last day of the initial stage, and  $K_{cb\ next}$  was the  $K_{cb}$  for the first day of the mid stage. For the late stage,  $K_{cb\ prev}$  was the  $K_{cb}$  for the last day of the mid stage, and  $K_{cb\ next}$  was the value for  $K_{cb\ end}$  ( $K_{cb}$  on the last day of the late stage).

The following example is for drought deciduous vegetation in an LG association on the first through third days of the late season stage, using data for the 1993 water year (Table D-24).

Table D-24. Parameter Values for Example Calculations of  $K_{cb}$  for the Late Season Stage

Parameter	Value	Source
$K_{cb\ prev}$	0.205	DTN: MO0606SPABASAL.001
$K_{cb\ next}$	0.108	DTN: MO0606SPABASAL.001
$\Sigma L_{prev}$	120 days	Table D-4
$L_{stage}$	15 days	Table D-4
First through third day of late season stage	121 to 123	Table D-4

$$\text{Day 91: } K_{cb121} = 0.205 + \left( \frac{121 - 120}{15} \right) (0.108 - 0.205) = 0.198$$

$$\text{Day 92: } K_{cb122} = 0.205 + \left( \frac{122 - 120}{15} \right) (0.108 - 0.205) = 0.192$$

$$\text{Day 93: } K_{cb123} = 0.208 + \left( \frac{123 - 120}{15} \right) (0.108 - 0.205) = 0.185$$

All  $K_{cb}$  calculations and results are available in Excel® spreadsheets in Output DTN: MO0606SPABASAL.001.

Daily  $K_{cb}$  values were set to zero outside the growing season for the three vegetation types (annuals, drought deciduous, and evergreen species) to represent the period of time when plants have completed their life cycle (annual species), are dormant (drought deciduous species), or physiologically inactive (evergreen species). The evaporation term ( $K_e$ ) of the dual transpiration coefficient controls the soil water balance under conditions when plants are not actively transpiring.

The impact of the  $RH_{min}$  and  $u_2$  corrections on  $K_{cb}$ s were assessed for representative above (1993 and 1998) and below (1990 and 2002) average precipitation years using data from the LG vegetation association. The monthly mean  $RH_{min}$  and  $u_2$  for the growing season (January through September; Table D-21) were substituted into the  $K_{cb}$  calculations for annuals, drought deciduous, and evergreen vegetation for Julian days 91 to 99. This time period corresponded to a subset of the midseason growth stage during which all three vegetation types were considered active in the  $K_{cb}$  calculations. No other input parameters were varied. The resulting  $K_{cb}$ s for those nine days are in Table D-25.

Comparisons of  $K_{cb}$ s in above average precipitation years showed that differences in  $RH_{min}$  and  $u_2$  translated into differences in  $K_{cb}$ s of 3% or less (Table D-25). For below average precipitation years, differences in  $RH_{min}$  and  $u_2$  translated into differences in  $K_{cb}$ s of 2.6% or less (Table D-25). Additionally, variation in  $K_{cb}$ s that were averaged across wet and dry years was low, ranging from less than 1% to 4% (Table D-25, CV). Allen et al. (1998 [DIRS 157311], p. 124) suggest that only approximations of  $RH_{min}$  and  $u_2$  are needed for the midseason growth stage because Equation 62, which has the same correction term as Equation D-1, is not sensitive to these values. The same argument applies to the initial and end of late season stages in this analysis, as Equation D-1 was used to calculate  $K_{cb}$ s for those stages. Thus, Equation D-1 is fairly insensitive to  $RH_{min}$  and  $u_2$ , and use of  $RH_{min}$  and  $u_2$  from different years had negligible impact on  $K_{cb}$ s.

Table D-25. Comparison of  $K_{cb}$ s Calculated with Mean Monthly Wind Speed and Minimum Relative Humidity from Representative Wet and Dry Years

$K_{cb}^1$ 1998	$K_{cb}^1$ 1993	Percent Difference <sup>2</sup>	$K_{cb}^1$ 2002	$K_{cb}^1$ 1990	Percent Difference <sup>3</sup>	Mean <sup>4</sup>	SD <sup>5</sup>	CV <sup>6</sup>
0.572	0.555	-3.0	0.593	NA <sup>7</sup>	NA <sup>7</sup>	0.576	0.017	2.88
0.557	0.563	1.0	0.602	0.598	-0.7	0.580	0.023	4.01
0.579	0.582	0.4	0.607	0.602	-0.7	0.593	0.014	2.37
0.585	0.602	2.7	0.606	0.599	-1.2	0.598	0.009	1.53
0.595	0.602	1.1	0.608	0.603	-0.8	0.602	0.005	0.89
0.593	0.599	1.0	0.608	0.599	-1.5	0.600	0.006	1.03
0.603	0.605	0.4	0.604	0.593	-1.8	0.601	0.006	0.92
0.601	0.604	0.5	0.609	0.593	-2.6	0.602	0.007	1.11
0.589	0.604	2.4	0.604	0.589	-2.6	0.597	0.009	1.45

<sup>1</sup> Transpiration coefficients ( $K_{cb}$ ) calculated using mean monthly minimum relative humidity ( $RH_{min}$ ) and wind speed ( $u_2$ ) from two representative wet (1998 and 1993) and two representative dry (2002 and 1996) years. Relative humidity and wind speed data used in the calculation are from Table D-22.

<sup>2</sup> Percent difference between  $K_{cb}$ s calculated using  $RH_{min}$  and  $u_2$  from 1998 and 1993 (two above average precipitation years).

<sup>3</sup> Percent difference between  $K_{cb}$ s calculated using  $RH_{min}$  and  $u_2$  from 1996 and 2002 (two below average precipitation years).

<sup>4</sup> Mean  $K_{cb}$  of 1998, 1993, 2002, and 1996.

<sup>5</sup> Standard deviation of mean  $K_{cb}$ .

<sup>6</sup> Coefficient of Variation = (SD/mean) × 100.

<sup>7</sup> No data were available for January 1990.

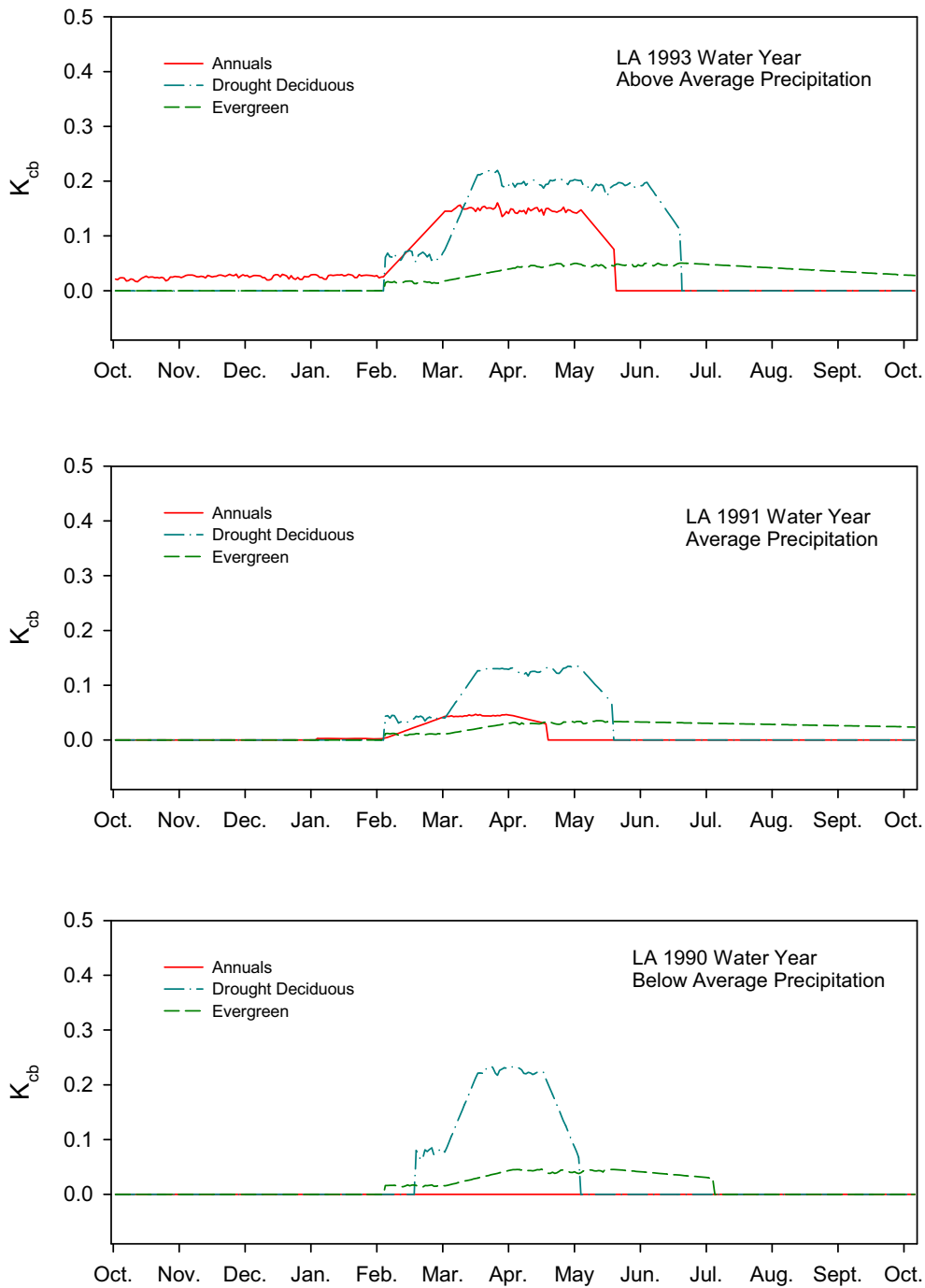
$K_{cb}$  profiles for the three vegetation types in the LA, LG, and LLG associations were generated for each water year (Figures D-4, D-5, and D-6, source data Output DTN: MO0606SPABASAL.001). The profiles showed that the magnitude of  $K_{cb}$ s for vegetation types was dependent on water year and vegetation association. Annuals were more important in the LLG association compared to LA and LG, and in the wet year compared to the average year for all associations. No annuals were recorded on plots during the dry year. These patterns reflect the relative importance of annuals in each of the associations with respect to water use. Cover was consistently greater for annuals on the LLG ESPs from 1991 to 1994, and consistently lower on the LA ESPs compared to the other associations over the same time period

(CRWMS M&O 1996 [DIRS 102235], p. 31, Figure 4-10). Drought deciduous vegetation was more important (higher  $K_{cbs}$ ) than evergreen vegetation during the midseason growth stage for LG and LA associations across water years, but the two vegetation types were similar for the LLG association across water years. While shorter growing seasons were developed for the drought year (Table D-4), making potential seasonal water use by plants low, mid stage  $K_{cbs}$  for drought deciduous vegetation were higher than in the average precipitation year (1991) for the three associations. The absence of annuals in the drought year may have resulted in more available water early in the season for drought deciduous species, which could have caused the higher mid stage cover values (Tables D-7 through D-9 and D-13 through D-15). Alternatively, higher cover values in the drought year could have been due to a time lag of the effects of the 1990 drought on the 1991 response of drought deciduous vegetation.

Because the three vegetation types were independent of each other (i.e., each contained unique information relevant to the association) and were important with respect to water use, it was appropriate to sum the annual, drought deciduous, and evergreen  $K_{cbs}$  to get one profile for each association (Figure D-7). This resulted in  $K_{cb}$  profiles for each water year and association that accounted for major sources of variation due to differences in growing season length, growth characteristics, physiological activity, and ground cover among vegetation types.

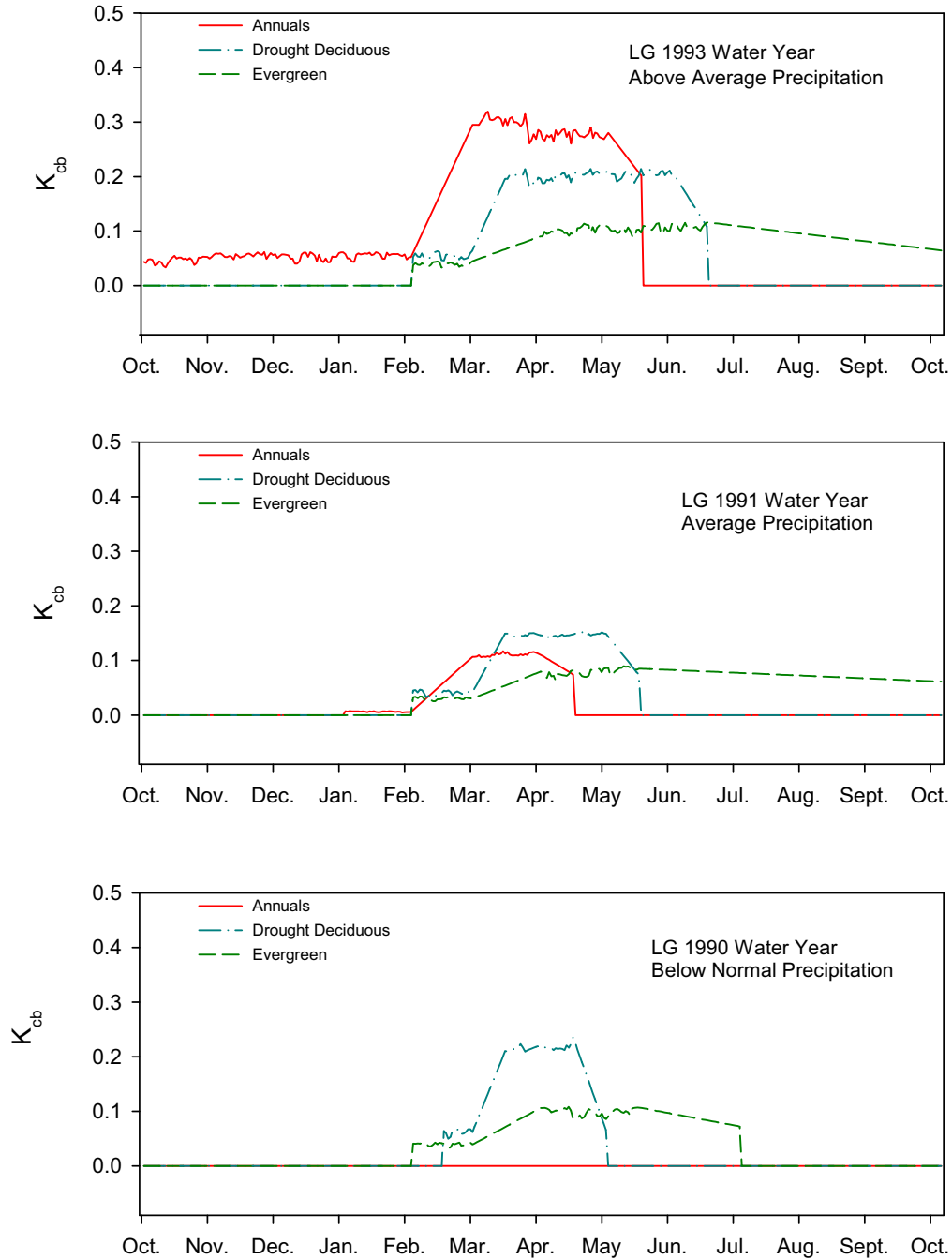
Regardless of the differences in potential water use among the vegetation types across associations, when  $K_{cbs}$  were summed to produce association totals, the values were very similar for LG and LLG over most of the profiles for 1998 and 2001 (Figure D-7). This was due to similarities in total vegetation cover on LG and LLG reference plots (Tables D-11, D-12, D-14, and D-15). The similarity of the association profiles indicates that regardless of species composition, potential water use is similar for the two associations during average and above average precipitation years.

Transpiration coefficients for the LA association were generally lower for the wet and average years than those calculated for the LG and LLG associations, reflecting the tendency toward lower cover of vegetation in the low elevation LA association (Figure D-6).  $K_{cb}$  profiles for the three associations tended to converge in the dry year (Figure D-6), reflecting water limitation to vegetation growth across associations.



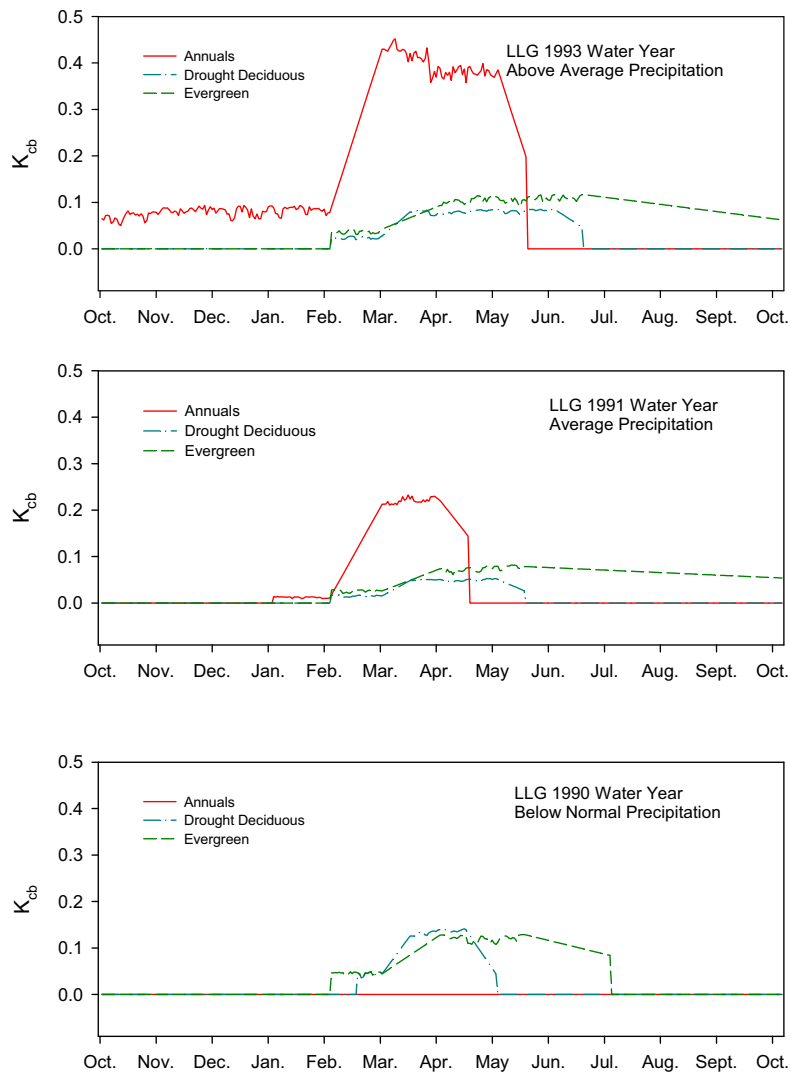
Source: Output DTN: MO0606SPABASAL.001.

Figure D-4. Transpiration Coefficient ( $K_{cb}$ ) Profiles for Three Vegetation Types (Annuals, Drought Deciduous, and Evergreen) for the *Larrea-Ambrosia* Vegetation Association



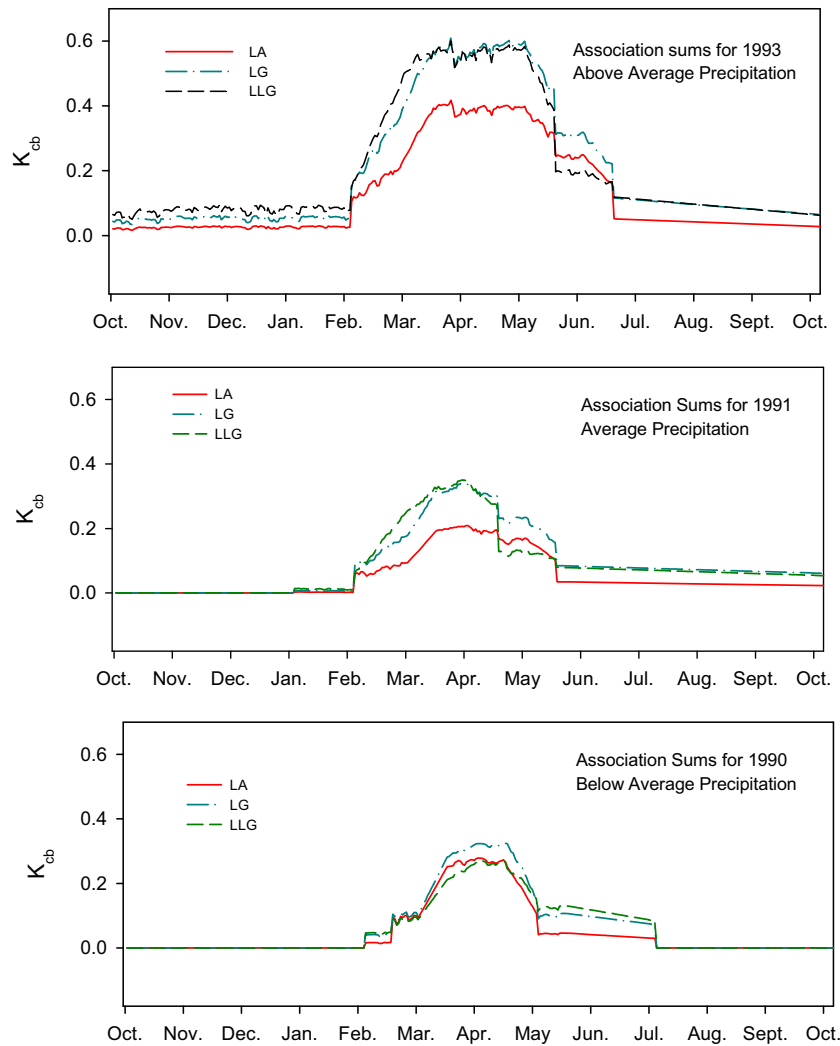
Source: Output DTN: MO0606SPABASAL.001.

Figure D-5. Transpiration Coefficient ( $K_{cb}$ ) Profiles for Three Vegetation Types (Annuals, Drought Deciduous, and Evergreen) for the *Lycium-Grayia* (LG) Vegetation Association



Source: Output DTN: MO0606SPABASAL.001.

Figure D-6. Transpiration Coefficient ( $K_{cb}$ ) Profiles for Three Vegetation Types (Annuals, Drought Deciduous, and Evergreen) for the *Larrea-Lycium-Grayia* (LLG) Vegetation Association



Source: Output DTN: MO0606SPABASAL.001.

Figure D-7. Transpiration Coefficient ( $K_{cb}$ ) Profiles Summed Across Three Vegetation Types (Annuals, Drought Deciduous, and Evergreen) for Three Vegetation Associations (LA, LG, and LLG)

Use of separate  $K_{cb}$ -NDVI' correlations for each vegetation association would require that each model cell be assigned to one of the three associations. This was not feasible due to lack of spatial data for vegetation associations and potential for vegetation change through time. As an alternative to using three separate  $K_{cb}$  profiles for the  $K_{cb}$ -NDVI' correlations, and for use in uncertainty analyses (Appendix I), upper and lower bounds for  $K_{cb}$ s were calculated for the LG association. This association was selected because it is representative of the vegetation directly above the proposed repository and is therefore most important with respect to the potential for water to infiltrate and reach interred waste containers. Upper and lower bounds were determined by using high and low input values for vegetation cover, plant height, and stomatal resistance for calculating daily  $K_{cb}$ s and generating the yearly profiles of uncertainty for the 1993 and 1991 water years. Inputs are described below. It was determined that the 1990 water year would not be used in the  $K_{cb}$ -NDVI' correlations, and so upper and lower bounds were not calculated for

that year (Appendix E). The same methods outlined above for calculating  $K_{cb}$ s were used to generate the uncertainty bounds.

Cover data from 1993 (wet year) and 1991 (average precipitation year) were evaluated to determine which ESPs from those years had the highest and lowest cover values. Ecological Study Plots LG3C and LG5C had the highest and lowest recorded cover, respectively, for 1993 (Table D-16). Ecological Study Plots LG2T and LG5T had the highest and lowest recorded cover, respectively, for 1991 (Table D-16). Source data for these plots were extracted from DTN: MO9907GCESPYMN.000 [DIRS 157659] and placed in Excel® spreadsheets (Output DTN: MO0606SPAVEGAS.001). The data were sorted per species and vegetation type. Mean percent cover per species was determined by summing the cover data per species and dividing by the number of transects sampled on the ESP. Cover per vegetation type was determined by summing the species specific data for each type. Cover data used to calculate the  $K_{cb}$  bounds for LG are in Tables D-26 through D-29.

Table D-26. Mean Cover from Ecological Study Plot LG3C

LG3C 1993					
Vegetation Type/Species	Life Form <sup>1</sup>	Cover (%)	Vegetation Type/Species	Life Form <sup>1</sup>	Cover (%)
<b>Annuals</b>			<b>Drought Deciduous</b>		
<i>Bromus madritensis</i> ssp. <i>rubens</i>	G	10.76	<i>Lycium andersonii</i>	S	3.49
Unknown		0.75	<i>Menodora spinescens</i>	S	3.25
<i>Lotus humistratus</i>	F	0.63	<i>Grayia spinosa</i>	S	1.37
<i>Cryptantha pterocarya</i>	F	0.38	<i>Ambrosia dumosa</i>	S	1.00
<i>Cryptantha</i> spp.	F	0.38	<i>Eriogonum fasciculatum</i>	S	0.88
<i>Cryptantha circumscissa</i>	F	0.25	<i>Pleuraphis jamesii</i> <sup>2</sup>	G	0.38
<i>Cryptantha nevadensis</i>	F	0.25	<i>Atriplex confertifolia</i>	S	0.38
<i>Phacelia fremontii</i>	F	0.25	<i>Stephanomeria pauciflora</i>	F	0.37
<i>Pectocarya platycarpa</i>	F	0.13	<i>Sphaeralcea ambigua</i>	F	0.25
<i>Chaenactis stevioides</i>	F	0.13	<i>Krascheninnikovia lanata</i> <sup>3</sup>	S	0.13
<i>Chorizanthe thurberi</i>	F	0.13	<i>Calochortus flexuosus</i>	F	0.13
<i>Eriogonum deflexum</i>	F	0.13	<i>Delphinium parishii</i>	F	0.13
<i>Lupinus flavoculatus</i>	F	0.13		Total	11.74
<i>Syntrichopappus fremontii</i>	F	0.13			
<i>Vulpia octoflora</i>	G	0.13			
	Total	14.51	<b>Evergreen</b>		



Table D-26. Mean Cover from Ecological Study Plot LG3C (Continued)

LG3C 1993					
Vegetation Type/Species	Life Form <sup>1</sup>	Cover (%)	Vegetation Type/Species	Life Form	Cover (%)
<b>Annuals</b>			<b>Drought Deciduous</b>		
			<i>Ephedra nevadensis</i>	S	6.00
			<i>Ericameria cooperi</i> <sup>4</sup>	S	2.88
			<i>Hymenoclea salsola</i>	S	1.25
			<i>Ericameria teretifolia</i> <sup>5</sup>	S	0.37
			Total		10.50
			Plot Total		36.75

Source: Output DTN: MO0606SPAVEGAS.001.

NOTE: Means are based on data collected from 8 transects on LG3C. Species are arranged in order of dominance within a vegetation type.

<sup>1</sup> G = grass, F = forb, S = shrub.

<sup>2</sup> Previous nomenclature: *Hilaria jamesii*.

<sup>3</sup> Previous nomenclature: *Ceretooides lanata*.

<sup>4</sup> Previous nomenclature: *Happlopapus cooperi*.

<sup>5</sup> Previous nomenclature: *Chrysothamnus teretifolius*.

Table D-27. Mean Cover from Ecological Study Plot LG5C

LG5C 1993					
Vegetation Type/Species	Life Form <sup>1</sup>	Cover (%)	Vegetation Type/Species	Life Form <sup>1</sup>	Cover (%)
<b>Annuals</b>			<b>Drought Deciduous</b>		
<i>Bromus madritensis ssp. rubens</i>	G	6.26	<i>Eriogonum fasciculatum</i>	S	2.61
<i>Cryptantha spp.</i>	F	1.00	<i>Grayia spinosa</i>	S	2.26
<i>Cryptantha pterocarya</i>	F	0.50	<i>Ambrosia dumosa</i>	S	1.38
<i>Syntrichopappus fremontii</i>	F	0.13	<i>Lycium andersonii</i>	S	1.25
<i>Stephanomeria exigua</i>	F	0.12	<i>Atriplex confertifolia</i>	S	1.00
	Total	8.01	<i>Eriogonum inflatum</i>	F	0.50
			<i>Achnatherum speciosum</i> <sup>2</sup>	G	0.25
			<i>Sphaeralcea ambigua</i>	F	0.25
			<i>Mirabilis bigelovii</i>	F	0.13
			<i>Stephanomeria pauciflora</i>	F	0.13
			Total		9.76
			<b>Evergreen</b>		
			<i>Ephedra nevadensis</i>	S	2.63
			<i>Hymenoclea salsola</i>	S	1.63
			<i>Ericameria teretifolia</i> <sup>3</sup>	S	0.50

Table D-27. Mean Cover from Ecological Study Plot LG5C (Continued)

LG5C 1993					
Vegetation Type/Species	Life Form <sup>1</sup>	Cover (%)	Vegetation Type/Species	Life Form	Cover (%)
<b>Annuals</b>			<b>Drought Deciduous</b>		
			<i>Ericameria nauseosa</i> <sup>4</sup>	S	0.25
			<i>Ericameria linearifolia</i> <sup>5</sup>	S	0.25
			<i>Larrea tridentata</i>	S	0.13
				Total	5.39
				Plot Total	23.15

Source: Output DTN: MO0606SPAVEGAS.001.

NOTE: Means are based on data collected from 8 transects on LG5C. Species are arranged in order of dominance within a vegetation type.

<sup>1</sup> G = grass, F = forb, S = shrub.<sup>2</sup> Previous nomenclature: *Stipa speciosa*.<sup>3</sup> Previous nomenclature: *Chrysothamnus teretifolius*.<sup>4</sup> Previous nomenclature: *Chrysothamnus nauseosus*.<sup>5</sup> Previous nomenclature: *Happlopapus linearifolius*.

Table D-28. Mean Cover from Ecological Study Plot LG2T

LG2T 1991					
Vegetation Type/Species	Life Form <sup>1</sup>	Cover (%)	Vegetation Type/Species	Life Form <sup>1</sup>	Cover (%)
<b>Annuals</b>			<b>Drought Deciduous</b>		
<i>Bromus madritensis ssp. rubens</i>	G	4.50	<i>Eriogonum fasciculatum</i>	S	1.40
<i>Salsola iberica</i>	F	1.60	<i>Grayia spinosa</i>	S	0.90
<i>Amsinckia tessellata</i>	F	1.50	<i>Salazaria mexicana</i>	S	0.90
<i>Sisymbrium altissimum</i>	F	0.70	<i>Lycium andersonii</i>	S	0.80
<i>Descurainia pinnata</i>	F	0.20	<i>Achnatherum speciosum</i> <sup>2</sup>	G	0.70
<i>Mentzelia obscura</i>	F	0.20	<i>Atriplex canescens</i>	S	0.40
<i>Phacelia fremontii</i>	F	0.20	<i>Atriplex confertifolia</i>	S	0.20
<i>Camissonia brevipes</i>	F	0.10	<i>Eriogonum inflatum</i>	F	0.10
<i>Lotus humistratus</i>	F	0.10	<i>Krascheninnikovia lanata</i> <sup>3</sup>	S	0.10
<i>Unknown</i>	F	0.10	<i>Encelia virginensis</i>	S	0.10
	Total	9.20	<i>Eriastrum eremicum</i>	S	0.10
			<i>Eriogonum microthecum</i>	S	0.10
				Total	5.80
			<b>Evergreen</b>		
			<i>Ephedra nevadensis</i>	S	2.70
			<i>Gutierrezia sarothrae</i>	S	1.20
			<i>Artemisia tridentata</i>	S	1.10
			<i>Ericameria teretifolia</i> <sup>4</sup>	S	0.70
			<i>Ephedra viridis</i>	S	0.60

Table D-28. Mean Cover from Ecological Study Plot LG2T (Continued)

LG2T 1991					
Vegetation Type/Species	Life Form <sup>1</sup>	Cover (%)	Vegetation Type/Species	Life Form	Cover (%)
<b>Annuals</b>			<b>Drought Deciduous</b>		
			<i>Ericameria cooperi</i> <sup>5</sup>	S	0.60
			<i>Hymenoclea salsola</i>	S	0.40
			<i>Ericameria nauseosa</i> <sup>6</sup>	S	0.30
			<i>Ericameria linearifolia</i> <sup>7</sup>	S	0.20
				Total	7.80
			Plot Total		22.80

Source: Output DTN: MO0606SPAVEGAS.001.

NOTE: Means are based on data collected from 12 transects on LG2T. Species are arranged in order of dominance within a vegetation type.

<sup>1</sup> G = grass, F = forb, S = shrub.

<sup>2</sup> Previous nomenclature: *Stipa speciosa*.

<sup>3</sup> Previous nomenclature: *Ceretooides lanata*.

<sup>4</sup> Previous nomenclature: *Chrysothamnus teretifolius*.

<sup>5</sup> Previous nomenclature: *Happlopapus cooperi*.

<sup>6</sup> Previous nomenclature: *Chrysothamnus nauseosus*.

<sup>7</sup> Previous nomenclature: *Happlopapus linearifolius*.

Table D-29. Mean Cover from Ecological Study Plot LG5T

LG5T 1991					
Vegetation Type/Species	Life Form <sup>1</sup>	Cover (%)	Vegetation Type/Species	Life Form	Cover (%)
<b>Annuals</b>			<b>Drought Deciduous</b>		
<i>Bromus madritensis ssp. rubens</i>	G	1.00	<i>Ambrosia dumosa</i>	S	2.30
<i>Amsinckia tessellata</i>	F	0.30	<i>Atriplex confertifolia</i>	S	1.40
<i>Salsola iberica</i>	F	0.30	<i>Lycium andersonii</i>	S	0.30
<i>Linanthus demissus</i>	F	0.20	<i>Achnatherum speciosum</i> <sup>2</sup>	G	0.30
<i>Sisymbrium altissimum</i>	F	0.20	<i>Krascheninnikovia lanata</i> <sup>3</sup>	S	0.20
<i>Unknown</i>	F	0.20	<i>Eriogonum fasciculatum</i>	S	0.20
<i>Lotus humistratus</i>	F	0.20	<i>Grayia spinosa</i>	S	0.20
<i>Cryptantha nevadensis</i>	F	0.10	<i>Salazaria mexicana</i>	S	0.20
<i>Chorizanthe thurberi</i>	F	0.10	<i>Lycium pallidum</i>	S	0.20
	Total	2.60	<i>Eriogonum inflatum</i>	F	0.10
				Total	5.40
			<b>Evergreen</b>		
			<i>Ephedra nevadensis</i>	S	2.10
			<i>Larrea tridentata</i>	S	0.90
			<i>Hymenoclea salsola</i>	S	0.40

Table D-29. Mean Cover from Ecological Study Plot LG5T (Continued)

LG5T 1991					
Vegetation Type/Species	Life Form <sup>1</sup>	Cover (%)	Vegetation Type/Species	Life Form	Cover (%)
<b>Annuals</b>			<b>Drought Deciduous</b>		
			<i>Ericameria nauseosa</i> <sup>4</sup>	S	0.20
			<i>Ericameria teretifolia</i> <sup>5</sup>	S	0.20
			<i>Ericameria cooperi</i> <sup>6</sup>	S	0.10
				Total	3.90
			Plot Total		11.90

Source: Output DTN: MO0606SPAVEGAS.001.

NOTE: Means are based on data collected from 10 transects on LG5T. Species are arranged in order of dominance within a vegetation type.

<sup>1</sup>G = grass, F = forb, S = shrub

<sup>2</sup>Previous nomenclature: *Stipa speciosa*

<sup>3</sup>Previous nomenclature: *Ceretooides lanata*

<sup>4</sup>Previous nomenclature: *Chrysothamnus nauseosus*

<sup>5</sup>Previous nomenclature: *Chrysothamnus teretifolius*

<sup>6</sup>Previous nomenclature: *Happlopapus cooperi*

Minimum and maximum values for stomatal resistance were determined from conductance values in Table D-18 for vegetation types and growth stages and used in upper and lower bound  $K_{cb}$  calculations (Table D-30). Because the bounds were calculated for the LG association and *Krameria erecta* was not recorded on ESPs sampled for LG, conductance values for this species were not considered for drought deciduous vegetation. One low conductance value for *Ericameria cooperi* (0.0011 m/s) was not considered for the midseason stage for evergreen vegetation because it would have made an unrealistic resistance value (909 s/m) for that time period.

Table D-30. Minimum and Maximum Stomatal Resistance for Vegetation Types

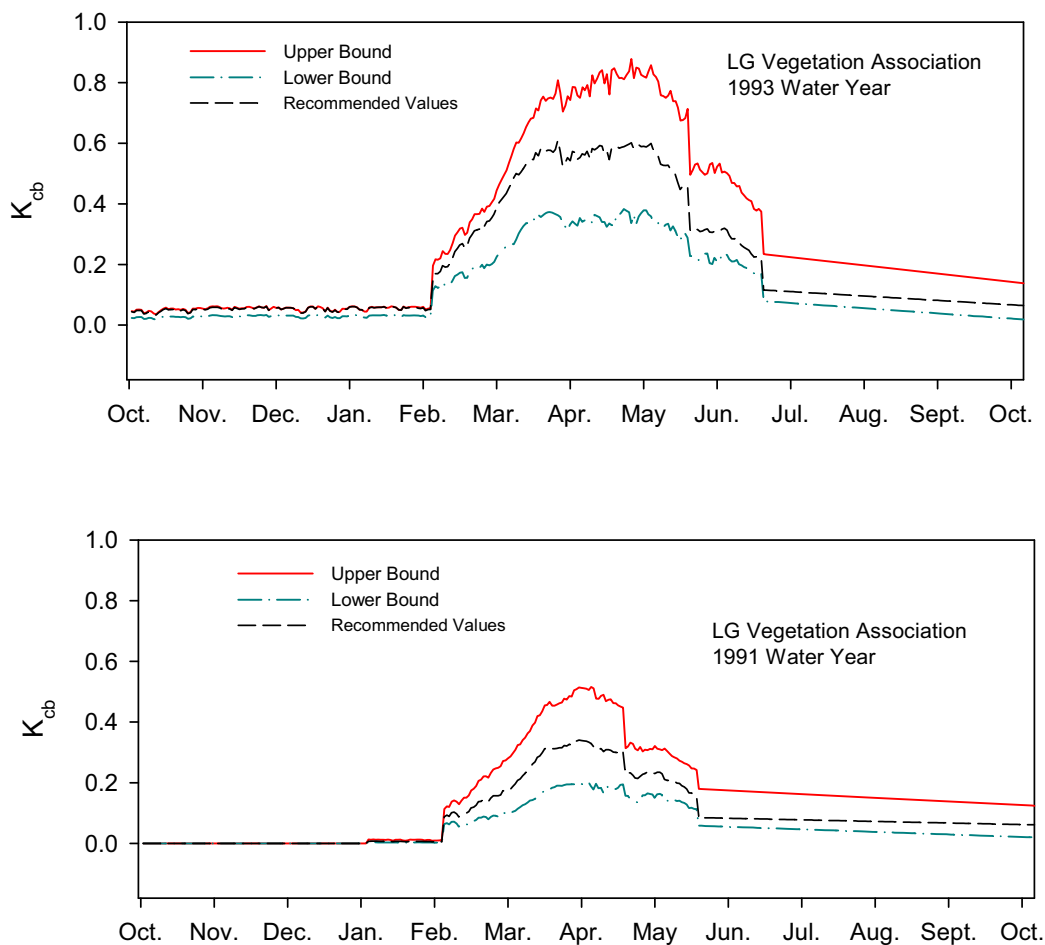
Vegetation Type	Growth Stage	Minimum $r_i$ (s/m) <sup>1</sup>	Maximum $r_i$ (s/m) <sup>2</sup>
Annual	Initial/End	345	357
	Mid	47	200
Drought Deciduous	Initial	385	385
	Mid	68	179
	End	714	714
Evergreen	Initial	323	417
	Mid	47	357
	End	400	2,500

<sup>1</sup> Minimum stomatal resistance for each vegetation type from Table D-19 used in upper bound calculation for transpiration coefficients.

<sup>2</sup> Maximum stomatal resistance for each vegetation type from Table D-19 used in lower bound calculation for transpiration coefficients.

Minimum and maximum plant heights were determined from Table D-5 and used for all vegetation types. The minimum height recorded in Table D-5 was 0.27 m (used in lower bound calculations). The maximum height was 0.51 m. Maximum height was rounded to 0.5 for calculations (used in upper bound calculations).

The upper and lower bounds for  $K_{cb}$ s for the 1998 and 2001 water years are in Figure D-8. The calculations and profile values are in Output DTN: MO0606SPABASAL.001. The uncertainty bounds for the LG association  $K_{cb}$  profiles encompassed the variation observed among association profiles. The LG  $K_{cb}$  profiles with uncertainty bounds were recommended and used in the NDVI- $K_{cb}$  correlations in Section 6.5.3.4.



Source: Output DTN: MO0606SPABASAL.001.

Figure D-8. Transpiration Coefficient Profiles for LG Vegetation Associations with Upper and Lower Uncertainty Bounds for Wet (1993) and Average Precipitation (1991) Years

## D5. FUTURE CLIMATE TRANSPIRATION COEFFICIENTS BASED ON AN EXOTIC GRASS MONOCULTURE

The Glacial Transition climate is expected to be colder and wetter than the modern interglacial climate at Yucca Mountain. Exotic grasses have invaded the current sagebrush steppes of the Great Basin and Columbia Plateau which have similar climate to that predicted for the Glacial Transition. Future climate  $K_{cb}$ s were calculated using *Bromus tectorum*. *Bromus madritensis* spp. *rubens* and *Bromus tectorum* are exotic annual grass species that were introduced to the western United States from Eurasia in the 1800s (Hunter 1991 [DIRS 129944], p. 176; Mack 1981 [DIRS 177164], pp. 145 and 146). Since their introduction, both species have become prominent invaders in cold deserts of the Great Basin and Columbia Plateau (*Bromus tectorum* (Mack 1981 [DIRS 177164], p. 157)) and across areas of the northern Mojave Desert (*Bromus madritensis* (Hunter 1991 [DIRS 129944], pp. 179 and 180)). The success of these two introduced grasses has been largely attributed to phenotypic plasticity, prolific seed production, early use of soil resources, and rapid establishment of root systems (Smith et al. 1997 [DIRS 103636], p. 202). Displacement of native perennial species by *Bromus tectorum* and *Bromus madritensis* is largely a consequence of opportunistic response to fire and their highly competitive nature once established (Smith et al. 1997 [DIRS 103636], p. 215). Both species mature early in the growing season and become extremely flammable, resulting in early season fires that are deleterious to metabolically active and fire intolerant species. Dense stands of *Bromus tectorum* have increased fire frequency in sagebrush steppe communities resulting in elimination of perennial shrubs in many of these habitats (Klemmedson and Smith 1964 [DIRS 177134], pp. 239 through 241). Conversion of sagebrush steppe to annual plant communities appears to be essentially irreversible.

*Bromus tectorum* and *Bromus madritensis* are present at Yucca Mountain in disturbed and undisturbed areas. *Bromus tectorum* occurs at higher elevations and can survive freezing temperatures, while *Bromus madritensis* is less tolerant of cold and killed by winter freeze. Studies have shown that densities of *Bromus madritensis* have increased over time on the NTS (e.g., Hunter 1991 [DIRS 129944]), and it has been the dominant annual species on ESPs during years of average and above average precipitation (Tables D-10 through D-15). Shifts in dominance of native perennial shrubs to exotic annual grasses have the potential to change net infiltration at Yucca Mountain. Maximum rooting depths of native shrub species in the Mojave Desert average about 2 m (Section 6.5.3.2), and studies have shown that native shrubs can extract water and nutrients to depths of two to three meters (Yoder and Nowak 1999 [DIRS 177167], p. 91, Figure 6; Jackson et al. 2002 [DIRS 177171], p. 624, Table 1). Mean maximum rooting depth for *Bromus tectorum* is about 1.0 m (Section 6.5.3.2), and studies have shown that water remains in the soil profile below about 0.5 to 0.6 m at the end of the growing season in brome dominated communities (Cline et al. 1977 [DIRS 177127], p. 200, Figure 3). The combination of shorter growing seasons and shallower root systems for *Bromus* spp. could result in increased net infiltration at Yucca Mountain should it become a brome dominated system.

Thus, with mechanisms that cause conversion from perennial shrub dominated communities to exotic annual communities already in place at Yucca Mountain and the potentially irreversible nature of these changes, a future climate scenario with a brome monoculture in place was considered for the infiltration model. Because the future climate is predicted to be colder and

wetter than the current climate, characteristics (timing of phenological events, rooting depths, and cover) of *Bromus tectorum* were used to calculate  $K_{cb}$ s. Additionally, increased fire frequencies and suppression of native perennial flora associated with *Bromus tectorum* invasions have been documented in southeastern Washington and areas around Spokane Washington (Mack 1981 [DIRS 177164], p. 151, Figure 1f; pp. 155 and 156), which is one of the future climate analogues (BSC 2004 [DIRS 170002], pp. 6-44 and 6-45, Table 6-1).

The equations and methods documented in the previous sections for calculating  $K_{cb}$ s were used to calculate  $K_{cb}$ s for the brome monoculture and therefore will not be repeated here. Inputs to  $K_{cb}$  calculations for the brome monoculture and the resulting  $K_{cb}$  profile are described below.

### D5.1. GROWTH STAGES AND VEGETATION HEIGHT

Growth stages for *Bromus tectorum* were developed from three sources: published values for timing of phenological stages; temperature requirements for growth established in Upadhyaya et al. (1986 [DIRS 177149], p. 695); and monthly mean temperatures from the future climate analogue weather station in Spokane, Washington.

Generally *Bromus tectorum* germinates in the fall and rapidly establishes a root system (Stewart and Hull 1949 [DIRS 177146], p. 58; Smith et al. 1997 [DIRS 103636], p. 210). It over-winters as a small basal rosette in a dormant to semi-dormant condition and initiates growth again in the spring as soon as temperatures allow (Klemmedson and Smith 1964 [DIRS 177134], p. 231). Stewart and Hull (1949 [DIRS 177146], p. 58) observed germination and leaf growth in Idaho from late September through October (Table D-31). Mack and Pyke (1983 [DIRS 177141], p. 89) observed emergence of *Bromus tectorum* in late August to early September when early rains occurred at sites in eastern Washington. However, early rains were commonly followed by dry periods and these cohorts usually died. Cohorts emerging in October were more likely to survive (Mack and Pyke 1983 [DIRS 177141], p. 89). When snow cover occurred at these sites, it lasted from the end of October through midFebruary (Mack and Pyke 1983 [DIRS 177141], p. 75, Figure 2). Link et al. (1990 [DIRS 177142], p. 511, Figure 6) observed initiation of spring growth in midFebruary to midMarch, flowering in mid to late April, and senescence in late May (Table D-31). Hulbert (1955 [DIRS 177129], p. 190, Figure 4) observed flowering at the end of April at Idaho sites and senescence was observed from early to late June (Table D-31).

Table D-31. Timing of Phenological Stages for *Bromus tectorum*

Reference	Germination and Leaf Growth	Winter Semi-Dormant Stage	Initiation of Spring Growth	Flowering Stage	Senescence
Hulbert 1955 [DIRS 177129] p. 190, Figure 4				End of April	By June 22
Link et al. 1990 [DIRS 177142], p. 511, Figure 6			Mid February to Mid March	Mid to late April	Late May
Stewart and Hull 1949 [DIRS 177146], p. 58	Late September to October				June 5 to 30
Mack and Pyke 1983 [DIRS 177141], pp. 83 and 75, Figure 2	Late August to October	October 31 to February 15			

Upadhyaya et al. (1986 [DIRS 177149], p. 695) described three seasonal growth phases for *Bromus tectorum* related to soil temperature (Table D-32).

Table D-32. Growth Phases for *Bromus tectorum*<sup>1</sup>

Growth Phase	Soil Temperature	Growth Description
Limited	1.9°C to 3.5°C	Growth is initiated
Unaffected	3.5°C to 15°C	Optimum growth
Inhibited	> 15°C	Retarded growth
Senescence	≈ 27°C	Growth ceases

<sup>1</sup> Growth phases are from Upadhyaya et al. 1986 [DIRS 177149], p. 695.

Using mean monthly air temperature from the Glacial Transition climate analogue station in Spokane (Table D-33) as a surrogate for soil temperature, the growth phases reported by Upadhyaya et al. (1986 [DIRS 177149], p. 695) correspond to following months:

- Limited phase – November and March
- Unaffected phase – April to May
- Inhibited phase – June to August.

Mean maximum air temperatures for the Glacial Transition climate analogue station reach 24°C in June and remain high July through September (Western Regional Climate Center 1997 [DIRS 152233]), which suggests that soil temperatures during this time period correspond to the senescence phase. Mean monthly air temperatures for December through February (Table D-33) are too cold for growth and suggest that *Bromus tectorum* would be quiescent during those months.

Table D-33. Average Monthly Weather Data for Glacial Transition Climate

Month	Temperature <sup>1</sup> (°C)	Month	Temperature (°C)
January	-2.7	July	20.4
February	0.7	August	20.2
March	3.7	September	14.9
April	7.7	October	8.5
May	12.2	November	1.7
June	16.7	December	-2.3

Source: Western Regional Climate Center (1997 [DIRS 152233]).

<sup>1</sup>Temperature was converted from °F to °C (°C = [°F-32]/1.8).

Based on the timing of phenological stages (Table D-31) and the comparison of growth phases to average monthly temperatures for the Glacial Transition climate, October 1 through 31, November 1 to February 28, March 1 to 31, April 1 to 30, May 1 to 15, and May 16 to May 30 were assigned to the initial, quiescent, initial, development, mid-, and late-growth stages, respectively, for *Bromus tectorum* (Table D-34).



Table D-34. Growth Stages for *Bromus tectorum*

Growth Stage	Annual
Initial	Oct. 1 to 31 DOY 274 to 304
Quiescent	Nov. 1 to Feb. 28 DOY 305 to 59
Initial	Mar. 1 to 31 DOY 60 to 90
Development	Apr. 1 to 30 DOY 91 to 120
Mid	May 1 to May 15 DOY 121 to 135
Late	May 16 to 31 DOY 136 to 151

**Vegetation Height**—In comprehensive reviews of *Bromus tectorum* ecology, Carpenter and Murray ([n.d.] [DIRS 174674], p. 7) reported fall growth of 2 to 4 cm (0.02 to 0.04 m) prior to the onset of winter dormancy, and Stewart and Hull (1949 [DIRS 177146], pp. 58 and 59) reported ordinary heights of mature plants of 12 to 20 inches (0.30 to 0.50 m), with 24 (0.60 m) or more inches under favorable conditions. For this analysis, a height of 0.03 m (the mean of values reported for fall growth) was selected for the initial growth stage and 0.46 m (the mean of values reported for mature plants rounded down to the nearest tenth of a meter) was selected for the mid season growth stage.

## D5.2. COVER DATA

To get estimates of potential ground cover for a brome monoculture scenario at Yucca Mountain, it was assumed that the grass would invade most areas that were not covered by gravel, cobble, or rock surfaces that would prevent or limit its ability to establish. Cover data collected from ESPs in 1990, 1991, and 1993 included measurement of percent of ground covered by gravel, cobble, and rock which were classified according to the following clast sizes:

- Gravel > 0.5 cm and  $\leq$  8 cm
- Cobble > 8 cm and  $\leq$  25 cm
- Rock > 25 cm.

Considering the range of particle size for gravel, it is unlikely that all gravel cover would omit brome establishment. However, there are other unmeasured factors that would exclude brome establishment including thin soils, rock outcrops, and soil surface crusts that form physical barriers. Therefore, gravel cover was included partly as a surrogate for these unmeasured factors.

Mean percent cover of gravel, cobble, and rock cover for ESPs representing the LA, LG, and LLG vegetation associations for 1990, 1991, and 1993 was determined using the same methods described for vegetation cover in Section D3.2.2. For each association, the means of gravel, cobble, and rock cover were summed to get a total cover for each year (Table D-35). Means and standard deviations based on the three years of data collection were calculated for each

association (Table D-35). The resulting mean values were subtracted from 100% to get the estimated potential cover of brome for each association for use in  $K_{cb}$  calculations (Table D-35).

Table D-35. Mean Cover of Gravel, Cobble, and Rock, and Potential Brome Cover

Vegetation Association	Mean Gravel Cover (%)	Mean Cobble Cover (%)	Mean Rock Cover (%)	Sum <sup>1</sup>	Mean of Years <sup>2</sup>	SD of Years <sup>3</sup>	Potential Brome Cover <sup>4</sup> (%)
LA 1990	38.13	1.11	0.84	40.08	33.91	5.423	66.09
LA 1991	28.03	1.33	0.54	29.9			
LA 1993	29.02	1.67	1.06	31.75			
LG 1990	27.69	9.06	15.43	52.18	48.413	5.713	51.59
LG 1991	25.67	9.29	16.26	51.22			
LG 1993	17.89	7.5	16.45	41.84			
LLG 1990	33.86	4.81	5.79	44.46	39.89	6.499	60.11
LLG 1991	32.41	5.06	5.29	42.76			
LLG 1993	20.94	5.12	6.39	32.45			

Source: Output DTN: MO0606SPAVEGAS.001.

<sup>1</sup> Sum of mean gravel, cobble, and rock cover for each year.

<sup>2</sup> Average of sums for 1990, 1991, and 1993.

<sup>3</sup> Standard deviation of sums for 1990, 1991, and 1993.

<sup>4</sup> Mean of years subtracted from 100.

### D5.3. STOMATAL RESISTANCE

Two sources that measured stomatal conductance in velocity units were used to estimate  $r_l$  for *Bromus tectorum* (Table D-36). Link et al. (1990 [DIRS 177142]) measured stomatal conductance of bromus plants grown at a field site in southeastern Washington. Mean maximal stomatal conductance measured on April 11 and 18 were used in the estimate for the midseason growth stage, and mean maximal stomatal conductance measured on May 1 was used in the estimate for initial and end of late season growth stages (Table D-36). Rice et al. (1992 [DIRS 177165]) measured stomatal conductance of bromus plants grown from seed sources collected in southeastern Washington and northern Idaho. Plants were grown in a glass house under controlled conditions. The ten highest values for conductance that were measured prior to the onset of water stress were selected to estimate  $r_l$  for the midseason growth stage (Rice et al. 1992 [DIRS 177165], p. 36, Figure 4). Seven lower values were selected to estimate  $r_l$  for the initial and end of late season growth stages (0.25 to 0.60 cm/s, Table D-36). Mean  $r_l$  was calculated according to Equation D-14 (Table D-36). Mean  $r_l$  for the initial and end of late season growth stages was used in Equation D-6 to correct  $K_{cbs}$  for stomatal resistance that was higher than that of agricultural species (Allen et al. 1998 [DIRS 157311], p. 191). Mean  $r_l$  for the mid season growth stage was less than 100 stomatal resistance; therefore, the resistance correction factor was not required (Allen et al. 1998 [DIRS 157311], p. 191).

Table D-36. Stomatal Conductance and Resistance for *Bromus tectorum*

Reference	Comments	$g^1$ (cm/s)	$g$ (m/s)	mean $g$ (m/s)	mean $r_1^2$ (s/m)
<b>Initial and Late Season Growth Stages</b>					
Link et al. 1990 [DIRS 177142], p. 508, Table 2	Measured May 1	0.62	0.0062	0.0048	208
Rice et al. 1992 [DIRS 177165], p. 36, Figure 4	Values from low end of graph (0.25 to 0.60). Value below 0.25 not used.	0.60	0.006		
		0.60	0.006		
		0.60	0.006		
		0.30	0.003		
		0.25	0.0025		
		0.25	0.0025		
<b>MidSeason Growth Stage</b>					
Link et al. 1990 [DIRS 177142], p. 508, Table 2	Mean Maximal $g$ measured Apr. 11 and 18; predawn water potentials indicate no stress.	0.78	0.0078	0.0140	71
Rice et al. 1992 [DIRS 177165], p. 36, Figure 4	Values from upper end of graph where no stress is indicated (1.48 to 1.75).	0.68	0.0068		
		1.75	0.0175		
		1.6	0.016		
		1.6	0.016		
		1.5	0.015		
		1.5	0.015		
		1.49	0.0149		
		1.49	0.0149		
		1.48	0.0148		
1.48	0.0148				
1.48	0.0148				

<sup>1</sup>  $g$  = stomatal conductance.<sup>2</sup>  $r_1$  = stomatal resistance (Equation D-14).

## D5.4 METEOROLOGICAL PARAMETERS

The upper bound Glacial Transition climate is semi-arid and characterized by cool, wet winters, and warm to cool dry summers relative to current conditions (BSC 2004 [DIRS 170002], Section 6.6.2). Recommended analogue weather stations for the upper bound Glacial Transition climate are Spokane, St. John, and Rosalia, Washington (BSC 2004 [DIRS 170002], Table 6-1 and Section 6.6.2). Daily temperature data from the Spokane weather station (DTN: MO0605SPASPOKA.000 [DIRS 177135]) were used as source data to calculate  $RH_{min}$  and  $\Delta$  for corrections to  $K_{cb}$ s. Daily data were averages of 10 to 13 years of data (DTN: MO0605SPASPOKA.000 [DIRS 177135]). Daily wind speed data from Yucca Mountain Meteorological Site 1 for water year 1998 were used in the  $K_{cb}$  calculation. As described in Section D3.2.4, wind speed data were corrected for a height of 2 m according to Equation D-15 (Output DTN: MO0603SPAREFET.000).

Average daily maximum temperatures ( $T_{max}$ ), average daily minimum air temperatures ( $T_{min}$ ), and average daily precipitation were extracted from the source file (DTN: MO0605SPASPOKA.000 [DIRS 177135]) and placed in an Excel® file (Output DTN: MO0605SPADAYWA.000 [DIRS 177135]). Temperature was converted from Fahrenheit to Celsius ( $^{\circ}\text{C} = 5/9 \times [^{\circ}\text{F}-32]$ ) and precipitation from inches to mm (1 inch = 25.4 mm). Minimum relative humidity was calculated according to the following equations (Allen et al. 1998 [DIRS 157311], p. 124, Equation 64, and p. 36, Equation 11):

$$RH_{\min} = \frac{e^{\circ}(T_{dew})}{e^{\circ}(T_{\max})} \times 100 \quad (\text{Eq. D-17})$$

and

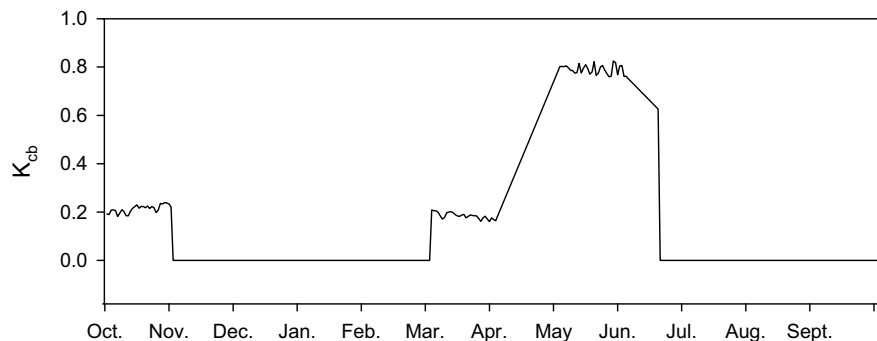
$$e^{\circ}(T) = 0.6108 \exp\left[\frac{17.27T}{T + 237.3}\right] \quad (\text{Eq. D-18})$$

where

- $e^{\circ}(T)$  = Saturation vapor pressure at temperature  $T$  (kPa),
- $T_{dew}$  = Minimum daily air temperature minus 2 degrees ( $^{\circ}\text{C}$ ),
- $T_{max}$  = Maximum daily air temperature,
- $\exp(x)$  = 2.7183 (base of natural logarithm) raised to the power ( $x$ ).

Average daily temperature was calculated from the mean of  $T_{max}$  and  $T_{min}$  (Output DTN: MO0605SPADAYWA.000) and used to calculate  $\Delta$  for use in the stomatal correction factor. As described in Section D3.2.4,  $\Delta$  was calculated according to Equation D-16 (Output DTN: MO0605SPADAYWA.000).

An average profile of the three associations (Figure D-9) was calculated in the Excel® spreadsheet in Output DTN: MO0606SPATRANS.000. This calculation was done using the Excel® AVERAGE command. Daily  $K_{cbs}$  and supporting calculations are in Output DTN: MO0606SPATRANS.000.



Source: Output DTN: MO0606SPATRANS.000.

Figure D-9. Transpiration Coefficients ( $K_{cb}$ ) for a *Bromus* Monoculture at Yucca Mountain

## D6. METHODS FOR CALCULATING REFERENCE EVAPOTRANSPIRATION FOR A GENERIC AREA AT YUCCA MOUNTAIN

To determine if reasonable values for plant water use in a desert environment were generated by the  $K_{cb}$  profiles,  $ET_0$  was needed for a generic area at Yucca Mountain to estimate potential transpiration ( $PT = ET_0 \times K_{cb}$  [Section 6.5.3.4]). Reference evapotranspiration was calculated as a function of slope and azimuth using the standardized FAO-56 Penman-Montieth equation in Appendix C for use in the infiltration model (Equation C-37). The  $ET_0$  values calculated in Appendix C are direct input to specific model grid cells. The results of this calculation show that the  $K_{cb}$  values estimated for the Yucca Mountain site result in a reasonable estimate of potential transpiration, which is consistent with comparable field data.

Reference evapotranspiration for a generic area at Yucca Mountain was also calculated according to methods described in Allen et al. (1998 [DIRS 157311]) using the FAO Penman-Monteith equation (Allen et al. 1998 [DIRS 157311], Equation 6, p. 24):

$$ET_0 = \frac{0.408\Delta(R_n - G) + \gamma \frac{900}{T + 273} u_2 (e_s - e_a)}{\Delta + \gamma(1 + 0.34u_2)} \quad (\text{Eq. D-19})$$

where

- $ET_0$  = Reference evapotranspiration (mm/day),
- $R_n$  = Net radiation at the crop surface ( $\text{MJ m}^{-2} \text{ day}^{-1}$ ),
- $G$  = Soil heat flux density ( $\text{MJ m}^{-2} \text{ day}^{-1}$ ),
- $T$  = Mean daily air temperature at 2 m height ( $^{\circ}\text{C}$ ),
- $u_2$  = Wind speed at 2 m height ( $\text{m s}^{-1}$ ),
- $e_s$  = Saturation vapor pressure (kPa),
- $e_a$  = Actual vapor pressure (kPa),
- $e_s - e_a$  = Saturation vapor pressure deficit (kPa),

$$\begin{aligned}\Delta &= \text{Slope vapor pressure curve (kPa } ^\circ\text{C}^{-1}\text{)}, \\ \gamma &= \text{Psychrometric constant (kPa } ^\circ\text{C}^{-1}\text{)}.\end{aligned}$$

Equation D-19 is the same as Equation C-37 used in Appendix C.

## D6.1 CALCULATION OF REFERENCE EVAPOTRANSPIRATION FOR A GENERIC AREA AT YUCCA MOUNTAIN

Meteorological factors that drive evapotranspiration include solar radiation, air temperature, air humidity, and wind speed. Climatological and physical parameters required to derive daily  $ET_0$  were either measured directly or derived from measured data. Daily  $ET_0$  was calculated using weather data from water years 1998, 2001, and 2002 to represent above average, average, and below average precipitation years, respectively. Reference  $ET$  was used with NDVI in Appendix E, and with  $K_{cbs}$  calculated in this appendix to estimate potential water use by desert vegetation for representative above average, average, and below average precipitation years. Weather data was used from Yucca Mountain Meteorological Site 1. The step-by-step methods to calculate  $ET_0$  are described and example calculations are provided below.

### D6.2 STEP-BY-STEP DESCRIPTION OF CALCULATIONS

Three atmospheric parameters were generated from meteorological data and used directly in the calculation of  $ET_0$ . These include the slope of the saturation vapor pressure curve ( $\Delta$ ), psychrometric constant ( $\gamma$ ), and vapor pressure deficit ( $e_s - e_a$ ). The slope of the saturation vapor pressure curve and  $\gamma$  were developed in Section D3.2.4. Values for  $\Delta$  for the 1998, 2001, and 2002 water years are in Output DTN: MO0603SPAREFET.000. A value of 0.059, which corresponds to the elevation of meteorological monitoring Site 1, was selected for  $\gamma$  (Section D3.2.4). Vapor pressure deficits are developed below.

#### D6.2.1 Vapor Pressure

**Vapor Pressure Deficit ( $e_s - e_a$ )**—The vapor pressure deficit ( $e_s - e_a$ ) is the difference between the saturation vapor pressure ( $e_s$ ) and the actual vapor pressure ( $e_a$ ) of the air. Essentially, it represents the evaporative power of the air. The air becomes dryer as the vapor pressure deficit increases.

Mean  $e_s$  is the average of the saturation vapor pressures calculated at the daily maximum ( $T_{max}$ ) and minimum ( $T_{min}$ ) air temperatures (Output DTN: MO0602SPAWEATH.000). The relationship of  $e_s$  to temperature is given by the following equations (Allen et al. 1998 [DIRS 157311], Equations 11 and 12, p. 36):

$$e^o(T) = 0.6108 \exp\left[\frac{17.27T}{T + 237.3}\right] \quad (\text{from Eq. D-18})$$

where

$e^{\circ}(T)$  = Saturation vapor pressure at temperature  $T$  (kPa),

$T$  = Air temperature ( $^{\circ}\text{C}$ ),

$\exp(x)$  = 2.7183 (base of natural logarithm) raised to the power ( $x$ ).

and

$$e_s = \frac{e^{\circ}(T_{\max}) + e^{\circ}(T_{\min})}{2} \quad (\text{Eq. D-20})$$

Example: For March 1, 1998 (day of year 60),  $T_{\max} = 13.9^{\circ}\text{C}$  and  $T_{\min} = 2.3^{\circ}\text{C}$  (Output DTN: MO0602SPAWEATH.000).

$$e^{\circ}(T_{\max}) = 0.6108 \exp\left[\frac{17.27(13.9)}{13.9 + 237.3}\right] = 0.6108 \exp 0.956 = 1.588 \text{ kPa} \quad (\text{from Eq. D-18})$$

$$e^{\circ}(T_{\min}) = 0.6108 \exp\left[\frac{17.27(2.3)}{2.3 + 237.3}\right] = 0.6108 \exp 0.166 = 0.721 \text{ kPa}$$

$$e_s = \frac{1.588 + 0.721}{2} = 1.154 \text{ kPa}$$

Daily  $e^{\circ}(T_{\max})$ ,  $e^{\circ}(T_{\min})$ , and  $e_s$  for the 1998, 2001, and 2002 water years are in Output DTN: MO0603SPAREFET.000.

Actual vapor pressure ( $e_a$ ) can be calculated from relative humidity ( $RH$ ), the dewpoint temperature ( $T_{dew}$ ), or psychrometric data. Monthly mean maximum and minimum  $RH$  values were available from meteorological monitoring Site 1. However, examination of  $RH$  values indicated they were not always representative of the expected conditions of the reference area defined for  $ET_0$  in FAO-56 methods (Allen et al. 1998 [DIRS 157311]). Under reference area conditions,  $RH_{\max}$  is expected to approach 90% to 100% (Allen et al. 1998 [DIRS 157311], Annex 6, pp. 257 to 262). At monitoring Site 1, daily  $RH_{\max}$  was less than 70% for up to 80% of the time, depending on the year (Output DTN: MO0602SPAWEATH.000). Use of such low  $RH$  values would result in overestimation of  $ET_0$ . Allen et al. (1998 [DIRS 157311], p. 36, and Annex 6, pp. 257 to 262) recommended use of  $T_{dew}$  calculated from daily minimum temperature rather than using unreliable or unrepresentative  $RH$  values or when no humidity data are available. Therefore, instead of using  $RH_{\max}$  to calculate  $e_a$ ,  $T_{dew}$  was estimated from  $T_{\min}$  (Allen et al. 1998 [DIRS 157311], Equation 6-6, p. 261):

$$T_{dew} = T_{\min} - K_o \quad (\text{Eq. D-21})$$

where  $K_o$  is a correction factor =  $2^{\circ}\text{C}$  for arid climates (Allen et al. 1998 [DIRS 157311], p. 261).

Use of Equation D-21 reflects the higher humidity anticipated under reference conditions. Dewpoint temperatures calculated with Equation D-21 are in Output DTN: MO0603SPAREFET.000.

The adjusted  $T_{dew}$  was used in the following equation to calculate daily values of  $e_a$  for the 1998, 2001, and 2002 water years (Allen et al. 1998 [DIRS 157311], Equation 14, p. 37):

$$e_a = e^o(T_{dew}) = 0.6108 \exp\left[\frac{17.27T_{dew}}{T_{dew} + 237.3}\right] \quad (\text{Eq. D-22})$$

Example: For March 1, 1998 (day of year 60),  $T_{min} = 2.3^\circ\text{C}$  (Output DTN: MO0602SPAWEATH.000) and  $T_{dew} = 0.3^\circ\text{C}$  (Output DTN: MO0603SPAREFET.000).

$$e_a = 0.6108 \exp\left[\frac{17.27 \times 0.3}{0.3 + 237.3}\right] = 0.6108 \exp(0.022) = 0.624 \text{ kPa} \quad (\text{from Eq. D-22})$$

Daily  $e_a$  values for 1998, 2001, and 2002 water years are in Output DTN: MO0603SPAREFET.000.

Using  $e_s$  and  $e_a$  calculated for March 1, 1998, the vapor pressure deficit is:

$$(e_s - e_a) = 1.154 - 0.580 = 0.574 \text{ kPa} \quad (\text{Eq. D-23})$$

Average daily ( $e_s$  and  $e_a$ ) values for the 1998, 2001, and 2002 water years are in Output DTN: MO0603SPAREFET.000.

## D6.2.2 Radiation

Net radiant energy is one of the main factors controlling the energy balance of a vegetated soil surface. Heat energy for  $ET$  is principally supplied by solar radiation, which can reach the plant canopy as direct sunlight or sunlight scattered by molecules and particles in the atmosphere. Both direct and scattered sunlight can be reflected by surroundings to the plant canopy. Net radiation ( $R_n$ ) represents the balance between energy absorbed, reflected, and emitted by the earth's surface and is used directly in the calculation of  $ET_0$ . Extraterrestrial radiation ( $R_a$ ), solar radiation ( $R_s$ ), clear sky radiation ( $R_{so}$ ), net shortwave radiation ( $R_{ns}$ ), and net longwave radiation ( $R_{nl}$ ) are required either directly or indirectly to calculate  $R_n$ .

**Extraterrestrial Radiation ( $R_a$ )**—Extraterrestrial radiation is the solar radiation received at the top of the earth's atmosphere on a horizontal surface. It is a function of latitude, date, and time of day. Daily  $R_a$  was calculated according to the following equations (Allen et al. (1998 [DIRS 157311], Equations 21 to 25, p. 46):

$$R_a = \frac{24(60)}{\pi} G_{sc} d_r [\omega_s \sin(\varphi) \sin(\delta) + \cos(\varphi) \cos(\delta) \sin(\omega_s)] \quad (\text{Eq. D-24})$$



where

$R_a$	=	Extraterrestrial radiation ( $\text{MJ m}^{-2} \text{ day}^{-1}$ ),
$G_{sc}$	=	Solar constant = $0.0820 \text{ (MJ m}^{-2} \text{ min}^{-1}\text{)}$ ,
$d_r$	=	Inverse relative distance Earth–Sun (Equation D-26),
$\varphi$	=	Latitude (rad) (Equation D-25),
$\omega_s$	=	Sunset hour angle (rad) (Equation D-28),
$\delta$	=	Solar declination (rad) (Equation D-27).

$$\varphi \text{ (radians)} = \frac{\pi}{180} [\text{latitude in decimal degrees}] \quad (\text{Eq. D-25})$$

$$d_r = 1 + 0.033 \cos\left(\frac{2\pi}{365} J\right) \quad (\text{Eq. D-26})$$

$$\delta = 0.409 \sin\left(\frac{2\pi}{365} J - 1.39\right) \quad (\text{Eq. D-27})$$

where  $J$  is the day of year.

$$\omega_s = \arccos[-\tan(\varphi)\tan(\delta)] \quad (\text{Eq. D-28})$$

Example: Using meteorological monitoring Site 1 (latitude =  $36^\circ 51'$ ) and March 1 (day of year 60), convert latitude from degrees and minutes to decimal degrees, then to radians.

$$36 + \frac{51}{60} = 36.85 \text{ (decimal degrees)}$$

$$\varphi [\text{Radians}] = \frac{\pi}{180} 36.85 = 0.64 \quad (\text{from Eq. D-25})$$

Calculate  $d_r$  and  $\delta$ .

$$d_r = 1 + 0.033 \cos\left(\frac{2\pi}{365} 60\right) = 1.017 \quad (\text{from Eq. D-26})$$

$$\delta = 0.409 \sin\left(\frac{2\pi}{365} 60 - 1.39\right) = -0.143 \quad (\text{from Eq. D-27})$$

Calculate  $\omega_s$ .

$$\omega_s = \arccos[-\tan(0.64)\tan(-0.143)] = 1.463 \quad (\text{from Eq. D-28})$$

Calculate  $R_a$ .

$$R_a = \frac{24(60)}{\pi} 0.082 \times 1.017 [1.463 \sin(0.64) \sin(-0.143) + \cos(0.64) \cos(-0.143) \sin(1.463)]$$

$$= 25.4 \text{ MJ m}^{-2} \text{ day}^{-1} \quad (\text{from Eq. D-24})$$

Daily  $R_a$  values for the 1998, 2001, and 2002 water years are in Output DTN: MO0603SPAREFET.000.

**Solar Radiation ( $R_s$ )**—Solar radiation ( $R_s$ ) measured at meteorological monitoring Site 1 for the 1998, 2001, and 2002 water years was used in  $ET_0$  calculations. See Section D3.2.4 for description and development of solar radiation data. Solar radiation data for the 1998, 2001, and 2002 water years are in Output DTN: MO0602SPAWEATH.000.

**Clear Sky Radiation ( $R_{so}$ )**—Clear sky radiation ( $R_{so}$ ) is the radiation that would hit a flat surface under cloudless conditions (Allen et al. 1998 [DIRS 157311], Equation 37, p. 51):

$$R_{so} = (0.75 + 2 \times 10^{-5} Z) R_a \quad (\text{Eq. D-29})$$

where

$$Z = \text{station elevation above sea level (m).}$$

Example: Station elevation for meteorological Site 1 = 1,143 m and  $R_a$  for March 1, 1998 (day of year 60) = 25.4 MJ m<sup>-2</sup> day<sup>-1</sup> (Output DTN: MO0603SPAREFET.000).

$$R_{so} = (0.75 + 2 \times 10^{-5} \times 1143) 25.4 = 19.6 \text{ MJ m}^{-2} \text{ day}^{-1} \quad (\text{from Eq. D-29})$$

Clear sky radiation is required to calculate net longwave radiation ( $R_{nl}$ ), which is used directly in the calculation of  $R_n$ . Daily  $R_{so}$  values are in Output DTN: MO0603SPAREFET.000.

**Net Solar (shortwave) Radiation ( $R_{ns}$ )**—Net solar radiation incorporates albedo (shortwave radiation reflected from the canopy of the grass reference crop) into incoming solar radiation and is used directly in the calculation of  $R_n$  (Allen et al. 1998 [DIRS 157311], Equation 38, p. 51):

$$R_{ns} = (1 - \alpha) R_s \quad (\text{Eq. D-30})$$

Where  $\alpha$  = albedo of grass reference crop = 0.23 (Allen et al. 1998 [DIRS 157311], p. 51).

Example: For March 1, 1998  $R_s = 18.1 \text{ MJ m}^{-2} \text{ day}^{-1}$  (Output DTN: MO0602SPAWEATH.000).

$$R_{ns} = (1 - 0.23) 18.1 = 13.9 \text{ MJ m}^{-2} \text{ day}^{-1} \quad (\text{from Eq. D-30})$$

Mean monthly  $R_{ns}$  values are in Output DTN: MO0603SPAREFET.000.

**Net Longwave Radiation ( $R_{nl}$ )**—Net loss of radiant energy ( $R_{nl}$ ) occurs primarily through thermal or longwave radiation. The Stefan-Boltzmann law predicts that black body radiation emission (radiation emitted by a perfect radiator) is proportional to surface temperature raised to the fourth power (Nobel 1983 [DIRS 159953], p. 347). Plants are virtually black body absorbers and emitters of longwave radiation. However, radiant energy is also absorbed and emitted by water vapor, carbon dioxide, ozone and clouds, which affects the outgoing energy flux. Because of this, the Stefan-Boltzmann law is corrected for humidity and cloudiness in the calculation of net outgoing longwave radiation ( $R_{nl}$  (Allen et al. 1998 [DIRS 157311], Equation 39, p. 52)):

$$R_{nl} = \sigma \left[ \frac{T_{max, K^4} + T_{min, K^4}}{2} \right] \left( 0.34 - 0.14 \sqrt{e_a} \right) \left[ 1.35 \frac{R_s}{R_{so}} - 0.35 \right] \quad (\text{Eq. D-31})$$

where

- $\sigma$  = Stefan-Boltzmann constant ( $4.903 \times 10^{-9} \text{ MJ K}^{-4} \text{ m}^{-2} \text{ day}^{-1}$ ),
- $T_{max}, K$  = maximum absolute temperature during the 24-hour period ( $K = ^\circ\text{C} + 273.16$ ),
- $T_{min}, K$  = minimum absolute temperature during the 24-hour period ( $K = ^\circ\text{C} + 273.16$ ),
- $e_a$  = actual vapor pressure (kPa),
- $R_s/R_{so}$  = relative shortwave radiation (limited to  $\leq 1.0$ ),
- $R_s$  = measured (Present-Day climate) or calculated (future climate) solar radiation ( $\text{MJ m}^{-2} \text{ day}^{-1}$ ),
- $R_{so}$  = calculated clear-sky radiation ( $\text{MJ m}^{-2} \text{ day}^{-1}$ ).

Example: For March 1, 1988,  $T_{max} = 13.9^\circ\text{C}$  and  $T_{min} = 2.3^\circ\text{C}$  (Output DTN: MO0602SPAWEATH.000);  $e_a = 0.580$  (Output DTN: MO0603SPAREFET.000);  $R_s = 18.1 \text{ MJ m}^{-2} \text{ day}^{-1}$  (Output DTN: MO0602SPAWEATH.000);  $R_{so} = 19.8 \text{ MJ m}^{-2} \text{ day}^{-1}$  (Output DTN: MO0603SPAREFET.000); and  $\sigma T_{max}, K^4 = 33.3$ ,  $\sigma T_{min}, K^4 = 28.2$  (Output DTN: MO0603SPAREFET.000).

$$\begin{aligned} R_{nl} &= \left[ \frac{33.3 + 28.2}{2} \right] \left( 0.34 - 0.14 \sqrt{0.580} \right) \left[ 1.35 \left( \frac{18.1}{19.8} \right) - 0.35 \right] \quad (\text{from Eq. D-31}) \\ &= 30.75 \times 0.233 \times 0.884 = 6.3 \text{ MJ m}^{-2} \text{ day}^{-1} \end{aligned}$$

Daily  $R_{nl}$  values are in Output DTN: MO0603SPAREFET.000.

**Net Radiation ( $R_n$ )**—Net Radiation is the balance between net shortwave radiation (both incoming and reflected) and net loss of longwave radiation (Allen et al. 1998 [DIRS 157311], Equation 40, p. 53):

$$R_n = R_{ns} - R_{nl} \quad (\text{Eq. D-32})$$

Example: For March 1, 1998,  $R_{ns} = 13.9$  and  $R_{nl} = 6.3$  (Output DTN: MO0603SPAREFET.000).

$$R_n = 13.9 - 6.3 = 7.6 \text{ MJ m}^{-2} \text{ day}^{-1} \quad (\text{from Eq. D-32})$$

Daily  $R_n$  values are in Output DTN: MO0603SPAREFET.000.

**Soil Heat Flux**—According to Allen et al. (1998 [DIRS 157311], Equation 42, p. 54) daily soil heat flux ( $G_{day}$ ) beneath the grass reference surface is small enough that it can be ignored:

$$G_{day} \approx 0 \quad (\text{Eq. D-33})$$

**Wind Speed ( $u_2$ )**—See Section D3.2 for description and correction of wind speed data. Daily wind speed values for the 1998, 2001, and 2002 water years are in Output DTN: MO0603SPAREFET.000.

### D6.3 REFERENCE EVAPOTRANSPIRATION AND POTENTIAL TRANSPIRATION

Using the humidity, radiation, and wind speed values generated in this appendix for March 1, 1998, mean daily  $ET_0$  can be calculated using Equation D-19.

Example: For March 1, 1998:

$$\Delta = 0.072$$

$$R_n = 7.5$$

$$G = 0$$

$$\gamma = 0.059$$

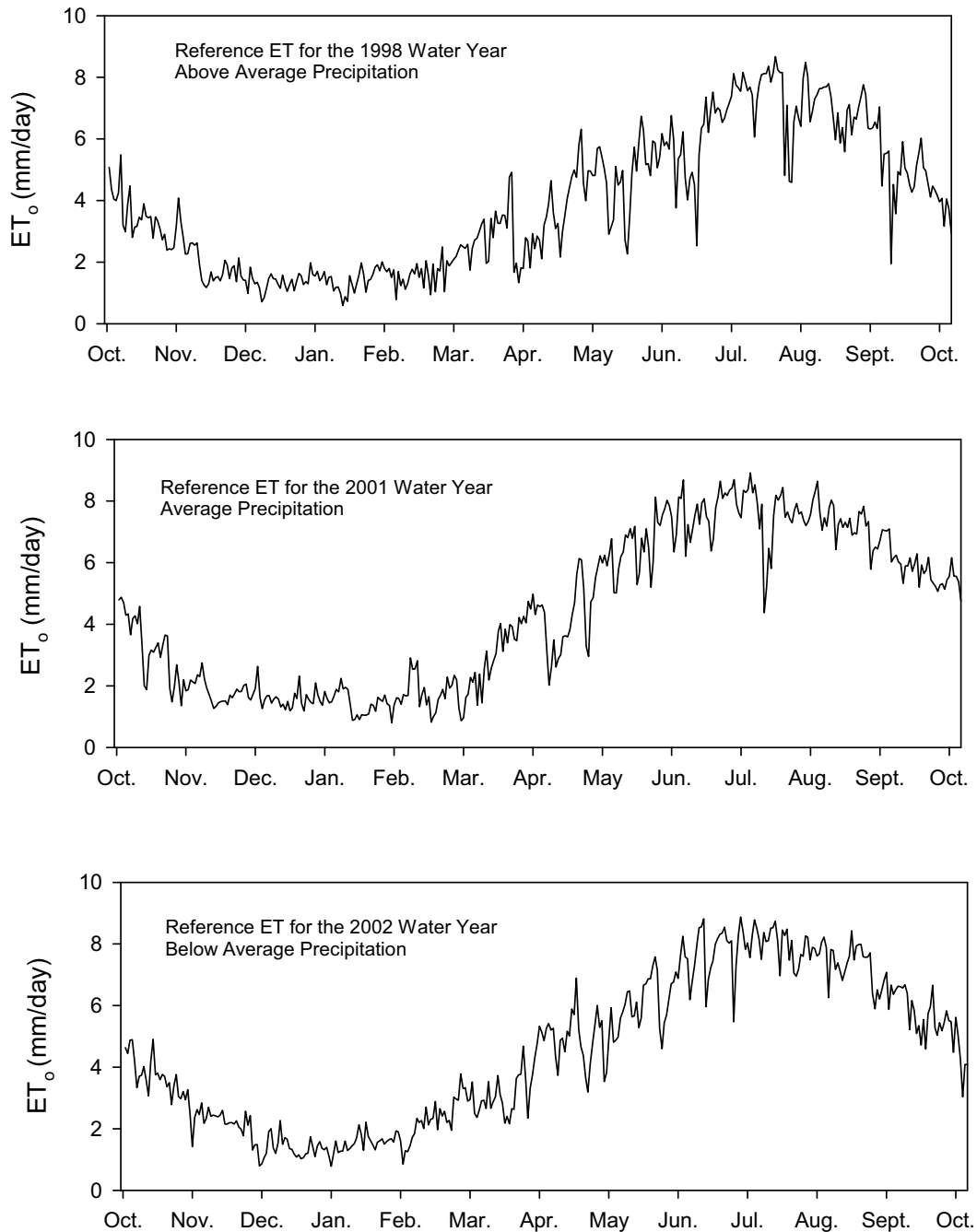
$$T = 7.8$$

$$u_2 = 1.7$$

$$(e_s - e_a) = 0.574$$

$$ET_0 = \frac{0.408 * 0.072(7.5 - 0.0) + 0.059 \frac{900}{7.8 + 273} 1.7(0.574)}{0.072 + 0.059(1 + 0.34 * 1.7)} = 2.5 \text{ mm/day} \quad (\text{from Eq. D-19})$$

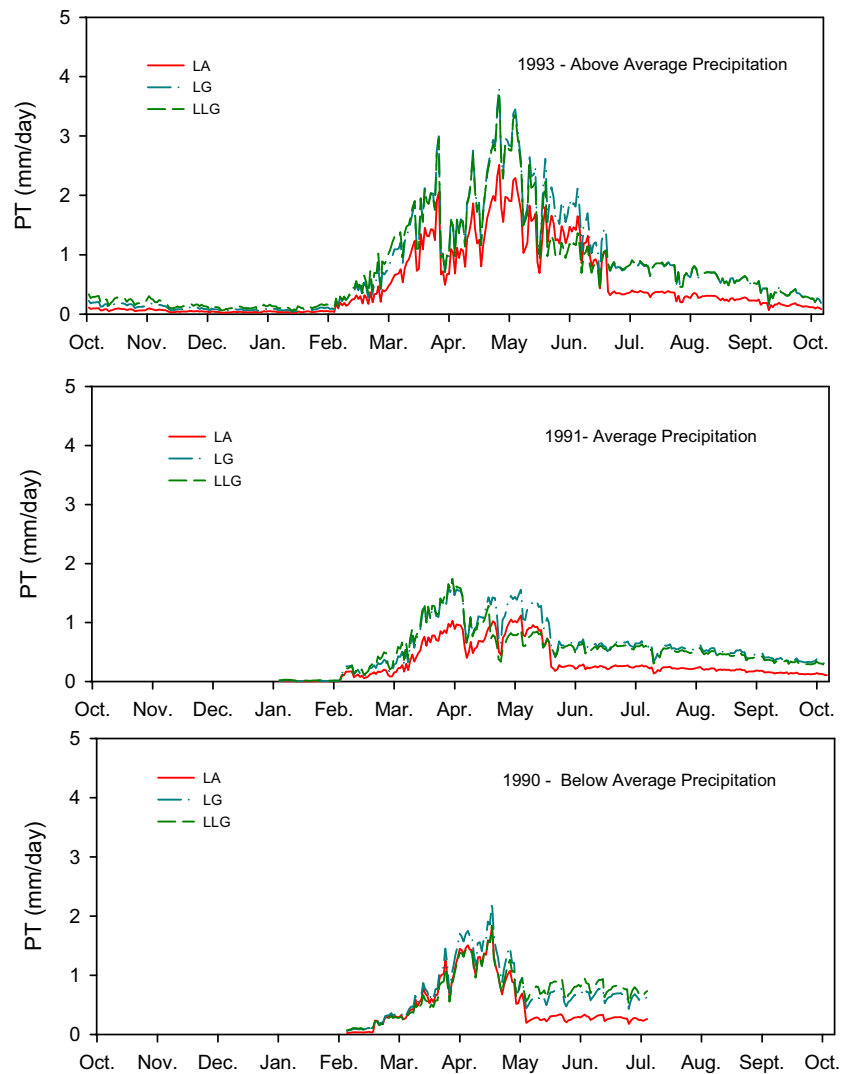
Daily  $ET_0$  for the 1998, 2001, and 2002 water years are in Output DTN: MO0603SPAREFET.000. Reference evapotranspiration profiles were generated for each water year (Figure D-10).



Source: Output DTN: MO0603SPAREFET.000.

Figure D-10. Reference Evapotranspiration ( $ET_0$ ) for the 1998, 2001, and 2002 Water Years

**Potential Transpiration Profiles**—PT profiles (Figure D-11) for the three vegetation associations, water years, and *Bromus* monoculture (profile not shown) were generated using Equation D-1 (Figure 6.5.3.6-5).



Source: Output DTN: MO0606SPABASAL.001.

Figure D-11. Potential Transpiration (PT) for the 1993, 1991, and 1990 Water Years for Three Vegetation Associations (LA = *Larrea-Ambrosia*, LG = *Lycium-Grayia*, LLG = *Larrea-Lycium-Grayia*)

Total *PT* for growing seasons was determined by summing the daily values in Figure D-11. There was little difference in total growing season *PT* between the LG and LLG associations across water years (Table D-37). Potential transpiration for the LA association ranged from about 54% to 68% of *PT* for the LG association. Even though the  $K_{cb}$  profiles for the 1990 water year appeared to converge, the greater cover of evergreen vegetation in the LG and LLG associations compared to the LA association resulted in about 36 mm more water use over the May through July time period (Table D-37).

Table D-37. Growing Season Potential Transpiration for Three Vegetation Associations

Vegetation Association	Potential Transpiration <sup>a</sup> for Growing Season
<b>Wet Year (240 mm)<sup>b</sup></b>	
<i>Larrea–Ambrosia</i>	180 mm
<i>Lycium–Grayia</i>	286 mm
<i>Larrea–Lycium–Grayia</i>	276 mm
<b>Average Year (150 mm)<sup>b</sup></b>	
<i>Larrea–Ambrosia</i>	87 mm
<i>Lycium–Grayia</i>	162 mm
<i>Larrea–Lycium–Grayia</i>	144 mm
<b>Dry Year (60 mm)<sup>b</sup></b>	
<i>Larrea–Ambrosia</i>	78 mm
<i>Lycium–Grayia</i>	113 mm
<i>Larrea–Lycium–Grayia</i>	108 mm
<b>Glacial Transition Climate (440 mm)<sup>c</sup></b>	
<i>Bromus tectorum</i> monoculture	276 mm

<sup>a</sup> Output DTN: MO0606SPABASAL.001.

<sup>b</sup> Approximate average annual precipitation for LA, LG, and LLG vegetation associations. Source: CRWMS M&O 1996 [DIRS 102235], p. 21, Figure 4-3.

<sup>c</sup> Average total yearly precipitation for Spokane, Washington. DTN: MO0605SPASPOKA.000 [DIRS 177135].

Potential transpiration for the *Bromus* monoculture was 276 mm, equal to that of the LLG association for the wet year. However, this amount was less than the mean annual precipitation estimates for the Glacial Transition climate state (about 440 mm) that the  $K_{cb}$ s were calculated for. This could indicate that cover for the *Bromus* monoculture at Yucca Mountain was underestimated by the methods used in Appendix D. It could also indicate that a *Bromus* monoculture would not use all the water available under Glacial Transition climate conditions. Under the right set of circumstances, this could result in available water for deeper rooted species to take hold in the system, perhaps preventing a monoculture from establishing. However, germination conditions for most Great Basin species do not occur until later in the spring when soil temperatures warm. *Bromus* is able to photosynthesize and use water at low temperatures, which could result in dry soils before germination of native species could occur.

**Appropriateness of  $K_{cb}$ s for Desert Vegetation**—To evaluate whether the magnitude of calculated  $K_{cb}$ s was reasonable for desert vegetation,  $PT$  was compared to average precipitation recorded on ESPs during WY1990, WY1991, and WY1993. Precipitation recorded on ESPs for those years were approximately 240 mm (1993), 150 mm (1991), and 60 mm (1990) (CRWMS M&O 1996 [DIRS 102235], p. 21, Figure 4-3). Potential transpiration exceeded precipitation by about 4 to 50 mm on the LG and LLG plots depending on the year (Table D-37). These amounts are minimal compared to variation in precipitation among sites that can occur at Yucca Mountain. It is important to note that the  $K_{cb}$  represents the potential water use for a given LAI or vegetation cover (i.e., water is not limiting for the green vegetation that is present on a site). Therefore,  $PT$  will generally be greater than actual transpiration. Actual transpiration is controlled in the infiltration model by soil water balance and  $K_s$  (Section 6.4.4).

$PT$  for the less productive LA sites was less than water year precipitation during the average and above average precipitation years. The LA sites support fewer annual species, which account for much of the increased cover on LLG and LG sites during average and above average precipitation years. Because precipitation is not directly used in  $K_{cb}$  or  $ET_0$  calculations, the correspondence between  $PT$  and precipitation provides an independent check suggesting that the  $K_{cb}$  values are appropriate for a desert system.

A second check on whether the magnitude of  $K_{cb}$ s was reasonable for a desert system was performed by comparing actual  $ET$  measured in the Mojave Desert to the  $PT$  values calculated for the three water years. In a study of plant water use by drought deciduous (*Ambrosia dumosa* and *Lycium pallidum*) and evergreen species (*Larrea tridentata* and *Ephedra nevadensis*), Yoder and Nowak (1999 [DIRS 177167], pp. 83 and 84) used soil moisture measurements (neutron probe) and soil water balance methods to estimate total annual  $ET$ . The study was conducted over a three-year time period (1995 to 1997) in the Mojave Desert vegetation zone on the Nevada Test Site. The elevation of field sites ranged from 950 to 1,150 m. Annual precipitation at the study sites ranged from 199 mm to 290 mm in 1995, 29 mm to 54 mm in 1996, and 79 to 125 mm in 1997, corresponding to above, below, and average precipitation years, respectively (Yoder and Nowak 1999 [DIRS 177167], pp. 84 and 85, Figure 1). Annual  $ET$  averaged for the study sites was about 225 mm in 1995, 50 mm in 1996, and 100 mm in 1997 (Yoder and Nowak 1999 [DIRS 177167], p. 88, Figure 3). These values were higher than  $PT$  estimated for the LA association for above average and average precipitation years by 47 mm and 13 mm, respectively, and lower than estimated  $PT$  for the remaining associations by 27 to 63 mm, depending on association and year. These differences are relatively small considering differences in water years, locations, and vegetation cover, and they provide additional evidence to suggest that the magnitude of  $K_{cb}$  values is reasonable for the Yucca Mountain area.

A third check on the appropriateness of the  $K_{cb}$  values was performed in Appendix E. In Section E7, actual  $ET$  for the LG association was simulated for the 1998 water year using  $ET_0$  and daily fitted values for NDVI that were scaled by precipitation (Figure E-25). Comparison of this estimated actual  $ET$  to the  $PT$  profile for LG (Figure E-26) showed remarkably good correspondence, suggesting that the  $K_{cb}$ s are appropriate for the Yucca Mountain system. See Appendix E for complete analysis.

***Criticisms on the Use of Transpiration Coefficients in Desert Environments***—Mata-Gonzalez et al. (2005 [DIRS 178523]) published a review paper criticizing the use of FAO-56 methods for calculating transpiration coefficients and the subsequent use of those coefficients to estimate  $ET$  for arid ecosystems. Their main criticisms were:

- $K_c$  estimated for nonstressed plants produces high values not representative of field conditions in arid environments. Use of the dual crop coefficient ( $K_c = K_{cb} + K_e$ ) does not adequately adjust for sparse vegetation because estimated  $K_{cb}$  values were not provided in FAO-56 for native desert vegetation. The water stress coefficient ( $K_s$ ) that adjusts for soil water availability causes  $ET$  to be underestimated.
- Leaf area is the only variable in FAO-56 methods that determines water use of a plant.



- Plants are assumed to have maximum foliage coverage throughout the growing season.
- The core methods do not consider stomatal regulation, and the correction provided for stomatal regulation for arid land species is too complicated. Estimation of  $K_e$  for the dual crop coefficient is too complicated.

The authors do not recognize that methods are provided in FAO-56 for calculating  $K_{cb}$  from LAI or effective ground cover. These methods are described in Chapter 9 of FAO-56, and Equations 98, 100, 101, and 102 (Allen et al. 1998 [DIRS 157311], pp. 183 to 194) and were used in this analysis to calculate  $K_{cbs}$  (Appendix D). The use of effective ground cover measured on reference area plots at Yucca Mountain directly accounted for the sparse vegetation typical of the Yucca Mountain area. The authors stated that "...transpiration rates of a species are constant for a given day of the year, since they are a function of the species inherent potential water use ( $K_c$ ) in relation to the maximum water use of a plant under ideal conditions ( $ET_0$ )...are inappropriate..." However, the assumption that ratios of  $ET$  by a specific vegetation to the climatic reference  $ET_0$  is relatively constant for a given amount of vegetation cover is a proven and long-standing tenet of crop coefficient practice.

Variables in addition to leaf area in FAO-56 methods that are used to calculate  $K_{cb}$ , and that were used in this analysis, included wind speed, minimum relative humidity, plant height, and stomatal resistance. Thus, while leaf area and effective ground cover are important variables used in FAO-56 methods to estimate plant water use, additional variables are also accounted for that influence transpiration.

The  $K_s$  is used to adjust for soil water availability in the infiltration model. The basis for the criticism that use of  $K_s$  underestimates  $ET$  is derived from the assumption that  $K_s$  goes to zero at a wilting point of  $-1.5$  MPa ( $-15$  bar) (Mata-Gonzalez et al. 2005 [DIRS 178523], p. 291). A wilting point of  $-1.5$  MPa is typical of many crop species. The authors point out that certain desert shrubs have been shown to maintain photosynthesis, extract soil moisture, and survive at much lower water potentials ( $-7.0$  to  $-12$  MPa [ $-70$  to  $-120$  bar], Mata-Gonzalez et al. 2005 [DIRS 178523], p. 291). That transpiration can occur in desert shrub species at lower water potentials than  $-1.5$  MPa is a valid point. FAO-56 never associates wilting point with a specific soil water potential, as this can vary with species. FAO-56 instead suggests that "Wilting point is the water content at which plants will permanently wilt" (Allen et al. 1998 [DIRS 157311, p. 162]), which is considered to be a true statement. However, the water potentials listed by the authors are extreme values, and it is not likely that transpiration occurs at any appreciable rate when soils are this dry. For the infiltration model, a wilting point of  $-6.0$  MPa ( $-60$  bars) was selected for desert vegetation (BSC 2006 [DIRS 176335]). This value was based on ranges of water potentials at which conductance and/or photosynthesis was determined to be zero for several Mojave Desert species. Thus, it is not likely that transpiration is underestimated by use of a wilting point that is realistic for desert plants.

Satellite based vegetation indices and observed fractions of ground cover have been applied during estimation of  $K_c$ . These indices and thus  $K_c$  vary over time to account for seasonal changes in ground cover and leaf area. Additionally, in the calculation of  $K_{cbs}$ , ground cover was reduced for the initial growth stage from the maximum observations used during the midseason

growth stage (Section D3.2.2). Thus, it was not assumed that plants have maximum foliage coverage throughout the growing season.

The basis for the last of these criticisms (methods being too complex) was that the objective of using FAO-56 methods to estimate  $ET$  in arid environments was to provide a widely accepted and simple approach for estimating water use by vegetation (Mata-Gonzales et al. 2005 [DIRS 178523], pp. 291 and 292). The authors recognized that partitioning evaporation and transpiration for arid systems and applying corrections for stomatal control are appropriate measures but suggest that the increase in level of complexity is such that these steps are rarely taken. Both were accounted for in the infiltration model.

## D7. NOMENCLATURE FOR EQUATIONS USED IN APPENDIX D

Symbol	Description	Units	Where Used*
$K_{cb}$	basal $K_{cb}$ when plant density and/or leaf areas are lower than for full cover conditions	dimensionless	Eq. D-1 (D-9)
$K_{c\ min}$	minimum $K_c$ for bare soil in the presence of vegetation ( $K_{c\ min} \approx 0$ )	dimensionless	Eq. D-1
$K_{cb\ full}$	estimated basal $K_{cb}$ during the midseason at peak plant size or height and full ground cover	dimensionless	Eq. D-1 (D-7)
$f_c$	observed fraction of soil surface that is covered by vegetation type (0.01–1)	dimensionless	Eq. D-1 (D-2)
$f_{c\ eff}$	effective fraction of soil surface covered or shaded by vegetation type (0.01–1)	dimensionless	Eq. D-1 (D-2)
$h$	plant height	m	Eq. D-1
$\sin(\eta)$	sine of the mean angle of the sun, $\eta$ , above the horizon during midday hours when maximum evapotranspiration is likely to occur	Sin(radians)	Eq. D-2 (D-3)
$\psi$	latitude	radians	Eq. D-3
$\delta$	solar declination	radians	Eq. D-3 (D-4, D-24, D-27)
$J$	day of year	dimensionless	Eq. D-4 (D-26, D-27)
$i$	day number within the growing season (1...length of the growing season)	dimensionless	Eq. D-5
$K_{cb, i}$	transpiration coefficient on day $i$	dimensionless	Eq. D-5
$K_{cb\ prev}$	$K_{cb}$ at the end of the previous stage	dimensionless	Eq. D-5
$K_{cb\ next}$	$K_{cb}$ at the beginning of the next stage	dimensionless	Eq. D-5
$L_{stage}$	length of the stage under consideration	days	Eq. D-5
$\Sigma L_{prev}$	sum of the length of all previous stages	days	Eq. D-5
$K_{cb, h}$	adjustment for the influence of vegetation height for $K_{cb}$ for full cover condition under standard climate	dimensionless	Eq. D-6
$K_{cb, h}$	$K_{cb}$ for full cover vegetation under a standard climate	dimensionless	Eq. D-7
$u_2$	mean wind speed at 2-m height	$\text{m s}^{-1}$	Eq. D-7, Eq. D-19 (D-15)
$RH_{min}$	minimum daily relative humidity	%	Eq. D-7 (D-17)

Symbol	Description	Units	Where Used*
$h$	mean maximum plant height	m	Eq. D-7 (D-6)
$F_r$	stomatal resistance correction factor	dimensionless	Eq. D-8 (D-9)
$\Delta$	slope of the saturation vapor pressure curve	kPa °C <sup>-1</sup>	Eq. D-8, Eq. D-19 (D-16)
$\gamma$	psychrometric constant	kPa °C <sup>-1</sup>	Eq. D-8, Eq. D-19
$r_l$	mean leaf resistance (stomatal) for the vegetation in question	s m <sup>-1</sup>	Eq. D-8 (D-14)
$CI$	confidence interval	dimensionless	Eq. D-10
$t$	t-table value for single tailed test with $\alpha = 0.10$ and $n-1$ degrees of freedom	dimensionless	Eq. D-10, Eq. D-11
$s_c$	standard deviation of cover data for ESPs	dimensionless	Eq. D-10 (D-11)
$n$	number of ESPs in mean calculation	dimensionless	Eq. D-10
$n_c$	the number of ESPs required to sample cover of an association to within 10% of the true population mean	dimensionless	Eq. D-11
$d$	precision that the true difference of the sample mean occurs from the population (= 0.10)	dimensionless	Eq. D-11
$x_c$	mean of cover data for ESPs	dimensionless	Eq. D-11
$g_v$	stomatal conductance in velocity units	m s <sup>-1</sup>	Eq. D-12 (D-14)
$g_m$	stomatal conductance in molar units	mol m <sup>-2</sup> s <sup>-1</sup>	Eq. D-12
$R$	universal gas constant	8.314 Pa m <sup>3</sup> mol <sup>-1</sup> K <sup>-1</sup>	Eq. D-12
$T_l$	leaf temperature	K	Eq. D-12
$P$	atmospheric pressure	Pa	Eq. D-12
$u_z$	wind speed measured at $z$ m aboveground surface	m s <sup>-1</sup>	Eq. D-15
$z$	height of measurement aboveground surface	m	Eq. D-15
$\exp(x)$	2.7183 (base of natural logarithm) raised to the power ( $x$ )	dimensionless	Eq. D-16 (D-18)
$e^\circ(T)$	saturation vapor pressure at temperature $T$	kPa	Eq. D-17, Eq. D-18, (D-20, D-22)
$T_{dew}$	minimum daily air temperature minus 2 degrees	°C	Eq. D-17 (D-21, D-22)
$T_{max}$	maximum daily air temperature	°C	Eq. D-17, Eq. D-20
$ET_0$	reference evapotranspiration	mm/day	Eq. D-19
$R_n$	net radiation at the crop surface	MJ m <sup>-2</sup> day <sup>-1</sup>	Eq. D-19 (D-32)
$G$	soil heat flux density	MJ m <sup>-2</sup> day <sup>-1</sup>	Eq. D-19
$T$	mean daily air temperature at 2 m height	°C	Eq. D-19
$e_s$	saturation vapor pressure	kPa	Eq. D-19 (D-20)
$e_a$	actual vapor pressure	kPa	Eq. D-19 (D-22, D-31)
$e_s - e_a$	saturation vapor pressure deficit	kPa	Eq. D-19 (D-23)
$T_{min}$	minimum daily air temperature	°C	Eq. D-20 (D-21)
$K_o$	correction factor (= 2°C for arid climates)	°C	Eq. D-21

<b>Symbol</b>	<b>Description</b>	<b>Units</b>	<b>Where Used*</b>
$R_a$	extraterrestrial radiation	$\text{MJ m}^{-2} \text{ day}^{-1}$	Eq. D-24 (D-29)
$G_{sc}$	solar constant = 0.0820	$\text{MJ m}^{-2} \text{ min}^{-1}$	Eq. D-24
$d_r$	inverse relative distance Earth–Sun	$\text{L}^{-1}$	Eq. D-24 (D-26)
$\phi$	latitude	rad	Eq. D-24 (D-25)
$\omega_s$	sunset hour angle	rad	Eq. D-24
$R_{so}$	calculated clear sky radiation	$\text{MJ m}^{-2} \text{ day}^{-1}$	Eq. D-29 (D-31)
$Z$	station elevation above sea level	m	Eq. D-29
$R_{ns}$	net solar (shortwave) radiation	$\text{MJ m}^{-2} \text{ day}^{-1}$	Eq. D-30 (D-32)
$\alpha$	albedo of grass reference crop (= 0.23)	dimensionless	Eq. D-30
$R_{nl}$	net outgoing longwave radiation	$\text{MJ m}^{-2} \text{ day}^{-1}$	Eq. D-31 (D-32)
$\sigma$	Stefan–Boltzmann constant	$\text{MJ K}^{-4} \text{ m}^{-2} \text{ day}^{-1}$	Eq. D-31
$T_{max}, K$	maximum absolute temperature during the 24–hour period	K	Eq. D-31
$T_{min}, K$	minimum absolute temperature during the 24–hour period	K	Eq. D-31
$R_s/R_{so}$	relative shortwave radiation (limited to $\leq 1.0$ )	dimensionless	Eq. D-31
$R_s$	measured (present–day climate) or calculated (future climate) solar radiation	$\text{MJ m}^{-2} \text{ day}^{-1}$	Eq. D-31 (D-30)
$G_{day}$	daily soil heat flux	$\text{MJ m}^{-2} \text{ D}^{-1}$	Eq. D-33

\* Defined in these equations. Equation numbers in parentheses show other equations where these terms are used but not redefined.

**APPENDIX E**  
**QUANTIFYING AND SIMULATING YUCCA MOUNTAIN VEGETATION RESPONSE**



## SUMMARY

One of the key issues in determining the net-infiltration at the Yucca Mountain repository is the ability to predict the interaction between vegetation and precipitation. Vegetation uses the moisture supplied from the atmosphere, allowing only the residual from this consumption to infiltrate into the media beyond the root zone – thus plant and canopy development is a surrogate measure of the water used. The net-infiltration model must capture this plant usage. To do this, vegetative patterns at the site were analyzed using remote sensor images, parameters governing these patterns were determined, and these parameters were then combined to simulate a seasonal, site specific response to moisture.

The principle behind vegetative analysis is simple. With the exception of green vegetation, most natural surfaces are about equally as bright in the red and near-infrared part of the spectrum. In vegetation, red light is strongly absorbed by photosynthetic pigments (such as chlorophyll) found in green leaves, while near-infrared light either passes through or is reflected by live leaf tissues. Thus, areas of bare soil having little or no green plant material will appear similar in both the red (R) and near-infrared (NIR) wavelengths, while areas with green vegetation will be very bright in the near-infrared and very dark in the red part of the spectrum. Because the remotely sensed images are 8-bit digital, every pixel corresponds to a number from 0 to 255 (zero being pure black and 255 being pure white). Vegetation indices are calculated using the pixel values for the red and near-infrared wavelengths. They are the reduction of multispectral scanning measurement to a single value for predicting and assessing vegetative characteristics such as plant leaf area, total biomass and general plant stress and vigor. This analysis used a normalized difference vegetation index (NDVI) that is calculated using near infrared and red spectral data from satellite images. Further, since the green response of vegetation is proportional to seasonal precipitation that is directly related to seasonal *ET*, NDVI as a surrogate measure for canopy response was used as a variable to help predict *ET* for the Mass Accounting System for Soil Infiltration and Flow (MASSIF) Model.

While the principle behind this vegetation analysis is simple, in practice there are many complications. In order to directly compare images taken on different dates, data must be:

- Adjusted for the gains and biases of each sensor (Section E2.1)
- Adjusted to account for the effect of having different solar zenith angles and compensated for different values of the exoatmospheric solar irradiances arising from spectral band differences (Section E2.1)
- Corrected for differing atmospheric conditions (Section E2.2)
- Corrected for nonsystematic variations, such as atmospheric opacity, soil albedo, ground level water content, atmospheric water content, and illumination geometry (Section E2.4)
- Aligned to a common geospatial coordinate system (Section E2.3).

In addition to the typical corrections mentioned above, the Yucca Mountain Site posed a unique challenge to data processing. Comparison between observed site vegetation and image analysis results showed there was a nonvegetation source that produced a strong depression in the red wavelength mimicking a vegetation response. It was concluded that the natural rock weathering processes over time produced desert varnish that caused this response. Because the site is very arid, the measured vegetation responses tend to be very low, and it was found that the signal from the desert varnish was high in comparison. Section E2.6 discusses the correction used for desert varnish.

A total of 33 images from three representative years (a very dry, an average, and a very wet year) were analyzed. The choice of image dates was made with regard to the satellite data available and ancillary data that were measured on and near Yucca Mountain. The images represented snapshots of the site during the growing season, emphasizing those times when the vegetation response was greatest (March through June of each year). These images were assembled to represent responses during a water year (WY), from October 1 through September 30 of subsequent years. A water year more naturally captures the cycle of winter precipitation and annual plant growth that is generally senescent in this environment during late summer.

The combined corrections discussed above resulted in a set of processing parameters for each image. These parameters were developed for the general site flora. As discussed in Appendix D, there are three predominant vegetation associations at the site. Analyses were completed to assure that the general processing parameters were appropriate for each of the three vegetation associations (Section E2.5). Analyses show that the corrected vegetation index, NDVI', has an inherent uncertainty of  $0.01 \pm 6\%$ .

Once images had been processed so that they were directly comparable, a seasonal response to precipitation was developed that contained an annual peak for vegetation (occurring in about mid April), as described in Section E3. General response curves were developed which captured the variability induced by slope and azimuth. Slope and azimuth combinations will result in different amounts of sunlight reaching the ground at different times of the year and thus, influence the magnitude and/or timing of the vegetation growth response at that location. These influences are irrespective of soil conditions at a specific point and were examined by comparing responses for various slope/azimuth combinations. The calculations used averages of pooled sample groups in order to determine overall trends. Comparison of a predicted vegetation response using the general response curves to image data from lowlands showed that the general response curves somewhat underestimate vegetation response. However, because the repository footprint is overlain by rocky uplands, the vegetation response curves were developed to be most accurate for these areas. The curves will conservatively estimate the proportion of precipitation that will be available from infiltration in the lowlands.

To account for spatially varying conditions at the site, such as amount of exposed rock, soil depth, and water holding capacity, a potential vegetation response (PVR) for each model grid cell was produced (Section E4). PVR is calculated per pixel (each 0.2 acres in size) using subtraction of the peak vegetation response from a critically dry year (2002) from that measured at the peak of a very wet year (1998). This measurement is thus an estimate of the capability for each pixel in the modeled region to support vegetation. The minimum NDVI values, measured during a critically dry year, represent the signal from desert varnish. PVR was normalized by



dividing each value by the average value for model grid cells for a subset area overlying the proposed repository. This area was chosen as a rectangle of 12,702 grid cells (11.43 km<sup>2</sup>). Normalization provided scaling to permit a better understanding of PVR distribution: a PVR of 1.0 represents the approximate average vegetation response overlying the repository.

An algorithm was developed to simulate vegetation for each model grid cell using results from the analyses. The general response curves provided the shape of the vegetation response through the growing season. They were then scaled for the general conditions for each growing year by a ratio of the precipitation of the year of interest to the wettest year (1998) that was used to fit the response curve. PVR was used as a scalar to represent plant growth potential within each model grid cell.

The uncertainty associated with the vegetation algorithm was only evaluated for the mathematical processing necessary to isolate the vegetation signal within the satellite data. Additional uncertainty associated with the response curve or the algorithm will be analyzed in the uncertainty of the MASSIF.

## **E1. GENERAL METHODS AND OVERVIEW FOR THEIR APPLICATION**

The present Yucca Mountain site climate is arid, with the vegetation cover being limited by meager precipitation. Vegetation responds to periods of precipitation by increasing the leaves within the canopy and consuming the available soil water through transpiration (Scanlon et al. 2005 [DIRS 175977]). Data obtained by satellite were used for characterizing this vegetation response.

This section outlines pertinent points of the analyses, starting with some general notes. Section E1 provides the guiding principles used in the analyses, Section E2 provides background information on vegetation signals and NDVI, Section E3 describes how the vegetation signal was isolated from the background signal, and Section E4 discusses which years were chosen for the analyses. Pertinent points in these analyses include:

1. As described in Appendix D, the vegetation at the site is a mix of species typical of the Mojave Desert and the Great Basin. Although there is a variety of species, they are simulated in this analysis as a lumped vegetation response. Each pixel of the satellite image represents an area many times larger than the individual plants making up the canopy.
2. Vegetation response was characterized according to its greenness, viewed at multiple points through each year. Chlorophyll, the molecule within plant leaves that moderates photosynthesis, is green, and the greenness captured within each pixel is determined by the overall chlorophyll content within the canopy viewed. This basic relationship permits using remote sensing for vegetation study (Asrar et al. 1992 [DIRS 176754]). As briefly described in Section D2, gas exchange for photosynthetic uptake of CO<sub>2</sub> is proportional to transpiration as mediated by the atmospheric demand, expressed as  $ET_0$ . Thus, as the numbers of leaves increase, the greenness and the rate at which water is used by the plants increase

proportionally. A measure of vegetation canopy expression, as greenness, is a surrogate measure of the transpiration rate.

3. Although several vegetation associations exist on Yucca Mountain, the mix of plant species was not evaluated separately using this remote-sensing approach. The parameterization that resulted was sensitive to the rise and fall of the annual growth cycle of the overall site flora. The relationships developed to characterize the site vegetation responses were calibrated for the rocky uplands that overlie the proposed repository to ensure the greatest level of accuracy for vegetation simulation there.
4. As described in Appendix D, there are three major vegetation associations on Yucca Mountain and the surrounding area that are characterized by the ecological study plots (ESPs). The principal vegetation covering the repository has been given the abbreviation LG for two dominant genera (*Lycium* and *Grayia*). The two other important regional assemblages are LA (*Larrea* and *Ambrosia*) and LLG (*Larrea*, *Lycium*, and *Grayia*). The equation developed for the lumped vegetation response was tested using data extracted from the ESPs to verify its appropriateness for these three vegetation associations.
5. The analyses and processing to develop the plant simulation are documented in a series of spreadsheets that are referenced in this appendix with appropriate data tracking numbers (DTNs).
6. The analyses contained in this appendix were made entirely with three software packages. Remote sensing analyses were performed using Environment for Visualizing Images software (ENVI + IDL, Version 4.2: STN: 11204-4.2-00). Spatial output from ENVI was analyzed and displayed in ArcGIS (ArcGIS Desktop Version 9.1: STN: 11205-9.1-00). ENVI and ArcGIS were both used for extraction of remote sensing data that were then analyzed and graphically displayed in Microsoft Excel™

Note that there are a series of citations contained in this document with associated DIRS (document input reference system) numbers. None of these citations were used for direct input. Further, uncertainty calculations are included as text boxes, shaded grey, in each section.

## **E1.1 ASSUMPTIONS**

Appendix E contains three assumptions. The first assumption was necessary for development of the processing parameters for atmospheric correction: the air mass overlying the region of Yucca Mountain at the time of each overpass was exemplified by the region chosen for estimation of the correction parameter. As part of the development of this correction parameter, it was also assumed that the properties of this air mass were evenly distributed over Yucca Mountain.

The two other assumptions concerned the development of an algorithm to simulate vegetation growth. The timing of the seasonal growth response for this algorithm was assumed to be represented by the response observed in WY1998. The final assumption concerns the

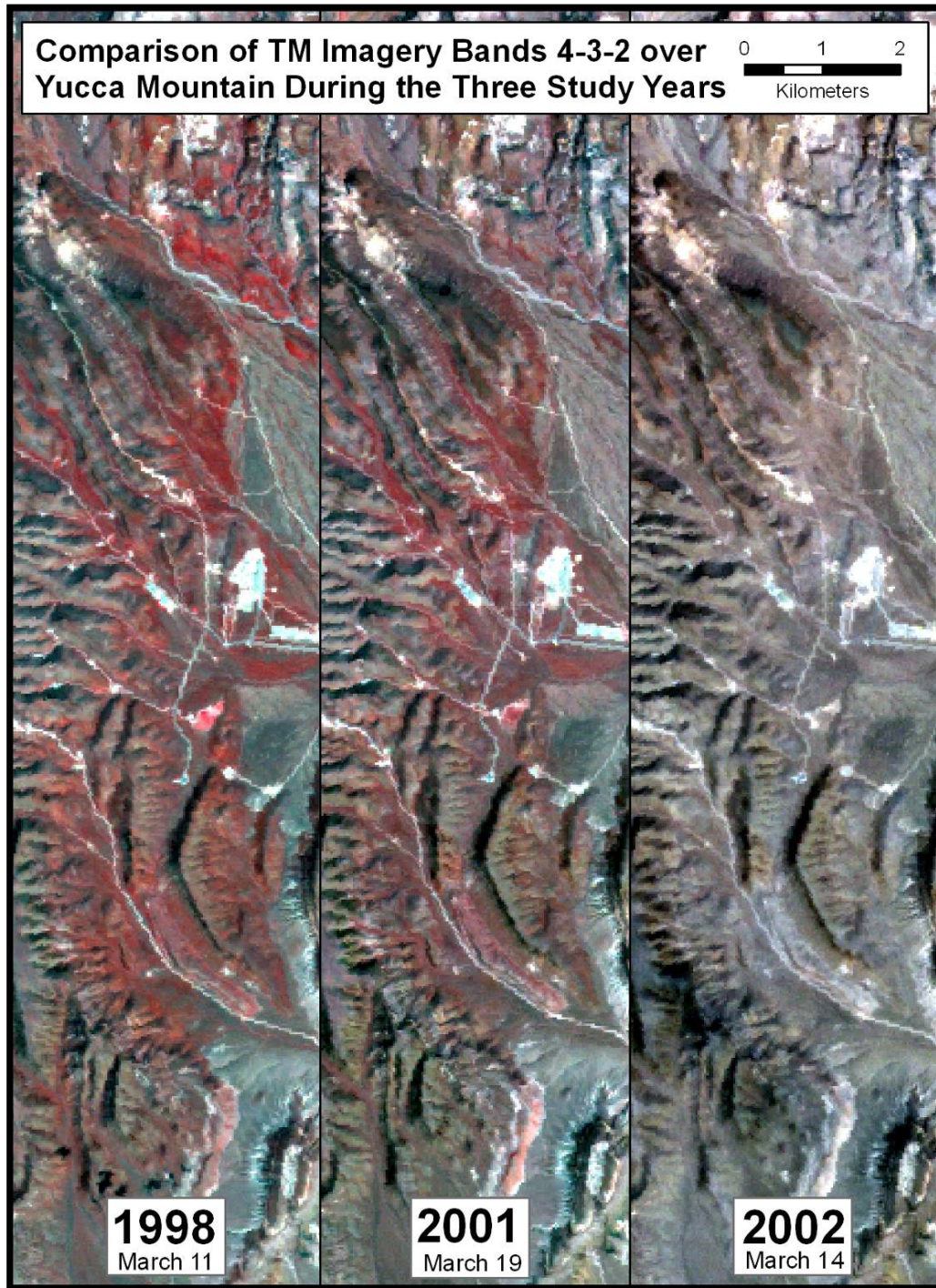
application of this algorithm: the vegetation algorithm developed should be generally applicable to related but different climates, either Monsoon or Glacial Transition.

## E1.2 GUIDING PRINCIPLES

There are several guiding principles that enable the analysis of *ET* using a vegetation canopy expression. These underscore the link for climate (i.e., long-term patterns of dryness and temperature from year to year) and weather, with shorter-term variations and the consequent vegetation response.

- The present Yucca Mountain climate is arid and the plants operate in deficit conditions for most of the year.
- Vegetation cover/expression on Yucca Mountain rises and falls with the magnitude of total annual precipitation.
- Seasonal total *ET* is also determined by precipitation, since, without precipitation there is virtually nothing to evapotranspire. Thus, an estimate of vegetation cover is a surrogate measure of relative *ET*.
- With the exception of small amounts of net infiltration that have escaped below the root zone, virtually all annual precipitation is expended as *ET* because precipitation is meager and the driving force for evaporation extremely high. In general, the amount of infiltrated water is very low or virtually nonexistent if the soil is deep.
- The timing of the seasonal growth response is assumed to be represented by the response observed in WY1998. This assumption is described in Section 5.
- Given the extent of our knowledge, the vegetation algorithm developed should be applicable to related but different climates, either Monsoon or Glacial Transition. This assumption is described in Section 5.

Vegetation response to precipitation is particularly evident for Yucca Mountain in the comparison of wet versus dry years on satellite data. Figure E-1 shows three views of Yucca Mountain taken by Landsat TM (thematic mapper) during the spring vegetation growth peak for the three years chosen for characterizing vegetation: a wet year (WY1998), an intermediate year (WY2001), and a dry year (WY2002).



Source: Output DTN: SN0608NDVILSTM.001.

NOTES: TM Bands 4, 3, and 2 are shown in red, green, and blue, respectively. Vigorous vegetation appears red. These images were produced from the geocorrected TM data Output DTN: SN0608NDVILSTM.001 without further processing using ENVI Software.

Figure E-1. Views of a Portion of the Yucca Mountain area during Wet (1998), Approximately Average (2001), and Critically Dry (2002) Antecedent Weather Displayed in False Color (Verdant Vegetation Appears Red)

### **E1.3 BACKGROUND FOR NDVI AND VEGETATION SIGNAL**

The regional scale of the infiltration model for Yucca Mountain (~50 square kilometers) is ideally suited for application of satellite data, particularly Landsat TM. Landsat TM has square pixels that are 28.5 m on a side; in area, each pixel is only about 1:140,000 of the area of the MASSIF model domain and constitutes an area of 0.2 acre. The wide spatial coverage (>100 km), digital form and high quality of TM data enable their use for the study of vegetation and its relationship to hydrology at the Yucca Mountain site.

Normalized difference vegetation index (NDVI) is an indicator of vegetation vigor often used for measurement of environmental response to landscape-scale hydrology, including global climate change (e.g., Running and Nemani 1991 [DIRS 176819]), rainfall (e.g., Wang et al. 2003 [DIRS 176761]), and evapotranspiration (*ET*) (e.g., Kustas et al. 1994 [DIRS 176757]; Seevers and Ottman 1994 [DIRS 176764]; Szilagyi et al. 1998 [DIRS 176839]; and Szilagyi 2002 [DIRS 176840]). For the TM sensor, Band 3 corresponds to the red wavelengths (R), while Band 4 corresponds to the near infrared wavelengths (NIR). NDVI utilizes the great difference between these two adjacent bands that occurs when viewing healthy green plants. Chlorophyll, responsible for the green color of plants, absorbs red light while leaf tissue reflects highly in near infrared (Buschmann and Nagel 1993 [DIRS 176736]). NDVI is calculated by subtracting the response in the red band from the reflectance in the near-infrared band and then dividing the sum of the reflectances for these two bands (Rouse et al. 1974 [DIRS 177246], Equation E-1).

$$\text{NDVI} = (\text{NIR} - \text{R}) / (\text{NIR} + \text{R}) \quad (\text{Eq. E-1})$$

Chlorophyll is a physiologically expensive molecule for plants to produce, and the amount of chlorophyll relates directly to the rate of photosynthesis (Sellers et al. 1992 [DIRS 176824]). Photosynthesis requires leaf conductance for uptake of carbon dioxide, and during this process water is evaporated to the atmosphere in the process of transpiration. Because of these linkages, NDVI can be used as a competent surrogate for the estimation of *ET* (Kustas et al. 1994 [DIRS 176757]; Seevers and Ottman 1994 [DIRS 176764]; Szilagyi 2000 [DIRS 176839]; and Szilagyi 2002 [DIRS 176840]).

### **E1.4 NDVI CALCULATION TO ISOLATE LOW-COVER VEGETATION SIGNAL**

The data set assembled for Yucca Mountain is multitemporal, with numerous time steps within each of the three years selected for analyses. Because the magnitude of NDVI in desert environments is very small, minute differences of NDVI are meaningful and must be discernible within the data. The challenge presented here was to employ processing methods to uncover the NDVI response from extremely low vegetation cover. These responses needed to be discernable from background signals. Desert varnish on ubiquitous rock surfaces also produces a positive NDVI signal, often in excess of the vegetation itself.

A common necessity for using multitemporal satellite data has been to minimize data set variability introduced by temporally changing conditions that affect individual data acquisitions. These include atmospheric opacity, soil albedo, ground-level and atmospheric water content, and illumination geometry (Huete and Liu 1994 [DIRS 176738]; Liu and Huete 1995 [DIRS 176739]; Carlson and Ripley 1997 [DIRS 176748]; and Song et al. 2001 [DIRS 176745]).

Soil background and atmospheric noise affecting NDVI may not be independent but interact in a complex manner since the atmosphere can also alter the soil background signal and vice versa (Liu and Huete 1995 [DIRS 176739]). Due to these complex interactions, when viewed temporally, raw NDVI tends to vary in a nonsystematic manner (Huete and Liu 1994 [DIRS 176738]; Liu and Huete 1995 [DIRS 176739]).

Nonsystematic scatter inherent in NDVI is nontrivial and, without correction, can mask vegetation response to changing hydrology, especially for vegetation of very low cover that consequentially produces a low NDVI signal. Fortunately, removing this scatter can be accomplished with a standard remote sensing technique. In the original correction described by Gillies et al. (1997 [DIRS 176763]), NDVI values were stretched to conform to a range from zero to one using Equation E-2:

$$\text{NDVI}^* = (\text{NDVI} - \text{NDVI}_0) / (\text{NDVI}_S - \text{NDVI}_0) \quad (\text{Eq. E-2})$$

where:  $\text{NDVI}_0$  = NDVI at zero vegetation cover,  
 $\text{NDVI}_S$  = NDVI at saturation.

Baugh and Groeneveld (2006 [DIRS 178678]) developed a modification to this correction called  $\text{NDVI}_{\text{offset}}$  that simply subtracts the value  $\text{NDVI}_0$  that is calculated by linear regression of the lowest linear portion of the cumulative distribution function.  $\text{NDVI}_S$ , representing peak vegetation expression, is often typified by cultivated fields. Although there are alfalfa fields in the Amargosa Valley adjacent to the YMP site, these do not reach a peak NDVI during winter months when they are cut, fallowed, or grazed. Calculation of  $\text{NDVI}^*$  is thus difficult for this site. However, of 12 vegetation indices, including simple NDVI,  $\text{NDVI}^*$ , and  $\text{NDVI}_{\text{offset}}$ , a comparison of the ability to predict a linear relationship with antecedent precipitation by Baugh and Groeneveld (2006 [DIRS 178678]), found that  $\text{NDVI}_{\text{offset}}$  and  $\text{NDVI}^*$  performed equally well and greatly outperformed all other indices, including simple NDVI. The formula for  $\text{NDVI}_{\text{offset}}$  is given as Equation E-3:

$$\text{NDVI}_{\text{offset}} = \text{NDVI} - \text{NDVI}_0 \quad (\text{Eq. E-3})$$

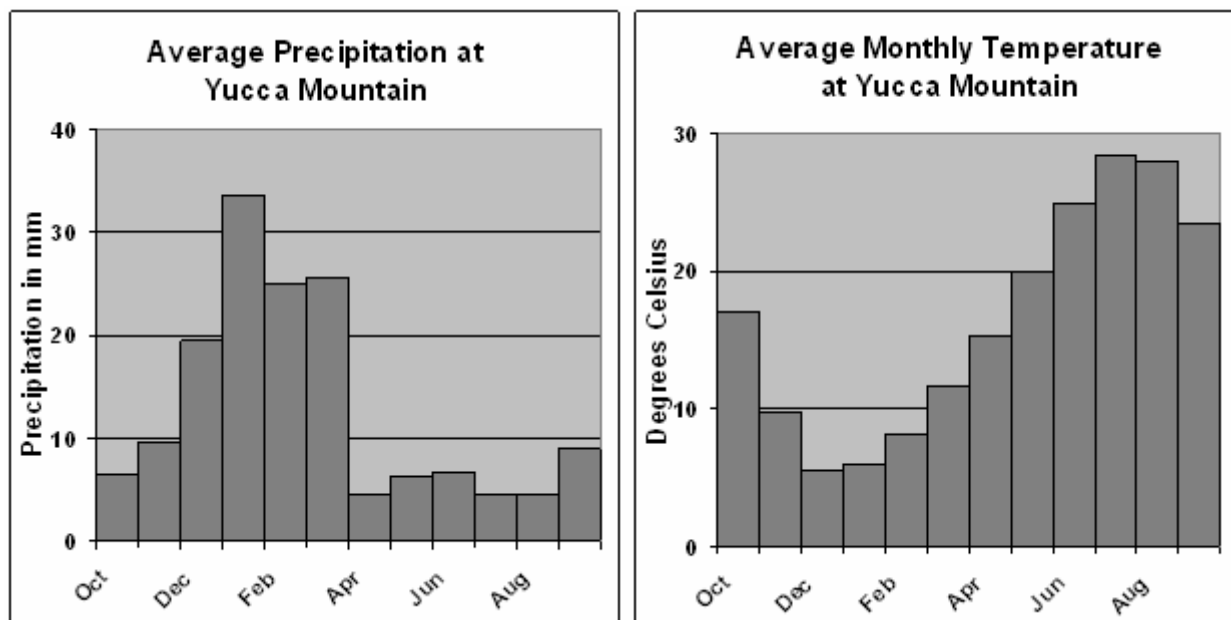
As explained later in this appendix, development of an algorithm to predict vegetation response for Yucca Mountain required one additional adaptation of NDVI, subtracting the lowest measured level of  $\text{NDVI}_{\text{offset}}$  that occurred during late summer of a very dry year, WY2002. This new index, given the convention NDVI', removed the  $\text{NDVI}_{\text{offset}}$  contributed by desert varnish and isolated the signal from the vegetation.

$\text{NDVI}_{\text{offset}}$  is calculated in Section E2.4 of this appendix.

## **E1.5 CHOICE OF DATA FOR ANALYSES: KEY YEARS – 1998, 2001, AND 2002**

There are two important trends in annual weather for Yucca Mountain that determine the pattern of vegetation growth that occurs. These are hot, dry summers and cool winters that tend to receive the greatest portion of annual precipitation (Figure E-2, a and b). Because of these influences, wintertime native vegetation passes through a dormant period that then responds with a flush of spring growth funded by overwinter precipitation. The hot dry summers create a second period of annual dormancy after all available soil water has been exhausted. In terms of

the annual hydrologic cycle, the hot dry months of summer are essentially a break between cycles. For this reason, the characterization of vegetation growth will be tracked on a water year basis starting October 1 (of the previous calendar year) and ending 364 days later on September 30. In this appendix, water year is abbreviated WY and individual days within each water year are numbered sequentially, 1 to 365, and abbreviated WYDOY for water year day of year.

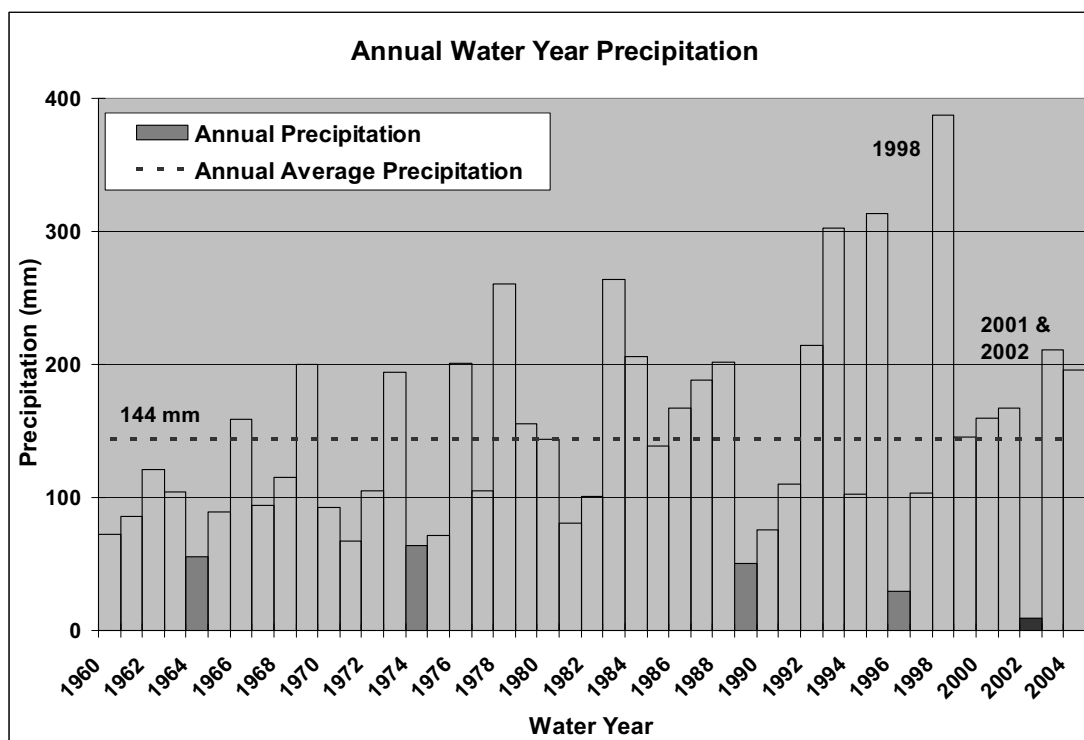


Source: DTN: MO9903CLIMATOL.001 [DIRS 116056]. Nine stations located at Yucca Mountain. Stations 1 to 5 from 1986 to 1997 and Stations 6 to 9 from 1993 to 1997.

NOTE: These data are presented only for illustration and were not used as direct inputs for the analyses.

Figure E-2. Yucca Mountain Average Monthly Precipitation (a) and Temperature (b) in Water Year Format as Background for Plant Growing Season and Precipitation Timing.

Three years were chosen for developing and testing the algorithm used to predict vegetation vigor using NDVI. These were an historic wet year (WY1998), an approximately average year (WY2001), and a very dry year (WY2002). Figure E-3 highlights these three years in the long term precipitation record for Station 4JA located 9 km from Yucca Mountain. During the wet year, WY1998, vegetation response was very high in comparison to the other two years. This is seen in the false color portrayals on Figure E-1. WY2002 was so dry that vegetation shows almost no response. This period of drought-induced quasi-zero vegetation cover is a baseline for minimal vegetation activity that was used in calculations to isolate the vegetation signal at Yucca Mountain. Vegetation expression during the record wet year (WY1998) was sufficiently robust for determining an ideal curve for annual vegetation response.



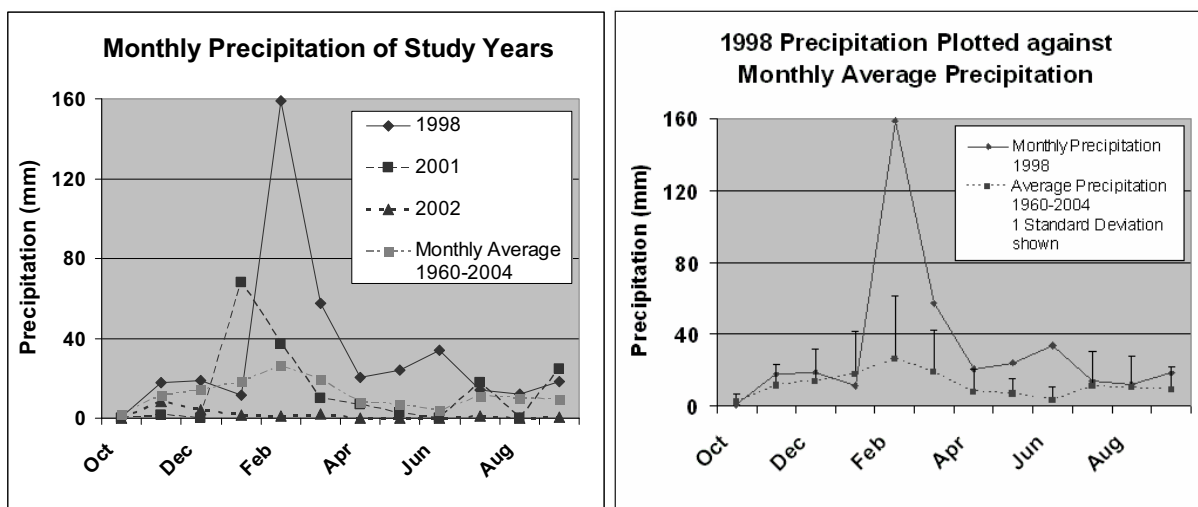
Source: 4JA east of Yucca Mountain 1959 to 2004: DTN: SN0601PRECPTMP.002 [DIRS 176122].

NOTE: These data were gathered sufficiently close to Yucca Mountain and have sufficient length of record to enable placing into context the three years that were chosen for analysis. All other data sets are either farther away from Yucca Mountain or have a comparatively short record. These data are presented only for illustration and were not used as direct inputs for the analyses.

Figure E-3. Water Year Total Precipitation Measured 12 km East of the Yucca Mountain Crest

Only three years were used for development and testing of the vegetation simulation and this small data set required characterization of seasonal growth response as a set response, hardwired for simplification, but scalable. Variations in plant growth according to intra-annual distribution of precipitation were, necessarily, not captured by the algorithm. Instead, as a simplification, vegetation growth will be fitted as proportional to antecedent precipitation occurring over the preceding winter. The peak precipitation, in March, also occurred in WY1998 (Figure E-4); however, for this year, precipitation was 2.6 times the annual average. Precipitation levels remained elevated through the summer of 1998.





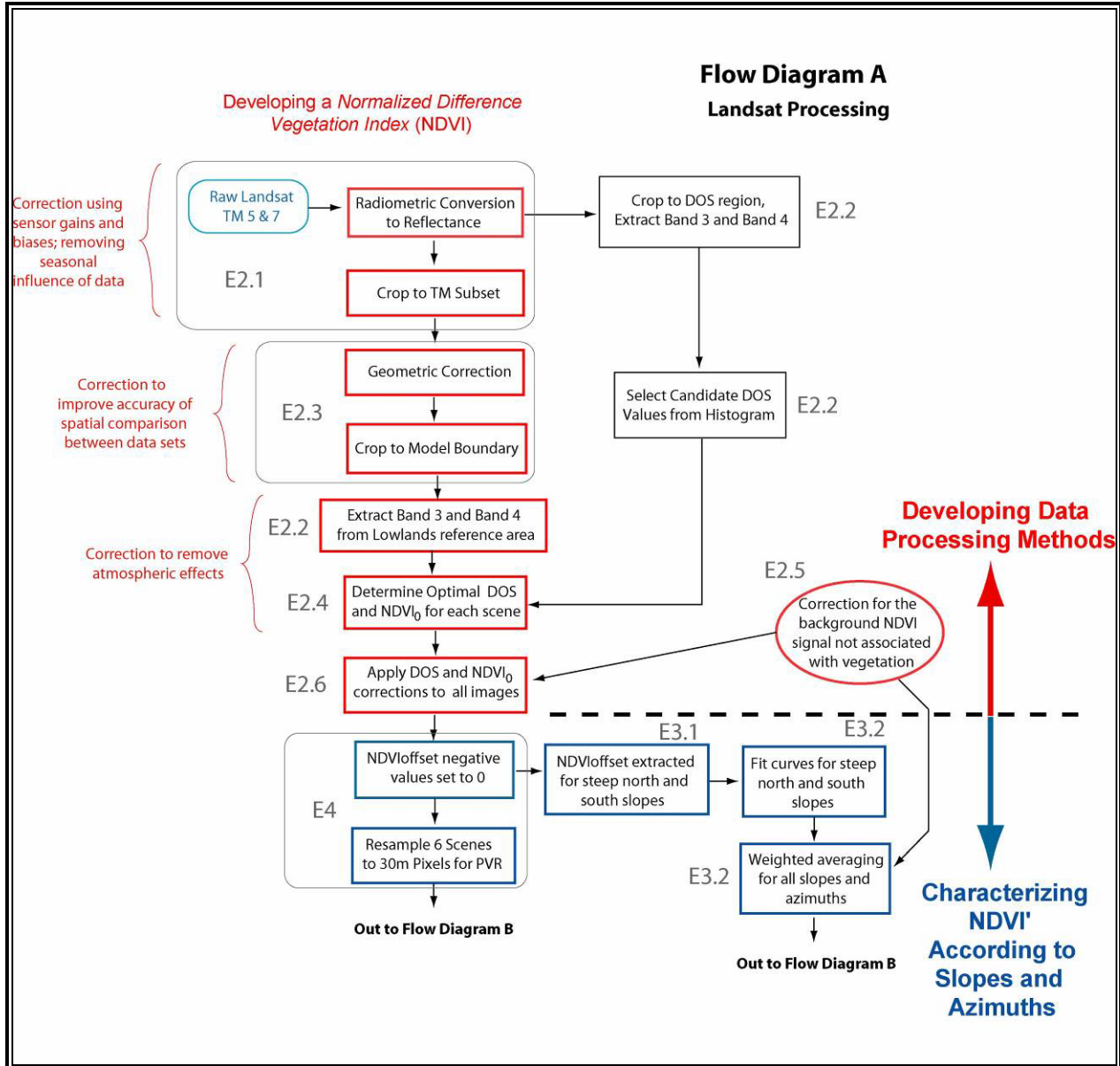
Source: Precipitation records from station 4JA east of Yucca Mountain 1959 to 2004:  
DTN: SN0601PRECPTMP.002 [DIRS 176122].

NOTE: These data are provided only for illustration and were not used as direct inputs.

Figure E-4. WY1998 Precipitation in Comparison to the Two Other Years (a) and the Statistics for Average Monthly Precipitation (b)

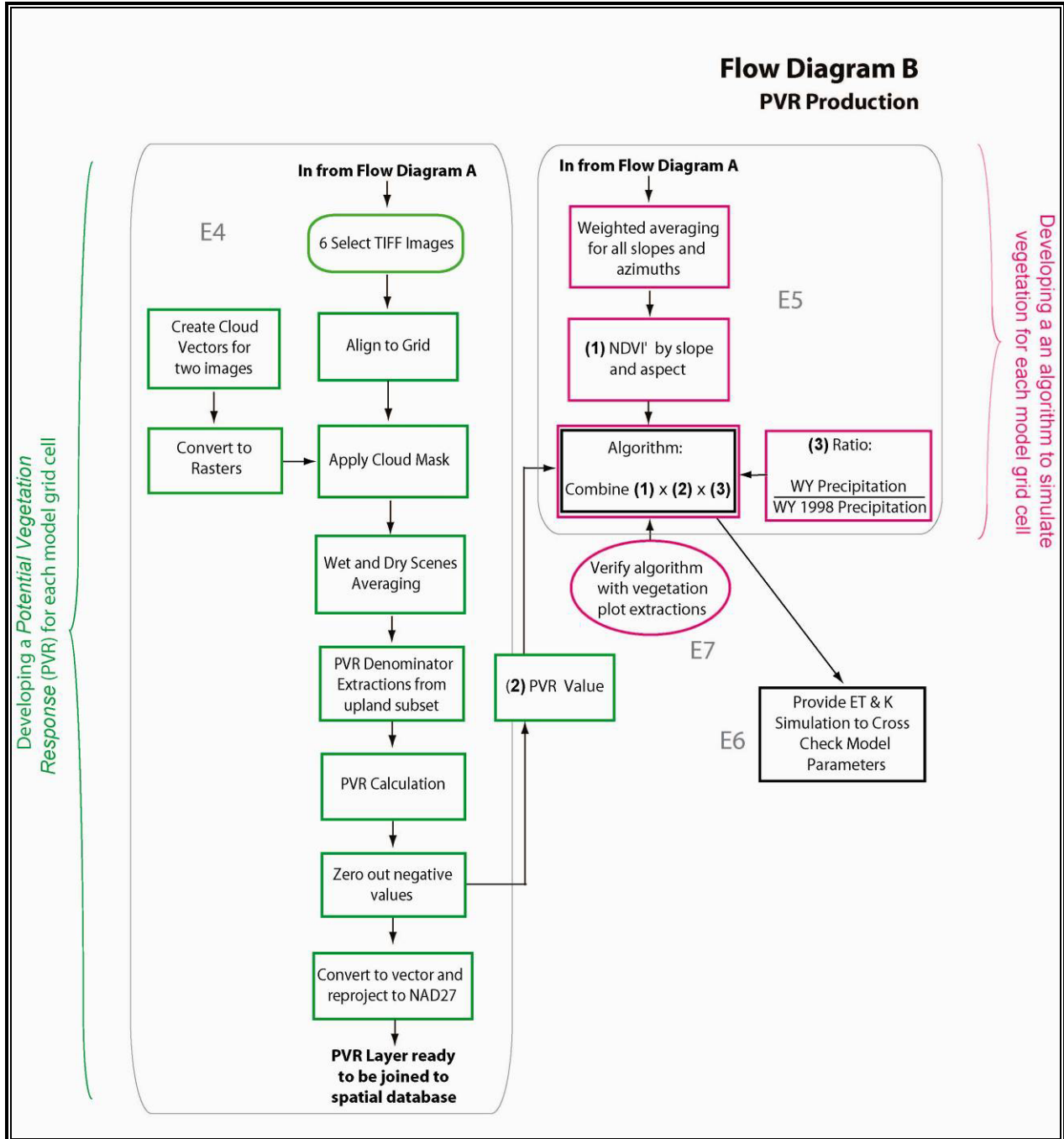
## E2. DATA PROCESSING AND FUNCTIONAL RELATIONSHIPS

In order to calculate NDVI as a function of location and time across the Yucca Mountain region, it was necessary to process the acquired Landsat TM data. This processing included the following major steps: (1) conversion of all TM images to units of reflectance, (2) correction for differing atmospheric conditions, (3) selection of  $NDVI_0$  to remove nonsystematic variation, and (4) geocorrection. A flow chart (Figure E-5) provides a visual map to follow the steps that are described in this section. The goal of the data processing was to isolate the vegetation signal by eliminating nonsystematic variation while selecting processing parameters in a nonarbitrary manner. A number of the data processing steps are standard, while others were developed specifically for the Yucca Mountain environment.



NOTE: Corroboration steps are given as ovals; processing and calculation as rectangles. Alpha-numeric designations are the sections in this appendix that describe these steps.

Figure E-5a. Flow Chart A for Processing and Analyzing Data Outputs that Feed to Flow Chart B



NOTE: Corroboration steps are given as ovals.

Figure E-5b. Flow Chart B for Processing and Analyzing Data Outputs from Flow Chart A

## E2.1 INITIAL PROCESSING STEPS

Thirty three images were used for algorithm development (Table E-1). For the period chosen for development of the algorithm, there were two Landsat TM satellites, TM5 and TM7. TM7 was launched during 1999 and TM5 in 1982. These sensors pass directly over the Yucca Mountain region every 16 days. This time spacing is optimal for evaluating the growth and development of vegetation. However, cloud cover often occludes viewing the area of interest. The collection of satellite images was chosen as a minimal set for establishing vegetation responses through each growing season.

Table E-1. Landsat TM Data Used for Characterization of Yucca Mountain

WY1998		WY2001		WY2002	
Filename	Sensor	Filename	Sensor	Filename	Sensor
T519971102	TM5	T520001009	TM5	T520011012	TM5
T519980121	TM5	T520010129	TM5	T720011004	TM7
T519980310	TM5	T520010318	TM5	T720011207	TM7
T519980411	TM5	T520010419	TM5	T720020124	TM7
T519980427	TM5	T520010505	TM5	T720020225	TM7
T519981529	TM5	T520010606	TM5	T720020329	TM7
T519980630	TM5	T520010724	TM5	T720020414	TM7
T519980716	TM5	T720001220	TM7	T720020430	TM7
T519980817	TM5	T720010326	TM7	T720020516	TM7
		T720010630	TM7	T720020601	TM7
		T720010817	TM7	T720020617	TM7
				T720020719	TM7
				T720020804	TM7

Source: Output DTN: SN0601ALANDSAT.001.

NOTE: Filenames list satellite, year, month, and day.

Sensor memory effects in TM bands 3 and 4 when passing across highly contrasting targets (Helder and Ruggles 2004 [DIRS 176740], Section IV) prompted exclusion of data from the TM5 satellite during WY2002 (Figure E-6). Analyses of pixel patterning for NDVI along the high-contrast scarp face of the Yucca Mountain crest (edges in shadow and full sunlight) were used to study this phenomenon. This method confirmed that the TM5 data from WY2001 (including data from 10/12/01 of WY2002) were free from this effect and were included in the sample. There were five TM images that were eliminated from the analyses of WY2002 due to memory effects: May 8, May 24, June 9, June 25, and August 12.

### Uncertainty Due to Integer Values for Digital Number

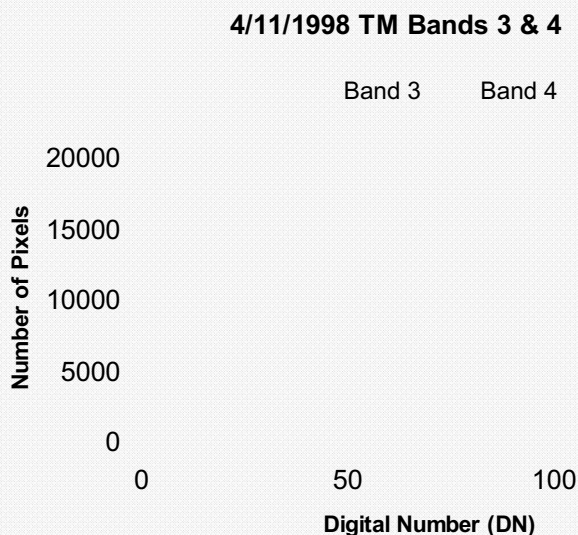
Details of the calculations are contained in Output DTN: SN0609LSTMPROC.001. In this appendix, details are provided for an example image. The example image was taken on 4/11/98, which is the peak of the growing season during a wet year. The statistics from this scene will be carried through the analyses to provide a measure of the greatest levels of uncertainty in the NDVI analyses.

Each image consists of raw digital numbers for each pixel and each band, supplemented by additional data, such as gain and bias corrections. Table E-Uncertainty-1 and Figure E-Uncertainty-1 indicate the range of values for the raw digital numbers for 4/11/1998. Truncation to an integer introduces a random uncertainty that is uniformly distributed over the range  $[-0.5, +0.5]$ . The standard uncertainty for that distribution is 0.3 (Appendix I). For each band, therefore, truncation produces a relative uncertainty that is random and is less than 1% of the mean measurement on 4/11/98 and less than 2% of the minimum measurement on that day.

Table E-Uncertainty-1. Landsat TM 5 04/11/1998 Pixel Value Statistics from within the Model Boundary

Band	Min	Max	Mean	Stdev
Band 3	20	196	61	12
Band 4	17	187	74	11

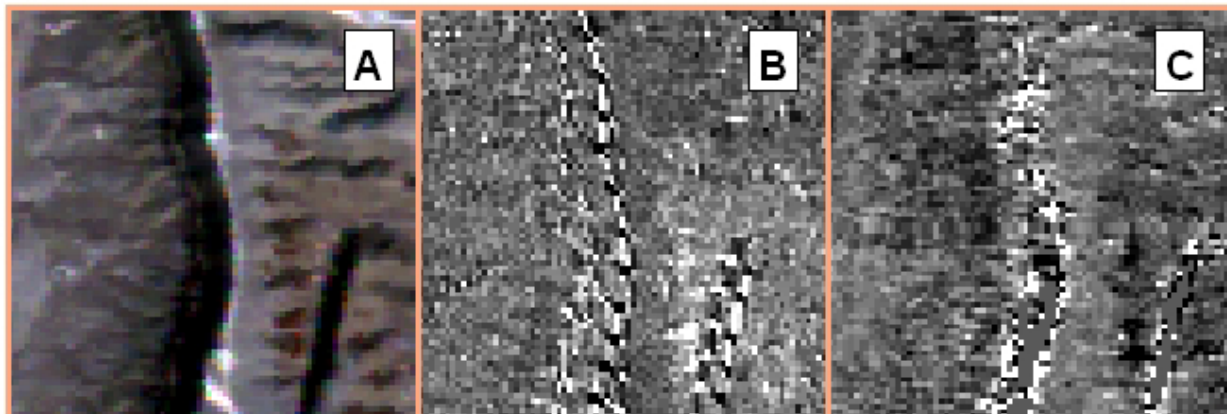
Source: Output DTN: SN0609LSTMPROC.001, *tm\_processing\_overview.xls*, worksheet *Process Steps*.



Source: Output DTN: SN0609LSTMPROC.001, *tm\_processing\_overview.xls*, worksheet *Process Steps*.

Figure E-Uncertainty-1. Histogram of Raw DN Numbers within the Model Boundary

Processing these TM data required an initial step to correct the data to radiance using the gains and biases of the sensors that accompany the satellite data. Radiance is the apparent light energy received at the satellite that is uncorrected for the strength of solar radiation incident to the target. The original signal from the satellite is output in digital numbers that are the readout from the sensors. The gains and offsets are, respectively, the slope and intercept of the linear relationship relating the radiance to the digital number. This correction removed the inherent differences between two sensors, Landsat TM5 and TM7, which were used in these analyses, and also corrected for sensor calibration drift (Markham and Barker 1987 [DIRS 177362]).



Source: Output DTN: SN0608NDVILSTM.001.

NOTES: A) A false color image from a TM 5 scene from May 8, 2002. B) The same showing NDVI. Note the systematic patterns along the crest and base of the shadowed slope due to the memory effect where high contrast existed between shaded and sunlit surfaces. C) The same location in a May 5, 2001, TM 5 scene exhibiting a normal NDVI response for comparison. The crest contains numerous high NDVI-response features.

Figure E-6. An Example of Observed Memory Effects in TM5 2002 Images

Development of a vegetation simulation for Yucca Mountain required evaluation of satellite images through the entire year. Thus, compensation for the differing solar radiation was necessary since the magnitude of solar radiation is much lower during the winter than the summer. Conversion to apparent (at satellite) reflectance is a step that effectively removes this seasonal influence by normalizing the measured data by the magnitude of solar radiation. This conversion process permits direct comparison of Landsat TM images taken throughout the year since, in essence, reflectance is radiance normalized by the strength of the solar irradiance. Each scene was converted to reflectance units using ENVI internal calibration utilities with the data for gains, offsets, and ephemeris from TM header files (Markham and Barker 1987 [DIRS 177362]). The formulae governing the calculation of radiance and reflectance are provided here in two steps (Equations E-4 and E-5), while the ENVI software provides this calculation in one step:

$$L_{\lambda} = Gain_{\lambda} DN_{\lambda} + Bias_{\lambda} \quad (\text{Eq. E-4})$$

where

- $L_\lambda$  = Exoatmospheric spectral reflectance
- $\lambda$  = Refers to either Band 3 or 4 value
- $Gain_\lambda$  = Vvalue included with the satellite header
- $DN_\lambda$  = Digital number output from the sensor
- $Bias_\lambda$  = Range of rescaled radiance in digital numbers.

$$\rho_\lambda = \frac{\pi L_\lambda d^2}{ESUN_\lambda \cos \theta_s} \quad (\text{Eq. E-5})$$

where

- $\rho_\lambda$  = Exoatmospheric reflectance (i.e., measured at the sensor)
- $d$  = Earth–Sun distance
- $ESUN_\lambda$  = Mean solar exoatmospheric irradiance
- $\theta_s$  = Solar zenith angle in degrees.

### Uncertainty for TM Band 3 and 4 Reflectance Calculation

The primary source of error influencing these calculations is in Equation E-4 because all of the inputs to Equation E-5 are matters of physics, are well known, and will tend to be small compared to the uncertainty involved in calibration. Table E-Uncertainty-2 lists the calibration coefficients for each of the images listed in Table E-1. These are colored to show that there are four groups with identical coefficients for all of the images that are in the same group. For the image on 4/11/98 (in the blue grouping), Gain<sub>3</sub> and Gain<sub>4</sub> are 1.04 and 0.87, while Bias<sub>3</sub> and Bias<sub>4</sub> are -1.17 and -1.51. Therefore, the value of  $L_\lambda$  is not much removed from the value of  $DN_\lambda$ .

Table E-Uncertainty-2. Calibration Coefficients for Images Used in this Appendix

TM Scene	Band3		Band4	
	Gain	Offset	Gain	Offset
t519971102	1.0398824	-1.1700000	0.8725882	-1.5100000
t519980121	1.0398824	-1.1700000	0.8725882	-1.5100000
t519980310	1.0398824	-1.1700000	0.8725882	-1.5100000
t519980411	1.0398824	-1.1700000	0.8725882	-1.5100000
t519980427	1.0398824	-1.1700000	0.8725882	-1.5100000
t519980529	1.0398824	-1.1700000	0.8725882	-1.5100000
t519980630	1.0398824	-1.1700000	0.8725882	-1.5100000
t519980716	1.0398824	-1.1700000	0.8725882	-1.5100000
t519980817	1.0398824	-1.1700000	0.8725882	-1.5100000
t520001009	1.0398824	-1.1700000	0.8725882	-1.5100000
t520010129	1.0398824	-1.1700000	0.8725882	-1.5100000
t520010318	1.0398824	-1.1700000	0.8725882	-1.5100000
t520010419	1.0398824	-1.1700000	0.8725882	-1.5100000
t520010505	1.0398824	-1.1700000	0.8725882	-1.5100000
t520010606	1.0398824	-1.1700000	0.8725882	-1.5100000
t520010724	1.0398824	-1.1700000	0.8725882	-1.5100000
t720001220	0.6216535	-5.6216431	0.6397638	-5.7397614
t720010326	0.9425197	-5.9425201	0.9692914	-6.0693054
t720010630	0.9425197	-5.9425201	0.9692914	-6.0693054
t720010328	0.9425197	-5.9425201	0.9692914	-6.0693054
t720010817	0.9425197	-5.9425201	0.9692914	-6.0693054
t520011012	1.0398824	-1.1700000	0.8725882	-1.5100000
t720011004	0.9425197	-5.9425201	0.9692914	-6.0693054
t720011207	0.9425197	-5.9425201	0.6397638	-5.7397614
t720020124	0.9425197	-5.9425201	0.6397638	-5.7397614
t720020225	0.9425197	-5.9425201	0.6397638	-5.7397614
t720020329	0.9425197	-5.9425201	0.9692914	-6.0693054
t720020414	0.9425197	-5.9425201	0.9692914	-6.0693054
t720020430	0.9425197	-5.9425201	0.9692914	-6.0693054
t720020516	0.9425197	-5.9425201	0.9692914	-6.0693054
t720020601	0.9425197	-5.9425201	0.9692914	-6.0693054
t720020617	0.9425197	-5.9425201	0.9692914	-6.0693054
t720020719	0.9425197	-5.9425201	0.9692914	-6.0693054
t720020804	0.9425197	-5.9425201	0.9692914	-6.0693054

Source: Output DTN: SN0609LSTMPROC.001; page "Gains\_and\_Offsets" of *tm\_processing\_overview.xls*.



### Uncertainty for TM Band 3 and 4 Reflectance Calculation – Continued

An analysis by Chander et al. (2004 [DIRS 177572]) evaluated the uncertainty in the Gain coefficients for TM5 using cross–correlation with TM7 and a calibration uncertainty of 3% for TM7. Data from 1999 (close in time to the combined data set for WY1998 that feeds relationships to the MASSIF model) were compared to image pairs for spectrally stable features on the Railroad Valley Playa that showed a repeatability of approximately  $\pm 2\%$ , and for Bands 3 (R) and 4 (NIR) that are used to generate NDVI, a one sigma value for exoatmospheric radiance uncertainty of about  $\pm 4\%$ . The Railroad Valley Playa is located about 70 km NNE of Yucca Mountain.

The exoatmospheric radiance uncertainty is a systematic uncertainty that applies to all of the values generated with the same values of Gain and Bias. The uncertainty from truncation is a random uncertainty.

Table E-Uncertainty–3 shows the range of values for radiance on 4/11/98, for individual pixels after processing through Equation E-5. Based on a relative uncertainty of 4%, the standard uncertainty of values near the mean is about 0.01, ranging from 0.002 at the minimum values to 0.02 at the maximum values.

Table E-Uncertainty–3. Reflectance Statistics of Pixel Values within the Model Boundary, Landsat TM5 4/11/1998

Band	Min	Max	Mean	Stdev
Band 3	0.05	0.52	0.16	0.03
Band 4	0.05	0.61	0.24	0.04

Source: DTN: SN0601ALANDSAT.001 [DIRS 177239]

Source: DTN: SN0609LSTMPROC.001, file *tm\_processing\_overview.xls*, worksheet "Process Steps."

## E2.2 ATMOSPHERIC CORRECTION

Up to this point, data processing produced values measured at the satellite sensor (exoatmospheric). Several steps were undertaken to remove the effects from the atmosphere through which light passed twice (incident and reflected). Atmospheric scatter due to the presence of airborne particles causes each of the TM bands to yield a higher reflectance than would be measured at the land surface in the absence of the entire atmospheric path. This scatter may especially confound radiometric measurement such as NDVI because different concentrations of airborne particles such as smoke, water droplets, and dust may be present at the time of overpass that would affect R and NIR bands differently. In order to accurately evaluate low vegetation cover within multiple time steps, the effects of this scatter were removed.

A technique to remove atmospheric scatter, called dark object subtraction (DOS), assumes that there exists at least one or more pixels within the scene that will have zero reflectance. This lowest measured reflectance (the DOS value) represents the scatter at the assumed zero reflectance and is simply subtracted from all pixels in the region of interest (Chavez 1988 [DIRS 176788]). Areas where zero reflectance would be expected include still, open water, or deep shadows, two features that are unfortunately rare within the Yucca Mountain region. There are water bodies within the TM scenes, including Ash Meadows and Pahrangat Valley, (45 and 140 km distant, respectively). Sensitivity analyses indicated that the water bodies in these locations were not suitable due to desiccation during the critically dry year of 2002. At other times these water bodies gave very high reflectance values, possibly due to the entrainment of sediments or specular reflectance from wind-driven waves.

Because of the lack of specific DOS targets in all images, correction for atmospheric influences was approached using histogram functions for all TM images (Chavez 1988 [DIRS 176788]). First, candidate values for DOS (i.e., lowest values for reflectance) were chosen by examining histograms for extracted values within the region overlying a region larger than Yucca Mountain, as shown in Figure E-7. The region chosen for the analysis of Bands 3 and 4 extends beyond the Yucca Mountain infiltration model domain to include areas with deep shadows and dark basalt (located to the north, but within a sufficiently small area so that it is still representative of the air mass overlying Yucca Mountain). Because close-tolerance geocorrection was not important for this step, it was conducted on images as received from Eros Data center, with geocorrection generally within several hundred meters.

The DOS correction for atmospheric scatter makes the assumption that the air mass overlying the region of Yucca Mountain at the time of each overpass was exemplified by the region chosen for the DOS determination. Further, it was assumed that the properties of this air mass were evenly distributed over Yucca Mountain.



Sources: Output DTNs: SN0608NDVIANAL.001 and SN0608NDVIAUXD.001 The net infiltration modeling domain is outlined in green for reference. The figure was developed from a TM image developed for explanatory purposes in *B3\_B4\_DOS\_ROI\_2.xls*. The blue and green polygons are defined by *dos\_region\_.evf* and *nad27\_boundary\_.evf*.

Figure E-7. Map Showing Candidate DOS Region (Blue Polygon)

For extraction of candidate DOS values, each scene was cropped to the larger polygonal region portrayed in Figure E-7. All pixel reflectance values for Bands 3 and 4 were extracted from this area and placed into histograms (i.e., pixel counts within reflectance bins). Two possible candidate values for DOS for each band were chosen:  $DOS_{min}$  was taken as the lowest reflectance where a single pixel appeared. If this reflectance represented less than three pixels, an alternate value,  $DOS_{alt}$ , was also chosen. This was done to constrain potential error. TM data may include a small number of pixels with erroneous data (Vogelmann et al. 2001 [DIRS 176746]), and extracting the data for over six million pixels within the DOS region of interest introduces a likelihood for including an errant low value. The average of  $DOS_{min}$  and

$DOS_{alt}$ , called  $DOS_{avg}$ , was used for the DOS value. The values for all TM images were developed in *B3\_B4\_DOS\_ROI.xls* (Output DTN: SN0608NDVIANAL.001).

### Uncertainty for Correction of Atmospheric Scatter (DOS)

For the image of 4/11/98, the lowest measured reflectance for Band 3 in the candidate DOS region was 0.034, which occurred in three pixels and became the value for  $DOS_3$ . For Band 4, the lowest value of 0.030 occurred in only one pixel and became  $DOS_{min}$ . The next higher value of 0.033 occurred in seven pixels and became  $DOS_{alt}$ . Therefore,  $DOS_4$  was 0.032. These values for DOS are smaller than any measured reflectance within the model domain.

Based on this example, the standard uncertainty in  $DOS_\lambda$  from random effects is about 0.001, which is consistent with the truncation error, which should be about 3% of these values. On the other hand, all of the calculated values carry the systematic errors in the calibrations of Gain and Bias. However, subtraction of DOS from the reflectance will cancel the Bias term and, therefore, remove any effects from the uncertainty in Bias. This follows from the confidence interval of  $L_\lambda$ , defined as  $CI(L_\lambda) = (Gain_\lambda \pm k\Delta G_\lambda)DN_\lambda + (Bias_\lambda \pm k\Delta B_\lambda)$  due to the uncertainty in gain and the uncertainty in bias.

We suppose that the function that transforms  $L_\lambda$  into  $\rho_\lambda$  does not bring any other uncertainty, so the confidence interval on  $\rho_\lambda$  is given by formulas described by Markham and Barker (1987 [DIRS 177362]):

$$CI(\rho_\lambda) = (Gain_\lambda \pm k_\theta \Delta G_\lambda) DN_\lambda \frac{\pi d^2}{ESUN_\lambda \cos \theta_\sigma} + (Bias_\lambda \pm k_\theta \Delta B_\lambda) \frac{\pi d^2}{ESUN_\lambda \cos \theta_\sigma}.$$

Thus, the error in bias does not stretch or compress the actual value of  $\rho_\lambda$ . It is an error in translation. When the DOS value is subtracted to  $\rho_\lambda$ , we move every value to a referential value and suppress the second term of the above equation (after the '+' sign). Therefore, this operation suppresses any error in bias term. The only uncertainty remaining is due to the uncertainty in gain ( $\Delta G_\lambda$ ).

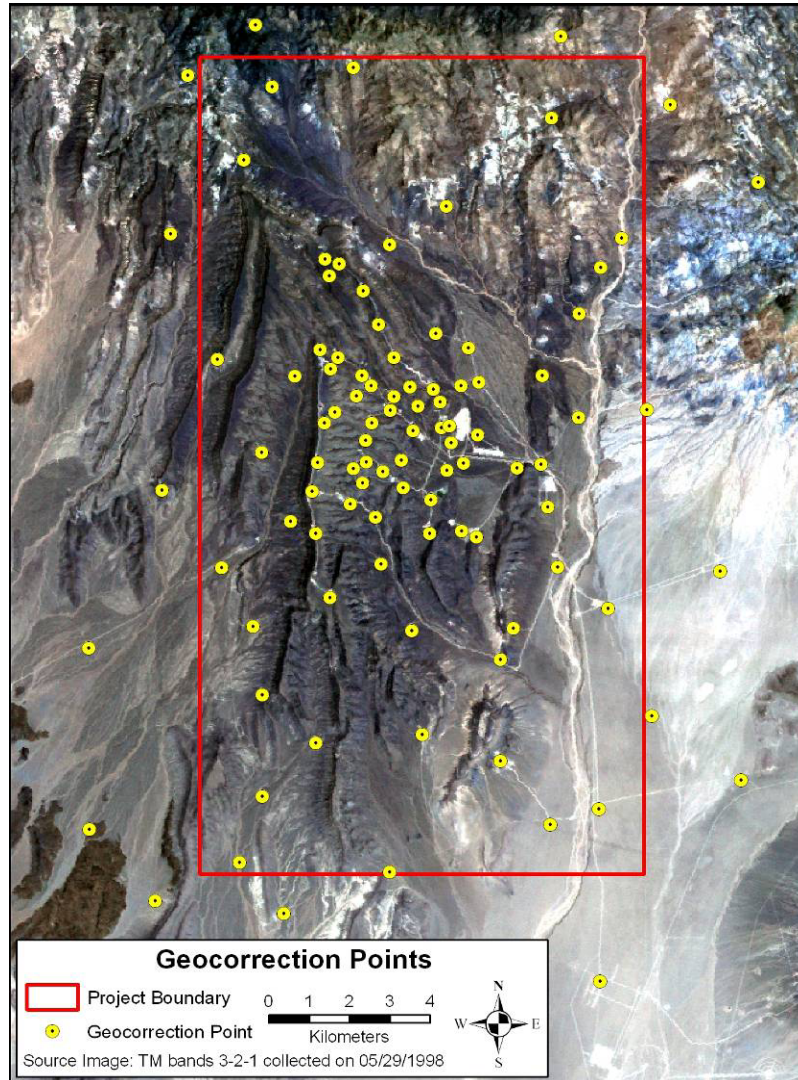
## E2.3 GEOCORRECTION

Landsat TM images are typically geocorrected by the Eros Data Center such that pixel locations may be correct to only several hundred meters, especially in mountainous terrain. In order to make comparisons among many images with fixed model grid cells of  $30 \times 30$  m, it was necessary to improve the accuracy of that initial geocorrection. Due to the high degree of elevation variation within the Yucca Mountain infiltration model boundary, a comprehensive set of 100 ground control points (GCPs) were collected from a large variety of elevations (Output DTN: SN0608NDVIAUXD.001). The highest concentration of points was placed in the region lying above the proposed repository.

The set of 100 points was an aggregate from three data sources: borehole coordinates (DTN: MO9906GPS98410.000 [DIRS 109059]), field-acquired points (DTN: MO0512COV05112.000 [DIRS 177249]), and points derived from U.S. Geological Survey Digital Ortho-Quarterquads (DOQQs) for areas inaccessible to vehicles (DTN: SN0601DOQQYM98.001 [DIRS 177240]). The points in this set were chosen to be highly visible on the majority of the TM images (Figure E-8). The large number of points allowed for a 4th order polynomial warp of the imagery to fit the complex Yucca Mountain surface.

Using the set of GCPs, reference pixel locations were visually mapped to geographic coordinate locations using the standard ENVI Image to Map registration tools. Points were visually matched on the TM images to the surveyed coordinates or selected DOQQ feature coordinates chosen in remote locations. All 100 GCPs were used for each of the Landsat scenes to maintain the greatest continuity in scene geometry. For points where unequivocal surface features were not identifiable, the ENVI predict function was used to place the point—this function uses the geometry of the remaining points as a reference. Points were carefully positioned until the average root mean square error (RMS) was less than 0.30 and each individual pixel RMS was less than 0.5.

This geocorrection process also was used to resample the 28.5 m data from the original TM pixels into 30 m grid cells of the infiltration model domain using the ENVI cubic convolution algorithm. Cubic convolution is a spatially weighted average of portions of the original pixels that fall within the 30 m boundaries of each model cell. All of the geocorrected data were projected in UTM, NAD83 Zone 11N (a positioning coordinate system described in the glossary of Appendix B).



NOTE: This figure displays a set of geocorrection points from the points folder (Output DTN: SN0608NDVIAUXD.001).

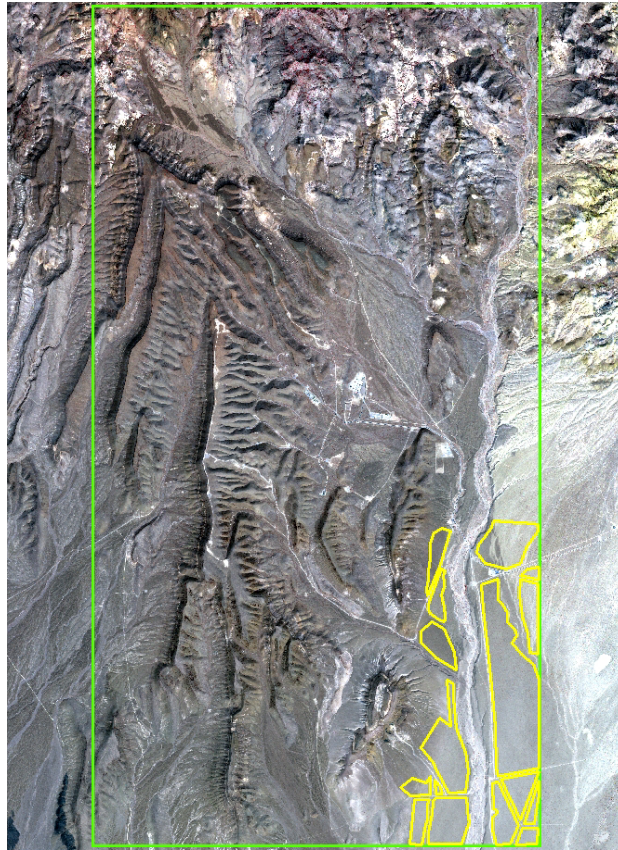
Figure E-8. Ground Control Points for the Infiltration Model Domain Region

#### E2.4 TM BAND 3 AND 4 ATMOSPHERIC CORRECTION AND DETERMINING $NDVI_0$ TO CORRECT FOR NONSYSTEMATIC VARIATION

Following geocorrection, each TM scene was cropped to the Yucca Mountain infiltration model boundary, and the  $DOS_{avg}$  values that were calculated during the step described in Section E2.2 were applied to Bands 3 and 4. Data from Bands 3 and 4 were then extracted from specially chosen reference polygons for selection of the parameter  $NDVI_0$  for calculation of  $NDVI_{offset}$  (Eq. E-3).

Reference polygons were chosen from false-color satellite imagery and digital elevation model data to have relatively homogeneous vegetation cover on low relief terrain, avoiding any influence of differential seasonal shadowing or bidirection reflectance functions that can strongly

influence NDVI (Walthall et al. 1985 [DIRS 176737]; Walter-Shea et al. 1997 [DIRS 176752]). Such influences would likely be detrimental for understanding the sparse vegetation cover and its seasonal progression on Yucca Mountain. Reference polygons, called lowlands, were selected within the model boundary as shown in Figure E-9.



NOTE: Reflectance values for Bands 3 and 4 were selected from within these polygons for iterative evaluation and selection of DOS values. This figure was created using Lowlands\_utm83.evf (Output DTN: SN0608NDVIAUXD.001), nad27\_boundary\_.evf (Output DTN: SN0608NDVIAUXD.001), and a TM scene (Output DTN: SN0608NDVILSTM.001).

Figure E-9. Yucca Mountain Infiltration Model Boundary (green) and a Series of Reference Polygons Representing Vegetation Cover on Low Relief Areas (Lowlands)

### Uncertainty for Estimation of NDVI<sub>0</sub>

In the example image of 4/11/98, there were 13,245 pixels that fell within one of the reference polygons representing lowlands. The NDVI values for those pixels were calculated in accordance with Equation E-1 after correcting NIR and R for the DOS values. Except for one pixel with NDVI of 0.11, the values ranged from 0.13 to 0.30, with a mean of 0.18.

Table E-Uncertainty-4 contains some example values and the resulting uncertainty. Because the subtraction of DOS eliminates any uncertainty in the Bias terms, only the uncertainty from truncation and the uncertainty in Gain are considered. The uncertainties in Gain<sub>3</sub> and Gain<sub>4</sub> are independent of each other and therefore combine (root-mean-square) when the bands are subtracted or added. As a result, the contribution of truncation uncertainty to NDVI uncertainty is negligible.

The uncertainty is dominated by the uncertainty in the numerator of Equation E-1. Everywhere within the lowland polygons, the uncertainty in NDVI is about 0.03. Choosing the lowest value of NDVI for NDVI<sub>0</sub> would introduce an uncertainty of 0.03.

Table E-Uncertainty-4. Example NDVI Calculations within Lowlands Polygons for 4/11/98

Pixel ID	$\rho_4^a$	$\rho_3^a$	$\rho_4\text{-DOS}_4^b$	$\rho_3\text{-DOS}_3^b$	NDVI Numerator <sup>c</sup>	NDVI Denominator <sup>c</sup>	NDVI
12,557	0.239 ±0.010	0.202 ±0.008	0.207 ±0.010	0.168 ±0.008	0.039 ±0.013	0.375 ±0.013	0.11 ±0.03
11,417	0.288 ±0.012	0.230 ±0.009	0.256 ±0.012	0.196 ±0.009	0.060 ±0.015	0.452 ±0.015	0.13 ±0.03
11,117	0.285 ±0.011	0.225 ±0.009	0.253 ±0.011	0.193 ±0.009	0.060 ±0.014	0.446 ±0.014	0.14 ±0.03
10,093	0.256 ±0.010	0.200 ±0.008	0.224 ±0.010	0.168 ±0.008	0.056 ±0.013	0.392 ±0.013	0.15 ±0.03
9,616	0.255 ±0.010	0.196 ±0.008	0.223 ±0.010	0.162 ±0.008	0.061 ±0.013	0.385 ±0.013	0.16 ±0.03
8,333	0.252 ±0.010	0.190 ±0.008	0.218 ±0.010	0.156 ±0.008	0.062 ±0.013	0.374 ±0.013	0.17 ±0.03
5	0.230 ±0.009	0.171 ±0.007	0.196 ±0.009	0.137 ±0.007	0.059 ±0.011	0.334 ±0.011	0.18 ±0.03
7,709	0.244 ±0.010	0.169 ±0.007	0.212 ±0.010	0.135 ±0.007	0.077 ±0.012	0.347 ±0.012	0.22 ±0.03
7,712	0.255 ±0.010	0.166 ±0.007	0.223 ±0.010	0.132 ±0.007	0.091 ±0.012	0.355 ±0.012	0.26 ±0.03
7,726	0.268 ±0.011	0.162 ±0.006	0.236 ±0.011	0.128 ±0.006	0.108 ±0.013	0.364 ±0.013	0.30 ±0.04

Source: The first three columns are from Output DTN: SN0609LSTMPROC.001, *tm\_processing\_overview.xls*, worksheet "4-11-1998 Intercept."

<sup>a</sup> Standard uncertainty estimated to be 4% of value.

<sup>b</sup> DOS<sub>3</sub> and DOS<sub>4</sub> are 0.034 and 0.032, respectively, with negligible uncertainty (Section E2.2).

<sup>c</sup> See Equation E-1. Standard uncertainty of sum or difference is root mean square of component uncertainties. Standard uncertainty of quotient is uncertainty in numerator divided by the value of denominator, which neglects uncertainty in denominator.



### Further Explanation of Uncertainty in the Numerator of Equation E-1

That uncertainty in the calculation of NDVI is dominated by the uncertainty in the numerator of Equation E-1 can be further explained. Equation E-1 can be rewritten to include uncertainties:

$$\rho_4 - DOS_4 = M_4 \pm \sigma_4$$

$$\rho_3 - DOS_3 = M_3 \pm \sigma_3$$

$$\text{With } 0 < M_3 < M_4$$

By considering  $\rho_4 - DOS_4$  and  $\rho_3 - DOS_3$  independent, the uncertainty on the numerator (N) and denominator (D) part of the estimate of NDVI can be estimated:

$$N = M_4 - M_3 \pm \sqrt{\sigma_4^2 + \sigma_3^2} \quad \text{and} \quad D = M_4 + M_3 \pm \sqrt{\sigma_4^2 + \sigma_3^2}$$

$$\text{Thus, } NDVI = \frac{N}{D} = \frac{M_4 - M_3 \pm \sqrt{\sigma_4^2 + \sigma_3^2}}{M_4 + M_3 \pm \sqrt{\sigma_4^2 + \sigma_3^2}} \quad (\text{Eq. E1-bis})$$

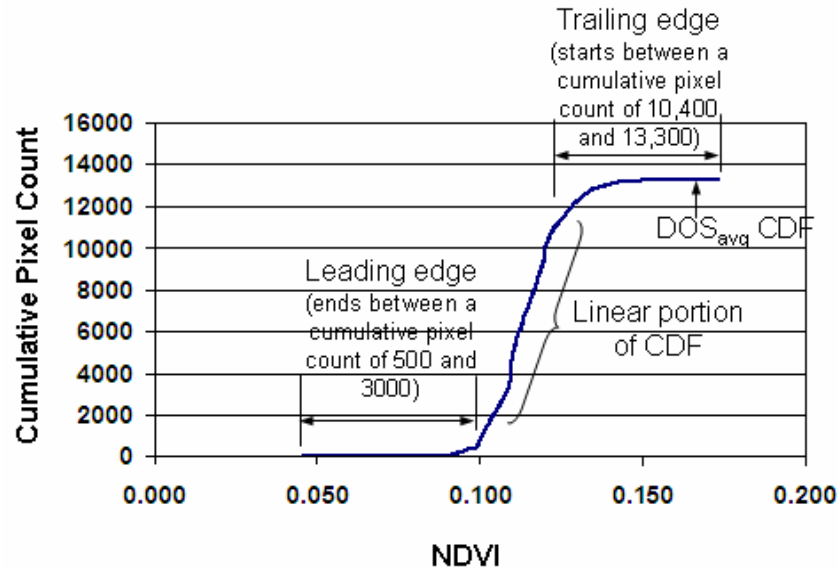
If  $M_4 - M_3 \ll M_4 + M_3$  and  $\sqrt{\sigma_4^2 + \sigma_3^2} \ll M_4 + M_3$ , then Equation E1-bis can be approximated with

$$NDVI \approx \frac{M_4 - M_3}{M_4 + M_3} \pm \frac{\sqrt{\sigma_4^2 + \sigma_3^2}}{M_4 + M_3}$$

In order to reduce the random uncertainty in  $NDVI_0$ , the extracted NDVI values (calculated after subtracting the atmospheric scatter,  $DOS_{avg}$ , were displayed as cumulative distribution functions (CDFs). These CDFs were analyzed by linear regression to determine the best fit for predicting an x-axis intercept ( $NDVI_0$ ) from the linear portion of the CDF (Baugh and Groeneveld 2006 [DIRS 178678]). The effect of these calculations is shown at the end of this section.

The cumulative pixel count for the CDFs typically varied between 0 and 15,000, with the leading edge of the curve ending between 500 and 3,000 and the trailing edge of the curve starting between 10,400 and 13,300. Figure E-10 shows a CDF typical of the data. The linear portion of the CDF for each data set was determined automatically for a number of cumulative pixel count ranges. A linear fit was made to the data in each range, and the range resulting in the best fit (that having the highest squared regression coefficient,  $R^2$ ) was used to define the linear portion of the CDF. As an example, Figure E-11 shows how the linear fit, and the resulting  $NDVI_0$  value, varies based on the chosen linear portion of the CDF curve. In this example, the linear portion of the curve would be defined as those data between the cumulative pixel count values

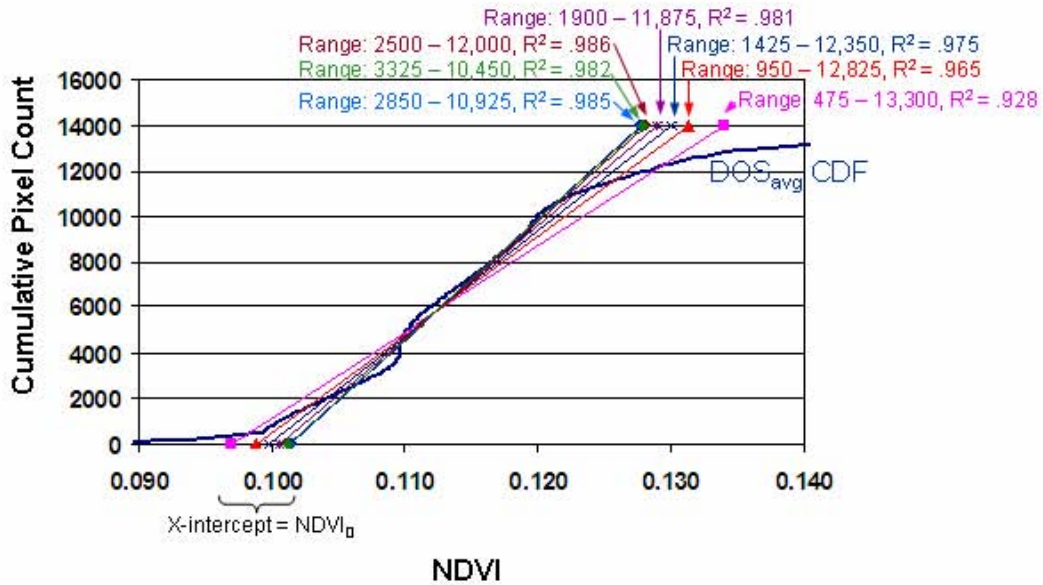
of 2,500 and 12,000. The ranges for calculating the linear regression relationships were standardized for use on all data sets by observation and optimization for the general curve shapes and ranges.



Source: Output DTN: SN0608NDVIANAL.001, *Atm\_Cor.xls*.

NOTE: The CDF was extracted from within the lowland polygons shown in Figure 9.

Figure E-10. Cumulative Distribution Function for 11/2/1997 Data Set Showing Typical Ranges for the Ending Points of the Leading Edge and the Starting Point of the Trailing Edge for YMP Data



The process for selecting the image processing parameters resulted in a table of final values for each water year in the study (Table E-2). These values were applied to the images for all subsequent steps. The workbook *Atm\_Cor.xls* (Output DTN: SN0608NDVIANAL.001) contains the analysis sheet, copies of the data for each image, and a summary of the resulting values. Table E-2 also indicates the standard deviation from several possible fits to the linear portion, indicating that the random uncertainty in  $NDVI_0$  is always less than 0.01.

Table E-2.  $DOS_{avg}$  Values in Reflectance Selected for TM5, Bands 3 and 4, and the Resulting  $NDVI_0$  and  $NDVI_{offset}$  for Each Image during all Three Water Years

	WY DOY	TM Date	TM Sensor	DOSavg Band 3	DOSavg Band 4	Average NDVI	$NDVI_0$ (Intercept)	$NDVI_{offset}$
WY 1998	33	11/2/1997	5	0.0180	0.0150	0.1145	0.1012	0.0133
	113	1/21/1998	5	0.0190	0.0150	0.1253	0.1041	0.0212
	161	3/10/1998	5	0.0240	0.0140	0.1493	0.1241	0.0252
	193	4/11/1998	5	0.0340	0.0315	0.1824	0.1504	0.0320
	209	4/27/1998	5	0.0405	0.0360	0.1998	0.1755	0.0242
	241	5/29/1998	5	0.0380	0.0315	0.1800	0.1626	0.0173
	273	6/30/1998	5	0.0360	0.0310	0.1521	0.1347	0.0173
	289	7/16/1998	5	0.0240	0.0280	0.1171	0.1025	0.0146
	321	8/17/1998	5	0.0280	0.0230	0.1312	0.1137	0.0174
WY 2001	9	10/9/2000	5	0.0050	0.0200	0.0591	0.0339	0.0252
	81	12/20/2000	7	0.0190	0.0145	0.1264	0.1017	0.0247
	121	1/29/2001	5	0.0370	0.0245	0.1492	0.1236	0.0256
	169	3/18/2001	5	0.0260	0.0135	0.1432	0.1179	0.0253
	177	3/26/2001	7	0.0275	0.0270	0.1493	0.1232	0.0261
	201	4/19/2001	5	0.0490	0.0370	0.1884	0.1628	0.0255
	217	5/5/2001	5	0.0375	0.0340	0.1488	0.1339	0.0148
	249	6/6/2001	5	0.0400	0.0285	0.1358	0.1204	0.0153
	273	6/30/2001	7	0.0445	0.0570	0.0865	0.0717	0.0147
297	7/24/2001	5	0.0325	0.0250	0.1242	0.1088	0.0154	
321	8/17/2001	7	0.0405	0.0425	0.1039	0.0892	0.0147	
WY 2002	4	10/4/2001	7	0.0220	0.0230	0.0986	0.0853	0.0133
	12	10/12/2001	5	0.0210	0.0145	0.1161	0.0995	0.0166
	68	12/7/2001	7	0.0060	0.0160	0.0869	0.0720	0.0149
	116	1/24/2002	7	0.0180	0.0150	0.1214	0.1058	0.0156
	148	2/25/2002	7	0.0190	0.0185	0.1238	0.1097	0.0141
	180	3/29/2002	7	0.0225	0.0250	0.0978	0.0848	0.0130
	196	4/14/2002	7	0.0310	0.0375	0.0823	0.0694	0.0130
	212	4/30/2002	7	0.0350	0.0330	0.1145	0.1023	0.0122
	228	5/16/2002	7	0.0490	0.0520	0.1051	0.0919	0.0132
	244	6/1/2002	7	0.0440	0.0395	0.1131	0.0999	0.0133
	260	6/17/2002	7	0.0475	0.0380	0.1321	0.1187	0.0133
292	7/19/2002	7	0.0240	0.0260	0.0865	0.0748	0.0117	
308	8/4/2002	7	0.0510	0.0575	0.0970	0.0860	0.0110	

Source: Output DTN: SN0608NDVIANAL.001, *atm\_cor.xls*.

NOTE: The value for standard deviation was calculated from all of the potential linear fits as illustrated in Figure E-11 as a maximal representation of the potential error associated with the linear fit method.

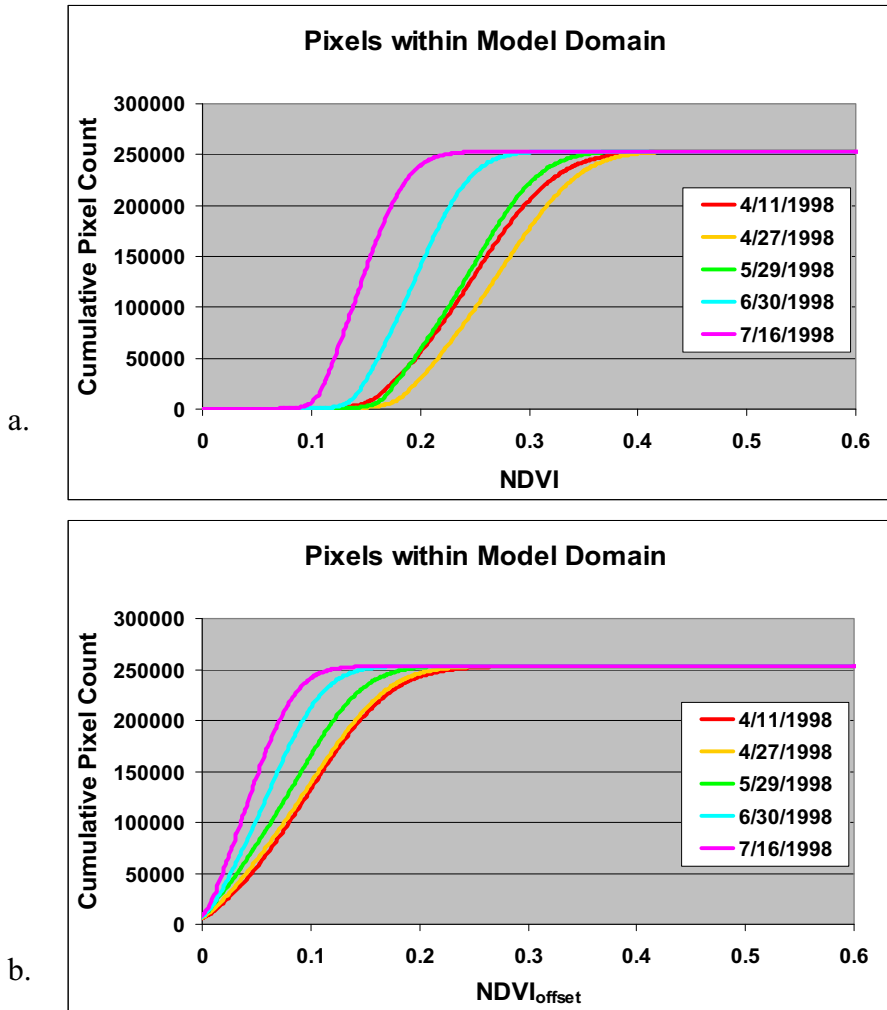
The values in Table E-2 were then used to calculate  $NDVI_{offset}$  according to Equation E-6.

$$NDVI_{offset} = [(B_4 - DOS_4) - (B_3 - DOS_3)] / [(B_4 - DOS_4) + (B_3 - DOS_3)] - NDVI_0 \quad (\text{Eq. E-6})$$

where subscripts 3 and 4 refer to the two bands.

$NDVI_0$  is the fitted intercept value as illustrated in Figure E-11.

Figure E-12 illustrates how calculation of  $NDVI_{offset}$  in Equation 6 corrects for nonsystematic variation in NDVI using five of the images from WY1998. By subtracting the intercept value, representing  $NDVI_0$ , this starts all of the curves at the same place and enables accurate comparison as was shown by Baugh and Groeneveld 2006 [DIRS 178678]



Source: Output DTN: SN0608NDVIANAL.001.

NOTE: The progression in plant phenology for this region had a peak in early April that declines through the growing season to midJuly. This progression is less apparent without removal of the nonsystematic scatter by subtraction of  $NDVI_0$ .  $NDVI_{offset}$  was calculated using the  $NDVI_0$  in Table E-2.

Figure E-12. CDFs for the Pixels of Five Images that Follow the Progression of the Growing Season within the Rectangular Area of the Model Domain Representing (a) as NDVI and (b) as  $NDVI_{offset}$

There are a couple of important factors to note relative to Figure E-12. First, for the five images chosen, the progression of plant phenology declines from the overall average peak expression on the first image, April 11, 1998, to lowest  $NDVI_{offset}$  expression during midsummer, July 16, 1998. Were the data not subjected to the calculation to derive  $NDVI_{offset}$ , the results would be not be in the correct order—a peak that declines to a minimum. In addition, these pixel data are extracted from the rectangular area of the model domain that contain large areas of lowlands where plant phenology is apparently accelerated over plant growth timing on the rocky uplands (hence, not equivalent to analyses for pixel extractions occurring later in this report).

A feature of  $NDVI_{offset}$  is that its magnitude is far less than  $NDVI$  due to the subtraction of  $NDVI_0$  and, thus, is not directly comparable to raw  $NDVI$  values. Though the range of  $NDVI_{offset}$  is changed by this calculation and the values decreased, this does not pose a problem because  $NDVI_{offset}$  is a dimensionless index that can be calibrated to other data, and this then enables spatial mapping.

### Uncertainty for NDVI<sub>offset</sub>

Table E-Uncertainty-5 shows sample calculations of NDVI<sub>offset</sub> for pixels measured on 4/11/98 within the model domain. For that day's image, NDVI<sub>0</sub> is 0.15 (Table E-2). The values of NDVI<sub>offset</sub> range from about -0.3 to about 0.4, though only about 2% of the pixels have negative values. These negative values correspond to graded roads, graded parking areas, and areas in deep shadow. For this image on 4/11/98, at about 10 a.m. local time, the sun is east and south of the zenith with an elevation of 52° (from the header file accompanying this image). The deep shadow is on steep northern and western slopes of the mountain. Negative values are set to zero before further processing. Table E-Uncertainty-5 also shows the propagation of estimated uncertainties. Through the calculation of NDVI, the uncertainty analysis is the same as that in Table E-Uncertainty-4. The dominant sources of uncertainty in both NDVI and NDVI<sub>0</sub> are the uncertainties in the two Bias values, with effects in the same direction. Therefore, the relative uncertainty in NDVI<sub>offset</sub> is approximately the relative uncertainty in NDVI but not less than the random uncertainty. The random uncertainty is dominated by the random uncertainty of 0.01 NDVI<sub>offset</sub>. The standard uncertainties for positive values of NDVI<sub>offset</sub> range from 0.01 to 0.03, being approximately 0.01 + 6% NDVI<sub>offset</sub>.

Table E-Uncertainty-5. Example NDVI<sub>offset</sub> Calculations within Model Domain on 4/11/98

Pixel ID	$\rho_4^a$	$\rho_3^b$	$\rho_4\text{-DOS}_4^c$	$\rho_3\text{-DOS}_3^c$	NDVI Numerator <sup>d</sup>	NDVI Denominator <sup>d</sup>	NDVI <sup>e</sup>	NDVI <sub>offset</sub> <sup>f</sup>
10,901	0.065 ±0.003	0.064 ±0.003	0.033 ±0.003	0.030 ±0.003	0.003 ±0.004	0.063 ±0.004	0.05 ±0.06	-0.10 ±0.12
253,574	0.259 ±0.011	0.201 ±0.008	0.227 ±0.011	0.167 ±0.008	0.060 ±0.014	0.394 ±0.014	0.15 ±0.04	0.00 ±0.01
116	0.202 ±0.008	0.152 ±0.006	0.170 ±0.008	0.118 ±0.006	0.052 ±0.010	0.288 ±0.010	0.18 ±0.03	0.03 ±0.01
136,394	0.225 ±0.009	0.161 ±0.006	0.193 ±0.009	0.127 ±0.006	0.066 ±0.015	0.320 ±0.015	0.21 ±0.05	0.06 ±0.01
212	0.207 ±0.008	0.144 ±0.006	0.175 ±0.008	0.110 ±0.006	0.065 ±0.010	0.285 ±0.010	0.23 ±0.04	0.08 ±0.01
253,447	0.263 ±0.011	0.171 ±0.007	0.231 ±0.011	0.137 ±0.007	0.094 ±0.013	0.368 ±0.013	0.26 ±0.04	0.11 ±0.02
234,601	0.226 ±0.009	0.150 ±0.006	0.194 ±0.009	0.116 ±0.006	0.078 ±0.011	0.310 ±0.011	0.25 ±0.04	0.10 ±0.02
147,056	0.199 ±0.008	0.124 ±0.005	0.167 ±0.008	0.090 ±0.005	0.077 ±0.009	0.257 ±0.009	0.30 ±0.04	0.15 ±0.02
147,067	0.234 ±0.009	0.131 ±0.005	0.202 ±0.009	0.097 ±0.005	0.105 ±0.010	0.299 ±0.010	0.35 ±0.03	0.20 ±0.02
136,365	0.299 ±0.012	0.147 ±0.006	0.267 ±0.012	0.113 ±0.006	0.154 ±0.013	0.380 ±0.013	0.41 ±0.03	0.26 ±0.02
42,795	0.204 ±0.008	0.098 ±0.004	0.172 ±0.008	0.064 ±0.004	0.108 ±0.009	0.236 ±0.009	0.46 ±0.04	0.31 ±0.03
24,753	0.196 ±0.008	0.082 ±0.003	0.164 ±0.008	0.048 ±0.003	0.116 ±0.009	0.212 ±0.009	0.55 ±0.04	0.40 ±0.03

<sup>a</sup> Source: Output DTN: SN0609LSTMPROC.001, 041198\_band4.txt. Standard uncertainty estimated to be 4%.

<sup>b</sup> Source: Output DTN: SN0609LSTMPROC.001, 041198\_band3.txt. Standard uncertainty estimated to be 4%.

<sup>c</sup> DOS<sub>3</sub> and DOS<sub>4</sub> are 0.034 and 0.032, respectively, with negligible uncertainty (Section E2.2).

<sup>d</sup> See Equation E-1. Standard uncertainty of sum or difference is root mean square of component uncertainties.

<sup>e</sup> Standard uncertainty of quotient is uncertainty in the numerator divided by the value of denominator, which neglects uncertainty in the denominator.

<sup>f</sup> The relative uncertainty in NDVI<sub>offset</sub> estimated to be the same as relative uncertainty in NDVI, but not less than 0.01.

### Uncertainty for NDVI<sub>offset</sub> (Continued)

The uncertainty associated with calculation of NDVI<sub>offset</sub> is considered to be the major source of uncertainty in the calculations and is equivalent to  $0.01 + 6\%$ . This estimate was made considering the sources of error within the calculations but does not acknowledge that uncertainty may be somewhat self correcting due the combinations of numbers that may be high combined with those that may be low, thus tending to force uncertainty to a more moderate value. This can be seen within the discussion of uncertainty contained in Section E7.4. The development of temporal (daily time step curves of expected NDVI' (developed from NDVI<sub>offset</sub> in Section E2.5 and E3) and spatial parameters PVR (potential vegetation response, Section E3) from NDVI<sub>offset</sub> are inputs for the MASSIF model and so, fall under modeling uncertainty. Uncertainty for these parameters is not estimated in this appendix.

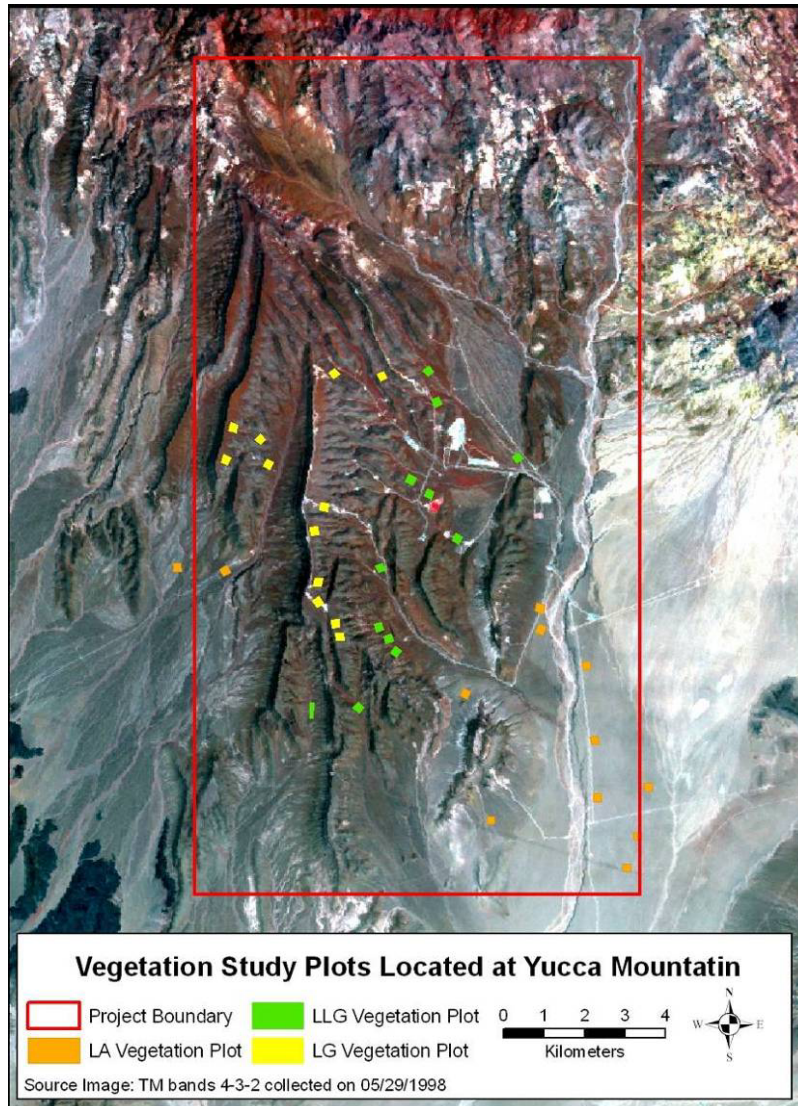
## E2.5 VERIFICATION OF PROCESSING PARAMETERS AND DEVELOPMENT OF NDVI'

The processing parameters for NDVI<sub>offset</sub> developed for the vegetation cover within the lowlands region shown on Figure E-9, were intended for application to all Yucca Mountain vegetation. Additional testing was performed to verify that the DOS parameters for NDVI measured over the “lowlands” region are appropriate for other vegetation cover closer to the repository footprint. This was accomplished using data from established ecological study plots.

There are 48 Ecological Study Plots (ESPs) for four vegetation associations established in and around Yucca Mountain where the vegetation growth was monitored during the late 1980s and early 1990s (CWRMS 1996 [DIRS 102235]). These plots, described at greater length in Appendix D, were established during 1988. Data for analyses using the vegetation plot data are listed within Output DTN: MO0606SPAVEGAS.001.

The three predominant Yucca Mountain vegetation associations were used for verification of the appropriateness of the processing parameters. Each of these vegetation associations contained 12 individual plots. These are shown on Figure E-13. For one of the associations, LA, 2½ plots lay outside of the infiltration model boundary and were excluded from consideration. As described in Appendix D, the names of the vegetation associations have changed since the plots were defined. The original naming convention will be used for these plots: LA for *Larrea–Ambrosia*, LLG for *Larrea–Lycium–Grayia*, and LG for *Lycium–Grayia*. The vegetation contained in the LG plots is most closely related to the vegetation of the rocky uplands that overly the repository and, thus, was of greater interest for verification and for later fitting of the simulation algorithm.





Source: Output DTN: SN0608NDVIANAL.001.

NOTE: The Yucca Mountain infiltration model boundary is shown in red (rectangle). Plots marked LG are most similar to the vegetation of the rocky uplands overlying the proposed repository. This figure was excerpted from *ESP\_NDVI\_simET-K3.xls*.

Figure E-13. Location of Ecological Study Plots Used to Verify Atmospheric Correction and Simulations of Vegetation Response

NDVI<sub>offset</sub> values were calculated for the different vegetation associations using the NDVI<sub>0</sub> parameters in Table E-2. Model grid cell values of NDVI<sub>offset</sub> were extracted from each of the ESPs and then lumped by each vegetation association into single statistical populations. These data are contained in the workbook *ESP\_NDVI\_simET-K.xls* (Output DTN: SN0608NDVIANAL.001). A description of the data extracted from the ESPs is contained in Table E-3.

Table E-3. Ecological Study Plots with Original Naming Convention and Measurements of the Total Pooled Area Evaluated for Verification

Original Name	Plots	30-m Grid Cells Extracted	Area in km <sup>2</sup>	Avg. Area/Plot (m <sup>2</sup> )
LA	9.5	445	0.401	42,200
LG	12	516	0.464	38,700
LLG	12	552	0.497	41,400

Source: Output DTN: SN0608NDVIANAL.001, *ESP\_NDVI'\_simET-K.xls*.

NOTE: If expressed as a square, on average, each ESP was approximately 200 m on a side.

Reasonable comparison of the curves formed by the calculated average NDVI<sub>offset</sub> values to the antecedent precipitation during each water year was taken to be confirmation that the processing parameters in Table E-2 were correct. The expected vegetation cycle, either remaining flat during the year with negligible precipitation (WY2002) or rising and falling through the growing season in the two years with average and significant precipitation (WY1998 and WY2001), were used to cross-check the NDVI<sub>offset</sub> curves. In all nine cases (3 vegetation associations \* 3 years), the processing parameters yielded curves that were reasonable. The individual values of NDVI<sub>offset</sub>, comprised of averages for the entire multiplot association, were well behaved and did not deviate greatly from the expected curve shapes, given the precipitation measured on Yucca Mountain. Because the same values of Gain were used for all pixels, averaging does not reduce the uncertainty.

Figure E-14 presents the results for the lumped LG plot data compared to the precipitation data for WY2002. Due to the intensity of the dryness and the lack of an effective precipitation event (events were less than 10 mm of rain, spaced widely apart in time), this year was expected to have near-zero vegetation response. For the NDVI<sub>offset</sub> calculated for these data, however, this is clearly not the case. Some other factor besides vegetation growth and canopy expression appears to be causing a background NDVI<sub>offset</sub> signal, and this signal significantly elevates the vegetation response curve well above the expected zero baseline. NDVI<sub>offset</sub> values above the baseline can be attributed to vegetation response to the precipitation (Figure E-15). This permanent nonvegetation factor causing upward zero-baseline displacement was identified as desert varnish that covers all undisturbed (in situ) exposed rock surfaces on Yucca Mountain. This effect, explained in Section E2.6, was known from the literature; however, the high magnitude of this response in comparison to the vegetation signal was unexpected.

To correct for the effect of the nonzero baseline, the lowest levels of expected vegetation cover measured on July 19 and August 4, 2002 (driest period during the driest year), were averaged and subtracted from all NDVI<sub>offset</sub> values through all years. This new NDVI parameter was given the designation NDVI'.

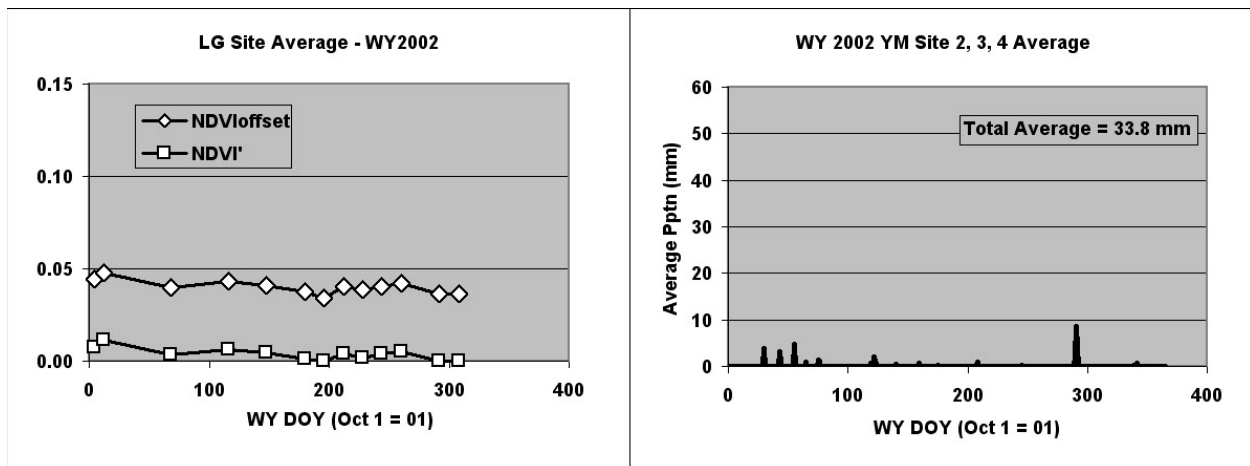
Values of NDVI' are also plotted on Figures E-14 and E-15 for WY2002 and WY1998. Since the promotional effect from desert varnish is not constant spatially, values of NDVI<sub>offset</sub> for a given area, for example the pooled ESP averages, must subtract the zero baseline developed for the same ground area (i.e., collections of pixels). Correcting for the permanent and highly variable concentration of desert varnish contained within each model grid cell (Section E2.6) is solved with the development of PVR (Section E4).

### Uncertainty for NDVI'

The values of Gain for three WY2001 dates, March 26, June 30, and August 17, were the same as those for WY 2002. After averaging over the pixels associated with a vegetation plot, the uncertainty in NDVI' is dominated by the uncertainty in Gain. As with the calculation of NDVI<sub>offset</sub> in Section E2.4, the effect is to make the standard uncertainty in NDVI' be approximately 6% of NDVI' for those three dates.

We consider here that the values for the lowest levels of expected vegetation are so low that the uncertainty is also relatively low. Its effect on NDVI' is negligible when compared to the effect of the uncertainty of NDVI<sub>offset</sub> for the selected period; thus, it can be ignored.

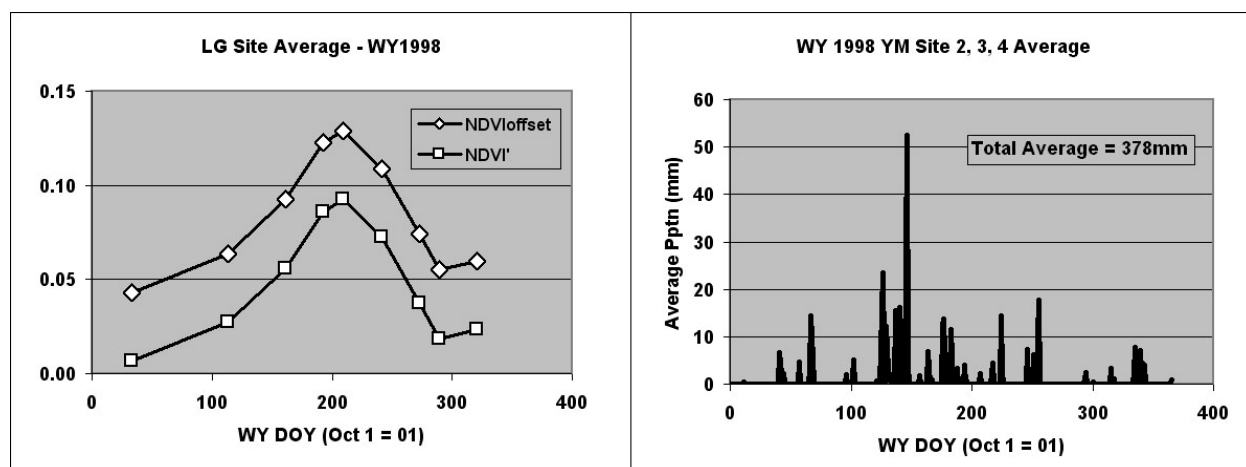
Because the values of Gain used for WY1998 and most of WY 2001 were different from the values used for WY 2002, the standard uncertainty in NDVI' for those dates is the root-mean-square of the two uncertainties. Because the values for WY 2002 are small, the standard uncertainty in NDVI' for those dates is approximately 0.01 + 6% NDVI'.



Source: Output DTN: SN0608NDVIANAL.001 (including average precipitation) *ESP\_NDVI'\_simET-K.xls*, worksheet "2. precip\_table."

NOTE: From this very dry year, a zero NDVI vegetation response is expected during summer. Values of NDVI<sub>offset</sub> were apparently promoted by about 0.04 NDVI<sub>offset</sub> that is represented by the last two values of WY2002 (about WYDOY 300). This interval was subtracted to yield NDVI'.

Figure E-14. NDVI<sub>offset</sub> and NDVI' for Lumped Samples for WY2002 LG Plots



Source: Output DTN: SN0608NDVIANAL.001, *ESP\_NDVI\_simET-K.xls*, worksheet "2. precip\_table."

NOTE: NDVI<sub>offset</sub> is promoted by a nonvegetation related factor that was determined from the data in Figure E-14. The same zero baseline subtracted for Figure E-14 was subtracted from these data to yield NDVI'.

Figure E-15. Plot of NDVI<sub>offset</sub> and NDVI' for Lumped Samples from LG Plots for WY1998

Again, these analyses and their results, represented by Figures E-14 and E-15, were used as a guide to subsequent analyses because they developed an understanding of Yucca Mountain vegetation responses and verified that the processing parameters for DOS and for NDVI<sub>0</sub> produced reasonable results. These analyses were not used as input to the algorithm to simulate Yucca Mountain vegetation.

## E2.6 NDVI SIGNAL FROM DESERT VARNISH

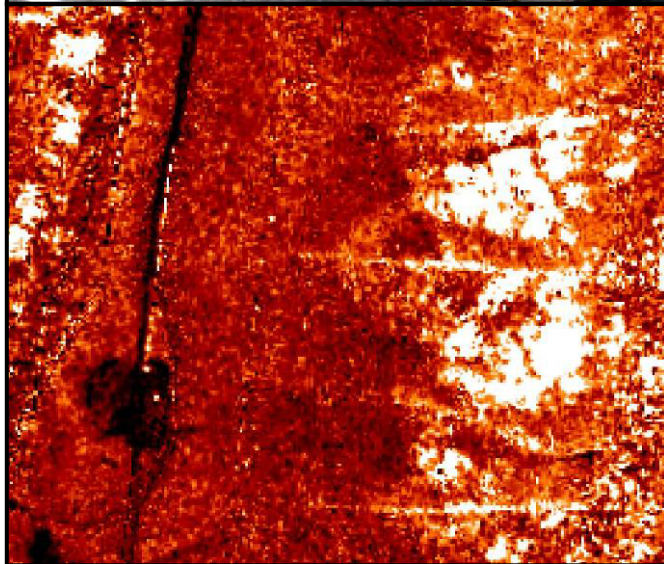
A Quickbird image (private sector satellite data collected by Digital Globe, Inc.) from August 30, 2002 (DTN: SN0601QBSAT802.001 [DIRS 177241]), was examined to confirm the source of the nonvegetation NDVI<sub>offset</sub> signal determined in Section E2.5. This multispectral image has high spatial resolution (2.4 m) pixels that were processed using ENVI Software to yield NDVI values. From observation of these data, it was concluded that the natural rock surfaces, devoid of vegetation and covered by desert varnish, produced the nonzero NDVI signal that was absent on nonvarnished rock surfaces such as the surfaces exposed for drill pads (Figure E-16). The NDVI signal from desert varnish has been identified by other researchers; however, the magnitude of the NDVI signal depends on the specific properties of the desert varnish and the rock (Spatz and Taranik 1989 [DIRS 176751]; Rivard et al. 1992 [DIRS 176758]; Rivard et al. 1993 [DIRS 176741]; and Kenea 2001 [DIRS 176760]). As can be seen in Figure E-16, the NDVI signal for Yucca Mountain desert varnish is of the same magnitude as the strength of the vegetation signal.

The desert varnish NDVI signal was removed in Section E2.5 by subtraction. For this calculation, the average NDVI<sub>offset</sub> extracted from the ESPs from the last two images in WY2002 (July 19 and August 4) were taken to represent only the NDVI from nonvegetation sources (desert varnish), since this was during a very dry year at a time when vegetation response would be expected to be near zero. This calculation was performed for the average NDVI<sub>offset</sub> values of each of the three vegetation associations for the verification step. This calculation used a mean

NDVI<sub>offset</sub> value calculated for the two approximated zero vegetation dates (July 19 and August 4, 2002) and was subtracted from all NDVI<sub>offset</sub> pixels of all images yielding a new adjusted index referred to as NDVI'. Because NDVI' has had all nonvegetation sources of NDVI removed, it represents only the NDVI response from vegetation expression.



a. False color view of a portion of the crest and eastern slopes of Yucca Mountain. Exposed rocks covered with desert varnish are visible on ridges to the right side of the view (dark brown). A roadway and drill pad, which were cut along the crest exposing fresh rock surfaces without desert varnish covering, are seen on the left side of the view (whitish).



b. The same scene displaying a colorized version of NDVI, where bright is high NDVI and black is zero response. The exposed rock areas with desert varnish (identified above) are the brightest portions of the image. In comparison, the freshly exposed rock along the crest has no NDVI response (black).

NOTE: The expected vegetation expression in this scene is near zero for all but scattered evergreen shrubs. These images were generated from data of Output DTN: SN0608NDVIQBIM.001.

Figure E-16. Quickbird Data from August 30, 2002, Following the Dry Summer during the Driest Year on Record for Yucca Mountain

The calculation of NDVI' does contain some bias because a small proportion of the canopy at the site is evergreen vegetation that would provide an NDVI signal even in a critically dry year. However, even the canopies of evergreen species can be expected to be at their lowest representation in late summer of a dry year, as is described in Section E4.

Identification of the NDVI signal in desert varnish and completion of the calculation methodology with NDVI' completed the first phase of the analyses—to determine how to process the data to isolate the vegetation signal. The next phase sought to develop an algorithm for simulating vegetation based upon its position on Yucca Mountain and its spatially discrete potential for growth response (measured as the difference between response to antecedent precipitation between wet, WY1998, and dry, WY2002, conditions).

### **E3. CHARACTERIZATION OF NDVI' ACCORDING TO SLOPE AND AZIMUTH**

NDVI' was predicted by an algorithm for any specified location, day of year, and history of total annual precipitation. Location is thought to affect vegetation in several ways. Slope and azimuth combinations will result in different amounts of sunlight reaching the ground at different times of the year and thus influence the magnitude and/or timing of the vegetation signal at that location. For example, in the northern hemisphere, north-facing slopes will tend to receive less solar radiation than south-facing slopes, and the ratio of the energy for evaporating water that is received by these two azimuths will change as a function of the time of year. This is a set influence that will affect vegetation growth no matter what condition of soils exist at the location.

In addition to effect of slope and azimuth, different locations will have specific properties that influence vegetation growth at that location. Areas with little to no soil present will not be able to support plant growth while areas of deep, well drained soils can.

The naming convention for slopes used in these analyses is N and S for north and south, which are equivalent to N- and S-facing slopes.

Previous analyses were accomplished sequentially to (1) determine the processing parameters for the TM imagery, DOS values, and NDVI<sub>0</sub>; (2) use the ESP data to verify the processing parameters and evaluate the generally curve shapes in response to seasonal timing and precipitation; and (3) to verify the effect of desert varnish on NDVI<sub>offset</sub> and develop a means to remove this effect (by calculating NDVI'). These three steps were accomplished with areas of homogeneous vegetation located on relatively low relief terrain, including the lowlands polygons (Figure E-9) and ESPs (Figure E-13).

In order to characterize the response of NDVI' on the complex topography overlying the proposed repository, data were extracted and processed on steep slopes to N and S azimuths. The results from this analysis were interpolated for the combinations of slope and azimuth that occur on Yucca Mountain.

#### **E3.1 EFFECT OF SLOPE AND AZIMUTH**

Creation of a simulation for vegetation growth represented by NDVI' (a surrogate for vegetation water use) required the vegetation response at Yucca Mountain be examined to determine its sensitivity to the orientation of the land surface. NDVI<sub>offset</sub> values were calculated for the model domain for extraction of data from grid cells on N versus S slopes (Output DTN: SN0608NSSLOPES.001). The suite of model grid cells that was sampled for this analysis is shown on Figure E-17. A total of 0.246 km<sup>2</sup> (273 model grid cells) were chosen from the model domain to represent north-facing slopes, and 0.364 km<sup>2</sup> (405 grid cells) were chosen

to represent south-facing slopes. The representative areas were chosen from the region of rocky uplands overlying the proposed repository in order to achieve the greatest accuracy in the most critical location.



Source: Output DTN: SN0608NDVIANAL.001, *ALL\_Years\_N\_S\_18\_24\_slope\_extractions3.xls*. The pixels indicating north- and south-facing slopes are identified in Output DTN: SN0608NSSLOPES.001.

Figure E-17. Model Grid Cells Sampled: S (orange); N (blue)

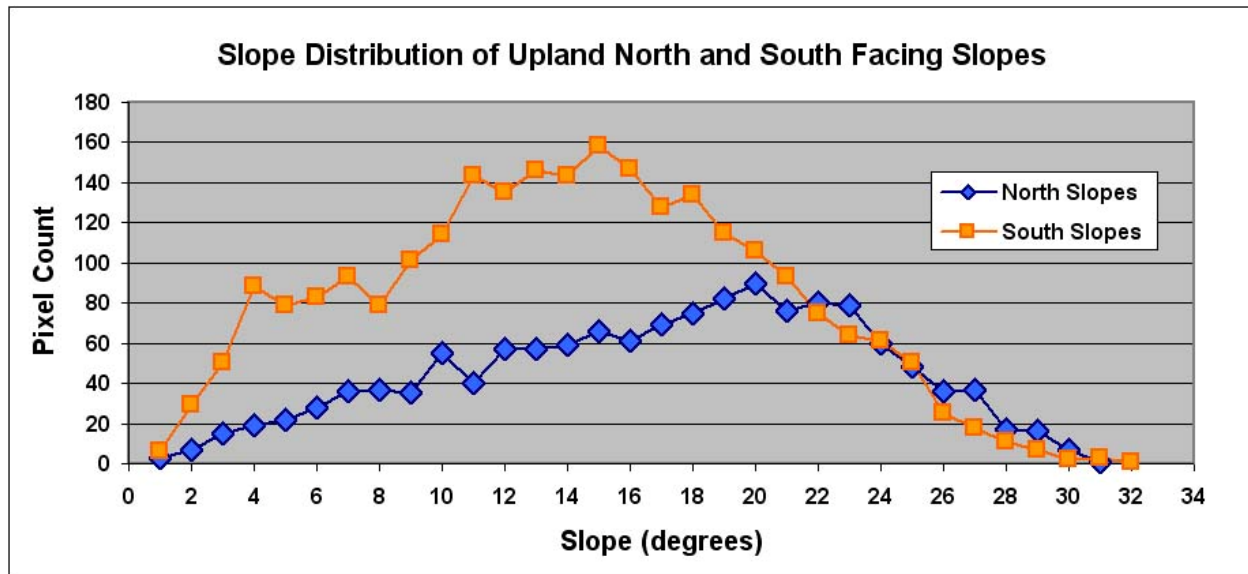
Figure E-18 represents the statistical distribution of model grid cells by slope for N and S slopes ( $30^\circ$  arcs to either side) on the Yucca Mountain rocky uplands. N and S slopes of  $18^\circ$  to  $24^\circ$  were selected as a lumped sample for extraction of  $NDVI_{offset}$  values to provide a population sufficient for characterizing the differences in temporal vegetation response. These slopes were selected because:

This slope range captured the peak of the cell distribution for the most limited sample of the two cardinal azimuths, N slopes.

Slopes of this steepness are at about the end of the distribution for normal vegetation growth, allowing any intermediate condition to be interpolated from these end members.

Slopes chosen to be any steeper than  $24^\circ$  would tend to have vegetation that is mostly constrained by rockiness

Note that further discussion concerning N and S slopes refers to the responses seen within the lumped sample for 18° to 24° grid cells that were extracted for analysis.



Source: Output DTN: SN0609AZSLPHST.001, north\_south\_slope\_distribution.

Figure E-18. Statistical Distribution of Landsat TM Pixels on N and S Slopes within a Region Overlying the Proposed Repository

The first step for slope-azimuth characterization was to define the region of interest overlying the proposed repository and to identify the 30-m model grid cells that had N and S alignment to within an arc of 60° (30° either side of cardinal direction). This pool of candidate model grid cell NDVI<sub>offset</sub> was then displayed as a partial transparency over the August 30, 2002, Quickbird image that had been processed to reveal NDVI (Figure E-16b). Multiple contiguous pixels (2.4-m each) of high NDVI response were taken to be exposed rock surfaces covered by desert varnish (Yucca Mountain vegetation is not distributed in this manner) and were eliminated from consideration for slope-azimuth characterization.

Rather than each slope-azimuth class for Yucca Mountain being measured and fitted individually, the relationships for the N- and S-slope endmembers were first characterized. Then, the relationships for intermediate slopes and azimuths were interpolated from these endmembers. A more comprehensive sampling investigation for vegetation response of all combinations of slopes and azimuths was rejected because of four factors: (1) poor statistical representation of some combinations of slope and azimuth (Figure E-18), (2) potential confounding influences due to bidirectional reflectance functions, (3) time and budget considerations, and (4) robustness for fitting all relationships from the two N- and S-slope endmembers.

A simplified conceptual model of vegetation distribution was used for slope and azimuth. Given that all other factors remain consistent, such as soil depth and surface rock expression, the following logical principles were made for characterizing NDVI' response to slope and azimuth:



**Logical Principle 1.** Vegetation of arid Yucca Mountain is usually critically short of water; thus, small differences in water availability are reflected in proportional differences in vegetation cover.

**Logical Principle 2.** Factors that influence vegetation growth are related primarily to the temporal availability of water—and secondarily to season of year. Water availability is governed by precipitation, any redistribution due to runoff/run-on, and the rates of its loss through evapotranspiration.

**Logical Principle 3.** N slopes present less atmospheric driving force and are less conducive to evaporation than S slopes. Thus, N slopes have higher vegetation cover than S slopes because water is available longer for plant uptake and photosynthesis. This relationship was suggested by Stothoff et al. (1999 [DIRS 176705]) who measured higher vegetation cover and leaf area index on the N slopes of Yucca Mountain.

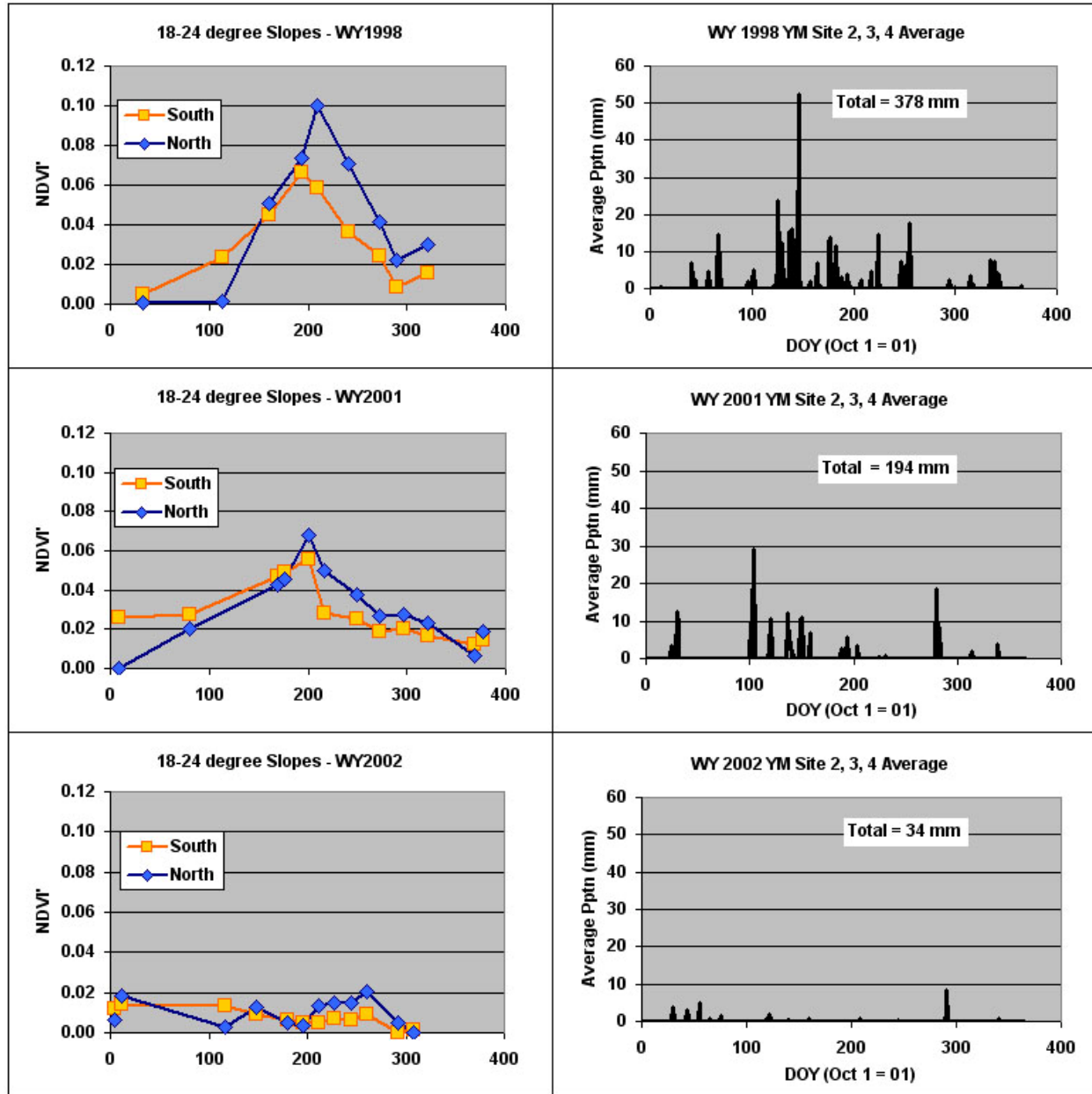
**Logical Principle 4.** Conditions affecting evaporation on east (E) and west (W) slopes represent an approximate average of the conditions that would exist on N and S slopes. Thus, vegetation on E and W slopes will be interpolated as a temporal average of N and S slopes.

**Logical Principle 5.** Vegetation response for flat and gentle slopes ( $<5^\circ$ ) are also averages between N and S slopes (and therefore, in this simple interpolation, equivalent to E and W slopes). Vegetation responses for all intermediate slopes and azimuths can be represented by weighted averaging between the endmember conditions for N and S slopes.

## **E3.2 CHARACTERIZING TEMPORAL VEGETATION RESPONSE**

As mentioned above, the analyses completed prior to this step were made using data derived on low-relief lands away from the rocky highlands overlying the proposed repository. These lands include both the lowland region used for developing processing parameters (Figure E-9) and the ESP sites that were mostly located away from the repository footprint on nearly level ground (Figure E-13). In contrast, this step to characterize NDVI' seasonal responses used data from the rocky region overlying the proposed repository (Figure E-17). Results provided a set of general response curves that capture the variability induced by slope and azimuth for the vegetation directly overlying the proposed repository.

Extractions from the areas depicted in Figure E-17 yielded a suite of pixels for  $NDVI_{offset}$  processed with the parameters developed in Section E2.4 for both N ( $n=273$ ) and S ( $N=405$ ) slopes. These values were placed into the workbook *ALL\_Years\_N\_S\_18\_24\_slope\_extractions.xls* (Output DTN: SN0608NDVIANAL.001). All N and S grid values for the point in time represented by each image were collected together in the workbook *Daily\_NDVI\_Estimation.xls* for further analyses (Output DTN: SN0606T0502206.012). Correction of the average  $NDVI_{offset}$  by subtracting the zero baseline (correcting for desert varnish) was completed as described in Section E2.4. The resulting values, 0.0298 for N slopes and 0.0316 for S slopes, were taken to represent average values for the zero baseline. When subtracted from all values of average  $NDVI_{offset}$  at each time step, this yielded average NDVI' that were graphed against the day of year for each of the three water years (Figure E-19).



Source: Output DTN: SN0606T0502206.012, *Daily\_NDVI\_Estimation.xls*.

NOTE: Points from the beginning of WY2002 (October 4 and 12, 2001) are plotted as the two endpoints for the WY2001 plots.

Figure E-19. NDVI' Calculated for N- and S-Slope Extractions (18° to 24°) for the Three Yucca Mountain Study Water Years, Paired with Average Daily Precipitation from Sites 2, 3, and 4

As previously discussed, calculation of NDVI' is a necessary step to remove the response induced by the content of desert varnish on the rock surfaces. While the response remains stable through time, there is some error introduced in the results due to geospatial uncertainty (the amount of desert varnish associated with individual cells varies naturally). Averaging of the populations of N (n=273) and S (n=405) slope cells was employed to minimize the associated error.

There are five key points about Yucca Mountain vegetation response and its detection that are illustrated in Figure E-19:

N slopes were confirmed to have greater NDVI' response during all growing seasons.

Early season (winter) growth on N slopes lags behind S slopes.

For the two years with sufficient precipitation to fund strong vegetation growth responses (1998 and 2001), the NDVI' peaks occurred at about the same time (approximately WYDOY = 200; April 18). For these same years, a difference in the timing of peak annual expression (WYDOY – 200) was not discernible between N and S slopes.

NDVI' values for the dry year (WY2002) show a slight promotion for N slope over S slope. However, these values are close to their probable zero. When coupled with the lack of effective precipitation, this suggests that the small curve responses for the N slope NDVI' that are visible in Figure E-19 for late WY2002 may be noise from the combined sources of error affecting NDVI' in this environment.

Intermediate levels of precipitation (WY2001) produced an intermediate NDVI' response. Thus, the expected vegetation response to precipitation for the three years falls in the correct order from low to high.

### **E3.3 FITTING NDVI' RESPONSE CURVES TO REPRESENT SLOPE AND AZIMUTH**

The NDVI' for WY1998 N and S slopes were selected for simulating vegetation annual response curves on Yucca Mountain. This year was chosen because it was extremely wet and vegetation canopy expression was at, or near, the potential maximum. This high vegetation response is desirable because it maximizes the signal to noise ratio for NDVI'.

Both N and S slope data for WY1998 (illustrated in the top-left graph of Figure 19) were spline-fitted to the ascending and descending limbs of NDVI'. The simplest mathematical function that provided a reasonable fit was chosen for each leg of the curve: 2nd Order polynomials. Expressed as curves they are:

18 to 24° North Slopes

Ascending Limb:  $NDVI' = 0.000000931x^2 + 0.000681033x - 0.086604350$

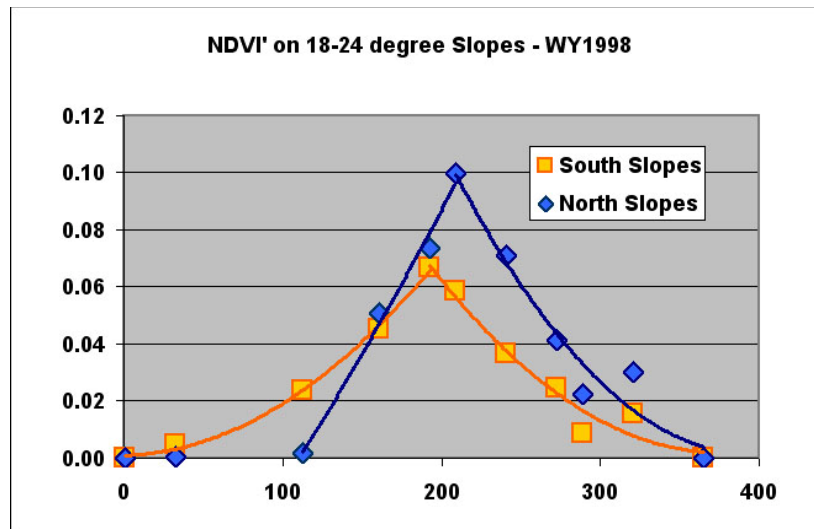
Descending Limb:  $NDVI' = 0.00000287x^2 - 0.00226123x + 0.44628979$

18° to 24° South Slopes

Ascending Limb:  $NDVI' = 0.00000167x^2 + 0.00001369x + 0.00096664$

Descending Limb:  $NDVI' = 0.00000198x^2 - 0.00148230x + 0.27967664$

These relationships were used to estimate NDVI' for both N and S slopes in daily time steps for WY1998 (Figure E-20). Curves to represent all classes of slopes and azimuths were then interpolated between these fitted relationships. These calculations are found in *Daily\_NDVI\_Estimation.xls* (Output DTN: SN0606T0502206.012).

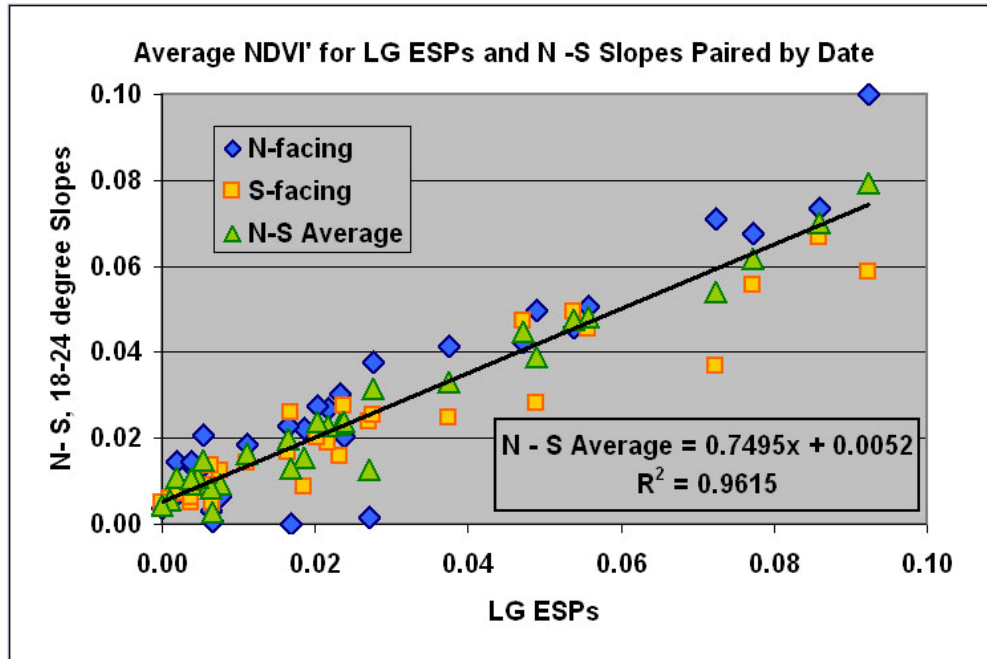


Source: Output DTN: SN0606T0502206.012, *Daily\_NDVI\_Estimation.xls*. The regression line was fitted to the N-S slope average.

Figure E-20. Plot of the Results for Calculation of NDVI' for the Pooled LG Vegetation Plots (x-axis) and for N and S Slopes and their Average

For characterization of vegetation for the class representing the combined flat-E-W slopes, the average per-time-step values of NDVI' for N and S slopes were combined as simple averages following Logical Principle 5, listed in Section E3.1. To test whether interpolating between N and S slopes was a reasonable approach for representation of quasi-level sites, these data were compared to the ESP data from LG sites. LG vegetation (dominated by genera *Lycium* and *Grayia*) predominates in the zone overlying the proposed repository.

Figure E-21 presents data paired by image time-step. The X-axis value is average NDVI' for the lumped pixels from LG ESPs (n=516). Paired with this are Y-axis values of average NDVI' for the steep N (n=273) and S (n=405) slopes and the N-S average (n=273+405). This results in three Y-values, WY1998, WY2001, and WY2002, for the n=31 unique X-axis values.



Source: Output DTN: SN0608NDVIANAL.001, *ESP\_NDVI'\_so, ET-K*; Output DTN: SN0606T0502206.012, *Daily\_NDVI'\_Estimation*. The regression line was fitted to the N-S slope average. This average represents a tighter data cloud than, and is intermediate to, N or S slopes.

Figure E-21. Plot of NDVI' for N and S Slopes and their Average for all Images Years Versus Average NDVI' Extracted for LG Vegetation Plots (x-axis)

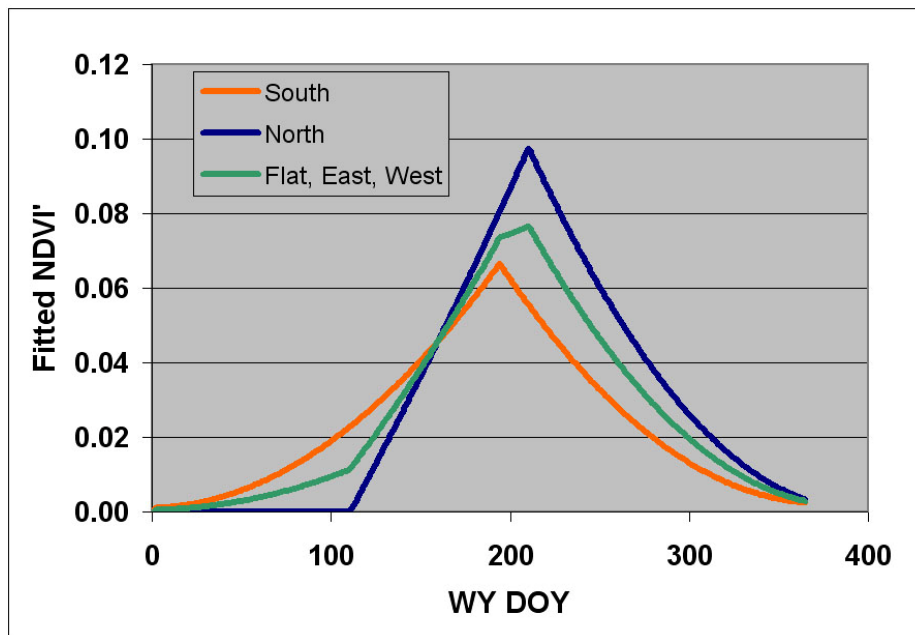
In Figure E-21, the N-S average is an intermediate condition between N and S endmembers. The slopes/azimuth for LG sites have low relief (i.e., nearly level) compared to the samples extracted for N and S slopes. As would be expected, there is a great deal more scatter for the N and S slope data than for their average. The S-slope data generally plots toward the lower side of the data cloud while N slopes plot above, again illustrating the predicted trend toward higher vegetation response on N slopes (Logical Principle 3, above).

A line fitted for the N-S average has a slope less than unity (about 0.76), indicating that the comparative strength of the upland vegetation response is lower than for the relatively flat sites that were chosen for LG ESPs. This reduction in vegetation for steep slopes of the rocky uplands may logically indicate that a proportion of precipitation is lost to runoff because soils are shallower and have limited water holding capacity compared to the gentle slopes of the LG ESPs. The shallow soils of the rocky uplands of Yucca Mountain limit the potential storage of incident precipitation (Stothoff et al. 1999 [DIRS 176705]).

Although the analysis in Figure E-21 shows that the LG sites and N-S slope average are not equivalent, they do have a strong linear relationship (Figure E-21). This confirms that the shape of the N-S average curve functions well as a predictor of the annual response for shallow slopes such as those presented by the LG vegetation plots (mostly  $<5^\circ$ ). However, and appropriately, the N-S slope NDVI' average is not equivalent (with a one-to-one relationship, nor would it be expected to be) to the NDVI' measured for the LG sites. The vegetation expression on Yucca Mountain is highly variable. Such spatial variability is addressed using a spatially correct scalar,

PVR, which was calculated for each model grid cell to adjust for the measured strength of the NDVI' response as the difference between wet and dry years (Section E4).

The daily time-step average of N- and S-slope curves that were used to represent environments that are nearly flat ( $<5^\circ$ ), and also for E and W slopes, are shown in Figure E-22. Table E-4 provides the calculation algorithms chosen for interpolating 13 unique slope-azimuth classes from the N-S slope results. E and W present roughly equivalent conditions. Thus, as an example, SW is equivalent to SE, NW to NE, and so forth. Figure E-23 presents the suite of curves to represent annual temporal NDVI' response for slope-azimuth combinations calculated with the algorithm in Table E-4 found in workbook *Daily\_NDVI\_Estimation.xls* (Output DTN: SN0606T0502206.012).



Source: Output DTN: SN0606T0502206.012, *Daily\_NDVI\_Estimation.xls*. By weighted averaging, these curves were adapted for various slope and azimuth combinations. The curve for flat, east, and west slopes is the temporal average of north and south and is calculated in file *Daily\_NDVI\_Estimation.xls*.

Figure E-22. Three Temporal Curves for NDVI' on Yucca Mountain

Table E-4. Algorithm for Calculating Slope- and Azimuth-weighted Temporal Average NDVI' Using Relationships Fitted for N- and S-facing Slopes (&gt;18°) and Their Temporal Average (A)

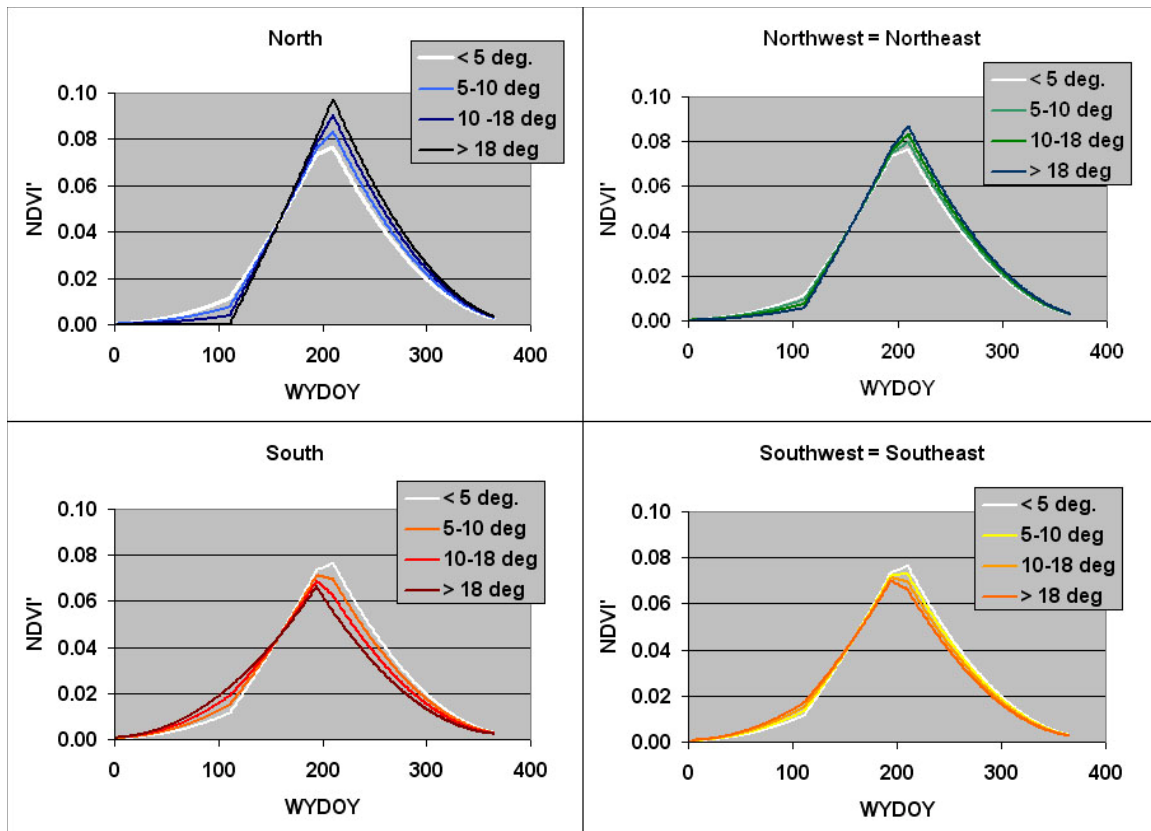
Cardinal Direction	Azimuth Start	Azimuth End	Azimuth Center	>18 deg	11-18 deg	5 - 10 deg	<5 deg
<b>N</b>	337.5	22.5	360	<b>N</b>	$(2N+A)/3$	<b>B</b> $(N+2A)/3$	<b>C</b> <b>A</b>
<b>NE</b>	22.5	67.5	45	$(N+A)/2$	$(A+B)/2$	$(A+C)/2$	<b>A</b>
<b>E</b>	67.5	112.5	90	<b>A</b>	<b>A</b>	<b>A</b>	<b>A</b>
<b>SE</b>	112.5	157.5	135	$(S+A)/2$	$(A+D)/2$	$(A+E)/2$	<b>A</b>
<b>S</b>	157.5	202.5	180	<b>S</b>	$(2S+A)/3$	<b>D</b> $(S+2A)/3$	<b>E</b> <b>A</b>
<b>SW</b>	202.5	247.5	225	$(S+A)/2$	$(A+D)/2$	$(A+E)/2$	<b>A</b>
<b>W</b>	247.5	292.5	270	<b>A</b>	<b>A</b>	<b>A</b>	<b>A</b>
<b>NW</b>	292.5	337.5	315	$(N+A)/2$	$(A+B)/2$	$(A+C)/2$	<b>A</b>

Source: Output DTN: SN0606T0502206.012, *Daily\_NDVI\_Estimation.xls*.

NOTE: Formulae for weighted averaging are defined as units B to E and are abbreviated for application to other cells.

The scheme for interpolating daily time steps of NDVI' in Table E-4 uses combinations of three relationships. These are the relationships for N, S (for slopes >18°), and E–W-flat slopes (given the abbreviation A, in Table 5). The interpolation for all intermediate slopes and azimuths combines various portions of these three curves for each daily time step (365). As an example for averaging the effect of slope for N aspects, the two endmembers across, N and A, are interpolated by weighted averaging;  $(2N+A)/3$  and  $(N+2A)/3$ . For brevity, these formulae were given the abbreviation B and C and thus formed endmembers for interpolation between N and NE and N and NW. In this simplified scheme, E and W were set to be equivalent (because they should receive about the same insolation) and so NW = NE and SW = SE.

As shown in Table E-4, the wide range of potential slopes and azimuths is characterized into four slope classes, >18°, 11° to 18°, 5° to 10°, and <5°, and by azimuths to the eight cardinal directions. The >18° class is represented by the curve shown in Figure E-20. The “flat” designation, <5°, was not classified as to azimuth. This system potentially gives rise to 25 separate classes; however, since the algorithm was simplified by choosing E = W, only 13 unique classes were created: [(4 azimuths × 3 slope classes) + 1 shallow-slope class at all azimuths].



Source: Output DTN: SN0606T0502206.012, *Daily\_NDVI\_Estimation.xls*.

NOTE: There are 13 unique combinations of curves. The curve representing level ground (<5°) and E and W slopes is reproduced (as the white curve) in each graph.

Figure E-23. Temporal Curves Developed by the Weighting Functions in Table E-4

#### E4. POTENTIAL VEGETATION RESPONSE – SCALAR VALUES FOR EACH MODEL GRID CELL

Up to this point, all calculations were largely independent of location. Section E2 determined how to process the satellite data, and Section E3 derived the shape of the annual response of NDVI' for all slopes and azimuths. Rather than being tied to any single model grid cell, these calculations employed averages of pooled sampled groups in order to determine overall trends. This final step, calculation of potential vegetation response (PVR), provided values for each model grid cell that are scaled to the strength of the actual vegetation response within that cell. The calculation of the PVR values for each grid cell is done in Output DTN: SN0608PVRATYMT.001.



As described in Section E2.6, there are highly variable amounts of desert varnish-covered rock that can occur within each cell. This potentially confounding problem was solved in the parameter-verification step in Section E2.5 and in the NDVI' curve-fitting of Section E3 by subtracting out the background values enhanced by the effects of desert varnish. These background values were taken as the recorded values during a critically dry year (WY2000). PVR is calculated as shown in Equation E-7:

$$PVR_i = \frac{(NDVI'_i)_{\max} - (NDVI'_i)_{\min}}{NDVI'_{\max-\min}} \quad (\text{Eq. E-7})$$

where  $(NDVI'_i)_{\max}$  and  $(NDVI'_i)_{\min}$  are the  $NDVI'$  values for pixel  $i$  with the maximum and minimum expected vegetation responses, respectively.  $NDVI'_{\max-\min}$  is the average difference between  $NDVI'$  values listed above for all pixels within the region of interest.

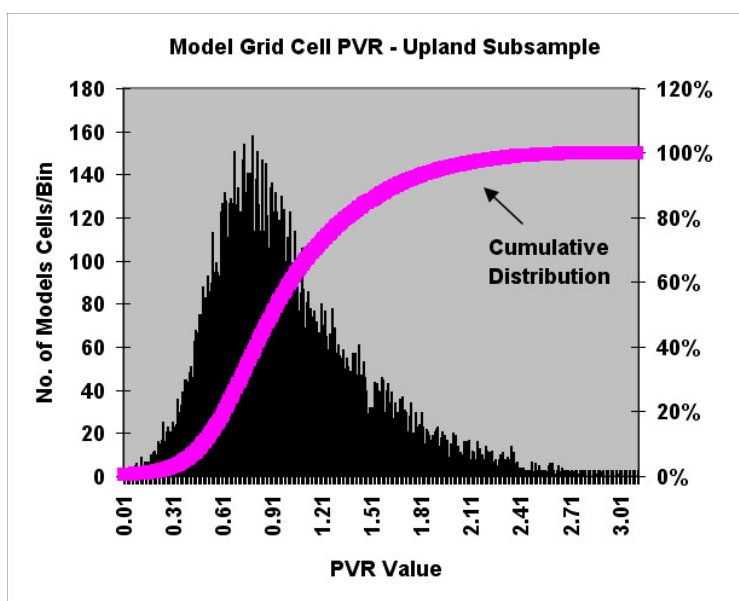
The denominator of PVR, the average value of grid cells within the area of interest, normalized the results for a subset area overlying the proposed repository. This area was chosen as a rectangle of 12,702 grid cells (11.43 km<sup>2</sup>). Normalization provided scaling to permit better understanding PVR distribution: a PVR of 1.0 represents the approximate average vegetation response overlying the repository (i.e., the denominator in Equation 7). It is important to note that PVR was normalized specifically for the region overlying the repository to permit additional analyses where the vegetation responses are of greater interest. In general, however, large areas of deeper soil may push the actual average for these repository-normalized PVR to a higher level within the entire MASSIF model domain. Mathematically, this is inconsequential because those areas do have higher responses, they are mathematically ordinal, and because the crop coefficients developed in Appendix D will be calibrated to the simulated NDVI'.

As a consideration for accuracy in the calculation of PVR (Equation E-7), the farther apart the conditions represented by the max and min precipitation years (i.e., very dry and very wet), the better resolution they provide for estimation of the potential for vegetation growth. For Yucca Mountain vegetation, the two years chosen for the characterization, WY1998 and WY2002, represent extremely wet and dry conditions (Figure E-3). For the dry conditions of WY2002, the average precipitation received for Sites 2, 3, and 4 was about 34 mm. Most of this precipitation was likely lost through evaporation as only small amounts of water were deposited during each precipitation period. Conditions were profoundly dry, and the expected vegetation expression was at, or near, the lowest level that can be attained in this system.

Rather than using the late summer zero baseline as the previous analyses had done for calculation of NDVI', calculation of PVR used NDVI' from periods of expected peak annual growth for both wet and dry years. For WY1998, the dates selected were March 10, April 11, and April 27. For WY2002, the dates selected were March 29, April 14, and April 30. Equivalent time periods were chosen to avoid any possible influence from solar angle. Data for the three before and after dates were averaged for each 30-m model grid cell in the model domain. The method for calculation of  $NDVI'_{\text{offset}}$  (subtracting  $NDVI_0$ ) can create slightly negative values for the lowermost, asymptotic portions of the NDVI curves. To avoid compounding errors in calculation, negative values were converted to zero (functionally correct, since vegetation cover and expression are never less than zero). Negative values occurred in

only 49 of the total grid cells (0.0039 of the rectangular sampled area). Within the rectangular subset area of 12,702 grid cells overlying the proposed repository, none of the values were negative.

The rectangular area overlying the repository was used for calculation of an appropriate average value for normalizing PVR. This normalized value was used to then investigate the statistical distribution of PVR values (*PVR-Max\_Min\_NDVI\_subset\_analysis.xls*, Output DTN: SN0608NDVIANAL.001). The average value of PVR for this subset, 0.071654, was divided into all pixels within the model domain: this was the denominator for normalizing PVR values (Equation E-7). Over the repository, the regionally normalized PVR ranged from zero to about three. Thus, for the repository region, normalized PVR had an average response of 1.0 and a peak response about 300% greater than average. In Figure E-24, a histogram of normalized PVR demonstrates the statistical distribution of PVR from within the subset area overlying the proposed repository.



Source: Output DTN: SN0608NDVIANAL.001, *PVR-Max\_Min\_NDVI\_subset\_analysis.xls*.

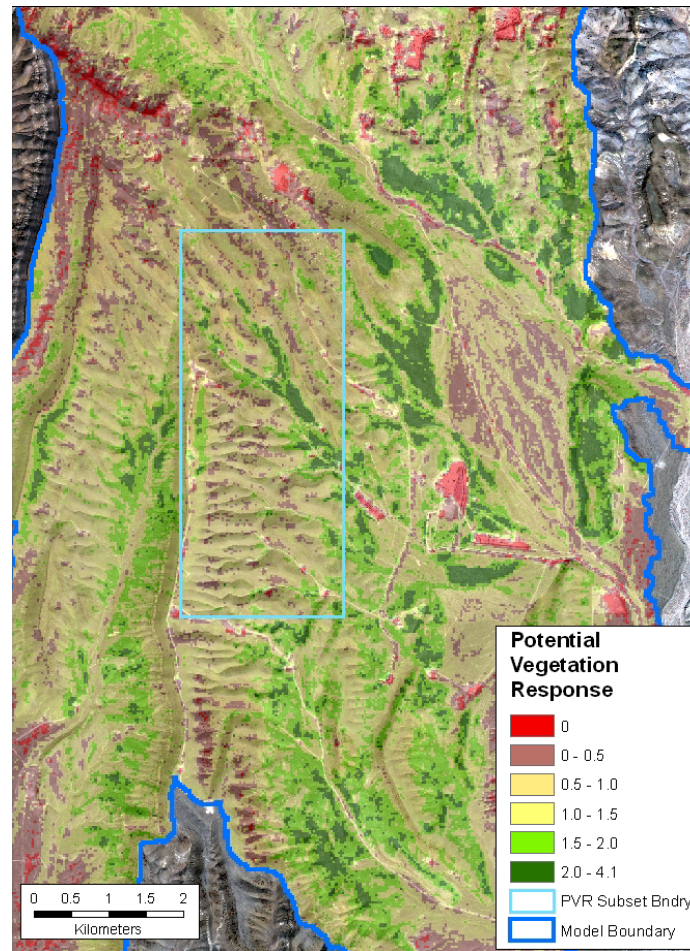
NOTE: The maximum PVR range for the full infiltration modeling domain is about 4, which is higher than for this subregion.

Figure E-24. Histogram of Normalized PVR from the Subset Area Overlying the Proposed Repository

Figure E-25 presents a graphic view of PVR distribution for the region overlying and surrounding the proposed repository. Comparison of the distribution of the higher PVR values to the brighter red signatures on the false color images for WY1998 (Figure E-1) confirmed that PVR captured the distribution of heavy vegetation response. A comparison of data from the vegetation plots disclosed that high PVR values are associated with heavy infestation by *Bromus madritensis* spp. *rubens*, (common name, “red chess”), a weedy annual grass introduced from Eurasia. A close look at the PVR values displayed over the DOQQ or Quickbird images indicates that that PVR correctly identifies areas of low (or no) vegetation activity in rocky locations.

To codify vegetation response as PVR for each grid cell, the minimum (critically dry) year should have a functionally zero vegetation signal. This may actually not be the case for many model grid cells because of partial leaf retention by evergreen species such as *Larrea divaricata*, *Ephedra* spp., and *Chrysothamnus* spp. that make up a portion of the vegetation on Yucca Mountain. The minimal canopies of these species would be present during the period chosen for the minimum expression and should be subtracted out. Fortunately, during extreme droughts these plants also lose leaves (Smith et al. 1995 [DIRS 103628]), reducing the potential error.

Though no data exist for recording the effect of uncounted evergreen species on the calculation of PVR, the potential bias due to evergreen species can be estimated. For the rocky uplands, only the *Ephedra* spp. and *Chrysothamnus* spp. are important since *Larrea* is excluded where soils are shallow. As an example, measurements by Stothoff et al. (1999 [DIRS 176705]) found one evergreen species (*Chrysothamnus teretifolius*) comprising about 10% of the perennial vegetation on the rocky uplands (0.03 of the 0.33 total cover). Thus, if the retained leaves during drought for this species were 10% of maximal canopy expression, the potential bias due to uncounted evergreen plants with leaves would be up to about 1% of the variation in the data (10% of 10%). This bias is insignificant in comparison to the uncertainty that exists in the data (discussed in Section E7). The bias associated with the LLG sites may be 2 or 3 times this amount due to a predominance of *Larrea*, though fortunately, is largely excluded from the target region for this simulation due to shallow soils in the rocky uplands overlying the proposed repository.



NOTE: Magnitude of PVR is reflected in the intensity of the green coloration. Pink areas are exposed rock or extremely low or near zero vegetation response. The irregular blue line is the boundary for watersheds included within the infiltration model. The light blue polygon is the region overlying the repository footprint selected for normalizing and evaluating the statistical distribution of PVR. The PVR values are calculated in Output DTN: SN0608PVRATYMT.001. The PVR Subset Boundary line is from *PVR\_subset\_evf* and *nad27\_boundary\_evf* in Output DTN: SN0608NDVIAUXD.001. Grayscale background is from a Quickbird image from DTN: SN0601QBSAT802.001 [DIRS 177241].

Figure E-25. PVR Located over the Region of the Proposed Repository

## E5. ALGORITHM TO SIMULATE VEGETATION FOR EACH MODEL GRID CELL

An algorithm to simulate annual vegetation response for each model grid cell was assembled from the resulting output from Sections E2, E3, and E4. In review, Section E2 established the proportionality for vegetation response to annual precipitation. In Section E3, a temporal curve for NDVI' was developed that was adjusted by weighted averaging to represent various classes of slope and azimuth. In Section E4, PVR was developed for each model grid cell to scale the magnitude of the vegetation response to antecedent precipitation, calibrating to the actual conditions that enhance or inhibit vegetation growth within that cell.

WY1998 was chosen for fitting all simulation parameters, including PVR, NDVI' slope/azimuth response curve, and a precipitation ratio for scaling the magnitude of the vegetation response. WY1998 is an ideal choice as the very high level of precipitation induced a maximal vegetation response. This maximal response corresponds to a strong signal in an environment that generally has a weak vegetation signal, hence maximizing the signal to noise ratio.

To simulate the strength of the vegetation response, the response curve is scaled using the total annual precipitation. This is accomplished by using the ratio of the annual precipitation of the year in question to the annual total WY1998 precipitation. Precipitation data were calculated as the average of three stations located on Yucca Mountain (Stations 2, 3, and 4). For WY1998, the yearly precipitation was 378 mm (in *ESP\_NDVI\_simET-K.xls*, 2. precip\_table (Output DTN: SN0608NDVIANAL.001)). It is noted that the WY1998 yearly precipitation value can be varied within the infiltration model; for example, a projection for WY1998 precipitation based upon elevation could be used instead

The resulting outputs were combined to estimate NDVI' for any day in the water year for any location within the model domain (Equation E-8):

$$\text{sim NDVI}'_i = \text{NDVI}'_{j, i\text{-curve}} * \text{PVR}_i * \text{WY precipitation (mm)} / 378 \text{ mm} \quad (\text{Eq. E-8})$$

where: sim denotes simulated,

j is the j<sup>th</sup> day of the water year,

i is the i<sup>th</sup> model grid cell,

i-curve denotes the NDVI'<sub>j</sub> curve values appropriate for the slope and azimuth of the i<sup>th</sup> cell.

This algorithm, along with the NDVI'<sub>j</sub> curve and PVR<sub>i</sub> data, are used as input for the MASSIF model.

## **E6. ET AND K FACTOR SIMULATION FOR COMPARISON TO OTHER MASSIF MODEL PARAMETERS AND ET ESTIMATION**

Although the data in this appendix were analyzed primarily to develop a simulation algorithm for vegetation response, they were also analyzed to enable comparison with the  $K_{cb}$  parameters developed and described in Appendix D.  $K_{cb}$ s are basal crop coefficients. These crop coefficients are multiplied by the reference  $ET$ ,  $ET_0$ , to yield an estimate of actual  $ET$ . The calculations for this comparison are contained within spreadsheets in the workbook entitled *ESP\_NDVI\_simET-K.xls* (Output DTN: SN0608NDVIANAL.001). This section provides scaled values of  $ET$  estimated using reference  $ET_0$  for comparison to the  $K_{cb}$  developed in Appendix D.

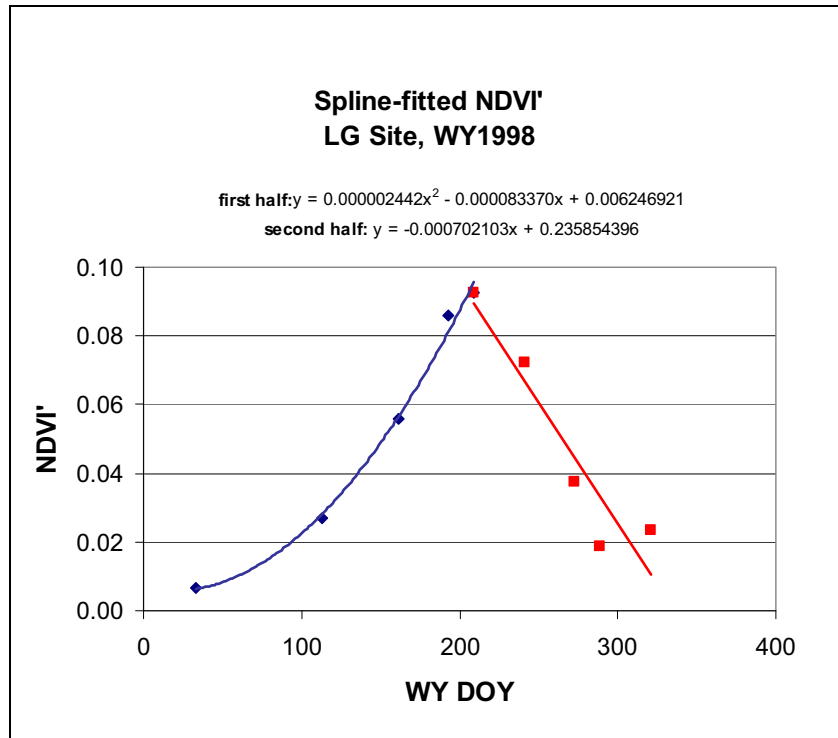
For this analysis, daily time steps of  $ET_j$  were simulated (where j denotes the j<sup>th</sup> day in the water year). In order to correlate the  $ET_j$  relationship from NDVI'<sub>j</sub>, polynomial functions were fitted to the NDVI' time steps to provide predictors for NDVI'<sub>j</sub>. As an example, the time-wise NDVI' data

shown on Figure E-19 for WY1998 were fitted with two polynomial relationships that enable estimation of daily time steps (Figure E-26).

NDVI<sub>j</sub> values predicted by the polynomial curves were multiplied in daily time steps by the daily  $ET_0$  estimated for Yucca Mountain using the FAO-56 Penman-Monteith method (Allen et al. 1998 [DIRS 157311]) in *Ref ET calcs\_2002 water year\_rev A2*, *Ref ET calcs\_2001 water year\_site 1 weatherdata\_rev A2*, and *Ref ET calcs\_2002 water year\_rev A2* (Output DTN: MO0603SPAREFET.000). To scale each time step to provide estimates of  $ET_j$ , these individual  $ET_{0j} * NDVI_j$  products were summed for the water year and divided into the total annual precipitation (all units in mm). This scalar value was then multiplied by the value of  $ET_{0j} * NDVI_j$  to simulate  $ET_j$  for the average vegetation NDVI' measured (Figure E-27). Note that this calculation provides values intended simply for guidance for expected  $ET_j$  because it  $ET$  is computed to all pass through plants (this results from scaling the total of the  $ET_j$  and NDVI<sub>j</sub> products by the total annual precipitation). This simplification does not account for the portion of water lost by evaporation at the soil surface or rock/canopy interception; however, these methods of water loss may be relatively small compared to the amount passing through the plants themselves. The  $ET_j$  relationship is given in Equation E-9.

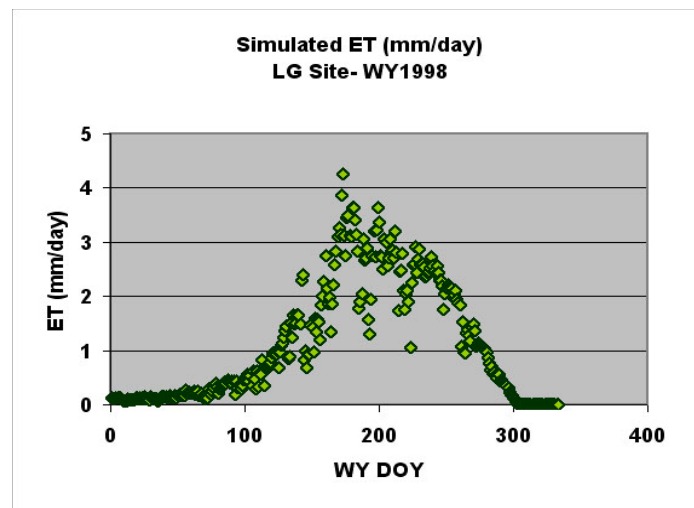
$$\text{sim } ET_j = (ET_{0j} * NDVI_j) * [\text{sum } (ET_{0j} * NDVI_j) / \text{sum precipitation}_j] \quad (\text{Eq. E-9})$$

Simulation of  $ET_j$  enabled the estimation of a simulated vegetation water use coefficient, a K factor (Allen et al. 1998 [DIRS 157311]). Daily time steps were calculated by simply dividing  $ET_j$  by  $ET_{0j}$ . The shape of this curve, again at daily time steps, is the same as the NDVI' curve in Figure E-26, except scaled by precipitation to the correct dimensions for  $ET_j$ . These curves of K were intended for comparison to the  $K_{cb}$  values that are described in Appendix D.



Source: Output DTN: SN0608NDVIANAL.001, *ESP\_NDVI'\_simET-K.xls*.

Figure E-26. Two Polynomial Curves, Ascending and Descending, Fitted to the NDVI' LG ESPs, WY1998, to Calculate Daily Time Steps through the Water Year



Source: Output DTN: SN0608NDVIANAL.001, *ESP\_NDVI'\_simET-K.xls*.

Figure E-27.  $ET_j$  Simulated for LG Sites in WY1998 Using  $ET_0$ , Daily Fitted Values for NDVI' and Scaled by the Water Available from Precipitation

## **E7. CORROBORATION OF THE NDVI' ALGORITHM AND OF THE POTENTIAL MAGNITUDE OF UNCERTAINTY**

The algorithm for simulating NDVI' was corroborated using three separate data sets. The data sets were extracted from the ESPs because these locations were used as input for estimation of *ET* and basal crop coefficient ( $K_{cb}$ ) relationships (Appendix D), they are locations where vegetation properties were measured, and they are a potential source for other meta-data such as average slope and aspect.

**Corroboration 1.** For the ESPs, simulated NDVI' was compared to measured NDVI' for WY1998, WY2001, and WY2002. The simulated NDVI' values were calculated using PVR data measured for the ESPs in the developed algorithm (Equation E-7). A total of nine comparisons were completed (three different vegetation types for years of above average, average, and dry levels of precipitation).

**Corroboration 2.** NDVI' simulations for WY1990, 1991, and 1993 were compared with  $K_{cb}$  values calculated in Appendix D. As seen in Section E6, NDVI' is a value that is closely related to crop coefficients (K factors).

**Corroboration 3.** Vegetation cover was measured on the ESPs during 1990, 1991, and 1993. Annual water year precipitation totals that were measured at three Yucca Mountain stations (2, 3, and 4) were combined with the PVR data extracted from the ESPs to estimate a peak NDVI' for comparison to measured cover.

Each of these corroboration efforts is described in more detail below.

### **E7.1. CORROBORATION 1: APPROPRIATENESS OF THE ALGORITHM FOR WY1998, WY2001, AND WY2002.**

NDVI' was simulated for daily time steps using Equation E-7 for the pooled samples of the three vegetation association-ESP sites (sampled locations on Figure E-13). For the simulation, the appropriate NDVI' curve was chosen to represent the average topographic slope and azimuth at each of the vegetation plots (typically <5 degrees). The daily time step curves were combined with average PVR values extracted for the model grid cells which fell within the vegetation plot boundaries. Sample sizes for PVR were robust: 445 cells for LA plots, 552 for LLG and 516 for LG. Data were averaged for the calculation of a single value to represent each of the three vegetation associations (Output DTN: SN0608NDVIANAL.001, workbook *Verify\_NDVI'\_Estimation.xls*). The resulting daily time-step curves were then compared with the average of NDVI' extracted and calculated for each image in Output DTN: SN0608NDVIANAL.001, workbook *ESP\_NDVI'\_simET-K*, as described in Section E2.5.

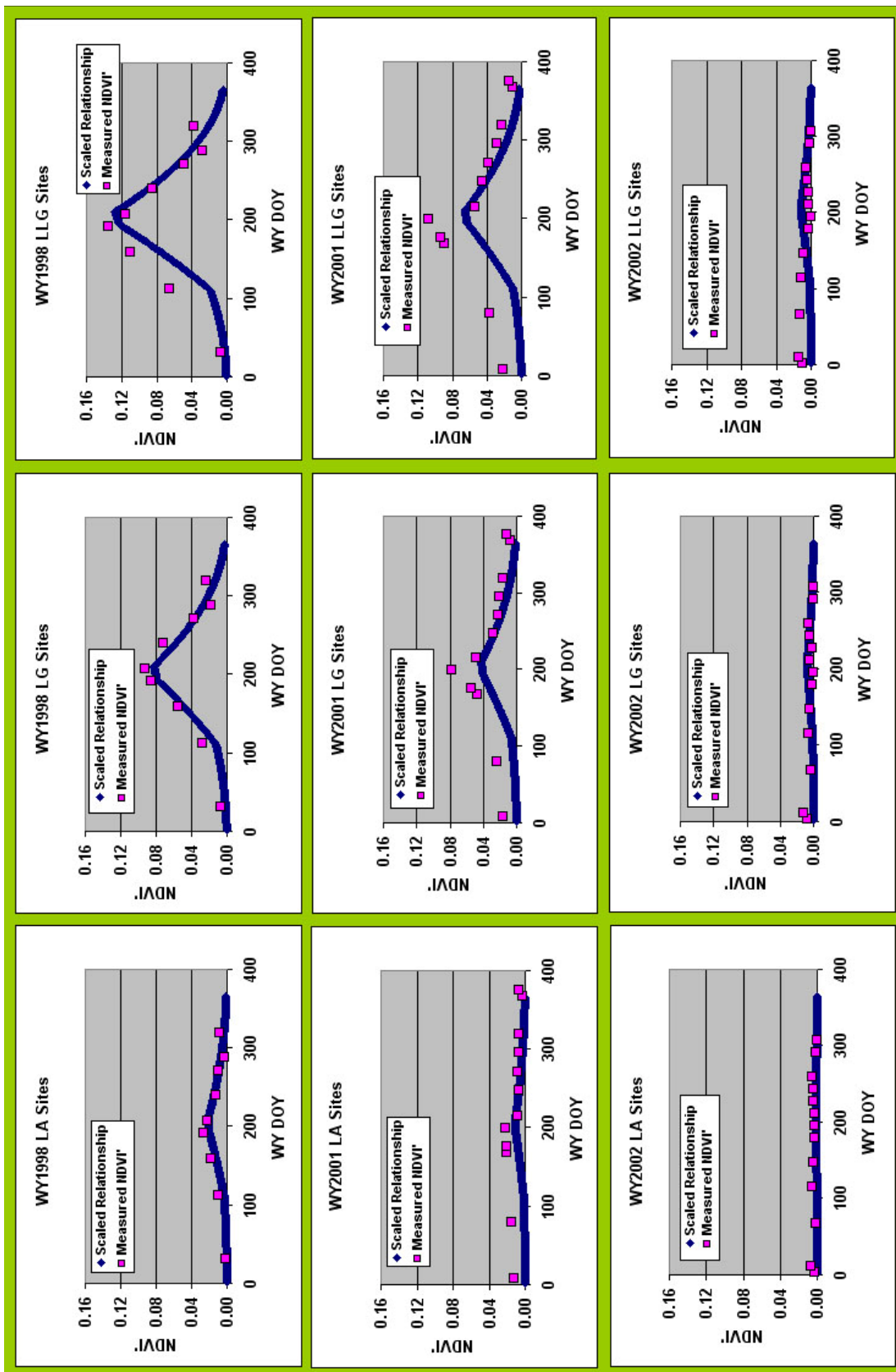
Figure E-28 provides a graphical comparison of simulated and measured NDVI' values. The comments here will be restricted to the LG vegetation that overlies the proposed repository. Of the two other vegetation types, LLG and LA, the simulation of LA appears to be qualitatively better than for the LLG type, while relative errors are greater in the early part of the season rather than in the latter portion for all three vegetation types.



Not surprisingly, the WY1998 simulation of LG vegetation is better than for WY2001. For example, the peak measured value for WY1998 NDVI' was 0.0924 while the simulated value for was 0.0852 (7.8% low). For peak point of the WY2001 growing season induced by moderate precipitation, the measured NDVI' was .0773, while the simulated value was 0.0422 resulting in an underprediction of about 45%. For the driest year, WY2002, the simulation correctly projected very low peak NDVI', 0.0073, that was less than 10% of either WY2001 or WY1998.

The simulation algorithm (Equation E-8) apparently induces a systematic underprediction during the first part of the WY relationships as can be seen in Figure E-28, where for LG plots, the estimation was about 1/2 of the measured values for WY2001. The declining leg of the simulated curve for WY2001 is closer, with the values at WYDOY 217 underpredicting the NDVI' by 25%.

Fortunately, the greatest potential for infiltration exists during the wet period where the simulation routine performs the best of the three cases.

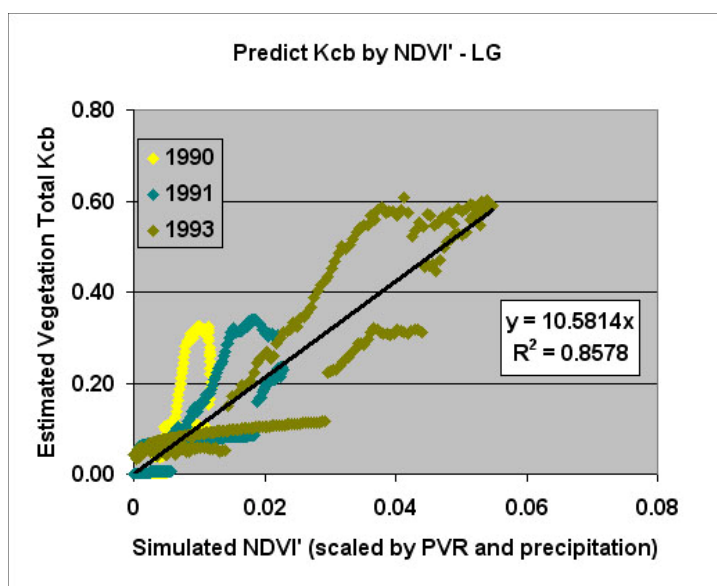


Source: Output DTN: SN0608NDVIANAL.001, Verify\_NDVI\_Estimation3.xls.

Figure E-28. Simulated (Curves) Versus Measured Values of NDVI on the Three Plots during the Three Years Chosen for Study

## E7.2. CORROBORATION 2: COMPARE NDVI' SIMULATIONS FOR WY1990, WY1991, AND WY1993 WITH $K_{cb}$ VALUES CALCULATED IN APPENDIX D

NDVI has been shown to be related linearly to  $K_{cb}$  in the literature (Hunsaker et al. 2003 [DIRS 176048], pp. 100 and 101, and Figure 6; Hunsaker et al. 2005 [DIRS 177302], pp. 10 and 11 and Figure 5). This step tested this linearity using the LG ESP data because it is most similar to the vegetation overlying the repository. The analysis used total water-year precipitation to scale the algorithm (total precipitation in desired year [mm]/total precipitation in wettest year [378 mm]). Three WYs were chosen (WY1990, WY1991 and WY1993). Results were applied to the lumped average PVR for each of the ESPs that were used for calculations in Section E7.1 from Output DTN: SN0608NDVIANAL.001, workbook *Verify\_NDVI'\_Estimation.xls*. Calculations are contained in Output DTN: SN0608NDVIANAL.001, workbook *ESP\_90,91,93,NDVI'\_simET-K.xls*. Figure E-29 shows the comparison for the LG plots of the  $K_{cb}$  values calculated for estimation of  $ET$  in Appendix D versus the simulated NDVI'.



Source: Output DTN: SN0608NDVIANAL.001, *ESP\_90,91,93,NDVI'\_simET-K.xls*.

NOTE: The regression line was forced through the origin.

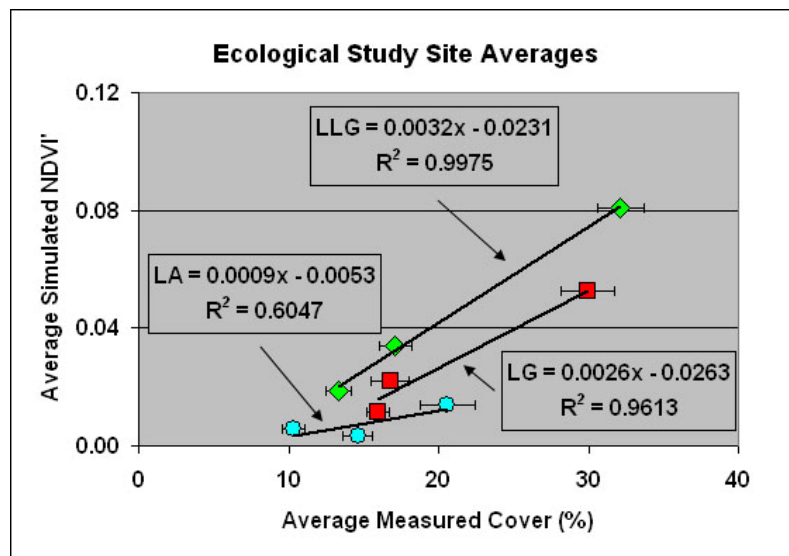
Figure E-29. Comparison of Simulated NDVI' to the  $K_{cb}$  Values, Paired by Daily Time Steps, for WY1990, WY1991, and WY1992 for the LG ESPs

Figure E-29 provides a linear relationship to relate the two data sets.  $K_{cb}$  is roughly a factor of ten higher than the simulated NDVI'. The systematic digressions from the NDVI' estimate occur as a hysteresis effect where the  $K_{cb}$  is higher during the early portion of the year when there is soil water available (plotting above the regression line), but much lower during the latter portions of the growing season when the plants are within a senescing cycle (below the regression line). All three years were lumped together to fit on this curve, and the driest year, WY1990, was distributed mostly above the predicted linear relationship.

### E7.3 CORROBORATION 3: COMPARE VEGETATION COVER MEASURED ON THE ESPS DURING 1990, 1991, AND 1993 WITH PEAK NDVI' SIMULATED BY THE ALGORITHM

Vegetation cover was measured on the ESPs starting in 1988, and measurements were discontinued after 1993 (CRWMS 1996 [DIRS 102235]), so there is no way to compare the NDVI' used in this analysis (1998, 2001, and 2002) directly to measured ESP cover. Instead, measured data from the ESPs (Output DTN: MO0606SPAVEGAS.001) were compared to peak NDVI' values simulated using the PVR values extracted for the corroboration step described in Section E7.1. These analyses are contained in Output DTN: SN0608NDVIANAL.001, workbook *ESP\_NDVI'sim\_v\_Cover.xls*.

As seen in all of the NDVI' response curves for Yucca Mountain vegetation (Figure E-19), the vegetation canopy expression is ephemeral. Therefore, the methods that were used to estimate vegetation counted each year's maximal canopy cover, whether green or senesced at the time of measurement (CRWMS 1996 [DIRS 102235]). Thus, measured cover at the ESPs represents peak vegetation standing crop. For this reason, ESP measured cover was compared to the peak NDVI' simulated with the algorithm. The NDVI' simulation employed PVR, precipitation scaling, and the peak NDVI' estimate provided by Equation E-8. For choosing the peak NDVI', the average slope and azimuth for each ESP was used to select the appropriate curve value from the suite of curves depicted in Figure E-23. Although the NDVI' values were calculated for each of the ESPs, only the lumped-average NDVI' is depicted for comparison to the lumped average cover measured for ESP vegetation associations (Figure E-30).



Source: This graph is excerpted from Output DTN: SN0608NDVIANAL.001, *ESP\_NDVI'sim\_v\_Cover.xls*.

NOTE: Each point represents an annual value in order from low to highest: 1990, 1991, and 1992. The error bars associated with each point are the 90% confidence interval for cover (Output DTN: MO0606SPAVEGAS.001).

Figure E-30. Comparison of Lumped-Average Simulated NDVI' to Lumped-Average Cover Measured on the ESPs

The linear fits in Figure E-30 for the simulated NDVI' and the measured cover offer further corroboration that the magnitude of NDVI' predicted by the algorithm generally follows the response of vegetation cover on Yucca Mountain.

The comparison of ESPs to NDVI for the LA vegetation type violated this during one year as can be seen on Figure E-30. This occurred for WY1991 when the lowest cover of the three years was measured for the LA ESPs even though the precipitation recorded on Yucca Mountain Sites 2, 3, and 4 was almost twice that recorded in WY1990 (Output DTN: MO0607SEPTOTAL.003)<sup>3</sup> and may have arisen in the ground truth measurements.

#### **E7.4 NUMERIC CORROBORATION OF RELATIVELY LOW UNCERTAINTY ASSOCIATED WITH SIMULATION OF NDVI'**

Although the three preceding parts of Section E7 provide corroboration that the algorithm for NDVI' provides simulations that mimic vegetation responses in nature, they do not provide an independent assessment of the uncertainty involved with calculation of the basic data that were used for fitting the NDVI' algorithm. Although uncertainty was evaluated in parts of Section E2, they require independent corroboration, especially the degree of error tails off at low values of NDVI'. Because of the complexity of the calculations and the potential for some of the calculations to be self correcting through the series of required steps (i.e., an estimate that is high or low is pushed toward the central tendency by subsequent calculations), this corroboration was approached as a thought problem that referenced the N- and S-slope data that were used to develop the algorithm.

An estimate of uncertainty was derived by looking at WY2002 and the data extracted for the steep slopes of the rocky uplands overlying the repository that were used for developing the response curves in the algorithm of Equation E-8 (curves shown in Figure E-23). During WY2002, a stable, near-zero vegetation response is expected because insufficient precipitation fell to be effective for vegetation growth. This near-zero response was simulated as NDVI' using the algorithm in Equation E-8 that matched the actual NDVI' vegetation responses, as can be seen in Figure E-28.

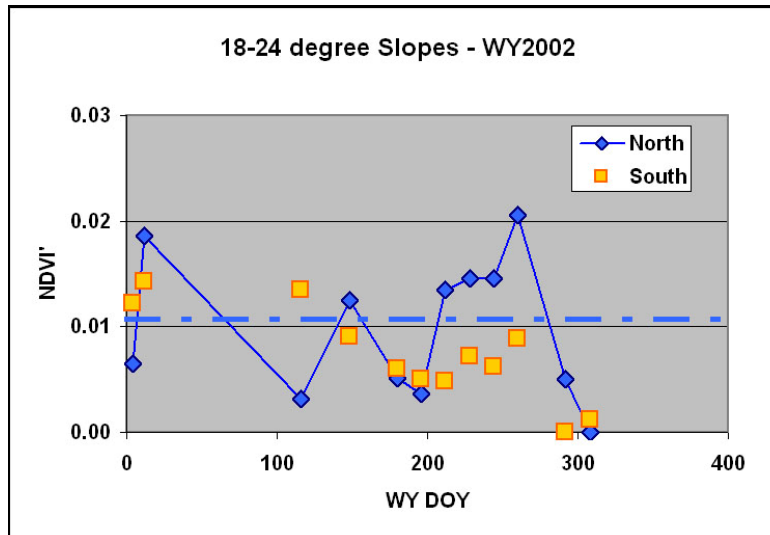
Zero vegetation response was expected due to the intense drought conditions, so the unexpected curve transgressions for NDVI' during WY2002 (Figure E-19) form the basis for an estimate of uncertainty. These values are averages of the extracted NDVI' developed using the processing parameters,  $DOS_{avg}$ , and  $NDVI_0$  developed in Section E2 and displayed in Table E-2.

Figure E-31 reproduces a rescaled version of the WY2002 data presented in Figure E-17. The N slope data have much higher fluctuations than S slope, possibly due to the influence of shading on the uncertainty of the estimates. Since the N slope has much larger fluctuations, this will be dealt with as a conservative worst case for estimating uncertainty. Fluctuations about a line for the average of nonzero N-slope values can be represented by the standard deviation. In this case,

---

<sup>3</sup> When the calculations were done, the source data was obtained from Output DTN: MO0605SEPTOTAL.001, which was later superseded by Output DTN: MO0605SEPTOTAL.002, that was subsequently superseded by Output DTN: MO0607SEPTOTAL.003. The source data used from the original DTN was not altered in the superseding DTNs as determined by a comparison check.

these digressions from the central tendency are 0.006 NDVI', thus showing that the degree of uncertainty tapers toward zero as the average NDVI' tapers toward zero.



Source: Ouput DTN: SN0606T0502206.012, *Daily\_NDVI\_Estimation.xls*.

NOTE: The dashed blue line is the approximate average for the north slope values shown.

Figure E-31. WY2002 Average NDVI' from N and S Slopes that Approach Zero Vegetation Response

## E8. CONCLUSIONS

These analyses developed a simple spatially and temporally appropriate algorithm to simulate vegetation response at the Yucca Mountain site during present climatic conditions. Precipitation is a potential source for infiltration at the proposed repository. Although vegetation cover is sparse at Yucca Mountain, most of the water supplied from the atmosphere is evaporated or transpired and only a small fraction is available for net infiltration. Thus, to be responsive to the actual physical conditions governing infiltration, the net-infiltration model must capture vegetation growth response as a function of both time and location. To do this, vegetation signatures were observed on satellite data and parameterized. These parameters were then combined to simulate responses to annual precipitation and seasonal factors, the two variables most influential to vegetation response.

In an arid environment such as Yucca Mountain, vegetation is dormant through much of the year. When water is present and growing temperatures are conducive, plants respond by growing leaves. Transpiration is a by-process to photosynthesis. In this context, plant and canopy development is an important factor in estimating the water used.

Vegetation water use is proportional to canopy leaf area. Green leaves can be detected using the Normalized Difference Vegetation Index (NDVI) and can be calculated using satellite data. Selected scenes from a 20-year archive of Landsat TM (thematic mapper) were chosen as the basis for characterizing Yucca Mountain vegetation.

This quantification and simulation of Yucca Mountain vegetation response first evaluated regional eco-hydrology, then characterized vegetation spatially on satellite data, and finally, assembled and corroborated an algorithm for simulating these responses. There were eight steps in this process:

- Characterizing the Yucca Mountain climate that drives the vegetation response. This was accomplished using precipitation and temperature data measured onsite.
- Choosing a set of years to capture vegetation response on which to base the simulation. This choice was made with regard to the satellite data available and ancillary data that were measured on and near Yucca Mountain. Three years were chosen: a wet year (WY1998), a critically dry year (WY2002), and a year with approximately average precipitation (WY2001). WY refers to water year, which corresponds to October 1 through September 30. The date is for the year most represented (i.e., WY1998 contains nine months in 1998 and only three months of 1997).
- Processing the satellite imagery for the chosen years to yield data in reflection units in their correct position on the landscape. Landsat TM imagery was used for the entire data suite. Images representing snapshots during the growing seasons of each year were selected to characterize vegetation canopy expression with an emphasis on the months when vegetation response was greatest (March through June of each year).
- Correcting the TM data to remove atmospheric effects (light scatter) and to remove nonsystematic variations inherent in the NDVI that was used to typify vegetation response. This resulted in a set of processing parameters that were unique to each image. These parameters were corroborated using data extracted from Ecological Study Plots (ESP) for three major vegetation associations typical of Yucca Mountain, and then applied to the entire data set.
- Fitting an annual relationship to characterize plant response, according to slope and azimuth, for the region overlying the proposed repository. This relationship used the wet year/high vegetation response: this maximal response was important because the vegetation signal is generally low due to Yucca Mountain’s arid climate.
- Developing an index to capture the potential vegetation growth within each 30-m model grid cell. This index was given the name PVR (potential vegetation response) and was calculated for every model grid cell by subtraction of the minimal vegetation response during the dry year from the maximal vegetation expression during the wet year. These measures were normalized by the PVR values from a zone overlying the proposed repository.
- Developing an algorithm to simulate vegetation response that combines annual curves characterized by (1) slope and azimuth with scaling, (2) a precipitation adjustment to enable projection for any year, and (3) PVR to scale this generalized vegetation response specifically for each model grid cell and the water availability of the year in question.

The algorithm was corroborated by comparison to data developed for the ESPs (1) with actual data extracted for WY1998, WY2001, and WY2002; (2) with basal crop coefficients,  $K_{cb}$ , developed for Appendix D; and (3) for measured cover during WY1990, WY1991, and WY1993. A final corroboration of the uncertainty associated with these measurements was then made based upon reasonable interpretation of the inherent data scatter at a time when the vegetation was at its lowest response (during the driest time, late summer, of the driest year, WY2002).

In conclusion, the corroborated vegetation algorithm provides a set annual response that is scaled by precipitation and position on the landscape for incorporation into the infiltration model, MASSIF. Inputs include (1) a table of daily time steps for any azimuth or slope specified for each 30-m model grid cell, (2) PVR values to typify the spatially correct potential for vegetation growth within each model grid cell, and (3) a simple means to scale plant response relative to the precipitation for each year.



**APPENDIX F**  
**DEVELOPMENT OF STOCHASTIC PRECIPITATION AND OTHER CLIMATE**  
**INPUT FILES**



This appendix supports Section 6.5.1, Weather Parameters for Anticipated Climate Episodes. Calculation of net infiltration requires an input file containing precipitation, temperature extremes, and mean wind speed on a daily basis. The MASSIF model varies precipitation and temperature with elevation and accepts input for an elevation of 1,524 m (5,000 ft), corresponding to the top of Yucca Mountain.

Section F1 is an explanation of the general methods for developing twelve precipitation parameters and twelve temperature parameters that together summarize the precipitation and temperature records at a meteorological station. Section F2 describes the application of these methods to the specific meteorological stations that are representative of each climate. Section F3 explains the development of twelve parameters for wind speed and the selection of 36 parameter uncertainty distributions to capture the range of uncertainty for each climate. Section F4 provides the general method for obtaining a weather input file from a particular set of parameter values.

In addition to the contents of the weather input file, this appendix provides the basis for the precipitation lapse rate. Section 6.5.1 provides the temperature lapse rate, two parameters of precipitation duration, and parameters of snowmelt and sublimation. Section 6.5.4 explains the selection of dew point parameters for each climate.

## **F1. PARAMETERIZATION OF PRECIPITATION AND TEMPERATURE RECORDS**

*Future Climate Analysis* (BSC 2004 [DIRS 170002], Table 6-1) identified specific meteorological stations as being representative of anticipated climate episodes at Yucca Mountain. *Data Analysis for Infiltration Modeling: Extracted Weather Station Data Used to Represent Present-Day and Potential Future Climate Conditions within the Vicinity of Yucca Mountain* (BSC 2006 [DIRS 177081], Table 7.3-1) qualified data from those meteorological stations.

This section describes the methods for developing parameters that characterize the relevant characteristics of each climate. For precipitation and temperature, the first step is development of a set of parameters for each meteorological station. These station-specific parameters approximate the multiyear record of daily measurements at that station. Section F1.1 describes the methods for developing parameters for precipitation. Section F.1.2 addresses temperature parameterization.

### **F1.1 PARAMETERIZATION OF PRECIPITATION RECORDS**

#### **F1.1.1 Background**

Precipitation may be characterized as a Markov process. This analysis models the sequence of wet and dry days as a first-order Markov process, which requires two parameters. The analysis models the amount of precipitation on a wet day as a random variable with a lognormal distribution, which requires two more parameters. The two parameters selected for the model of wet-day precipitation are the mean precipitation,  $\lambda$ , and the mean of the logarithm of precipitation,  $m$ . That is, the probability density for the amount of precipitation,  $P$ , is

$$p(P) = \frac{1}{Ps\sqrt{2\pi}} \exp\left[-\frac{1}{2s^2}(\ln P - m)^2\right] \quad (\text{Eq. F-1})$$

where

$$s^2 = 2(\ln \lambda - m) \quad (\text{Eq. F-2})$$

Section 6.5.1 and this appendix describe twelve precipitation parameters that are arranged in four groups of three parameters. Each group of three parameters provides coefficients of a Fourier series for one of the following four functions of the day of the year,  $d$ , for  $d$  from 1 through 365 (March 1 through February 28):

- $p_{00}(d)$ : the probability that day  $d$  is dry, given that day  $D-1$  is dry,
- $p_{10}(d)$ : the probability that day  $d$  is dry, given that day  $D-1$  is wet,
- $\lambda(d)$ : mean of the probability distribution for amount of precipitation on day  $d$ , given that it is a wet day,
- $m(d)$ : mean of the probability distribution for the natural logarithm of the amount of precipitation on day  $d$ , given that it is a wet day.

The Fourier series representation of a continuous function  $f(t)$  with domain  $(0, 2\pi)$  is:

$$f(t) = a + \sum_{n=1}^{\infty} v_n \sin nt + \sum_{n=1}^{\infty} w_n \cos nt = a + \sum_{n=1}^{\infty} b_n \sin(\theta_n + nt) \quad (\text{Eq. F-3})$$

where the first expression is the usual textbook form and the second is the polar form. The formulas for the coefficients are:

$$a = \frac{1}{2\pi} \int_0^{2\pi} f(t) dt \quad (\text{Eq. F-4})$$

$$v_n = \frac{1}{\pi} \int_0^{2\pi} f(t) \sin(nt) dt \quad (\text{Eq. F-5})$$

$$w_n = \frac{1}{\pi} \int_0^{2\pi} f(t) \cos(nt) dt \quad (\text{Eq. F-6})$$

$$b_n = \sqrt{v_n^2 + w_n^2} \quad (\text{Eq. F-7})$$

$$\theta_n = \arctan(w_n/v_n) \quad (\text{Eq. F-8})$$

The sign of  $b_n$  must be consistent with the quadrant chosen for  $\theta_n$ . The formulas derive their simplicity from the orthogonality of the trigonometric functions in Equation F-3; the integral of the product of two functions vanishes unless both functions are the same.

Fourier series can represent a finite set of observations,  $f(t_i)$ ,  $i = 1, 2, \dots, I$ , but the Fourier series becomes finite. Once the number of coefficients is equal to the number of observations, the series fits every point exactly and all higher terms are zero. The first few terms in a finite Fourier series reflect the general trend of the observations. In many cases, the next few terms are small. However, the last terms are larger as they create an exact fit to variations in the data; these last coefficients tend to be artifacts of the particular data set that is chosen. Consequently, Fourier representations of observations are usually truncated after a few terms.

However, when the formulas for the coefficients are based on a finite number of observations, the  $t_i$  must have a special distribution in  $(0, 2\pi)$ , such as a uniform distribution. A difficulty in representing a first-order Markov probability by a truncated Fourier series is that the observations are not uniformly distributed.

For a Markov-chain model of precipitation, each day's observation provides data for only one of the two probabilities, depending on whether the previous day was wet or dry. Some authors dealt with this problem by constructing, for each of the 365 days of a year, an average over several years, with special treatment of leap years. Barring bad luck, such as never having a wet day on January first, these averages provide a uniformly distributed set that can be used to evaluate up to 365 Fourier coefficients. However, this procedure gives the 365 averages equal weights, whereas they may be based on widely varying numbers of observations.

Woolhiser and Pegram (1979 [DIRS 176108], pp. 34 and 35) argued that least-squares estimates of Fourier coefficients are undesirable because the days of the year have unequal sample sizes. Instead, they used optimization software to maximize a likelihood function, either using software that solved for all parameters simultaneously or software that found only one parameter at a time and had to be iterated. Most of the subsequent literature is based on variations of this approach.

For the Yucca Mountain Project, it is desirable to have a procedure that is more transparent than optimization software. To develop the stochastic parameters, this model for Total System Performance Assessment for the License Application (TSPA-LA) uses a least-squares method that accounts for the unequal sample sizes. Instead of treating the average for each day,  $d$ , as the basic data for the Fourier analysis, this method takes the individual daily records, year by year, as the input to the Fourier analysis. This appendix develops the modified formulas for the Fourier coefficients.

### **F1.1.2 Least-Squares Formulas**

For each of the four stochastic functions, a truncated Fourier series represents its variation with  $d$ , as follows:

$$p_{00}(d) = a_{00} + b_{00,1} \sin(\theta_{00,1} + d') + b_{00,2} \sin(\theta_{00,2} + 2d') \quad (\text{Eq. F-9})$$

$$p_{10}(d) = a_{10} + b_{10,1} \sin(\theta_{10,1} + d') + b_{10,2} \sin(\theta_{10,2} + 2d') \quad (\text{Eq. F-10})$$

$$\lambda(d) = a_{\lambda} + b_{\lambda,1} \sin(\theta_{\lambda,1} + d') + b_{\lambda,2} \sin(\theta_{\lambda,2} + 2d') \quad (\text{Eq. F-11})$$

$$m(d) = a_m + b_{m,1} \sin(\theta_{m,1} + d') + b_{m,2} \sin(\theta_{m,2} + 2d') \quad (\text{Eq. F-12})$$

where

$$d' = 2\pi d / 365 \quad (\text{Eq. F-13})$$

In each case, the last term is used only for estimating the uncertainty caused by truncating the series.

This appendix generalizes the three parameters in the form:

$$f(d) = a + b_1 \sin(\theta_1 + d') + b_2 \sin(\theta_2 + 2d') \quad (\text{Eq. F-14})$$

The observations are available on a domain  $D_f$ ; that is,  $D_f$  contains all pairs  $(d, y)$  for which there is an applicable observation. Here,  $d$  varies from 1 through 365, and  $y$  varies from 1 through the number of full years of observation.

In this least-squares approach, the coefficients for the polar form were evaluated one term at a time. First,  $a$  is chosen to minimize the sum of the squares of the deviations from  $a$ . That is, the derivative of the sum of squares with respect to  $a$  must be zero:

$$0 = \frac{\partial}{\partial a} \sum_{(d,y) \in D_f} [f(d,y) - a]^2 = -2 \sum_{(d,y) \in D_f} [f(d,y) - a] \quad (\text{Eq. F-15})$$

Therefore,

$$a = \text{Mean}_{(d,y) \in D_f} [f(d,y)] \quad (\text{Eq. F-16})$$

Next, general formulas for  $b_n$  and  $\theta_n$  were developed having chosen all preceding coefficients. That is, minimizing:

$$\sum_{(d,y) \in D_f} [\hat{f}_{n-1}(d,y) - b_n \sin(\theta_n + nd')]^2$$

where  $\hat{f}_{n-1}(d,y)$  is  $f(d,y)$  reduced by the preceding terms:

$$f'_1(d) = f(d) - a \quad (\text{Eq. F-17})$$

$$\hat{f}_{n-1}(d) = f(d) - a - \sum_{m=1}^{n-1} b_m \sin(\theta_m + md'), \quad n > 2 \quad (\text{Eq. F-18})$$

Minimizing with respect to  $b_n$ ,

$$0 = \frac{\partial}{\partial b_n} \sum_{(d,y) \in D_f} [\hat{f}_{n-1}(d,y) - b_n \sin(\theta_n + nd')]^2 \quad (\text{Eq. F-19})$$

$$0 = -2 \sum_{(d,y) \in D_f} [\hat{f}_{n-1}(d,y) - b_n \sin(\theta_n + nd')] \sin(\theta_n + nd') \quad (\text{Eq. F-20})$$

$$b_n = \frac{\sum_{(d,y) \in D_f} \hat{f}_{n-1}(d,y) \sin(\theta_n + nd')}{\sum_{(d,y) \in D_f} \sin^2(\theta_n + nd')} \quad (\text{Eq. F-21})$$

$$b_n = \frac{\sum_{(d,y) \in D_f} \hat{f}_{n-1}(d,y) (\sin \theta_n \cos nd' + \cos \theta_n \sin nd')}{\sum_{(d,y) \in D_f} (\sin \theta_n \cos nd' + \cos \theta_n \sin nd')^2} \quad (\text{Eq. F-22})$$

$$b_n = \frac{\sin \theta_n \sum_{(d,y) \in D_f} \hat{f}_{n-1}(d,y) \cos nd' + \cos \theta_n \sum_{(d,y) \in D_f} \hat{f}_{n-1}(d,y) \sin nd'}{\sin^2 \theta_n \sum_{(d,y) \in D_f} \cos^2 nd' + 2 \sin \theta_n \cos \theta_n \sum_{(d,y) \in D_f} \sin nd' \cos nd' + \cos^2 \theta_n \sum_{(d,y) \in D_f} \sin^2 nd'} \quad (\text{Eq. F-23})$$

$$b_n \cos \theta_n = \frac{\tan \theta_n \sum_{(d,y) \in D_f} \hat{f}_{n-1}(d,y) \cos nd' + \sum_{(d,y) \in D_f} \hat{f}_{n-1}(d,y) \sin nd'}{\tan^2 \theta_n \sum_{(d,y) \in D_f} \cos^2 nd' + 2 \tan \theta_n \sum_{(d,y) \in D_f} \sin nd' \cos nd' + \sum_{(d,y) \in D_f} \sin^2 nd'} \quad (\text{Eq. F-24})$$

Minimizing with respect to  $\theta_n$ ,

$$0 = \frac{\partial}{\partial \theta_n} \sum_{(d,y) \in D_f} [\hat{f}_{n-1}(d,y) - b_n \sin(\theta_n + nd')]^2 \quad (\text{Eq. F-25})$$

$$0 = -2 \sum_{(d,y) \in D_f} [\hat{f}_{n-1}(d,y) - b_n \sin(\theta_n + nd')] b_n \cos(\theta_n + nd') \quad (\text{Eq. F-26})$$

For  $b_n \neq 0$ ,

$$b_n = \frac{\sum_{(d,y) \in D_f} [\hat{f}_{n-1}(d,y) \cos(\theta_n + nd')] }{\sum_{(d,y) \in D_f} [\sin(\theta_n + nd') \cos(\theta_n + nd')] } \quad (\text{Eq. F-27})$$

$$b_n = \frac{\sum_{(d,y) \in D_f} \hat{f}_{n-1}(d,y) [\cos \theta_n \cos nd' - \sin \theta_n \sin nd'] }{\sum_{(d,y) \in D_f} [\sin \theta_n \cos nd' + \cos \theta_n \sin nd'] [\cos \theta_n \cos nd' - \sin \theta_n \sin nd'] } \quad (\text{Eq. F-28})$$

$$b_n = \frac{\cos \theta_n \sum_{(d,y) \in D_f} \hat{f}_{n-1}(d,y) \cos nd' - \sin \theta_n \sum_{(d,y) \in D_f} \hat{f}_{n-1}(d,y) \sin nd' }{\sum_{(d,y) \in D_f} [\cos \theta_n \sin \theta_n \cos^2 nd' - \sin^2 \theta_n \cos nd' \sin nd'] } + \frac{\sum_{(d,y) \in D_f} [\cos^2 \theta_n \sin nd' \cos nd' - \sin \theta_n \cos \theta_n \sin^2 nd'] }{\sum_{(d,y) \in D_f} [\cos^2 \theta_n \sin nd' \cos nd' - \sin \theta_n \cos \theta_n \sin^2 nd'] } \quad (\text{Eq. F-29})$$

$$b_n \cos \theta_n = \frac{\sum_{(d,y) \in D_f} f'_{n-1}(d,y) \cos nd' - \tan \theta_n \sum_{(d,y) \in D_f} f'_{n-1}(d,y) \sin nd' }{\tan \theta_n \sum_{(d,y) \in D_f} (\cos^2 nd' - \sin^2 nd') + (1 - \tan^2 \theta_n) \sum_{(d,y) \in D_f} \sin nd' \cos nd' } \quad (\text{Eq. F-30})$$

Equating the right-hand sides of Equations F-24 and F-30,

$$\frac{\tan \theta_n \sum_{(d,y) \in D_f} \hat{f}_{n-1}(d,y) \cos nd' + \sum_{(d,y) \in D_f} \hat{f}_{n-1}(d,y) \sin nd' }{\tan^2 \theta_n \sum_{(d,y) \in D_f} \cos^2 nd' + 2 \tan \theta_n \sum_{(d,y) \in D_f} \sin nd' \cos nd' + \sum_{(d,y) \in D_f} \sin^2 nd' } = \frac{\sum_{(d,y) \in D_f} \hat{f}_{n-1}(d,y) \cos nd' - \tan \theta_n \sum_{(d,y) \in D_f} \hat{f}_{n-1}(d,y) \sin nd' }{\tan \theta_n \sum_{(d,y) \in D_f} [\cos^2 nd' - \sin^2 nd'] + [1 - \tan^2 \theta_n] \sum_{(d,y) \in D_f} \sin nd' \cos nd' } \quad (\text{Eq. F-31})$$



$$\begin{aligned}
 & \left. \begin{aligned}
 & \left[ \tan \theta_n \sum_{(d,y) \in D_f} \hat{f}_{n-1}(d,y) \cos nd' + \sum_{(d,y) \in D_f} \hat{f}_{n-1}(d,y) \sin nd' \right] \\
 & \times \left[ \tan \theta_n \sum_{(d,y) \in D_f} [\cos^2 nd' - \sin^2 nd'] + [1 - \tan^2 \theta_n] \sum_{(d,y) \in D_f} \sin nd' \cos nd' \right] \\
 & = \left[ \sum_{(d,y) \in D_f} \hat{f}_{n-1}(d,y) \cos nd' - \tan \theta_n \sum_{(d,y) \in D_f} \hat{f}_{n-1}(d,y) \sin nd' \right] \\
 & \times \left[ \tan^2 \theta_n \sum_{(d,y) \in D_f} \cos^2 nd' + 2 \tan \theta_n \sum_{(d,y) \in D_f} \sin nd' \cos nd' + \sum_{(d,y) \in D_f} \sin^2 nd' \right]
 \end{aligned} \right\}
 \end{aligned}$$

(Eq. F-32)

$$\begin{aligned}
 & \left. \begin{aligned}
 & \tan^3 \theta_n \left( - \sum_{(d,y) \in D_f} \hat{f}_{n-1}(d,y) \cos nd' \sum_{(d,y) \in D_f} \sin nd' \cos nd' \right) \\
 & + \tan^2 \theta_n \left( - \sum_{(d,y) \in D_f} \hat{f}_{n-1}(d,y) \sin nd' \sum_{(d,y) \in D_f} \sin nd' \cos nd' \right. \\
 & \quad \left. + \sum_{(d,y) \in D_f} \hat{f}_{n-1}(d,y) \cos nd' \sum_{(d,y) \in D_f} [\cos^2 nd' - \sin^2 nd'] \right) \\
 & + \tan \theta_n \left( \sum_{(d,y) \in D_f} \hat{f}_{n-1}(d,y) \cos nd' \sum_{(d,y) \in D_f} \sin nd' \cos nd' \right. \\
 & \quad \left. + \sum_{(d,y) \in D_f} \hat{f}_{n-1}(d,y) \sin nd' \sum_{(d,y) \in D_f} [\cos^2 nd' - \sin^2 nd'] \right) \\
 & + \sum_{(d,y) \in D_f} \hat{f}_{n-1}(d,y) \sin nd' \sum_{(d,y) \in D_f} \sin nd' \cos nd'
 \end{aligned} \right\} \\
 = & \left\{ \begin{aligned}
 & \tan^3 \theta_n \left( - \sum_{(d,y) \in D_f} \hat{f}_{n-1}(d,y) \sin nd' \sum_{(d,y) \in D_f} \cos^2 nd' \right) \\
 & + \tan^2 \theta_n \left( \sum_{(d,y) \in D_f} \hat{f}_{n-1}(d,y) \cos nd' \sum_{(d,y) \in D_f} \cos^2 nd' \right. \\
 & \quad \left. - 2 \sum_{(d,y) \in D_f} \hat{f}_{n-1}(d,y) \sin nd' \sum_{(d,y) \in D_f} \sin nd' \cos nd' \right) \\
 & + \tan \theta_n \left( 2 \sum_{(d,y) \in D_f} \hat{f}_{n-1}(d,y) \cos nd' \sum_{(d,y) \in D_f} \sin nd' \cos nd' - \sum_{(d,y) \in D_f} \hat{f}_{n-1}(d,y) \sin nd' \sum_{(d,y) \in D_f} \sin^2 nd' \right) \\
 & \sum_{(d,y) \in D_f} \hat{f}_{n-1}(d,y) \cos nd' \sum_{(d,y) \in D_f} \sin^2 nd'
 \end{aligned} \right\}
 \end{aligned}$$

(Eq. F-33)

$$\left. \begin{aligned}
& \tan^3 \theta_n \left( \begin{array}{l} \sum_{(d,y) \in D_f} \hat{f}_{n-1}(d,y) \sin nd' \quad \sum_{(d,y) \in D_f} \cos^2 nd' \\ - \sum_{(d,y) \in D_f} \hat{f}_{n-1}(d,y) \cos nd' \quad \sum_{(d,y) \in D_f} \sin nd' \cos nd' \end{array} \right) \\
& + \tan^2 \theta_n \left( \begin{array}{l} \sum_{(d,y) \in D_f} \hat{f}_{n-1}(d,y) \sin nd' \quad \sum_{(d,y) \in D_f} \sin nd' \cos nd' \\ - \sum_{(d,y) \in D_f} \hat{f}_{n-1}(d,y) \cos nd' \quad \sum_{(d,y) \in D_f} \sin^2 nd' \end{array} \right) \\
& + \tan \theta_n \left( \begin{array}{l} \sum_{(d,y) \in D_f} \hat{f}_{n-1}(d,y) \sin nd' \quad \sum_{(d,y) \in D_f} \cos^2 nd' \\ - \sum_{(d,y) \in D_f} \hat{f}_{n-1}(d,y) \cos nd' \quad \sum_{(d,y) \in D_f} \sin nd' \cos nd' \end{array} \right) \\
& + \sum_{(d,y) \in D_f} \hat{f}_{n-1}(d,y) \sin nd' \quad \sum_{(d,y) \in D_f} \sin nd' \cos nd' - \sum_{(d,y) \in D_f} \hat{f}_{n-1}(d,y) \cos nd' \quad \sum_{(d,y) \in D_f} \sin^2 nd'
\end{aligned} \right\} = 0$$

(Eq. F-34)

The left-hand side has a factor of  $(1 + \tan^2 \theta_n)$  because that factor must be greater than zero.

$$\left. \begin{aligned}
& \tan \theta_n \left( \begin{array}{l} \sum_{(d,y) \in D_f} \hat{f}_{n-1}(d,y) \sin nd' \quad \sum_{(d,y) \in D_f} \cos^2 nd' - \sum_{(d,y) \in D_f} \hat{f}_{n-1}(d,y) \cos nd' \quad \sum_{(d,y) \in D_f} \sin nd' \cos nd' \end{array} \right) \\
& + \sum_{(d,y) \in D_f} \hat{f}_{n-1}(d,y) \sin nd' \quad \sum_{(d,y) \in D_f} \sin nd' \cos nd' - \sum_{(d,y) \in D_f} \hat{f}_{n-1}(d,y) \cos nd' \quad \sum_{(d,y) \in D_f} \sin^2 nd'
\end{aligned} \right\} = 0$$

(Eq. F-35)

$$\theta_n = \arctan \left[ \frac{\sum_{(d,y) \in D_f} \hat{f}_{n-1}(d,y) \cos nd' \quad \sum_{(d,y) \in D_f} \sin^2 nd' - \sum_{(d,y) \in D_f} \hat{f}_{n-1}(d,y) \sin nd' \quad \sum_{(d,y) \in D_f} \sin nd' \cos nd'}{\sum_{(d,y) \in D_f} \hat{f}_{n-1}(d,y) \sin nd' \quad \sum_{(d,y) \in D_f} \cos^2 nd' - \sum_{(d,y) \in D_f} \hat{f}_{n-1}(d,y) \cos nd' \quad \sum_{(d,y) \in D_f} \sin nd' \cos nd'} \right]$$

(Eq. F-36)

Notice that if the observations were uniformly distributed, Equation F-36 would have the form of Equation F-9.

### F1.1.3 Implementation Notes

The treatment of leap year data follows the suggestion of Woolhiser and Pegram (1979 [DIRS 176108], p. 36). A year of observations begins on March 1 ( $d=1$ ). The previous day ( $d=0$ ) is the last day of February, whether the 28th or 29th. Thus, the estimation does not use observations on February 29th, except for defining the Markov probability to which the March 1

observation applies. A year qualifies for inclusion in the set of observations only if data are available from the last day of February through February 28.

Note that the arctan function can take either of two values over a range of  $2\pi$ . In this case, the choice of  $\theta_n$  determines the sign of  $b_n$ . That is,

$$b_n \sin(\theta_n + nd') = -b_n \sin(\theta_n \pm \pi + nd') \quad (\text{Eq. F-37})$$

If the coefficients estimated from two similar sets of data seem to be quite different, it may be that one set should be adjusted in accordance with Equation F-37.

#### F1.1.4 Precipitation Frequency and Mean Annual Precipitation

The probability that day  $d$  is dry is:

$$p_d(d) = p_{00}(d)p_d(d-1) + p_{10}(d)[1 - p_d(d-1)] \quad (\text{Eq. F-38})$$

Because  $p_{00}$  and  $p_{10}$  change slowly from one day to the next, their values for one day are approximately the same as for the previous day. Therefore,  $p_d(d-1)$  is approximately the same as  $p_d(d)$ , so:

$$p_d(d) \cong p_{00}(d)p_d(d) + p_{10}(d)[1 - p_d(d)] \quad (\text{Eq. F-39})$$

(

$$p_d(d) \cong p_{10}(d)/[1 - p_{00}(d) + p_{10}(d)] \quad (\text{Eq. F-40})$$

Making the further approximation of replacing each parameter with its mean value over the year, the fraction of days that are wet is approximately:

$$f_w \cong [1 - \frac{a_{10}}{1 - a_{00} + a_{10}}] = \frac{1 - a_{00}}{1 - a_{00} + a_{10}} \quad (\text{Eq. F-41})$$

The expected mean annual precipitation (MAP) is:

$$MAP \cong 365 f_w a_\lambda \quad (\text{Eq. F-42})$$

## F1.2 PARAMATERIZATION OF TEMPERATURE RECORDS

Output DTN: SN0608T0502206.019 contains MathCAD files for the calculation of parameters to best-fit daily temperature data as a function of day of year, using a least-squares approach. There are four temperature models, one each for minimum temperature on wet days, minimum temperature on dry days, maximum temperature on wet days, and maximum temperature on dry days. Each temperature model is in the form of a sine function described by three parameters,  $\alpha$ ,

$\beta$ , and  $\gamma$ , representing respectively the magnitude of the first-order term, the phase of the first-order term, and the zero-order term, as follows:

$$T_{wet\_min} = \alpha_{wet\_min} \sin\left(\frac{x - \beta_{wet\_min}}{365/2\pi}\right) + \gamma_{wet\_min} \quad (\text{Eq. F-43})$$

$$T_{dry\_min} = \alpha_{dry\_min} \sin\left(\frac{x - \beta_{dry\_min}}{365/2\pi}\right) + \gamma_{dry\_min} \quad (\text{Eq. F-44})$$

$$T_{wet\_max} = \alpha_{wet\_max} \sin\left(\frac{x - \beta_{wet\_max}}{365/2\pi}\right) + \gamma_{wet\_max} \quad (\text{Eq. F-45})$$

$$T_{dry\_max} = \alpha_{dry\_max} \sin\left(\frac{x - \beta_{dry\_max}}{365/2\pi}\right) + \gamma_{dry\_max} \quad (\text{Eq. F-46})$$

The parameters for this model have the following significance:

- $x$  is the day of year from 1 to 365 (January 1 through December 31; February 29 on leap years is ignored).
- $\alpha$  represents half the annual difference in temperature (minimum or maximum) between summer and winter values, according to the model. It is the amplitude of the sine function and is in units of temperature.
- $\beta$  represents the calendar day of the year (DOY) when the model temperature is rising and passes through its central value.
- $\gamma$  is the mean value for the temperature, according to the model.

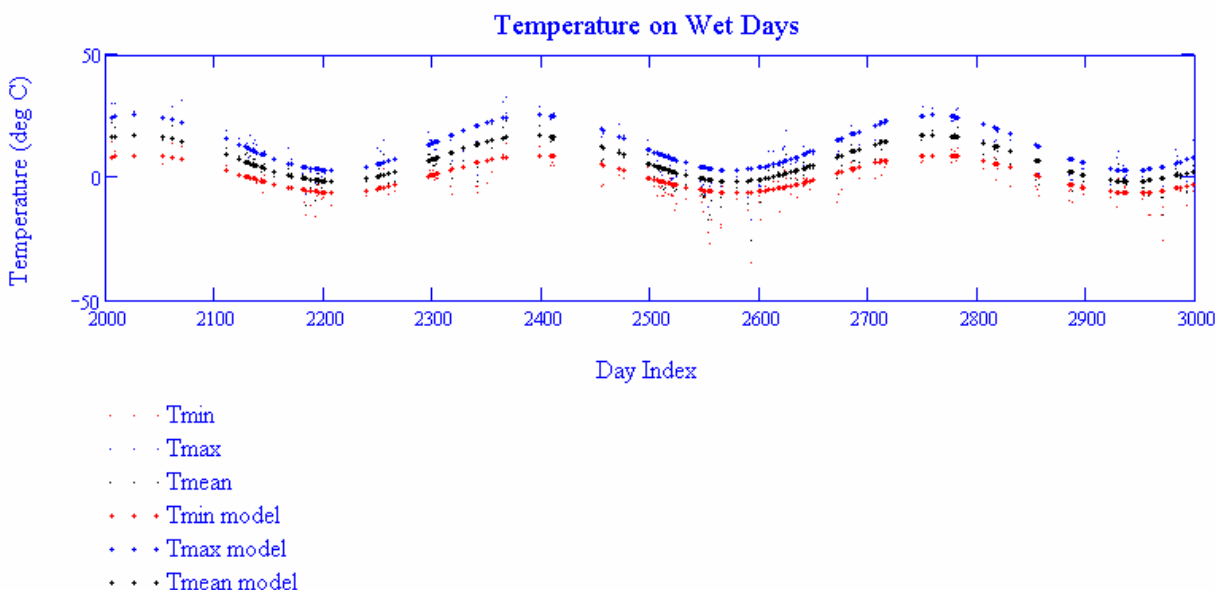
MathCAD routines were developed to organize the proxy climate site temperature data, including daily minima and maxima. Temperature records were organized by wet days and dry days for each of the proxy sites. For each meteorological station and each temperature model, the DTN includes derivation of values for  $\alpha$ ,  $\beta$ , and  $\gamma$  to best fit the minimum and maximum temperatures as a function of day of year using a least-squares approach. The three parameters are the result of applying the MathCAD function *minerr* to minimize the sum of the squares of the differences between the measured temperatures and the model temperatures.

As in the precipitation analysis, there are multiple equivalent solutions for the three parameters, with the values for the  $\beta$  parameter separated by half of a year and with the  $\alpha$  parameter alternating between positive and negative. However, because all of the proxy sites are in the temperate region of the Northern hemisphere, the functions are very similar, and the initial values could be chosen such that the calculated values of the  $\beta$  parameter would all fall near DOY 115. The initial for  $\alpha$ ,  $\beta$ , and  $\gamma$  were 20°C, DOY 80, and 30°C, respectively.

Unlike the precipitation analysis, this procedure generates parameters that are not stochastic. In this temperature model, the temperature extremes depend only on the day of the year and whether or not there is precipitation on that day.

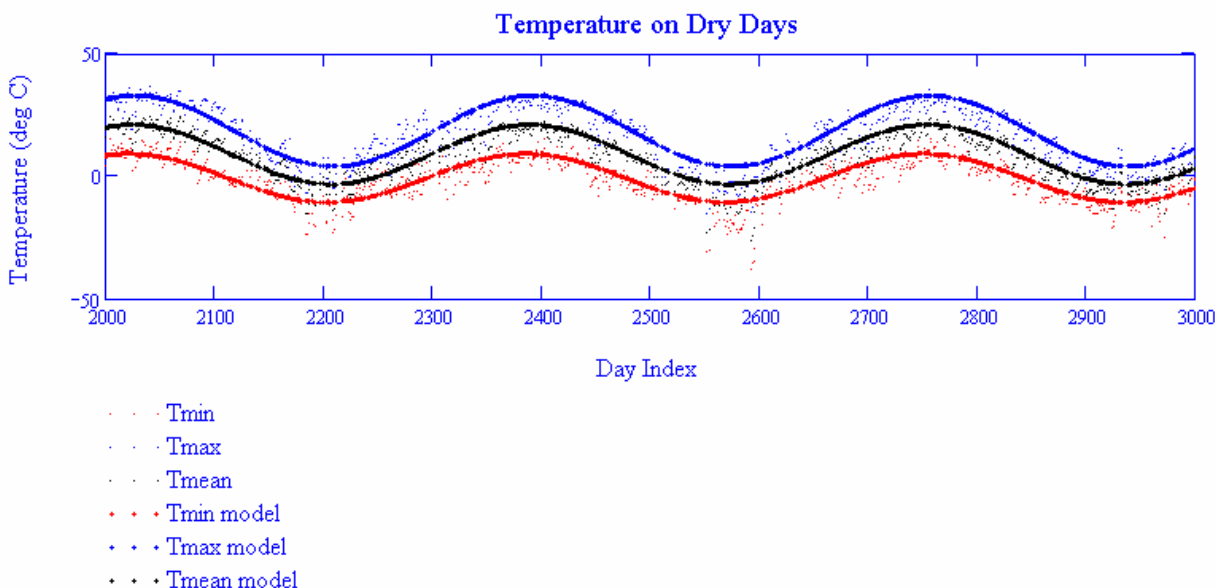
There is another aspect in which this analysis differs slightly from that of the precipitation analysis in Section F1.1. That analysis determined each zero-order term as the mean of its data, then the higher-order terms were developed without modifying the lower-order terms. This temperature analysis solves for the zero-order and first-order terms simultaneously. Therefore, although the zero-order term is the mean annual temperature (MAT) for the model, it may not be exactly the mean of the data. Nevertheless, the MathCAD application estimates the standard uncertainty for each zero-order term by making the same calculation that would be used for the standard error using the  $\gamma$  parameter in lieu of the mean of the data.

As an example of the results of this analysis, Figure F-1 shows the modeled and measured temperature extremes for wet days in the record for Beowawe, Nevada. Modeled versus measured temperatures for recorded dry days are shown in Figure F-2. The modeled temperatures do apply to all days of the year, not just those for which the record has applicable data. Similar figures for each of the proxy sites are contained in Output DTN: SN0608T0502206.019.



Source: Output DTN: SN0608T0502206.019.

Figure F-1. Model versus Measured Temperatures for Wet Days, Beowawe, Nevada



Source: Output DTN: SN0608T0502206.019.

Figure F-2. Model versus Measured Temperatures for Dry Days, Beowawe, Nevada

Applying the approximations of F1.1.4, the MAT is approximately

$$MAT = \frac{a_{10}}{1 - a_{00} + a_{10}} \frac{\gamma_{dry_{min}} + \gamma_{dry_{min}}}{2} + \frac{1 - a_{00}}{1 - a_{00} + a_{10}} \frac{\gamma_{wet_{min}} + \gamma_{wet_{min}}}{2} \quad (\text{Eq. F-47})$$

## F2. PARAMETERS FOR REPRESENTATIVE METEOROLOGICAL STATIONS

Data from ten site and regional meteorological stations, representing the range of weather anticipated during the remainder of the Present-Day climate, have been qualified in an analysis report (BSC 2006 [DIRS 177081]).

### F2.1 STATIONS REPRESENTING THE PRESENT-DAY CLIMATE

DTNs: SN0601PRECPTMP.002 [DIRS 176122] and SN0608WEATHER1.005 [DIRS 177912] comprise the qualified precipitation records from the ten representative stations. Output DTN: SN0609T0502206.023 contains the Excel workbooks that performed the Fourier analyses of the ten precipitation records. Tables F-1 and F-2 report results of these analyses. The phase parameters are rounded to one hundredth of a radian (about half a day); the remaining parameters are rounded to a level of precision consistent with the standard error. Although the subsequent analysis omits second-order terms, these two tables provide their magnitudes ( $b_{00,2}$ ,  $b_{10,2}$ , etc.).

Equations F-41 and F-42 provide a method for calculating the approximate MAP implied by the zero-order coefficients. For corroboration of the analyses, Table F-2a compares the MAP implied by the coefficients with the actual MAP at each station. In each case, the MAPs agree to within 10%.

Table F-1. Fourier Parameters for  $p_{00}$  and  $p_{10}$  at Stations Representing the Present-Day Climate

Station	Station Elevation (m)	$a_{00}$	$a_{00}$ Standard Error	$b_{00,1}$	$\theta_{00,1}$ (Radians)	$b_{00,2}$	$a_{10}$	$a_{10}$ Standard Error	$b_{10,1}$	$\theta_{10,1}$ (Radians)	$b_{10,2}$
4JA	1,043	0.939	0.002	0.024	-1.26	0.010	0.621	0.013	0.043	-1.24	0.067
40 MN	1,469	0.929	0.002	0.022	-1.43	0.012	0.514	0.011	0.046	-1.36	0.059
A12	2,283	0.911	0.003	0.025	-1.35	-0.015	0.504	0.011	0.026	-1.54	0.052
Amargosa Farms	747	0.955	0.002	0.023	-1.17	0.016	0.661	0.019	-0.039	+0.53	0.069
Cane Spring	1,219	0.934	0.002	0.028	-1.24	0.013	0.582	0.013	0.052	-1.34	0.072
YM Site 1	1,143	0.937	0.004	0.031	-1.20	-0.009	0.66	0.03	0.09	-1.48	0.09
YM Site 2	1,478	0.941	0.004	0.025	-1.30	0.015	0.60	0.03	0.10	-1.44	0.06
YM Site 3	1,279	0.937	0.004	0.029	-1.39	0.011	0.61	0.02	0.06	-1.42	0.05
YM Site 6	1,315	0.937	0.004	0.030	-1.34	0.017	0.63	0.02	0.06	-1.29	0.06
YM Site 9	838	0.947	0.004	0.031	-1.39	-0.006	0.67	0.03	-0.10	+1.47	-0.06

Source: Output DTN: SN0609T0502206.023.

Table F-2. Fourier Parameters for  $\lambda$  and  $m$  at Stations Representing the Present-Day Climate

Station	$a_{\lambda}$ (mm)	$a_{\lambda}$ Standard Error (mm)	$b_{\lambda,1}$ (mm)	$\theta_{\lambda,1}$ (Radians)	$b_{\lambda,2}$ (mm)	$a_m$ (mm)	$a_m$ Standard Error (ln mm)	$b_{m,1}$ (ln mm)	$\theta_{m,1}$ (Radians)	$b_{m,2}$ (ln mm)
4JA	4.42	0.17	-0.75	-0.38	-0.88	0.64	0.04	-0.22	-0.40	-0.16
40 MN	4.68	0.16	-0.54	+0.81	-0.99	0.68	0.03	-0.10	+0.04	-0.16
A12	5.75	0.17	-0.90	-0.64	-1.22	0.92	0.03	-0.19	-0.82	-0.15
Amargosa Farms	5.1	0.3	-0.3	-0.80	-1.1	0.90	0.05	-0.15	-0.84	-0.15
Cane Spring	5.3	0.2	-0.8	-0.36	-1.1	0.82	0.04	-0.17	-0.52	-0.20
YM Site 1	4.9	0.4	-0.8	-0.71	-1.3	0.71	0.08	-0.16	-1.04	-0.20
YM Site 2	5.4	0.4	0.6	+1.46	-1.03	0.85	0.07	-0.10	-1.31	0.20
YM Site 3	5.7	0.4	-0.8	-1.07	-1.49	0.90	0.07	-0.12	-0.91	-0.28
YM Site 6	5.9	0.4	-1.1	-1.27	-1.15	0.95	0.07	-0.10	-0.93	0.26
YM Site 9	3.7	0.3	-0.6	-0.49	-0.62	0.48	0.08	-0.20	-0.36	-0.13

Source: Output DTN: SN0609T0502206.023.

Table F-2a. Mean Annual Precipitation at Site and Regional Stations Compared with Values Implied by Fourier Coefficients

Meteorological Station	Station Elevation (m)	Measured MAP (mm)	MAP Implied by Coefficients (mm)	Years Used for Fourier Analysis (Mar. 1 to Feb. 28)
Amargosa Farms	747	$1.1 \times 10^2$	$1.2 \times 10^2$	26 years: 1968, 1969, 1979 to 2000, 2002, 2003
YM Site 9	838	$1.1 \times 10^2$	$1.0 \times 10^2$	11 years: 1993 to 2003
4JA	1,043	$1.4 \times 10^2$	$1.4 \times 10^2$	45 years: 1959 to 2003
YM Site 1	1,143	$1.8 \times 10^2$	$1.6 \times 10^2$	10 years: 1993 to 1998, 2000 to 2003
Cane Spring	1,219	$2.0 \times 10^2$	$2.0 \times 10^2$	39 years: 1965 to 2003
YM Site 3	1,279	$2.1 \times 10^2$	$1.9 \times 10^2$	11 years: 1993 to 2003

Table F-2a. Mean Annual Precipitation at Site and Regional Stations Compared with Values Implied by Fourier Coefficients (Continued)

YM Site 6	1,315	$2.1 \times 10^2$	$2.0 \times 10^2$	11 years: 1993 to 2003
40 MN	1,469	$2.1 \times 10^2$	$2.1 \times 10^2$	43 years: 1961 to 2003
YM Site 2	1,478	$1.9 \times 10^2$	$1.8 \times 10^2$	11 years: 1993 to 2003
A12	2,283	$3.2 \times 10^2$	$3.1 \times 10^2$	41 years: 1960 to 1994, 1998 to 2003

Source: BSC 2006 [DIRS 177081], Table 6.1.4; Section 6.2.5.1 (Measured MAPs); from Equations F-41 and F-42, using values from Tables F-1 and F-2 (Implied MAPs); Output DTN: SN0609T0502206.023 (Elevations and data years).

Adjustment to an elevation of 1524 m requires a lapse rate for each first-order precipitation parameter. For each station, Table F-3 shows its elevation and each first-order parameter, with parameter lapse rates and uncertainties calculated by the Excel function LINEST.

Generally, the frequency of dry days decreases with elevation and the average wet-day precipitation increases with elevation. However, the MASSIF model makes the approximation that all elevations have wet or dry days when the top of the mountain has a wet or dry day. Therefore, total annual precipitation is adjusted for elevation using an input lapse rate. Table F-3 includes the expected MAP for each station, calculated in accordance with Equation F-42, and a precipitation lapse rate and uncertainty calculated by the Excel function LINEST. The table also shows the MAP extrapolated to 1,524 m with the Excel function FORECAST and the precipitation lapse rate expressed as a percentage of the extrapolated value. Thus, the nominal precipitation lapse rate is equal to 134 mm/km divided by 213 mm, which gives 6.3%/100 m. The standard error on this lapse rate is calculated by dividing the standard error on the slope (14 mm/km) by 213 mm, which gives 0.7%/100 m.

Table F-3. Lapse Rates for Parameters of the Present-Day Climate

Station	Station Elevation (m)	$a_{00}$	$a_{10}$	$a_{\lambda}$ (mm)	$a_m$ (ln mm)	Elevation in 100s of Meters	Expected MAP (mm)
4JA	1,043	0.939	0.621	4.42	0.64	10.43	144
40 MN	1,469	0.929	0.514	4.68	0.68	14.69	207
A12	2,283	0.911	0.504	5.75	0.92	22.83	315
Amargosa Farms	747	0.955	0.661	5.1	0.90	7.47	119
Cane Spring	1,219	0.934	0.582	5.3	0.82	12.19	197
YM Site 1	1,143	0.937	0.66	4.9	0.71	11.43	156
YM Site 2	1,478	0.941	0.60	5.4	0.85	14.78	176



Table F-3. Lapse Rates for Parameters of the Present-Day Climate (Continued)

Station	Station Elevation (m)	$a_{00}$	$a_{10}$	$a_{\lambda}$ (mm)	$a_m$ (ln mm)	Elevation in 100s of Meters	Expected MAP (mm)
YM Site 3	1,279	0.937	0.61	5.7	0.90	12.79	195
YM Site 6	1,315	0.937	0.63	5.9	0.95	13.15	196
YM Site 9	838	0.947	0.67	3.7	0.03	8.38	99
Lapse Rate		-0.025 $\pm 0.004$ /km	-0.11 $\pm 0.03$ /km	0.9 $\pm 0.5$ mm/km	0.15 $\pm 0.14$ mm/km		134 $\pm 14$ mm/km
Extrapolated	1,524						213 mm
Percentage Lapse Rate							6.3 $\pm 0.7$ %/100m

NOTE: Data for stations is from Tables F-1 and F-2, except last column calculated using Equations F-41 and F-42. Lapse rates and their uncertainties are  $m$  and  $se1$ , calculated with the Excel function LINEST by setting the *known\_y's* to the station values and the *known\_x's* to station elevations. Extrapolated MAP calculated with the Excel function FORECAST by setting  $x$  to 1524 m, the *known\_y's* to station values of MAP (mm) and the *known\_x's* to station elevations. Percentage lapse rate for MAP calculated by dividing lapse rate and uncertainty by extrapolated MAP and dividing by ten to convert from km to 100 m (and multiplying by one hundred to get percentage).

In order to avoid exaggerating the range of uncertainty of each parameter, this section adjusts the values from the various stations to make them comparable. This is particularly necessary for the first-order terms, which have multiple equivalent forms, separated in phase by  $\pi$ . In Tables F-1 and F-2, some of the coefficients of the first-order terms ( $b_{00}$  and  $b_{10}$ ) are negative. Tables F-4 and F-5 include adjustment of the first-order terms in accordance with Equation F-37, so that all of the coefficients are positive. In some cases, the phase has been adjusted by  $2\pi$  to bring it closer to the adjusted phase values at other stations. The phases of the first-order terms correspond to relatively more winter than summer precipitation.

Tables F-4 and F-5 also include adjustment of the zero-order terms ( $a_{00}$  and  $a_{10}$ ) to the reference elevation of 5,000 ft (1,524 m), using lapse rates from Table F-3. The following equation was used for adjusting values to the reference elevation:

$$\text{adjusted value} = \text{initial value} + (\text{ref elev} - \text{stn elev}) * \text{lapse rate} \quad (\text{Eq. F-48})$$

where *ref elev* is the reference elevation of 5,000 ft (1,524 m), *stn elev* is the elevation for the station where the initial value was based, and *lapse rate* is the value from Table F-3.

Almost every summary value in Table F-4 or F-5 is used in Section F3.1 either directly in a parameter uncertainty distribution or indirectly in selecting a distribution. The parameters in the last line of each table are used in Section F3.2 to represent the lower bound of the Monsoon climate.

Table F-6 provides two additional properties for each station. One is the probability of a wet day, adjusted to the top of the mountain, calculated in accordance with Equation F-39, and rounded to the nearest 1%. The other is the adjusted value for MAP (Equation F-40). After adjustment to the top of the mountain, the range of MAP is about 170 to 250 mm, with only relatively short records falling below 190 mm.

Table F-4. Parameters for  $p_{00}$  and  $p_{10}$  at Stations Representing the Present-Day Climate Adjusted to an Elevation of 1,524 m

Station	Station Elevation (m)	$a_{00}$ <sup>a</sup>	$a_{00}$ Standard Error <sup>b</sup>	$b_{00,1}$ <sup>b</sup>	$\theta_{00,1}$ (Radians) <sup>b</sup>	$a_{10}$ <sup>a</sup>	$a_{10}$ Standard Error <sup>b</sup>	$b_{10,1}$ <sup>b</sup>	$\theta_{10,1}$ (Radians) <sup>b</sup>
4JA	1,043	0.927	0.002	0.024	-1.26	0.568	0.013	0.043	-1.24
40 MN	1,469	0.928	0.002	0.022	-1.43	0.508	0.011	0.046	-1.36
A12	2,283	0.930	0.003	0.025	-1.35	0.587	0.011	0.026	-1.54
Amargosa Farms	747	0.936	0.002	0.023	-1.17	0.576	0.019	0.039 <sup>c</sup>	-2.61 <sup>c</sup>
Cane Spring	1,219	0.926	0.002	0.028	-1.24	0.548	0.013	0.052	-1.34
YM Site 1	1,143	0.927	0.004	0.031	-1.20	0.62	0.03	0.09	-1.48
YM Site 2	1,478	0.940	0.004	0.025	-1.30	0.60	0.03	0.10	-1.44
YM Site 3	1,279	0.931	0.004	0.029	-1.39	0.58	0.02	0.06	-1.42
YM Site 6	1,315	0.932	0.004	0.030	-1.34	0.61	0.02	0.06	-1.29
YM Site 9	838	0.930	0.004	0.031	-1.39	0.59	0.03	0.10 <sup>c</sup>	-1.67 <sup>c</sup>
Mean		0.931		0.027	-1.31	0.58		0.06	-1.5
Standard Deviation		0.004		0.003	0.09	0.03		0.03	0.4
Minimum After Subtracting One Standard Error		0.924				0.50			
Maximum After Adding One Standard Error		0.944				0.65			
Maximum Plus One Standard Deviation				0.034				0.13	

<sup>a</sup> From Table F-1, adjusted in accordance with Equation F-48.<sup>b</sup> From Table F-1, except as noted.<sup>c</sup> Sign changed on  $b$ , and  $\theta$  shifted by  $\pi$ .Table F-5. Parameters for  $\lambda$  and  $m$  at Stations Representing the Present-Day Climate Adjusted to an Elevation of 1,524 m

Station	Station Elevation (m)	$a_\lambda$ (mm) <sup>a</sup>	$a_\lambda$ Standard Error (mm) <sup>b</sup>	$b_{\lambda,1}$ (mm) <sup>b</sup>	$\theta_{\lambda,1}$ (Radians) <sup>b</sup>	$a_m$ (ln mm) <sup>a</sup>	$a_m$ Standard Error (ln mm) <sup>b</sup>	$b_m$ (ln mm) <sup>b</sup>	$\theta_{m,1}$ (Radians) <sup>b</sup>
4JA	1,043	4.85	0.17	0.75 <sup>c</sup>	+2.76 <sup>c</sup>	0.71	0.04	0.22 <sup>c</sup>	+2.74 <sup>c</sup>
40 MN	1,469	4.73	0.16	0.54 <sup>c</sup>	+3.95 <sup>c</sup>	0.69	0.03	0.10 <sup>c</sup>	+3.18 <sup>c</sup>
A12	2,283	5.07	0.17	0.90 <sup>c</sup>	+2.50 <sup>c</sup>	0.80	0.03	0.19 <sup>c</sup>	+2.32 <sup>c</sup>
Amargosa Farms	747	5.8	0.3	0.3 <sup>c</sup>	+2.34 <sup>c</sup>	1.02	0.05	0.15 <sup>c</sup>	+2.30 <sup>c</sup>
Cane Spring	1,219	5.6	0.2	0.8 <sup>c</sup>	+2.78 <sup>c</sup>	0.87	0.04	0.17 <sup>c</sup>	+2.62 <sup>c</sup>
YM Site 1	1,143	5.2	0.4	0.8 <sup>c</sup>	+2.43 <sup>c</sup>	0.77	0.08	0.16 <sup>c</sup>	+2.10 <sup>c</sup>
YM Site 2	1,478	5.4	0.4	0.6	+1.46	0.86	0.07	0.10 <sup>c</sup>	+1.83 <sup>c</sup>
YM Site 3	1,279	5.9	0.4	0.8 <sup>c</sup>	+2.07 <sup>c</sup>	0.94	0.07	0.12 <sup>c</sup>	+2.23 <sup>c</sup>

Table F-5. Parameters for  $\lambda$  and  $m$  at Stations Representing the Present-Day Climate Adjusted to an Elevation of 1,524 m (Continued)

Station	Station Elevation (m)	$a_\lambda$ (mm) <sup>a</sup>	$a_\lambda$ Standard Error (mm) <sup>b</sup>	$b_{\lambda,1}$ (mm) <sup>b</sup>	$\theta_{\lambda,1}$ (Radians) <sup>b</sup>	$a_m$ (ln mm) <sup>a</sup>	$a_m$ Standard Error (ln mm) <sup>b</sup>	$b_m$ (ln mm) <sup>b</sup>	$\theta_{m,1}$ (Radians) <sup>b</sup>
YM Site 6	1,315	6.1	0.4	1.1 <sup>c</sup>	+1.87 <sup>c</sup>	0.98	0.07	0.10 <sup>c</sup>	+2.21 <sup>c</sup>
YM Site 9	838	4.3	0.3	0.6 <sup>c</sup>	+2.65 <sup>c</sup>	0.58	0.08	0.20 <sup>c</sup>	+2.78 <sup>c</sup>
Mean		5.3		0.7	+2.5	0.82		0.15	+2.4
Standard Deviation		0.6		0.2	0.7	0.14		0.04	0.4
Minimum After Subtracting One Standard Error		4.0				0.50			
Maximum After Adding One Standard Error		6.5				1.07			
Maximum Plus One Standard Deviation				1.3				0.26	

<sup>a</sup> From Table F-2, adjusted in accordance with Equation F-48.

<sup>b</sup> From Table F-2, except as noted.

<sup>c</sup> Sign changed on  $b$ , and  $\theta$  shifted by  $\pi$ .

Table F-6. Wet Day Fraction and Mean Annual Precipitation Implied by Parameters Adjusted to an Elevation of 1,524 –m

Meteorological Station	Fraction of Days that are Wet, $f_w$ (%)	Adjusted MAP (mm)	Years Used for Fourier Analysis (Mar. 1 to Feb. 28)
4JA	11	$1.9 \times 10^2$	45 years: 1959 to 2003
40 MN	12	$2.1 \times 10^2$	43 years: 1961 to 2003
A12	11	$2.0 \times 10^2$	41 years: 1960 to 1994, 1998 to 2003
Amargosa Farms	10	$2.1 \times 10^2$	26 years: 1968, 1969, 1979 to 2000, 2002, 2003
Cane Spring	12	$2.5 \times 10^2$	39 years: 1965 to 2003
YM Site 1	11	$2.1 \times 10^2$	10 years: 1993 to 1998, 2000 to 2003
YM Site 2	9	$1.8 \times 10^2$	11 years: 1993 to 2003
YM Site 3	11	$2.4 \times 10^2$	11 years: 1993 to 2003
YM Site 6	10	$2.2 \times 10^2$	11 years: 1993 to 2003
YM Site 9	11	$1.7 \times 10^2$	11 years: 1993 to 2003

NOTE:  $f_w$  and MAP from Equations F-41 and F-42, using values from Tables F-4 and F-5. Data years from Output DTN: SN0609T0502206.023.

DTN: SN0608WEATHER1.005 [DIRS 177912] contains the qualified temperature records from the Yucca Mountain meteorological stations. Excel files in Output DTN: SN0608T0502206.019 contain temperature records extracted for Yucca Mountain Sites 1, 2, 3, and 6. The output DTN also contains the MathCAD workbooks that analyzed the four temperature records. Tables F-7 and F-8 report the results of these analyses. The phase parameters are rounded to the nearest day; the remaining parameters are rounded to 0.1°C.

Section F3 uses the ranges of these coefficients as a guide to the uncertainty distributions for the Present-Day climate and for the Monsoon climate. For ease of reference, Tables F-7 and F-8 show the minimum and maximum values for each of the coefficients of the first-order terms.

Table F-7. Fourier Parameters for Wet Day Temperatures at Stations Representing the Present-Day Climate

Station	$\gamma_{wet_{min}}$ (°C)	$\gamma_{wet_{min}}$ Standard Error (°C)	$\alpha_{wet_{min}}$ (°C)	$\beta_{wet_{min}}$ (DOY)	$\gamma_{wet_{max}}$ (°C)	$\gamma_{wet_{max}}$ Standard Error (°C)	$\alpha_{wet_{max}}$ (°C)	$\beta_{wet_{max}}$ (DOY)
YM Site 1	9.2	0.4	9.0	123	18.3	0.5	12.0	118
YM Site 2	8.2	0.4	9.6	124	15.8	0.5	12.4	117
YM Site 3	9.0	0.4	9.0	122	16.9	0.5	12.1	117
YM Site 6	7.9	0.4	8.6	121	16.5	0.5	11.8	116
Minimum			8.6	121			11.8	116
Maximum			9.6	124			12.4	118

Source: Output DTN: SN0608T0502206.019; folder Present-Day-Temperature; files BSC1\_parameters, BSC2\_parameters, BSC3\_parameters, and BSC6\_parameters.

Table F-8. Fourier Parameters for Dry Day Temperatures at Stations Representing the Present-Day Climate

Station	$\gamma_{dry_{min}}$ (°C)	$\gamma_{dry_{min}}$ Standard Error (°C)	$\alpha_{dry_{min}}$ (°C)	$\beta_{dry_{min}}$ (DOY)	$\gamma_{dry_{max}}$ (°C)	$\gamma_{dry_{max}}$ Standard Error (°C)	$\alpha_{dry_{max}}$ (°C)	$\beta_{dry_{max}}$ (DOY)
YM Site 1	10.8	0.1	10.0	114	23.3	0.2	12.0	110
YM Site 2	12.2	0.1	10.0	116	21.0	0.2	12.4	109
YM Site 3	11.6	0.1	9.9	114	21.8	0.2	12.0	110
YM Site 6	9.1	0.1	9.4	114	21.6	0.1	11.9	110
Minimum			9.4	114			11.9	109
Maximum			10.0	116			12.4	110

Source: Output DTN: SN0608T0502206.019; folder Present-Day-Temperature; files BSC1\_parameters, BSC2\_parameters, BSC3\_parameters, and BSC6\_parameters.

Before comparing the zero-order coefficients, they are adjusted to an elevation of 1,524 m using a temperature lapse rate of  $-10^{\circ}\text{C}/\text{km}$  (dry lapse rate from Maidment (1993 [DIRS 125317], p. 3.3)), as shown in Table F-9. That table also shows the minimum and maximum of these adjusted zero-order coefficients extended by one standard error in each direction.

Table F-9. Zero-Order Temperature Parameters for Stations Representing the Present-Day Adjusted to an Elevation of 1,524 m

Station	Station Elevation (m)	$\gamma_{wet,min}$ (°C)	$\gamma_{wet,max}$ (°C)	$\gamma_{dry,min}$ (°C)	$\gamma_{dry,max}$ (°C)
YM Site 1	1,143	5.4	14.5	7.0	19.5
YM Site 2	1,478	7.7	15.3	11.7	20.5
YM Site 3	1,279	6.6	14.5	9.2	19.4
YM Site 6	1,315	5.8	14.4	7.0	19.5
Minimum Less One Standard Error		5.0	13.9	6.9	19.2
Maximum Plus One Standard Error		8.1	15.8	11.8	20.7

NOTE: Values from Tables F-7 and F-8, adjusted in accordance with Equation F-48, using a lapse rate of  $-10^{\circ}\text{C}/\text{km}$ .

## F.2.2 STATIONS REPRESENTING AN UPPER BOUND FOR THE MONSOON CLIMATE

*Future Climate Analysis* selected meteorological stations to represent lower and upper bounds of precipitation during the Monsoon climate, including multiple stations for each extreme in order to minimize local effects on the climate parameters (BSC 2004 [DIRS 170002], p. 6-50). The site and regional stations presented in Section F.2.1 represent the lower bound of Monsoon precipitation. For an upper bound, *Future Climate Analysis* selected meteorological stations at Hobbs, New Mexico, and Nogales, Arizona (DTN: GS000308315121.003 [DIRS 151139]).

DTN: SN0603DWEATHER.002 [DIRS 177917] contains the qualified precipitation records from the two stations. Output DTN: SN0609T0502206.023 contains the Excel workbooks that performed the Fourier analyses of the two precipitation records. Tables F-10 and F-11 report results of these analyses. The phase parameters are rounded to one hundredth of a radian (about half a day); the remaining parameters are rounded to a level of precision consistent with the standard error. For corroboration of the analyses, Table F-2a compares the MAP implied by the coefficients with the actual MAP at each of the two stations. In each case, the MAPs agree to within 3%.

Table F-10. Fourier Parameters for  $p_{00}$  and  $p_{10}$  at Stations Representing the Upper-Bound Monsoon Climate

Station	$a_{00}$	$a_{00}$ Standard Error	$b_{00,1}$	$\theta_{00,1}$ (Radians)	$b_{00,2}$	$a_{10}$	$a_{10}$ Standard Error	$b_{10,1}$	$\theta_{10,1}$ (Radians)	$b_{10,2}$
Hobbs	0.903	0.003	-0.042	-0.89	0.010	0.662	0.011	0.027	1.35	-0.020
Nogales	0.899	0.003	-0.059	-1.40	0.092	0.521	0.012	-0.069	-0.84	0.078

Source: Output DTN: SN0609T0502206.023.

Table F-11. Fourier Parameters for  $\lambda$  and  $m$  at Stations Representing the Upper-Bound Monsoon Climate

Station	$a_\lambda$ (mm)	$a_\lambda$ Standard Error (mm)	$b_{\lambda,1}$ (mm)	$\theta_{\lambda,1}$ (Radians)	$b_{\lambda,2}$ (mm)	$a_m$ (ln mm)	$a_m$ Standard Error (ln mm)	$b_{m,1}$ (ln mm)	$\theta_{m,1}$ (Radians)	$b_{m,2}$ (ln mm)
Hobbs	8.7	0.3	3.2	-1.09	1.2	1.28	0.03	0.36	-1.17	0.11
Nogales	7.1	0.2	-1.4	1.13	-0.3	1.24	0.03	-0.14	1.36	-0.11

Source: Output DTN: SN0609T0502206.023.

Table F-11a. Mean Annual Precipitation at Stations Representing the Upper-Bound Monsoon Climate Compared with Values Implied by Fourier Coefficients

Meteorological Station	Measured MAP (mm)	MAP Implied by Coefficients (mm)	Years Used for Fourier Analysis (Mar. 1 to Feb. 28)
Hobbs	$4.0 \times 10^2$	$4.1 \times 10^2$	37 years: 1952, 1954, 1955, 1957, 1959 to 1967, 1969 to 1980, 1982, 1983, 1985 to 1988, 1990, 1992 to 1994, 1996, 1998
Nogales	$4.2 \times 10^2$	$4.2 \times 10^2$	29 years: 1948, 1951, 1953 to 1958, 1960, 1962 to 1965, 1967 to 1982

Source: BSC 2006 [DIRS 177081], Section 6.3.5.1 (Measured MAPs); Equations F-41 and F-42 using values from Tables F-10 and F-11 (Implied MAPs); Output DTN: SN0609T0502206.023 (Data Years).

In Tables F-10 and F-11, some of the coefficients of the first-order terms ( $b_{00}$ ,  $b_{10}$ , etc.) are negative. Tables F-12 and F-13 include adjustment of the first-order terms in accordance with Equation F-35 so that all of the coefficients are positive. Because these stations were chosen for their values of temperature and MAP without consideration of their elevation, they each represent conditions at the reference Yucca Mountain elevation of 5,000 ft (1,524 m) and need no adjustment for elevation.

Tables F-12 and F-13 also contain the average of each parameter for the upper-bound stations. For the zero-order parameters, the tables show the wetter value, reflecting the larger number of wet days at Nogales and the greater precipitation per wet day at Hobbs.

Table F-12. Adjusted Parameters for  $p_{00}$  and  $p_{10}$  at Stations Representing the Upper-Bound Monsoon Climate

Station	$a_{00}$ <sup>a</sup>	$a_{00}$ Standard Error <sup>a</sup>	$b_{00,1}$ <sup>a</sup>	$\theta_{00,1}$ (Radians) <sup>a</sup>	$a_{10}$ <sup>a</sup>	$a_{10}$ Standard Error <sup>a</sup>	$b_{10,1}$ <sup>a</sup>	$\theta_{10,1}$ (Radians) <sup>a</sup>
Hobbs	0.903	0.003	0.042 <sup>b</sup>	2.25 <sup>b</sup>	0.662	0.011	0.027	1.35
Nogales	0.899	0.003	0.059 <sup>b</sup>	1.74 <sup>b</sup>	0.521	0.012	0.069 <sup>b</sup>	2.30 <sup>b</sup>
Average Upper Bound	0.901	0.003	0.050	2.0	0.59	0.012	0.05	1.8
Standard Deviation	0.003		0.012	0.4	0.10		0.03	0.7
Wetter Value	0.899				0.521			
Minimum After Subtracting One Standard Error	0.896				0.509			
Maximum After Adding One Standard Error	0.906				0.673			

<sup>a</sup> From Table F-10, except as noted.<sup>b</sup> Sign changed on  $b$ , and  $\theta$  shifted by  $\pi$ .

Table F-13. Adjusted Parameters for  $\lambda$  and  $m$  at Stations Representing the Upper-Bound Monsoon Climate

Station	$a_\lambda$ (mm) <sup>a</sup>	$a_\lambda$ Standard Error (mm) <sup>a</sup>	$b_{\lambda,1}$ (mm) <sup>a</sup>	$\theta_{\lambda,1}$ (Radians) <sup>a</sup>	$a_m$ (ln mm) <sup>a</sup>	$a_m$ Standard Error (ln mm) <sup>a</sup>	$b_{m,1}$ (ln mm) <sup>a</sup>	$\theta_{m,1}$ (Radians) <sup>a</sup>
Hobbs	8.7	0.3	3.2	-1.09	1.28	0.03	0.36	-1.17
Nogales	7.1	0.2	1.4 <sup>b</sup>	-2.01 <sup>b</sup>	1.24	0.03	0.14 <sup>b</sup>	-1.78 <sup>b</sup>
Average Upper Bound	7.9	0.3	2.3	-1.55	1.26	0.03	0.25	-1.47
Standard Deviation	1.1		1.3	0.7	0.03		0.16	0.4
Wetter Value	8.7				1.28			
Minimum After Subtracting One Standard Error	6.9				1.21			
Maximum After Adding One Standard Error	9.0				1.31			

<sup>a</sup> From Table F-11, except as noted.

<sup>b</sup> Sign changed on  $b$ , and  $\theta$  shifted by  $\pi$ .

DTN: SN0603DWEATHER.002 [DIRS 177917] contains qualified temperature records from the Hobbs and Nogales stations. Excel files in Output DTN: SN0605T0502206.019 contain temperature records extracted for these two stations. The output DTN also contains the MathCAD workbooks that analyzed the two temperature records. Tables F-14 and F-15 report the results of these analyses. The phase parameters are rounded to the nearest day; the remaining parameters are rounded to 0.1°C. Tables F-20 and F-21 also contain the minimum and maximum for each parameter. For the zero-order parameters, the extremes include extension by the maximum of the standard errors.

Table F-14. Fourier Parameters for Wet Day Temperatures at Stations Representing the Upper-Bound Monsoon Climate

Station	$\gamma_{wet_{min}}$ (°C)	$\gamma_{wet_{min}}$ Standard Error (°C)	$\alpha_{wet_{min}}$ (°C)	$\beta_{wet_{min}}$ (DOY)	$\gamma_{wet_{max}}$ (°C)	$\gamma_{wet_{max}}$ Standard Error (°C)	$\alpha_{wet_{max}}$ (°C)	$\beta_{wet_{max}}$ (DOY)
Hobbs	8.5	0.2	10.5	119	20.6	0.2	12.4	112
Nogales	9.5	0.2	8.2	122	22.2	0.2	10.5	116
Minimum	8.3 <sup>a</sup>		8.2	119	20.4 <sup>a</sup>		10.5	112
Maximum	9.7 <sup>a</sup>		10.5	122	22.4 <sup>a</sup>		12.4	116

Source: Output DTN: SN0608T0502206.019; folder Future\_Climate\_Temperature; *Hobbs\_Parameters.xls* and *Nogales\_Parameters.xls*.

<sup>a</sup> Minimum and maximum for  $\gamma_{wet_{min}}$  and  $\gamma_{dry_{min}}$  are extended by one standard error.

Table F-15. Fourier Parameters for Dry Day Temperatures at Stations Representing the Upper-Bound Monsoon Climate

Station	$\gamma_{dry_{min}}$ (°C)	$\gamma_{dry_{min}}$ Standard Error (°C)	$\alpha_{dry_{min}}$ (°C)	$\beta_{dry_{min}}$ (DOY)	$\gamma_{dry_{max}}$ (°C)	$\gamma_{dry_{max}}$ Standard Error (°C)	$\alpha_{dry_{max}}$ (°C)	$\beta_{dry_{max}}$ (DOY)
Hobbs	8.9	0.1	11.0	115	25.3	0.1	10.4	110
Nogales	4.9	0.1	9.7	120	26.8	0.1	8.4	117
Minimum	4.8 <sup>a</sup>		9.7	115	25.2 <sup>a</sup>		8.4	110
Maximum	9.0 <sup>a</sup>		11.0	120	26.9 <sup>a</sup>		10.4	117

Source: Output DTN: SN0608T0502206.019; folder Future\_Climate\_Temperature; *Hobbs\_Parameters.xls* and *Nogales\_Parameters.xls*.

<sup>a</sup> Minimum and maximum for  $\gamma_{wet_{min}}$  and  $\gamma_{dry_{min}}$  are extended by one standard error.

### F2.3 STATIONS REPRESENTING THE GLACIAL TRANSITION CLIMATE

Five meteorological stations represent the range of precipitation anticipated during the Glacial Transition climate, three for the upper bound and two for the lower bound (DTN: GS000308315121.003 [DIRS 151139]). DTN: SN0603DWEATHER.002 [DIRS 177917] contains the qualified precipitation records from the five stations. Output DTN: SN0609T0502206.023 contains the Excel workbooks that performed the Fourier analyses of the five precipitation records. Tables F-16 and F-17 report the results of these analyses. The phase parameters are rounded to one hundredth of a radian (about half a day); the remaining parameters are rounded to a level of precision consistent with the standard error. For corroboration of the analyses, Table F-17a compares the MAP implied by the coefficients with the actual MAP at each of the five stations. In each case, the MAPs agree to within 3%.

Table F-16. Fourier Parameters for  $p_{00}$  and  $p_{10}$  at Stations Representing the Glacial Transition Climate

Station	$a_{00}$	$a_{00}$ Standard Error	$b_{00,1}$	$\theta_{00,1}$ (Radians)	$b_{00,2}$	$a_{10}$	$a_{10}$ Standard Error	$b_{10,1}$	$\theta_{10,1}$ (Radians)	$b_{10,2}$
Beowawe	0.884	0.006	0.074	-1.30	-0.012	0.56	0.02	0.02	-0.76	-0.02
Delta	0.870	0.004	0.028	-1.23	-0.016	0.608	0.011	-0.053	0.31	-0.044
Rosalia	0.794	0.005	0.090	-1.10	-0.044	0.477	0.009	0.063	-0.82	-0.029
Spokane	0.784	0.004	0.104	-1.04	0.048	0.489	0.007	0.112	-0.75	0.019
St. John	0.805	0.005	0.102	-1.05	0.051	0.534	0.011	0.108	-0.29	-0.021

Source: Output DTN: SN0609T0502206.023.



Table F-17. Fourier Parameters for  $\lambda$  and  $m$  at Stations Representing the Glacial Transition Climate

Station	$a_\lambda$ (mm)	$a_\lambda$ Standard Error (mm)	$b_{\lambda,1}$ (mm)	$\theta_{\lambda,1}$ (Radians)	$b_{\lambda,2}$ (mm)	$a_m$ (ln mm)	$a_m$ Standard Error (ln mm)	$b_{m,1}$ (ln mm)	$\theta_{m,1}$ (Radians)	$b_{m,2}$ (ln mm)
Beowawe	3.84	0.18	1.05	-0.52	0.73	0.80	0.04	0.16	-0.83	0.16
Delta	3.22	0.09	0.44	-0.95	0.50	0.51	0.03	0.09	-0.59	0.11
Rosalia	4.13	0.08	-0.36	0.22	-0.41	0.904	0.019	-0.161	-0.10	-0.077
Spokane	3.75	0.06	-0.26	0.74	-0.36	0.665	0.016	-0.089	-0.12	0.074
St. John	4.41	0.11	0.14	0.09	-0.45	0.86	0.03	0.08	1.54	-0.06

Source: Output DTN: SN0609T0502206.023.

Table F-17a. Mean Annual Precipitation at Stations Representing the Glacial Transition Climate Compared with Values Implied by Fourier Coefficients

Meteorological Station	Measured MAP (mm)	MAP Implied by Coefficients (mm)	Years Used for Fourier Analysis (Mar. 1 to Feb. 28)
Beowawe	$2.4 \times 10^2$	$2.4 \times 10^2$	10 years: 1983, 1986 to 1989, 1993 to 1995, 1999, 2001
Delta	$2.1 \times 10^2$	$2.1 \times 10^2$	29 years: 1972, 1973, 1975, 1976, 1978 to 1981, 1983 to 2003
Rosalia	$4.6 \times 10^2$	$4.5 \times 10^2$	28 years: 1953, 1956, 1958 to 1960, 1963 to 1971, 1973, 1975 to 1978, 1980 to 1983, 1985 to 1988, 1993
Spokane	$4.2 \times 10^2$	$4.2 \times 10^2$	52 years: 1948 to 1952, 1954 to 1994, 1998 to 2003
St. John	$4.3 \times 10^2$	$4.3 \times 10^2$	22 years: 1964 to 1969, 1972 to 1981, 1987, 1989 to 1991, 1994, 2001

Source: Measured MAPs from BSC 2006 [DIRS 177081], Section 6.3.5.1; implied MAPs from Equations F-41 and F-42 using values from Tables F-16 and F-17; data years from Output DTN: SN0609T0502206.023.

In Tables F-16 and F-17, some of the coefficients of the first-order terms ( $b_{00}$ ,  $b_{10}$ , etc.) are negative. Tables F-18 and F-19 include adjustment of the first-order terms in accordance with Equation F-35 so that all of the coefficients are positive. In some cases, the phase has been adjusted by  $2\pi$  to bring it closer to the adjusted values at other stations. Because these stations were chosen for their values of temperature and MAP without consideration of their elevation, they each represent conditions at the reference Yucca Mountain elevation of 5,000 ft (1,524 m) and need no adjustment for elevation.

Tables F-18 and F-19 also contain two averages for each parameter, one for the lower-bound stations and one for the upper-bound stations. For some first-order terms, these averages omit one of the stations. The lower-bound averages of  $b_{10,1}$  and  $\theta_{10,1}$  omit Beowawe because the magnitude of this first-order term is no larger than the standard error. The upper bound averages of  $b_{\lambda,1}$ ,  $\theta_{\lambda,1}$ ,  $b_{m,1}$ , and  $\theta_{m,1}$  omit St. John because these first-order terms are out of phase with Rosalia and Spokane and because St. John has larger standard errors. For the zero-order parameters, the tables show the extent to which one standard error would extend the range of the parameter.

Because the magnitude of the first-order terms are larger for some of these stations than for stations previously considered, the choice of phase required further attention. The phase is more relevant when the amplitude is larger. Therefore, Tables F-18 and F-19 include weighted means of the phases and weighted standard deviations using the amplitudes as weighting factors.

Table F-18. Adjusted Parameters for  $p_{00}$  and  $p_{10}$  at Stations Representing the Glacial Transition Climate

Station	$a_{00}$ <sup>a</sup>	$a_{00}$ Standard Error <sup>a</sup>	$b_{00,1}$ <sup>a</sup>	$\theta_{00,1}$ (Radians) <sup>a</sup>	$a_{10}$ <sup>a</sup>	$a_{10}$ Standard Error <sup>a</sup>	$b_{10,1}$ <sup>a</sup>	$\theta_{10,1}$ (Radians) <sup>a</sup>
Beowawe	0.884	0.006	0.074	-1.30	0.56	0.02	0.02	-0.76
Delta	0.870	0.004	0.028	-1.23	0.608	0.011	0.053 <sup>b</sup>	-2.83 <sup>b</sup>
Rosalia	0.794	0.005	0.090	-1.10	0.477	0.009	0.063	-0.82
Spokane	0.784	0.004	0.104	-1.04	0.489	0.007	0.112	-0.75
St. John	0.805	0.005	0.102	-1.05	0.534	0.011	0.108	-0.29
Minimum	0.78 <sup>c</sup>		0.028		0.468 <sup>c</sup>		.02	
Maximum	0.89 <sup>c</sup>		0.104		0.619 <sup>c</sup>		.112	
Weighted Average <sup>d</sup>				-1.12				-0.93
Weighted Standard Deviation <sup>d</sup>				0.10				0.84

<sup>a</sup> From Table F-16, except as noted.

<sup>b</sup> Sign changed on  $b$ , and  $\theta$  shifted by  $\pi$ .

<sup>c</sup> Minimum and maximum for  $a_{00}$  and  $a_{10}$  are extended by one standard error.

<sup>d</sup> Average and standard deviation values for  $\theta$  are weighted by values of  $b$ .

Table F-19. Adjusted Parameters for  $\lambda$  and  $m$  at Stations Representing the Glacial Transition Climate

Station	$a_\lambda$ (mm) <sup>a</sup>	$a_\lambda$ Standard Error (mm) <sup>a</sup>	$b_{\lambda,1}$ (mm) <sup>a</sup>	$\theta_{\lambda,1}$ (Radians) <sup>a</sup>	$a_m$ (ln mm) <sup>a</sup>	$a_m$ Standard Error (ln mm) <sup>a</sup>	$b_{m,1}$ (ln mm) <sup>a</sup>	$\theta_{m,1}$ (Radians) <sup>a</sup>
Beowawe	3.84	0.18	1.05	-0.52	0.80	0.04	0.16	-0.83
Delta	3.22	0.09	0.44	-0.95	0.51	0.03	0.09	-0.59
Rosalia	4.13	0.08	0.36 <sup>b</sup>	-2.92 <sup>b</sup>	0.904	0.019	0.161 <sup>b</sup>	-3.24 <sup>b</sup>
Spokane	3.75	0.06	0.26 <sup>b</sup>	-2.40 <sup>b</sup>	0.665	0.016	0.089 <sup>b</sup>	-3.26 <sup>b</sup>
St. John	4.41	0.11	0.14	0.09	0.86	0.03	0.08	1.54
Minimum	3.13 <sup>c</sup>		0.14		0.48 <sup>c</sup>		0.08	
Maximum	4.52 <sup>c</sup>		1.05		0.923 <sup>c</sup>		0.161	
Weighted average <sup>d</sup>				-1.2				-1.5
Weighted standard deviation <sup>d</sup>				1.0				1.7

<sup>a</sup> From Table F-17, except as noted.

<sup>b</sup> Sign changed on  $b$ , and  $\theta$  shifted by  $\pi$ .

<sup>c</sup> Minimum and maximum for  $a_\lambda$  and  $a_m$  are extended by one standard error.

<sup>d</sup> Average and standard deviation values for  $\theta$  are weighted by values of  $b$ .

For the five stations that represent the Glacial Transition climate, DTN: SN0603DWEATHER.002 [DIRS 177917] contains qualified temperature data. Output DTN: SN0608T0502206.019 contains the MathCAD files that record the calculations of the temperature parameters for each station. Tables F-20 and F-21 report the results of these analyses. The phase parameters are rounded to the nearest day; the remaining parameters are rounded to 0.1°C.

Tables F-20 and F-21 also contain the minimum and maximum for each parameter. For the zero-order parameters, the extremes include extension by the maximum of the standard errors.

Table F-20. Parameters of Minimum Temperature at Stations Representing the Glacial Transition Climate

Station	$\alpha_{wet_{min}}$ (°C)	$\beta_{wet_{min}}$ (DOY)	$\gamma_{wet_{min}}$ (°C)	$\gamma_{wet_{min}}$ Standard Uncertainty (°C)	$\alpha_{dry_{min}}$ (°C)	$\beta_{dry_{min}}$ (DOY)	$\gamma_{dry_{min}}$ (°C)	$\gamma_{dry_{min}}$ Standard Uncertainty (°C)
Beowawe	7.6	114	1.4	0.2	9.9	106	-0.7	0.1
Delta	10.4	116	2.9	0.2	11.6	112	0.7	0.1
Rosalia	6.3	118	2.9	0.1	8.3	112	1.8	0.1
Spokane	7.9	116	3.5	0.1	10.0	116	2.5	0.1
St. John	6.4	114	3.8	0.1	7.5	111	1.6	0.1
Minimum	6.3	114	1.2 <sup>a</sup>		7.5	106	-0.8 <sup>a</sup>	
Maximum	10.4	118	3.9 <sup>a</sup>		11.6	116	2.6 <sup>a</sup>	

Source: Output DTN: SN0608T0502206.019; folder Future\_Climate\_Temperature; files *Beowawe\_Parameters.xls*, *Delta\_Parameters.xls*, *Rosalia\_Parameters.xls*, *Spokane\_Parameters.xls*, and *StJohn\_Parameters.xls*.

<sup>a</sup> Minimum and maximum for  $\gamma_{wet_{min}}$  and  $\gamma_{dry_{min}}$  are extended by one standard error using the maximum standard error.

Table F-21. Parameters of Maximum Temperature at Stations Representing the Glacial Transition Climate

Station	$\alpha_{wet_{max}}$ (°C)	$\beta_{wet_{max}}$ (DOY)	$\gamma_{wet_{max}}$ (°C)	$\gamma_{wet_{max}}$ Standard Uncertainty (°C)	$\alpha_{dry_{max}}$ (°C)	$\beta_{dry_{max}}$ (DOY)	$\gamma_{dry_{max}}$ (°C)	$\gamma_{dry_{max}}$ Standard Uncertainty (°C)
Beowawe	11.2	112	14.2	0.2	14.5	112	18.4	0.1
Delta	13.4	115	15.7	0.2	15.0	112	19.5	0.1
Rosalia	10.1	115	12.6	0.1	13.8	117	15.0	0.1
Spokane	10.8	113	11.8	0.1	14.8	115	14.7	0.1
St. John	10.4	111	14.3	0.1	13.8	114	16.6	0.1
Minimum	10.1	111	11.7 <sup>a</sup>		13.8	112	14.6 <sup>a</sup>	
Maximum	13.4	115	15.9 <sup>a</sup>		15.0	117	19.6 <sup>a</sup>	

Source: Output DTN: SN0608T0502206.019; folder Future\_Climate\_Temperature; *Beowawe\_Parameters.xls*, *Delta\_Parameters.xls*, *Rosalia\_Parameters.xls*, *Spokane\_Parameters.xls*, and *StJohn\_Parameters.xls*.

<sup>a</sup> Minimum and maximum for  $\gamma_{wet_{max}}$  and  $\gamma_{dry_{max}}$  are extended by one standard error using the maximum standard error.

### F3. SELECTION OF PARAMETER RANGES FOR EACH CLIMATE

For each meteorological station, Section F2 reports the station's parameters, adjusted as appropriate to be applicable to an elevation equivalent to the top of Yucca Mountain (5,000 ft or 1,524 m). The section you are now reading reports the development of a range of uncertainty for each climate parameter, first for the remainder of the Present-Day climate, then for the Monsoon climate, and finally for the Glacial Transition climate.

Each climate parameter represents an estimate of the value that would result if the analyses of Section F2 could be performed on the future record of a meteorological station located at the top of the mountain. Thus, the ranges of the parameters represent the full potential range of integrated weather over the future period, not the parameters for individual years. Standard uncertainties are calculated in accordance with formulas in Section I2.2. Values are rounded to accuracies consistent with the standard uncertainties.

Analyses with the MASSIF model require precipitation amounts and intensities, maximum and minimum temperatures, and wind speeds. Potential climates do not fit onto a linear scale. One climate may be hot, wet, and windy, with intense storms; another may be cold, wet, and windy, with long, slow snowfalls; and a third may be cold, dry, and still, with slow snowfalls. Where *Future Climate Analysis* refers to lower- and upper-bound representatives of a climate, those bounds refer to precipitation, not necessarily to any other parameter.

#### F3.1 PARAMETER RANGES FOR THE PRESENT-DAY CLIMATE

This section presents the nominal value and uncertainty for each weather parameter of the Present-Day climate. For precipitation and temperature parameters, the analyses of individual meteorological station records, which are reported in Section F2.1, provide the basis. However, for the analyses of wind speed and precipitation duration, meteorological stations are treated as a group, not separately.

Output DTN: SN0610T0502206.030 contains a MathCAD application that calculates monthly wind speeds averaged over four Yucca Mountain meteorological stations, Site 1, Site 2, Site 3, and Site 6. The calculation uses wind speed data from DTN: SN0608WEATHER1.005 [DIRS 177912].

This calculation converts these measurements to equivalent wind speed at 2 meters height, using the following equation (Allen et al. 1998 [DIRS 157311], Eq. 47):

$$u_2(u, z) = u \frac{4.87}{\ln(67.8z - 5.42)} \quad (\text{Eq. F-49})$$

where  $u$  is the wind speed measured at a height of  $z$  meters aboveground and  $u_2$  is the equivalent wind speed at 2 m. The application calculates monthly averages, omitting days with no wind speed data, and determines the standard error in each average.

Table F-22 lists the nominal value and uncertainty for each parameter of the Present-Day climate. The approximate uncertainty distribution for each zero-order precipitation parameter

( $a_{00}$  and  $a_{10}$ ) is a uniform distribution. The extremes of the distribution are the minimum and the maximum values among those obtained by analysis of the ten stations, extended by one standard error. These values also appear in Tables F-4 and F-5. The nominal value is the midpoint between these extremes. For a uniform distribution that ranges from  $x$  to  $y$ , the standard uncertainty is  $(y - x)/\sqrt{12}$ . Section I2.2 provides the derivation of this formula.

Using Equations F-41 and F-42 and the nominal values of the zero-order parameters yields a value of  $1.9 \times 10^2$  mm as a nominal MAP for the Present-Day climate. Section 7.1.1.3 discusses the uncertainty distribution for MAP during the remainder of the modern interglacial climate.

For each of the eight first-order precipitation parameters, the nominal value is the mean of the values for the ten meteorological stations. The approximate uncertainty distribution is usually a normal distribution, established by the mean and standard deviation for the 10 stations. The one exception is  $b_{10,1}$ , which is only two standard deviations above zero, so that a uniform distribution, defined by the extreme values from the 10 stations, is a more representative distribution of this nonnegative parameter. The values for the phase parameters are consistent with peak precipitation in the winter.

All of the temperature parameters have uncertainty distributions that are uniform, with a range determined by the minimum and maximum values for the four sites, as given in Tables F-8 through F-10. Each nominal value is at the center of its range.

The wind speed averages have normal distributions, based on the mean and standard error calculated in Output DTN: SN0610T0502206.030.

Table F-22. Nominal Values and Uncertainties for Parameters of the Weather Input File during the Present-Day Climate

Parameter Symbol	Nominal Value	Uncertainty Range	Uncertainty Distribution	Standard Uncertainty
$a_{00}$	0.934	0.924 to 0.944	uniform	0.006
$b_{00,1}$	0.027	$0.027 \pm 0.003$	normal	0.003
$\theta_{00,1}$	-1.31 radians	$-1.31 \pm 0.09$ radians	normal	0.09 radians
$a_{10}$	0.58	0.50 to 0.65	uniform	0.04
$b_{10,1}$	0.06	0.03 to 0.10	uniform	0.02
$\theta_{10,1}$	-1.5 radians	$-1.5 \pm 0.4$ radians	normal	0.4 radians
$a_{\lambda}$	5.2 mm	4.0 to 6.5 mm	uniform	0.7
$b_{\lambda,1}$	0.7 mm	$0.7 \pm 0.2$ mm	normal	0.2 mm
$\theta_{\lambda,1}$	+2.5 radians	$+2.5 \pm 0.7$ radians	normal	0.7 radians
$a_m$	0.78 mm	0.50 to 1.07 ln mm	uniform	0.16 ln mm
$b_{m,1}$	0.15 mm	$0.15 \pm 0.04$ ln mm	normal	0.04 ln mm
$\theta_{m,1}$	+2.4 radians	$+2.4 \pm 0.4$ radians	normal	0.4 radians
$\alpha_{wet_{min}}$	9.1°C	8.6°C to 9.6°C	uniform	0.3°C

Table F-22. Nominal Values and Uncertainties for Parameters of the Weather Input File During the Present-Day Climate (Continued)

Parameter Symbol	Nominal Value	Uncertainty Range	Uncertainty Distribution	Standard Uncertainty
$\beta_{wet_{min}}$	122 days	121 to 124 days	uniform	1 day
$\gamma_{wet_{min}}$	6.6°C	5.0°C to 8.1°C	uniform	0.9°C
$\alpha_{dry_{min}}$	9.7°C	9.4°C to 10.0°C	uniform	0.2°C
$\beta_{dry_{min}}$	115 days	114 to 116 days	uniform	1 day
$\gamma_{dry_{min}}$	9.4°C	6.9°C to 11.8°C	uniform	1.4°C
$\alpha_{wet_{max}}$	12.1°C	11.8°C to 12.4°C	uniform	0.2°C
$\beta_{wet_{max}}$	117 days	116 to 118 days	uniform	1 day
$\gamma_{wet_{max}}$	14.8°C	13.9°C to 15.8°C	uniform	0.6°C
$\alpha_{dry_{max}}$	12.2°C	11.9°C to 12.4°C	uniform	0.1°C
$\beta_{dry_{max}}$	110 days	109 to 110 days	uniform	0.3 days
$\gamma_{dry_{max}}$	20.0°C	19.2°C to 20.7°C	uniform	0.4°C
$u_2(1)$	2.36 m/s	2.36 ± 0.03 m/s	normal	0.03 m/s
$u_2(2)$	2.67 m/s	2.67 ± 0.04 m/s	normal	0.04 m/s
$u_2(3)$	2.84 m/s	2.84 ± 0.03 m/s	normal	0.03 m/s
$u_2(4)$	3.22 m/s	3.22 ± 0.04 m/s	normal	0.04 m/s
$u_2(5)$	2.97 m/s	2.97 ± 0.03 m/s	normal	0.03 m/s
$u_2(6)$	2.90 m/s	2.90 ± 0.02 m/s	normal	0.02 m/s
$u_2(7)$	2.75 m/s	2.75 ± 0.02 m/s	normal	0.02 m/s
$u_2(8)$	2.71 m/s	2.71 ± 0.02 m/s	normal	0.02 m/s
$u_2(9)$	2.64 m/s	2.64 ± 0.02 m/s	normal	0.02 m/s
$u_2(10)$	2.61 m/s	2.61 ± 0.03 m/s	normal	0.03 m/s
$u_2(11)$	2.47 m/s	2.47 ± 0.03 m/s	normal	0.03 m/s
$u_2(12)$	2.48 m/s	2.48 ± 0.03 m/s	normal	0.03 m/s

Source: Precipitation parameters from Tables F-4 and F-5; temperature values from Tables F-7 through F-9; wind speeds from Output DTN: SN0610T0502206.030.

### F3.2 PARAMETER RANGES FOR THE MONSOON CLIMATE

According to *Future Climate Analysis*, the Monsoon climate is characterized in the Owens Lake record by species that imply a monsoon sufficient to generate diluting surface flow in the Owens River. As noted in Section F2.2, however, *Future Climate Analysis* selected the Present-Day sites and regional stations to represent one bound for the Monsoon climate. This bound has lower precipitation with more winter than summer precipitation (BSC 2004 [DIRS 170002], pp. 6-47 to 6-50).

An upper-bound value for the monsoon precipitation must have MAP higher than the range of values at the Haiwee station near Owens Lake (up to 270 mm) and MAT as high or higher than Owens Lake today. *Future Climate Analysis* selected the stations at Hobbs, New Mexico and Nogales, Arizona, reported to have MAP levels of 418 mm and 414 mm, respectively, but noted that the MAP at these sites may not be high enough to generate the appropriate lake in the Owens Basin. An expansion of the summer rain regime to the Owens Basin region also would have expanded well north of Yucca Mountain. Because Yucca Mountain would be more centrally

located within such a summer rain regime it may experience upper-bound levels of MAP that are higher than those identified from the analogue meteorological stations (BSC 2004 [DIRS 170002], pp. 6-47 to 6-50).

For the Monsoon climate, one limit of precipitation behavior is wettest in the winter, whereas the other limit is wettest in the summer. For temperature, on the other hand, both limits are hottest in the summer. Therefore, the development of distributions for monsoon precipitation parameters differs from the procedure for monsoon temperature parameters. Furthermore, lacking qualified wind speed data from Hobbs or Nogales, the wind speed parameters are approximated by the parameters for the Present-Day climate.

For each parameter of the Monsoon climate, Table F-23 contains the nominal value and the uncertainty distribution for the Yucca Mountain analysis. Table F-23 also shows the standard uncertainty for each distribution. For a uniform distribution that ranges from  $x$  to  $y$ , the standard uncertainty is  $(y - x)/\sqrt{12}$ . Section I2.2 provides the derivation of this formula. Values in the table have been rounded to the level of accuracy indicated by the standard uncertainty.

For the zero-order precipitation terms, the uncertainty distribution is uniform. To ensure that the extremes capture the full range of uncertainty, the range is defined by the minimum and maximum of all values from the analyses of Present-Day (Tables F-4 and F-5) and upper bound Monsoonsites (Tables F-12 and F-13), extended by one standard error. The nominal value is the midpoint between these extremes.

For example, the zero-order parameter,  $a_{10}$ , in Table F-23 is defined by a uniform distribution between 0.50 to 0.67. The lower bound is the minimum value of this parameter after reduction by one standard error, considering all of the stations in Table F-4 and Table F-12. Station 40 MN has the minimum value after reduction by one standard error, 0.497 (0.508 minus 0.011, Table F-4). This result is rounded to the level of accuracy indicated by the standard uncertainty (see below). The upper bound is the maximum value of this parameter after addition of one standard error, 0.673 (Hobbs, 0.662 plus 0.11, Table F-12). The standard uncertainty is  $(0.673 - 0.497)/\sqrt{12} = 0.05$ , indicating a level of accuracy of two decimal places. Thus the range is 0.50 to 0.67.

Using Equations F-41 and F-42 and the nominal values of the zero-order parameters yields a value of  $2.9 \times 10^2$  mm as a nominal MAP for the Monsoon climate. Section 7.1.1.4 discusses the uncertainty distribution for MAP during the Monsoon climate.

As forecast in *Future Climate Analysis*, the typical Monsoon climate is a climate where winter precipitation exists, but does not dominate MAP. However, by specifying that local and regional stations be used as a lower bound, *Future Climate Analysis* suggests that the climate during the monsoon period would vary from episodes of intense summer rain to Present-Day-like climates with relatively more winter and less summer precipitation (BSC 2004 [DIRS 170002], p. 6-50). Therefore, although the magnitude of the first-order precipitation term is uncertain, the phase of the first-order term must be that of the summer-precipitation upper-bound stations, not the winter-precipitation Yucca Mountain stations.

A Monsoon climate has strong seasonal variation in precipitation, which makes the first-order terms more important than for other climates. The amplitudes for the first-order terms differ greatly between the two upper-bound stations. Nogales has the greater seasonal variation in the probability that a day is wet. Hobbs has the greater variation in the average precipitation on wet days. Tables F-12 and F-13 show that the values for the two stations differ by more than a factor of two for  $b_{10,1}$ ,  $b_{\lambda,1}$ , and  $b_{m,1}$ . Those tables also report standard deviations for  $b_{00,1}$ ,  $b_{\lambda,1}$ , and  $b_{m,1}$  that are larger than the standard deviations in the corresponding zero-order terms.

Because *Future Climate Analysis* describes these stations as “the best choices available” (BSC 2004 [DIRS 170002], p. 6-49), it is not clear that the two values for a first-order amplitude, as different as they are, actually capture the full range of uncertainty. An alternate interpretation is that these stations are just two samples of potential upper-bound stations. In this interpretation, the potential upper-bound stations have a distribution for each parameter that may be approximated as a normal distribution, with the average and standard deviation for the two stations providing estimates for the mean and variance of the distribution. A range from one standard deviation below the lower value to one standard deviation above the upper value captures about 90% of this hypothetical distribution for the climate upper bound. This observation guides the selection of a range for each first-order magnitude.

However, the magnitude of a first-order term is subject to constraints. The magnitude of a first-order term must be less than the magnitude of the zero-order term because neither a Markov probability nor an average precipitation can be less than zero. Also, the first-order term may not cause a Markov probability to exceed 1.0. Therefore, an approximate uncertainty distribution for the magnitude of a first-order term for the upper-bound Monsoon climate is a uniform distribution from one standard deviation below the lower value to one standard deviation above the upper value, subject to constraints.

Because the first-order terms for the lower-bound stations are completely out of phase with the first-order terms for the upper-bound stations, they may be represented by negative values of the  $b$ 's. In Table F-23 the complete range for the amplitude of a first-order term may range from the largest value for the Present-Day climate (Table F-3), plus one standard deviation, but taken as negative, to the larger of the values from the upper-bound stations, plus one standard deviation, taken as positive. For  $b_{00,1}$ , the range is from  $-0.03$  to  $+0.07$ , with the larger value bringing  $p_{00}$  to greater than 1.0 when  $a_{00}$  takes on its largest value of 0.944. The constraint that  $p_{00}$  remain less than or equal to 1.0, must be observed in downstream use of these values. For  $b_{10,1}$ , the range is from  $-0.06$  to  $+0.08$ , with no applicable constraints. For  $b_{\lambda,1}$  the range is from  $-0.7$  mm to  $+3.6$  mm. For  $b_{m,1}$  the range is from  $-0.15$  ln mm to  $+0.30$  ln mm.

The uncertainty distribution for the phase of each first-order precipitation term is a uniform distribution. The extreme values are the values for the two upper-bound stations.

For the temperature parameters, uncertainty distributions are uniform, with the limits determined by the extreme values from among all of the Present-Day and upper-bound monsoon stations. For wet-day temperature parameters, ranges of station values appear in Tables F-7 and F-14. The ranges for dry day parameters are in Tables F-8 and F-15. As before, the zero-order parameters are extended by one standard error; Table F-9 summarizes the effects of that extension for Present-Day stations. The parameter  $\gamma_{dry_{min}}$  provides an example. After extension



by one standard error, the values at the stations range from 4.8°C (Table F-15) to 11.8°C (Table F-9). Because the standard uncertainty for this uniform distribution is 2.0°C, Table F-23 shows the values rounded to 5°C and 12°C.

Table F-23. Nominal Values and Uncertainties for Parameters of the Monsoon Climate

Parameter Symbol	Nominal Value	Uncertainty Range	Uncertainty Distribution	Standard Uncertainty
$a_{00}$	0.920	0.896 to 0.944	uniform	0.014
$b_{00,1}$	0.02	-0.03 to +0.07	uniform	0.03
$\theta_{00,1}$	+2.00 radians	+1.74 to +2.25 radians	uniform	0.15 radians
$a_{10}$	0.58	0.50 to 0.67	uniform	0.05
$b_{10,1}$	-0.02	-0.13 to +0.10	uniform	0.07
$\theta_{10,1}$	+1.8 radians	+1.4 to +2.3 radians	uniform	0.3 radians
$a_{\lambda}$	6.5 mm	4.0 to 9.0 mm	uniform	1.4 mm
$b_{\lambda,1}$	1.6 mm	-1.3 to 4.5 mm	uniform	1.7 mm
$\theta_{\lambda,1}$	-1.6 radians	-2.0 to -1.1 radians	uniform	0.3
$a_m$	0.9 mm	0.5 to 1.3 ln mm	uniform	0.2 ln mm
$b_{m,1}$	0.1 mm	-0.3 to 0.5 ln mm	uniform	0.2 ln mm
$\theta_{m,1}$	-1.48 radians	-1.78 to -1.17 radians	uniform	0.18 radians
$\alpha_{wet_{min}}$	9.4°C	8.2°C to 10.5°C	uniform	0.7°C
$\beta_{wet_{min}}$	122 days	119 to 124 days	uniform	1 day
$\gamma_{wet_{min}}$	7.4°C	5.0°C to 9.7°C	uniform	1.4°C
$\alpha_{dry_{min}}$	10.2°C	9.4°C to 11.0°C	uniform	0.5°C
$\beta_{dry_{min}}$	117 days	114 to 120 days	uniform	2 days
$\gamma_{dry_{min}}$	8°C	5°C to 12°C	uniform	2°C
$\alpha_{wet_{max}}$	11.4°C	10.5°C to 12.4°C	uniform	0.5°C
$\beta_{wet_{max}}$	115 days	112 to 118 days	uniform	2 days
$\gamma_{wet_{max}}$	18°C	14°C to 22°C	uniform	2°C
$\alpha_{dry_{max}}$	10.4	8.4°C to 12.4°C	uniform	1.2°C
$\beta_{dry_{max}}$	113 days	109 to 117 days	uniform	2 days
$\gamma_{dry_{max}}$	23°C	19°C to 27°C	uniform	2°C
$u_2(1)$	2.36 m/s	2.36 ± 0.03 m/s	normal	0.03 m/s
$u_2(2)$	2.67 m/s	2.67 ± 0.04 m/s	normal	0.04 m/s
$u_2(3)$	2.84 m/s	2.84 ± 0.03 m/s	normal	0.03 m/s
$u_2(4)$	3.22 m/s	3.22 ± 0.04 m/s	normal	0.04 m/s
$u_2(5)$	2.97 m/s	2.97 ± 0.03 m/s	normal	0.03 m/s
$u_2(6)$	2.90 m/s	2.90 ± 0.02 m/s	normal	0.02 m/s
$u_2(7)$	2.75 m/s	2.75 ± 0.02 m/s	normal	0.02 m/s
$u_2(8)$	2.71 m/s	2.71 ± 0.02 m/s	normal	0.02 m/s
$u_2(9)$	2.64 m/s	2.64 ± 0.02 m/s	normal	0.02 m/s
$u_2(10)$	2.61 m/s	2.61 ± 0.03 m/s	normal	0.03 m/s
$u_2(11)$	2.47 m/s	2.47 ± 0.03 m/s	normal	0.03 m/s
$u_2(12)$	2.48 m/s	2.48 ± 0.03 m/s	normal	0.03 m/s

Source: Precipitation parameters from Tables F-4, F-5, F-12, and F-13; temperature values from Tables F-7 through F-9, F-14, and F-15; wind speeds from Output DTN: SN0610T0502206.030.

### F3.3 PARAMETER RANGES FOR THE GLACIAL TRANSITION CLIMATE

Judged from the Owens Lake record, the change to the Glacial Transition climate was large and fast, shifting from a strong monsoon system dominated by summer precipitation to a winter regime with sufficient effective moisture to sustain a fresh and spilling Owens Lake. Therefore, the polar front must be resident in the region during much of the winter, lowering the MAT. The genesis of greater snowpack with a resident polar mass must also lower temperature and increase MAP at Yucca Mountain, but the cooler climate never becomes very cold with high effective moisture as was true of the last two full-glacial periods. The climate during the Glacial Transition period was typically a cool, usually wet winter season with warm (not hot) to cool summers that were usually dry relative to the Present-Day summers. The MAT should be no colder and preferably warmer than 8°C. The MAP should be higher than the 309 mm recorded near Owens Lake, because even the high historic discharge levels of that year would not be sufficient to fill and spill the lake as implied by the microfossil record. The three selected stations in eastern Washington, Rosalia, St. John, and Spokane, fit all of the criteria for the upper-bound Glacial Transition climate (BSC 2004 [DIRS 170002], pp. 6-50 to 6-52).

However, there are indications that there were also episodes during this climate period that were relatively warm and dry, thus demonstrating some degree of climate variability. The stations representing the lower bound should have a higher temperature, but lower than that for the Owens Lake Basin today. They may have MAP values that are similar to or even lower than Present-Day Owens Lake Basin, but dominated by winter precipitation. The set of meteorological data for Delta, Utah, fits all of these criteria. The site at Beowawe, Nevada, was added as a lower-bound station to avoid using a single site and because its data met most of the requirements (BSC 2004 [DIRS 170002], pp. 6-50 to 6-53).

Lacking qualified wind speed data from any of these five stations, the wind speed parameters are approximated by the parameters for the Present-Day climate.

For each parameter of the Glacial Transition climate, Table F-24 contains the nominal value and the uncertainty distribution for the Yucca Mountain analysis. Most of the uncertainty distributions for precipitation and temperature parameters are uniform, with the ranges determined in Section F2.3, extended by one standard error where applicable, and the nominal values are the means of the distributions. The exceptions are the phase coefficients for precipitation. The table assigns a normal distribution to the phase coefficients for the Markov probabilities, using the weighted average and standard deviation from Table F-18. In the case of the phase coefficients for the amount of precipitation of a wet day (Table F-19), however, the weighted standard deviations are so large that no nominal value seemed justified. These last two phase coefficients are considered as completely uncertain so that any value is possible.

Table F-24 also shows the standard uncertainty for each distribution. For a uniform distribution that ranges from  $x$  to  $y$ , the standard uncertainty is  $(y - x)/\sqrt{12}$ . Section I2.2 provides the derivation of this formula. Values in the table have been rounded to the level of accuracy indicated by the standard uncertainty or by a relevant standard error.

Table F-24. Nominal Values and Uncertainties for Parameters of the Glacial Transition Climate

Parameter Symbol	Nominal Value	Uncertainty Range	Uncertainty Distribution	Standard Uncertainty
$a_{00}$	0.84	0.78 to 0.89	uniform	0.03
$b_{00,1}$	0.066	0.028 to 0.104	uniform	0.02
$\theta_{00,1}$	-1.12 radians	$-1.12 \pm 0.10$ radians	normal	0.010 radians
$a_{10}$	0.54	0.47 to 0.62	uniform	0.04
$b_{10,1}$	0.07	0.02 to 0.11	uniform	0.03
$\theta_{10,1}$	-0.93 radians	$-0.93 \pm 0.84$ radians	normal	0.84 radians
$a_{\lambda}$	3.8 mm	3.1 to 4.5 mm	uniform	0.4 mm
$b_{\lambda,1}$	0.6 mm	0.1 to 1.0 mm	uniform	0.3 mm
$\theta_{\lambda,1}$	N/A	$-\pi$ to $\pi$ radians	uniform	N/A
$a_m$	0.70 mm	0.48 to 0.92 ln mm	uniform	0.13 ln mm
$b_{m,1}$	0.12 mm	0.08 to 0.16 ln mm	uniform	0.02 ln mm
$\theta_{m,1}$	N/A	$-\pi$ to $\pi$ radians	uniform	N/A
$\alpha_{wet,min}$	8.4°C	6.3°C to 10.4°C	uniform	1.2°C
$\beta_{wet,min}$	DOY 116	DOY 114 to 118	uniform	1 day
$\gamma_{wet,min}$	2.6°C	1.2°C to 3.9°C	uniform	0.8°C
$\alpha_{dry,min}$	9.6°C	7.5°C to 11.6°C	uniform	1.2°C
$\beta_{dry,min}$	DOY 111	DOY 106 to 116	uniform	3 days
$\gamma_{dry,min}$	0.9°C	-0.8°C to 2.6°C	uniform	1.0°C
$\alpha_{wet,max}$	11.8°C	10.1°C to 13.4°C	uniform	1.0°C
$\beta_{wet,max}$	DOY 113	DOY 111 to 115	uniform	1 day
$\gamma_{wet,max}$	13.8°C	11.7°C to 15.9°C	uniform	1.2°C
$\alpha_{dry,max}$	14.4°C	13.8°C to 15.0°C	uniform	0.3°C
$\beta_{dry,max}$	DOY 114	DOY 112 to 117	uniform	1 day
$\gamma_{dry,max}$	17.1°C	14.6°C to 19.6°C	uniform	1.4°C
$u_2(1)$	2.36 m/s	$2.36 \pm 0.03$ m/s	normal	0.03 m/s
$u_2(2)$	2.67 m/s	$2.67 \pm 0.04$ m/s	normal	0.04 m/s
$u_2(3)$	2.84 m/s	$2.84 \pm 0.03$ m/s	normal	0.03 m/s
$u_2(4)$	3.22 m/s	$3.22 \pm 0.04$ m/s	normal	0.04 m/s
$u_2(5)$	2.97 m/s	$2.97 \pm 0.03$ m/s	normal	0.03 m/s
$u_2(6)$	2.90 m/s	$2.90 \pm 0.02$ m/s	normal	0.02 m/s
$u_2(7)$	2.75 m/s	$2.75 \pm 0.02$ m/s	normal	0.02 m/s
$u_2(8)$	2.71 m/s	$2.71 \pm 0.02$ m/s	normal	0.02 m/s
$u_2(9)$	2.64 m/s	$2.64 \pm 0.02$ m/s	normal	0.02 m/s
$u_2(10)$	2.61 m/s	$2.61 \pm 0.03$ m/s	normal	0.03 m/s
$u_2(11)$	2.47 m/s	$2.47 \pm 0.03$ m/s	normal	0.03 m/s
$u_2(12)$	2.48 m/s	$2.48 \pm 0.03$ m/s	normal	0.03 m/s

Source: Precipitation parameters from Tables F-18 and F-19; temperature values from Tables F-20 and F-21; wind speeds from Output DTN: SN0610T0502206.030.

Using Equations F-41 and F-42 and the nominal values of the zero-order parameters yields a value of  $3.2 \times 10^2$  mm as a nominal MAP for the Glacial Transition climate. Section 7.1.1.5 discusses the uncertainty distribution for MAP during the Glacial Transition climate.

## F4. GENERATION OF A WEATHER INPUT FILE FROM A SET OF CLIMATE PARAMETERS

This section discusses the general method for developing a weather input file from a set of climate parameters. Appendix I presents the sample values used for calculations and the development of a specific weather input file for each set of sample values.

### F4.1 GENERATION OF PRECIPITATION INPUT

#### F4.1.1 Stochastic Precipitation Model

The stochastic algorithm proceeds as follows to develop a 1,000-year sample of daily precipitation,  $P(d, y)$ , for  $d$  from 1 to 365 and  $y$  from 1 to 1,000.

For  $d$  from 1 to 365, evaluate the formulas in Equations F-9 through F-12 and Equation F-2.

Set  $P(0,1)$  to 0.001 (starting with a wet day to avoid underestimating precipitation).

For each  $y$  from 1 to 1,000,

For each  $d$  from 1 to 365

If  $P(d-1, y)$  is zero, select a random number,  $0 < R < 1$ .

If  $R < p_{oo}(d)$ , set  $P(d, y)$  to zero.

Else, set  $P(d, y)$  such that:

$$\int_0^{P(d,y)} \frac{e^{-[\ln x - m(d)]^2 / 2[s(d)]^2}}{xs(d)\sqrt{2\pi}} dx = R \quad (\text{Eq. F-50})$$

If using a built-in inverse lognormal function, verify the result.

Else, select a random number,  $0 < R < 1$ .

If  $R < p_{1o}(d)$ , set  $P(d, y)$  to zero.

Else, set  $P(d, y)$  such that:

$$\int_0^{P(d,y)} \frac{e^{-[\ln x - m(d)]^2 / 2[s(d)]^2}}{xs(d)\sqrt{2\pi}} dx = R \quad (\text{Eq. F-51})$$

If using a built-in inverse lognormal function, verify the result.

$$\text{Set } T(y) \text{ to } \sum_{d=1}^{365} P(d, y).$$

$$\text{Set } P(0, y+1) \text{ to } P(365, y).$$

(Sort  $y$ ) Create  $Y(i)$ ,  $i = 1$  to 1,000, such that  $T[Y(i)] \geq T[Y(i+1)]$ ,  $i = 1$  to 1,000.

#### **F4.1.2 Developing a Representative Subsample**

This procedure groups the 1,000 sample years into bins. The first bin contains just the year with the greatest precipitation. The next bin contains the next two wettest years. Subsequent bins contain seven, twenty, and seventy years. The remaining 900 years are divided into five bins of 180 years each.

(Weights for sample years)

Set  $W(1)$  to 0.001 (1,000-year event).

Set  $W(2)$  to 0.002 (300-year event).

Set  $W(3)$  to 0.007 (100-year event).

Set  $W(4)$  to 0.02 (30-year event).

Set  $W(5)$  to 0.07 (10-year event).

For  $i$  from 6 through 10, set  $W(i)$  to 0.18.

(Select subsample years)

Set  $S(1)$  to  $Y(1)$ .

Select a random number,  $0 < R < 1$ , and set  $S(2)$  to  $Y(2 + 2R)$ , truncating index.

Select a random number,  $0 < R < 1$ , and set  $S(3)$  to  $Y(4 + 7R)$ , truncating index.

Select a random number,  $0 < R < 1$ , and set  $S(4)$  to  $Y(11 + 20R)$ , truncating index.

Select a random number,  $0 < R < 1$ , and set  $S(5)$  to  $Y(31 + 70R)$ , truncating index.

For  $i$  from 6 through 10, select a random number,  $0 < R < 1$ , and set  $S(i)$  to  $Y(101 + 180(i - 6) + 180R)$ , truncating index.

## F4.2 GENERATION OF TEMPERATURE INPUT

This section steps through how the daily minimum and maximum temperatures are determined for the 10 representative years generated in Section F4.1.

For  $x$  from 1 to 365, use the least squares approach to best fit each of the four temperature models defined by Equations F-43 through F-46 for each of the meteorological stations. Initial values for  $\alpha$ ,  $\beta$ , and  $\gamma$  are 20°C, DOY 80, and 30°C, respectively.

Determine the  $\alpha$ ,  $\beta$ , and  $\gamma$  values for each of the four temperature models for each of the three anticipated climate episodes. This is done by calculating the midpoint of the range for the  $\alpha$ ,  $\beta$ , and  $\gamma$  values calculated in Step I for the meteorological stations in each climate.

Using Equations F-43 through F-46 for  $x$  from 1 to 365, apply the  $\alpha$ ,  $\beta$ , and  $\gamma$  values to the 10 representative years generated in Section F4.1 for each of the three anticipated climates to obtain the daily minimum and maximum temperatures for dry or wet days as appropriate.

## F4.3 GENERATION OF WIND SPEED INPUT

Wind speeds are calculated by averaging the monthly wind data collected at the four Yucca Mountain meteorological stations: Sites 1, 2, 3, and 6. These values are then converted to equivalent wind speed at 2 meters aboveground level using Equation F-49. Each monthly average is applied at the middle of the month and the wind speeds for other days are interpolated between two monthly averages. Output DTN: SN0610T0502206.030 contains details of the interpolation.

Since there is no qualified wind speed data for the Monsoon climate and Glacial Transition analogue sites, those daily wind speed values are approximated by the Present-Day climate.

## F5. NOMENCLATURE FOR EQUATIONS USED IN APPENDIX F

Symbol	Description	Units	Where Used*
$P$	Precipitation		Eq. F-1
$p$	Probability density		Eq. F-1
$m$	Mean of the logarithm of precipitation		Eq. F-1 (F-2)
$s$			Eq. F-1 (F-2)
$\lambda$	Mean precipitation		Eq. F-2
$f(t)$	Any continuous function of time	varies	Eq. F-3 (F-4; F-5; F-6)
$a$	Zero-order term in a Fourier series	varies	Eq. F-3 (F-4; F-14; F-15; F-16; F-17; F-18)
$v_n$	Coefficient of nth-order sine term in a Fourier series	varies	Eq. F-3 (F-5; F-7; F-8)
$n$	Index of term in a Fourier series	none	Eq. F-3 (F-5; F-6)

Symbol	Description	Units	Where Used*
$w_n$	Coefficient of nth-order cosine term in a Fourier series	varies	Eq. F-3 (F-6; F-7; F-8)
$b_n$	Coefficient of nth-order term in polar form of a Fourier series	varies	Eq. F-3
$\theta_n$	Phase of nth-order term in polar form of a Fourier series	radians	Eq. F-3 (F-8)
$p_{00}(d)$	The probability that day $d$ is dry, given that day $D-1$ is dry	none	Eq. F-9 (F-38; F-39; F-40)
$p_{10}(d)$	The probability that day $d$ is dry, given that day $D-1$ is wet	none	Eq. F-10 (F-38; F-39; F-40)
$\lambda(d)$	Mean of the probability distribution for amount of precipitation on day $d$ , given that it is a wet day	mm	Eq. F-11
$m(d)$	Mean of the probability distribution for the natural logarithm of the amount of precipitation on day $d$ , given that it is a wet day	In mm	Eq. F-12
$a_{00}$	Zero-order term in Fourier series for $p_{00}(d)$	none	Eq. F-9 (F-41; F-42; F-47)
$a_{10}$	Zero-order term in Fourier series for $p_{10}(d)$	none	Eq. F-10 (F-41; F-42; F-47)
$b_{00,1}$	Coefficient of first-order term in Fourier series for $p_{00}(d)$ (polar form)	none	Eq. F-9
$b_{00,2}$	Coefficient of second-order term in Fourier series for $p_{00}(d)$ (polar form)	none	Eq. F-9
$\theta_{00,1}$	Phase of first-order term in Fourier series for $p_{00}(d)$ (polar form)	radians	Eq. F-9
$d'$	$2\pi d / 365$	radians	Eq. F-9 (F-10; F-11; F-12; F-13; F-14; F-33)
$\theta_{00,2}$	Phase of second-order term in Fourier series for $p_{00}(d)$ (polar form)	radians	Eq. F-9 (F-10)
$b_{10,1}$	Coefficient of first-order term in Fourier series for $p_{10}(d)$ (polar form)	none	Eq. F-10
$\theta_{10,1}$	Phase of first-order term in Fourier series for $p_{10}(d)$ (polar form)	radians	Eq. F-10
$b_{10,2}$	Coefficient of second-order term in Fourier series for $p_{10}(d)$ (polar form)	none	Eq. F-10
$\theta_{10,2}$	Phase of second-order term in Fourier series for $p_{10}(d)$ (polar form)	radians	Eq. F-10
$a_\lambda$	Zero-order term in Fourier series for $\lambda(d)$	mm	Eq. F-11 (F-42)
$b_{\lambda,1}$	Coefficient of first-order term in Fourier series for $\lambda(d)$ (polar form)	mm	Eq. F-11
$\theta_{\lambda,1}$	Phase of first-order term in Fourier series for $\lambda(d)$	radians	Eq. F-11
$b_{\lambda,2}$	Coefficient of second-order term in Fourier series for $\lambda(d)$ (polar form)	mm	Eq. F-11
$\theta_{\lambda,2}$	Phase of second-order term in Fourier series for $\lambda(d)$	radians	Eq. F-11
$a_m$	Zero-order term in Fourier series for $m(d)$	In mm	Eq. F-12

Symbol	Description	Units	Where Used*
$b_{m,1}$	Coefficient of first-order term in Fourier series for $m(d)$ (polar form)	In mm	Eq. F-12
$\theta_{m,1}$	Phase of first-order term in Fourier series for $m(d)$	radians	Eq. F-12
$b_{m,2}$	Coefficient of second-order term in Fourier series for $m(d)$ (polar form)	In mm	Eq. F-12
$\theta_{m,2}$	Phase of second-order term in Fourier series for $m(d)$	radians	Eq. F-12
$F(d)$	A precipitation parameter as a function of $d$	varies	Eq. F-14
$d$	Day of the year beginning with March 1	days	Eq. F-15 (F-16; F-17; F-18; F-20)
$y$	Year index	none	Eq. F-15 (F-16; F-20)
$f_1(d)$	Residue of after subtracting zero-order term: $f(d) - a$	varies	Eq. F-17
$\hat{f}_{n-1}(d, y)$	Residue after subtracting terms through $n-1$ : $f(d) - a - \sum_{m=1}^{n-1} b_m \sin(\theta_m + md')$	varies	Eq. F-18 (F-19; F-20; F-21; F-22; F-23; F-24; F-25; F-26; F-27; F-28; F-29; F-30; F-31; F-32; F-33; F-34; F-35; F-36)
$p_d(d)$	Probability that day $d$ is dry	none	Eq. F-38 (F-39; F-40)
$T_{wet_{min}}$	Minimum temperature on wet days	°C	Eq. F-43
$a_{wet_{min}}$	Magnitude of sine term in sine function for $T_{wet_{min}}$	°C	Eq. F-43
$\beta_{wet_{min}}$	Spring day of zero sine term for $T_{wet_{min}}$	days	Eq. F-43
$x$	Day of year from January 1, ignoring February 29	days	Eq. F-43 (F-44; F-45; F-46)
$\gamma_{wet_{min}}$	Zero-order term in sine function for $T_{wet_{min}}$	°C	Eq. F-43 (F-47)
$T_{dry_{min}}$	Minimum temperature on dry days	°C	Eq. F-44
$a_{dry_{min}}$	Magnitude of sine term in sine function for $T_{dry_{min}}$	°C	Eq. F-44
$\beta_{dry_{min}}$	Spring day of zero sine term for $T_{dry_{min}}$	days	Eq. F-44
$\gamma_{dry_{min}}$	Zero-order term in sine function for $T_{dry_{min}}$	°C	Eq. F-42 (F-47)
$T_{wet_{max}}$	Maximum temperature on wet days	°C	Eq. F-45
$a_{wet_{max}}$	Magnitude of sine term in sine function for $T_{wet_{max}}$	°C	Eq. F-45
$\beta_{wet_{max}}$	Spring day of zero sine term for $T_{wet_{max}}$	days	Eq. F-45
$\gamma_{wet_{max}}$	Zero-order term in sine function for $T_{wet_{max}}$	°C	Eq. F-45
$T_{dry_{max}}$	Maximum temperature on dry days	°C	Eq. F-46
$a_{dry_{max}}$	Magnitude of sine term in sine function for $T_{dry_{max}}$	°C	Eq. F-46
$\beta_{dry_{max}}$	Spring day of zero sine term for $T_{dry_{max}}$	days	Eq. F-46
$\gamma_{dry_{max}}$	Zero-order term in sine function for $T_{dry_{max}}$	°C	Eq. F-46
$u_2$	Wind speed at 2 m aboveground	m/s	Eq. F-49



<b>Symbol</b>	<b>Description</b>	<b>Units</b>	<b>Where Used*</b>
$u$	Wind speed measured at a height of $z$ meters aboveground	m/s	Eq. F-49
$z$	Height aboveground at which wind speed is measured	m	Eq. F-49
$P(d,y)$	Precipitation for day $d$ (1 to 365) of year, $y$	mm	Eq. F-50 (F-51)
$s$	Parameter of lognormal distribution $s^2 = 2(\ln \lambda - m)$	ln mm	Eq. F-50 (F-51)
$R$	Random number between 0 and 1	none	Eq. F-50 (F-51)
$f_w$	Fraction of days that are wet	none	Eq. F-41

\* Defined in these equations. Equation numbers in parentheses show other equations where these terms are used but not redefined.

INTENTIONALLY LEFT BLANK

**APPENDIX G**  
**DESCRIPTION OF THE MASSIF ROUTINES**



## **PREFACE**

The purpose of Appendix G is to document the MASSIF routines. It does not contain a listing or rationale for the property values, initial values, or options used for specific calculations. These are contained in the model and property descriptions of the report, or in the calculation results section.

Appendix G is a nearly exact reproduction of the electronic Mathcad file “Massif Documentation.xmcd”, in which the MASSIF routines are documented step-by-step. The electronic file contains hypertext links to the actual MASSIF routines. The MASSIF routines contain reciprocal hypertext links to the documentation file as well as to tables of variable definitions, and to the primary FAO-56 references in electronic form. Appendix G **contains** pointers to sections of the model report that are **not** contained in the electronic version. The electronic version does not contain the pointers to the model report for two reasons:

- 1) Editing the report can result in changes in the sections numbers. Since it is desirable to “freeze” the electronic files before the report editing is complete, the electronic files do not contain most of the pointers.
- 2) Future revisions of the report may result in changes of the section numbers. Corresponding revisions of the electronic files should not be required unless there are accompanying changes in the model implementation.

Because the primary purpose of the electronic file is on-line documentation, the file and Appendix G have certain traits worth noting:

- 1) The variable names are identical to those in the Mathcad files but may be somewhat different than those used in other parts of the model report.
- 2) The documentation of the routines is organized according to phenomenological topic. Within each topic group, the primary routine is listed first. Secondary routines which are used by the primary routine follow within the group. One exception to this is the explanation of the water balance model. The balance model is explained first; the “group-balance” model that links the individual cells together is listed second.

## G1. INTRODUCTION

MASSIF (**M**ass **A**ccounting **S**ystem for **S**oil **I**nfiltration and **F**low) is designed to provide an estimate of the net infiltration of water into the fractured rock which underlies the soil at Yucca Mountain. The core of MASSIF is a daily water balance for each cell in the watershed (Section 6.4). The daily water balance for the soil in each cell ( $30 \text{ m} \times 30 \text{ m}$ ) is:

$$R_{off} = P_{rain} + R_{on} + SM - \Delta\theta - ET - NI \quad (\text{Eq. G-1a})$$

where

$R_{off}$	=	runoff
$P_{rain}$	=	precipitation as rain
$R_{on}$	=	run-on
$SM$	=	snowmelt
$\Delta\theta$	=	change in water storage in the soil
$ET$	=	evapotranspiration
$NI$	=	net infiltration.

The water balance is written as a calculation for the runoff from the cell. All the quantities to the right of the equals sign are computed from submodels. MASSIF deals only with self-contained watersheds that have no run-on from sources outside the watershed boundary.

The daily water balance on the snowpack for each cell is:

$$\Delta SP = P_{snow} - SUB - SM \quad (\text{Eq. G-1b})$$

where

$\Delta SP$	=	change in the water storage of the snowpack
$P_{snow}$	=	precipitation as snow
$SUB$	=	sublimation
$SM$	=	snowmelt.

The model for the snowpack is simple (Appendix G3.5). Precipitation accumulates in the snow layer when the temperature is sufficiently low. While the temperature remains low, part of the snow sublimates. When the temperature increases, the snow melts and releases water into the soil.

The structure of MASSIF parallels that of FAO-56 (Allen et al. 1998 [DIRS 157311]), which is also the source of the submodel for evapotranspiration (ET). The water balance in FAO-56 utilizes the field capacity concept described in Section 6.2.2 of the modeling report. In the FAO-56 implementation of this concept, water in excess of the soil field capacity flows downward freely without rate restrictions. The daily water balance is performed in two steps. The first step (Appendix G3) handles the precipitation (or irrigation) event, and results in a calculation of net infiltration (NI) and the change in the water stored in the soil ( $\Delta\theta$ ). The duration of the precipitation event is included in this step, and the periods during and after the event are modeled separately (Appendix G3.2). The second step deals with the

evapotranspiration (ET) and results in another adjustment to the water stored in the soil ( $\Delta\Theta$ ) (Appendix G4).

Water flow rate limits in the soil and rock can result in water runoff ( $R_{\text{off}}$ ) when the rain intensity is sufficiently high. MASSIF uses saturated soil and rock conductivities to limit water flow between soil nodes (Figure G-1) and between the soil–rock interface. Runoff from a particular cell in the watershed appears as run-on in the cell immediately downstream. The calculation of runoff is part of the calculation step that deals with precipitation.

MASSIF is a collection of Mathcad “routines.” The following sections describe each routine in detail. The highest-level routine, the “driver” is named *Massif* (note the italics). Examination of *Massif* reveals the architecture of the calculation. Details of the component parts “called” in *Massif* are contained in appropriate sections. This documentation is contained in both Appendix G and in the appropriate Mathcad files. Mathcad users are encouraged to begin with the Table of Contents file (*MASSIF Table of Contents.xmcd*). This file contains (double click) hyperlinks (indicated by underlined bold blue text) to all sections in all of files that are a direct part of the MASSIF calculation. Examination of the Mathcad files allows the user to understand the exact implementation of the constituent parts of the infiltration analysis. A table of MASSIF routines and the Mathcad files in which they are located is provided in Section G6.

The *Massif* driver is executed in Mathcad files called “front ends.” These files feed the input stream into the *Massif* driver for the specific problem being examined. Results of the calculation are stored either in the front-end file in the form of embedded Excel worksheets, or as external ASCII files. Whenever the calculation in the front end is time-consuming, the call to the *Massif* driver is disabled; the disabled part of the front-end is colored pink. Documentation of these “front end” files and the associated postprocessing is included in *Massif Results Documentation.xmcd*.

Provisions have been made so that the user or reviewer can spot-check time-consuming calculations. Each of the front-ends used for the sensitivity analyses calculates the infiltration for ten (10) precipitation years in all eleven (11) watersheds in the domain for one realization in the Latin Hypercube Sampling (LHS) analysis. The CPU time for one of these files ranges from about 22 to 36 hours, depending upon the speed of the computer and the parameters of the LHS sample. Checking the entire calculation for a single realization would represent a considerable investment in time. In order to shorten and simplify the review process, the *Massif* driver is implemented for a single watershed and a single precipitation year specified by the user/reviewer. CPU time for this calculation can range from about 30 seconds for the smallest watershed to about 80 minutes for the largest watershed. Results of the spot check are displayed along with the results stored in the external ASCII file.

The structure of the MASSIF calculation is designed to realize three attributes of QUALITY consisting of TRANSPARENCY, TRACEABILITY AND REPRODUCIBILITY. TRANSPARENCY is facilitated by including explanatory text adjacent to the Mathcad implementation of the modeled equations. Mathcad's graphical interface enables a quicker grasp of the specifics of implementation that is elusive in scripted languages such as FORTRAN or C. TRACEABILITY is facilitated by the hyperlinked directory structure containing both the calculation files and the results of the calculation. REPRODUCIBILITY is possible because

specific portions of the front-ends can be reenabled and the results compared directly the archived results in the associated subdirectories.

## G2. THE MASSIF DRIVER

The *Massif* driver consists of two sections. The first section includes the calculations that need be calculated only once. The second section includes the calculation of values that change daily. The following steps are executed in the *Massif* routine:

### G2.1 SECTION 1: ONE-TIME EVALUATIONS

**Step 1:** Extract a subset of inputs from the input vectors/matrices.

**Explanation:** The input string to *Massif* consists of the name of the watershed (*Wshed*) and a series of vectors and matrices that contain the calculation inputs. The calculation inputs were condensed into vectors and matrices in order to keep the length of the variable string manageable. In many cases, the vectors and matrices are passed into called routines directly. However, some of the inputs must be extracted within the main driver (*Massif*).

**Step 2:** Read the watershed characteristics.

**Explanation:** *Wshed* is the name of the watershed file. The ID number, latitude, elevation, ID number of downstream cell, slope, azimuth, soil depth zone, soil type zone, rock zone (or type), and potential vegetative response is read for each cell in the watershed. The development of the Yucca Mountain watershed files are described in Section 6.5.2.1 and Appendix B.

**Step 3:** Calculate layer properties and assign initial conditions.

**Explanation:** The routine *LayerProps* calculates soil layer depths and extrinsic properties for each cell from the intrinsic soil properties and the soil depths. Additionally, the initial soil water levels are calculated for each node in each cell.

**Step 4:** Initialize the infiltration, total infiltration, snow level, monitored watershed output, and monitored cell output to zero at the start of the calculation.

**Explanation:** A vector of zeros and length equal to the number of cells is created by multiplying the vector *MaxInfil\_rk* by zero. The initial daily infiltration (*Infil*), the cumulative infiltration (*Total*), and the snow level for each cell (*Slevel*) are then set to this zero vector. Next, the initial values of the monitored watershed values are set to zero. Finally, if no cell quantities are to be monitored (*icell\_1=-1*), then the first (and only) element of the cell monitor vector (*Monitor\_cell\_1*) is set to zero.

**Step 5:** Calculate the psychrometric constant for each cell.

**Explanation:** The routine  $\gamma_{c\_fcn}$  calculates the psychrometric constant as a function of elevation. The Mathcad vectorizing function (the arrow) is applied to



$\gamma_{c\_fcn}$  because the variable  $elev$  is a vector containing the elevation for each cell in the watershed.

**Step 6:** Calculate the column indices for the  $R_b$  constant for each cell.

**Explanation:** The  $R_b$  constant is used to calculate the partitioning between direct and diffuse radiation. An external look-up table contains the value of  $R_b$  for specific combinations of surface slope and aspect (columns of table) for each day of the calendar year (rows of the table). The routine  $Index\_Rb\_fcn$  calculates the four columns of the  $R_b$  look-up table that apply to a specific cell. The Mathcad vectorizing function (the arrow) is applied to  $Index\_Rb\_fcn$  so that the four columns in the  $R_b$  look-up table that apply to a specific cell are computed for each cell in the watershed.

**Step 7:** Calculate the interpolation constants for  $R_b$  for each cell.

**Explanation:** The value of  $R_b$  for a particular cell on a particular day is calculated by interpolating the four bounding values. The interpolation is conducted over the slope/azimuth space. Hence the interpolating coefficients calculated in the routine  $CRb\_fcn$  are calculated once at the beginning of the infiltration calculation. The Mathcad vectorizing function (the arrow) is applied to  $CRb\_fcn$  so that the interpolation coefficients that apply to a specific cell are computed for each cell in the watershed.

**Step 8:** Calculate the column indices for the NDVI table for each cell.

**Explanation:** An external look-up table contains the NDVI values for various ranges of surface slope and azimuth (columns of table) for each day in the calendar year. The routine  $Index\_NDVI\_fcn$  determines the index of the NDVI look-up table that applies for a particular slope/azimuth combination. The Mathcad vectorizing function (the arrow) is applied to  $Index\_NDVI$  so that the index that applies to a specific cell is computed for each cell in the watershed.

**Step 9:** Find the upstream nodes that contribute to run-on.

**Explanation:** The geospatial file describing the watershed contains the ID of the single downstream cell to which runoff can move. However, run-on to a particular cell may come from multiple contributing cells. The routine  $UpStream3$  produces a list of cells that contribute run-on for each cell in the watershed.

**Step 10:** Calculate the annual precipitation used to scale the NDVI/ $K_{cb}$  correlation.

**Explanation:** The relationship between the vegetative coefficient ( $K_{cb}$ ) and the NDVI measurement is adjusted for the cumulative amount of precipitation in the water year. The routine  $precip\_Kcb\_fcn$  sums up the precipitation for the water year(s) being modeled.

**G2.2 SECTION 2: EVALUATIONS CONDUCTED FOR EACH DAY OF THE ANALYSIS**

**Step 11:** Calculate the average, maximum, minimum, and dew temperatures for each cell in the watershed.

**Explanation:** The daily maximum and minimum temperatures specified in the weather file apply to a specific reference elevation (*elev\_ref*). The routine *T<sub>elev\_cor</sub>* produces the average, maximum, minimum, and dew temperature for a given elevation. The Mathcad vectorizing function (the arrow) is applied to *T<sub>elev\_cor</sub>* so that the temperature vector that applies to a specific cell is computed for each cell in the watershed.

**Step 12:** Generate the temperatures for the average elevation of the watersheds.

**Explanation:** The air properties used to calculate the incident solar radiation are based upon temperatures computed at the average elevation (*elev\_avg*) of the modeled region (Appendix C1.1).

**Step 13:** Generate the daily precipitations for each cell.

**Explanation:** The daily precipitations listed in the weather file apply to a specific reference elevation (*elev\_ref*). The routine *Precip<sub>elev\_cor</sub>* produces the daily precipitation adjusted for the elevation of the cell of interest. The Mathcad vectorizing function (the arrow) is applied to *Precip<sub>elev\_cor</sub>* so that the temperature vector that applies to a specific cell is computed for each cell in the watershed.

**Step 14:** Calculate the “crop” coefficients and the vegetative canopy coefficients and adjust water levels of nodes in top layer due to varying canopy coefficient for each cell in the watershed.

**Explanation:** The top layer of soil is subdivided into two nodes. Node 1 models the bare soil. Node 2 models the soil under the vegetative canopy. The fraction of the soil covered by the vegetative canopy is described by the vegetative canopy coefficient (*f<sub>c</sub>*). The input to the *Massif* driver permits two options for the canopy coefficient. If an invariant canopy coefficient is specified ( $0 \leq f_{c\_switch} \leq 1$ ) the canopy coefficient is set equal to *f<sub>c\_switch</sub>*. If the correlation for vegetative canopy coefficient (*f<sub>c</sub>*) is used (*f<sub>c\_switch</sub>*=-1), the canopy coefficient changes from day to day (calculated for each cell in the watershed in routine *K<sub>cb\_fcn</sub>*). The change in the relative size of Nodes 1 and 2 necessitates a transfer of water from the shrinking node to the expanding node in order to conserve water. This transfer of water between Nodes 1 and 2 is performed in routine *Varying<sub>f<sub>c</sub></sub>*.

**Step 15:** Calculate the reference evapotranspiration for the day.

**Explanation:** The reference evapotranspiration (*ET<sub>0</sub>*) is calculated for each cell in the watershed in routine *ET<sub>0</sub>*.

**Step 16:** Calculate the accumulation of snow and its influence on the water available to the soil.

**Explanation:** When the temperature is sufficiently low, precipitation will accumulate above the soil in the form of snow. When the temperature is sufficiently high, accumulated snow will melt and supply water to the soil. Routine *SnowB* calculates the snow level (*Slevel*), amount of precipitation that reaches the soil (*NetPrecip*), snow sublimation (*Sublimation*), and snowmelt (*SnowMelt*) for each cell in the watershed.

**Step 17:** Calculate changes in water levels, runoff, and run-on due to water redistribution for each cell in the watershed.

**Explanation:** The field-capacity model of water flow through soils permits water to instantaneously flow downward when the “water level” of a layer exceeds the field capacity. This soil flow model is implemented in the routine *Balance*. The routine *GroupBalance* implements the *Balance* routine on every cell in the watershed and keeps track of the amount of runoff and run-on for each cell.

**Step 18:** Calculate changes in water levels due to evaporation and transpiration for each cell in the watershed.

**Explanation:** The amount of transpiration and evaporation that occurs in the day is calculated and subtracted from the appropriate water levels in routine *ET*.

**Step 19:** Check global water conservation for the day and keep track of spatially integrated water values.

**Explanation:** The integrated amount of water leaving the watershed is subtracted from the integrated amount of water entering the watershed in routine *Masscheck\_fcn*. The difference should be a small number that reflects the machine precision limitations of the algebraic operations. The individual components of the global balance equation are saved in an array (*addition1*) for output from the *Massif* routine.

The watershed output from *Massif* is contained in the matrix *Monitor<sub>WS</sub>*. The information content of this matrix is decided by the user. If the user assigns a value of  $-1$  to the input variable *i<sub>WS</sub>*, then *Massif* returns cumulative values of the reported components for the modeled time period. If the user assigns a value of  $1$  to *i<sub>WS</sub>*, *Massif* returns daily values of the reported components. A list of the reported quantities is contained with the routine *Masscheck\_fcn*.

**Step 20:** Assemble calculated quantities for the monitored cells.

**Explanation:** If there is a list of monitored cells, append the monitored daily quantities assembled in *Monitor<sub>cell\_fcn</sub>* to the list of those quantities for previous days.

**Routine Output:** Return the output from the routine.

**Explanation:** *Massif* returns eight sets of calculated values:

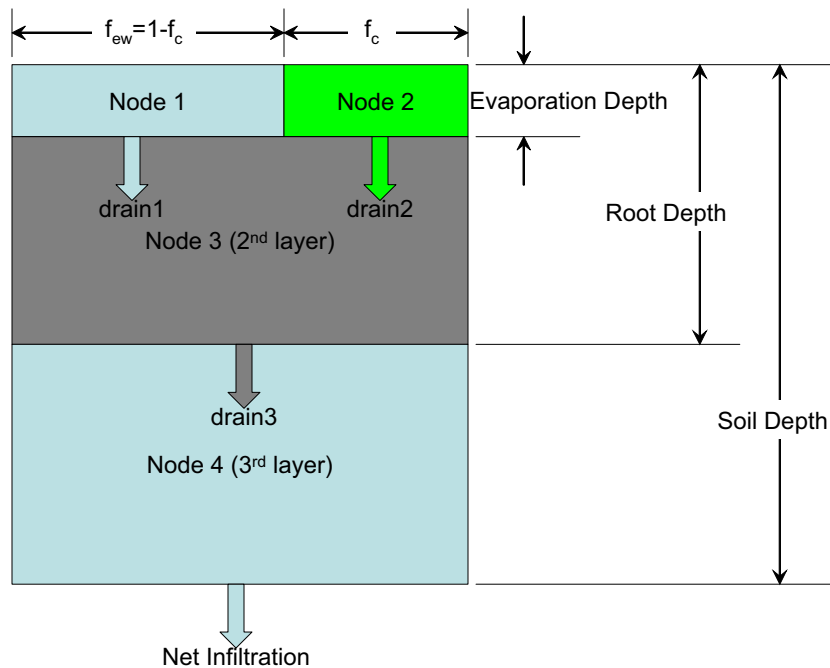
- 1) Average annual net infiltration into the bedrock for each cell in the watershed
- 2) Average annual precipitation for each cell in the watershed
- 3) Average annual run-on for each cell in the watershed
- 4) Average annual runoff for each cell in the watershed
- 5) Global mass check for each day of the calculation
- 6) Monitored quantities for each monitored cell
- 7) Monitored watershed quantities
- 8) Clock time needed to complete the calculation.

### **G3. WATER FLOW**

#### **G3.1 THE CELL BALANCE MODEL**

The cell “balance” model is a water conservation model in which water in excess of the field capacity flows into the underlying layer subject to the constraints of saturated conductivities. Fractured bedrock, characterized by rock saturated flow conductivity, underlies the bottom soil layer. The soil is divided into three layers. The thickness of the top layer is defined by the evaporation depth. The thickness of the second layer is defined by the difference between the rooting depth and the evaporation depth. The thickness of the third layer is defined by the difference between the soil depth and the rooting depth. When the soil depth is less than the rooting depth, the thickness of Layer 3 is zero. When the soil depth is less than the evaporation depth, the thickness of Layer 2 is zero. The thickness of Layer 1 is always finite, but it can be less than the evaporation depth. In such cases, the thickness of the top layer is equal to the soil depth.

The cell balance model in this analysis consists of four soil nodes (Figure G-1). The top layer is divided into two nodes. Node 1 is the evaporation region, which is not protected by the vegetation canopy. Node 2 lies under the vegetation canopy. Nodes 3 and 4 consist of the middle and bottom soil layers, respectively. Water from precipitation and runoff is added to the water levels of Nodes 1 and 2 before the balance model is “called.” The balance model is called only when the water level in at least one of the nodes is greater than the layer field capacity.



Source: Output DTN: SN0701T0502206.037.

Figure G-1. Water Infiltration in the Cell Balance Model

The balance model calculates, for a given water inventory in the nodes, the amount of water that flows into the underlying bedrock, and the amount that flows off the cell in the form of “runoff.” It calculates these quantities in a two-stage calculation procedure. In the first stage, water is allowed to flow downward subject to saturated conductivity limits into the underlying node without regard to the capacity of the underlying node to hold the water. The net infiltration into the bedrock is calculated at the end of this stage. In the second stage, the capacity of the nodes to hold water is examined, and water that cannot fit within the node is passed upward into the overlying node. The runoff from the cell is calculated at the end of the second stage.

The two stage calculation procedure is merely an efficient numerical tool for the solution of the equations for water motion. The numerical artifices of overfilling a node with water and then pushing the excess water upward are not real physical processes. They are simply used as a method of applying volumetric constraints on a flow equation with split boundary conditions.

The use of two nodes in the top layer presents a complicating factor. It is possible that one of the top nodes might have an excess of water at the end of the second stage while the adjacent node is not fully filled. In this event, the excess water in one of the top nodes is first applied to fill the adjacent node. Only after the adjacent node is filled will excess water be applied to “runoff,” which will migrate to the adjacent cell. This is justified because there will be several plants, each with its own evaporation zone and canopy zone, in a single 30-m × 30-m cell.

The following are the computational steps of the cell balance model (routine *Balance*). Note that the water available to the cell has already been added to the surface layer (Nodes 1 and 2) before the call to *Balance*.

**Step 1:** Calculate the amount of water that can drain from Node 1.

**Explanation:** The water level for Node 1 ( $W_{level1}$ ) is compared against the field capacity for that layer ( $FC_{layer1}$ ). The drainage from Node 1 ( $drain1$ ) is then set to the difference between the water level and the field capacity. The drainage is then limited to the soil conductivity limit adjusted for the time period of the precipitation episode ( $MaxInfil_{sl\_mod}$ ). Finally, the drainage is subtracted from the water level.

**Step 2:** Calculate the amount of water that can drain from Node 2.

**Explanation:** The water level for Node 2 ( $W_{level2}$ ) is compared against the field capacity for that layer ( $FC_{layer2}$ ). The drainage from Node 2 ( $drain2$ ) is then set to the difference between the water level and the field capacity. The drainage is then limited to the soil conductivity limit adjusted for the time period of the precipitation episode ( $MaxInfil_{sl\_mod}$ ). Finally, the drainage is subtracted from the water level.

**Step 3:** Transfer excess water from Node 1 to Node 2 if the drainage from Node 2 is less than the episodic soil conductivity limit.

**Explanation:** If there is excess water remaining in Node 1 and the drainage from Node 2 was not maximized, part or all of the excess water is transferred to Node 2. First, the drainage from Node 2 is restored to the node. The excess water in Node 1 ( $\Delta W_{level1\_max}$ ) is calculated. Then the change in the Node 2 water level needed to realize the flow limit ( $\Delta W_{level2\_max}$ ) is calculated. The actual change in the water level ( $\Delta W_{level2}$ ) of Node 2 is the minimum of the  $\Delta W_{level1\_max}$  corrected for the canopy fraction ( $f_c$ ), and  $\Delta W_{level2\_max}$ . The water level of Node 2 is increased by the amount  $\Delta W_{level2}$ . The drainage from Node 2 ( $drain2$ ) is then calculated as the difference between the new Node 2 water level and the Node 2 field capacity ( $FC_{layer2}$ ). The drainage is subtracted from Node 2. Finally, the transferred water is subtracted from Node 1.

**Step 4:** Transfer excess water from Node 2 to Node 1 if the drainage from Node 1 is less than the episodic soil conductivity.

**Explanation:** If there is excess water remaining in Node 2 and the drainage from Node 1 was not maximized, part or all of the excess water is transferred to Node 1. First, the drainage from Node 1 is restored to the node. The excess water in Node 2 ( $\Delta W_{level2\_max}$ ) is calculated. Then the change in the Node 1 water level needed to realize the flow limit ( $\Delta W_{level1\_max}$ ) is calculated. The actual change in the water level ( $\Delta W_{level1}$ ) of Node 1 is the minimum of the  $\Delta W_{level2\_max}$  corrected for the canopy fraction ( $f_c$ ), and  $\Delta W_{level1\_max}$ . The water level of Node 1 is increased by the amount

$\Delta W_{level1}$ . The drainage from Node 1 (*drain1*) is then calculated as the difference between the new Node 1 water level and the Node 1 field capacity ( $FC_{layer1}$ ). The drainage is subtracted from Node 1. Finally, the transferred water is subtracted from Node 2.

**Step 5:** Add the drainage from Nodes 1 and 2 to Node 3.

**Explanation:** The drainage from Nodes 1 and 2, weighted for the canopy fraction, is added to the water level of Node 3 ( $W_{level3}$ ).

**Step 6:** Excess water in Node 3 drains into Node 4.

**Explanation:** If the water level of Node 3 ( $W_{level3}$ ) exceeds the Node 3 field capacity ( $FC_{layer3}$ ), then let the excess water flow downward. First the drainage from Node 3 (*drain3*) is calculated as the difference between the water level and the node field capacity. Then the drainage is corrected for the soil saturated conductivity ( $MaxInfil_{sl}$ ). The drainage is subtracted from the Node 3 water level. Finally, the drainage is added to the Node 4 water level.

**Step 7:** Excess water in Node 4 drains into the bedrock.

**Explanation:** If the water level of Node 4 ( $W_{level4}$ ) exceeds the Node 4 field capacity ( $FC_{layer4}$ ), then let the excess water flow downward into the underlying fracture rock. First the drainage from Node 4 (*Infil*) is calculated as the difference between the water level and the node field capacity. Then the drainage is corrected for the soil saturated conductivity ( $MaxInfil_{sl}$ ). Next the drainage is corrected for the rock saturated conductivity ( $MaxInfil_{rk}$ ). The drainage is subtracted from the Node 4 water level.

**Step 8:** If the water content of Node 4 exceeds the pore volume, pass the excess water up into Node 3.

**Explanation:** If the water level of Node 4 ( $W_{level4}$ ) exceeds the pore volume of Node 4 ( $Pore_{sl4}$ ), pass the excess water up into Node 3.

**Step 9:** If the water content of Node 3 exceeds the pore volume, pass the excess water up into Nodes 1 and 2.

**Explanation:** If the water level of Node 3 ( $W_{level3}$ ) exceeds the pore volume of Node 4 ( $Pore_{sl3}$ ), pass the excess water ( $\Delta W_{level3}$ ) up into Nodes 1 and 2. The excess water is prorated between Nodes 1 and 2 according to the amounts that originally drained into Node 3 during **Step 5**.

**Step 10:** Transfer excess water in Node 1 into Node 2 before computing runoff.

**Explanation:** If the water level in Node 1 ( $W_{level1}$ ) is greater than the pore volume of Node 1 ( $Pore_{sl1}$ ) and the water level in Node 2 is less than the pore volume in Node 2 ( $Pore_{sl2}$ ) and the canopy fraction ( $f_c$ ) is greater than zero, transfer as much excess water to Node 2 before computing the runoff. First, compute the maximum amount of water that can be transferred from Node 1 ( $DW_{level1\_max}$ ). The actual change in the water level of Node 2 ( $\Delta W_{level2}$ ) is the minimum of  $\Delta W_{level1\_max}$  adjusted for the canopy fraction and the amount of water necessary to maximize the water content of Node 2 ( $Pore_{sl2} - W_{level2}$ ). The actual change is added to the water level of Node 2. Finally, the actual change, adjusted for the canopy fraction, is subtracted from Node 1.

**Step 11:** Transfer excess water in Node 2 into Node 1 before computing runoff.

**Explanation:** If the water level in Node 2 ( $W_{level2}$ ) is greater than the pore volume of Node 2 ( $Pore_{sl2}$ ) and the water level in Node 1 is less than the pore volume in Node 1 ( $Pore_{sl1}$ ) and the canopy fraction ( $f_c$ ) is greater than zero, transfer as much excess water to Node 1 before computing the runoff. First, compute the maximum amount of water that can be transferred from Node 2 ( $\Delta W_{level2\_max}$ ). The actual change in the water level of Node 1 ( $\Delta W_{level1}$ ) is the minimum of  $\Delta W_{level2\_max}$  adjusted for the canopy fraction, and the amount of water necessary to maximize the water content of Node 1 ( $Pore_{sl1} - W_{level1}$ ). The actual change is added to the water level of Node 1. Finally, the actual change, adjusted for the canopy fraction, is subtracted from Node 2.

**Step 12:** Transfer excess water in Node 1 to runoff.

**Explanation:** If the water level of Node 1 ( $W_{level1}$ ) is greater than the pore volume of Node 1 ( $Pore_{sl1}$ ), transfer the excess water to runoff. The canopy fraction ( $f_c$ ) is used to compute the weighted contribution of Node 1 to the runoff.

**Step 13:** Transfer excess water in Node 2 to runoff.

**Explanation:** If the water level of Node 2 ( $W_{level2}$ ) is greater than the pore volume of Node 1 ( $Pore_{sl2}$ ), transfer the excess water to runoff. The canopy fraction ( $f_c$ ) is used to compute the weighted contribution of Node 2 to the runoff.

**Routine Output:** The routine returns the water level for each node, the net infiltration into the bedrock, and the runoff from the cell.



### G3.2 THE GROUP BALANCE MODEL

With the exception of the outlet cell in the watershed, runoff from one cell becomes run-on for another cell. Run-on is an additional source of water for infiltration into the soil. MASSIF keeps track of runoff and run-on for each cell. The cell indices of upstream contributors, computed by the *Upstream* routine, is contained in the vector *Upstream*. The water available for infiltration in an individual cell consists of the runoff from these upstream contributors, the cell precipitation, and the cell snowmelt.

The *GroupBalance* routine models the run-on/runoff connection between the individual cells in the watershed. The routine begins at the top of the watershed and computes the infiltration/runoff for this top-most cell using the cell balance model (*Balance*). It then proceeds to the next lower cell in the watershed and does the same for it. The routine proceeds through the entire watershed and ends at the lowest cell. Runoff from this last cell exits the watershed. Because the cells in the geospatial files describing the watersheds are ordered according to elevation, the progression from highest to lowest elevation cells occurs naturally.

The calculation of runoff and infiltration from individual cells when available water exists (i.e., when it rains or when there is snowmelt) is accomplished by two calls to the *Balance* routine. The first call accounts for infiltration and runoff during the precipitation event. In this call, both runoff and infiltration can take place. Soil saturated conductivity limits create the possibility of water contents greater than the field capacity at the end of a storm. Therefore, water can still drain from the soil after the storm has ended. The second call to *Balance* deals with this “drainage” stage. Although infiltration is possible during this second stage, addition runoff is not possible.

The steps in the group balance model (*GroupBalance*) are listed below. Only the processes within the loop that proceeds through the cells in the watershed are enumerated. The initialization and output that occurs before and after the loop are obvious. Note that a certain amount of logic has been added to avoid unnecessary calls to the *Balance* routine. This is done to minimize execution time.

**Step 1:** The runoff and run-on for the cell are each initialized to 0 mm.

**Step 2:** Calculate the run-on to the cell.

**Explanation:** *Upstream* is a vector of vectors. The vector component  $Upstream_n$  is, itself, a vector that contains the indices of the upstream contributors to cell  $n$ . The first contributor is listed as the second element of this vector; the second contributor is listed as the third element, and so on. There are no upstream contributors if this vector ( $Upstream_n$ ) has only one element. If the length of  $Upstream_n$  is greater than one, the run-on to cell  $n$  is set equal to the sum of the runoff of the upstream contributors.

**Step 3:** Compute the water available to the soil.

**Explanation:** The water available to the soil is the sum of the precipitation (when it does not appear as snow), the snowmelt, and the run-on. Note that the variable *NetPrecip<sub>n</sub>* is equal to zero when precipitation occurs as snow, and is equal to the cell precipitation when precipitation occurs as rain.

**Step 4:** Compute the fraction of the day during which precipitation takes place.

**Explanation:** This calculation is performed in anticipation of the calls to the *Balance* routine. It denotes the fraction of the day when the available water is exposed to the soil surface. Note that special provision is made for the case when precipitation is absent and snowmelt is present. For this specific case, the precipitation duration (normally set to zero in the absence of precipitation) is set to 12 hours. This allows a 12-hour exposure time for snowmelt to seep into the soil when precipitation does not occur.

**Step 5:** Add the available water to the nodes in Layer 1 (Nodes 1 and 2).

**Explanation:** The sum of the runon, snowmelt, and rainfall constitutes the water available for infiltration. This available water is added to Nodes 1 and 2. This is the initial condition at the start of the day. Note that the available water may exceed the holding capacity of the soil in this layer. This condition is examined in the following steps. Excess water is manifested as either infiltration or runoff in the subsequent portion of the calculation.

**Step 6:** If any water level of the current node exceeds the field capacity, implement the balance routine.

**Explanation:** There is no need to redistribute water using the *Balance* routine if the field capacity in at least one of the soil nodes is not exceeded.

**Step 6a:** If there is water available to the soil surface, separate the precipitation/snowmelt event from the subsequent drainage phase.

**Explanation:** When water is available, the soil-filling phase is separated from the subsequent soil-draining phase. The first call to *Balance* computes net infiltration and runoff during the precipitation/snowmelt event. The second call to *Balance* computes net infiltration during the draining phase. No runoff can occur during the draining phase.

**Step 6b:** If there is no precipitation or snowmelt, the entire day is a drainage period.

**Explanation:** This condition can occur if draining and evapotranspiration that took place during the previous day was insufficient to lower the water levels in the soil to the field capacity. Only one call to *Balance* is needed under these circumstances.

**Routine Output:** The *GroupBalance* routine returns the water level for the four nodes, the net infiltration, run-on, and runoff for the day for every cell in the watershed.

### G3.3 UPSTREAM CONTRIBUTORS TO RUN-ON

The run-on to a specific cell is equal to the runoff from the “upstream” cells that are above it. To calculate run-on, one needs a list of the contributing “upstream” cells for every cell in the watershed. However, the geospatial file describing the watershed lists the ID number of a single “downstream” cell for every cell in the watershed, to which the runoff flows. Only the last cell in the geospatial file, the exit cell, lacks a “downstream” cell. For this last cell, the “downstream” cell ID is listed as “-3.”

The *Upstream* routine creates a vector of cell indices of the “upstream” cells that contribute to run-on for each cell in the watershed. It is easiest to describe this vector by an example. Suppose that the 50th cell in the watershed is the cell of interest and that the 25th, 35th, and 49th cells are the “upstream” cells that contribute to the run-on to the 50th cell. The upstream vector for the 50th cell would be:

$$\text{upstream}_{50} = \begin{pmatrix} 50 \\ 25 \\ 35 \\ 49 \end{pmatrix} \quad (\text{Eq. G-2})$$

This vector contains four elements. The first element is the index of the cell for which the run-on is to be calculated. The remaining elements of the vector are the indices of the upstream contributing cells. The lengths of the actual vectors vary with the number of upstream contributors.

Some cells in the watershed have no “upstream” cells that contribute to run-on. The 1st cell in the watershed is such a cell because it has the highest elevation in the watershed. The upstream vector for the 1st cell in the watershed is always a vector with a single element:

$$\text{upstream}_1 = (1) \quad (\text{Eq. G-3})$$

It is important to note that the cell ID number is not the cell index. The cell ID number has meaning only in the context of the software used to generate the geospatial file.

The steps in the *Upstream* routine are:

**Step 1:** Create the first element in the upstream vector of cell  $n$  for all cells.

**Explanation:** The first element of the upstream vector is the index of the cell.

**Step 2:** Find the downstream cell to which cell  $n$  contributes to run-on.

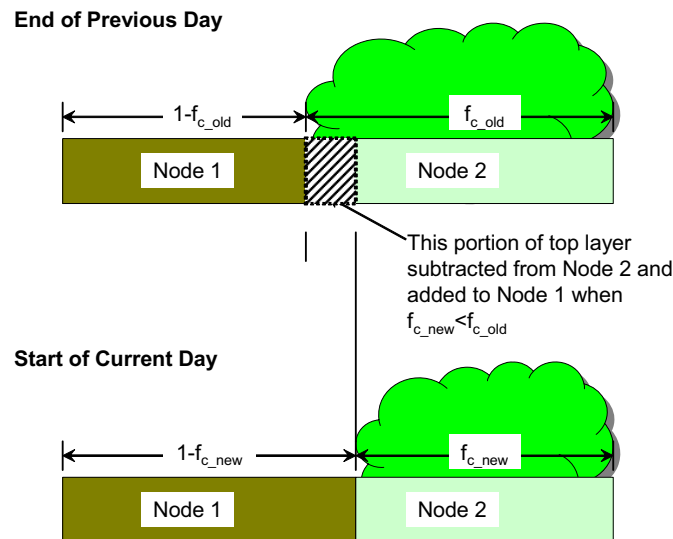
**Explanation:** Beginning with the 1st cell in the watershed, search for the ID number of the downstream cell. Because the cells are sorted by elevation, the downstream cell must have an index greater than the contributing cell ( $m > n$ ). If the ID number of the downstream cell ( $DnStn$ ) is the same as the cell ID number of the cell being checked ( $locidm$ ), the index of the

contributing cell is added to the upstream vector of cell  $m$  (*upstream $m$* ). If the downstream cell ID has not been found after examining the last cell in the watershed (*Ncells*), an error message is generated that states that the geospatial file had not been sorted correctly at the time of its generation and the calculation is terminated.

**Routine Output:** The *Upstream* routine creates a vector for each cell that lists the indices of the contributors to run-on.

### G3.4 WATER ADJUSTMENT FOR THE VARYING CANOPY COEFFICIENT ( $f_c$ )

The canopy coefficient can change from day to day when it is coupled to the crop coefficient ( $K_{cb}$ ). In order to conserve water, the water level in the expanding node in the top soil layer must be adjusted to account for the water being transferred from the shrinking node in the top soil layer (Figure G-2).



Source: Output DTN: SN0701T0502206.037.

Figure G-2. Daily Variation of Vegetative Canopy

Consider the case where the new canopy coefficient is less than the old canopy coefficient ( $f_{c\_new} < f_{c\_old}$ ). The water level of Node 2 (the canopy region) remains the same. However, the water level of Node 1 (the evaporation region) must be adjusted. Before the change, the water is Node 1 is:

$$\text{Water\_old}_1 = A \cdot (1 - f_{c\_old}) \cdot \text{Wlevel\_old}_1 \quad (\text{Eq. G-4})$$

where A is the area of of the node. The water “transferred” from Node 2 to Node 1 is:

$$\Delta Water = A \cdot (f_{c\_old} - f_{c\_new}) \cdot Wlevel_2 \quad (\text{Eq. G-5})$$

The new water level in Node 1 is:

$$Wlevel\_new_1 = \frac{Water\_old_1 + \Delta Water}{A \cdot (1 - f_{c\_new})}$$

$$Wlevel\_new_1 = \frac{[(1 - f_{c\_old}) \cdot Wlevel\_old_1 + (f_{c\_old} - f_{c\_new}) \cdot Wlevel_2]}{(1 - f_{c\_new})} \quad (\text{Eq. G-6})$$

Now consider the alternate case where the new canopy coefficient is greater than the old canopy coefficient ( $f_{c\_new} > f_{c\_old}$ ). The water level of Node 1 (the evaporation region) remains the same. However, the water level of Node 2 (the canopy region) must be adjusted. Before the change, the water in Node 2 is:

$$Water\_old_2 = A \cdot f_{c\_old} \cdot Wlevel\_old_2 \quad (\text{Eq. G-7})$$

The water “transferred” from Node 1 to Node 2 is:

$$\Delta Water = A \cdot [(1 - f_{c\_old}) - (1 - f_{c\_new})] \cdot Wlevel_1$$

$$\Delta Water = A \cdot (f_{c\_new} - f_{c\_old}) \cdot Wlevel_1 \quad (\text{Eq. G-8})$$

The new water level in Node 2 is:

$$Wlevel\_new_2 = \frac{Water\_old_2 + \Delta Water}{A \cdot f_{c\_new}}$$

$$Wlevel\_new_2 = \frac{f_{c\_old} \cdot Wlevel\_old_2 + (f_{c\_new} - f_{c\_old}) \cdot Wlevel_1}{f_{c\_new}} \quad (\text{Eq. G-9})$$

### G3.5 THE SNOW MODEL

The snow model in MASSIF is simple. When the average temperature for the day is less than or equal to 0°C, precipitation occurs in the form of snow, and the “net precipitation” (i.e., the precipitation that can enter the soil) is equal to zero. When the average daily temperature is greater than 0°C, precipitation is manifested as rain, and the “net precipitation” is equal to the daily precipitation. Accumulated snow melts at a rate that is linearly proportional to the average

daily temperature (in °C). Snowmelt is tracked separately from net precipitation, even though both are available to the soil surface.

Sublimation is crudely modeled in MASSIF. The reference for sublimation of snow packs gives an estimate of the fraction of the snowpack that is lost over the entire snow season; no estimate of daily loss to sublimation is given. In the absence of a phenomenological model or a correlation, the sublimation fraction is applied at the time of precipitation (Section 6.4.2). As an example, suppose the seasonal sublimation fraction is 0.1. If the precipitation is 10 mm for a particular day, 9 mm of snow is added to the snow level. The remaining 1 mm of precipitation is credited to sublimation.

The routine *SnowB* computes the snow level for each cell in the watershed. The steps for each cell in *SnowB* are:

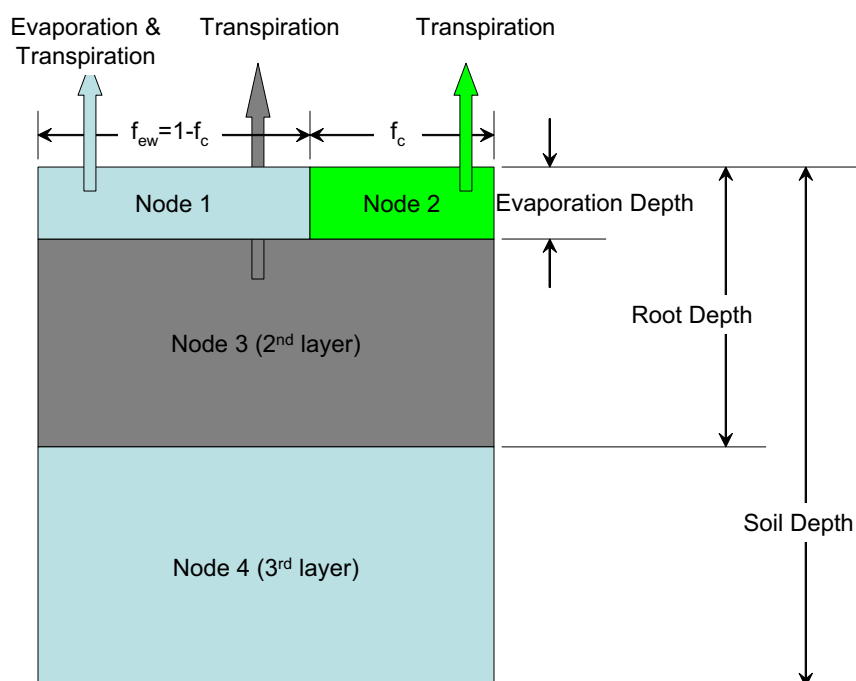
- Step 1:** Initialize the  $SnowMelt_n$  and  $Sublimation_n$  to zero. Initialize the  $NetPrecip_n$  to the precipitation.
- Step 2:** If the average temperature of the day ( $T_{avg}$ ) for the cell is less than or equal to zero, then
- Set the sublimation for cell n ( $Sublimation_n$ ) to the product of the precipitation for cell n ( $precip_n$ ) and the sublimation coefficient ( $C_{sublime}$ ).
  - Add the precipitation ( $precip_n$ ) to the snow level ( $Slevel_n$ ) and subtract the sublimation ( $Sublimation_n$ ) to get the new snow level.
  - Set the net precipitation ( $NetPrecip_n$ , precipitation available for infiltration) to zero.
- Step 3:** If the average temperature of the day ( $T_{avg}$ ) for the cell is greater than zero and the snow level for cell n ( $SnowMelt_n$ ) is greater than zero, then
- Set the snowmelt for cell n ( $SnowMelt_n$ ) to the minimum of
    - the product of the average temperature ( $T_{avg}$ ) and the snowmelt coefficient ( $C_{snowmelt}$ ), or
    - the total amount of snow for cell n ( $Slevel_n$ ).

**Routine Output:** *SnowB* returns the snow level, net precipitation, sublimation, and snowmelt for every cell in the watershed.

#### G4. EVAPOTRANSPIRATION

Evapotranspiration is the term applied for the transport of water to the atmosphere from the soil. It is so named because the mechanisms of evaporation from the soil and moisture transport through the plant structure and from the plant surfaces are difficult to completely separate. Hence the term implies an approach in which both phenomena are modeled within a single analytic framework.

The evapotranspiration paths, as contained in MASSIF, are shown below (Figure G-3). Nodes 1, 2, and 3 collectively describe the root zone. Node 4 extends from the bottom of the root zone to the bedrock. The top layer of the soil is divided into two nodes. Node 1 describes the near-surface bare soil region that lies outside of the vegetative canopy. Within Node 1, short term evaporative processes are modeled explicitly. Under the vegetative canopy (Node 2), the soil is shaded and evaporation rates are slower. The evaporative mechanisms in Nodes 2 and 3 are actually integrated into the correlations for transpiration. Transpiration is also attributed to the bare soil region (Node 1). This is because plant roots extend radially beyond the surface vegetative cover.



Source: Output DTN: SN0701T0502206.037.

Figure G-3. Evaporation and Transpiration in a Soil Cell

The foundation for the evapotranspiration model in MASSIF is the dual crop coefficient approach described in FAO-56 (Allen et al. 1998 [DIRS 157311], Chapter 7), and in a subsequent publication (Allen et al. 2005 [DIRS 176207]) that supports FAO-56. Within the FAO-56 procedure, water is presumed to drain without limitation to the field capacity whenever a surplus of water is introduced into the soil. The curve number approach can be used directly with the FAO-56 models when runoff is of interest. However, MASSIF utilizes saturated conductivity limits for the rock and soil to determine runoff. To accommodate this approach, the FAO-56 procedure has been adapted to the structure of MASSIF.

In FAO-56, the primary water balance is applied to the root zone, which is a combination of Nodes 1, 2, and 3 in the MASSIF calculation. MASSIF deals with evaporation in the bare soil region (Node 1) in the same way as FAO-56. The difference is that FAO-56 does not deal with the zone described by Node 2 explicitly. MASSIF must model Node 2 explicitly in order to deal

with the flow limits within the soil. This impacts the partitioning of transpiration within the root zone. Publications subsequent to FAO-56 (Allen et al. 2005 [DIRS 176207]) correlate the fraction of the transpiration that takes place in the evaporation zone (Node 1). A similar approach has been used to predict the fraction of transpiration that takes place in Node 2.

#### **G4.1 REFERENCE EVAPOTRANSPIRATION**

The reference evapotranspiration ( $ET_0$ ) is the evapotranspiration that takes place for a reference vegetation (the reference grass) under the condition of adequate soil moisture content. It takes into account the amount of solar insolation and reference atmospheric conditions that affect the transport of water. Actual evapotranspiration (ET) is calculated by modifying the reference evapotranspiration ( $ET_0$ ) for actual soil moisture contents and actual atmospheric conditions. The calculation of  $ET_0$  is documented in Appendix C, which is used as the reference for the equations used in MASSIF. The steps enumerated in Appendix C have been parsed into several routines in MASSIF for reasons of calculation efficiency. The steps numbers that follow in this section correspond to the steps in the individual MASSIF routines and should not be confused with the step numbers in Appendix C.

##### **G4.1.1 Calculation of Reference ET**

The steps of the routine that actual produces  $ET_0$  are examined first. The steps of individual supporting routines are enumerated after that.

The steps of the  $ET_0$  routine are:

**Step 1:** Calculate the actual vapor pressure for the entire domain (Equation C-2).

**Explanation:** This quantity is used in the calculation of diffuse and direct components of the solar insolation. A single value is used to model the air mass through which the scattering takes place.

**Step 2:** Calculate the solar insolation on a horizontal surface.

**Explanation:** The solar insolation on a horizontal surface is calculated in routine *R<sub>smhor\_func</sub>*.

**Step 3:** Calculate the diffuse and direct components of solar insolation

**Explanation:** The diffuse and direct components of solar insolation are calculated in routine *DiffuseDirect*. Breaking solar insolation into diffuse and direct components is done in preparation for computing solar insolation on inclined surfaces.

**The following steps take place for each cell in the watershed:**

**Step 4:** Calculate the slope/aspect correction for direct beam radiation for cell n.

**Explanation:** The correction is calculated in routine *Rb\_fn*.



- Step 5:** Calculate the mean vapor pressure for cell n (Equation C-29a).  
**Explanation:** The mean vapor pressure is used in the calculation of the estimated actual vapor pressure (Step 6).
- Step 6:** Calculate the estimated actual vapor pressure for cell n (Equation C-31).  
**Explanation:** The estimated actual vapor pressure is used to calculate the reference ET.
- Step 7:** Calculate the net solar radiation on the inclined surface of cell n.  
**Explanation:** The net solar radiation on the inclined surface is calculated in routine *SolarRad\_inc*.
- Step 8:** Calculate the slope of the saturation vapor pressure curve for cell n (Equation C-32).  
**Explanation:** Equation C-32 incorporates the equation for vapor pressure. The function for vapor pressure ( $e0$ ) is used in the MASSIF implementation.
- Step 9:** Calculate the reference evapotranspiration ( $ET_0$ ) using the Penman Monteith method for cell n (Equation C-37).  
**Routine Output:** Routine *ET0* returns the reference ET for a 24-hour day in mm of water for every cell in the watershed for the day being analyzed.

#### G4.1.2 Calculation of Vapor Pressure from Temperature

The vapor pressure is used in the calculation of the Reference ET (Steps 1 and 5 of routine *ET0*). It is written as a simple function of temperature as specified by Equation C-2 in. In Equation C-2, the temperature of interest is a particular temperature: the general dew point temperature. Because the MASSIF implementation uses this vapor pressure in several capacities, the vapor pressure function has been written with a nonspecific temperature. The vapor pressure routine is named  $e0$ .

#### G4.1.3 Calculation of “Actual” Solar Insolation on a Horizontal Surface

In Step 2 of the *ET0* routine, the solar insolation on a horizontal surface is calculated from the clear sky solar flux in routine *R<sub>smhor\_func</sub>*. The steps in routine *R<sub>smhor\_func</sub>* are:

- Step 1:** Calculate the clear sky solar flux on a horizontal surface.  
**Explanation:** The clear sky solar flux is calculated in routine *R<sub>sohor\_func</sub>*.
- Step 2:** Calculate the estimated “actual” solar flux on a horizontal surface (Equation C-13).  
**Explanation:** This step corrects the clear sky radiation flux for weather conditions.
- Step 3:** Limit “actual” solar radiation to the value of the clear sky solar flux (sentence following Equation C-13).  
**Explanation:** The clear sky solar radiation is an upper bound for the incident flux.

**Routine Output:** Routine  $R_{smhor\_fcn}$  returns a vector containing 1) the extraterrestrial radiation on a horizontal surface, the clear sky radiation, and 2) the estimated “actual” radiation on a horizontal surface.

In **Step 1** of routine  $R_{smhor\_func}$ , the clear sky solar insolation on a horizontal surface is calculated by a call to routine  $R_{sohor\_func}$ . The steps in routine  $R_{sohor\_func}$  are:

**Step 1:** Calculate the orbit eccentricity of the earth (Equation C-3).

**Step 2:** Calculate the solar declination (Equation C-4).

**Step 3:** Calculate the sunset hour angle (Equation C-5).

**Step 4:** Calculate the extraterrestrial radiation for daily periods (Equation C-6).

**Explanation:** The extraterrestrial solar radiation is calculated from the distance between the sun and the earth and the daylight period at a specific location on earth.

**Step 5:** Calculate the sine of the mean solar elevation weighted by extraterrestrial radiation (Equation C-7).

**Step 6:** Calculate the atmospheric pressure at the average elevation (station) (Equation C-8).

**Explanation:** This pressure is used to calculate the transmissivity of the air in the weather mass overlying the site on a given day. The average elevation of the domain is used to characterize the weather mass properties.

**Step 7:** Calculate the precipitable water for the weather mass (Equation C-9).

**Step 8:** Calculate the 24-hr transmissivity for beam radiation (Equation C-10).

**Step 9:** Calculate the 24-hr transmissivity for diffuse radiation (Equation C-11).

**Step 10:** Calculate the clear sky solar radiation over a 24 hour period (Equation C-12).

**Routine Output:** Routine  $R_{sohor\_fcn}$  returns a vector containing 1) the extraterrestrial radiation on a horizontal surface and 2) the clear sky radiation.

#### **G4.1.4 Partition the Total Incident Radiation into Diffuse and Direct Components**

In Step 3 of the  $ETO$  routine, the solar insolation on a horizontal surface is partitioned into diffuse and direct components. The direct component can be partially or totally obscured from particular surface depending upon the slope and azimuth of the surface. The diffuse component reaches all surfaces independent of the surface orientation.

The routine  $DiffuseDirect$  performs the partitioning. The steps in  $DiffuseDirect$  are:

**Step 1:** Calculate the total short wave transmissivity (Equation C-14).

- Step 2:** Calculate the diffuse radiation transmissivity (Equation C-15).
- Step 3:** Calculate the direct beam transmissivity (Equation C-16).
- Step 4:** Calculate direct beam radiation on a horizontal surface (Equation C-17).
- Step 5:** Calculate diffuse radiation on a horizontal surface (Equation C-18).
- Step 6:** Calculate the anisotropic index (Equation C-21).
- Step 7:** Calculate the modulating function for horizontal brightness (Equation C-22).

**Routine Output:** Routine *DiffuseDirect* returns a matrix that contains the direct beam radiation, the diffuse radiation, the anisotropic index, and the modulating function.

#### G4.1.5 Calculation of the Slope/Azimuth Correction Factor for Direct Beam Radiation

In Step 4 of routine *ET0*, the correction factor for direct beam radiation for cell *n* ( $R_b$ ) is calculated. The quantity  $R_b$  is the fraction of daily direct beam radiation for a horizontal surface that occurs on an inclined surface. The calculation of  $R_b$ , documented in Appendix C2, is performed in an Excel workbook (*Rb\_ver1.2.03.xls*, Output DTN: SN0602T0502206.003), which is located in the Massif directory. The worksheet *Rb\_LUT\_ET0* contains a look-up table of  $R_b$  values. A portion of this worksheet is shown below (Table G-1) to make the description easier.

Table G-1. A Portion of the  $R_b$  Look-up Table

ID	1	2	3	4	5
Azimuth (deg)	0	0	0	0	0
Slope (deg)	0	2.5	7.5	15	25
DOY (J) \ K1	0	2.5	7.5	15.0	25.0
1	1.00	0.90	0.71	0.42	0.10
2	1.00	0.90	0.71	0.42	0.10
3	1.00	0.90	0.71	0.43	0.10
4	1.00	0.90	0.71	0.43	0.10
5	1.00	0.90	0.71	0.43	0.11
6	1.00	0.90	0.71	0.43	0.11

Source: Output DTN: SN0602T0502206.003, worksheet *Rb\_LUT\_ET0*.

Each row of the worksheet contains values of  $R_b$  for a particular day of the calendar year. Each column of the worksheet contains values of  $R_b$  for a specific slope/azimuth combination.

To use this worksheet, one first determines the four slope/azimuth columns listed in the table that bound the slope/azimuth of the cell of interest. Given the day of the year, one now has four

values of  $R_b$  for four slope/azimuth combinations. An interpolation routine is then used to determine the value of  $R_b$  for the cell of interest.

To maximize computational efficiency, the four columns appropriate to each cell are calculated in Step 6 of the *Massif* driver. The interpolation coefficients are calculated in Step 7 of the *Massif* driver. Both of these steps are executed before the daily calculations are executed, thereby eliminating redundant calculations. Only the final interpolation for  $R_b$  is conducted daily within the *ET0* routine.

The actual reading of the  $R_b$  look-up table takes place in *RefET.xmcd*. After the table is read into a variable called *Rb\_lookup*, the table is cropped so that only the tabulated values of  $R_b$  remain; values of slope, aspect, and day of year are eliminated. These values are “hard wired” into the routine that finds the column indices. The Excel file that is read (*Rb\_ver1.2.03.xls*) is identical to the one entered into Output DTN: SN0602T0502206.003.

Routine *Index\_Rb\_fcn* finds the four columns in the  $R_b$  look-up table that bound the slope/azimuth combination of a particular cell. This routine contains the following steps:

**Step 1:** Define Slope and Azimuth in terms of degrees.

**Explanation:** The default “unit” in Mathcad for angular displacement is radians. The angles in the look-up table are in degrees. The variables “azimuth” and “slope” are divided by the Mathcad unit “deg” so that their numerical value reflects an implied unit of degrees.

**Step 2:** Determine the slope indices that bound the input value of “slope.”

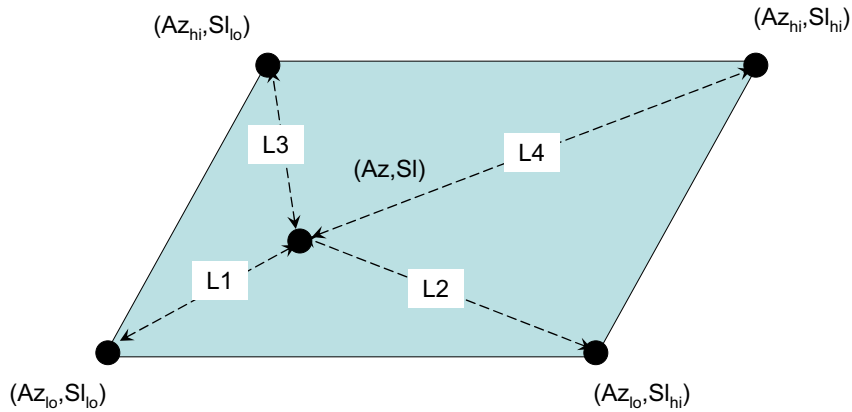
**Explanation:** The look-up table contains values of  $R_b$  for slope values of 0, 2.5, 7.5, 15, 25, and 40 degrees. For a given value of “slope”, the correct slope index pair is selected.

**Step 3:** Determine the azimuth indices that bound the input value of “azimuth.”

**Explanation:** The look-up table contains values of  $R_b$  for azimuth values of 0, 30, 60, 90, 120, 150, 180, 210, 270, 300, 330, and 360 degrees. For a given value of “azimuth”, the correct azimuth index pair is selected.

**Routine Output:** The four column indices that bound the input values of “slope” and “azimuth” are returned as a vector containing four elements.

The interpolation scheme (Figure G-4) used to obtain a value for  $R_b$  is a “nearest neighbor approach in which the weighted contribution of the four nearest neighbors is inversely proportional to the normalized distance to the “neighbor.” The interpolation space is defined by the low and high slope and azimuth values ( $Az_{lo}$ ,  $Az_{hi}$ ,  $Sl_{lo}$ ,  $Sl_{hi}$ ) extracted from the  $R_b$  look-up table for a specific day of the year. The distances from the slope/azimuth combination of interest ( $Az$ ,  $Sl$ ) are  $L1$ ,  $L2$ ,  $L3$ , and  $L4$  (see diagram below).



Source: Output DTN: SN0701T0502206.037.

Figure G-4. Interpolation Point Surrounded by Nearest Neighbors

The interpolated value in the Z direction ( $Z(Az, Sl)$ ), using the nearest neighbor approach, is:

$$Z(Az, Sl) = \frac{\frac{Z(Az_{lo}, Sl_{lo})}{L1} + \frac{Z(Az_{lo}, Sl_{hi})}{L2} + \frac{Z(Az_{hi}, Sl_{lo})}{L3} + \frac{Z(Az_{hi}, Sl_{hi})}{L4}}{\frac{1}{L1} + \frac{1}{L2} + \frac{1}{L3} + \frac{1}{L4}} \quad (\text{Eq. G-10})$$

where

$$\begin{pmatrix} L1 \\ L2 \\ L3 \\ L4 \end{pmatrix} = \begin{pmatrix} \sqrt{(Az - Az_{lo})^2 + (Sl - Sl_{lo})^2} \\ \sqrt{(Az - Az_{lo})^2 + (Sl - Sl_{hi})^2} \\ \sqrt{(Az - Az_{hi})^2 + (Sl - Sl_{lo})^2} \\ \sqrt{(Az - Az_{hi})^2 + (Sl - Sl_{hi})^2} \end{pmatrix}$$

This can be written as:

$$Z(Az, Sl) = C_{Rb} \cdot \begin{pmatrix} Z(Az_{lo}, Sl_{lo}) \\ Z(Az_{lo}, Sl_{hi}) \\ Z(Az_{hi}, Sl_{lo}) \\ Z(Az_{hi}, Sl_{hi}) \end{pmatrix} \quad (\text{Eq. G-11})$$

where

$$C_{Rb} = \frac{1}{\left(\frac{1}{L1} + \frac{1}{L2} + \frac{1}{L3} + \frac{1}{L4}\right)} \cdot \begin{pmatrix} L1^{-1} \\ L2^{-1} \\ L3^{-1} \\ L4^{-1} \end{pmatrix}$$

The formulation shows that the interpolation coefficients ( $C_{Rb}$ ) can be calculated separately from the actual interpolation. The interpolation coefficients are calculated in the routine  $C_{Rb\_fcn}$ . The steps in this routine are as follows:

**Step 1:** Define Slope and Azimuth in terms of degrees.

**Explanation:** The default “unit” in Mathcad for angular displacement is radians. The angles in the look-up table are in degrees. The variables “azimuth” and “slope” are divided by the Mathcad unit “deg” so that their numerical value reflects an implied unit of degrees.

**Step 2:** Define the low and high ends of Azimuth.

**Explanation:** The  $R_b$  look-up table has  $R_b$  values for azimuths in 30-degree increments. The low bounding value of azimuth ( $Azimuth_{lo}$ ) in the table is equal to the input value rounded down to the nearest integer multiple of 30. The high bounding value of azimuth ( $Azimuth_{hi}$ ) is equal to  $Azimuth_{lo}$  plus 30.

**Step 3:** Define the low and high ends of Slope.

**Explanation:** The look-up table contains values of  $R_b$  for slope values of 0, 2.5, 7.5, 15, 25, and 40 degrees. The values of  $Slope_{lo}$  and  $Slope_{hi}$  bound the input value of “slope”.

**Step 4:** Calculate the interpolation distances ( $L1$ ,  $L2$ ,  $L3$ , and  $L4$ ).

**Explanation:** These are the distances to the four nearest neighbors.

**Routine Output:** The routine returns a vector containing the four interpolation coefficients. When all of the interpolation distances are nonzero, the formula derive above is used. When one of the distances is zero, the standard formula contains a singularity. This situation occurs when one of the four bounding slope/azimuth combinations in the table is identical to the cell slope/azimuth pair. In this case, the interpolation coefficient vector must contain three zeros and one element of unity. This is performed in this routine by returning a vector of logical statements of the form “ $L*=0$ ”. When this logical statement is true, the statement returns a value of unity. When this logical statement is false, the statement returns a value of zero.

The actual calculation of  $R_b$  for cell  $n$  on a particular day of the year is performed in routine *Rb\_fcn*. The calculation is performed in a single step. The interpolation coefficients ( $C_{Rb}$ ), interpolation indices (*Index\_Rb*), and day of the year (*DOY*) are passed into the routine. The routine returns the sum of the product of the interpolation coefficients and the appropriate values from the  $R_b$  look-table.

#### **G4.1.6 Calculation of Solar Radiation on an Inclined Surface**

The calculation of solar radiation on an inclined surface is performed in routine *SolarRad\_inc*. The steps in this routine are as follows:

**Step 1:** Calculate the direct beam radiation on the inclined surface (Equation C-20).

**Step 2:** Calculate the diffuse radiation on the inclined surface (Equation C-23).

**Step 3:** Calculate the reflected radiation from lower lying terrain (Equation C-24).

**Step 4:** Calculate the total radiation received by the inclined surface (Equation C-25).

**Step 5:** Project the total radiation to a horizontal equivalent (Equation C-26).

**Step 6:** Calculate the horizontal equivalent for net short-wave radiation (Equation C-34).

**Step 7:** Calculate the net outgoing long-wave radiation (Equation C-35).

**Step 8:** Calculate the net radiation from the surface (Equation C-36).

**Routine Output:** This routine returns the net solar radiation on a single inclined surface.

#### **G4.2 EVAPOTRANSPIRATION**

Evapotranspiration from the soil is based upon the FAO-56 formulation. Short-term evaporation is extracted from a thin layer of soil lying outside the vegetative canopy cover (Node 1). Transpiration is extracted from the entire root zone (Nodes 1, 2, and 3). A paper by Allen et al. (2005 [DIRS 176207]) expands upon the FAO-56 procedure and presents a partition function that predicts the fraction of transpiration that comes from the evaporation layer (Node 1). This partitioning function has been extended in MASSIF to predict the fraction of transpiration that comes from the canopy zone (Node 2).

### G4.2.1 Calculation of ET

The routine *ET* calculates evapotranspiration for all the cells in the watershed for a given day. All of the steps enumerated in this description apply to individual cells in the watershed. The steps in routine *ET* are:

**Step 1:** If the thickness of the 1st layer is zero, the evaporation and transpiration are each zero.

**Explanation:** When the soil depth for a particular cell is zero, the thicknesses of all the nodes in that cell are all set to zero in the *cdepth* routine. In the absence of soil, there is no storage of water in soil and, consequently, neither evaporation nor transpiration.

**Step 2:** Calculate the evaporation depletion depth.

**Explanation:** The evaporation depletion depth is calculated in routine *De\_fcn*. The evaporation depletion depth is used in the calculation of evaporation from Node 1.

**Step 3:** Calculate the daily evaporation.

**Explanation:** For evaporation to occur in the evaporation layer (Node 1), the water level in that node must be greater than the half of the wilting point (Allen et al. 1998 [DIRS 157311], Figure 38 and discussion of soil evaporation reduction coefficient on pp. 144 to 146). Also, the snow level must equal zero because the presence of snow will strongly inhibit evaporation. When these conditions are met, the soil evaporation is calculated in three steps.

**Step 3a:** Calculate the evaporation reduction coefficient (Allen et al. 1998 [DIRS 157311], Equation 74 and Figure 38).

**Explanation:** The evaporation reduction coefficient is calculated in routine *Kr\_fcn*.

**Step 3b:** Compute the evaporation coefficient (Allen et al. 1998 [DIRS 157311], Equation 71).

**Explanation:** The evaporation coefficient is calculated in routine *Ke\_fcn*.

**Step 3c:** Calculate the daily evaporation (Allen et al. 1998 [DIRS 157311], Equation 69).

**Explanation:** The daily evaporation flux is equal to the product of the evaporation coefficient ( $K_e$ ) and the reference evapotranspiration ( $ET_0$ ). This is a flux that has been “smeared” over both Nodes 1 and 2. Evaporation can reduce the water level in Node 1 only to the wilting point. Therefore, the upper limit to the daily evaporation is the water content in Node 1 in excess of the wilting point multiplied by the complement of the vegetative canopy ( $f_c$ ).



**Step 4:** Subtract the daily evaporation from the water level in the evaporation node.

**Explanation:** The daily evaporation flux is a quantity that has been “smeared” over both Nodes 1 and 2. However, the water comes only from Node 2. Hence, the flux must be divided by the complement of the vegetative canopy ( $f_c$ ) before it is subtracted from the water level in Node 1.

**Step 5:** Compute the upper limits for transpiration from each node.

**Explanation:** Transpiration can reduce the water level in a node only to the wilting point. The **max** function with a lower limit of 0 mm is used in case the machine precision of the previous calculations has reduced the water level to something slightly below the wilting point.

**Step 6:** Compute the maximum value of total transpiration.

**Explanation:** The maximum possible transpiration in the cell is equal to the sum of the maximum possible transpirations in each node in that cell.

**Step 7:** Compute the total transpiration.

**Explanation:** When the maximum possible total transpiration is greater than zero, the total transpiration is computed in four steps.

**Step 7a:** Calculate the root zone depletion depth (Allen et al. 1998 [DIRS 157311], p. 167).

**Explanation:** The root zone depletion depth is calculated in routine  $D_r_{fcn}$ . It is based upon all the water in the entire root zone (Nodes 1, 2 and 3).

**Step 7b:** Calculate the unadjusted evapotranspiration (Allen et al. 1998 [DIRS 157311], Equation 69).

**Explanation:** “Unadjusted” means that the transpiration portion has not yet been adjusted for water stress.

**Step 7c:** Calculate the water stress coefficient (Allen et al. 1998 [DIRS 157311], Equation 84).

**Explanation:** The water stress coefficient is calculated in routine  $K_s_{fcn}$ .

**Step 7d:** Calculate the total daily transpiration (Allen et al. 1998 [DIRS 157311], Equation 80).

**Explanation:** The total daily transpiration is limited by the amount of water in the root zone in excess of the wilting point.

**Step 8:** Initialize the transpiration partition by placing all of the transpiration in the 2nd layer (Node 3).

**Explanation:** This is an initial guess that will be modified per the transpiration partitioning algorithms.

**Step 9:** Calculate the transpiration in the evaporation zone (Node 1) if the water level in the node is greater than the integrated wilting point.

**Explanation:** The fraction of the transpiration that comes from the evaporation layer ( $K_{tp}$ ) is computed according to a paper by Allen et al. (2005 [DIRS 176009]) that expands the FAO-56 procedure. Equation 29 of that paper states that the partitioning coefficient (calculated in routine  $K_{tp\_fcn}$ ) is:

$$K_{tp} = \left( \frac{1 - \frac{D_{ep}}{TEW}}{1 - \frac{D_r}{TAW}} \right) \cdot \left( \frac{Z_e}{Z_r} \right)^{0.6} \quad (\text{Eq. G-12})$$

Because there is no irrigation in the MASSIF calculation, the evaporation depletion depth ( $D_e$ ) used in this calculation is identical to the evaporation precipitation-depletion depth ( $D_{ep}$ ) cited in the paper.

The transpiration in the evaporation layer (Node 1) is equal to the product of the partition coefficient ( $K_{tp}$ ) and the total transpiration. The transpiration in the evaporation node (Node 1) is limited to the maximum possible transpiration computed in Step 6.

**Step 10:** Calculate the transpiration in the canopy zone (Node 2) if the water level in the node is greater than the integrated wilting point.

**Explanation:** As mentioned earlier, neither FAO-56 (Allen et al. 1998 [DIRS 157311]) nor subsequent expansions of the procedure deal explicitly with the zone described by Node 2. Therefore MASSIF treats this zone in a manner directly analogous to the evaporation zone. First a depletion depth is calculated for the canopy node ( $D_c$ ) using the same formula used to compute  $D_e$ . Then a partitioning function is computed for the canopy zone ( $K_{tp\_c}$ ) using the same formula used for  $K_{tp}$  (above) with  $D_c$  substituted for  $D_e$ . The transpiration in the canopy node (Node 2) is limited to the maximum possible transpiration computed in Step 6.

**Step 11:** Recalculate the transpiration in the 2nd layer (Node 3).

**Explanation:** The transpiration in Node 3 is set equal to the total transpiration minus the sum of the transpiration in the evaporation and canopy nodes (Nodes 1 and 2). The upper bound on transpiration in the 2nd layer, computed in Step 6, is enforced.

**Step 12:** Recalculate the total transpiration.

**Explanation:** The total transpiration is set equal to the sum of the transpiration in Nodes 1, 2, and 3. This step is necessary because of the upper limit on transpiration enforced on Node 3 in Step 11.

**Step 13:** Subtract the transpiration from the water level in Node 1.

**Step 14:** Subtract the transpiration from the water level in Node 2.

**Step 15:** Subtract the transpiration from the water level in Node 3.

**Routine Output:** This routine returns the new water levels (*Wlevel*), amount of transpiration (*Transpiration*), and amount of evaporation (*Evaporation*) for each cell for the day examined.

#### G4.2.2 Evaporation

Evaporation (Section 6.4.4.2) from the evaporation layer (Node 1) is modeled in FAO-56 (Allen et al. 1998 [DIRS 157311], p. 142) as:

$$\text{Evaporation} = K_e \cdot ET_0 \quad (\text{Eq. G-13})$$

where  $K_e$  is the evaporation coefficient and  $ET_0$  is the reference evapotranspiration (Section G4.1). It is important to note that, even though this component of evaporation comes only from the fraction of soil surface that is both exposed and wetted ( $f_{ew}$ ), the flux computed by this equation applies to the entire soil surface (i.e., both the exposed and canopy regions). The actual flux from the exposed and wetted surface is:

$$\text{Evaporation}_{\text{exposed\_wetted}} = \frac{K_e \cdot ET_0}{f_{ew}} \quad (\text{Eq. G-14})$$

Also note that, because MASSIF does not include irrigation, the exposed and wetted fraction of the soil surface ( $f_{ew}$ ) is equal to the complement of the canopy coefficient ( $1-f_c$ , Allen et al. 1998 [DIRS 157311], pp. 147 to 149 including Table 20).

The evaporation coefficient ( $K_e$ , calculated in routine  $K_{e\_fcn}$ ) is a function of the water in the evaporation layer (Node 1) and the vapor transport limitations at the soil surface. FAO-56 (Allen et al. 1998 [DIRS 157311], Equation 71) models this as:

$$K_e = \min[K_r \cdot (K_{c\_max} - K_{cb}), f_{ew} \cdot K_{c\_max}] \quad (\text{Eq. G-15})$$

where  $K_r$  is the evaporation reduction coefficient that is a function of the evaporation layer water content,  $K_{cb}$  is the basal crop coefficient, and  $K_{c\_max}$  is the maximum value of the evapotranspiration coefficient ( $K_c = K_e + K_{cb}$ ) following rain.

The evaporation reduction coefficient ( $K_r$ , calculated in routine  $K_r\_fcn$ ) accounts for water depletion in the evaporation layer (Node 1). It is discussed in FAO-56 (Allen et al. 1998 [DIRS 157311], pp. 144 to 146). It is modeled in FAO-56 (Allen et al. 1998 [DIRS 157311], Equation 74, Figure 38) as:

$$K_r = \max\left(0, \min\left(\frac{TEW - D_e}{TEW - REW}, 1\right)\right) \quad (\text{Eq. G-16})$$

where  $D_e$  is the evaporation depletion depth, TEW is the total evaporable water, and REW is the readily evaporable water. REW, a property of the soil, is the amount of water that can be evaporated without water transport processes in the soil kicking in. TEW is the total amount of water available for evaporation in a well drained soil. The depletion depth ( $D_e$ ) is the difference between the water content and the extrinsic field capacity in the evaporation layer. When the evaporation layer is filled to field capacity, the depletion depth is zero. When the evaporation is down to half of the wilting point, the depletion depth is equal to TEW (Allen et al. 1998 [DIRS 157311], Equations 73 and 78). The depletion depth is calculated in routine  $D_e\_fcn$ .

### G4.2.3 Transpiration

Transpiration, nominally, is water transport from the root zone (Nodes 1, 2, and 3 in MASSIF) to the atmosphere through the plant. In FAO-56 (Allen et al. 1998 [DIRS 157311], p. 135), the transpiration component of ET also includes “a residual diffusive evaporation component supplied by soil water below the dry surface and by soil water from beneath dense vegetation.” The equation for transpiration is (Allen et al. 1998 [DIRS 157311], Equation 80):

$$\text{Transpiration} = K_s \cdot K_{cb} \cdot ET_0 \quad (\text{Eq. G-17})$$

where  $ET_0$  is the reference ET,  $K_{cb}$  is the basal “crop” coefficient, and  $K_s$  is the water stress coefficient.

#### G4.2.3.1 Water Stress Coefficient

The water stress coefficient ( $K_s$ ) models the behavior of plant transpiration as the water content in the root zone drops below “optimum” levels (Allen et al. 1998 [DIRS 157311], Chapter 1). It is modeled in FAO-56 (Allen et al. 1998 [DIRS 157311], Equations 83 and 84) as:

$$K_s = \frac{TAW - D_r}{TAW - RAW} \quad (\text{Eq. G-18})$$

where  $RAW = p_{adj} \cdot TAW$

where TAW is the total available water in the root zone, RAW is the readily available water,  $p_{adj}$  is the fraction of TAW that a “crop” can extract from the root zone without suffering water

stress, and  $D_r$  is the root zone depletion depth. The “p” is adjusted according to the text at the bottom of page 162 of FAO-56 (Allen et al. 1998 [DIRS 157311]). Calculation of  $K_s$  is performed in routine  $K_{s\_fcn}$ , which has the following steps:

**Step 1:** Calculate the adjusted  $p$ .

**Explanation:** The value of  $p$  is a function of the vegetation type (Section 6.4.4.2). However,  $p$  is also a function of the “evaporative power of the atmosphere.” The text at the bottom of page 162 of FAO-56 (Allen et al. 1998 [DIRS 157311]) states: “A numerical approximation for adjusting  $p$  for  $ET_c$  rate is

$$p = p_{\text{Table\_22}} + 0.04 \cdot (5 - ET_c) \quad (\text{Eq. G-19})$$

where the adjusted  $p$  is limited to  $0.1 \leq p \leq 0.8$  and  $ET_c$  is in mm/day.”

**Step 2:** Calculate the readily available water (Allen et al. 1998 [DIRS 157311], Equation 83).

**Step 3:** Return a value of unity for the water stress coefficient if the root zone depletion depth is less than  $RAW$ .

**Explanation:** If there is sufficient water in the root zone, there is no water stress ( $K_s=1$ ).

**Step 4:** Return a value for the water stress coefficient according to Equation 84 of FAO-56 (Allen et al. 1998 [DIRS 157311]).

**Explanation:** The lower bound of 0 for  $K_s$  is not enforced here because the upper bound (TAW) for the root zone depletion depth ( $D_r$ ) is enforced at its calculation.

The root zone depletion depth (routine  $D_{r\_fcn}$ ) is the water deficit for the entire root zone. The water levels for Nodes 1, 2 (weighted by the canopy coefficient  $f_c$ ) and 3 are added, and that sum is subtracted from the integrated field capacity (product of soil field capacity and rooting depth) for the root zone. The difference is the root zone depletion depth.

#### G4.2.3.2 Calculation of “Crop” Coefficient ( $K_{cb}$ ) and Canopy Coefficient ( $f_c$ )

MASSIF uses the results of satellite imagery coupled with studies of native vegetation to deduce the value of  $K_{cb}$  for every cell in the model domain (Section 6.4.4.1). The details of the satellite and plant studies are located in Section 6.5.3 and Appendices D and E. This discussion simply contains the basic implementation aspects.

The basal crop coefficient ( $K_{cb0}$ ) is linearly related to a corrected satellite signature ( $NDVI_{\text{corrected}}$ ):

$$K_{cb0} = C_1 + C_2 \cdot NDVI_{\text{corrected}} \quad (\text{Eq. G-20})$$

$$NDVI_{corrected} = NDVI_{table} \cdot \frac{Annual\_Precip}{Annual\_Precip_{1998}} \cdot PVR$$

where

The quantity  $NDVI_{table}$  is extracted from an “NDVI table” in which the satellite signature has been correlated by slope, aspect, and day of the 1998 water year (Output DTN: SN0606T0502206.012). The ratio of the water year precipitations ( $Annual\_Precip/Annual\_Precip_{1998}$ ) adjusts the quantity extracted from the NDVI table for precipitation. The quantity PVR (potential vegetative response) adjusts the NDVI signature for the specific cell in the watershed. The PVR constants are found in the geospatial files describing the watersheds. Tabulated quantities normally used in FAO-56 are corrected for actual wind speeds and relative humidities (RHs) (Allen et al. 1998 [DIRS 157311], Equation 70). Because satellite observations are direct, actual wind speeds and RHs are integral and implicit in the NDVI table and PVR adjustments.

The lower bound of  $K_{cb0}$  is zero. The upper limit is set to the general upper bound for tall vegetation adjusted for wind speed ( $u_2$ ), relative humidity ( $RH_{min}$ ), and plant height ( $h_{plant}$ ) (Allen et al. 1998 [DIRS 157311], Equation 100 and text following Equation 101 on p. 189). That is:

$$K_{cb0} \leq 1.2 + \text{adjust} \quad (\text{Eq. G-21})$$

$$\text{adjust} = \left[ 0.04 \cdot (u_2 - 2) - 0.004 \cdot (RH_{min} - 45) \right] \cdot \left( \frac{h_{plant}}{3} \right)^{0.3}$$

where

The calculation of  $K_{cb0}$  for a single cell is performed in routine  $K_{cb0\_fcn}$ .

The “crop” coefficient is calculated in every cell in the watershed in routine  $K_{cb\_fcn}$ . In addition, this routine calculates the canopy coefficient for every cell from the cell “crop” coefficient using a correlation supplied by FAO-56. Finally, the routine calculates the maximum evapotranspiration coefficient. The steps in routine  $K_{cb\_fcn}$  are:

**Step 1:** Calculate the ratio of annual precipitations.

**Explanation:** The satellite signatures are corrected for the cumulative precipitation of the water year of interest ( $precip\_Kcb$ ). The reference water year for the NDVI table is 1998. The cumulative precipitation for that water year is  $PrecipRef_{NDVI}$ .

**Step 2:** Calculate the day of the water year from the day of the calendar year.

**Explanation:** The precipitation file gives the day of the calendar year ( $DOY$ ). The NDVI table is listed in terms of the day of the water year ( $DOWY$ ). The routine  $DOWY\_fcn$  calculates the day of the water year from the day of the calendar year based upon a 365 day calendar year.

**The following steps apply to each cell in the watershed:**

**Step 3:** Calculate the minimum relative humidity from the cell temperatures.

**Explanation:** The minimum relative humidity for the day is based on the ratio of the actual vapor pressure for the day and the saturation vapor pressure for the maximum temperature ( $T_{max}$ ) for the day (Allen et al. 1998 [DIRS 157311], Equation 10). The actual vapor pressure is calculated from the dew temperature ( $T_{dew}$ ) of the day (Allen et al. 1998 [DIRS 157311], Equation 14).

**Step 4:** Calculate the adjustment to the maximum basal crop coefficient (Allen et al. 1998 [DIRS 157311], Equation 100).

**Step 5:** Calculate  $K_{cb}$ ,  $K_{c\_max}$ , and  $f_c$  when  $PVR=0$ .

**Explanation:** When  $PVR=0$ , there is no vegetation on the cell. Intermediate calculations are not necessary. The “crop” coefficient ( $K_{cb}$ ) is set to the minimum value ( $K_{c\_min}$ ), which accounts for diffusive evaporation from the soil. The canopy coefficient ( $f_c$ ) is set to either 0.0001 ( $f_{c\_switch}=-1$ ) or to the user-specified value.  $K_{c\_max}$  is set to the adjusted value (Allen et al. 1998 [DIRS 157311], Equation 100). The loop proceeds to the next cell after these assignments are made.

**Step 6:** Calculate the basal “crop” coefficient from the NDVI data.

**Explanation:** Routine  $K_{cb0}$  (discussed above) is implemented to produce the basal crop coefficient from the NDVI data for the day of interest.

**Step 7:**  $K_{cb}$  is the maximum of  $K_{cb0}$  and  $K_{c\_min}$ .

**Explanation:** The satellite signature detects the presence of active plants. When the plants are completely dormant or very sparse, the signature is null. Diffusive evaporation from the soil below the evaporation layer cannot be detected by the satellite measurement and is therefore not implicitly part of the correlation for  $K_{cb0}$ . Because this component is small for plants at peak transpiration,  $K_{c\_min}$  is used as a lower bound for  $K_{cb}$ .

**Step 8:** Calculate the upper bound coefficient for ET ( $K_{c\_max}$ , Allen et al. 1998 [DIRS 157311], Equation 72).

**Step 9:** Calculate the canopy coefficient,  $f_c$  (user specified or FAO-56, Equation 76).

**Explanation:** The user has the option of specifying a constant, uniform canopy coefficient or using the correlation specified by FAO-56 (Allen et al. 1998 [DIRS 157311], Equation 76) with the *Massif* input variable  $f_{c\_switch}$ . If  $f_{c\_switch}$  is equal to  $-1$ , the FAO-56 correlation is used. Otherwise,  $f_c$  is set equal to the value of  $f_{c\_switch}$ . When the correlation is used, the canopy coefficient can be no less than  $10^{-4}$ . This prevents singularity from occurring in another part of the calculation.

**Routine Output:** The routine returns  $K_{cb}$ ,  $K_{c\_max}$ , and  $f_c$  for every cell in the watershed.

#### G4.2.3.3 Calculation of Column Indices for the NDVI Table

The NDVI table, which tabulates the correlation of satellite signature with the slope and azimuth of the terrain, consists of 365 rows and 25 columns. Cell slopes are grouped into 4 bins: 1) less than 5 degrees, 2) five to ten degrees, 3) ten to eighteen degrees, and 4) greater than eighteen degrees. The azimuths are grouped into eight bins: 1) North, 2) Northeast, 3) East, 4) Southeast, 5) South, 6) Southwest, 7) West, and 8) Northwest.

A small portion of the table is shown below (Table G-2). The column that precedes the table lists the days of the water year, which starts on October 1. The first column of the table consists of the correlated satellite signature for cells having a slope less than 5 degrees. Because the slope is small, the correlation with azimuth is negligible. Columns 2 thru 9 correspond to slopes between 5 and 10 degrees. Columns 10 thru 17 correspond to slopes between 10 and 18 degrees. Columns 18 thru 25 correspond to slopes greater than 18 degrees.

Table G-2. A Portion of the NDVI Table

	A'	C'	(A'+C')/2	A'	(A'+E')/2	E'	(A'+E')/2
	Flat	North	NorthEast	East	SouthEast	South	SouthWest
Day	(<5 deg)	5-10 deg	5-10 deg	5-10 deg	5-10 deg	5-10 deg	5-10 deg
1	0	0	0	0	0	0	0
2	0.0005	0.000334	0.000417	0.0005	0.000584	0.000667	0.000584
3	0.000511	0.000341	0.000426	0.000511	0.000597	0.000682	0.000597
4	0.000524	0.000349	0.000437	0.000524	0.000611	0.000699	0.000611
5	0.000538	0.000359	0.000449	0.000538	0.000628	0.000718	0.000628

Source: Output DTN: SN0701T0502206.037.

For a specific cell, only the row of the table, corresponding to the day of the water year, changes throughout the calculation; the index of the column remains constant. To save calculation time, the appropriate NDVI column index is determined at the beginning of the *Massif* routine; that index is carried into the ET calculation as a routine argument. The routine *Index\_NDVI\_fcn* determines the appropriate column for a given slope and azimuth.



#### G4.2.3.4 Transpiration Partition Coefficients

A paper by Allen et al. (2005 [DIRS 176009], Equation 29) presents an algorithm for the fraction of the transpiration ( $K_{tp}$ ) that comes from the evaporation layer (Node 1):

$$K_{tp} = \left( \frac{1 - \frac{D_{ep}}{TEW}}{\frac{D_r}{1 - \frac{TAW}{D_r}}} \right) \cdot \left( \frac{Z_e}{Z_r} \right)^{0.6} \quad (\text{Eq. G-22})$$

where  $D_{ep}$  is the depletion depth in the portion of the evaporation zone that does not experience irrigation,  $D_r$  is the root zone depletion depth, TEW is the total evaporable water, TAW is the total available water,  $Z_e$  is the evaporation layer thickness, and  $Z_r$  is the root zone depth. The numerator and denominator of the first part of the expression are required to be greater than 0.001. The maximum value of  $K_{tp}$  is unity.

A number of slight modifications are required to implement this expression into MASSIF.

- 1) Because MASSIF is not concerned with irrigation, the evaporation depletion depth ( $D_e$ ) is identical to  $D_{ep}$ .
- 2) In thin soil regions, the actual soil depth can be less than the rooting depth. Therefore, the thickness of Node 1 ( $Thick_1$ ) is substituted for the evaporation layer thickness ( $Z_e$ ), and the sum of the thicknesses of Nodes 1 and 3 ( $Thick_1 + Thick_3$ ) is substituted for the rooting depth ( $Z_r$ ).
- 3) The description in the paper by Allen et al. (2005 [DIRS 176009]) requires that the minimum value of both the numerator and the denominator in the first part of the expression be greater than 0.001. The reason for limiting the denominator is obvious. When the depletion depth approaches TAW, the denominator becomes very small and the equation approaches a singularity (infinity). The problem is strictly mathematical, because the upper value of  $K_{tp}$  is unity.

The limitation on the numerator appears to be unnecessary and causes a problem with the conservation of water in MASSIF. When the evaporation depletion depth equals TEW, no further transpiration is allowed. If, however, the numerator is numerically kept above 0.001, a portion of the transpiration will be assigned to the evaporation node but will not actually be subtracted from the node; the water will be “lost.” Because the limitation in the numerator serves no practical or physical purpose, it is not implemented in MASSIF.

These modifications are implemented in the routine  $K_{tp\_fcn}$ . This routine implements the partitioning coefficient as:

$$K_{tp} = \min \left[ \left( \frac{1 - \frac{D_e}{TEW}}{\max \left( 1 - \frac{D_r}{TAW}, 0.001 \right)} \right) \left( \frac{Thick_1}{Thick_1 + Thick_3} \right)^{0.6}, 1 \right] \quad (\text{Eq. G-23})$$

As stated earlier, FAO-56 does not explicitly model the canopy region (Node 2). However, because of the way that MASSIF enforces soil saturated conductivity limits, the water balance for Node 2 must be explicit and complete. This requires that a transpiration partitioning coefficient be developed for Node 2.

The structure of the partitioning coefficient has two parts. The first part compares the water content of the evaporation node to the total water content of the root zone. If most of the water lies in the evaporation zone, then most of the transpiration should come from the evaporation zone; if the evaporation zone is relative dry, most of the transpiration should come from the balance of the root zone. The second part of the partitioning coefficient shows a dependency upon the relative thickness of the evaporation zone and the rooting depth. The exponent of 0.6 is related to a “root extraction pattern” that relates the location of transpiration with the depth of the root section.

Both of these elements are implemented in a partitioning coefficient for the canopy region ( $K_{tp\_c}$ ) by substituting a “canopy depletion depth” ( $D_c$ ) for the evaporation depletion depth. Otherwise, the equation remains the same. The routine  $K_{tp\_c\_fcn}$  calculates the partitioning coefficient for the canopy region (Node 2) as:

$$K_{tp\_c} = \min \left[ \left( \frac{1 - \frac{D_c}{TEW}}{\max \left( 1 - \frac{D_r}{TAW}, 0.001 \right)} \right) \left( \frac{Thick_1}{Thick_1 + Thick_3} \right)^{0.6}, 1 \right] \quad (\text{Eq. G-24})$$

The canopy depletion depth ( $D_c$ ) is calculated using the same formula as for  $D_e$ , with the Node 2 water level used instead of the Node 1 water level. The calculation of  $D_c$  is performed in routine  $D_c\_fcn$ .

#### G4.2.3.5 Annual Cumulative Precipitation

The calculation of the “crop” coefficient from the NDVI table requires that the baseline value be adjusted for the cumulative precipitation over the water year (Section G4.2.3.2). Calculation of the cumulative precipitation is performed in routine  $precip\_Kcb\_fcn$ . The calculation requires

that the precipitation/weather file 1) begins on October 1, and 2) has at least 365 days. The steps in *precip\_Kcb\_fcn* are:

**Step 1:** Calculate the number of full water years in the weather file.

**Explanation:** The precipitation may include more than one water year. When actual weather data is used, one of the years may have 366 days rather than 365. Additionally, the weather file may include part of a water year in addition to one or more complete water years. The year count (*Nyears*) calculated in this step is the number of complete water years in the weather file.

**Step 2:** Assign a cumulative annual precipitation to each day in the weather file.

**Explanation:** This process takes place within a loop that counts the years in the weather file. The counter is *nyr*.

**Step 2a:** Calculate the number of days in the weather file that precedes the year.

**Explanation:** When starting with the 1st year, the number of preceding days is zero. Otherwise, the number of preceding days is the sum of the days in each of the preceding years.

**Step 2b:** Calculate the number of days in year *nyr*.

**Explanation:** There are either 365 or 366 days in the year. The last day of the water year is September 30. If the day of the month of the 365th day of year *nyr* is 30, then water year *nyr* has 365 days. Otherwise, it has 366 days.

**Step 2c:** Calculate the reference annual precipitation for year *nyr*.

**Explanation:** The daily reference precipitation is summed over the number of days in year *nyr*.

**Step 2d:** Assign the lapse-corrected annual precipitation to every day in year *nyr*.

**Explanation:** The reference annual precipitation is lapse-corrected to the elevation used in the NDVI formulation (*elev\_NDVI*). The corrected value is assigned to every day in year *nyr*.

**Step 2e:** If the weather file ends with a partial water year, the annual precipitation from the previous year is applied to the days of the partial water year.

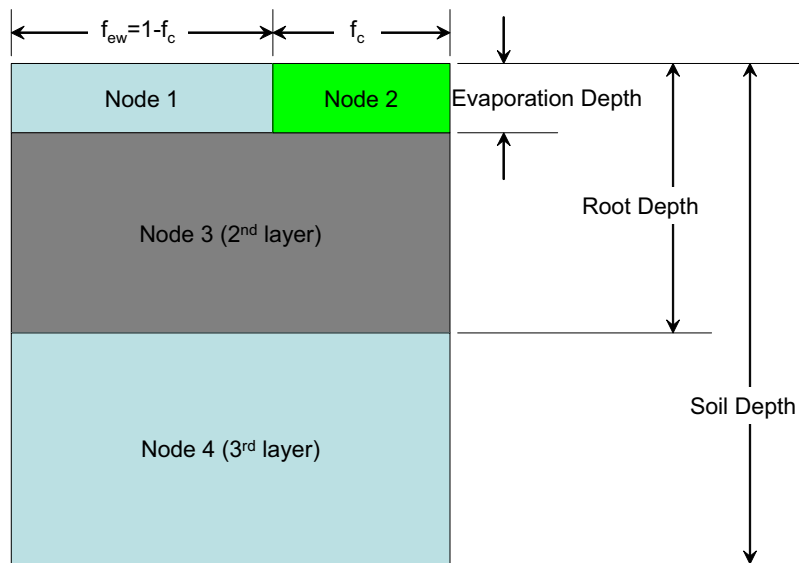
**Explanation:** The annual precipitation for a partial water year cannot be calculated. Therefore, the annual precipitation from the previous water year is applied to the partial water year. This provision is made so that data from the end of a calendar year can be appended to the end of the last water year.

**Routine Output:** This routine returns a vector of length equal to the length of the weather file. The vector contains the annual precipitation for each day in the weather file.

## G5. ANCILLARY ROUTINES

### G5.1 LAYER DEPTHS AND PROPERTIES

The routine *cdepth* calculates the soil layer depths for each node in an individual cell (Figure G-5). When the soil depth is greater than the maximum root depth, the two nodes in the first layer have a thickness equal to the evaporation layer thickness, the second layer has a thickness equal to the difference between the root depth and the evaporation layer thickness, and the third layer contains the balance of the soil thickness. When the soil depth of a cell is less than root depth of the evaporation layer thickness, then the layer thickness(es) are truncated accordingly. In the extreme case where the soil depth is zero, the three layer thicknesses are equal to zero.



Source: Output DTN: SN0701T0502206.037.

Figure G-5. Soil Discretization in MASSIF

The routine *cdepth* contains the following steps:

- Step 1:** When the soil depth is less than the evaporation layer depth, the thickness of the two nodes in the first layer are set to the soil thickness. The thicknesses of 3rd and 4th nodes are set to zero.
- Step 2:** When the soil depth is less than the root depth and greater than the evaporation layer depth, the thickness of the two nodes in the first layer are set to the evaporation depth. The thickness of 3rd node is set equal to the difference between the soil depth and the evaporation layer thickness. The thickness of the 4th node is set to zero.

**Step 3:** When the soil depth is greater than the root depth, the thickness of the two nodes in the first layer are set to the evaporation depth. The thickness of 3rd node is set equal to the difference between the root depth and the evaporation layer thickness. The thickness of the 4th node is set to the difference between the soil depth and the root depth.

The routine *LayerProps* calculates extrinsic properties for each cell from the intrinsic soil properties and the soil depths. Additionally, the initial soil water levels are calculated for each node in each cell of the watershed. The following steps are contained in routine *LayerProps*:

**Step 1:** Determine the soil depth for cell n.

**Explanation:** The geospatial file for the watershed characterizes each cell with a depth zone number. The vector *depthsoils* contains the soil depths for each of the depth zones.

**Step 2:** Calculate the node thicknesses for cell n.

**Explanation:** The thickness of each node in the cell is calculated from the cell soil depth, the evaporation layer thickness, and the root depth. The calculation is performed in routine *cdepth*. The vector element *thick<sub>n</sub>* is, itself, a vector containing four elements: the thicknesses of Nodes 1, 2, 3, and 4 of cell n.

**Step 3:** Calculate the layer water content associated with field capacity.

**Explanation:** The water content (level) associated with field capacity is the product of the node thickness and the field capacity for the cell. Each cell in the geospatial file is characterized by a soil zone number. The vector *fieldcap* contains the field capacities for each of the soil zones.

**Step 4:** Compute maximum daily infiltrations for cell n.

**Explanation:** The daily flow limit through a soil layer is the product of the soil conductivity (m/s) and the duration of a day (24 hrs). The daily flow limit into the bedrock is the product of the rock conductivity (m/s) and the duration of a day (24 hrs).

**Step 5:** Set the initial water content in each node of cell n.

**Explanation:** The user supplies values for a four-element vector, IC, which specifies the fractional distance between the wilting point and the field capacity for each node (4) in every cell of the watershed. Unless there is measured data to the contrary, the user should make the fourth element of the vector equal to 1 (*IC<sub>4</sub>=1*). This is because there are no mechanisms in MASSIF that extract water from Node 4 below the field capacity. The first three elements of the vector (*IC<sub>1</sub>*, *IC<sub>2</sub>*, *IC<sub>3</sub>*) can be any value between 0 and 1.

**Step 6:** Set the maximum possible water content for the nodes in cell n.

**Explanation:** The maximum water level in a node is the product of the thickness of that node and the saturated water content of the soil (*soilporo*). **Note:** Originally, the creator of these Mathcad files thought the cell porosity was being specified. This accounts for the variable name *soilporo*. In fact, the saturated water content is being specified, but the variable name remains unchanged.

**Step 7:** Calculate the water level associated with the wilting point for the four nodes of cell n.

**Explanation:** The water level associated with the wilting point (*Wilt\_layer*) is the product of the layer thickness and the wilting point.

**Step 8:** Calculate the total evaporable water (*TEW*; Allen et al. 1998 [DIRS 157311], Equation 73) for cell n.

**Explanation:** The total evaporable water is the product of the thickness of the evaporation layer and the difference between the field capacity and half of the wilting point.

**Step 9:** Set the readily evaporable water of cell n (*REW<sub>n</sub>*) to the user-specified value (*rew*).

**Step 10:** Calculate the total available water (*TAW*; Allen et al. 1998 [DIRS 157311], Equation 82) for cell n.

**Explanation:** FAO-56 defines the total available water as the product of the root depth and the difference between the field capacity and the wilting point. MASSIF allows soil depths that are less than the rooting depth. Hence the sum of the thicknesses of Layers 1 and 2 (i.e., Nodes 1 and 3) are used in place of the rooting depth to calculate TAW.

**Routine output:** This routine returns the node thicknesses, initial node water levels, maximum daily water flows through the soil and rock, TEW, REW, TAW, integrated node field capacities, integrated node wilting points, and maximum pore volumes for every cell in the watershed.

## G 5.2 WEATHER ROUTINES

### G5.2.1 Estimate of the Daily Dew Temperature

The daily dew temperature (*T<sub>dew</sub>*) is calculated as an offset from the minimum temperature for the day (*T<sub>min</sub>*). The offset for winter (*K<sub>winter</sub>*) is different than the offset for the rest of the year (*K<sub>rest</sub>*). Winter starts on the calendar year day *K<sub>winter\_start</sub>* and ends on the calendar year day *K<sub>winter\_end</sub>*. The parameters *K<sub>winter</sub>*, *K<sub>rest</sub>*, *K<sub>winter\_start</sub>*, and *K<sub>winter\_end</sub>*, are inputs to *Massif* and are described under *Miscellaneous Parameters* in Section 6.5. The dew temperature is calculated in routine *T<sub>dew\_fcn</sub>*.

### G5.2.2 Correction of Temperature for Elevation

The temperatures in the weather files ( $T_{airRef_{max}}$ ,  $T_{airRef_{min}}$ ) are for a specific elevation ( $elev_{ref}$ ). The temperatures for a specific cell (elevation  $elev$ ) are calculated from these reference temperatures using a lapse rate correction for elevation ( $C_{Tcor}$ ). Temperature corrections are performed in  $T_{elev\_cor}$ . The steps in routine  $T_{elev\_cor}$  are:

**Step 1:** Calculate the lapse rate correction.

**Explanation:** The lapse rate correction is linear in temperature.

**Step 2:** Calculate the corrected maximum temperature.

**Explanation:** The corrected maximum air temperature is the reference maximum air temperature minus the lapse rate correction.

**Step 3:** Calculate the corrected minimum temperature.

**Explanation:** The corrected minimum air temperature is the reference minimum air temperature minus the lapse rate correction.

**Step 4:** Compute the mean daily temperature.

**Explanation:** The mean daily temperature is the average of the maximum and minimum daily temperatures (Allen et al. 1998 [DIRS 157311], Equation 9).

**Step 5:** Compute the dew point temperature.

**Explanation:** The dew point temperature is computed using routine  $T_{dew\_fcn}$ .

### G5.2.3 Correction of Precipitation for Elevation

The daily precipitation in the weather files is for a specific elevation ( $elev_{ref}$ ). The precipitation for a specific cell (elevation  $elev$ ) is calculated from this reference precipitation using a lapse rate correction for elevation ( $C_{Precipcor}$ ). Precipitation corrections are performed in routine  $Precip_{elev\_cor}$ .

### G5.2.4 Estimate of the Duration of the Precipitation Event

The duration of a precipitation event is estimated from a linear correlation of measured daily durations as a function of measured daily precipitation amounts (Section 6.5.1). The daily duration is no less than zero and no greater than 24 hrs. The duration of the precipitation event is calculated in routine  $Duration\_fcn$ .

### G5.3 READING THE WEATHER/PRECIPITATION FILE

The routine *Weather* is used to read the stochastically generated weather files (Section 6.5) used to model the three climates (present day, monsoon, and glacial). These weather files are Excel workbooks. The information on the first spreadsheet in the workbook is used in the infiltration calculation. The steps in *Weather* are:

**Step 1:** Read the reference elevation for the weather.

**Explanation:** The reference elevation is contained in row 2 of column 1 in the spreadsheet.

**Step 2:** Read the number of weather years.

**Explanation:** The number of weather years is located in row 2 of column 2 in the spreadsheet.

**Step 3:** Read the weight of each weather year.

**Explanation:** The relative probability of a weather year is its “weight.” The “weights” are in column 2 and begin in row 5.

**Step 4:** Read the time information.

**Explanation:** The time information includes month, day of month, sequential year number, and day of the calendar year. The data begins in row 2 and extend to the end of the file. The time data is included in columns 3 through 6.

**Step 5:** Read the weather information for each weighted precipitation year.

**Explanation:** The weather information consists of daily precipitation, maximum temperature, minimum temperature, and wind speed at 2 m. This set of four adjacent columns is repeated for all the weighted weather years.

**Step 6:** Create a weather set for each of the weighted precipitation years.

**Explanation:** The weather set includes the time data, read in **Step 4**, and the weather data, read in Step 5.

**Routine Output:** The routine returns a vector of weather sets; each weather set is a matrix. It also returns the “weights” (or probabilities) of each weighted weather year, and the reference elevation.

### G5.4 MONITORED OUTPUT

#### G5.4.1 Watershed-scale Monitored Quantities

On the scale of the watershed, *Massif* returns the:

- 1) Change in the water stored in the soil of the watershed
- 2) Change in the snow level for the watershed
- 3) Sum of the precipitation over the watershed
- 4) Sum of the evapotranspiration over the watershed



- 5) Sum of the infiltration over the watershed
- 6) Sum of the snow sublimation over the watershed
- 7) Runoff from the watershed.

When the user specifies a value of  $-1$  for the input flag  $i_{ws}$ , the reported changes and sums are cumulative for the entire water year(s) of the calculation. If the user specifies a value of  $1$  for the input flag  $i_{ws}$ , the reported changes and sums are reported for each day of the water year(s) of the calculation. In addition, *Massif* returns the difference between all of the sources and sinks of water for the watershed. The magnitude of this “error” should always be approximately equal to the number of cell times the machine precision. For small watersheds, this is about  $10^{-14}$ . For large watersheds, this is about  $10^{-7}$ .

The daily watershed-scale mass check and its component parts are in routine *Masscheck\_fcn*. The steps in *Masscheck\_fcn* are:

**Step 1:** Calculate the change in the stored water.

**Explanation:** The daily change in the water content of an individual cell is computed using the daily changes in water levels for each of the four nodes that comprise the cell:

$$\begin{aligned} \Delta W_{level} = & \Delta W_{level_{Node1}} \cdot (1 - f_c) + \Delta W_{level_{Node2}} \cdot f_c \dots & \text{(Eq. G-25)} \\ & + \Delta W_{level_{Node3}} + \Delta W_{level_{Node4}} \end{aligned}$$

The change for the entire watershed is the sum of the cell changes for all the cells in the watershed.

**Step 2:** Calculate the change in snow levels, and cumulative values of precipitation, evapotranspiration, runoff, net infiltration, and sublimation.

**Explanation:** All of these quantities vary from cell to cell. The watershed totals are merely sums over all the cells in the watershed. As in the case of runoff, the only interest is in runoff from the watershed. Therefore, the cell runoff is summed only for cells that have no downstream cells ( $DnSt_n = -3$  in the geospatial file describing the watershed).

**Step 3:** Compute the change in water inventory.

**Explanation:** The change in water inventory (*Masscheck*) is calculated as:

$$\begin{aligned} \text{Masscheck} = & (-\text{Precip\_sum} - \text{ET\_sum} - \text{Infil\_sum} - \text{Sublimation\_sum} - \text{Runoff\_sum}) \dots \\ & + \Delta W_{level\_sum} + \Delta S_{level\_sum} & \text{(Eq. G-26)} \end{aligned}$$

This quantity should deviate from zero only due to machine precision limitations. The actual magnitude of *Masscheck* will be proportional to the number of cells in the watershed.

**Step 4:** Assemble the component part of the mass check.

**Explanation:** The component parts of the mass check are placed in the output variable  $Monitor_{ws}$ .

**Routine Output:** This routine returns the values for the daily mass check and the component parts of that mass check.

#### G5.4.2 Cell-scale Monitored Quantities

The user can also specify specific cells to monitor. The list of cells to be monitored is specified by the user in the vector  $i_{cell}$ . If, for instance, the user wishes to monitor cell numbers 1, 100, and 1,000, the user specifies:

$$i_{cell} := \begin{pmatrix} 1 \\ 100 \\ 1000 \end{pmatrix} \quad (\text{Eq. G-27})$$

The monitored quantities are returned in the vector  $Monitor_{cell}$  (see the output of the *Massif* driver). Each element of the output vector contains a matrix of monitored quantities for each monitored cell. For the example specified above,  $Monitor_{cell_1}$  is a matrix that contains the monitored quantities for cell 1,  $Monitor_{cell_2}$  is a matrix that contains the monitored quantities for cell 100, and  $Monitor_{cell_3}$  is a matrix that contains the monitored quantities for cell 1,000. The rows of each matrix correspond to the days listed in the precipitation file. A 1-year precipitation would have 365(6) rows; a 2-year precipitation file would have 730(1) rows. The columns in each matrix correspond to the cell-monitored quantities. These quantities are shown in Table G-3.

Table G-3. Quantities Returned by  $Monitor_{cell\_fcn}$

Column	Variable Name	Quantity
1	Wlevel <sub>1</sub>	Water level in Node 1
2	Wlevel <sub>2</sub>	Water level in Node 2
3	Wlevel <sub>3</sub>	Water level in Node 3
4	Wlevel <sub>4</sub>	Water level in Node 4
5	Slevel	Snow level (equivalent water height)
6	Runon	Run-on from upstream cells
7	Runoff	Runoff to downstream cells
8	Infil	Infiltration into rock
9	precip	Precipitation (adjusted for elevation)
10	NetPrecip	Amount of precipitation/snowmelt that is available to the soil
11	SnowMelt	Snowmelt for the day
12	ET0	Reference ET
13	Evaporate	Evaporation from the evaporation layer
14	Transpire	Transpiration from the root zone

Table G-3. Quantities Returned by Monitor<sub>cell\_fcn</sub> (Continued)

Column	Variable Name	Quantity
15	Sublimation	Snow sublimation
16	FC_layer <sub>1</sub>	Product of layer thicknesses and field capacity for Layer 1 (Nodes 1 and 2)
17	FC_layer <sub>3</sub>	Product of layer thicknesses and field capacity for Layer 2 (Node 3)
18	Wilt_layer <sub>1</sub>	Product of layer thickness and wilting point for Layer 1 (Nodes 1 and 2)
19	Wilt_layer <sub>3</sub>	Product of layer thickness and wilting point for Layer 2 (Node 3)
20	Masscheck_cell	Check of water conservation for the cell
21	MaxInfil_sl	Maximum daily (24 hr) water flow in the soil
22	MaxInfil_rk	Maximum daily (24 hr) water flow in the underlying rock
23	Pore_sl <sub>1</sub>	Soil pore volume of Node 1
24	f <sub>c_new</sub>	Vegetative canopy coefficient
25	K <sub>cb</sub>	Adjusted crop coefficient
26	PVR	Potential vegetative response
27	Tmax	Maximum temperature (adjusted for elevation)
28	Tmin	Minimum temperature (adjusted for elevation)
29	Precip <sub>total</sub>	Daily precipitation (adjusted for elevation) for the entire repository)

Source: Output DTN: SN0701T0502206.037.

The mass check for the individual monitored cells and the compilation of monitored cell properties is performed in the routine *Monitorcell\_fcn*. The formulation for the individual cell mass check is explained in the description of the routine *Masscheck\_fcn* (above).

## G5.5 INPUT FILES: CONSTANTS AND NOMINAL INPUT VALUES

Numerical constants and nominal values of input parameters are included in a total of four Mathcad files. Constants are located in *Constants.xmcd*. Nominal soil properties are located in *SoilProperties.xmcd*. Nominal rock properties are located in *Rock Properties.xmcd*. The balance of most nominal input parameters is located in *Inputs Values.xmcd*. These files contain tables of numerical values as well as the references for those values. These values should be compared to Section 4.

The constants file is “referenced” in the MASSIF files where needed. The rock and soil properties files are referenced in the input values files so that only *Input Values.xmcd* need be referenced. When the user constructs a “front end” for the *Massif* routine, the user typically “references” the input values file. The user will then selectively supersede any of the nominal values listed in these files with the specific values of interest to the particular analysis. Other input values, such as the weather files, site elevation, and site latitude, are provided in the “front end” and are not part of the input files listed here.

## G6. FILES AND ROUTINES

Table G-4 shows a list of the MASSIF routines and their corresponding Mathcad file names.

Table G-4. List of MASSIF Routines and Corresponding Mathcad File Names

<b>MASSIF ROUTINE</b>	<b>MATHCAD FILE NAME</b>
Balance	<i>Balance Model.xmcd</i>
cdepth	<i>Layer Depths and Properties.xmcd</i>
C <sub>Rb</sub> fcn	<i>RefET.xmcd</i>
D <sub>c</sub> fcn	<i>ET.xmcd</i>
D <sub>e</sub> fcn	<i>ET.xmcd</i>
DiffuseDirect	<i>RefET.xmcd</i>
DOWY_fcn	<i>ET.xmcd</i>
D <sub>r</sub> fcn	<i>ET.xmcd</i>
Duration_fcn	<i>Weather Correction.xmcd</i>
e0	<i>ET.xmcd and RefET.xmcd</i>
ET	<i>ET.xmcd</i>
ET <sub>0</sub>	<i>RefET.xmcd</i>
GroupBalance	<i>Balance Model.xmcd</i>
Index_NDVI_fcn	<i>ET.xmcd</i>
Index_Rb_fcn	<i>RefET.xmcd</i>
K <sub>cb</sub> fcn	<i>ET.xmcd</i>
K <sub>cb0</sub> fcn	<i>ET.xmcd</i>
K <sub>e</sub> fcn	<i>ET.xmcd</i>
K <sub>r</sub> fcn	<i>ET.xmcd</i>
K <sub>s</sub> fcn	<i>ET.xmcd</i>
K <sub>tp_c</sub> fcn	<i>ET.xmcd</i>
K <sub>tp</sub> fcn	<i>ET.xmcd</i>
LayerProps	<i>Layer Depths and Properties.xmcd</i>
Masscheck_fcn	<i>Monitored IO.xmcd</i>
Massif	<i>Massif extended.xmcd</i>
Monitorcell_fcn	<i>Monitored IO.xmcd</i>
precip_Kcb_fcn	<i>AnnualCumulativePrecip.xmcd</i>
Precip <sub>elev_cor</sub>	<i>Weather Correction.xmcd</i>
Rb_fcn	<i>RefET.xmcd</i>
R <sub>smhor</sub> func	<i>RefET.xmcd</i>
R <sub>sohor</sub> func	<i>RefET.xmcd</i>
SnowB	<i>Snow.xmcd</i>
SolarRad_inc	<i>RefET.xmcd</i>
T <sub>dew</sub> fcn	<i>Weather Correction.xmcd</i>
T <sub>elev_cor</sub>	<i>Weather Correction.xmcd</i>
Upstream3	<i>Upstream Contributors.xmcd</i>
Varying_fc	<i>Balance Model.xmcd</i>
Weather	<i>Read Weather Routines.xmcd</i>
γ <sub>c</sub> fcn	<i>RefET.xmcd</i>

Source: Output DTN: SN0701T0502206.037.

**APPENDIX H**  
**SENSITIVITY ANALYSIS OF MEAN ANNUAL INFILTRATION**



## H1. METHODOLOGY

### H1.1 INTRODUCTION

The purpose of uncertainty and sensitivity analysis is primarily to increase our understanding of a complex system. Formally, any system can be presented as:

$$\mathbf{y} = f(\mathbf{x})$$

where

- $\mathbf{y} = (y_1, y_2, \dots, y_k)$  represents a vector of output data of the model (the quantities to be estimated). In this case, the output data considered is the spatially averaged mean annual net infiltration over the infiltration modeling domain (Section 6.5.7).
- $\mathbf{x} = (x_1, x_2, \dots, x_n)$  represents a vector of input data
- $f$  represents a function or set of functions, which is generally complex.

Uncertainty analysis is defined as the study of the uncertainty of  $\mathbf{y}$  due to the uncertainty in the set of inputs  $\mathbf{x}$ . In other words, because of uncertainty of the input values, uncertainty is induced in the output value (response). It is desirable to quantify and represent this uncertainty in order to know what could be the possible range (and distribution) of each element of  $\mathbf{y}$ .

Sensitivity analysis is complementary to uncertainty analysis and is defined as the study of how the uncertainty in  $\mathbf{y}$  can be apportioned to the uncertainty in each element of  $\mathbf{x}$ . It is important to know how each input uncertainty affects a given element of  $\mathbf{y}$ .

Ultimately, the sensitivity analysis helps in verifying the model by checking whether the influential uncertain parameters are concordant with what was expected from the equations. It is also a very good tool for planning a new set of experiments by indicating what benefit could be obtained (i.e., which reduction of uncertainty can be expected in a given element of  $\mathbf{y}$ ) by reducing the uncertainty in an element of  $\mathbf{x}$ .

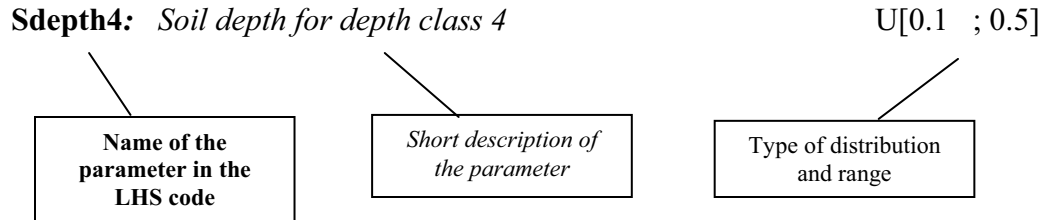
Different methods have been developed for performing sensitivity analysis such as local sensitivity analysis (based on derivatives), screening methods, reliability methods (e.g., FORM/SORM). The one used in this appendix is a sampling based method (Monte Carlo analysis).

A Monte Carlo analysis consists in sampling the input space in order to determine the distribution of the output space. This provides the tools necessary for both uncertainty and sensitivity analysis. Different techniques can be used to sample the input space. The technique chosen is the Latin Hypercube Sampling (LHS), which provides good coverage of the distribution of each parameter, due to its stratification.

Due to the high cost (in computer time and memory) of the MASSIF (Mass Accounting System for Soil Infiltration and Flow) code, the sample size chosen is relatively low ( $n=20$ ). However, two replicates have been created in order to study the stability of the results.

## H1.2 LIST OF CONSIDERED INPUTS

Appendix I lists the range of each uncertain parameter and provides the screening of parameters that are considered as uncertain in this analysis. This list of considered uncertain parameters is displayed below. The format is the following:



The acronyms for the type of distribution are:

- U Uniform minimum and maximum values are given
- LU Loguniform minimum and maximum values are given
- N Normal 0.001 and 0.999 quantiles values are given
- CDF Cumulative distribution function.

Certain precipitation parameters are represented as a first order Fourier series parameterized with three fitting parameters. The meaning of the precipitation parameters and the fitting parameters are defined below.

Precipitation parameters:

$p_{00}(d)$  Probability of a dry day given the previous day was dry (dimensionless)

$p_{01}(d)$  Probability of a dry day given the previous day was wet (dimensionless)

$\lambda(d)$  Mean of the probability distribution for the amount of precipitation on day,  $d$ , given that it is wet (mm)

$m(d)$  Mean of the probability distribution for the natural logarithm of the amount of precipitation on day,  $d$ , given that it is wet (ln(mm)).

Fitting parameters:

$a$  Annual mean value

$b$  Amplitude of the annual variation (equal to one half of the annual variation)

$\theta$  Phase shift for the seasonal variation.

Thus, to parameterize daily precipitation twelve stochastic parameters must be defined ( $a$ ,  $b$ , and  $\theta$  for each of the four precipitation parameters). An alternative way to analyze precipitation parameter sensitivity is to focus not on the individual stochastic parameters separately but rather to use the mean annual precipitation (MAP) resulting from the stochastic simulation. Both analysis methods are used in this appendix.



### H1.2.1 Climate Independent Parameters

<b>Sdepth4</b>	Soil depth for depth class 4 (m)	U[0.1 ; 0.5]
<b>Z_e</b>	Evaporation depth (m)	U[0.1 ; 0.2]
<b>KC_min</b>	Minimum basal crop coefficient (dimensionless)	CDF
<b>HC_579</b>	Holding capacity for soil group 5/7/9 ( $m^3/m^3$ )	U[0.09 ; 0.17]
<b>ln Rks_405</b>	Natural log of rock conductivity for rock type 405 (Ln(m/s))	U[-16.39 ; -12.25]
<b>ln Rks_406</b>	Natural log of rock conductivity for rock type 406 (Ln(m/s))	U[-17.68 ; -11.77]
<b>REW</b>	Readily evaporable water (mm)	U[2.0 ; 10.0]
<b>Ckcb2</b>	Slope of the linear relationship between NDVi and $K_{cb}$ (dimensionless)	N[3.2 ; 16.2].

### H1.2.2 Modern Interglacial Climate Parameters

<b>Z_r</b>	Rooting depth (m)	U[0.6 ; 2.6]
<b>h_plant</b>	Plant height (m)	U[0.2 ; 0.6]
<b>a<sub>m</sub></b>	Annual average of $m(d)$ (ln(mm))	U[0.5 ; 1.07].

Moreover,  $a_\lambda$  (average over the year of expected precipitation) is defined as a function of  $a_m$ . Thus  $a_m$  represent the influence of the couple  $(a_m, a_\lambda)$

### H1.2.3 Monsoon Climate Parameters

<b>Z_r</b>	Rooting depth (m)	U[0.6 ; 2.6]
<b>h_plant</b>	Plant height (m)	U[0.2 ; 0.6]
<b>a<sub>m</sub></b>	Annual average of $m(d)$ (ln(mm))	U[0.5 ; 1.3]
<b>a<sub>00</sub></b>	Annual average $p_{00}(d)$ (dimensionless)	U[0.896 ; 0.944]
<b>b<sub>m</sub></b>	Amplitude of the annual variation in $m(d)$ (ln(mm))	U[-0.3 ; 0.5]
<b>gTmaxwet</b>	Annual average of daily maximum temperature on days with precipitation ( $^{\circ}C$ )	U[14 ; 22]
<b>PDur_S</b>	Slope of the linear relationship between precipitation duration and precipitation amount (mm/hr)	U[0.14 ; 0.43].

Moreover,  $a_\lambda$ ,  $b_\lambda$ ,  $b_m$ ,  $b_{00}$ , and  $b_{10}$  are defined as a function of  $a_m$ . Thus  $a_m$  represent the influence of the group  $(a_m, a_\lambda)$ , and  $b_m$  represents the influence of the group  $(b_\lambda, b_m, b_{00}, b_{10})$ .

The sampling of  $b_m$  and linear interpolation of other amplitude values conditional on  $b_m$ , may sometimes induce nonphysical results in the precipitation generation. The two possible nonphysical results are:

- The probability  $p_{00}(d)$  being greater than one
- $\lambda(d)$  being lower than  $m(d)$ .

The first item is unlikely to happen, but samples have been screened in order to be sure that such nonphysical results do not occur.

The second occurrence is more likely. In order to reduce its likelihood, a small positive correlation ( $=0.2$ ) has been imposed between  $a_m$  and  $b_m$ .

### H1.2.4 Glacial Transition Climate Parameters

<b>Z<sub>r</sub></b>	Rooting depth (m)	U[1.0 ; 4.0]
<b>h<sub>plant</sub></b>	Plant height (m)	U[0.6 ; 1.8]
<b>a<sub>00</sub></b>	Annual average $p_{00}(d)$ (dimensionless)	U[0.78 ; 0.89]
<b>a<sub>m</sub></b>	Annual average of $m(d)$ (ln(mm))	U[0.48 ; 0.92]
<b>θ<sub>m</sub></b>	Phase of annual variation in $m(d)$ (radians)	U[-3.14 ; 3.14]
<b>(Theta<sub>m</sub>)</b>		
<b>PDur<sub>S</sub></b>	Slope of the linear relationship between precipitation duration and precipitation amount (mm/hr)	U[0.32 ; 0.71].

Moreover,  $a_\lambda$  is defined as a function of  $a_m$ . Thus  $a_m$  represents the influence of the coupled parameters,  $a_m$  and  $a_\lambda$ .  $\theta_\lambda$  is defined as a function of  $\theta_m$ . Thus  $\theta_m$  represents the influence of the coupled parameters,  $\theta_\lambda$  and  $\theta_m$ .

### H1.3 DATA TRANSFORM

The methods used for sensitivity analysis quantify linear relationships that may exist between the input parameters and the output results of a calculation or model. It is possible to extend these methods to quantifying monotonic relationships by working with the rank of the data instead of the raw values. For each parameter (whether it is input or output), rank values are obtained by assigning the rank of 1 to the highest value, 2 to the next highest value, and so on. Identical values are assigned with the same rank number.

### H1.4 STEPWISE REGRESSION APPROACH

The stepwise regression used on raw data quantifies the linear relationship between the inputs and the output.

The stepwise regression used on rank data quantifies the monotonic relationship between the inputs and the output.

The stepwise regression analysis works as follows:

- Step 1: Pick the most important variable and create a regression model
- Step 2: Pick the next most important variable and add it to the regression model
- Step 3: Pick the next most important variable and add it to the regression model
- Repeat until adding additional variables does not result in an improved regression model.

The degree of importance of the variables is defined by the coefficient of determination of the regression model once the variable is added. In other words, the most important variable is the variable that gives the “best” regression model using a single variable. The next most important variable is the variable that gives the “best” regression model using two variables including the first variable, and so forth.

The determination of influence is based on what is called an alpha cutoff. At each step, an alpha value is calculated. This value represents the probability that an input variable is considered as influential when in fact it is not. The alpha cutoff considered is equal to 0.10, which means that there is a 10% chance of having a noninfluential parameter considered as influential.

Moreover, a color coding has been used – if alpha is lower than 0.05 (i.e., less than a 5% chance of spurious correlation), then the number is in black. If alpha is between 0.05 and 0.10, then the number is shown in red. When alpha is above 0.10, the parameter is not included in the list because the regression model is not improved by including additional parameters.

The relevant parameters calculated are:

- $R^2$ : Coefficient of determination of the regression model. It represents the fraction of uncertainty (percentage of variance) explained by the regression model. It indicates how good the regression model is and how well understood the input parameters influence is.
- SRC: Standardized Regression Coefficients of the regression model. They are standardized to suppress the “unit” effect (i.e., having the same results whether the input is in meters, millimeters or kilometers).
- SRRC: Standardized Rank Regression Coefficients. These are calculated as for the SRC, but are based on the rank of the data instead of raw data themselves.

The software used for this analysis is MVIEW 4.0 (STN: 10072-4.0-00) [DIRS 173438].

## H1.5 SCATTERPLOT ANALYSIS

Scatterplot analysis is visual. Figures are created with plots whose abscissa corresponds to the input parameter value and whose ordinate corresponds to the mean net infiltration results, listed as the weighted mean annual net infiltration over the entire modeling domain. If net infiltration is sensitive to a given input parameter, a pattern should be seen in the scatterplot. Otherwise, the scatterplots will look like random distributions. Only input data explaining more than 10% of the infiltration variance are presented, as an influence of 10% and lower is generally not discernable.

## H2. PRESENT-DAY CLIMATE

### H2.1 STUDY OF REPLICATE 1 – ALEATORY UNCERTAINTY VARYING

Table H-1. Stepwise Regression (linear and rank) on Average Infiltration for Replicate 1: Present-Day Climate (aleatory uncertainty varying)

Step	Stepwise Regression (linear)				Stepwise Regression (rank)			
	Variable	tot. $R^2$	inc. $R^2$	SRC	Variable	tot. $R^2$	inc. $R^2$	SRRC
1	Sdepth4	0.33	0.33	-0.61	Sdepth4	0.37	0.37	-0.63
2	$a_m$	0.63	0.30	0.50	HC_579	0.66	0.28	-0.49
3	HC_579	0.82	0.19	-0.44	$a_m$	0.83	0.17	0.43
4	REW	0.86	0.04	0.19	REW	0.88	0.05	0.22

Source: Output DTN: SN0701T0502206.044, *Stepwise\_Analysis\_R1\_MIC\_VA.xls*.

### H2.1.1 Linear Regression

The linear regression results for Replicate 1 of the Present-Day climate are shown in Table H-1. Soil Depth Class 4 explains 33% of the variance in net infiltration and has a strong negative effect ( $SRC = -0.61$ ). The negative effect of soil depth is expected, since a deeper soil layer can store more water, which is later lost to evapotranspiration, resulting in less infiltration.  $a_m$  ranks second in importance with a positive effect ( $SRC=0.50$ ).  $HC\_579$  ranks third with a small negative effect. Readily evaporable water ( $REW$ ) ranks fourth with a very small positive influence ( $R^2$  increment of 4%). However, the red text in Table H-1 indicates that this influence may be due to spurious correlation, with a probability higher than 5%.

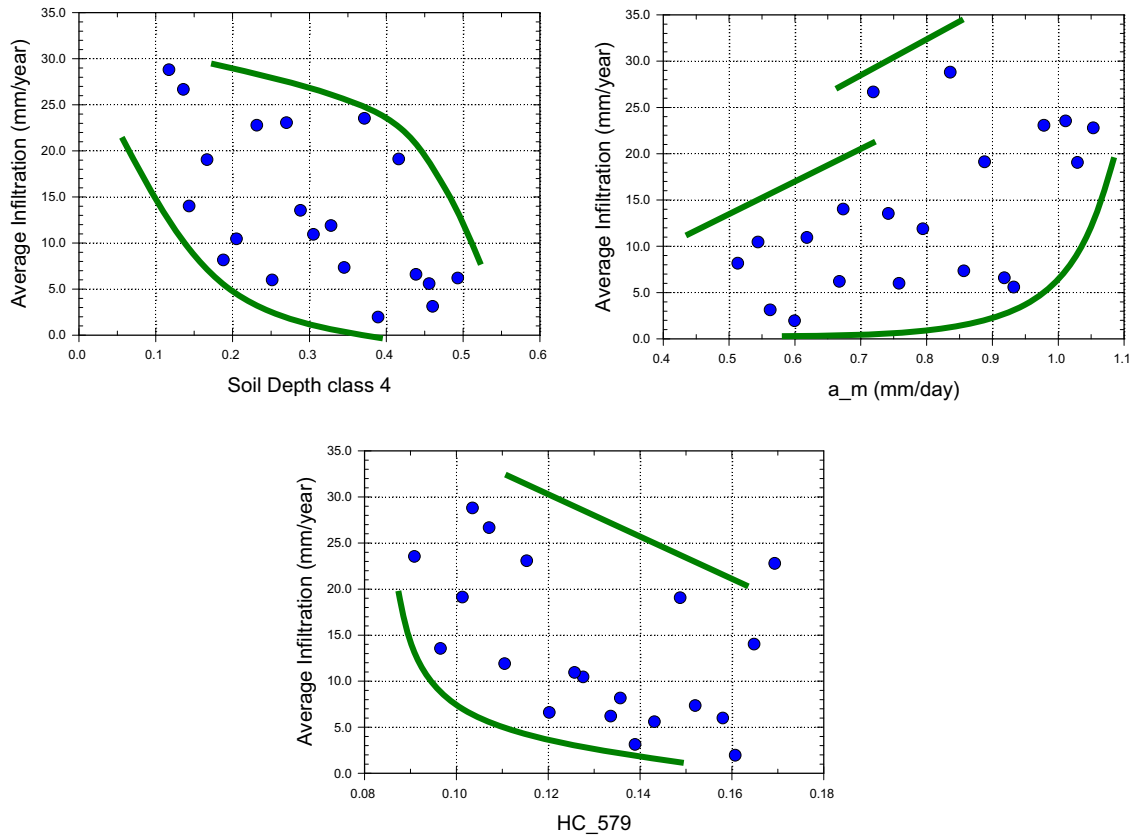
Analysis performed while replacing the precipitation parameter with mean annual precipitation ( $MAP$ ) values gives similar results and is therefore not presented here.

### H2.1.2 Rank Regression

The rank regression results for Replicate 1 of the Present-Day climate are also shown in Table H-1. Soil Depth Class 4 is the top contributor, explaining 37% of the variance in average net infiltration. It has a strong negative effect ( $SRRC=-0.63$ ).  $HC\_579$  and  $a_m$  also contribute, explaining an additional 28% and 17% of the net infiltration variance, respectively. Readily evaporable water ( $REW$ ) explains 5% of the variance, with a small positive effect. However, the influence may be due to spurious correlation.

Analysis performed while replacing the precipitation parameter with  $MAP$  values gives similar results, and is therefore not presented here.

### H2.1.3 Scatterplots



Source: Output DTN: SN0701T0502206.044, *scatterplots\_R1\_MIC-VA.JNB*.

Figure H-1. Scatterplots of Average Infiltration Versus Soil Depth Class 4 (upper left frame),  $a_m$  (upper right frame), and HC\_579 (lower frame) - Replicate 1 - Present-Day Climate (aleatory uncertainty varying)

Scatterplot analysis (Figure H-1) shows clearly the influence of Soil Depth Class 4. The other parameters show less influence.

## H2.2 STUDY OF REPLICATE 2 – ALEATORY UNCERTAINTY VARYING

Table H-2. Stepwise Regression (linear and rank) on Average Infiltration for Replicate 2: Present-Day Climate (aleatory uncertainty varying)

Step	Stepwise Regression (linear)				Stepwise Regression (rank)			
	Variable	tot. R <sup>2</sup>	inc. R <sup>2</sup>	SRC	Variable	tot. R <sup>2</sup>	inc. R <sup>2</sup>	SRRC
1	Sdepth4	0.50	0.50	-0.74	Sdepth4	0.50	0.50	-0.74
2	$a_m$	0.85	0.35	0.58	$a_m$	0.83	0.33	0.57
3	HC_579	0.90	0.05	-0.21	HC_579	0.86	0.04	-0.19
4	REW	0.91	0.01	-0.12				

Source: Output DTN: SN0701T0502206.044, *Stepwise\_Analysis\_R2\_MIC\_VA.xls*.

### H2.2.1 Linear Regression

The linear regression results for Replicate 2 of the Present-Day climate are shown in Table H-2. Soil Depth Class 4 explains 50% of the variance in net infiltration. It has a strong negative effect on infiltration ( $SRC = -0.74$ ).

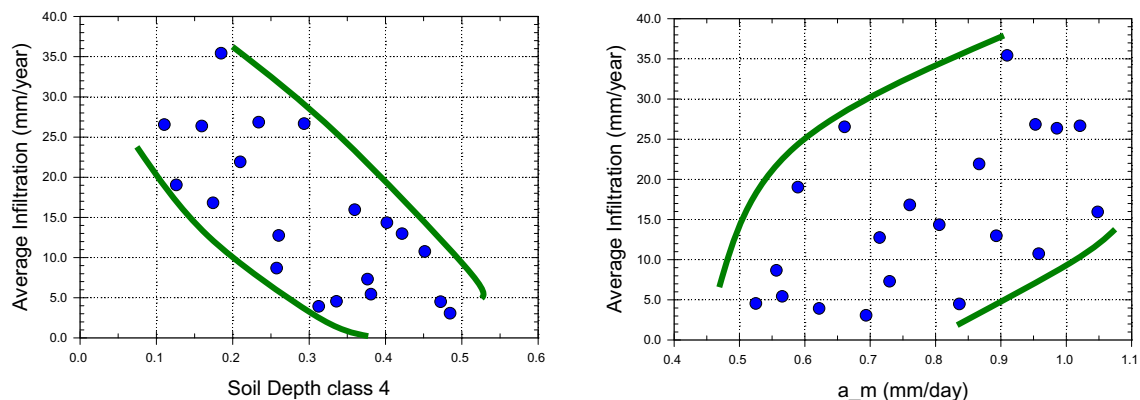
$a_m$  has a positive effect on the average net infiltration ( $SRC=0.58$ ), explaining an additional 35% of the variance. The positive influence of  $a_m$  is expected. By increasing the precipitation (and thus  $a_m$ ), the water available at the surface and the resulting net infiltration are increased.

HC\_579 has a negative effect, explaining an additional 5% in the variance of net infiltration. Readily Evaporable Water ( $REW$ ) has a very small negative influence, explaining 1% of the variance of net infiltration, but it has more than a 5% chance of being due to spurious correlation.

### H2.2.2 Rank Regression

The rank regression results for Replicate 2 of the Present-Day climate are also shown in Table H-2. The rank regression is identical to the linear regression, without the inclusion of  $REW$ . HC\_579 (holding capacity for soil group 5/7/9) is highlighted in red, indicating that the influence is so small that it could be spurious.

### H2.2.3 Scatterplots



Source: Output DTN: SN0701T0502206.044, *scatterplots\_R2\_MIC-VA.JNB*.

Figure H-2. Scatterplots of Average Infiltration Versus Soil Depth Class 4 (left frame),  $a_m$  (right frame) Replicate 2 - Present-Day Climate (aleatory uncertainty varying)

Figure H-2 shows clearly the influence of Soil Depth Class 4 and  $a_m$ . The other parameters show less influence.

## H2.3 CONCLUSION OF STUDY OF ORIGINAL DATA (ALEATORY UNCERTAINTY VARYING)

Sensitivity analyses on Replicates 1 and 2 of the Present-Day climate agree on the most influential parameters – Soil Depth Class 4 and  $a_m$ . They also agree on the relative importance of each parameter ( $R^2$  increment of  $\sim 0.5$  for Soil Depth Class 4 and  $\sim 0.2$  for  $a_m$ ). The third most important parameter is HC\_579.

One of the problems of current analysis is that infiltration results are influenced by the precipitation years generated. Each set of 10 years is different for each LHS run. In other words, a different future is considered for each realization.

It is reasonable to consider a different future because the future is uncertain (random). However, it makes the sensitivity analysis of the physical parameters (system properties that can be physically measured) harder to interpret.

One possible solution is to eliminate the uncertainty in the future for the sensitivity analysis. In other words, the same set of 10 precipitation years is considered for any LHS run in MASSIF. In such a “Fixed Aleatory” scenario, only the physical parameters are varied. This scenario should provide a cleaner sensitivity analysis for the physical parameters but will ignore the influence of stochastic precipitation parameters.

### Replicate 1 – Aleatory Uncertainty Fixed

Table H-3. Stepwise Regression (linear and rank) on Average Infiltration for Replicate 1: Present-Day Climate (aleatory uncertainty fixed)

Step	Stepwise Regression (linear)				Stepwise Regression (rank)			
	Variable	tot. $R^2$	inc. $R^2$	SRC	Variable	tot. $R^2$	inc. $R^2$	SRRC
1	Sdepth4	0.66	0.66	-0.85	Sdepth4	0.77	0.77	-0.90
2	HC_579	0.90	0.24	-0.46	HC_579	0.93	0.16	-0.40
3	CKcb2	0.93	0.03	-0.15				
4	h_plant	0.95	0.02	0.15				

Source: Output DTN: SN0701T0502206.044, *Stepwise\_Analysis\_R1\_MIC\_FA.xls*.

### H2.3.1 Linear Regression

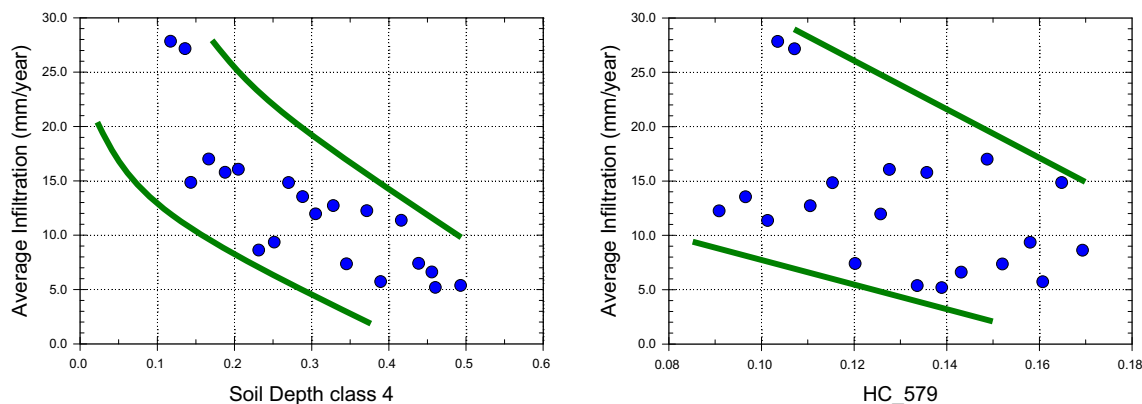
The linear regression results for Replicate 1, Fixed Aleatory, of the Present-Day climate are shown in Table H-3. Soil Depth Class 4 explains 66% of the variance. It has a strong negative effect on infiltration (SRC =  $-0.85$ ). HC\_579 has some negative effect, explaining 24% of the variance. CKcb2 and h\_plant explain an additional 3% and 2% of the variance of infiltration, respectively.

### H2.3.2 Rank Regression

The rank regression results for Replicate 1, Fixed Aleatory, of the Present-Day climate are also shown in Table H-3. Regression on the rank gives similar results to that of regression on raw

values for Soil Depth Class 4 (explaining 77% of the variance) and HC\_579 (16% of the variance).

### H2.3.3 Scatterplots



Source: Output DTN: SN0701T0502206.044, *scatterplots\_R1\_MIC\_FA.JNB*.

Figure H-3. Scatterplots of Average Infiltration Versus Soil Depth Class 4 (left frame), and HC\_579 (right frame) - Replicate 1 - Present-Day Climate (aleatory uncertainty fixed)

Scatterplot analysis (Figure H-3) clearly shows the influence of Soil Depth Class 4. The other parameters show less influence. This is mainly due to the strong influence of Soil Depth Class 4, which explains almost 80% of the variance of net infiltration.

## H2.4 REPLICATE 2 – ALEATORY UNCERTAINTY FIXED

Table H-4. Stepwise Regression (linear and rank) on Average Infiltration for Replicate 2: Present-Day Climate (aleatory uncertainty fixed)

Stepwise Regression (linear)					Stepwise Regression (rank)			
Step	Variable	tot. R <sup>2</sup>	inc. R <sup>2</sup>	SRC	Variable	tot. R <sup>2</sup>	inc. R <sup>2</sup>	SRRC
1	Sdepth4	0.63	0.63	-0.80	Sdepth4	0.82	0.82	-0.91
2	HC_579	0.89	0.26	-0.49	HC_579	0.92	0.10	-0.32
3	lnRks_406	0.91	0.02	-0.16				

Source: Output DTN: SN0701T0502206.044, *Stepwise\_Analysis\_R2\_MIC\_FA.xls*.

### H2.4.1 Linear Regression

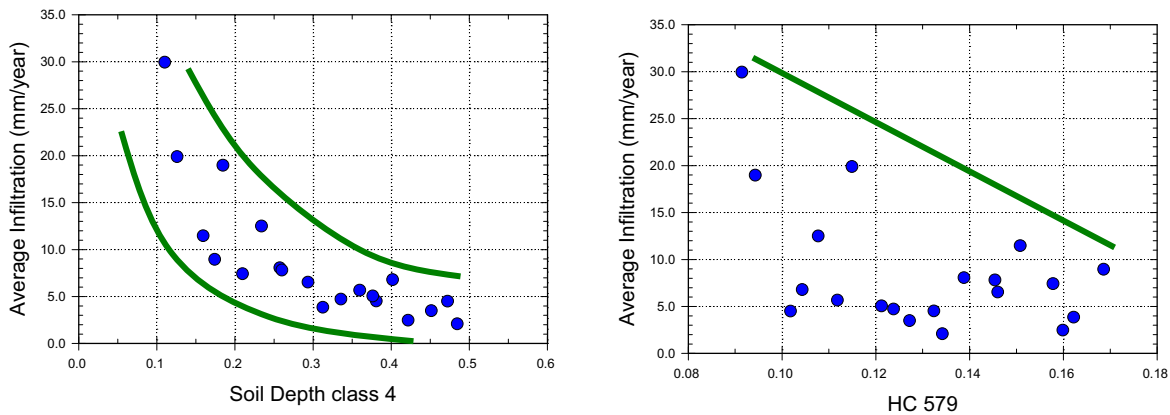
The linear regression results for Replicate 2, Fixed Aleatory, of the Present-Day climate are shown in Table H-4. Soil Depth Class 4 explains 63% of the variance. It has a strong negative effect on infiltration (SRC = -0.80). HC\_579 has some negative effect, explaining 26% of the variance on infiltration. lnRks\_406 seems to have a small negative effect on infiltration. However, the influence is negligible (increment in R<sup>2</sup> ~ 2%).



### H2.4.2 Rank Regression

The rank regression results for Replicate 1, Fixed Aleatory, of the Present-Day climate are also shown in Table H-4. Regression on the rank gives similar results to that of regression on raw values for the two most important parameters.

### H2.4.3 Scatterplots



Source: Output DTN: SN0701T0502206.044, *scatterplots\_R2\_MIC\_FA.JNB*.

Figure H-4. Scatterplots of Average Infiltration Versus Soil Depth Class 4 (left frame) and HC\_579 (right frame) - Replicate 2 - Present-Day Climate (aleatory uncertainty fixed)

Scatterplot analysis (Figure H-4) clearly shows the influence of Soil Depth Class 4. The other parameters show less influence.

## H2.5 CONCLUSIONS

When aleatory uncertainty is allowed to vary (different futures are considered) the results of the sensitivity analysis are more difficult to interpret because it is hard to distinguish between the influence of the variation in physical parameters (epistemic uncertainty) and the influence of randomness in future precipitation (aleatory uncertainty). These analyses shows the importance of Soil Depth Class 4 and precipitation amount (represented by the variation in  $a_m$ ), but little can be discerned about the relative importance of the other physical parameters. When aleatory uncertainty is fixed, the importance of HC\_579 is identified.

In conclusion, two physical parameters can be considered important and explain about 90% of the variance in infiltration when future weather is fixed: Soil Depth Class 4 and HC\_579. In addition to these two parameters, the weather parameter  $a_m$  should be added since it controls the MAP and is an influential parameter in the varying aleatory uncertainty study.

### H3. MONSOON CLIMATE (MC)

#### H3.1 REPLICATE 1 – ALEATORY UNCERTAINTY VARYING

Table H-5. Stepwise Regression (linear and rank) on Average Infiltration for Replicate 1: MC (aleatory uncertainty varying)

Step	Stepwise Regression (linear)				Stepwise Regression (rank)			
	Variable	tot. R <sup>2</sup>	inc. R <sup>2</sup>	SRC	Variable	tot. R <sup>2</sup>	inc. R <sup>2</sup>	SRRC
1	a <sub>m</sub>	0.46	0.46	0.57	a <sub>m</sub>	0.51	0.51	0.62
2	Sdepth4	0.79	0.33	-0.58	Sdepth4	0.81	0.30	-0.57
3	HC_579	0.87	0.08	-0.25	HC_579	0.91	0.11	-0.33
4	a <sub>00</sub>	0.91	0.04	-0.19	a <sub>00</sub>	0.94	0.03	-0.15
5	PDur_S	0.93	0.01	0.15	Ze	0.96	0.02	-0.15
6	Kc_min	0.94	0.01	-0.15	Kc_min	0.97	0.01	-0.12
7	Z <sub>e</sub>	0.95	0.01	-0.13				
8	Z <sub>r</sub>	0.96	0.01	-0.10				

Source: Output DTN: SN0701T0502206.044, *Stepwise\_Analysis\_R1\_MC\_VA.xls*.

Table H-6. Stepwise Regression (linear and rank) on Average Infiltration for Replicate 1, Where all Precipitation Parameters Have Been Replaced by Average Annual Precipitation: MC (aleatory uncertainty varying)

Step	Stepwise Regression (linear)				Stepwise Regression (rank)			
	Variable	tot. R <sup>2</sup>	inc. R <sup>2</sup>	SRC	Variable	tot. R <sup>2</sup>	inc. R <sup>2</sup>	SRRC
1	Sdepth4	0.46	0.46	-0.63	PPT_R1	0.44	0.44	0.57
2	PPT_R1	0.78	0.32	0.55	Sdepth4	0.75	0.31	-0.57
3	HC_579	0.86	0.08	-0.28	HC_579	0.86	0.11	-0.34

Source: Output DTN: SN0701T0502206.044, *Stepwise\_Analysis\_R1\_Precipitation\_MC\_VA.xls*.

#### H3.1.1 Linear Regression

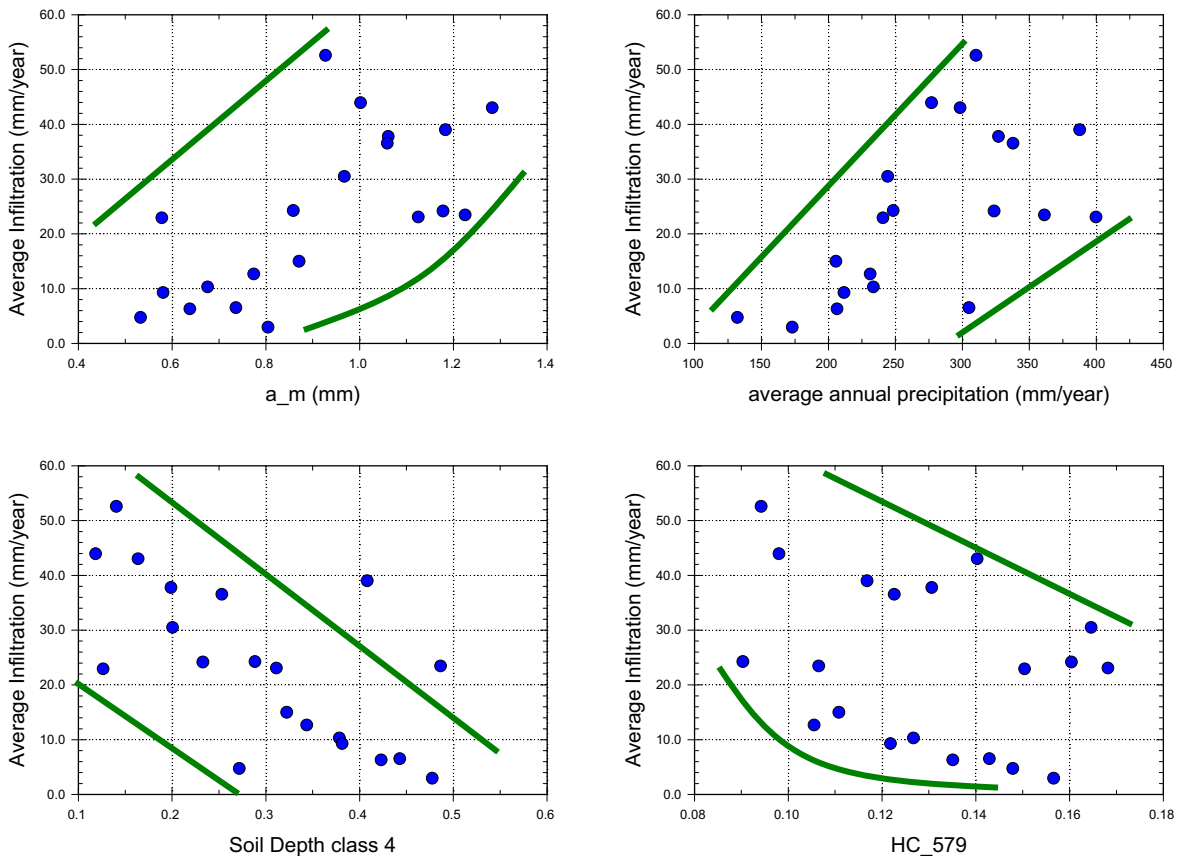
The linear regression results for Replicate 1 of the Monsoon climate are shown in Table H-5.  $a_m$  is the most important parameter, explaining 46% of the variance of infiltration. It has a positive effect, as expected. The next most important parameter is Soil Depth Class 4, with a negative effect on infiltration (SRC=-0.58). The third most important parameter is HC\_579, with a small negative effect (R<sup>2</sup> increment of 8%; SRC=-0.25). The other parameters in the table have negligible influence that may be due to spurious correlation.

MAP for the Monsoon climate is a function of the three independently sampled precipitation parameters ( $a_m$ ,  $a_{00}$ , and  $b_m$ ). A second stepwise regression analysis was performed to test the importance of this quantity (PPT\_R1 in Table H-6). In this case, Soil Depth Class 4 is the most important parameter, explaining 46% of the variance. The next two most important parameters are MAP and HC\_579.

### H3.1.2 Rank Regression

The rank regression results for Replicate 1 of the Monsoon climate are also shown in Tables H-5 and H-6. The rank analysis results in the same top three parameters:  $a_m$  (or MAP) ranks first in importance, followed by Soil Depth Class 4 and HC\_579.

### H3.1.3 Scatterplots



Source: Output DTN: SN0701T0502206.044, *scatterplots\_R1\_MC\_VA.JNB*.

Figure H-5. Scatterplots of Average Infiltration versus  $a_m$  (upper left frame), MAP (upper right frame), Soil Depth Class 4 (lower left frame), and HC\_579 (lower right frame) - Replicate 1 - MC (aleatory uncertainty varying)

Scatterplot analysis (Figure H-5) shows the influence of  $a_m$  and MAP on infiltration to be positive and significant. Soil Depth Class 4 has a visible negative effect on infiltration. The effect of HC\_579 is discernable but very small.

### H3.2 REPLICATE 2 – ALEATORY UNCERTAINTY VARYING

Table H-7. Stepwise Regression (linear and rank) on Average Infiltration for Replicate 2: MC (aleatory uncertainty varying)

Step	Stepwise Regression (linear)				Stepwise Regression (rank)			
	Variable	tot. R <sup>2</sup>	inc. R <sup>2</sup>	SRC	Variable	tot. R <sup>2</sup>	inc. R <sup>2</sup>	SRRC
1	a <sub>m</sub>	0.44	0.44	0.60	a <sub>m</sub>	0.58	0.58	0.76
2	Sdepth4	0.69	0.25	-0.41	Sdepth4	0.81	0.23	-0.39
3	a <sub>00</sub>	0.74	0.05	-0.23	Z <sub>e</sub>	0.88	0.07	-0.28
4	HC_579	0.79	0.05	-0.21	a <sub>00</sub>	0.92	0.04	-0.21
5	b <sub>m1</sub>	0.84	0.04	0.21	gTmaxwet	0.94	0.02	0.13
6	REW	0.87	0.04	-0.19				
7	lnRks_406	0.90	0.03	-0.20				
8	h_plant	0.93	0.02	-0.15				

Source: Output DTN: SN0701T0502206.044, *Stepwise\_Analysis\_R2\_MC\_VA.xls*.

Table H-8. Stepwise Regression (linear and rank) on Average Infiltration for Replicate 2, Where all Precipitation Parameters Have Been Replaced by Average Annual Precipitation: MC (aleatory uncertainty varying)

Step	Stepwise Regression (linear)				Stepwise Regression (rank)			
	Variable	tot. R <sup>2</sup>	inc. R <sup>2</sup>	SRC	Variable	tot. R <sup>2</sup>	inc. R <sup>2</sup>	SRRC
1	PPT_R2	0.57	0.57	0.76	PPT_R2	0.58	0.58	0.78
2	Sdepth4	0.84	0.27	-0.48	Sdepth4	0.83	0.25	-0.46
3	HC_579	0.89	0.05	-0.20	Z <sub>e</sub>	0.86	0.03	-0.18
4	h_plant	0.91	0.02	-0.16	gTmaxwet	0.88	0.02	0.14
5	REW	0.93	0.01	-0.13	HC_579	0.90	0.02	-0.14
6	lnRks_406	0.94	0.01	-0.11				

Source: Output DTN: SN0701T0502206.044, *Stepwise\_Analysis\_R2\_precipitation\_MC\_VA.xls*.

#### H3.2.1 Linear Regression

The linear regression results for Replicate 2 of the Monsoon climate are shown in Table H-7 (Section H3.2).  $a_m$  is the most important parameter, explaining 44% of the variance of infiltration. Soil Depth Class 4 comes next, explaining an additional 25% of the variance in infiltration, with a negative effect. The next parameter is a precipitation parameter,  $a_{00}$ , with a negative effect as expected. HC\_579 comes next, explaining an additional 5% of the infiltration variance. The remaining parameters in Table H-7 have a very small influence on the variance of infiltration and may be due to spurious correlation.

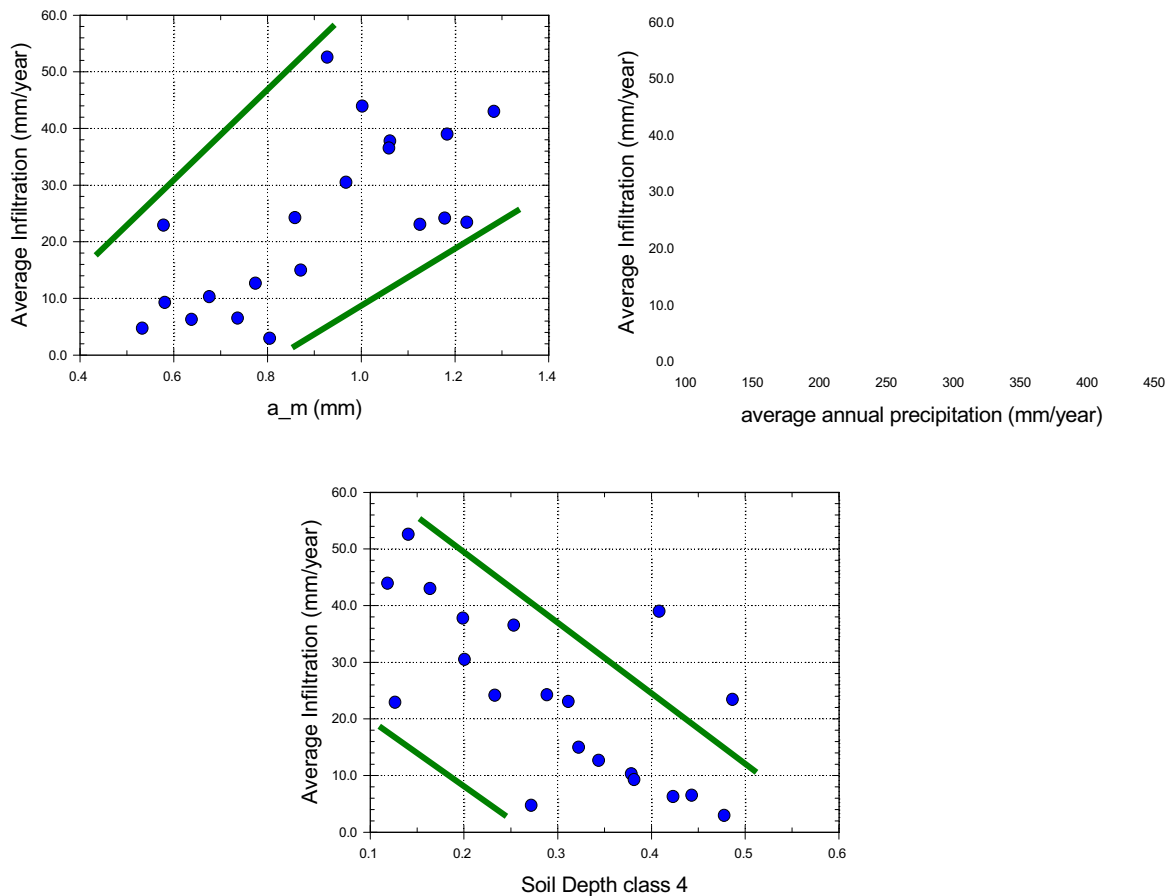
When MAP (PPT\_R2 in Table H-8)) is used as a replacement of the precipitation parameters, it becomes the most important parameter, explaining 57% of the variance in infiltration with a positive effect (as expected). The next most important parameter is Soil Depth Class 4, explaining 27% of the infiltration variance, with a negative effect (SRC=-0.52). HC\_579 comes next, explaining an additional 5% of the infiltration variance. The next three parameters listed have a negligible influence.

### H3.2.2 Rank Regression

The rank regression results for Replicate 2 of the Monsoon climate are also shown in Table H-7. The results of the rank regression are in agreement with linear regression for the two most important parameters,  $a_m$  and Soil Depth Class 4. The third most important parameter  $Z_e$  is different than for the linear regression but explains only 7% of the variance, which may be due to spurious correlation. The influence of the other parameters is negligible.

When precipitation parameters are replaced with the rank of MAP in the input set (PPT\_R2 in Table H-8), it represents the most important parameter. Soil Depth Class 4 ranks next in importance. These top two parameters explain 80% of the variance in infiltration. The next three parameters explain 3%, 2%, and 2%, respectively.

### H3.2.3 Scatterplots



Source: Output DTN: SN0701T0502206.044, *scatterplots\_R2\_MC\_VA.JNB*.

Figure H-6. Scatterplots of Average Infiltration versus  $a_m$  (upper left frame), MAP (upper right frame), and Soil Depth Class 4 (lower frame) - Replicate 2 - MC (aleatory uncertainty varying)

Scatterplot analysis (Figure H-6) shows a positive influence of  $a_m$  and MAP. The negative effect of Soil Depth Class 4 is also evident.

### H3.3 CONCLUSION OF STUDY OF ORIGINAL DATA (ALEATORY UNCERTAINTY VARYING)

For Monsoon Climate, the two major contributors in the infiltration variance are the annual precipitation and the Soil Depth Class 4. The relative ranking of the top two parameters switches between replicates when MAP is substituted for the precipitation parameters. This result is not surprising given the small sample size used in the analysis and is not considered significant. Fixing the aleatory uncertainty helps to identify the importance of the other physical parameters and is discussed next for this climate.

### H3.4 REPLICATE 1 – ALEATORY UNCERTAINTY FIXED

Table H-9. Stepwise Regression (linear and rank) on Average Infiltration for Replicate 1: MC (aleatory uncertainty fixed)

Step	Stepwise Regression (linear)				Stepwise Regression (rank)			
	Variable	tot. R <sup>2</sup>	inc. R <sup>2</sup>	SRC	Variable	tot. R <sup>2</sup>	inc. R <sup>2</sup>	SRRC
1	Sdepth4	0.63	0.63	-0.77	Sdepth4	0.65	0.65	-0.77
2	HC_579	0.89	0.26	-0.47	HC_579	0.86	0.21	-0.41
3	Z_r	0.92	0.03	-0.19	Kc_min	0.89	0.03	-0.20
4	Kc_min	0.94	0.02	-0.17	CKcb2	0.92	0.03	0.18
5	REW	0.95	0.01	-0.11	lnRks_406	0.93	0.02	-0.13
6					REW	0.95	0.01	-0.14
7					Z_r	0.96	0.02	-0.14
8					h_plant	0.97	0.01	-0.13
9					PDur_S	0.98	0.01	0.08
10					Z_e	0.99	0.01	0.07
11					gTmaxwet	0.99	0.00	0.07

Source: Output DTN: SN0701T0502206.044, *Stepwise\_Analysis\_R1\_MC\_FA.xls*.

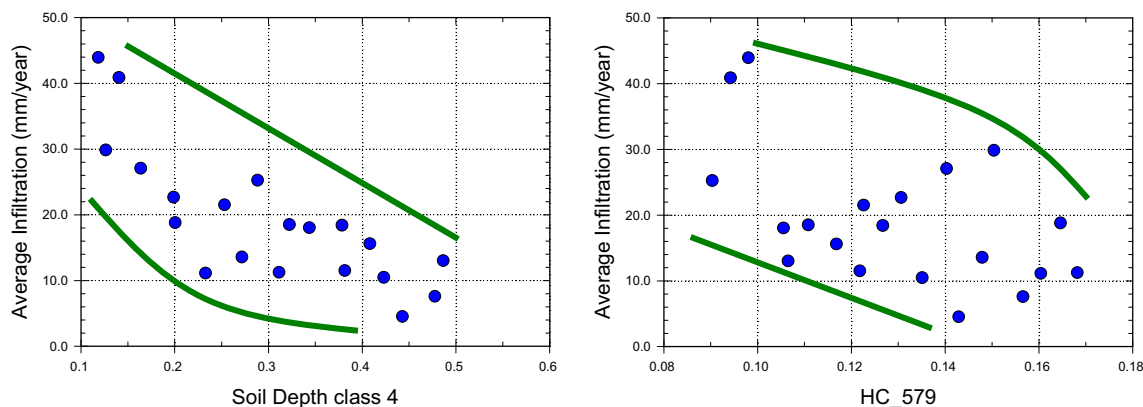
#### H3.4.1 Linear Regression

The linear regression results for Replicate 1, Fixed Aleatory, of the Monsoon climate are shown in Table H-9. Soil Depth Class 4 is the most important parameter, explaining 63% of the infiltration variance, with a strong negative influence (SRC=-0.77). HC\_579 ranks second in importance, with a negative influence, and explaining an additional 26% of the variance in infiltration. The influence of the other parameters displayed in the table is insignificant.

#### H3.4.2 Rank Regression

The rank regression results for Replicate 1, Fixed Aleatory, of the Monsoon climate are also shown in Table H-9. Results using rank transform are similar for the two most important parameters identified in the linear regression. Nine other parameters are displayed in Table H-9, but all of them have a small influence (3% or lower). Some of these parameters (in red) may be identified due to spurious correlations.

### H3.4.3 Scatterplots



Source: Output DTN: SN0701T0502206.044, *scatterplots\_R1\_MC\_FA.JNB*.

Figure H-7. Scatterplots of Average Infiltration Versus Soil Depth Class 4 (left frame), and HC\_579 (right frame) - Replicate 1 - MC (aleatory uncertainty fixed)

Scatterplot analysis (Figure H-7) clearly shows the negative influence of Soil Depth Class 4. A less obvious negative influence of HC\_579 is also illustrated.

### H3.5 REPLICATE 2 – ALEATORY UNCERTAINTY FIXED

Table H-10. Stepwise Regression (linear and rank) on Average Infiltration for Replicate 2: MC (aleatory uncertainty fixed)

Step	Stepwise Regression (linear)				Stepwise Regression (rank)			
	Variable	tot. R <sup>2</sup>	inc. R <sup>2</sup>	SRC	Variable	tot. R <sup>2</sup>	inc. R <sup>2</sup>	SRRC
1	Sdepth4	0.58	0.58	-0.74	Sdepth4	0.57	0.57	-0.70
2	HC_579	0.84	0.26	-0.44	HC_579	0.81	0.23	-0.46
3	Z_r	0.88	0.04	-0.23	Z_r	0.89	0.08	-0.28
4	REW	0.91	0.03	-0.15	REW	0.92	0.03	-0.17
5	CKcb2	0.93	0.02	-0.13	PDur_S	0.94	0.02	0.16
6	PDur_S	0.95	0.02	0.13				
7	InRks_405	0.96	0.01	0.13				
8	Kc_min	0.97	0.01	-0.13				
9	InRks_406	0.98	0.01	0.10				

Source: Output DTN: SN0701T0502206.044, *Stepwise\_Analysis\_R2\_MC\_FA.xls*.

#### H3.5.1 Linear Regression

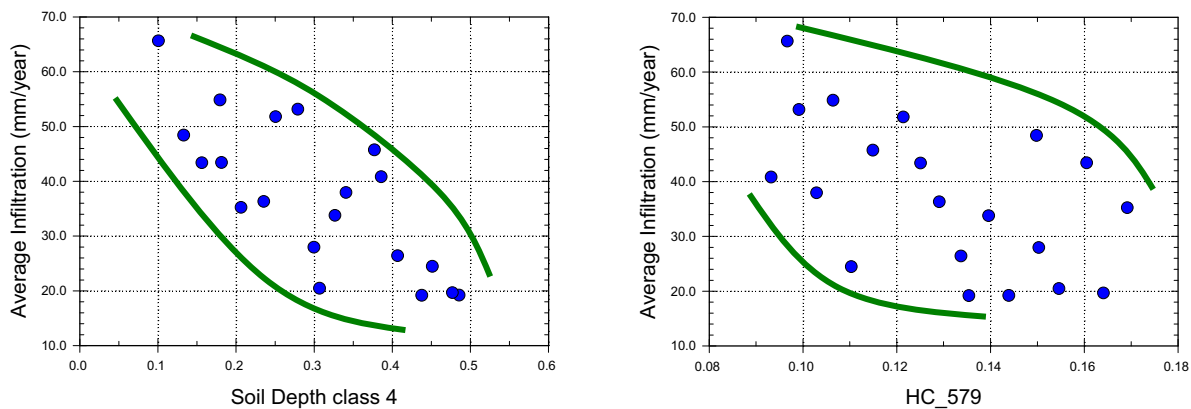
The linear regression results for Replicate 2, Fixed Aleatory, of the Monsoon climate are shown in Table H-10. Soil Depth Class 4 is the most important parameter, explaining 58% of the variance in infiltration, with a strong negative effect (SRC=-0.74). HC\_579 ranks second in importance, explaining 26% of the remaining variance with a negative effect. The other

parameters found in Table H-10 have negligible influence (4% and lower), which indicates that this may be due to spurious correlations.

### H3.5.2 Rank Regression

The rank regression results for Replicate 2, Fixed Aleatory, of the Monsoon climate are also shown in Table H-10. Results from rank regression are similar to the result of linear regression, with Soil Depth Class 4 and HC\_579 identified as the first and second most important parameters. Rooting Depth ( $Z_r$ ) has a small negative influence ( $R^2$  increment of 8%). Other parameters have negligible influence.

### H3.5.3 Scatterplots



Source: Output DTN: SN0701T0502206.044, *scatterplots\_R2\_MC\_FA.JNB*.

Figure H-8. Scatterplots of Average Infiltration Versus Soil Depth Class 4 (left frame), and HC\_579 (right frame) - Replicate 2 - MC (aleatory uncertainty fixed)

Scatterplot analysis (Figure H-8) shows the influence of Soil Depth Class 4 and HC\_579.

## H3.6 CONCLUSIONS

The influence of the physical parameters on net infiltration for the Monsoon climate is similar to that observed for the Present-Day climate simulations, especially when aleatory uncertainty is fixed. This result increases confidence that the uncertainty in Soil Depth Class 4 and HC\_579 are driving the uncertainty in infiltration, when future weather uncertainty is neglected (held constant). When future weather uncertainty is allowed to vary,  $a_{00}$  and  $a_m$ , which controls the MAP, are also important for estimating net infiltration.



## H4. GLACIAL TRANSITION CLIMATE (GTC)

### H4.1 REPLICATE 1 – ALEATORY UNCERTAINTY VARYING

Table H-11. Stepwise Regression (linear and rank) on Average Infiltration for Replicate 1: GTC (aleatory uncertainty varying)

Step	Stepwise Regression (linear)				Stepwise Regression (rank)			
	Variable	tot. R <sup>2</sup>	inc. R <sup>2</sup>	SRC	Variable	tot. R <sup>2</sup>	inc. R <sup>2</sup>	SRRC
1	Sdepth4	0.28	0.28	-0.51	Sdepth4	0.22	0.22	-0.42
2	a <sub>00</sub>	0.53	0.25	-0.52	a <sub>00</sub>	0.42	0.21	-0.46
3	Theta_m	0.67	0.14	0.41	a <sub>m</sub>	0.59	0.17	0.40
4	a <sub>m</sub>	0.80	0.13	0.36	Theta_m	0.71	0.12	0.35
5	CKcb2	0.90	0.10	-0.31	CKcb2	0.81	0.10	-0.31
6	Z_e	0.95	0.05	0.23	lnRks_406	0.86	0.05	0.23
7	lnRks_406	0.96	0.01	0.13				
8	PDurS	0.97	0.01	0.10				

Source: Output DTN: SN0701T0502206.044, *Stepwise\_Analysis\_R1\_GTC\_VA.xls*.

Table H-12. Stepwise Regression (linear and rank) on Average Infiltration for Replicate 1, Where All Precipitation Parameters Have Been Replaced by Average Annual Precipitation: GTC (aleatory uncertainty varying)

Step	Stepwise Regression (linear)				Stepwise Regression (rank)			
	Variable	tot. R <sup>2</sup>	inc. R <sup>2</sup>	SRC	Variable	tot. R <sup>2</sup>	inc. R <sup>2</sup>	SRRC
1	PPT_R1	0.43	0.43	0.67	PPT_R1	0.38	0.38	0.65
2	Sdepth4	0.73	0.30	-0.53	Sdepth4	0.65	0.27	-0.48
3	CKcb2	0.79	0.06	-0.26	CKcb2	0.73	0.08	-0.29
4	Z_e	0.83	0.03	0.18				

Source: Output DTN: SN0701T0502206.044, *Stepwise\_Analysis\_R1\_Precipitation\_GTC\_VA.xls*.

#### H4.1.1 Linear Regression

The linear regression results for Replicate 1 of the Glacial Transition climate are shown in Table H-11. Soil Depth Class 4 is the most important parameter, explaining 28% of the variance with, as expected, a strong negative effect (SRC=-0.51) (see Table H-11). Next in importance are the three precipitation parameters.  $a_{00}$  ranks second in importance, explaining 25% of the variance in infiltration. It has a strong negative effect (SRC = -0.52). Higher values of  $a_{00}$  result in a lower frequency of precipitation, and consequently, it reduces average infiltration.  $\theta_m$  and  $a_m$ , explain 14% and 13% of the variance of infiltration, respectively. CKcb2 has a small negative influence, explaining an additional 10% of the variance. Other parameters have negligible influence.

MAP for the Glacial Transition Climate is a function of the three independently sampled precipitation parameters ( $a_m$ ,  $a_{00}$ , and  $\theta_m$ ). A second stepwise regression analysis was performed to test the importance of MAP (PPT\_R1 in Table H-12). In this analysis, MAP becomes the most important parameter, explaining 43% of the infiltration variance. Soil Depth Class 4 and CKcb2 rank second and third in importance, explaining 30% and 6% of the variance,

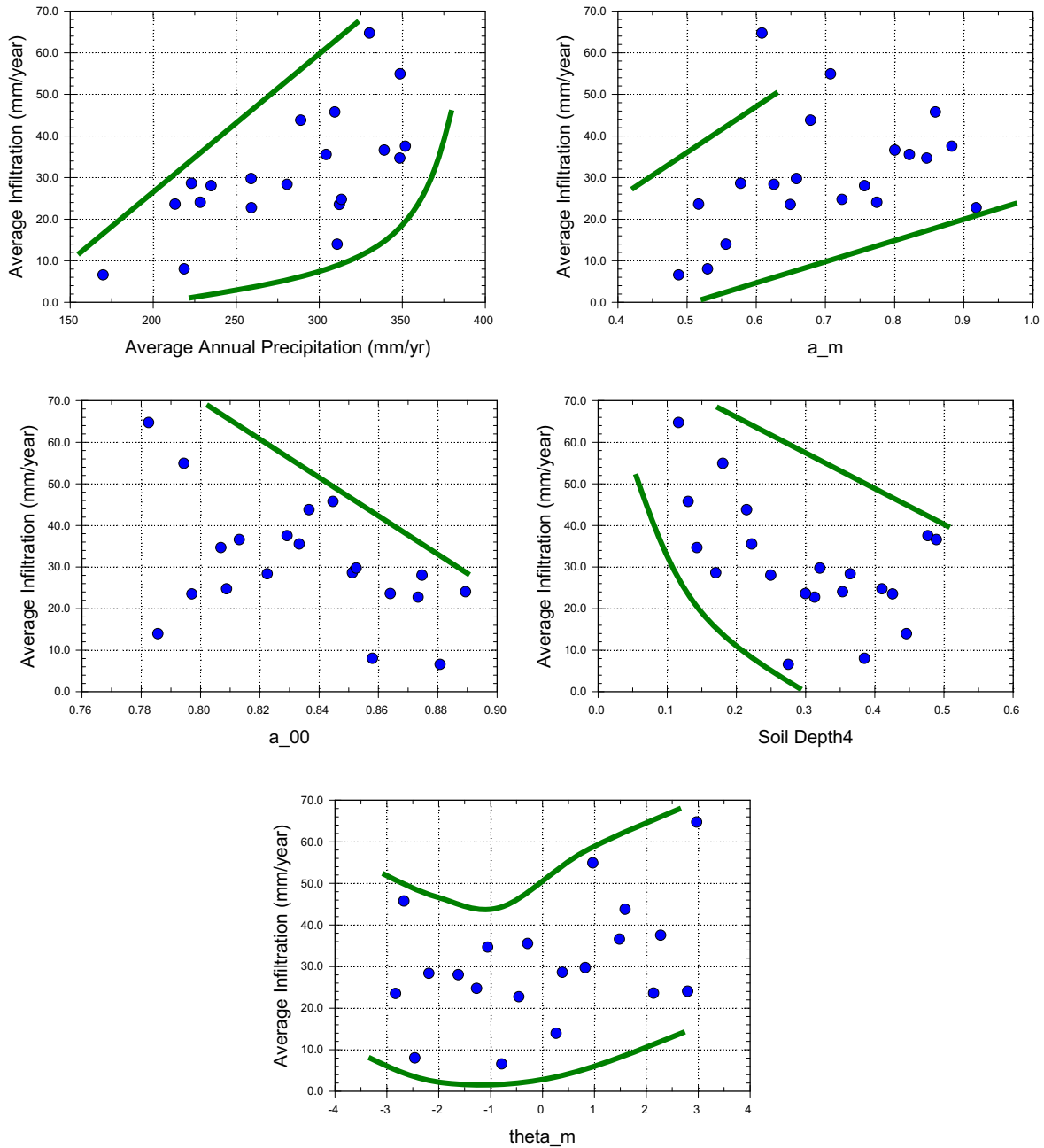
respectively. The last parameter listed,  $Z_e$  (evaporation depth) explains only 3% of the variance and has more than 5% chance of being due to spurious correlation.

#### **H4.1.2 Rank Regression**

The rank regression results for Replicate 1 of the Glacial Transition climate are also shown in Table H-11. Results of the rank regression are similar to results of the linear regression, with Soil Depth Class 4 explaining 22% of the variance. The next three parameters are all precipitation parameters, explaining together 50% of the remaining variance. CKcb2 ranks next in importance, explaining 10% of the variance in infiltration. lnRks\_406 accounts for 5% of the variance.

When precipitation parameters are replaced with MAP (PPT\_R1 in Table H-12), average annual precipitation becomes the most important parameter, explaining 38% of the variance. Soil Depth Class 4 and CKcb2 are ranked next in importance, explaining 27% and 8% of the variance of infiltration, respectively.

### H4.1.3 Scatterplots



Source: Output DTN: SN0701T0502206.044, scatterplots\_R1\_GTC\_VA.JNB.

Figure H-9. Scatterplots of Average Infiltration versus MAP (upper left frame),  $a_m$  (upper right frame),  $a_{00}$  (middle left frame), Soil Depth Class 4 (middle right frame) and  $\theta_m$  (lower frame) - Replicate 1 - GTC (aleatory uncertainty varying)

Scatterplot analysis (Figure H-9) shows the influence of Soil Depth Class 4,  $a_{00}$ ,  $a_m$  and, MAP. The importance of Theta\_m ( $\theta_m$ ) is not clear in the figure.

## H4.2 REPLICATE 2 – ALEATORY UNCERTAINTY VARYING

Table H-13. Stepwise Regression (linear and rank) on Average Infiltration for Replicate 2, Where All Precipitation Parameters Have Been Replaced by Average Annual Precipitation (MAP): GTC (aleatory uncertainty varying)

Step	Stepwise Regression (linear)				Stepwise Regression (rank)			
	Variable	tot. R <sup>2</sup>	inc. R <sup>2</sup>	SRC	Variable	tot. R <sup>2</sup>	inc. R <sup>2</sup>	SRRC
1	Sdepth4	0.43	0.43	-0.68	Sdepth4	0.41	0.41	-0.63
2	a <sub>00</sub>	0.57	0.14	-0.37	a <sub>m</sub>	0.61	0.20	0.51
3	a <sub>m</sub>	0.70	0.13	0.41	a <sub>00</sub>	0.75	0.13	-0.33
4	HC_579	0.79	0.09	-0.33	Kc_min	0.79	0.04	-0.21
5	Z_e	0.86	0.07	-0.24	CKcb2	0.83	0.04	-0.19
6	Kc_min	0.90	0.04	-0.16	PDurS	0.86	0.04	0.19
7	CKcb2	0.92	0.02	-0.16	HC_579	0.89	0.03	-0.17
8	PDurS	0.95	0.03	0.16				
9	Theta_m	0.96	0.01	0.12				

Source: Output DTN: SN0701T0502206.044, *Stepwise\_Analysis\_R2\_GTC\_VA.xls*.

Table H-14. Stepwise Regression (linear and rank) on Average Infiltration for Replicate 2, Where All Precipitation Parameters Have Been Replaced by Average Annual Precipitation: GTC (aleatory uncertainty varying)

Step	Stepwise Regression (linear)				Stepwise Regression (rank)			
	Variable	tot. R <sup>2</sup>	inc. R <sup>2</sup>	SRC	Variable	tot. R <sup>2</sup>	inc. R <sup>2</sup>	SRRC
1	Sdepth4	0.43	0.43	-0.68	Sdepth4	0.41	0.41	-0.64
2	PPT_R2	0.70	0.27	0.54	PPT_R2	0.73	0.32	0.58
3	HC_579	0.81	0.12	-0.37	HC_579	0.78	0.05	-0.22
4	Z_e	0.88	0.07	-0.25	CKcb2	0.82	0.04	-0.19
5	CKcb2	0.91	0.03	-0.17				
6	PDurS	0.93	0.02	0.13				
7	Kc_min	0.95	0.01	-0.12				

Source: Output DTN: SN0701T0502206.044, *Stepwise\_Analysis\_R2\_Precipitation\_GTC\_VA.xls*.

### H4.2.1 Linear Regression

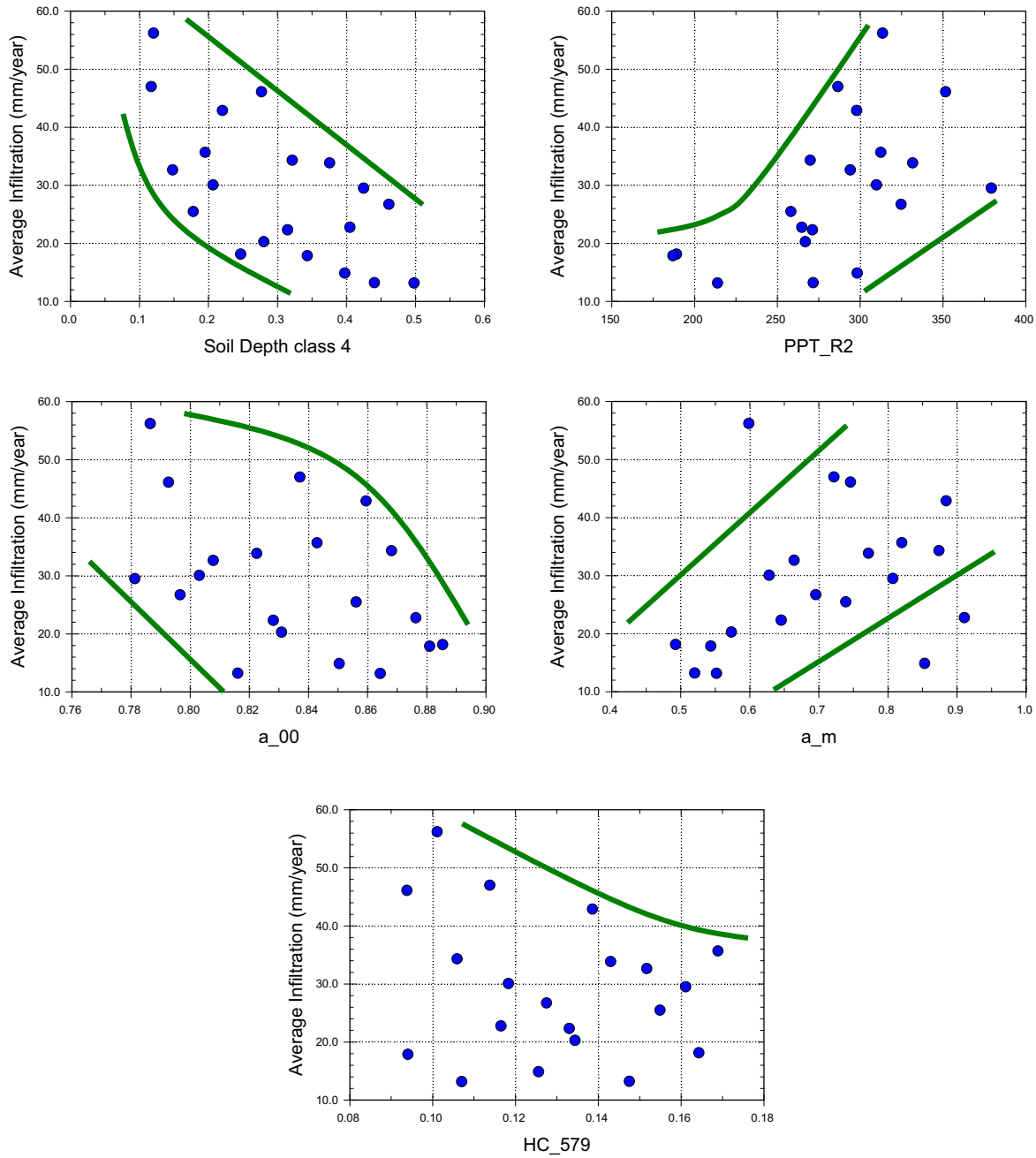
The linear regression results for Replicate 2 of the Glacial Transition climate are shown in Table H-13. Soil Depth Class 4 is the most important parameter, explaining 43% of the variance. The parameters ranked second and third in importance are,  $a_{00}$  and  $a_m$ , explaining 14% and 13% of the variance, respectively. HC\_579 is ranked next, explaining 9% of the variance, followed by Z\_e, with 7% of the variance explained. The other parameters listed in Table H-13 have negligible influence.

If MAP (PPT\_R2 in Table H-14) is used in place of the precipitation parameters, Soil Depth Class 4 is the most important parameter, with 43% of the variance of infiltration explained. It is followed in importance by MAP (incremental R<sup>2</sup> of 27%) and HC\_579 (incremental R<sup>2</sup> of 12%). Z\_e has a small negative influence and explains 7% of the variance. The other parameters have negligible influence.

#### **H4.2.2 Rank Regression**

The rank regression results for Replicate 2 of the Glacial Transition climate are also shown in Table H-13. Results of rank regression are similar to results of the linear regression. Soil Depth Class 4 and the precipitation parameters are the most important. No other parameters are found to be influential.

### H4.2.3 Scatterplots



Source: Output DTN: SN0701T0502206.044, *scatterplots\_R2\_GTC\_VA.JNB*.

Figure H-10. Scatterplots of Average Infiltration Versus Soil Depth Class 4 (upper left frame), MAP (upper right frame),  $a_{00}$  (middle left frame),  $a_m$  (middle right frame), and HC\_579 (lower frame) - Replicate 2 - GTC (aleatory uncertainty varying)

Scatterplot analysis (Figure H-10) shows the influence of Soil Depth Class 4 and average annual precipitation. The influence of  $a_{00}$  and  $a_m$  is also evident. The influence of HC\_579 is not that evident.

### H4.3 CONCLUSION OF STUDY OF ORIGINAL DATA (ALEATORY UNCERTAINTY VARYING)

Sensitivity analyses done for Replicates 1 and 2 of the Glacial Transition climate result are generally consistent between replicates, in that the same top two parameters are identified for both replicates. Theta\_m ranks third in importance for the linear regression results for Replicate 1, explaining 14% of the incremental variance. This may be a random result or it may reflect a genuine sensitivity. However, even with this question unresolved, it is clear that Soil Depth Class 4 and precipitation are the most important parameters for this climate.

The relative ranking of the top two parameters switches between replicates when MAP is substituted for the precipitation parameters. This result is not surprising given the small sample size used in the analysis and is not considered significant. Fixing the aleatory uncertainty helps to identify the importance of the other physical parameters and is discussed next for this climate.

### H4.4 REPLICATE 1 – ALEATORY UNCERTAINTY FIXED

Table H-15. Stepwise Regression (linear and rank) on Average Infiltration for Replicate 1: GTC (aleatory uncertainty fixed)

Step	Stepwise Regression (linear)				Stepwise Regression (rank)			
	Variable	tot. R <sup>2</sup>	inc. R <sup>2</sup>	SRC	Variable	tot. R <sup>2</sup>	inc. R <sup>2</sup>	SRRC
1	Sdepth4	0.77	0.77	-0.87	Sdepth4	0.81	0.81	-0.88
2	HC_579	0.93	0.16	-0.41	HC_579	0.93	0.11	-0.36
3	CKcb2	0.95	0.02	-0.18	InRks_406	0.94	0.01	0.11
4	Kc_min	0.97	0.01	-0.11	Z_e	0.95	0.01	-0.09
5	REW	0.98	0.01	-0.10	CKcb2	0.95	0.01	-0.09
6	Z_r	0.98	0.01	-0.08				

Source: Output DTN: SN0701T0502206.044, Stepwise\_Analysis\_R1\_GTC\_FA.xls.

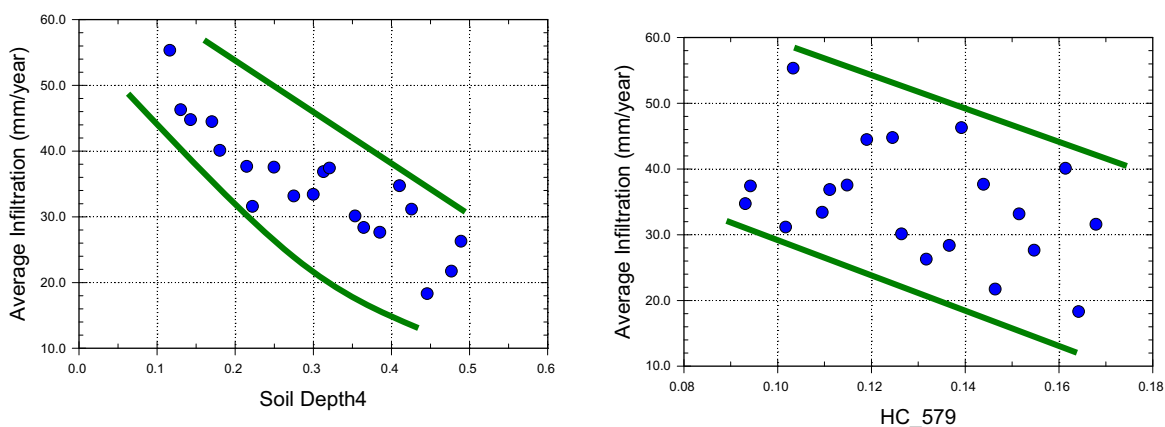
#### H4.4.1 Linear Regression

The linear regression results for Replicate 1, Fixed Aleatory, of the Glacial Transition climate are shown in Table H-15. The most important parameter is Soil Depth Class 4. It has a strong negative effect and explains 77% of the variance of mean infiltration. The next most important parameter is HC\_579 with a negative influence on infiltration, explaining 16% of the variance. All other parameters explain 2% or less of the variance of infiltration and may be due to spurious correlation.

#### H4.4.2 Rank Regression

The rank regression results for Replicate 1, Fixed Aleatory, of the Glacial Transition climate are also shown in Table H-15. Rank regression results are similar to the results of the linear regression. The top two parameters are Soil Depth Class 4 and HC\_579, explaining 81% and 11% of the variance, respectively.

#### H4.4.3 Scatterplots



Source: Output DTN: SN0701T0502206.044, *scatterplots\_R1\_GTC\_FA.JNB*.

Figure H-11. Scatterplots of Average Infiltration Versus Soil Depth Class 4 (left frame), and HC\_579 (right frame) - Replicate 1 - GTC (aleatory uncertainty fixed)

Scatterplot analysis (Figure H-11) indicates a strong relationship between Soil Depth Class 4 and average infiltration. The influence of HC\_579 is not as strong but is discernable.

#### H4.5 REPLICATE 2 – ALEATORY UNCERTAINTY FIXED

Table H-16. Stepwise Regression (linear and rank) on Average Infiltration for Replicate 2: GTC (aleatory uncertainty fixed)

Step	Stepwise Regression (linear)				Stepwise Regression (rank)			
	Variable	tot. R <sup>2</sup>	inc. R <sup>2</sup>	SRC	Variable	tot. R <sup>2</sup>	inc. R <sup>2</sup>	SRRC
1	Sdepth4	0.69	0.69	-0.89	Sdepth4	0.75	0.75	-0.90
2	HC_579	0.89	0.20	-0.46	HC_579	0.87	0.12	-0.32
3	CKcb2	0.95	0.06	-0.25	CKcb2	0.90	0.02	-0.18
4	Z_e	0.97	0.01	-0.10	Kc_min	0.93	0.03	-0.18
5	Kc_min	0.97	0.01	-0.08				
6	Z_r	0.98	0.01	-0.07				

Source: Output DTN: SN0701T0502206.044, *Stepwise\_Analysis\_R2\_GTC\_FA.xls*.



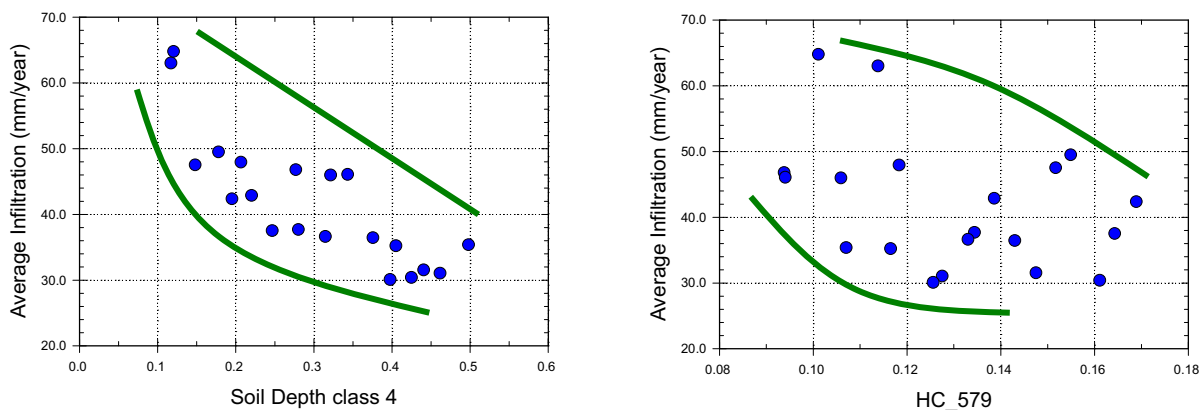
### H4.5.1 Linear Regression

The linear regression results for Replicate 2, Fixed Aleatory, of the Glacial Transition climate are shown in Table H-16. Soil Depth Class 4 is the most important parameter, explaining 69% of the variance in net infiltration. HC\_579 explains 20% of the variance. CKcb2 seems to have a small effect on infiltration, explaining 6% of the variance. The influence of the other parameters is negligible.

### H4.5.2 Rank Regression

The rank regression results for Replicate 2, Fixed Aleatory, of the Glacial Transition climate are also shown in Table H-16. Results of the rank regression are very similar to the results of the linear regression, with Soil Depth Class 4 and HC\_579 explaining 75% and 12% of the variance, respectively. CKcb2 and Kc\_min rank third and fourth in importance but with very little influence.

### H4.5.3 Scatterplots



Source: Output DTN: SN0701T0502206.044, *scatterplots\_R2\_GTC\_FA.JNB*.

Figure H-12. Scatterplots of Average Infiltration Versus Soil Depth Class 4 (left frame) and HC\_579 (right frame) - Replicate 2 - GTC (aleatory uncertainty fixed)

Scatterplot analysis (Figure H-12) shows the influence of Soil Depth Class 4. The influence of HC\_579 is not as pronounced but is discernable.

## H4.6 CONCLUSIONS

The fixed aleatory analysis arrives at similar results to those obtained for the Present-Day and Monsoon climates. Soil Depth Class 4 and HC\_579 together explain approximately 90% of the variance in net infiltration. When aleatory uncertainty is allowed to vary, and precipitation parameters (i.e.  $a_{00}$ ,  $a_m$ ,  $\theta_m$ ... etc.) are allowed to vary individually, the precipitation parameters are second in importance only to Soil Depth Class 4. If precipitation parameters are replaced by the MAP, the analysis suggests precipitation is as important as soil depth.

INTENTIONALLY LEFT BLANK

**APPENDIX I**  
**TREATMENT OF UNCERTAINTIES**



This appendix addresses various details related to uncertainty analysis. Section I1 addresses the screening of parameters in order to select those included in the detailed analysis of parameter uncertainty. Section I2 presents background information on uncertainty, including definitions, commonly used uncertainty distributions, and key properties of those distributions.

## **I1. SCREENING OF PARAMETERS FOR UNCERTAINTY ANALYSIS**

The first step in the uncertainty analysis was the elimination of parameters that do not have a large contribution to uncertainty in net infiltration. This step considered two properties associated with each parameter, its relative uncertainty and its influence on the average net infiltration.

In several places, the MASSIF model uses a formula that is an approximation for a function. Section I1.1, Parameters Included in Model Uncertainty, evaluates how the uncertainty in such approximations contributes to the uncertainty in calculated net infiltration. The concern in each case is the uncertainty of the approximate formula as a whole, not the uncertainty in the coefficients of the formula. Therefore, the sensitivity studies did not vary any coefficients of function approximations. The section identifies the coefficients that were not considered individually in the sensitivity studies but rather were included in model uncertainty.

Of the remaining parameters, some have different values for different climates. Others may have the same nominal values but different uncertainties. Parameters in either of these categories require a separate treatment for each climate.

First, however, Section I1.2 provides screening results for those parameters for which neither the nominal value nor its uncertainty varies appreciably for the three climates of interest. Sections I1.3, I1.4, and I1.5 summarize the screening for parameters specific to the Present-Day, Monsoon, and Glacial Transition climate, respectively.

Nominal values and limits have been rounded to be consistent with the standard uncertainty. The standard uncertainty is the uncertainty expressed as a standard deviation (ANSI/NCSL Z540-2-1997 [DIRS 157394], p. 3). Standard uncertainty has been rounded to one significant digit, except that a second significant digit may be included if the first digit is 1. Section I2.2 contains formulas for calculating standard uncertainty for various distributions.

A parameter is excluded from the sensitivity studies without further explanation if its standard uncertainty is less than 15% of a relevant value (relative uncertainty), often its nominal value, or if it is expected to have less than 15% influence on average net infiltration. A value of 15% was chosen arbitrarily for the sole reason that it resulted in a manageable number of parameters that were screened into the uncertainty analysis. Because of the time required to run the MASSIF calculation and the computer resources available, it was decided that approximately 40 realizations per climate could be accommodated. As described in Section 6.5.5, Latin Hypercube Sampling (LHS) was used to create a Monte Carlo analysis with which uncertainty in net infiltration could be estimated for each climate. LHS sampling works best when the number of realizations is less than 4/3 the number of sampled parameters. Therefore, a 15% cutoff, which resulted in between 11 and 15 sampled parameters, was chosen. Because there is no a priori basis upon which to choose a particular percent cutoff, it was deemed necessary to validate

the choice of the 15% value in a separate sensitivity study. This study, described in Section 7, applied a lower relative uncertainty cutoff which resulted in many more parameters being sampled by LHS. Two hundred realizations were generated and the MASSIF model was run on a single watershed (Drill Hole Wash), which covers the repository footprint. A global sensitivity study was performed on the results of this calculation and the parameters for which net infiltration is most sensitive were identified. The results of this study supported the use of the 15% cutoff for the uncertainty analysis for each climate, because the same parameters were identified as being most important in the larger LHS study as in uncertainty analyses using the 15% cutoff (see Section 7 for a detailed description of this validation study).

## **II.1 PARAMETERS INCLUDED IN MODEL UNCERTAINTY**

The formulas in this section contain over 50 coefficients. Each formula is a model approximation, the effects of which are considered as part of model uncertainty. Therefore, the parameter uncertainty analysis does not vary any of the coefficients in the following formulas or tables (see Section 6.4 and Appendix C):

- Formula for inverse relative distance Earth-Sun (Eq. C-3)
- Formula for solar declination (Eq. C-4)
- Formula for sine of mean solar elevation (Eq. C-7)
- Formula for total evaporable water (Eq. 6.4.4.2-2)
- Formula for atmospheric pressure (Eq. C-8)
- Formula for psychrometric constant (Eq. C-33b)
- Formula for saturation vapor pressure (Eq. C-2)
- Formula for precipitable water (Eq. C-9)
- Formula for 24-hour transmissivity for beam radiation (Eq. C-10)
- Table of slope-aspect corrections for direct beam radiation (Section C2)
- Formula for 24-hour transmissivity for diffuse radiation (Eq. C-11)
- Formula for diffuse radiation transmissivity for horizontal surface (Eq. C-15)
- Formula for diffuse radiation on inclined surface (Eq. C-23)
- Formula for net long wave radiation (Eq. C-35)
- Formula for reference evapotranspiration (Penman-Monteith equation) (Eqs. C-37 and 6.4.5-1)

- Formula for adjusting depletion factor for the evaporative power of the atmosphere (Eq. 6.4.4.2-6)
- Formula for vegetative cover fraction (canopy coefficient) (Eq. 6.4.4.1-3)
- Formula for upper limit on evaporation and transpiration (Eq. 6.4.4.1-1)
- Table of normalized differences between red and near-infrared bands as a function of DOY, slope, and azimuth, as measured at the Yucca Mountain site during reference year,  $NDVI_{table}$
- Formula for fraction of transpiration that takes place in each node of the surface layer (Eqs. 6.4.4.2-8 and 6.4.4.2-9).

The following parameters are represented on a cell-by-cell basis within the MASSIF model. Being represented on a cell-by-cell basis means that each cell is assigned a unique value. Considering there are 139,092 cells in the infiltration modeling domain (Section 6.5.2.1), random uncertainty in these parameters will be small due to the large sample size used to obtain averages. Any systematic effects from the following parameters are contributors to model uncertainty, not parameter uncertainty.

- Precipitation during reference year for NDVI table,  $PrecipRefNDVI$
- Potential Vegetative Response,  $PVR$
- Slope,  $slope$
- Azimuth,  $azimuth$
- Elevation,  $elev$
- Latitude,  $lat$
- Longitude,  $long$ .

## II.2 SCREENING OF CLIMATE-INDEPENDENT PARAMETERS

This section lists the climate-independent parameters that are not coefficients of model approximations. For each such parameter that is excluded from the detailed uncertainty analysis, the current section provides information on its nominal value and either its uncertainty or its influence.

This section provides screening information for over 90 climate-independent parameters. Of these, the following eight meet the requirement for inclusion in the detailed uncertainty analysis:

- Soil depth of Depth Soil Class 4
- Saturated hydraulic conductivities of bedrock units 405 and 406 ( $K_{sat\_rock}$ )
- Soil water holding capacity for soil group 5/7/9 ( $\theta_{HC}$ )
- Readily evaporable water ( $REW$ ) and the evaporation layer depth ( $Z_e$ )
- The minimum  $K_c$  for dry soil with no crop cover ( $K_{cmin}$ )
- The slope of the relationship between NDVI' and  $K_{cb}$  ( $CK_{cb2}$ ).

These parameters are compiled in tables of included parameters for each climate and can be found in Sections I1.3, I1.4, and I1.5.

Table I-1 lists the remaining climate-independent parameters, those that are excluded from the detailed analysis of parameter uncertainty. The holding capacity is not an input to the model; it is a surrogate for the field capacity, which is the sum of the wilting point and the holding capacity.



Table I-1. Climate Independent Parameters Excluded from the Uncertainty Analysis

Parameter Description	Parameter Symbol	Nominal Value	Low Range	High Range	Stand. Uncert.	Units	Relative Uncert.	Dist.	Reference	Reason for Exclusion
Terrain albedo	$\alpha_T$	0.22	0.15	0.35	0.06	none	27%	Uniform	Table 6.5.4.1-4	Low influence; $\alpha_T$ has only a small impact on the solar radiation estimate and $E_{T_0}$ (Section C1.3)
Intercept of linear fit of NDVI' and $K_{cb}$	$C_{Kcb1}$	-0.05	NA	NA	0.05	none	100%	Normal	Section 6.5.3.7	Low influence; at small values of NDVI', $K_{c,min}$ overrides $C_{Kcb1}$ ; at large values of NDVI', uncertainty in $C_{Kcb2}$ dominates (see Section 6.5.3.7.2)
Dew point offset from $T_{min}$ , winter months	$K_{O,winter}$	2	0	10	3	°C	140%	Uniform	Table 6.5.4.1-2	Low influence (extremes of uncertainty range cause less than 15% variation in standard evapotranspiration, $E_{T_0}$ ; Section 6.5.4.1)
Dew point offset from $T_{min}$ , rest of year	$K_{O,rest}$	4.5	0	10	3	°C	60%	Uniform	Table 6.5.4.1-2	Low influence (extremes of uncertainty range cause less than 15% variation in standard evapotranspiration, $E_{T_0}$ ; Section 6.5.4.1)
Precipitation lapse rate	$C_{Precipior}$	6.3	NA	NA	0.7	%/100m	11%	Normal	Table F2.1-3	Low uncertainty
Maximum daily precipitation		983	NA	NA	NA	mm	NA	NA	Section 6.5.1 and Maidment 1993 [DIRS 125317], p. 3.36, Table 3.10.2	Low influence; this parameter was introduced to ensure that unrealistically high daily precipitation was not included in the analysis
Temperature lapse rate (dry adiabatic lapse rate)	LR	0.010	0.0095	0.0105	0.0003	°C/m	3%	Uniform	Maidment 1993 [DIRS 125317], p. 3.3	Low uncertainty
Fraction of snowfall that eventually sublimates	$C_{sublime}$	0.1	0	0.2	0.06	none	6%	Uniform	Table 6.5.1.7-1	Low uncertainty; uncertainty relative to total snowfall (1.0)

Table I-1. Climate Independent Parameters Excluded from the Uncertainty Analysis (Continued)

Parameter Description	Parameter Symbol	Nominal Value	Low Range	High Range	Stand. Uncert.	Units	Relative Uncert.	Dist.	Reference	Reason for Exclusion
Rate of increase of snowmelt with temperature	$C_{\text{snowmelt}}$	2	1	3	0.6	mm/day/ °C	30%	Uniform	Table 6.5.1.7-1	Low influence; difference in snowmelt rate affects days in which snowmelt is added to rainfall, does not affect total snowmelt
Adjustment coefficient in Hargreaves' radiation formula	$K_{Rs}$	0.19	0.15	0.22	0.02	°C <sup>-0.5</sup>	11%	Uniform	Table 6.5.4.1-3	Low uncertainty
Average fraction of TAW that can be depleted from the root zone before reduction in ET	$p$	0.65	0.50	0.80	0.09	none	14%	Uniform	Table 6.5.4.2-3	Low uncertainty
Solar constant	$G_{sc}$	0.0820	0.0819	0.0821	0.0002	MJ/m <sup>2</sup> /min	0.1%	Uniform	Table 6.5.4.1-5	Low uncertainty
Turbidity coefficient	$K_{\text{turb}}$	1.0	0.80	1.1	0.09	none	9%	Uniform	Table 6.5.4.1-6	Low uncertainty
Saturated hydraulic conductivity (cm/s)	$K_{\text{sat\_soil}}(1)$	$8.0 \times 10^{-5}$	NR	NR	NR	cm/s	NR	NR	Table 6.5.2.3-1	Low influence; soil group less than 15% of UZ grid (Table 6.5.2.2-2)
	$K_{\text{sat\_soil}}(2/6)$	$1.1 \times 10^{-4}$	NR	NR	NR	cm/s	NR	NR		
	$K_{\text{sat\_soi}}(3/4)$	$7.0 \times 10^{-5}$	NR	NR	NR	cm/s	NR	NR		
	$K_{\text{sat\_soil}}(5/7/9)$	$6.8 \times 10^{-5}$	NA	NA	8%	cm/s	8%	Lognormal		
Saturated water content	$\theta_s(1)$	0.23	NR	NR	NR	m <sup>3</sup> /m <sup>3</sup>	NR	NR	Table 6.5.2.3-1	Low influence; soil group less than 15% of UZ grid (Table 6.5.2.2-2)
	$\theta_s(2/6)$	0.21	NR	NR	NR	m <sup>3</sup> /m <sup>3</sup>	NR	NR		
	$\theta_s(3/4)$	0.16	NR	NR	NR	m <sup>3</sup> /m <sup>3</sup>	NR	NR		
	$\theta_s(5/7/9)$	0.23	NA	NA	0.01	m <sup>3</sup> /m <sup>3</sup>	4%	Normal		
Soil wilting point	$\theta_{\text{wip}}(1)$	0.040	NR	NR	NR	m <sup>3</sup> /m <sup>3</sup>	NR	NR	Table 6.5.2.3-1	Low influence; soil group less than 15% of UZ grid (Table 6.5.2.2-2)
	$\theta_{\text{wip}}(2/6)$	0.037	NR	NR	NR	m <sup>3</sup> /m <sup>3</sup>	NR	NR		
	$\theta_{\text{wip}}(3/4)$	0.024	NR	NR	NR	m <sup>3</sup> /m <sup>3</sup>	NR	NR		
	$\theta_{\text{wip}}(5/7/9)$	0.039	NA	NA	0.002	m <sup>3</sup> /m <sup>3</sup>	5%	Normal		

Table I-1. Climate Independent Parameters Excluded from the Uncertainty Analysis (Continued)

Parameter Description	Parameter Symbol	Nominal Value	Low Range	High Range	Stand. Uncert.	Units	Relative Uncert.	Dist.	Reference	Reason for Exclusion
Soil water holding capacity	$\theta_{HC}(1)$	0.115	NR	NR	NR	m <sup>2</sup> /m <sup>3</sup>	NR	NR	Table 6.5.2.3-2	Low influence; soil group less than 15% of UZ grid (Table 6.5.2.2-2)
	$\theta_{HC}(2/6)$	0.114	NR	NR	NR	m <sup>3</sup> /m <sup>3</sup>	NR	NR		
	$\theta_{HC}(3/4)$	0.076	NR	NR	NR	m <sup>3</sup> /m <sup>3</sup>	NR	NR		
Depth of soil	$depth_{soil}(1)$	95	NR	NR	NR	m	NR	NR	Table 6.5.2.4-2	Low influence; soil depth class less than 15% of UZ grid (Table 6.5.2.4-1)
	$depth_{soil}(2)$	16.5	NA	NA	1.8	m	11%	Normal	Table 6.5.2.4-2	Low uncertainty
Bulk saturated hydraulic conductivity of bedrock	$depth_{soil}(3)$	3.3	NR	NR	NR	m	NR	NR	Table 6.5.2.4-2	Low influence; soil depth class less than 15% of UZ grid (Table 6.5.2.4-1)
	$depth_{soil}(5)$	0	NR	NR	NR	m	NR	NR		
	$K_{sat\_rock}(401)$	$1.80 \times 10^{-6}$	NR	NR	NR	m/s	NR	NR	Table 6.5.2.6-1	Low influence; IHU less than 15% of the UZ grid (Table 6.5.2.5-1)
	$K_{sat\_rock}(402)$	$1.20 \times 10^{-6}$	NR	NR	NR	m/s	NR	NR	Table 6.5.2.6-1	
	$K_{sat\_rock}(403)$	$1.80 \times 10^{-6}$	NR	NR	NR	m/s	NR	NR	Table 6.5.2.6-1	
	$K_{sat\_rock}(404)$	$7.70 \times 10^{-7}$	NR	NR	NR	m/s	NR	NR	Table 6.5.2.6-1	
	$K_{sat\_rock}(407)$	$1.10 \times 10^{-6}$	NR	NR	NR	m/s	NR	NR	Table 6.5.2.6-1	
	$K_{sat\_rock}(408)$	$1.70 \times 10^{-6}$	NR	NR	NR	m/s	NR	NR	Table 6.5.2.6-1	
	$K_{sat\_rock}(409)$	$9.20 \times 10^{-7}$	NR	NR	NR	m/s	NR	NR	Table 6.5.2.6-1	
	$K_{sat\_rock}(410)$	$2.70 \times 10^{-6}$	NR	NR	NR	m/s	NR	NR	Table 6.5.2.6-1	
	$K_{sat\_rock}(411)$	$1.40 \times 10^{-5}$	NR	NR	NR	m/s	NR	NR	Table 6.5.2.6-1	
	$K_{sat\_rock}(412)$	$4.90 \times 10^{-6}$	NR	NR	NR	m/s	NR	NR	Table 6.5.2.6-1	Low influence; IHU less than 15% of repository footprint (Table 6.5.2.5-1)
	$sat\_rock(413)$	$3.90 \times 10^{-6}$	NR	NR	NR	m/s	NR	NR	Table 6.5.2.6-1	
	$sat\_rock(414)$	$3.10 \times 10^{-6}$	NR	NR	NR	m/s	NR	NR	Table 6.5.2.6-1	
	$sat\_rock(415)$	$9.40 \times 10^{-6}$	NR	NR	NR	m/s	NR	NR	Table 6.5.2.6-1	

Table I-1. Climate Independent Parameters Excluded from the Uncertainty Analysis (Continued)

Parameter Description	Parameter Symbol	Nominal Value	Low Range	High Range	Stand. Uncert.	Units	Relative Uncert.	Dist.	Reference	Reason for Exclusion
<i>Bulk saturated hydraulic conductivity of bedrock (continued)</i>	<i>K<sub>sat rock</sub></i> (416)	1.70 × 10 <sup>-5</sup>	NR	NR	NR	m/s	NR	NR	Table 6.5.2.6-1	Low influence; IHU less than 15% of repository footprint (Table 6.5.2.5-1) (continued)  Low influence; IHU less than 15% of the UZ grid (Table 6.5.2.5-1)
	<i>K<sub>sat rock</sub></i> (417)	3.30 × 10 <sup>-5</sup>	NR	NR	NR	m/s	NR	NR	Table 6.5.2.6-1	
	<i>K<sub>sat rock</sub></i> (418)	1.50 × 10 <sup>-6</sup>	NR	NR	NR	m/s	NR	NR	Table 6.5.2.6-1	
	<i>K<sub>sat rock</sub></i> (419)	1.20 × 10 <sup>-6</sup>	NR	NR	NR	m/s	NR	NR	Table 6.5.2.6-1	
	<i>K<sub>sat rock</sub></i> (420)	9.00 × 10 <sup>-7</sup>	NR	NR	NR	m/s	NR	NR	Table 6.5.2.6-1	
	<i>K<sub>sat rock</sub></i> (421)	1.30 × 10 <sup>-6</sup>	NR	NR	NR	m/s	NR	NR	Table 6.5.2.5-1	
	<i>K<sub>sat rock</sub></i> (422)	1.20 × 10 <sup>-6</sup>	NR	NR	NR	m/s	NR	NR	Table 6.5.2.6-1	
	<i>K<sub>sat rock</sub></i> (423)	1.70 × 10 <sup>-6</sup>	NR	NR	NR	m/s	NR	NR	Table 6.5.2.6-1	
	<i>K<sub>sat rock</sub></i> (424)	8.50 × 10 <sup>-7</sup>	NR	NR	NR	m/s	NR	NR	Table 6.5.2.6-1	
	<i>K<sub>sat rock</sub></i> (425)	8.00 × 10 <sup>-6</sup>	NR	NR	NR	m/s	NR	NR	Table 6.5.2.6-1	
	<i>K<sub>sat rock</sub></i> (426)	9.40 × 10 <sup>-7</sup>	NR	NR	NR	m/s	NR	NR	Table 6.5.2.6-1	
	<i>K<sub>sat rock</sub></i> (427)	1.00 × 10 <sup>-5</sup>	NR	NR	NR	m/s	NR	NR	Table 6.5.2.6-1	
	<i>K<sub>sat rock</sub></i> (428)	9.40 × 10 <sup>-7</sup>	NR	NR	NR	m/s	NR	NR	Table 6.5.2.6-1	
	<i>K<sub>sat rock</sub></i> (429)	2.00 × 10 <sup>-4</sup>	NR	NR	NR	m/s	NR	NR	Table 6.5.2.6-1	
	<i>K<sub>sat rock</sub></i> (430)	9.40 × 10 <sup>-7</sup>	NR	NR	NR	cm/s	NR	NR	Table 6.5.2.6-1	
	<i>K<sub>sat rock</sub></i> (432)	9.40 × 10 <sup>-7</sup>	NR	NR	NR	cm/s	NR	NR	Table 6.5.2.6-1	
	<i>K<sub>sat rock</sub></i> (434)	9.40 × 10 <sup>-6</sup>	NR	NR	NR	cm/s	NR	NR	Table 6.5.2.6-1	
	<i>K<sub>sat rock</sub></i> (435)	1.50 × 10 <sup>-6</sup>	NR	NR	NR	cm/s	NR	NR	Table 6.5.2.6-1	
	<i>K<sub>sat rock</sub></i> (436)	1.20 × 10 <sup>-6</sup>	NR	NR	NR	cm/s	NR	NR	Table 6.5.2.6-1	
	<i>K<sub>sat rock</sub></i> (437)	6.40 × 10 <sup>-7</sup>	NR	NR	NR	cm/s	NR	NR	Table 6.5.2.6-1	
<i>K<sub>sat rock</sub></i> (438)	2.10 × 10 <sup>-6</sup>	NR	NR	NR	cm/s	NR	NR	Table 6.5.2.6-1		

NOTE: Uncertainty distribution not reported (NR) in this table for material properties that affect less than 15% of UZ grid.

### II.3 SCREENING OF PRESENT-DAY CLIMATE PARAMETERS

For the Present-Day climate, Table I-2 summarizes the eleven parameters varied independently in the uncertainty analysis (the eight climate-independent parameters plus three additional parameters). Two plant parameters were varied (the mean plant height and the maximum effective rooting depth).

One weather parameter,  $a_m$ , was also varied. Another weather parameter,  $a_\lambda$ , was not varied independently, but rather was correlated with  $a_m$  (Table I-3). Although the relative uncertainty in  $a_\lambda$  is somewhat less than the arbitrary 15% criterion, it was included in the uncertainty analysis so that its value would remain consistent with the value of  $a_m$ .

Approximately 30 other climate dependent parameters were screened. Table I-4 lists those parameters that are excluded from the detailed analysis of parameter uncertainty.

Table I-2. Parameters Varied Independently in Uncertainty Analysis for Present-Day Climate

Parameter Description	Parameter Symbol	Nominal Value	Low Range	High Range	Stand. Uncert.	Units	Relative Uncert.	Dist.	Reference	Comments
Constant term in Fourier series for $m(d)$	$a_m$	0.78	0.50	1.07	0.16	ln mm	20%	Uniform	Table F.3.1-2	
Mean plant height	$h_{plant}$	0.40	0.20	0.60	0.12	m	30%	Uniform	Table 6.5.3.3-1	
Maximum effective rooting depth	$Z_r$	1.6	0.6	2.6	0.6	m	38%	Uniform	Table 6.5.3.2-1	
Depth of soil	$depth_{soil}(4)$	0.3	0.1	0.5	0.12	m	40%	Uniform	Section 6.5.2.4	Midpoint selected as nominal value; not used in calculations
Bulk saturated hydraulic conductivity of bedrock	$K_{sat\_rock}(405)$	$1.1 \times 10^{-6}$	$7.6 \times 10^{-8}$	$4.8 \times 10^{-6}$	factor of 3	m/s	factor of 3	Loguniform	Table 6.5.2.6-1	
	$K_{sat\_rock}(406)$	$1.3 \times 10^{-6}$	$2.1 \times 10^{-8}$	$7.7 \times 10^{-6}$	factor of 5	m/s	factor of 5	Loguniform	Table 6.5.2.6-1	
Soil water holding capacity	$\theta_{HC}(5/7/9)$	0.13	0.09	0.17	0.02	$m^3/m^3$	15%	Uniform	Table 6.5.2.3-2	
Readily evaporable water	$REW$	6	2	10	2	mm	30%	Uniform	Table 6.5.4.2-5	
Minimum $K_c$ for dry soil with no crop cover	$K_{c\_min}$	0	0	0.2	0.06	none	30%	50% 0.0, 50% triangular	Table 6.5.4.2-2	Uncertainty relative to maximum
Evaporation layer depth	$Z_e$	0.15	0.1	0.2	0.03	m	19%	Uniform	Table 6.5.4.2-4	
Slope of relationship between $K_{cb}$ to $NDVI\_cor$	$C_{Kcb2}$	9.7	NA	NA	2.1	none	20%	Normal	Section 6.5.3.7	

Table I-3. Parameters Correlated with Other Parameters that Varied Independently in Uncertainty Analysis for Present-Day Climate

Parameter Description	Parameter Symbol	Nominal Value	Low Range	High Range	Stand. Uncert.	Units	Relative Uncert.	Dist.	Reference	Comments
Constant term in Fourier series for $I(d)$	$a_1$	5.20	4.0	6.5	0.7	mm	13%	Uniform	Table F3.1-1	Included; correlated with $a_m$

Table I-4. Parameters Excluded from Uncertainty Analysis for Present-Day Climate

Parameter Description	Parameter Symbol	Nominal Value	Low Range	High Range	Stand. Uncert.	Units	Relative Uncert.	Dist.	Reference	Comments	Reason for Exclusion
Constant term in Fourier series for $p_{00}(d)$	$a_{00}$	0.934	0.924	0.944	0.006	none	9%	Uniform	Table F3.1-1	Uncertainty relative to $1-a_{00}$	Low uncertainty
Magnitude of first order-term in Fourier series for $p_{00}(d)$	$b_{00,1}$	0.027	NA	NA	0.003	none	5%	Normal	Table F3.1-1	Uncertainty relative to $1-a_{00}$	Low uncertainty
Phase of first-order term in Fourier series for $p_{00}(d)$	$\theta_{00,1}$	-1.31	NA	NA	0.09	radians	3%	Normal	Table F3.1-1	Uncertainty relative to $\pi$	Low uncertainty
Constant term in Fourier series for $p_{10}(d)$	$a_{10}$	0.58	0.50	0.65	0.04	none	10%	Uniform	Table F3.1-1	Uncertainty relative to $1-a_{10}$	Low uncertainty
Magnitude of first-order term in Fourier series for $p_{10}(d)$	$b_{10,1}$	0.06	0.03	0.10	0.02	none	5%	Uniform	Table F3.1-1	Uncertainty relative to $1-a_{10}$	Low uncertainty
Phase of first-order term in Fourier series for $p_{10}(d)$	$\theta_{10,1}$	-1.5	NA	NA	0.4	radians	13%	Normal	Table F3.1-1	Uncertainty relative to $\pi$	Low uncertainty

Table I-4. Parameters Excluded from Uncertainty Analysis for Present-Day Climate (Continued)

Parameter Description	Parameter Symbol	Nominal Value	Low Range	High Range	Stand. Uncert.	Units	Relative Uncert.	Dist.	Reference	Comments	Reason for Exclusion
Magnitude of first-order term in Fourier series for $l(d)$	$b_{\lambda,1}$	0.7	NA	NA	0.2	mm	4%	Normal	Table F3.1-1	Uncertainty relative to $a_{\lambda}$	Low uncertainty
Phase of first-order term in Fourier series for $l(d)$	$\theta_{\lambda,1}$	2.5	NA	NA	0.7	radians	22%	Normal	Table F3.1-1	Uncertainty relative to $\pi$	Low influence; first order term less than 15% of magnitude of constant term
Magnitude of first-order term in Fourier series for $m(d)$	$b_{m,1}$	0.15	NA	NA	0.04	In mm	5%	Normal	Table F3.1-1	Uncertainty relative to $a_m$	Low uncertainty
Phase of first-order term in Fourier series for $m(d)$	$\theta_{m,1}$	2.4	NA	NA	0.4	radians	13%	Normal	Table F3.1-1	Uncertainty relative to $\pi$	Low uncertainty
Starting DOY (calendar day) for winter dew point		335	274	335	18	days	10%	Uniform	Table 6.5.4.1-2	Uncertainty relative to 182 days	Low uncertainty
Ending DOY (calendar day) for winter dew point		90	90	151	18	days	10%	Uniform	Table 6.5.4.1-2	Uncertainty relative to 182 days	Low uncertainty
Magnitude of first-order term in Fourier series for $T_{wet,min}(d)$	$\alpha_{wet,min}$	9.1	8.6	9.6	0.3	°C	4%	Uniform	Table F3.1-1	Uncertainty relative to $\beta_{wet,max} - \beta_{wet,min}$	Low uncertainty
Phase of first-order term in Fourier series for $T_{wet,min}(d)$	$\beta_{wet,min}$	122	121	124	1	days	0.5%	Uniform	Table F3.1-1	Uncertainty relative to 182 days	Low uncertainty



Table I-4. Parameters Excluded from Uncertainty Analysis for Present-Day Climate (Continued)

Parameter Description	Parameter Symbol	Nominal Value	Low Range	High Range	Stand. Uncert.	Units	Relative Uncert.	Dist.	Reference	Comments	Reason for Exclusion
Constant term in Fourier series for $T_{wet,min}(d)$	$\gamma_{wet,min}$	6.6	5.0	8.1	0.9	°C	11%	Uniform	Table F3.1-1	Uncertainty relative to $\gamma_{wet,max} - \gamma_{wet,min}$	Low uncertainty
Magnitude of first-order term in Fourier series for $T_{dry,min}(d)$	$\alpha_{dry,min}$	9.7	9.4	10.0	0.2	°C	2%	Uniform	Table F3.1-1	Uncertainty relative to $\gamma_{dry,max} - \gamma_{dry,min}$	Low uncertainty
Phase of first-order term in Fourier series for $T_{dry,min}(d)$	$\beta_{dry,min}$	115	114	116	1	days	0.5%	Uniform	Table F3.1-1	Uncertainty relative to 182 days	Low uncertainty
Constant term in Fourier series for $T_{dry,min}(d)$	$\gamma_{dry,min}$	9.4	6.9	11.8	1.4	°C	13%	Uniform	Table F3.1-1	Uncertainty relative to $\gamma_{dry,max} - \gamma_{dry,min}$	Low uncertainty
Magnitude of first-order term in Fourier series for $T_{wet,max}(d)$	$\alpha_{wet,max}$	12.1	11.8	12.4	0.2	°C	2%	Uniform	Table F3.1-1	Uncertainty relative to $\gamma_{wet,max} - \gamma_{wet,min}$	Low uncertainty
Phase of first-order term in Fourier series for $T_{wet,max}(d)$	$\beta_{wet,max}$	117	116	118	1	days	0.5%	Uniform	Table F3.1-1	Uncertainty relative to 182 days	Low uncertainty
Constant term in Fourier series for $T_{wet,max}(d)$	$\gamma_{wet,max}$	14.8	13.9	15.8	0.6	°C	7%	Uniform	Table F3.1-1	Uncertainty relative to $\gamma_{wet,max} - \gamma_{wet,min}$	Low uncertainty
Magnitude of first-order term in Fourier series for $T_{dry,max}(d)$	$\alpha_{dry,max}$	12.2	11.9	12.4	0.10	°C	1.3%	Uniform	Table F3.1-1	Uncertainty relative to $\gamma_{dry,max} - \gamma_{dry,min}$	Low uncertainty
Phase of first-order term in Fourier series for $T_{dry,max}(d)$	$\beta_{dry,max}$	110	109	110	0.3	days	0.2%	Uniform	Table F3.1-1	Uncertainty relative to 182 days	Low uncertainty
Constant term in Fourier series for $T_{dry,max}(d)$	$\gamma_{dry,max}$	20.0	19.2	20.7	0.4	°C	4%	Uniform	Table F3.1-1	Uncertainty relative to $\gamma_{dry,max} - \gamma_{dry,min}$	Low uncertainty

Table I-4. Parameters Excluded from Uncertainty Analysis for Present-Day Climate (Continued)

Parameter Description	Parameter Symbol	Nominal Value	Low Range	High Range	Stand. Uncert.	Units	Relative Uncert.	Dist.	Reference	Comments	Reason for Exclusion
Wind speed at height of 2m during month m	$u_2(1)$	2.36	NA	NA	0.03	m/s	1.3%	Normal	Table F3.1-1	<9% of year	low uncertainty
	$u_2(2)$	2.67	NA	NA	0.04	m/s	1.5%	Normal	Table F3.1-1	<9% of year	low uncertainty
	$u_2(3)$	2.84	NA	NA	0.03	m/s	1.1%	Normal	Table F3.1-1	<9% of year	low uncertainty
	$u_2(4)$	3.22	NA	NA	0.04	m/s	1.2%	Normal	Table F3.1-1	<9% of year	low uncertainty
	$u_2(5)$	2.97	NA	NA	0.03	m/s	1.0%	Normal	Table F3.1-1	<9% of year	low uncertainty
	$u_2(6)$	2.90	NA	NA	0.02	m/s	0.7%	Normal	Table F3.1-1	<9% of year	low uncertainty
	$u_2(7)$	2.75	NA	NA	0.02	m/s	0.7%	Normal	Table F3.1-1	<9% of year	low uncertainty
	$u_2(8)$	2.71	NA	NA	0.02	m/s	0.7%	Normal	Table F3.1-1	<9% of year	low uncertainty
	$u_2(9)$	2.64	NA	NA	0.02	m/s	0.8%	Normal	Table F3.1-1	<9% of year	low uncertainty
	$u_2(10)$	2.61	NA	NA	0.03	m/s	1.1%	Normal	Table F3.1-1	<9% of year	low uncertainty
	$u_2(11)$	2.47	NA	NA	0.03	m/s	1.2%	Normal	Table F3.1-1	<9% of year	low uncertainty
	$u_2(12)$	2.48	NA	NA	0.03	m/s	1.2%	Normal	Table F3.1-1	<9% of year	low uncertainty
Minimum precipitation duration (intercept to 1)		1.07	NA	NA	NA	hr	NA	NA	Table 6.5.1.7-3		uncertainty captured in rate of duration increase with precipitation
Rate of duration increase with precipitation (slope)		0.38	NA	NA	0.05	hr/mm	13%	Normal	Table 6.5.1.7-3		low uncertainty

## II.4 SCREENING OF MONSOON CLIMATE PARAMETERS

Tables I-5 and I-6 summarize the 19 parameters varied in the uncertainty analysis for the monsoon climate, including the eight parameters that are climate-independent. Two plant parameters were varied (the mean plant height and the maximum effective rooting depth). The slope of precipitation duration versus amount of precipitation was varied for this climate.

Four weather parameters were varied directly. Four additional weather parameters were not varied independently but rather were correlated with  $a_m$  and  $b_{m1}$ . These seven weather parameters provided variation in the weather input files for model calculations.

The monsoon climate is described in *Future Climate Analysis* (BSC 2004 [DIRS 170002]) as being something between the current desert climate (with most of the rain in winter) and a classical monsoon climate (with most of the rain in summer). This uncertainty has been modeled by fixing the phase of the seasonal variation (all  $\theta$  values) such that most of the rain falls in summer, and authorizing the amplitude (all  $b$  values) to vary between positive values (keeping most of the rain in summer) and negative values (switching the largest amount of rain to winter period).

One of the amplitude values,  $b_m$ , is varied independently. All the other amplitudes are estimated using simple linear regression. Even though there is no correlation between annual average ( $a$  values) and amplitude ( $b$  values), the resulting weather parameters have to be checked in order to suppress any physical impossibilities:

- First,  $b_{00,1}$  cannot be higher than  $1-a_{00}$  (as it will create a probability of having a dry day bigger than 1).
- Next,  $b_\lambda$  cannot be higher than  $a_\lambda$ , as it will create a negative value for some daily amounts of rain.

These configurations are unlikely to happen. Therefore, in the event that sampling results one vector that contains a physically impossible set of values, the entire set of sample vectors is discarded.

Table I-7 lists those parameters that are excluded from the detailed analysis of parameter uncertainty.

Table I-5. Parameters Varied Independently in Uncertainty Analysis for Monsoon Climate

Parameter Description	Parameter Symbol	Nominal Value	Low Range	High Range	Stand. Uncert.	Units	Relative Uncert.	Dist.	Reference	Comments
Constant term in Fourier series for $p_{soil}(d)$	$a_{00}$	0.920	0.896	0.944	0.014	none	18%	Uniform	Table F3.2-1	Uncertainty relative to $1-a_{00}$
Constant term in Fourier series for $m(d)$	$a_m$	0.9	0.5	1.3	0.2	ln mm	20%	Uniform	Table F3.2-1	
Magnitude of first-order term in Fourier series for $m(d)$	$b_{m,1}$	0.1	-0.3	0.5	0.2	ln mm	20%	Uniform	Table F3.2-1	Uncertainty relative to $a_m$
Constant term in Fourier series for $T_{wet,max}(d)$	$\gamma_{wet,max}$	18	14	22	2	°C	18%	Uniform	Table F3.2-1	Uncertainty relative to $\gamma_{wet,max} - \gamma_{wet,min}$
Mean plant height	$h_{plant}$	0.4	0.2	0.6	0.12	m	30%	Uniform	Table 6.5.3.3-1	
Maximum effective rooting depth	$Z_r$	1.6	0.6	2.6	0.6	m	38%	Uniform	Table 6.5.3.2-1	
Rate of duration increase with precipitation (slope)		0.28	0.14	0.43	0.08	hr/mm	30%	Uniform	Table 6.5.1.7-4	Extremes extended by one standard error
Depth of soil	$depth_{soil}(4)$	0.3	0.1	0.5	0.12	m	40%	Uniform	Section 6.5.2.4	Midpoint selected as nominal value; not used in calculations
Bulk saturated hydraulic conductivity of bedrock	$K_{sat\_rock}(405)$ $K_{sat\_rock}(406)$	$1.1 \times 10^{-6}$ $1.3 \times 10^{-6}$	$7.6 \times 10^{-8}$ $2.1 \times 10^{-8}$	$4.8 \times 10^{-6}$ $7.7 \times 10^{-6}$	factor of 3 factor of 5	m/s m/s	factor of 3 factor of 5	Loguniform Loguniform	Table 6.5.2.6-1 Table 6.5.2.6-1	
Soil water holding capacity	$\theta_{HC}(5/7/9)$	0.13	0.09	0.17	0.02	$m^3/m^3$	15%	Uniform	Table 6.5.2.3-2	

Table I-5. Parameters Varied Independently in Uncertainty Analysis for Monsoon Climate (Continued)

Parameter Description	Parameter Symbol	Nominal Value	Low Range	High Range	Stand. Uncert.	Units	Relative Uncert.	Dist.	Reference	Comments
Readily evaporable water	$REW$	6	2	10	2	mm	30%	Uniform	Table 6.5.4.2-5	
Minimum $K_c$ for dry soil with no crop cover	$K_{c\_min}$	0	0	0.2	0.06	none	30%	50% 0.0, 50% Triangular	Table 6.5.4.2-2	Uncertainty relative to maximum
Evaporation layer depth	$Z_e$	0.15	0.1	0.2	0.03	m	19%	Uniform	Table 6.5.4.2-4	
Slope of relationship between $K_{cb}$ to $NDVI\_cor$	$C_{K_{cb}2}$	9.7	NA	NA	2.1	none	20%	Normal	Section 6.5.3.7	

Table I-6. Parameters Correlated with Other Parameters that Varied Independently in Uncertainty Analysis for Monsoon Climate

Parameter Description	Parameter Symbol	Nominal Value	Low Range	High Range	Stand. Uncert.	Units	Relative Uncert.	Dist.	Reference	Comments
Constant term in Fourier series for $I(d)$	$a_4$	6.50	4.0	9.0	1.4	mm	22%	Uniform	Table F3.2-1	Correlated with $a_m$
Magnitude of first-order term in Fourier series for $I(d)$	$b_{A,1}$	1.6	-1.3	4.5	1.7	mm	26%	Uniform	Table F3.2-1	Uncertainty relative to $a_{A,i}$ ; correlated with $b_{m,1}$
Magnitude of first-order-term in Fourier series for $p_{00}(d)$	$b_{00,1}$	0.02	-0.03	0.07	0.03	none	38%	Uniform	Table F3.2-1	Uncertainty relative to $1-a_{00,i}$ ; correlated with $b_{m,1}$
Magnitude of first-order term in Fourier series for $p_{10}(d)$	$b_{10,1}$	-0.02	-0.13	0.10	0.07	none	17%	Uniform	Table F3.2-1	Uncertainty relative to $1-a_{10,i}$ ; correlated with $b_{m,1}$

Table I-7. Parameters Excluded from Uncertainty Analysis for Monsoon Climate

Parameter Description	Parameter Symbol	Nominal Value	Low Range	High Range	Stand. Uncert.	Units	Relative Uncert.	Dist.	Reference	Comments	Reason for Exclusion
Phase of first-order term in Fourier series for $p_{so}(d)$	$\theta_{00,1}$	2.00	1.74	2.25	0.15	radians	5%	Uniform	Table F3.2-1	Uncertainty relative to $\pi$	Low uncertainty
Constant term in Fourier series for $p_{so}(d)$	$a_{10}$	0.58	0.50	0.67	0.05	none	12%	Uniform	Table F3.2-1	Uncertainty relative to $1-a_{10}$	Low uncertainty
Phase of first-order term in Fourier series for $p_{so}(d)$	$\theta_{10,1}$	1.8	1.4	2.3	0.3	radians	10%	Uniform	Table F3.2-1	Uncertainty relative to $\pi$	Low uncertainty
Phase of first-order term in Fourier series for $l(d)$	$\theta_{\lambda,1}$	-1.6	-2.0	-1.1	0.3	radians	10%	Uniform	Table F3.2-1	Uncertainty relative to $\pi$	low uncertainty
Phase of first-order term in Fourier series for $m(d)$	$\theta_{m,1}$	-1.48	-1.78	-1.17	0.18	radians	6%	Uniform	Table F3.2-1	Uncertainty relative to $\pi$	Low uncertainty
Starting DOY (calendar day) for winter dew point		335	274	335	18	days	10%	Uniform	Table 6.5.4.1-2	Uncertainty relative to 182 days	Low uncertainty
Ending DOY (calendar day) for winter dew point		90	90	151	18	days	10%	Uniform	Table 6.5.4.1-2	Uncertainty relative to 182 days	Low uncertainty
Magnitude of first-order term in Fourier series for $T_{wet_{min}}(d)$	$\alpha_{wet_{min}}$	9.4	8.2	10.5	0.7	°C	7%	Uniform	Table F3.2-1	Uncertainty relative to $\gamma_{wet_{max}}-\gamma_{wet_{min}}$	Low uncertainty
Phase of first-order term in Fourier series for $T_{wet_{min}}(d)$	$\beta_{wet_{min}}$	122	119	124	1	days	0.5%	Uniform	Table F3.2-1	Uncertainty relative to 182 days	Low uncertainty
Constant term in Fourier series for $T_{wet_{min}}(d)$	$\gamma_{wet_{min}}$	7.4	5.0	9.7	1.4	°C	13%	Uniform	Table F3.2-1	Uncertainty relative to $\gamma_{wet_{max}}-\gamma_{wet_{min}}$	low uncertainty
Magnitude of first-order term in Fourier series for $T_{dry_{min}}(d)$	$\alpha_{dry_{min}}$	10.2	9.4	11.0	0.5	°C	3%	Uniform	Table F3.2-1	Uncertainty relative to $\gamma_{dry_{max}}-\gamma_{dry_{min}}$	Low uncertainty
Phase of first-order term in Fourier series for $T_{dry_{min}}(d)$	$\beta_{dry_{min}}$	117	114	120	2	days	1.1%	Uniform	Table F3.2-1	Uncertainty relative to 182 days	Low uncertainty
Constant term in Fourier series for $T_{dry_{min}}(d)$	$\gamma_{dry_{min}}$	8	5	12	2	°C	13%	Uniform	Table F3.2-1	Uncertainty relative to $\gamma_{dry_{max}}-\gamma_{dry_{min}}$	Low uncertainty

Table I-7. Parameters Excluded from Uncertainty Analysis for Monsoon Climate (Continued)

Parameter Description	Parameter Symbol	Nominal Value	Low Range	High Range	Stand. Uncert.	Units	Relative Uncert.	Dist.	Reference	Comments	Reason for Exclusion
Magnitude of first-order term in Fourier series for $T_{wetmax}(d)$	$\alpha_{wetmax}$	11.4	10.5	12.4	0.5	°C	5%	Uniform	Table F3.2-1	Uncertainty relative to $\gamma_{wetmax} - \gamma_{wetmin}$	Low uncertainty
Phase of first-order term in Fourier series for $T_{wetmax}(d)$	$\beta_{wetmax}$	115	112	118	2	days	1.1%	uniform	Table F3.2-1	Uncertainty relative to 182 days	Low uncertainty
Magnitude of first-order term in Fourier series for $T_{drymax}(d)$	$\alpha_{drymax}$	10.4	8.4	12.4	1.2	°C	8%	uniform	Table F3.2-1	Uncertainty relative to $\gamma_{drymax} - \gamma_{drymin}$	Low uncertainty
Phase of first-order term in Fourier series for $T_{drymax}(d)$	$\beta_{drymax}$	113	109	117	2	days	1.1%	uniform	Table F3.2-1	Uncertainty relative to 182 days	Low uncertainty
Constant term in Fourier series for $T_{drymax}(d)$	$\gamma_{drymax}$	23	19	27	2	°C	13%	uniform	Table F3.2-1	Uncertainty relative to $\gamma_{drymax} - \gamma_{drymin}$	Low uncertainty
Wind speed at height of 2m during month m	$u_2(1)$	2.36	NA	NA	0.03	m/s	1.3%	normal	Table F3.2-1	<9% of year	Low uncertainty
	$z(2)$	2.67	NA	NA	0.04	m/s	1.5%	normal	Table F3.2-1	<9% of year	Low uncertainty
	$z(3)$	2.84	NA	NA	0.03	m/s	1.1%	normal	Table F3.2-1	<9% of year	Low uncertainty
	$z(4)$	3.22	NA	NA	0.04	m/s	1.2%	normal	Table F3.2-1	<9% of year	Low uncertainty
	$z(5)$	2.97	NA	NA	0.03	m/s	1.0%	normal	Table F3.2-1	<9% of year	Low uncertainty
	$z(6)$	2.90	NA	NA	0.02	m/s	0.7%	normal	Table F3.2-1	<9% of year	Low uncertainty
	$z(7)$	2.75	NA	NA	0.02	m/s	0.7%	normal	Table F3.2-1	<9% of year	Low uncertainty
	$z(8)$	2.71	NA	NA	0.02	m/s	0.7%	normal	Table F3.2-1	<9% of year	Low uncertainty
	$z(9)$	2.64	NA	NA	0.02	m/s	0.8%	normal	Table F3.2-1	<9% of year	Low uncertainty
	$z(10)$	2.61	NA	NA	0.03	m/s	1.1%	normal	Table F3.2-1	<9% of year	Low uncertainty

Table I-7. Parameters Excluded from Uncertainty Analysis for Monsoon Climate (Continued)

Parameter Description	Parameter Symbol	Nominal Value	Low Range	High Range	Stand. Uncert.	Units	Relative Uncert.	Dist.	Reference	Comments	Reason for Exclusion
Wind speed at height of 2m during month m (Continued)	$u_2(11)$	2.47	NA	NA	0.03	m/s	1.2%	normal	Table F3.2-1	<9% of year	Low uncertainty
	$u_2(12)$	2.48	NA	NA	0.03	m/s	1.2%	normal	Table F3.2-1	<9% of year	Low uncertainty
Minimum precipitation duration		0.91	0.76	1.07	0.09	hr	10%	uniform	Table 6.5.1.7-4		Low uncertainty



## **II.5 SCREENING OF GLACIAL TRANSITION CLIMATE PARAMETERS**

A total of 17 parameters were varied for the Glacial Transition climate, as listed in Tables I-8 and I-9. Eight of these were climate-independent. Two plant parameters were varied (the mean plant height and the maximum effective rooting depth). For this climate, the analyses varied both parameters of the precipitation duration model, but only one was varied independently, so that they could be correlated.

Three weather parameters were varied directly. Two additional weather parameters were not varied independently but rather were correlated (Table I-9). These five weather parameters provided variation in the weather input files for model calculations.

Table I-10 lists the parameters excluded from the detailed uncertainty analysis.

Table I-8. Parameters Varied Independently in Uncertainty Analysis for Glacial Transition Climate

Parameter Description	Parameter Symbol	Nominal Value	Low Range	High Range	Stand. Uncert.	Units	Relative Uncert.	Dist.	Reference	Comments
Constant term in Fourier series for $p_{soil}(d)$	$a_{00}$	0.84	0.78	0.89	0.03	none	19%	Uniform	Table F3.3-1	Uncertainty relative to $1-a_{00}$
Constant term in Fourier series for $m(d)$	$a_m$	0.70	0.48	0.92	0.13	in mm	19%	Uniform	Table F3.3-1	
Phase of first-order term in Fourier series for $l(d)$	$\theta_{\lambda,1}$	NA	$-\pi$	$+\pi$	NA	radians	NA	Uniform	Table F3.3-1	
Rate of duration increase with precipitation		0.52	0.32	0.71	0.11	hr/mm	20%	Uniform	Table 6.5.1.7-4	
Mean plant height	$h_{plant}$	1.3	0.6	1.8	0.3	m	30%	Uniform	Table 6.5.3.3-2	
Maximum effective rooting depth	$Z_r$	2.5	1.0	4.0	0.9	m	40%	Uniform	Table 6.5.3.2-2	
Depth of soil	$depth_{soil}(4)$	0.3	0.1	0.5	0.12	m	40%	Uniform	Section 6.5.2.4	Midpoint selected as nominal value; not used in calculations
Bulk saturated hydraulic conductivity of bedrock	$K_{sat\_rock}(405)$	$1.1 \times 10^{-6}$	$7.6 \times 10^{-8}$	$4.8 \times 10^{-6}$	factor of 3	m/s	factor of 3	Loguniform	Table 6.5.2.6-1	
Soil water holding capacity	$K_{sat\_rock}(406)$	$1.3 \times 10^{-6}$	$2.1 \times 10^{-8}$	$7.7 \times 10^{-6}$	factor of 5	m/s	factor of 5	Loguniform	Table 6.5.2.6-1	
Readily evaporable water	$\theta_{HC}(5/7/9)$	0.13	0.09	0.17	0.02	$m^3/m^3$	15%	Uniform	Table 6.5.2.3-2	
Minimum $K_c$ for dry soil with no crop cover	$REW$	6	2	10	2	mm	30%	Uniform	Table 6.5.4.2-5	
Evaporation layer depth	$K_{c\_min}$	0	0	0.2	0.06	none	30%	50% 0.0, 50% Triangular	Table 6.5.4.2-2	Uncertainty relative to maximum
Slope of relationship between $K_{cb}$ to NDVI <sub>cor</sub>	$Z_e$	0.15	0.1	0.2	0.03	m	19%	Uniform	Table 6.5.4.2-4	
	$C_{Kcb2}$	9.7	NA	NA	2.1	none	20%	Normal	Section 6.5.3.7	

Table I-9. Parameters Correlated with Other Parameters that Varied Independently in Uncertainty Analysis for Glacial Transition Climate

Parameter Description	Parameter Symbol	Nominal Value	Low Range	High Range	Stand. Uncert.	Units	Relative Uncert.	Dist.	Reference	Comments
Constant term in Fourier series for $\lambda(d)$	$a_1$	3.8	3.1	4.5	0.4	mm	11%	Uniform	Table F3.3-1	Included; correlated with $a_m$
Phase of first-order term in Fourier series for $m(d)$	$\theta_{m,1}$	NA	$-\pi$	$+\pi$	NA	radians	NA	Uniform	Table F3.3-1	Included; correlated with $\theta_{\lambda,1}$
Minimum precipitation duration (Intercept - 1)		0.96	0.70	1.22	0.15	hr	16%	Uniform	Table 6.5.1.7-4	Uncertainty captured in rate of duration increase with precipitation

Table I-10. Parameters Excluded from Uncertainty Analysis for Glacial Transition Climate

Parameter Description	Parameter Symbol	Nom. Value	Low Range	High Range	Stand. Uncert.	Units	Relative Uncert.	Dist.	Reference	Comments	Reason for Exclusion
Magnitude of first-order term in Fourier series for $\lambda(d)$	$b_{\lambda,1}$	0.6	0.1	1.0	0.3	mm	8%	Uniform	Table F3.3-1	Uncertainty relative to $a_1$	Low uncertainty
Magnitude of first order-term in Fourier series for $p_{\infty}(d)$	$b_{00,1}$	0.066	0.028	0.104	0.02	none	13%	Uniform	Table F3.3-1	Uncertainty relative to $1-a_{00}$	Low uncertainty
Phase of first-order term in Fourier series for $p_{\infty}(d)$	$\theta_{00,1}$	-1.12	NA	NA	0.010	radians	0.3%	Normal	Table F3.3-1	Uncertainty relative to $\pi$	Low uncertainty
Constant term in Fourier series for $p_{10}(d)$	$a_{10}$	0.54	0.47	0.62	0.04	none	9%	Uniform	Table F3.3-1	Uncertainty relative to $1-a_{10}$	low uncertainty
Magnitude of first-order term in Fourier series for $p_{10}(d)$	$b_{10,1}$	0.07	0.02	0.11	0.03	none	7%	Uniform	Table F3.3-1	Uncertainty relative to $1-a_{10}$	Low uncertainty
Phase of first-order term in Fourier series for $p_{10}(d)$	$\theta_{10,1}$	-0.93	NA	NA	0.84	radians	26%	Normal	Table F3.3-1	Uncertainty relative to $\pi$	Low influence; $b_{10,1}$ is barely 15% of $1-a_{10}$
Magnitude of first-order term in Fourier series for $m(d)$	$b_{m,1}$	0.12	0.08	0.16	0.02	In mm	3%	Uniform	Table F3.3-1	Uncertainty relative to $a_m$	Low uncertainty
Starting DOY (calendar day) for winter dew point		274	244	274	9	days	5%	Uniform	Table 6.5.4.1-2	Uncertainty relative to 182 days	Low uncertainty

Table I-10. Parameters Excluded from Uncertainty Analysis for Glacial Transition Climate (Continued)

Parameter Description	Parameter Symbol	Nom. Value	Low Range	High Range	Stand. Uncert.	Units	Relative Uncert.	Dist.	Reference	Comments	Reason for Exclusion
Ending DOY (calendar day) for winter dew point		120	120	151	9	days	5%	Uniform	Table 6.5.4.1-2	Uncertainty relative to 182 days	Low uncertainty
Magnitude of first-order term in Fourier series for $T_{wet,min}(d)$	$\alpha_{wet,min}$	8.4	6.3	10.4	1.2	°C	11%	Uniform	Table F3.3-1	Uncertainty relative to $\gamma_{wet,max} - \gamma_{wet,min}$	Low uncertainty
Phase of first-order term in Fourier series for $T_{wet,min}(d)$	$\beta_{wet,min}$	116	114	118	1	days	0.6%	Uniform	Table F3.3-1	Uncertainty relative to 182 days	Low uncertainty
Constant term in Fourier series for $T_{wet,min}(d)$	$\gamma_{wet,min}$	2.6	1.2	3.9	0.8	°C	7%	Uniform	Table F3.3-1	Uncertainty relative to $\gamma_{wet,max} - \gamma_{wet,min}$	Low uncertainty
Magnitude of first-order term in Fourier series for $T_{dry,min}(d)$	$\alpha_{dry,min}$	9.6	7.5	11.6	1.2	°C	7%	Uniform	Table F3.3-1	Uncertainty relative to $\gamma_{dry,max} - \gamma_{dry,min}$	Low uncertainty
Phase of first-order term in Fourier series for $T_{dry,min}(d)$	$\beta_{dry,min}$	111	106	116	3	days	2%	Uniform	Table F3.3-1	Uncertainty relative to 182 days	Low uncertainty
Constant term in Fourier series for $T_{dry,min}(d)$	$\gamma_{dry,min}$	0.9	-0.8	2.6	1.0	°C	6%	Uniform	Table F3.3-1	Uncertainty relative to $\gamma_{dry,max} - \gamma_{dry,min}$	Low uncertainty
Magnitude of first-order term in Fourier series for $T_{wet,max}(d)$	$\alpha_{wet,max}$	11.8	10.1	13.4	1.0	°C	9%	Uniform	Table F3.3-1	Uncertainty relative to $\gamma_{wet,max} - \gamma_{wet,min}$	Low uncertainty
Phase of first-order term in Fourier series for $T_{wet,max}(d)$	$\beta_{wet,max}$	113	111	115	1	days	0.6%	Uniform	Table F3.3-1	Uncertainty relative to 182 days	Low uncertainty
Constant term in Fourier series for $T_{wet,max}(d)$	$\gamma_{wet,max}$	13.8	11.7	15.9	1.2	°C	11%	Uniform	Table F3.3-1	Uncertainty relative to $\gamma_{wet,max} - \gamma_{wet,min}$	Low uncertainty
Magnitude of first-order term in Fourier series for $T_{dry,max}(d)$	$\alpha_{dry,max}$	14.4	13.8	15.0	0.3	°C	2%	Uniform	Table F3.3-1	Uncertainty relative to $\gamma_{dry,max} - \gamma_{dry,min}$	Low uncertainty
Phase of first-order term in Fourier series for $T_{dry,max}(d)$	$\beta_{dry,max}$	114	112	117	1	days	0.6%	Uniform	Table F3.3-1	Uncertainty relative to 182 days	Low uncertainty
Constant term in Fourier series for $T_{dry,max}(d)$	$\gamma_{dry,max}$	17.1	14.6	19.6	1.4	°C	9%	Uniform	Table F3.3-1	Uncertainty relative to $\gamma_{dry,max} - \gamma_{dry,min}$	Low uncertainty

Table I-10. Parameters Excluded from Uncertainty Analysis for Glacial Transition Climate (Continued)

Parameter Description	Parameter Symbol	Nom. Value	Low Range	High Range	Stand. Uncert.	Units	Relative Uncert.	Dist.	Reference	Comments	Reason for Exclusion
<i>Wind speed at height of 2m during month m</i>	$u_2(1)$	2.36	NA	NA	0.03	m/s	1.3%	Normal	Table F3.3-1	< 9% of year	Low uncertainty
	$u_2(2)$	2.67	NA	NA	0.04	m/s	1.5%	Normal	Table F3.3-1	< 9% of year	Low uncertainty
	$u_2(3)$	2.84	NA	NA	0.03	m/s	1.1%	Normal	Table F3.3-1	< 9% of year	Low uncertainty
	$u_2(4)$	3.22	NA	NA	0.04	m/s	1.2%	Normal	Table F3.3-1	< 9% of year	Low uncertainty
	$u_2(5)$	2.97	NA	NA	0.03	m/s	1.0%	Normal	Table F3.3-1	< 9% of year	Low uncertainty
	$u_2(6)$	2.90	NA	NA	0.02	m/s	0.7%	Normal	Table F3.3-1	< 9% of year	Low uncertainty
	$u_2(7)$	2.75	NA	NA	0.02	m/s	0.7%	Normal	Table F3.3-1	< 9% of year	Low uncertainty
	$u_2(8)$	2.71	NA	NA	0.02	m/s	0.7%	Normal	Table F3.3-1	< 9% of year	Low uncertainty
	$u_2(9)$	2.64	NA	NA	0.02	m/s	0.8%	Normal	Table F3.3-1	< 9% of year	Low uncertainty
	$u_2(10)$	2.61	NA	NA	0.03	m/s	1.1%	Normal	Table F3.3-1	< 9% of year	Low uncertainty
	$u_2(11)$	2.47	NA	NA	0.03	m/s	1.2%	Normal	Table F3.3-1	< 9% of year	Low uncertainty
	$u_2(12)$	2.48	NA	NA	0.03	m/s	1.2%	Normal	Table F3.3-1	< 9% of year	Low uncertainty

## 12. BACKGROUND ON UNCERTAINTY AND UNCERTAINTY DISTRIBUTIONS

### 12.1 DEFINITIONS

There is no standard for the expression of uncertainty in predictions made with algorithms. However, algorithms are used to predict measurements. The treatment of uncertainty in this report is based on ANSI/NCSL Z540-2-1997, *American National Standard for Calibration —U.S. Guide to the Expression of Uncertainty in Measurement* [DIRS 157394]. The following are adapted from definitions that appear in the standard:

1. The **measurand** is the particular quantity subject to measurement and therefore to prediction. Its definition may require specification of the conditions under which the quantity is measured. The standard avoids the phrase “true value of the measurand” because the word “true” is viewed as redundant. The “true value of the measurand” is simply the value of the measurand (ANSI/NCSL Z540-2-1997 [DIRS 157394], p. 41).
2. The **measurement error** is the result of the measurement minus the value of the measurand (ANSI/NCSL Z540-2-1997 [DIRS 157394], p. 34). As used in this appendix, the **prediction error** is the result of the prediction minus the value of the measurand.
3. A **random component** of prediction error is an effect that, for multiple predictions with varying inputs, produces a mean error that is small relative to the standard deviation of the error from that effect. An example of a random component is the residual error after a formula has been adjusted to correlate with data.
4. A **systematic component** of prediction error is an effect that is not a random component.
5. If the systematic component of prediction error includes a systematic effect that is quantifiable, one may add a **correction** to the prediction to compensate for that effect. However, the necessary correction may not be practical in the intended application of the prediction.
6. The **uncertainty** of the result of a prediction is an estimate of the likelihood of nearness to the best value that is consistent with presently available knowledge (adapted from ANSI/NCSL Z540-2-1997 [DIRS 157394], p. 41). Components of uncertainty include estimates of random error, uncertainties in corrections, and estimates of uncorrected or unrecognized systematic effects.
7. **Standard uncertainty**  $u(x)$ , of a predicted value  $x$  is the uncertainty of the result of a prediction expressed as a standard deviation. It does not correspond to a high level of confidence.
8. A **Type A evaluation** of uncertainty is an evaluation by statistical analysis of a series of observations. A **Type B evaluation** of uncertainty is an evaluation by any other method. A Type B evaluation is founded on an a priori distribution of the possible values (ANSI/NCSL Z540-2-1997 [DIRS 157394], p. 3).

9. If the result of a prediction is a function of the values of a number of other quantities, the standard uncertainty in the prediction is the **combined standard uncertainty**.
10. For contributions to uncertainty that are independent, the **law of propagation of uncertainty** (ANSI/NCSL Z540-2-1997 [DIRS 157394], p. 19) determines the combined standard uncertainty. For  $y = f(x_1, \dots, x_n)$ , the combined standard uncertainty  $u_c(y)$  is given by:

$$u_c^2(y) = \sum_{i=1}^N \left( \frac{\partial f}{\partial x_i} \right)^2 u^2(x_i) \quad (\text{Eq. I-1})$$

1. In some applications, it may be necessary to have a measure of uncertainty that encompasses a large fraction of the values that one could reasonably attribute to the measurand. If necessary, the user may multiply the standard uncertainty by a **coverage factor** to obtain an **expanded uncertainty**. In general, the coverage factor will be in the range 2 to 3 (ANSI/NCSL Z540-2-1997 [DIRS 157394], p. 24). This appendix uses a coverage factor of 2 to approximate a 95% confidence interval (ASME PTC 19.1-1998 [DIRS 153195], p. 95).
2. The **relative combined standard uncertainty** in a predicted positive value  $y$  is  $u_c(y)/y$  (ANSI/NCSL Z540-2-1997 [DIRS 157394], p. 25, Sect. 7.2.1).
3. For nonzero values of the  $x_i$ , Equation I-1 may be rewritten for propagation of relative uncertainty:

$$\left[ \frac{u_c(y)}{y} \right]^2 = \sum_{i=1}^N \left( \frac{x_i}{y} \frac{\partial f}{\partial x_i} \right)^2 \left[ \frac{u(x_i)}{x_i} \right]^2 \quad (\text{Eq. I-2})$$

## I2.2 UNCERTAINTY DISTRIBUTIONS

Most of the uncertainty distributions in this report are normal, uniform, or loguniform. The properties of normal distributions are available in any standard statistics text. The standard uncertainty is the square root of the variance of the distribution.

In general, the variance of a distribution that has a probability density  $p_X(X)$  and a mean value  $\mu_X$  is:

$$\sigma_X^2 = \int_{x_1}^{x_2} p_X(X)(X - \mu_X)^2 dX = \int_{x_1}^{x_2} p_X(X)(X^2 - 2\mu_X X + \mu_X^2) dX \quad (\text{Eq. I-3})$$

so that:

$$\sigma_X^2 \begin{cases} = \int_{X_1}^{X_2} p_X(X) X^2 dX - 2\mu_X \int_{X_1}^{X_2} p_X(X) X dX + \mu_X^2 \int_{X_1}^{X_2} p_X(X) dX \\ = \int_{X_1}^{X_2} p_X(X) X^2 dX - \mu_X^2 \end{cases} \quad (\text{Eq. I-4})$$

which is a well-known relationship.

### Uniform Distribution

This report assigns a uniform uncertainty distribution to many parameters. That is, the parameter is a random variable,  $X$ , which is equally likely to be anywhere within its range, from  $X_1$  to  $X_2$ . Therefore, the cumulative probability distribution for  $X$  is:

$$P_X(X) = \frac{X - X_1}{X_2 - X_1}, \quad X_1 \leq X \leq X_2 \quad (\text{Eq. I-5})$$

The probability density function for  $X$  is:

$$p_X(X) = \frac{\partial P_X(X)}{\partial X} = \frac{1}{[X_2 - X_1]}, \quad X_1 \leq X \leq X_2 \quad (\text{Eq. I-6})$$

with the mean value of:

$$\mu_X = (X_1 + X_2)/2 \quad (\text{Eq. I-7})$$

Therefore,

$$\int_{X_1}^{X_2} p_X(X) X^2 dX = \frac{1}{X_2 - X_1} \int_{X_1}^{X_2} X^2 dX = \frac{X_2^3 - X_1^3}{3[X_2 - X_1]} = \frac{X_2^2 + X_2 X_1 + X_1^2}{3} \quad (\text{Eq. I-8})$$

Applying Equation I-4,

$$\sigma_X^2 = \frac{X_2^2 + X_2 X_1 + X_1^2}{3} - \frac{(X_1 + X_2)^2}{4} = \frac{(X_2 - X_1)^2}{12} \quad (\text{Eq. I-9})$$

and the standard uncertainty is  $(X_2 - X_1)/\sqrt{12}$ .



### Loguniform Distribution

Next the properties of a log uniform distribution are considered. Let a random variable,  $X$ , have a loguniform distribution from  $X_1$  to  $X_2$ , which means that the logarithm of  $X$  has a uniform distribution. That is, defining a random variable  $Y$  that is equal to  $\ln(X)$ ,  $Y$  has a uniform distribution from  $Y_1 = \ln(X_1)$  to  $Y_2 = \ln(X_2)$ .

The median of the distribution for  $X$  is the geometric mean of the extremes,  $\sqrt{X_1 X_2}$ .

The standard uncertainty of the distribution for  $Y$  is  $(Y_2 - Y_1)/\sqrt{12}$ . In this report, the standard uncertainty in  $X$  is expressed as a factor of  $\left(\frac{X_2}{X_1}\right)^{1/\sqrt{12}}$ . Factors below 1.2 are expressed as a relative percent.

### Special Triangular Distribution

The uncertainty distribution for the parameter  $K_{c\_min}$  has the following cumulative probability distribution:

$$P(0) = 0.5 \quad (\text{Eq. I-10})$$

$$P(x) = 1 - \frac{(0.2 - x)^2}{2(0.2)^2} \quad (\text{Eq. I-11})$$

$$p(x) = \frac{dP(x)}{dx} = \frac{(0.2 - x)}{(0.2)^2} \quad (\text{Eq. I-12})$$

The root-mean-square deviation from the median value of zero is an estimate of the standard uncertainty,  $u$ . Therefore,

$$u^2 = \int_{x=0}^{0.2} x^2 \frac{(0.2 - x)}{(0.2)^2} dx = \int_{x=0}^{0.2} \frac{(0.2x^2 - x^3)}{(0.2)^2} dx \quad (\text{Eq. I-13})$$

$$u^2 = \frac{(0.2)^4}{3(0.2)^2} - \frac{(0.2)^4}{4(0.2)^2} = \frac{(0.2)^2}{12} = 0.0033 \quad (\text{Eq. I-14})$$

$$u = 0.06 \quad (\text{Eq. I-15})$$

INTENTIONALLY LEFT BLANK

**APPENDIX J**  
**SUPPORTING INFORMATION ON VALIDATION OF EVAPOTRANSPIRATION**  
**USING SOIL WATER STORAGE MEASUREMENTS IN WEIGHING LYSIMETERS**



This appendix provides supporting information regarding the site-specific data, modeling setup, calculations, and modeling results for validation of the evapotranspiration study presented in Section 7.1.2.

Two lysimeter sites are considered in Section 7.1.2. The first lysimeter site is located in Area 5 Radioactive Waste Management Site (RWMS) of the Nevada Test Site (NTS) and represents an analogue to the present-day climate conditions at the Yucca Mountain. This site will be referred to further in this appendix as the NTS lysimeter site. The second site is located in Reynolds Creek Experimental Watershed (RCEW) in southwestern Idaho and represents a potential analogue to the future glacial transition climate conditions at Yucca Mountain. This site will be referred to further in this appendix as the RCEW lysimeter site. The sections within this appendix provide details for each of the two sites.

The data, modeling setup, calculations and results for the NTS lysimeter site is described in Section J1. Details of the NTS bare-soil and vegetated lysimeter simulations can be found in Sections J1.1 and J1.2, respectively. Section J1.3 describes an optimization process that was set up to estimate evapotranspiration and soil parameters by minimizing differences between the calculated and measured daily water storage values in both bare soil and vegetated lysimeters. Section J1.4 describes the details of the model simulations using HYDRUS-1D and MASSIF compared to the lysimeter storage data.

The data, modeling setup, calculations and results for the RCEW lysimeter site is described in Section J2. Details of the climate data are described in Section J2.1. Details of the geospatial data are described in Section J2.2. Other relevant data are discussed in Section J2.3. Section J2.4 describes the details of the model simulations using HYDRUS-1D and MASSIF compared to the lysimeter storage data.

Although direct comparisons between MASSIF and an alternative model, HYDRUS 1D, are documented in Sections 7.2.2 and in Appendix K, comparisons between MASSIF, HYDRUS-1D, and lysimeter field data are also presented in Section 7.1.2 and in Sections J1.4 and J2.4 in order to demonstrate that the comparisons between MASSIF and field data are similar to comparisons between HYDRUS-1D and field data. These comparisons show that a field capacity model such as MASSIF can closely simulate field data as well as a more physics-based flow model such as HYDRUS-1D.

## **J1. AREA 5 RADIOACTIVE WASTE MANAGEMENT SITE (RWMS) NEVADA TEST SITE (NTS)**

The Area 5 RWMS is located in the northern Frenchman Flat on the NTS in southern Nevada. Frenchman Flat is a closed basin. The RWMS is at an elevation of 976 m on a bajada of the Massachusetts Mountains at the intersection of three alluvial fans on a slope of about 1° (Levitt et al. 1999 [DIRS 177521]). The lysimeter site is located 400 m west of the Area 5 RWMS. The lysimeter site coordinates are: 36° 51' 9.13" (latitude) and 115° 56' 56.06" (longitude) (Scanlon et al. 2005 [DIRS 175977]).

The NTS lysimeter site is located approximately 40 km from the eastern boundary of the MASSIF model domain. The site elevation (976 m) is approximately the same as the lowest elevation of the MASSIF model domain (964 m). The predominant vegetation found at the lysimeter site is the same as found in the Larrea–Ambrosia vegetation association described in Appendix D. Given these similarities, the NTS lysimeter site is a good analogue to the low elevation areas of the Yucca Mountain model domain.

Two weighing lysimeters were installed at this site in 1994 to conduct water balance studies. Each lysimeter is a 2-m by 4-m by 2-m deep steel tank filled with native alluvium at a bulk density of about 1.5 kg/m<sup>3</sup> (Scanlon et al. 2005 [DIRS 175977]). The lysimeter schematics are shown in Figure 7.1.2-1 in Section 7.1.2. One lysimeter is vegetated with the creosote bush, four-wing salt bush, and annual grasses at the approximate density of the surrounding landscape (Desotell et al. 2006 [DIRS 176858]). This lysimeter will be referred as vegetated lysimeter. Another lysimeter is maintained under bare soil conditions and is referred to as bare soil lysimeter.

Eighteen core samples were collected throughout the lysimeter depth profile in 10-cm increments. The measured soil hydraulic properties are reported by Desotell et al. (2006 [DIRS 176858]) and include:

- Saturated hydraulic conductivity (geometric mean): 14 cm/hr
- Residual moisture content: 0.04 m<sup>3</sup>/m<sup>3</sup>
- Porosity: 0.357 m<sup>3</sup>/m<sup>3</sup>
- van Genuchten parameter alpha: 0.0328 cm<sup>-1</sup>
- van Genuchten parameter n: 1.57.

Based on these parameters, the field capacity is 0.117 m<sup>3</sup>/m<sup>3</sup> (calculated using pressure of  $-1/3$  bar), and wilting point is 0.044 m<sup>3</sup>/m<sup>3</sup> (calculated using pressure of  $-60$  bars). Since a higher pressure may be more appropriate for the coarse-grained textured soils (up to  $-1/10$  bars) than the pressure of  $-1/3$  bars (medium textured soils), the bare soil lysimeter storage data were analyzed during periods with heavy precipitation over a few or more consecutive days. The largest storage value was 277.3 mm. This corresponds to the moisture content of 0.139 m<sup>3</sup>/m<sup>3</sup> and a pressure of  $-2/10$  bars. This is consistent with the pressure range of  $-1/3$  bars to  $-1/10$  bars at which field capacity is calculated.

The lysimeter storage observations are available for the period of time from 03/30/94 until 12/31/04. The storage data were copied from Di Sanza (2006 [DIRS 178797]) into the file *NTSLysimeter.xls* (NTS folder in the Validation Output DTN: SN0607T0502206.016). The precipitation data are available for the lysimeter site. They were obtained from the file (Di Sanza 2006 [DIRS 178797]) and copied into the worksheet *Original Climate Data* in *NTSLysimeter.xls* (NTS folder in the Validation Output DTN: SN0607T0502206.016).

The temperature data were not available for the lysimeter site. The daily minimum, maximum, and average temperatures collected at Well 5B located 1.5 km from the lysimeter site were used instead. These data were downloaded from DTN: MO0607SEPMED94.000 [DIRS 178079] into the worksheet *Original Climate Data* in *NTSLysimeter.xls* (NTS folder in the Validation Output DTN: SN0607T0502206.016). The temperature data in this data set are not available for some

dates. The data gaps were filled with the temperatures that were calculated using linear interpolation between the closest points in which the data were available. The interpolated values are outlined in yellow in the *Original Climate Data* worksheet.

Since the MASSIF model can be run only for the whole number of the water years, the bare soil lysimeter simulations were for the period of time from 10/01/94 to 09/30/05. The climate data for the period of time from 01/01/05 to 09/30/05 were filled with the corresponding data from the previous year. This was done to satisfy MASSIF input requirements (whole water year). The results of the calculations for this period of time were not used. This does not affect in any way the results of the calculations for the period of time prior to 01/01/05. The climate data and the bare soil lysimeter storage data are in *BS Input Data* worksheet in *NTSLysimeter.xls*. These data were copied into the built-in Excel files in the MASSIF interfaces *Bare Soil Lysimeter* and *BS and Veget Optimization*. The data are in the format required by MASSIF and corresponding MASSIF interfaces.

The vegetated lysimeter was irrigated for about a year to establish the vegetation cover, but the irrigation rates are not available, and it took about 1.5 years for the transplanted vegetation to equilibrate with moisture conditions in the lysimeter box. Consequently, the period of observations for the vegetated lysimeter was from 10/01/95 until 09/30/05. As in the case of the bare soil lysimeter, the climate data for the period of time from 01/01/05 to 09/30/05 were filled with the corresponding data from the previous year. The climate data and the vegetated lysimeter storage data are in *Veg Input Data* worksheet in *NTSLysimeter.xls*. These data were copied into the built-in Excel files in the MASSIF interfaces *Vegetated Lysimeter* and *BS and Veget Optimization*. The data are in the format required by MASSIF and corresponding MASSIF interfaces.

Three MASSIF interfaces were designed to simulate NTS lysimeters. The input data used in these interfaces and the interface functions are described below.

### **J1.1 MASSIF INTERFACE BARE SOIL LYSIMETER**

The interface is located in folder *Validation Analyses/Lysimeter* in the MASSIF package (Output DTN: SN0701T0502206.037). This interface was specifically designed to simulate soil water storage measured in the bare soil lysimeter. The interface reads the embedded Excel file with the climate and storage data. As discussed above, these data were copied into this file from *BS Input Data* worksheet in *NTSLysimeter.xls* (NTS folder in Validation Output DTN: SN0607T0502206.016).

The interface reads an external Excel file with the geospatial data provided in the format required by MASSIF. The file name is *NTS\_location.csv*. It is located in the same directory *Lysimeter*, in which the interface is located. The file consists of two lines; each line represents one watershed cell. The lysimeter site is represented by the first cell in this file (the first line). The second cell is not used in the analysis. The geospatial information includes the cell identification number (arbitrary number in this case), site latitude and longitude in degrees and UTM coordinates in meters, site elevation in meters, slope in degrees, aspect, soil type, soil depth class, bedrock type, *PVR* (potential vegetation response), and an identification number of the cell from which runoff is routed to this cell (it is set to -3 to exclude the run-on component using the

corresponding MASSIF option). The site longitude, latitude, and elevation are defined as described above. The slope at the site is  $1^\circ$  (as described above). Soil type is set equal to 5, soil depth class is set equal to 2, and bedrock type is set equal to 406. The  $PVR$  is set equal to 1. As described in Section 7.1.2, the parameter  $PVR$  can be set equal to an arbitrary value as long as the  $K_{cb}$  value is estimated by adjusting  $C_{kcb}$ . The  $PVR$  was set equal to 1 for convenience.

The other parameters required to run MASSIF are defined directly within the interface as follows:

- Reference elevation is set equal to site elevation (976 m) to avoid correction of temperature and precipitation with regard to the reference elevation.
- The albedo is set equal to 0.22 (see Sections 6.3.3 and 6.3.4)
- Weather parameters, such as first and last day of winter and precipitation duration coefficients were set equal to the values defined for the Present-Day climate (Sections 6.3.3 and 6.3.4).
- Dew point offset parameters were set equal to the default MASSIF values.
- Soil porosity and hydraulic conductivity of soil type 5 are set equal to the following values: porosity is  $0.357 \text{ m}^3/\text{m}^3$  and hydraulic conductivity is 14 cm/hr. This redefines the values that MASSIF reads from the built-in look-up table with the soil properties for soil type 5.
- Bedrock hydraulic conductivity of bedrock type 406 is set equal to  $10^{-10}$  m/s. This redefines the value that MASSIF reads from the built-in look-up table with the bedrock properties. This initial value was changed within a range from 0 to  $4 \times 10^{-5}$  m/s as a part of a sensitivity analysis. The high end of this range corresponds to the maximum hydraulic conductivity of the bedrock at the Yucca Mountain site. The low end of this range is consistent with a sealed bottom boundary of the lysimeter. The bedrock hydraulic conductivity did not affect the results of the calculations.
- The soil depth of the Soil Depth Class 2 is set equal to 2.00 m.
- The rooting depth was specified equal to 2.00 m.
- The vegetation cover is set equal to 0 (there is no vegetation).
- $C_{kcb}$  coefficients (interception and slope of the  $\text{NDVI}'-K_{cb}$  linear regression line) are set equal to 0 (there is no vegetation).
- The plant height is set equal to 0.0 m (there is no vegetation).
- The water stress parameter  $p$  is set equal to 0.0.



- The evaporation depth  $Z_e$  is set equal to 100 mm (this parameter is not a part of the optimization scheme; however, it can be manually adjusted if needed).
- Readily evaporable water  $rew_l$  is set equal to 6 mm (this parameter is not a part of the optimization scheme; however, it can be manually adjusted if needed).
- The diffusive evaporation parameter  $K_{c\_min}$  is set equal to 0.0135 based on the results of optimization implemented in MASSIF interface **BS and Veget Optimization**. This parameter can also be adjusted manually.
- Sublimation and snowmelt coefficient are set equal to default MASSIF values ( $C_{sublime} = 0.1$  and  $C_{snowmelt} = 2.0$ ).
- The initial moisture content in each layer is calculated as the lysimeter storage measured on 10/01/94 divided by the lysimeter depth. The resulting moisture content was  $0.084 \text{ m}^3/\text{m}^3$ .
- The field capacity ( $\theta_l$ ) and wilting point ( $\theta_2$ ) are calculated using (Simunek et al. 2005 [DIRS 178140], Equation 2.26):

$$\theta_i = \theta_r + s_i \times (\theta_s - \theta_r), \quad i=1,2 \quad (\text{Eq. J-1})$$

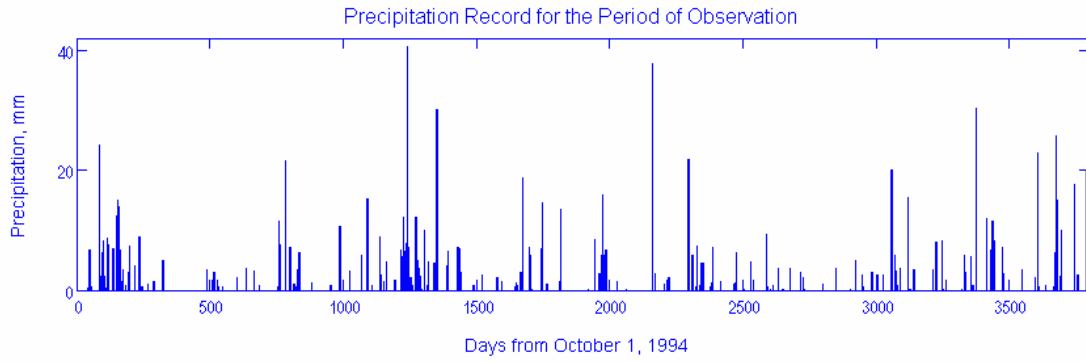
$$s_i = [(1 + (h_i \times \alpha)^n)^{-m}]$$

$$m = 1 - 1/n$$

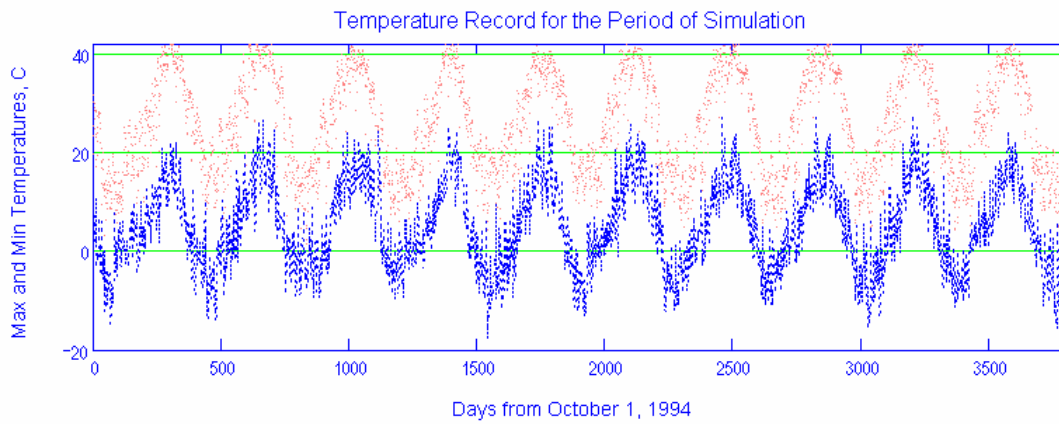
$$h_1 = -336.6 \text{ cm } (-1/3 \text{ bar}) \text{ and } h_2 = -61,200 \text{ cm } (-60 \text{ bars})$$

- where  $\theta_r$  is residual porosity,  $\theta_s$  is saturated porosity, and  $\alpha$ ,  $n$ , and  $m$  are van Genuchten parameters defined by Simunek et al. (2005 [DIRS 178140]). The resulting field capacity and wilting point are  $0.117 \text{ m}^3/\text{m}^3$  and  $0.044 \text{ m}^3/\text{m}^3$ , respectively.
- Field capacity and wilting point of soil type 5 are set equal to  $0.117 \text{ m}^3/\text{m}^3$  and  $0.044 \text{ m}^3/\text{m}^3$ . This redefines the values that MASSIF reads from the built-in look-up table with the soil properties for soil type 5.

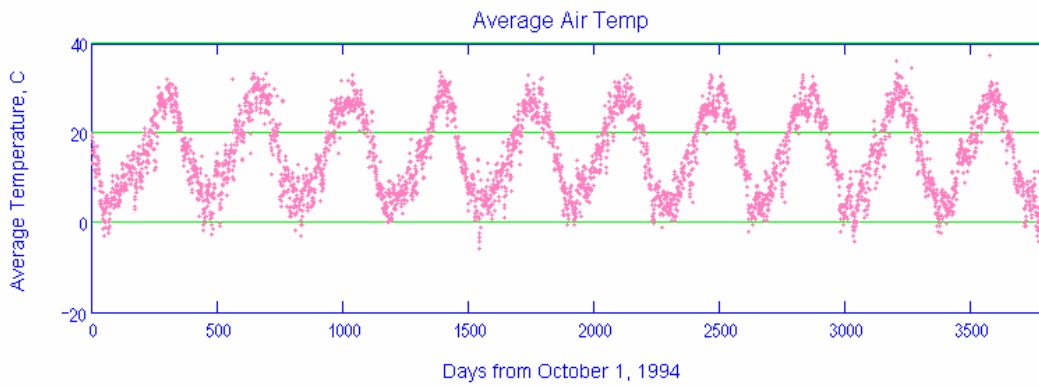
The interface performs the following functions. The interface displays the climate data. This includes the plots of the daily precipitation record and minimum, maximum, and average daily air temperatures. The percentage of time when mean daily temperature is below  $0^\circ\text{C}$  is calculated (1.3%). The examples are shown in the Figure J-1.



(a)



(b)

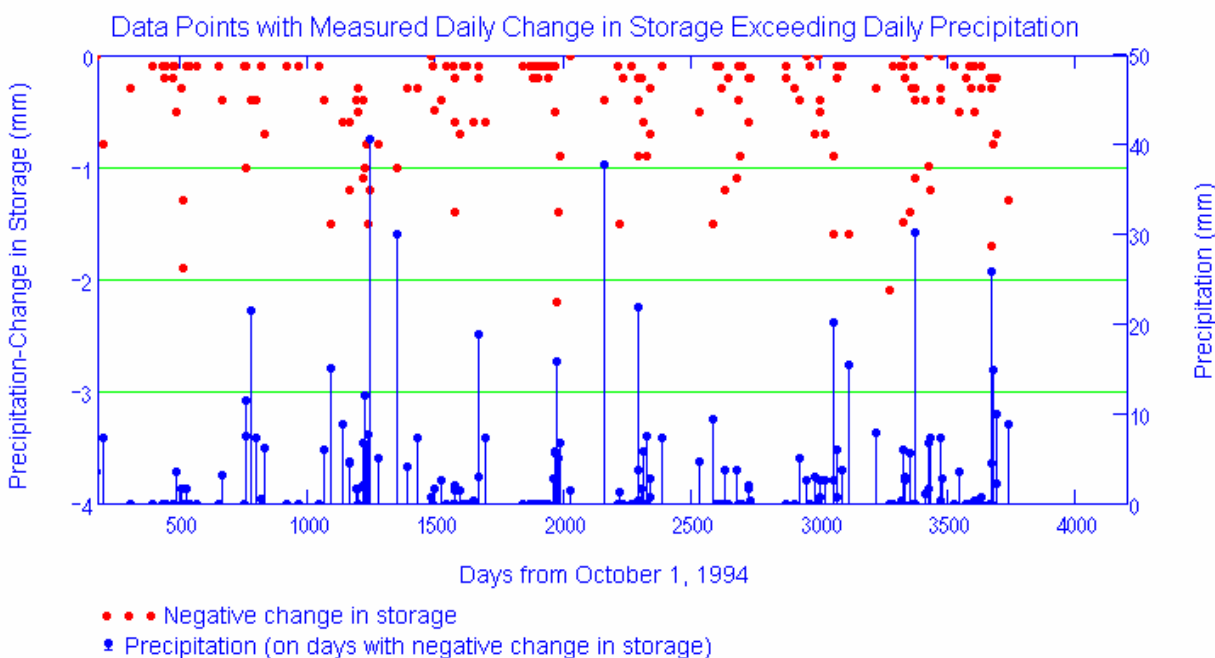


(c)

Source: Output DTN: SN0701T0502206.037, *Welcome to Massif\Massif\Validation Analyses\Lysimeter\Bare Soil Lysimeter.xmcd*.

Figure J-1. Climate Data Plots for the MASSIF Simulation of Storage in the Bare Soil Lysimeter

The interface calculates the difference between the daily precipitation and the daily change in lysimeter storage. This difference should be either equal to 0 (if there is no evaporation) or be greater than 0 (if there is evaporation). The negative difference indicates that the precipitation was underestimated. The data points in which this difference is negative are shown in Figure J-2. Both the difference between the precipitation and storage and precipitation are shown.



Source: Output DTN: SN0701T0502206.037, *Welcome to Massif\Massif\Validation Analyses\Lysimeter\Bare Soil Lysimeter.xmcd*.

Figure J-2. Days with Negative Daily Difference between Precipitation and Change in Storage Calculated using MASSIF Bare Soil Lysimeter Interface

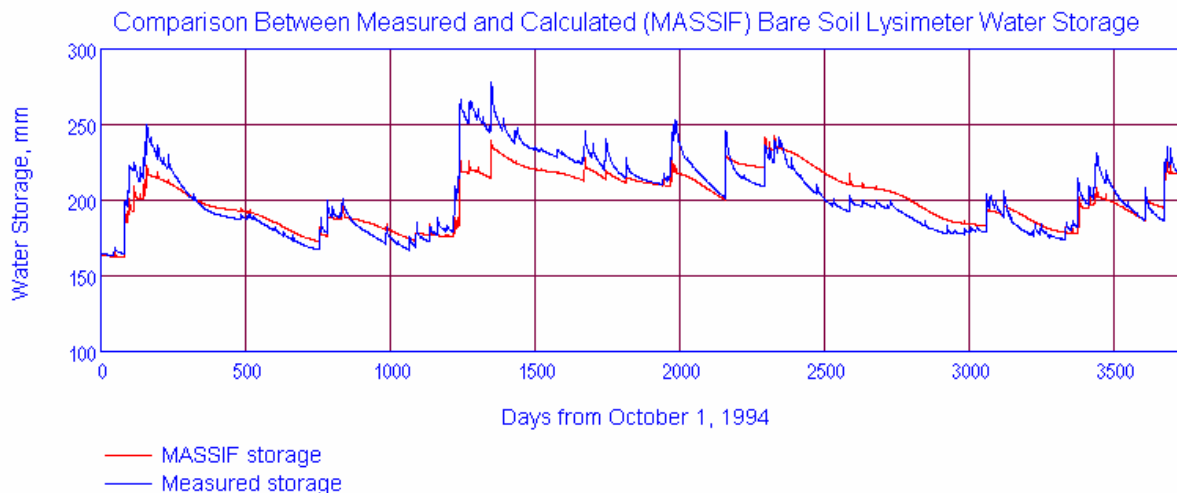
There are 196 points (5% of the data) in which precipitation was underestimated. This is consistent with the fact that rain gauges are subject to under-measurement caused by (1) splash out of drops, (2) blow-by of drops due to Venturi effects, and (3) evaporation of intercepted drops along the sides of the collector (Sevruk 1992 [DIRS 177480]). As can be seen from this figure, these points coincide in many cases with the large intensity precipitation events. The mean intensity of the precipitation events in these points is 6.9 mm, and the mean intensity of the precipitation events based on all precipitation data is 4.2 mm. The maximum negative difference was 3.4 mm. Since evaporation is calculated as the difference between precipitation and storage, the same error in precipitation measurement will result in the corresponding error in the evaporation estimate.

The interface runs MASSIF, stores the results of calculations, and calculates the lysimeter storage as a sum of the water depths within the four model layers. The interface displays the measured and calculated daily lysimeter storage. An example is shown in Figure J-3. The

parameters placed in the yellow box located just above the storage plot can be manually adjusted. Each adjustment results in a recalculation and a display of newly calculated storage values in the storage plot. This function was used in the sensitivity analysis. For the period of simulation, the interface calculates the water balance constituents such as total precipitation, total evaporation, total run-on, total runoff, and total infiltration. The total run-on is always zero since the lysimeter cell is not connected to any other cell in the geospatial file. The interface calculates the objective function value using Equation 7.1.2-2.

#### Adjustable Evaporation Parameters

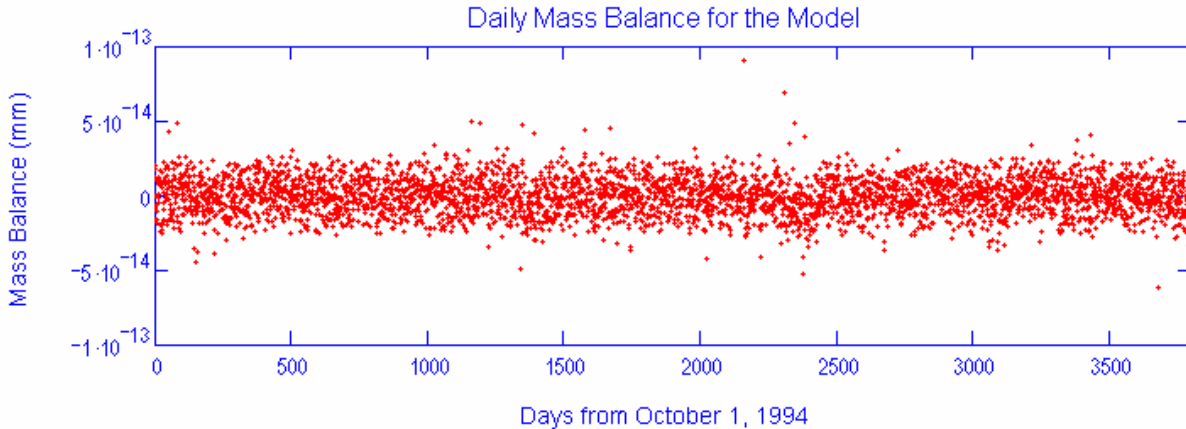
Param1 = 100-mm - Evaporation Depth  
 Param2 = 0.0135 - Diffusive Evaporation Parameter  
 Param3 = 6-mm - Readily Evaporable Water  
 Param4 = 0.117 - Field Capacity  
 Param5 = 0.044 - Wilting Point



Source: Output DTN: SN0701T0502206.037, *Welcome to Massif\Massif\Validation Analyses\Lysimeter\Bare Soil Lysimeter.xmcd*.

Figure J-3. Calculated versus Measured Lysimeter Storage using MASSIF Bare Soil Lysimeter Interface

The interface then checks the daily mass balance for the simulation and displays it as shown in Figure J-4.

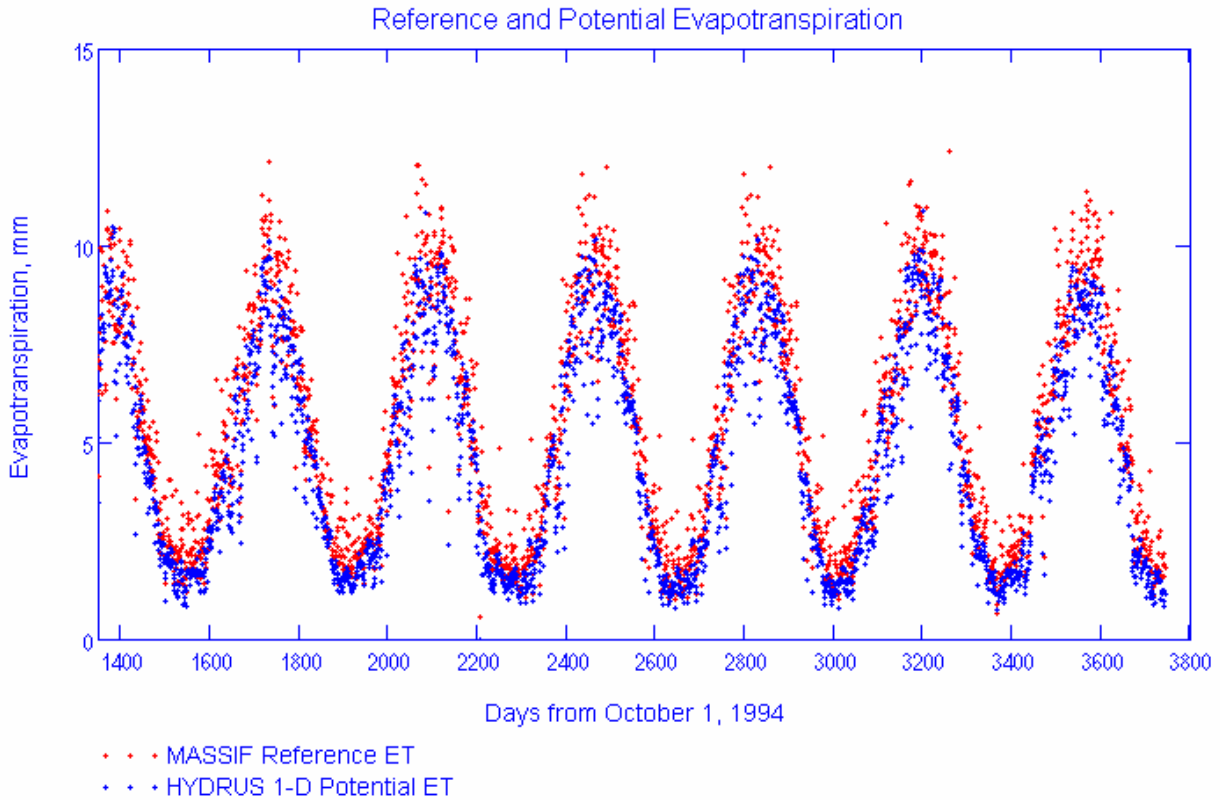


Source: Output DTN: SN0701T0502206.037, *Welcome to Massif\Massif\Validation Analyses\Lysimeter\Bare Soil Lysimeter.xmcd*.

Figure J-4. Daily Mass Balance Displayed by MASSIF Bare Soil Lysimeter Interface

The interface reads an external Excel file *Hydrus1D Data&Results.xls* that contains HYDRUS-1D input data (including potential evapotranspiration) and modeling results (daily storage and infiltration). These data are in worksheet *Bare Soil*. The description of the HYDRUS-1D modeling setup and details on how the potential evapotranspiration was calculated are provided below.

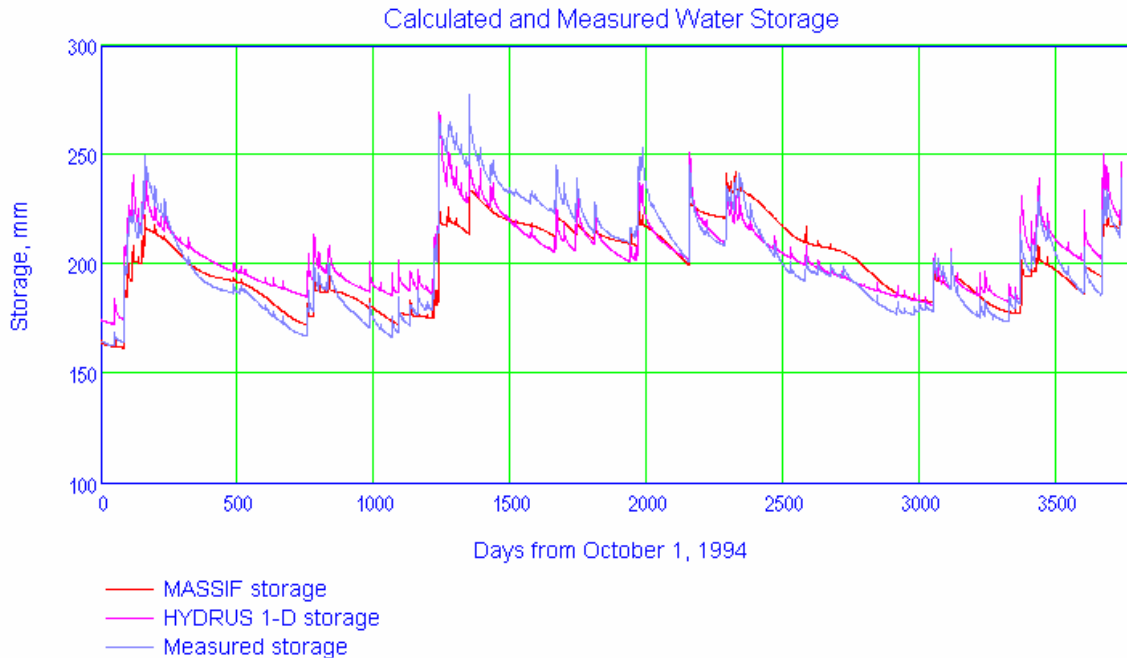
The interface displays the reference evapotranspiration calculated by MASSIF and potential evapotranspiration used as HYDRUS-1D boundary condition. An example is shown in Figure J-5.



Source: Output DTN: SN0701T0502206.037, *Welcome to Massif\Massif\Validation Analyses\Lysimeter\Bare Soil Lysimeter.xmcd*.

Figure J-5. Reference Evapotranspiration calculated with MASSIF and Potential Evapotranspiration Calculated using HYDRUS-1D.

The interface displays the observed lysimeter storage and lysimeter storage calculated with MASSIF and HYDRUS-1D as shown in Figure J-6.



Source: Output DTN: SN0701T0502206.037, *Welcome to Massif\Massif\Validation Analyses\Lysimeter\Bare Soil Lysimeter.xmlcd*.

Figure J-6. Calculated (MASSIF and HYDRUS) and Measured Lysimeter Storage Displayed by MASSIF Bare Soil Lysimeter Interface

## J1.2 MASSIF INTERFACE *VEGETATED LYSIMETER*

The interface is located in folder *Validation Analyses/Lysimeter* in the MASSIF package (Output DTN: SN0701T0502206.037). This interface was specifically designed to simulate the vegetated lysimeter. The interface reads the embedded Excel file with the climate and storage data. As discussed above, these data were copied into this file from the *Veg Input Data* worksheet in *NTSLysimeter.xls* (*NTS* folder in the Validation Output DTN: SN0607T0502206.016). The interface reads an external Excel file *NTS\_location.csv* with the geospatial data provided in a format required by MASSIF. The lysimeter site is represented by the second cell in this file (the second line). This is the same file used for bare soil lysimeter. The input data provided in the second line of this file are the same as described above under the interface *Bare Soil Lysimeter*.

The other parameters required to run MASSIF are defined directly within the interface. These parameters are described below. Only the parameters that differ from the ones described under the bare soil lysimeter interface are provided below.

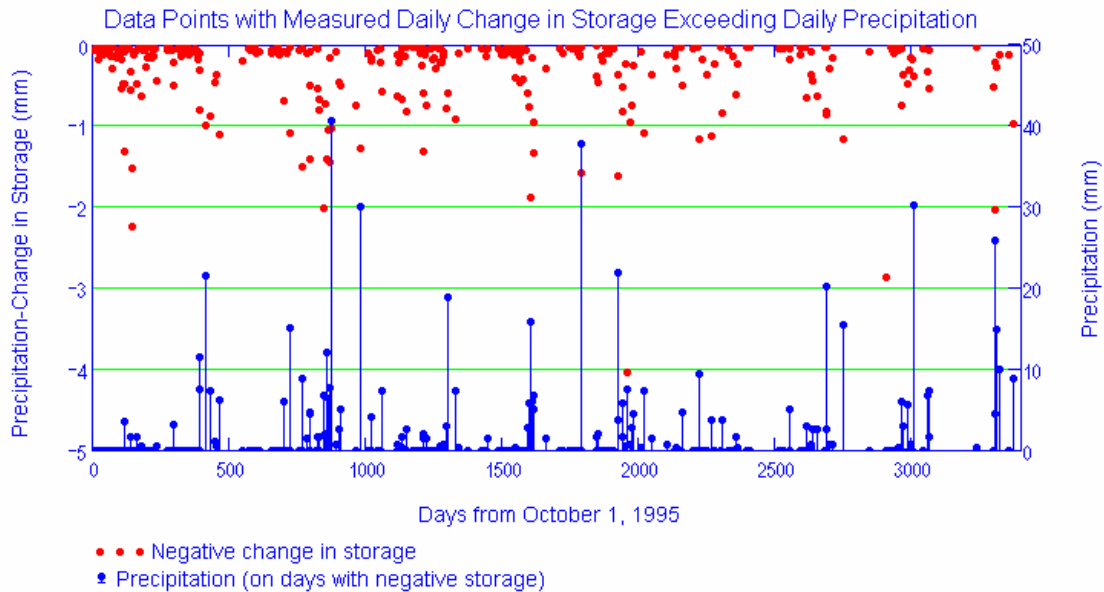
- The vegetation cover is set equal to 0.26 based on the results of optimization implemented in MASSIF interface *BS and Veget Optimization*. This parameter can also be adjusted manually.

- The  $C_{kcb}$  coefficient for slope is set equal to 2.4 based on the results of optimization implemented in MASSIF interface ***BS and Veget Optimization***. This parameter can be manually adjusted if needed. The  $C_{kcb}$  coefficient for intercept is set equal to 0.
- The plant height is set equal to 0.3 m (this is a site-specific parameter).
- The water stress parameter  $p$  is set equal to the default value of 0.65 (see Sections 6.3.3 and 6.3.4).
- The initial moisture content in each layer is calculated as the lysimeter storage measured on 10/01/95 divided by the lysimeter depth. The resulting moisture content is  $0.053 \text{ m}^3/\text{m}^3$ .

The interface performs the following functions. The interface displays the climate data. This includes the plot of the daily precipitation record and minimum, maximum, and average daily air temperatures. The percentage of time when mean daily temperature is below  $0^\circ\text{C}$  is calculated (1.3%). The plots are the same as the ones shown above using the MASSIF interface ***Bare Soil Lysimeter***.

The interface calculates the difference between the daily precipitation and daily change in lysimeter storage. This difference should be either equal to 0 (if there is no evapotranspiration) or be greater than 0 (if there is evapotranspiration). The negative difference indicates that the precipitation was underestimated. The data points in which this difference is negative are shown in Figure J-7. Both the daily precipitation and the difference between the precipitation and change in storage are shown.





Source: Output DTN: SN0701T0502206.037, *Welcome to Massif\Massif\Validation Analyses\Lysimeter\Vegetated Lysimeter.xmcd*.

Figure J-7. Data Points with Negative Daily Difference between Precipitation and Change in Storage Using the MASSIF Vegetated Lysimeter Interface

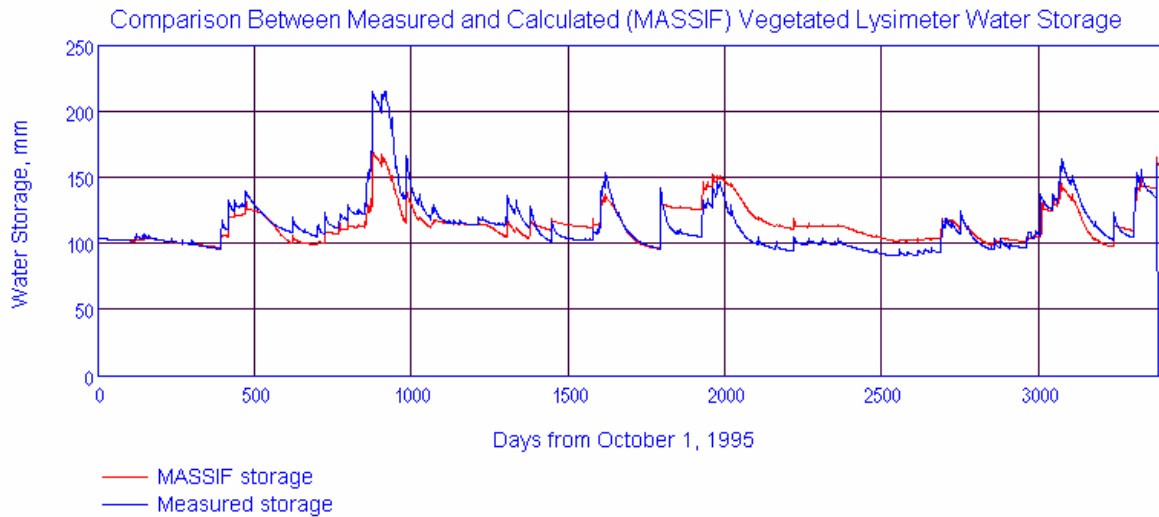
There are 341 points (10% of the data) in which precipitation was underestimated. As in the bare soil lysimeter case, these points coincide with large intensity precipitation events. The maximum negative difference is 4.1 mm. Since the ET is calculated as the difference between precipitation and storage, the same error in precipitation measurement will result in a corresponding error in the ET estimate.

The interface runs MASSIF, stores the results of calculations, and calculates the lysimeter storage as a sum of the water depths within the four model layers. The interface displays the measured and calculated daily lysimeter storage. An example is shown in Figure J-8. The parameters placed in the yellow box located just above the storage plot can be manually adjusted. Each adjustment results in a recalculation and a display of newly calculated storage values in the storage plot. This function is used in the sensitivity analysis.

For the period of simulation, the interface calculates the water balance constituents such as total precipitation, total evapotranspiration, total run-on, total runoff, and total infiltration. The total run-on is always zero since the lysimeter cell is not connected to any other cell in the geospatial file.

**Adjustable Evaporation Parameters**

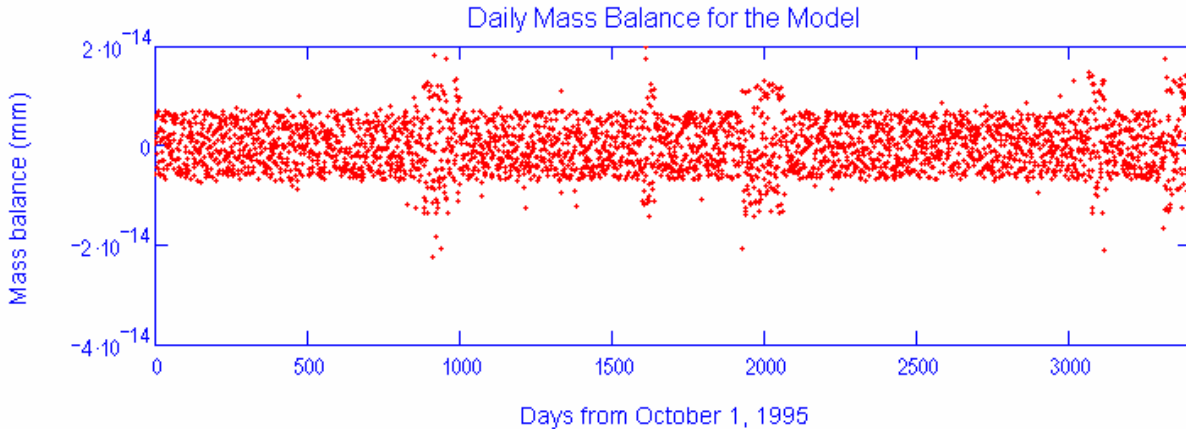
Param1 = 0.26 - Canopy fraction  
Param2 = 2.40 - NDVI-Kcb slope  
Param3 = .0135 - Diffusive evaporation parameter  
Param8 = 0.65 parameter p  
Param5 = 6 Readily evaporable water  
Param6 = 0.117 Field capacity  
Param7 = 0.044 Wilting point



Source: Output DTN: SN0701T0502206.037, *Welcome to Massif\Massif\Validation Analyses\Lysimeter\Vegetated Lysimeter.xmcd*.

Figure J-8. Calculated versus Measured Lysimeter Storage Plot Displayed by *Vegetated Lysimeter* Interface

The interface then checks the daily mass balance for the simulation and displays it as shown in Figure J-9.



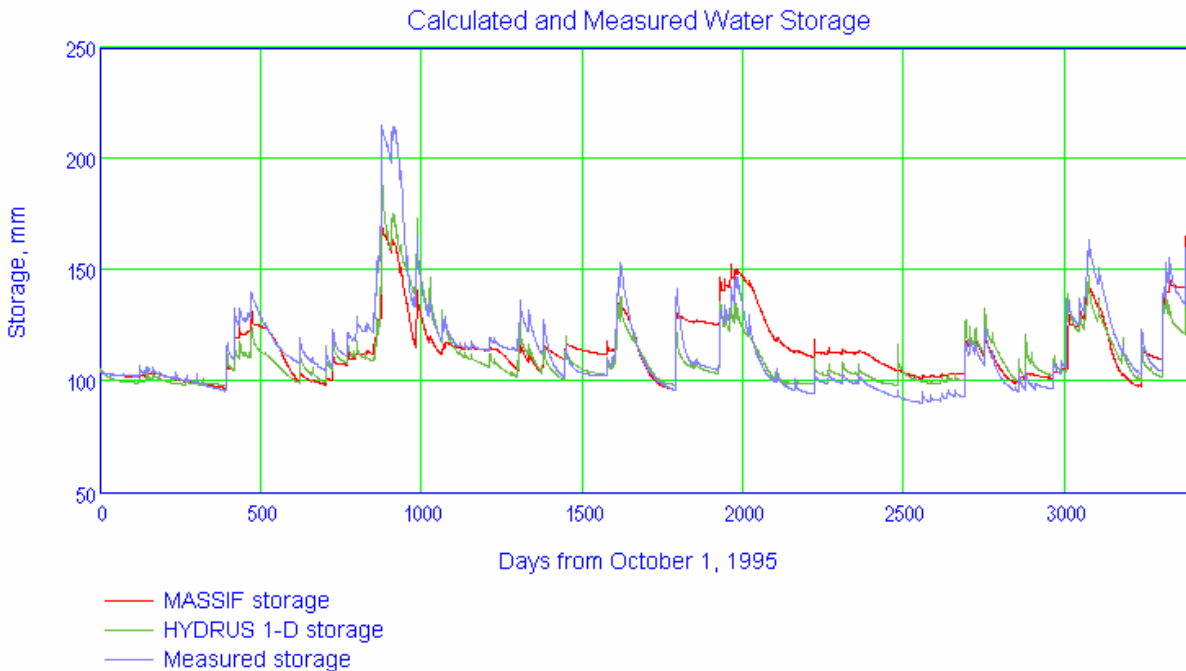
Source: Output DTN: SN0701T0502206.037, *Welcome to Massif\Massif\Validation Analyses\Lysimeter\Vegetated Lysimeter.xmcd*.

Figure J-9. Daily Mass Balance Displayed by *Vegetated Lysimeter* Interface

The interface reads an external Excel file *Hydrus1D Data&Results.xls* that contains HYDRUS-1D input data (including potential evapotranspiration) and modeling results (daily storage and infiltration). These data are in worksheet *Vegetated*. The description of HYDRUS-1D modeling setup and details on how the potential evapotranspiration was calculated are provided below.

The interface displays the reference evapotranspiration calculated by MASSIF and the potential evapotranspiration used as HYDRUS-1D boundary condition. The plot is the same as the ones shown above under the MASSIF interface *Bare Soil Lysimeter*.

The interface displays the observed lysimeter storage and the lysimeter storage calculated with MASSIF and HYDRUS-1D as shown in Figure J-10.



Source: Output DTN: SN0701T0502206.037, *Welcome to Massif\Massif\Validation Analyses\Lysimeter\Vegetated Lysimeter.xmlcd*.

Figure J-10. Calculated (MASSIF and HYDRUS-1D) and Measured Lysimeter Storage Displayed by Vegetated Lysimeter Interface

The interface calculates the mean root square error between the observed storage values and those calculated with MASSIF and HYDRUS-1D, and also between storage values calculated with MASSIF and those calculated with HYDRUS-1D. It displays the differences between the calculated and measured values in the form of histograms. The discussion of these results is provided in Section 7.1.2.

### J1.3 MASSIF INTERFACE *BS AND VEGET OPTIMIZATION*

The interface is located in folder *Validation Analyses/Lysimeter* in the MASSIF package (Output DTN: SN0701T0502206.037). This interface was specifically designed to estimate evapotranspiration and soil parameters by minimizing differences between the calculated and measured daily water storage values in both bare soil and vegetated lysimeters. The interface reads the two embedded Excel files with the climate and storage data for the bare soil and vegetated lysimeters. The data for the bare soil lysimeter are from the *BS Input Data* worksheet in *NTSLysimeter.xls* and the data for the vegetated lysimeter are from the *Veg Input Data* worksheet in *NTSLysimeter.xls* (*NTS* folder in Validation Output DTN: SN0607T0502206.016). These are the same data used in the simulation performed by interfaces *Bare Soil Lysimeter* and *Vegetated Lysimeter*.

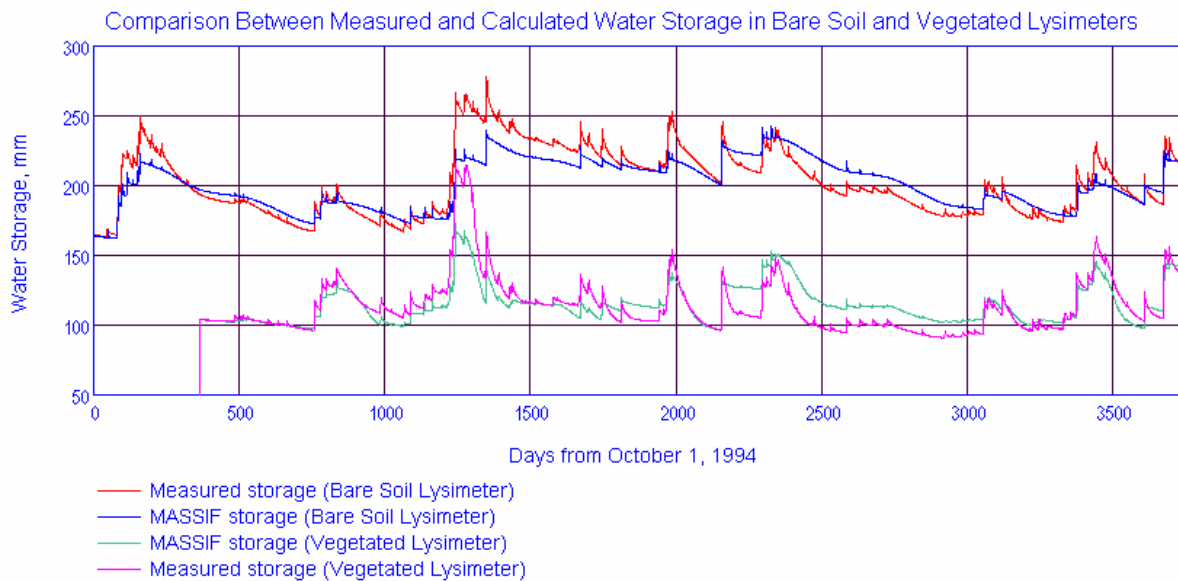
The interface reads an external Excel file *NTS\_location.csv* with the geospatial data provided in a format required by MASSIF. The bare soil lysimeter site is represented by the first cell in this file and the vegetated lysimeter site by the second cell. As explained above, the input data in these two cells are the same. This is the same file used in *Bare Soil Lysimeter* and *Vegetated Lysimeter* interfaces. The input data read from this file are described above under the interface *Bare Soil Lysimeter*.

The other parameters required to run MASSIF are defined directly within the interface as described above under the *Bare Soil Lysimeter* and *Vegetated Lysimeter* interfaces. The interface performs the following functions. The interface defines two optimization schemes in accordance with Equations 7.1.2-2 and 7.1.2-3. This includes the definition of the objective functions and initial values and ranges for the parameters to be estimated.

The optimization parameters for Scheme 1 are diffusive evaporation parameter  $K_{c\_min}$ , vegetated lysimeter canopy fraction  $f_c$ , and vegetated lysimeter parameter  $C_{kcb}$ . The optimization parameters for Scheme 2 are diffusive evaporation parameter  $K_{c\_min}$ , vegetated lysimeter canopy fraction  $f_c$ , vegetated lysimeter parameter  $C_{kcb}$ , and field capacity  $\theta_f$ .

The interface runs the conjugate gradient minimization procedure, which is a built-in MathCAD function. The minimization procedure returns the values of the optimization scheme parameters that result in the minimum value of the corresponding objective functions. The interface lets the user define the optimization scheme parameters based on the result of the optimization. It then performs the final runs, one for the bare soil lysimeter and one for the vegetated soil lysimeter. The interface then calculates the mean root square error for the bare soil and the vegetated lysimeters.

The interface displays the observed bare soil and vegetated lysimeter storage values and the calculated bare soil and vegetated lysimeter storage values. An example is shown in Figure J-11.



Source: Output DTN: SN0701T0502206.037, *Welcome to Massif\Massif\Validation Analyses\Lysimeter\BS and Veget Optimization.xmcd*.

Figure J-11. Calculated and Measured Lysimeter Storage Displayed by BS and Veget Lysimeter Interface

The interface outputs the observed daily storage values and those calculated with MASSIF for bare soil and vegetated lysimeters into an embedded Excel file to assist in further data processing and display. These data were used to generate Figure 7.1.2.1-3 in Section 7.1.2. A discussion of these results is provided in Section 7.1.2.

#### J1.4 HYDRUS-1D MODELING SETUP

The MASSIF simulations were compared to the simulations performed using HYDRUS-1D code (Šimunek et al. 2005 [DIRS 178140]). The HYDRUS-1D program numerically solves the Richards' equation for one-dimensional variably saturated water flow and heat and solute transport. The short description of HYDRUS-1D is provided in Section 6.2.4.1.

HYDRUS-1D was obtained from the Yucca Mountain Project Software Configuration Manager. The related communication and installation record are in **HYDRUS\_Gen** directory (Validation Output DTN: SN0607T0502206.016). All the input and output HYDRUS-1D files for the bare soil lysimeter are in subdirectory **NTSBar\_P** in the **HYDRUS\_Model** directory in **NTS** folder in Validation Output DTN: SN0607T0502206.016. The input and output files in this subdirectory were created by running the HYDRUS-1D file **NTSBar\_P.h1d** located in the **HYDRUS\_Model** directory. All the input and output HYDRUS-1D files for the vegetated lysimeter are in subdirectory **VL\_90\_10\_Snow** in the **HYDRUS\_Model** directory in the **NTS** folder in Validation Output DTN: SN0607T0502206.016. The input and output files in this subdirectory were created by running HYDRUS-1D file **VL\_90\_10\_Snow.h1d** located in the **HYDRUS\_Model** directory.

The HYDRUS-1D modeling setup is described as follows. The simulated processes are water flow (including snow hydrology) and heat transport. The root uptake is simulated as the vegetated lysimeter. The depth of the soil profile is 200 cm. It is represented with 101 nodes. The first node is at the land surface ( $z = 0$  cm) and the last node is at the lysimeter bottom (200 cm). The nodes are 2 cm apart. The soil profile is homogeneous. The initial moisture content is 0.08765 calculated as the lysimeter storage on 03/30/94 divided by the lysimeter depth. The initial temperature is 20°C. The van Genuchten model in HYDRUS-1D is used to represent relationships between the saturation and pressure head and between the saturation and hydraulic conductivity. The soil parameters are:

- saturated hydraulic conductivity is 336 cm/d
- saturated porosity is 0.357
- residual moisture content is 0.04
- van Genuchten parameter  $\alpha$  is 0.0328 1/cm
- van Genuchten parameter  $n$  is 1.57
- pore connectivity parameter  $l$  is 0.5. Šimunek et al. (2005 [DIRS 178140]) suggest leaving this parameter at its default value of 0.5.

The upper boundary is an atmospheric boundary with specified daily potential evaporation, potential transpiration (for the vegetated lysimeter only), precipitation, and temperature. The daily values of these parameters are defined for the entire period of simulation, which are 3,930 days for the bare soil lysimeter (03/30/94 to 12/31/04) and 3,380 days for the vegetated lysimeter (10/01/95 to 12/31/04).

The potential evapotranspiration  $ET_p$  was calculated using the Hargreaves formula (Jensen et al. 1997 [DIRS 177103]). This method was selected because the only site data required are daily average, maximum, and minimum air temperatures.

$$ET_p = 0.0023R_a (T_m + 17.8)\sqrt{TR} \quad (\text{Eq. J-2})$$

where  $R_a$  is the extraterrestrial radiation in the same units as  $ET_p$  (e.g., mm d<sup>-1</sup> or J m<sup>-2</sup>s<sup>-1</sup>),  $T_m$  is the daily mean air temperature, (°C), and  $TR$  is the temperature range between mean daily maximum and minimum air temperatures (°C). The extraterrestrial radiation,  $R_a$  (J m<sup>-2</sup>s<sup>-1</sup>), can be calculated as follows:

$$R_a = \frac{G_{sc}}{\pi} d_r (\omega_s \sin \varphi \sin \delta + \cos \varphi \cos \delta \sin \omega_s) \quad (\text{Eq. J-3})$$

where  $G_{sc}$  is the solar constant (J m<sup>-2</sup>s<sup>-1</sup>; 1,360 W m<sup>-2</sup>),  $\varphi$  is the site latitude (rad),  $\omega_s$  is the sunset hour angle (rad),  $d_r$  is the relative distance between Earth and Sun (-), and  $\delta$  is the solar declination (rad). The last three variables are calculated as follows:

$$\omega_s = \arccos(-\tan \varphi \tan \delta) \quad (\text{Eq. J-4})$$

$$d_r = 1 + 0.033 \cos\left(\frac{2\pi}{365} J\right) \quad (\text{Eq. J-5})$$

$$\delta = 0.409 \sin\left(\frac{2\pi}{365} J - 1.39\right) \quad (\text{Eq. J-6})$$

where  $J$  is the number of the day in the year (-).

The solar constant  $G_{sc}$  can be converted from  $\text{J m}^{-2}\text{s}^{-1}$  to  $\text{m s}^{-1}$  as follows:

$$\begin{aligned} G_{sc} &= \lambda ET_0 = \lambda \rho_w G_{sc}^* \\ \lambda &= 2.501 * 10^6 - 2369.2T \\ G_{sc}^* &= \frac{G_{sc}}{\lambda \rho_w} = \frac{G_{sc}}{\rho_w (2.501 * 10^6 - 2369.2T)} = \\ &= \frac{1360}{10^3 * 2.454 * 10^6} = 5.54 * 10^{-7} \text{ m/s} = 4.789 \text{ cm/d} \end{aligned} \quad (\text{Eq. J-7})$$

where  $\lambda ET_0$  is the latent heat flux of evaporation ( $\text{J m}^{-2}\text{s}^{-1}$ ),  $\lambda$  is the latent heat of vaporization of water ( $\text{J kg}^{-1}$ ,  $\text{ML}^2\text{T}^{-2}\text{M}^{-1}$ ,  $\text{L}^2\text{T}^{-2}$ ),  $T$  is temperature ( $^\circ\text{C}$ ), and  $\rho_w$  is the density of liquid water ( $\text{ML}^{-3}$ ).

The input data used in these calculations and the resulting potential evapotranspiration values are in worksheet *PET* of *NTSLysimeter.xls* (*NTS* folder in Validation Output DTN: SN0607T0502206.016). The potential transpiration was assumed to be equal to 0.1 of the potential evapotranspiration. This corresponds to a vegetation fraction of 10 percent. The vegetation fractions of the LA association are 0.11, 0.15, and 0.21 for dry, average, and wet years, respectively (Appendix D). The NTS lysimeter site is drier than most of the Yucca Mountain model domain (based on elevation), so the use of a vegetation fraction of 10% is reasonable. In addition, a value of 20% was used and there was little change in soil water storage.

The potential evaporation is equal to potential evapotranspiration in the case of the bare soil lysimeter. The potential evapotranspiration values were copied into the built-in HYDRUS-1D time-dependent boundary condition spreadsheet for the bare soil lysimeter. The potential evaporation and transpiration values were copied into the built-in HYDRUS-1D time-dependent boundary condition spreadsheet for the vegetated lysimeter. The daily precipitation, mean daily temperature, and daily temperature amplitude values were copied from the *PET* worksheet as well.



The lower boundary is defined as a seepage boundary for flow and as a zero gradient boundary for the heat transport. The seepage boundary condition assumes that a zero-flux boundary condition applies as long as the local pressure head at the bottom of the soil profile is negative. However, a zero pressure head will be used as soon as the bottom of the profile becomes saturated. This type of boundary condition often applies to finite lysimeters that are allowed to drain under the gravity.

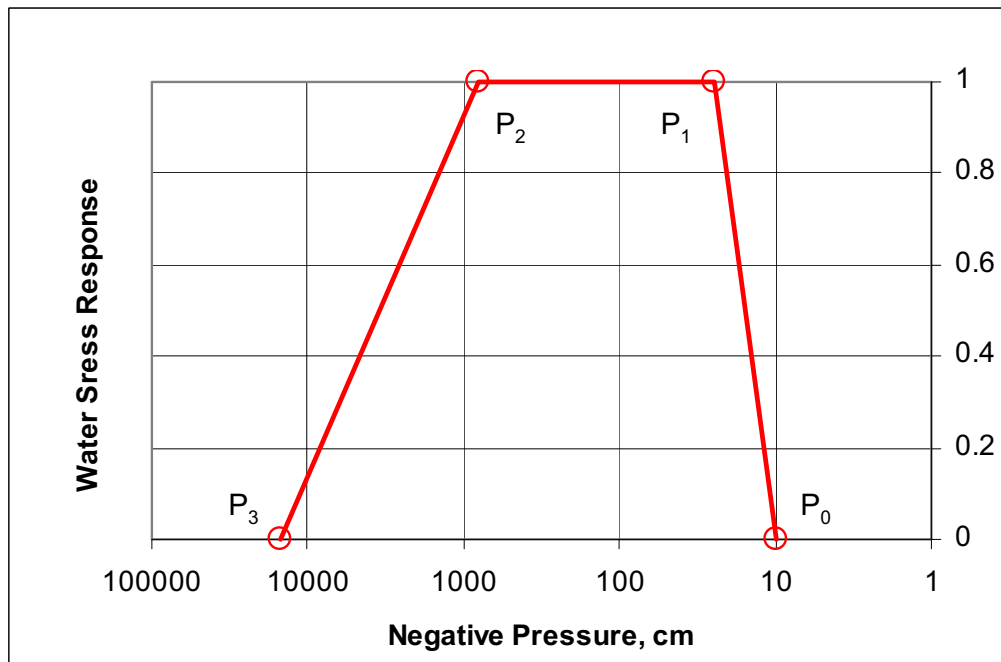
Heat transport was turned on in NTS and RCEW lysimeter simulations. The heat transport module must be turned on to simulate snow hydrology with HYDRUS-1D even when the heat transport is not of interest. The average daily temperature specified in this module was used in HYDRUS-1D to calculate whether the precipitation should be treated as snow and to maintain snow cover during the freezing periods. The snow hydrology has no impact on the NTS as temperatures rarely fall below freezing. However, this was a significant factor for the RCEW lysimeter where the snow cover may exist for 3 to 4 months during the winter.

The root water uptake is considered for the vegetated lysimeter only throughout 200 cm of the soil profile. The roots are uniformly distributed within this depth. The Feddes model in HYDRUS-1D is used for the stress response function (see Figure J-12). Water uptake is assumed to be zero when close to saturation (pressure head  $P_0$ ). Root water uptake is also zero for pressure head  $P_3$  which is less than the wilting point. Water uptake is considered optimal between pressure heads  $P_1$  and  $P_2$ , whereas for the pressure heads between  $P_2$  and  $P_3$ , water uptake decreases linearly with pressure head. The parameters describing this function were taken from HYDRUS-1D database. The most common values were used. The sensitivity analysis showed that the Feddes model parameters have little impact on the calculations. The parameter values are provided below.

- Value of the pressure head below which roots start to extract water from the soil ( $P_0$ ) is  $-10$  cm
- Value of the pressure head below which roots extract water at the maximum possible rate ( $P_1$ ) is  $-25$  cm.
- Value of the limiting pressure head below which roots can no longer extract water at the maximum rate assuming a potential transpiration rate of  $0.5$  cm/d ( $P_{2h}$ ) is  $-200$  cm (this value is not used in calculations since the maximum potential transpiration during the period of simulation was  $0.11$  cm/day).
- Value of the limiting pressure head below which roots cannot longer extract water at the maximum rate assuming a potential transpiration rate of  $0.1$  ( $P_{2l}$ ) is  $-800$  cm.
- Value of the pressure head below which root water uptake ceases ( $P_3$ ) is  $-15,000$  cm. The maximum negative pressure under which the plants can extract water did not impact the calculations because the moisture in the soil profile was always higher than the limiting moisture.

The resulting water stress function is shown in Figure J-12. The water stress function plays the role similar to  $K_{cb}$ —it decreases the potential transpiration. The major difference is that the

Feddes water stress function reduces potential transpiration based on the pressure head in the soil profile (saturation), and the  $K_{cb}$  function reduces the potential transpiration based on the season of the year. Although saturation is low during the dry part of the year and high during the wet part, there is no direct translation from one function to the other.



Source: Šimůnek et al. 2005 [DIRS 178140], Figure 2.1a, p. 15.

Figure J-12. Feddes Model Water Stress Function Used in HYDRUS-1D Modeling

HYDRUS-1D input and output files (all these files are text files) for the final runs are located in the subdirectories *NTSBar\_P* (bare soil lysimeter) and *VL\_90\_10\_Snow* (vegetated lysimeter) in the *HYDRUS\_Model* directory in the *NTS* folder in Validation Output DTN: SN0607T0502206.016.

The input files have the extension *in* or *dat*. The output files have the extension *out*. The results presented in Section 7.1.2 are from the output files *T\_LEVEL.OUT*. These files provide the daily values of all the water balance components, including storage (column “*volume*”) and infiltration (column “*vBot*”) in centimeters. The storage values were copied from this file into *HYDRUS1D Data&Results.xls* that is an external file read by the interfaces *Bare Soil Lysimeter* and *Vegetated Lysimeter*, as explained above. Comparison of the HYDRUS-1D results and MASSIF results is performed within the interface.

The HYDRUS-1D results for the vegetated lysimeter run (from *NOD\_INF.OUT* in *VL\_90\_10\_Snow* subdirectory in the *HYDRUS\_Model* directory in the *NTS* folder in Validation Output DTN: SN0607T0502206.016) were used to plot the moisture profiles shown in Figure 7.1.2.1-3. A discussion of the HYDRUS-1D results is provided in Section 7.1.2.

## J2. REYNOLDS CREEK EXPERIMENTAL WATERSHED LYSIMETER SITE

The Reynolds Creek Experimental Watershed (RCEW) data were collected by the U.S. Department of Agriculture (USDA) Northwest Watershed Research Center (NWRC), Boise, Idaho. The data are available from [ftp.nwrc.ars.usda.gov](http://ftp.nwrc.ars.usda.gov). The data used in this analysis were obtained directly from USDA NWRC. The information included in a CD provided by the USDA NWRC is submitted as DTN: SN0608T0502206.020 [DIRS 179875].

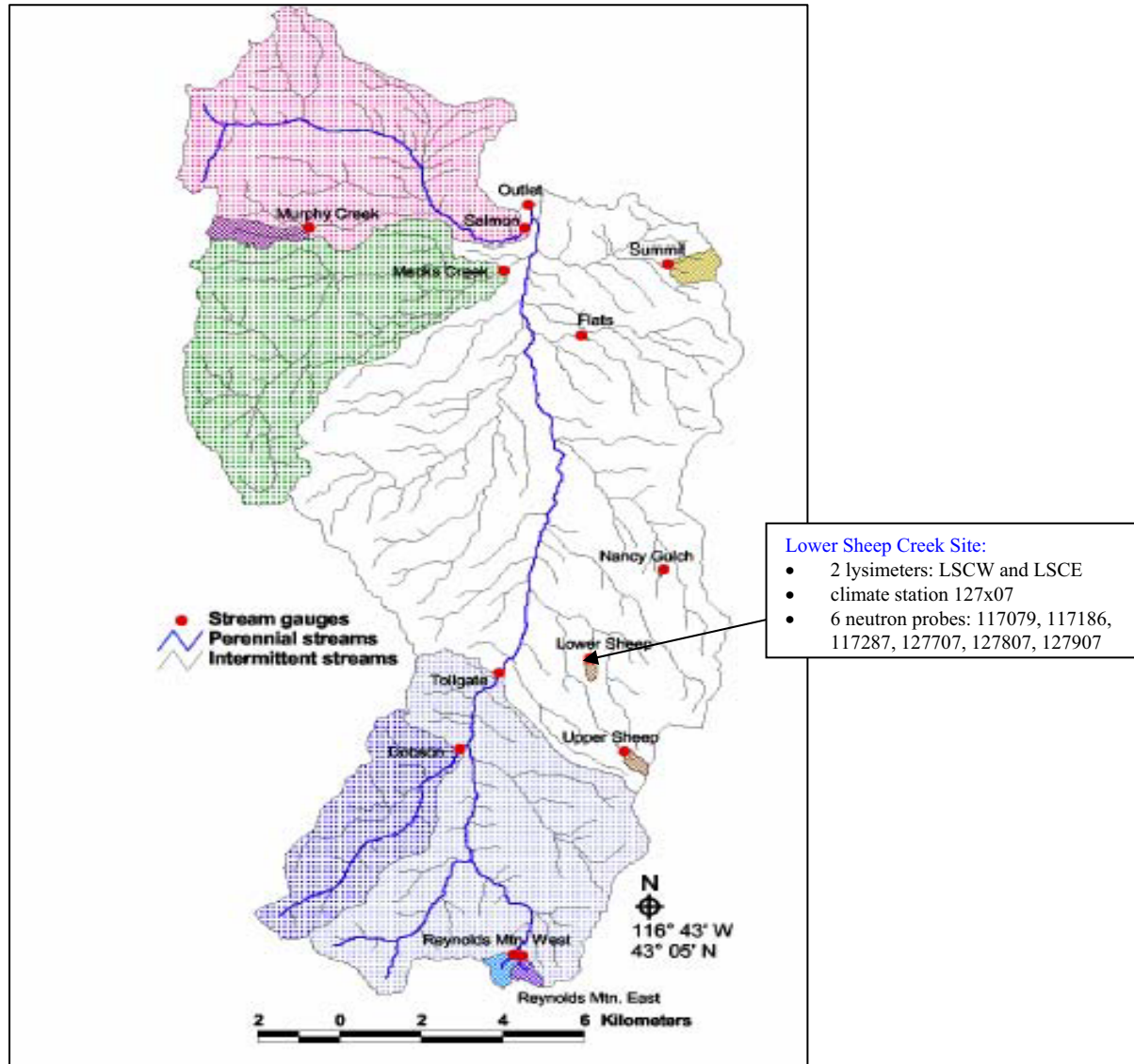
The RCEW occupies 239 km<sup>2</sup> in the Owyhee Mountain region located in the southwestern Idaho, 80 km southwest of Boise (Hanson et al. 2001 [DIRS 177509]). Two pairs of soil lysimeters were installed in the RCEW in 1967, one pair at the Lower Sheep Creek climate station (designated the “east” and “west” lysimeters) and the other one at the Reynolds Mountain climate station (designated “north” and “south”). The long-term lysimeter database is described by Seyfried et al (2001 [DIRS 177515]). The database includes the lysimeter description, calibration, data collection, and data availability. The RCEW lysimeters are hydraulic weighing lysimeters in which an inner cylindrical tank containing soil is set within a slightly larger outer cylinder. The inner cylinder rests on a coil of 0.05-m-diameter butyl tubing filled with liquid (different low freezing point liquids were used). The inner cylinder was 1.22-m deep and 1.47 m in diameter.

The Lower Sheep Creek (LSC) lysimeter site (elevation 1,656 m) was selected for this analysis because the climatic conditions at this site are closer to the glacial transition climate conditions predicted for Yucca Mountain. The Reynolds Mountain lysimeter site is located at a much higher elevation (2,098 m) and is under significantly colder and wetter conditions than the glacial transition climate.

The mean precipitation at the LSC lysimeter site is 349 mm (Wight et al. 1986 [DIRS 177104]) and the mean annual temperature is 7.4°C (Wight and Hanson 1990 [DIRS 177113]). About 21% of precipitation comes from snow. The lysimeter latitude is 43° 08' 24.088", longitude is 116° 43' 57.732", and elevation is 1,656 m (DTN: SN0608T0502206.020 [DIRS 179875]).

The LSC lysimeter site is located next to the climate station 127x07 (see Figure J-13). The minimum and maximum temperatures and precipitation data are available for this climate station. The daily temperature data were taken from *daily127x07climate.txt* located in the directory *climate* (DTN: SN0608T0502206.020 [DIRS 179875]). The precipitation data were collected hourly. These data were taken from *hourly127x07precipitation.txt* located in the directory *precipitation* (DTN: SN0608T0502206.020 [DIRS 179875]). The daily precipitation was calculated from hourly precipitation data. Based on the availability of the lysimeter data, the considered period of observation was from 01/10/77 through 09/30/84. October 1, 1977 was selected as the beginning of the observation period to satisfy MASSIF input requirements (the data set must start at the beginning of the water year). The temperature and precipitation data were converted to a format required by MASSIF. The formatted data are in *RCEWLysimeter.xls (worksheet “Climate Data”)* (DTN: SN0608T0502206.020 [DIRS 179875]). This file contains month number, day of the month number, day of the year number, year number, daily precipitation in mm, daily maximum temperature in degrees C, daily minimum temperature in degrees C, and daily average wind speed in m/s. The daily average wind speed was set to 2 m/s for the entire period of observation since no wind speed data were available.

The LSC site has two lysimeters LSCW (west lysimeter) and LSCE (east lysimeter) and six neutron probes. Three neutron probes (117079, 117186, and 117287) are installed at the LSCE lysimeter site, and three neutron probes are installed at the LSCW lysimeter site (127707, 127807, and 127907). The comparison between the lysimeter data and the neutron probe data is provided in Seyfried et al. (2001 [DIRS 177515]; 2001 [DIRS 177506]). It was shown that the LSCW lysimeter data are in good agreement with the neutron probe data. The LSCE lysimeter data differ from the LSCW lysimeter data (even though it is located only 3.6 m away) and are not in a good agreement with the neutron probe data. Based on this conclusion, the LSCW lysimeter was selected for the analysis.



Source: Seyfried et al. 2001 [DIRS 177501], Figure 3.

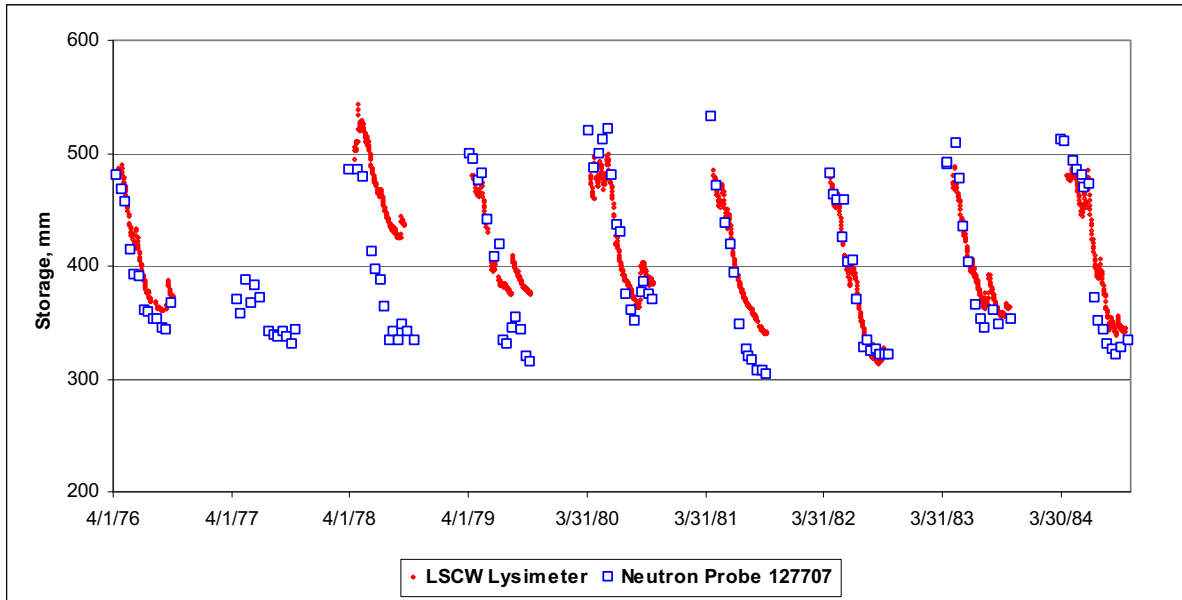
Figure J-13. Locations of the 13 Weirs in the RCEW with Long-term Data

The LSCW lysimeter data were taken from *daily127x07lysimeter.txt* located in the directory *soilmoisture* (DTN: SN0608T0502206.020 [DIRS 179875]). These data represents the changes in lysimeter soil water storage in mm with regard to the storage measured on 04/13/1976. The data were taken irregularly during the no snow part of the year and were not taken during the snow season.

To convert the changes in lysimeter storage into the actual daily storage values, the initial storage must be known. The initial storage was calculated using the neutron probe data. These data were taken from *neutronprobesoilwater127707.txt* located in the directory *soilmoisture* (DTN: SN0608T0502206.020 [DIRS 179875]). This file contains data for the neutron probe 127707, which is 0.91 m deep. This probe was selected based on the analysis in Seyfried et al. (2001 [DIRS 177515], Figure 1) since probe 127707 data are in very good agreement with the LSCW lysimeter data. The moisture content in this file is provided for the following four readings: 15, 31, 61, and 91 cm. As suggested by Seyfried et al. (2001 [DIRS 177506]), the 15 cm reading represents soil water from 0 to 23 cm, the 31 cm reading represents soil water from 23 to 46 cm, the 61 cm reading represents soil water from 46 to 75 cm, and the 91 cm reading represents soil water from 75 to 106 cm. The lysimeter is 122-cm deep. It was assumed that the moisture within the last 16 cm of the lysimeter is the same as that within the 75- to 106-cm interval. The moisture contents measured in neutron probe 127707 were converted to the lysimeter storages (s) using the following formula:

$$s = \theta_1 \times \Delta z_1 + \theta_2 \times \Delta z_2 + \theta_3 \times \Delta z_3 + \theta_4 \times \Delta z_4 \quad (\text{Eq. J-8})$$

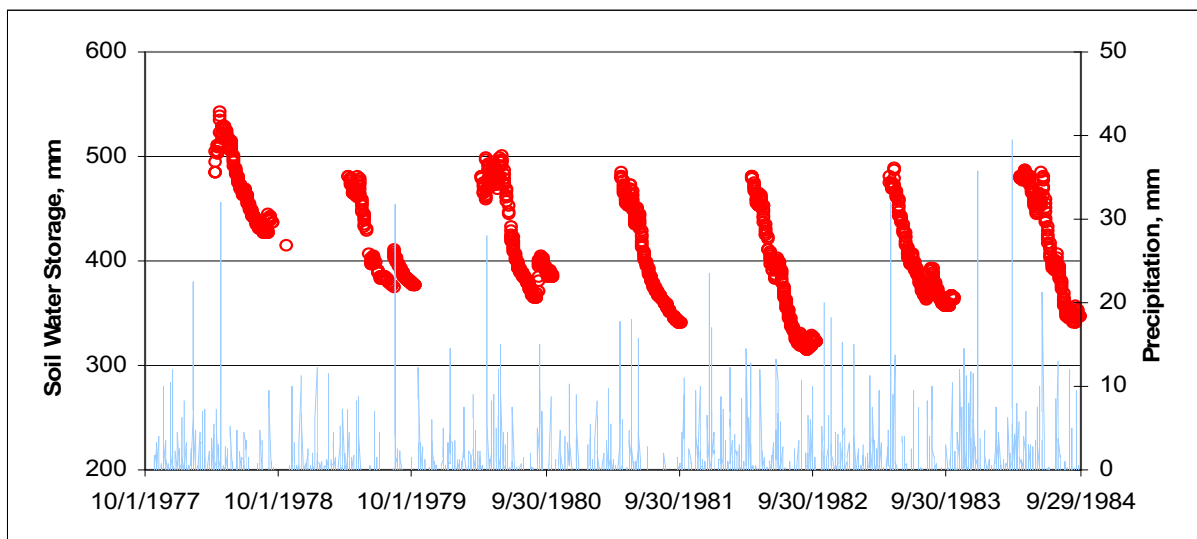
where  $\Delta z_1$ ,  $\Delta z_2$ ,  $\Delta z_3$ , and  $\Delta z_4$  are the depth interval thicknesses (23 cm, 23 cm, 29 cm, and 46 cm from the top interval down) and  $\theta_1$ ,  $\theta_2$ ,  $\theta_3$ , and  $\theta_4$  are the corresponding measured moisture contents. The data and the calculations are in worksheet "*NP127707*" of *RCEWLysimeter.xls* (*RCEW* folder in Validation Output DTN: SN0607T0502206.016). Plotted in Figure J-14 are the lysimeter storages from LSCW data and from neutron probe 127707 data. The lysimeter data are in good agreement with the neutron probe data except in the summers of 1978 and 1981.



Source: Validation Output DTN: SN0607T0502206.016.

Figure J-14. Soil Moisture Storage in RCEW Lysimeter LSCW

The lysimeter storage data and precipitation are shown in Figure J-15. The storage data were added to the MASSIF input file because these data are required by the MASSIF interface *“Reynolds Creek”* that performs the analysis of the RCEW lysimeter data. These data are in worksheet *“Climate Data”* of *RCEWLysimeter.xls* (RCEW folder in Validation Output DTN: SN0607T0502206.016). The lysimeter calibration is described in Seyfried et al. (2001 [DIRS 177515]). As is concluded in this publication, the lysimeter observations have the precision of  $\pm 8$  mm ( $\pm 2.2$  % of the mean annual precipitation).

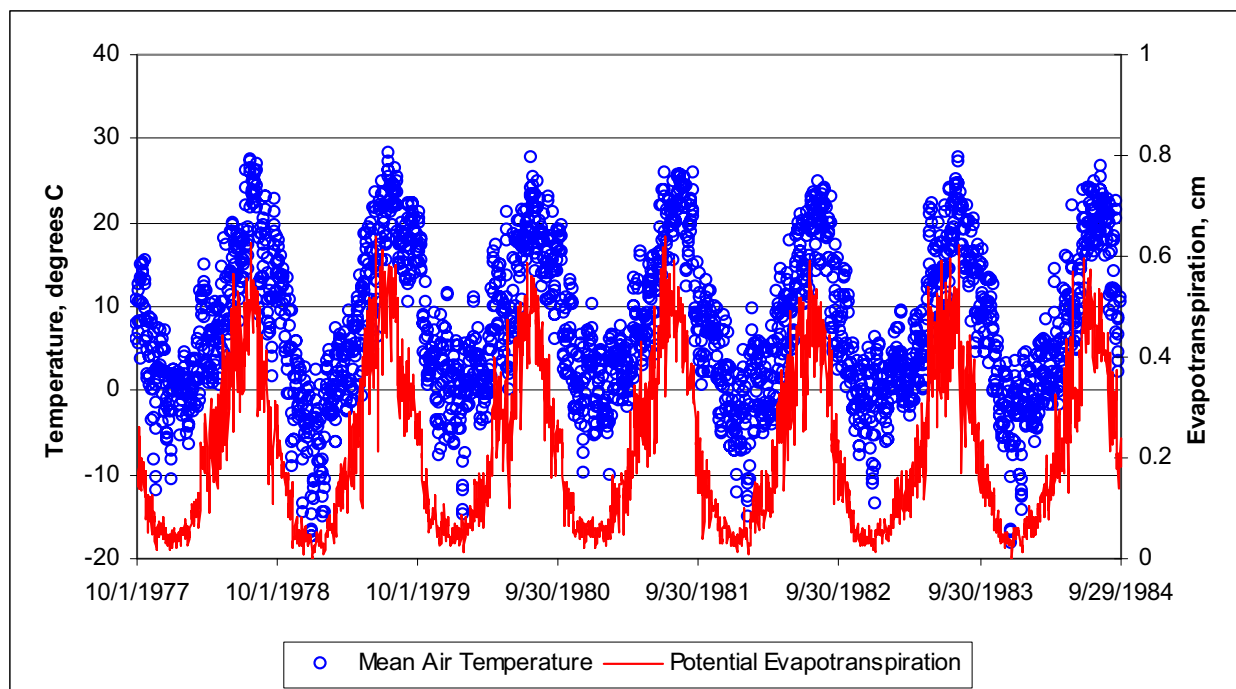


Source: Validation Output DTN: SN0607T0502206.016.

Figure J-15. RCEW LSCW Lysimeter Soil Water Storage and Precipitation Data Used in the Analysis

The maximum lysimeter storage during this period of observation is 542.7 mm. This corresponds to the moisture content of 0.445. The minimum lysimeter storage is 313.9 mm. This corresponds to the moisture content of 0.257.

The climate data in worksheet *Climate Data* of *RCEWLysimeter.xls* (*RCEW* folder in the Validation Output DTN: SN0607T0502206.016) are used to calculate potential evapotranspiration, which constitutes the upper boundary condition in the HYDRUS-1D model. The calculations of the potential evapotranspiration are implemented the same way as described above for the NTS lysimeter site. The Hargreaves formula (Jensen et al. 1997 [DIRS 177103]) is used in these calculations. The input data to these calculations are minimum, maximum, and average daily temperatures, and the site latitude. The average temperature is calculated from minimum and maximum temperatures. The transpiration is assumed to be 50% of evapotranspiration based on the estimate of the mean vegetation cover including live plants and litter at the site over the 11 years of observations provided in Wight et al. (1986 [DIRS 177104]). The input data and the calculations are in worksheet *Potential ET* of *RCEWLysimeter.xls* (*RCEW* folder in Validation Output DTN: SN0607T0502206.016). The average temperature and calculated potential evapotranspiration are shown in Figure J-16.



Source: Validation Output DTN: SN0607T0502206.016.

Figure J-16. Average Air Temperature and Calculated Potential Evapotranspiration at the RCEW LSCW Lysimeter Site

The remaining input parameters are initial moisture content, soil and bedrock properties and the vegetation parameters.

The initial conditions apply to 10/01/77, which is the beginning of the simulation. No storage data are available for this date. The storage measured on 09/15/78 was 435.5. This corresponds to an integrated water content within the profile of  $0.36 \text{ m}^3/\text{m}^3$ . The initial water content on 10/01/77 was likely to be higher, because the water year of 1977 was the highest in storage. Consequently, the initial moisture was set equal to  $0.39 \text{ m}^3/\text{m}^3$ . The initial moisture should not have a great effect on the calculations.

The soil properties were taken from *neutronprobesoils.dbf* located in the directory *soilmoisture* (DTN: SN0608T0502206.020 [DIRS 179875]). The soil properties were obtained from the neutron tube 127907, which is 183-cm deep. Nine soil horizons were described at this location. The soil data include the depth and thickness of each horizon; percent sand, clay, and silt; bulk density; field capacity (at  $-1/3$  bars); wilting point (at  $-15$  bars); parent material; texture; average slope; and other properties. Based on these data, the first 10.2 cm of the lysimeter site consists of loam/silty loam, the next 48.3 cm is clay/clay loam, and the remaining soil is loam/sandy loam. The bedrock at the site is basalt (which is the parent material for the lysimeter soils). The average slope is 4 degrees.

No information is available on the horizon saturated hydraulic conductivity, residual moisture content, porosity, van Genuchten parameters *alpha* and *n*, and bedrock saturated hydraulic conductivity. These parameters were obtained from the HYDRUS-1D module that allows for



estimating these soil properties using Rosetta Lite 1.1, June 2003. The horizon saturated hydraulic conductivity, residual moisture content, porosity, van Genuchten parameters  $\alpha$  and  $n$  were estimated from percent sand, silt, and clay and bulk density, field capacity, and wilting point, except for horizons 2 and 4. The information on bulk density and field capacity was not available for these horizons, and only the available data on percent sand, silt, and clay were used. The original soil properties and estimated soil properties are in worksheet ***Soils*** of ***RCEWlysimeter.xls*** (***RCEW*** folder in the Validation Output DTN: SN0607T0502206.016).

Since MASSIF is not designed to simulate heterogeneous soils, the soil properties were averaged over the 122 cm of the lysimeter depth. The geometric weighted mean (Fetter 2001 [DIRS 156668], p. 88) and inverse value mean were used for the hydraulic conductivities (Fetter 2001 [DIRS 156668]). These calculations are in worksheet ***Soils*** of ***RCEWlysimeter.xls*** (***RCEW*** folder in the Validation Output DTN: SN0607T0502206.016). The averaged soil properties are summarized in Table J-1. The only situation in which soil saturated hydraulic conductivity can affect the MASSIF results is when there is runoff at the site. No noticeable runoff occurred at this site because it was designed to prevent both runoff and run-on. The residual moisture content and van Genuchten parameters  $\alpha$  and  $n$  are not inputs to MASSIF. They are required for HYDRUS-1D simulations only. The saturated hydraulic conductivity of the bedrock is not available. The range considered was from  $10^{-9}$  cm/s to  $10^{-7}$  cm/s. This range is suggested for dense and vesicular basalt hydraulic conductivity by Freeze and Cherry (1979 [DIRS 101173], p. 162, Table 4.1). The bedrock hydraulic conductivity is a MASSIF parameter and is not a HYDRUS-1D parameter. In the HYDRUS-1D simulation the lower boundary is set at the bottom of the lysimeter, and a seepage boundary condition is defined in the same way as described above for the NTS lysimeter site.

The vegetation parameters are rooting depth, vegetation cover, plant height, water stress parameter  $p$ , the potential vegetation response parameter  $PVR$ , and transpiration parameter  $C_{kcb}$ . Note that the last four parameters are MASSIF inputs only. As described above,  $C_{kcb}$  is the slope of the linear regression line representing the  $NDVI'-K_{cb}$  relationship (see Appendix E for details). Parameter  $PVR$  can be defined arbitrarily (it was set equal to 1), as explained in Section 7.1.2, because the optimization scheme estimates the product of  $K_{cb}$  and  $PVR$ .

As described by Seyfried et al. (2001 [DIRS 177515]), the vegetation at the lysimeter site is dominated by low sagebrush that grows to a height of about 0.3 m and is accompanied by perennial bunchgrasses and forbs. The lysimeter site contains a mature shrub along with the naturally associated plants with a slightly higher vegetation density than the surrounding landscape. The rooting depth is specified equal to 122 cm, which is the lysimeter depth. The vegetation cover used in HYDRUS-1D is set equal to 0.5. The vegetation cover in MASSIF is a parameter in the optimization scheme. There is no data to define  $C_{kcb}$ , which is the MASSIF input. It is a parameter in the optimization scheme as well. The plant height is set equal to 0.3 m and water stress is set to 0.8 in MASSIF calculations.

The default MASSIF values are used for the evaporation depth  $Z_e$  (100 mm), readily evaporable water  $rew_1$  (6 mm), and sublimation and snowmelt coefficient. The terrain albedo was set equal to 0.15 based on the information from a journal article by Wight et al. (1986 [DIRS 177104]).

Table J-1. Averaged Soil Properties Used in MASSIF and HYDRUS-1D Calculations

Soil Property	Units	Input Category	Weighted Mean	Min	Max
Soil Porosity	m <sup>3</sup> /m <sup>3</sup>	H, M	0.467	0.422	0.506
Soil Field Capacity	m <sup>3</sup> /m <sup>3</sup>	M	0.332	0.273	0.415
Soil Wilting Point	m <sup>3</sup> /m <sup>3</sup>	M	0.187	0.118	0.267
Soil Saturated Hydraulic Conductivity (average of the inverse values)	cm/d	H, M	17.678	3.930	74.470
Soil Saturated Hydraulic Conductivity (geometric average)	cm/d	H, M	4.128	3.930	74.470
Soil van Genuchten alpha	1/cm	H	0.014	0.0059	0.0218
Soil van Genuchten n	–	H	1.335	1.24	1.59
Soil Residual Moisture	m <sup>3</sup> /m <sup>3</sup>	H	0.064	0.05	0.081
Bedrock Saturated Hydraulic Conductivity	cm/s	M	–	1.0 × 10 <sup>-9*</sup>	1.0 × 10 <sup>-7*</sup>

Source: Validation Output DTN: SN0607T0502206.016.

\*Values from Freeze and Cherry 1979 [DIRS 101173], p. 162, Table 4.1).

H stands for HYDRUS-1D; M stands for MASSIF.

The site coordinates and elevation, climate data, soil and bedrock properties, and vegetation parameters described above are incorporated in the MASSIF interface (MathCAD file **Reynolds Creek**). The geospatial data are in a separate text file. The climate data are embedded within the interface Excel file. The other data are directly defined within the interface. This is explained below.

## J2.1 CLIMATE DATA

The interface reads the embedded Excel file with the climate data provided in the format required by MASSIF. The climate data are copied to this file from the worksheet **Climate Data** in **RCEWlysimeter.xls** (**RCEW** folder in the Validation Output DTN: SN0607T0502206.016). In addition to the climate data required to run MASSIF (first 8 columns in the file), this file contains the lysimeter storage in mm required by the interface (10th column).

## J2.2 GEOSPATIAL DATA

The interface reads an external Excel file with the geospatial data provided in a format required by MASSIF. The file name is **RCEW\_location.csv**. It is located in the same directory (**Lysimeter**) in which the interface is located. The file consists of two lines; each line represents one watershed cell. The lysimeter site is represented by the first cell in this file (the first line). The second cell is not used in the analysis. The geospatial information includes the cell identification number (arbitrary number in this case), site latitude and longitude in degrees and UTM coordinates in meters, site elevation in meters, slope in degrees, aspect, soil type, soil depth class, bedrock type, *PVR*, and an identification number of the cell from which the runoff is routed to this cell (it is set to -3 to exclude the run-on component using the corresponding MASSIF option). The site longitude, latitude, and elevation are defined as described above. The slope at the site is 4° (as described above). Soil type is set equal to 5, soil depth class is set equal to 2, and bedrock type is set equal to 406. The *PVR* is set equal to 1. As described above the

$PVR$  can be set equal to an arbitrary value as long as the  $K_{cb}$  value is estimated by adjusting  $C_{kcb}$ . The  $PVR$  is set equal to 1 for the sake of convenience.

### J2.3 OTHER PARAMETERS

The other parameters required to run MASSIF and discussed above are defined directly within the interface as follows:

- Reference elevation is set equal to site elevation to avoid correction of temperature and precipitation with regard to the reference elevation.
- The albedo is set equal to 0.15.
- Weather parameters, such as first and last day of winter and precipitation duration coefficients, were set equal to the values defined for the glacial transition climate (Sections 6.3.3 and 6.3.4).
- Dew point offset parameters were set equal to the default MASSIF values.
- Soil properties such as porosity, hydraulic conductivity, and wilting point of the soil type 5 are set equal to the weighted mean values defined in Table J-1 (inverse value mean is used for hydraulic conductivity). This redefines the values that MASSIF reads from the built-in look-up table with the corresponding soil properties for the soil type 5.
- Bedrock hydraulic conductivity of the bedrock type 406 is set equal to  $10^{-9}$  cm/s (the lower bound defined above). This redefines the value that MASSIF reads from the built-in look-up table with the bedrock properties. This initial value was changed within the range considered above as part of the sensitivity analysis.
- The soil depth of the Soil Depth Class 2 is set equal to 183 cm.
- The rooting depth was specified equal to 122 cm.
- The vegetation cover is set equal to 0.5. The vegetation cover is a parameter in the optimization scheme and can also be adjusted manually.
- $C_{kcb}$  coefficient representing the regression line slope is a parameter in the optimization scheme and can also be adjusted manually.  $C_{kcb}$  coefficient representing the regression line intercept is set equal to 0.
- The plant height is set equal to 0.3 m.
- The water stress parameter  $p$  is set equal to 0.65 (this parameter is not a part of the optimization scheme; however, it can be manually adjusted if needed).
- The evaporation depth  $Z_e$  is set equal to 100 mm (this parameter is not a part of the optimization scheme, however, it can be manually adjusted if needed).

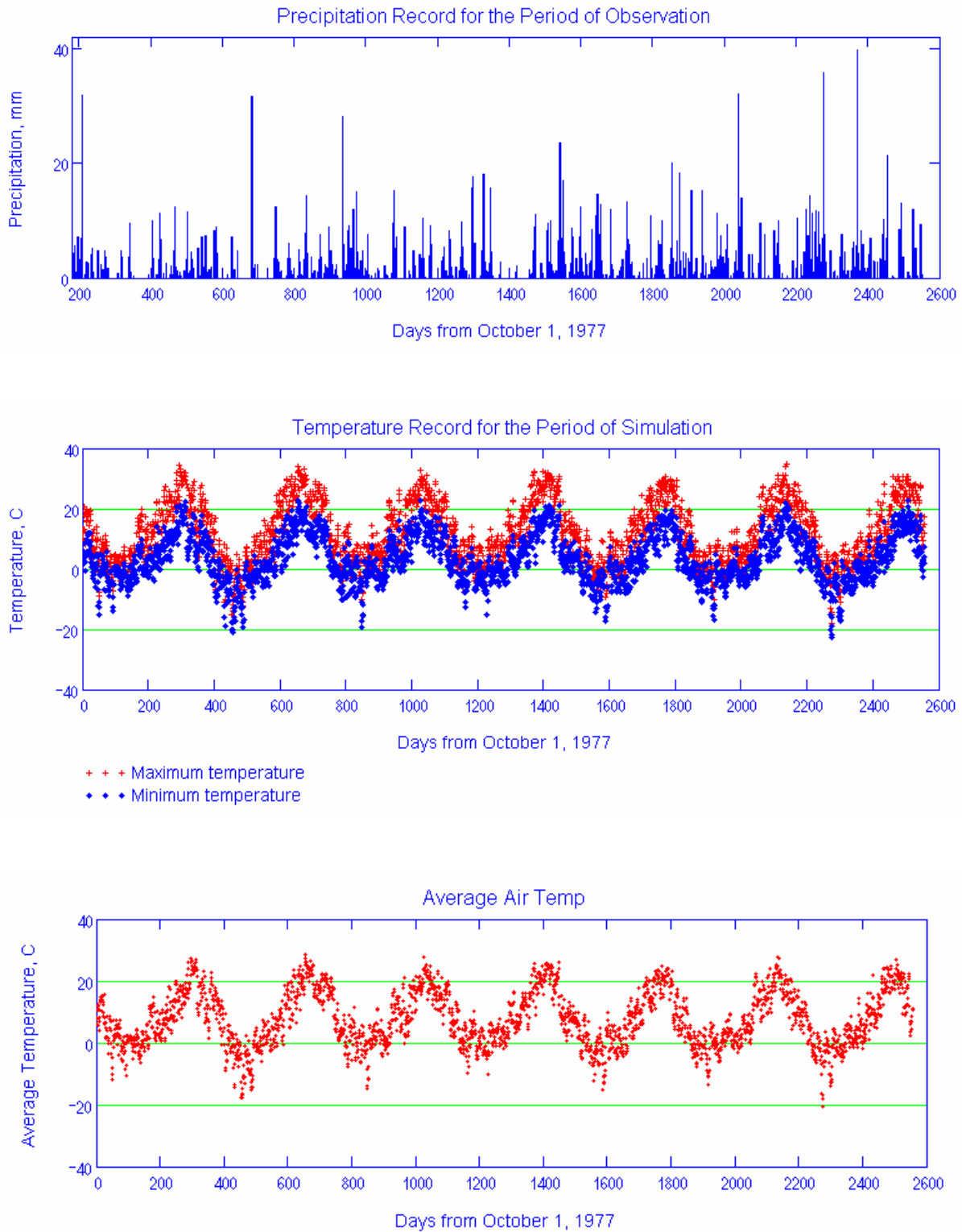
- Readily evaporable water  $rew_I$  is set equal to 6 mm (this parameter is not a part of the optimization scheme; however, it can be manually adjusted if needed).
- The diffusive evaporation parameter  $K_{c\_min}$  is set equal to 0.0. This parameter is a parameter in the optimization scheme and can also be adjusted manually.
- Sublimation and snowmelt coefficients are set equal to the default MASSIF values.
- The initial moisture content in each layer is set equal to  $0.39 \text{ m}^3/\text{m}^3$ .

The functions performed by the interface are described as follows. The interface displays the climate data read for the period of simulation. This includes the plot of the daily precipitation record and minimum, maximum, and average daily air temperatures. The percentage of time when mean daily temperature is below  $0^\circ\text{C}$  is calculated (20.6 %). The examples are shown in the Figure J-17.

The interface runs MASSIF, stores the results of calculations, and calculates the lysimeter storage as a sum of the water depths within the three upper layers (top 122 cm of soil profile where the lysimeter is located).

The interface displays the measured and calculated daily lysimeter storage. An example is shown in Figure J-18. The parameters placed in the yellow box located just above the storage plot can be manually adjusted. Each adjustment results in recalculation and display of new calculated storage values in the storage plot. This function was used in the sensitivity analysis and in further adjustment of the parameters obtained via optimization scheme. The interface calculates the objective function value using Equation 7.1.2-4.

For the period of simulation, the interface calculates the water balance constituents such as total precipitation, total evaporation, total transpiration, total run-on, total runoff, and total infiltration. Note that the total run-on is always zero since the lysimeter cell is not connected to any other cell in the geospatial file. The interface checks the daily mass balance for the simulation and displays it as shown in Figure J-19.

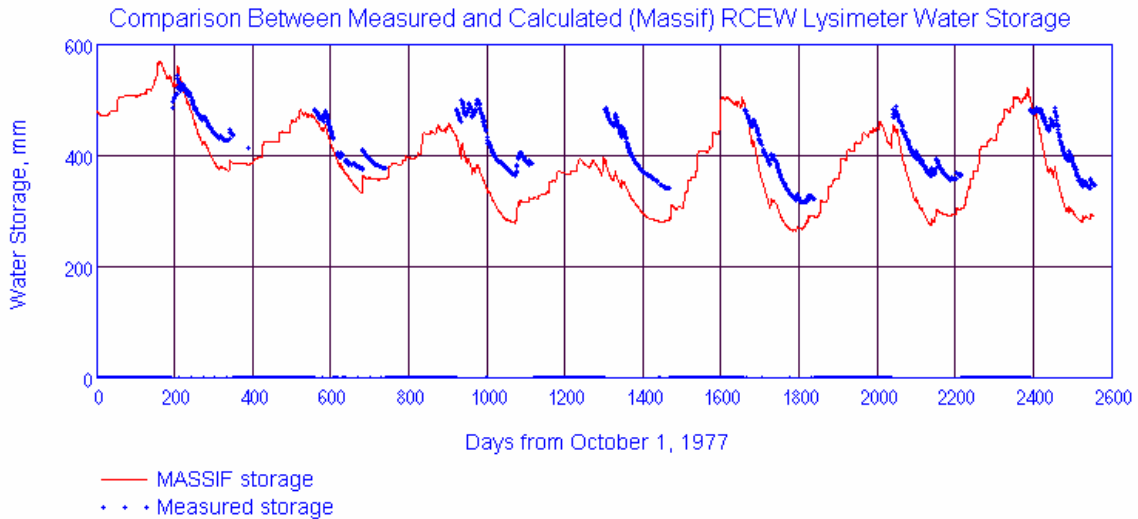


Source: Output DTN: SN0701T0502206.037, *Welcome to Massif\Massif\Validation Analyses\Lysimeter\Reynolds Creek.xmlcd*.

Figure J-17. Climate Data Plots for the RCEW Lysimeter Site Displayed by Reynolds Creek Interface

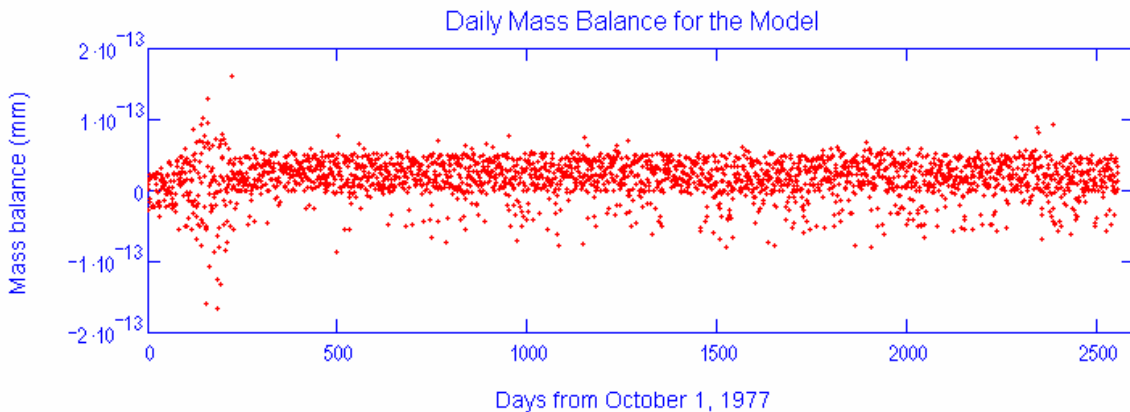
**Adjustable Evaporation Parameters**

- Param1 = 0.70 - Canopy fraction
- Param2 = 13.685 - NDVI-K<sub>cb</sub> slope (C<sub>kcb</sub>)
- Param3 = .0 - Diffusive evaporation parameter (K<sub>c\_min</sub>)
- Param8 = 0.65 - depletion factor (p)
- Param5 = 6 - Readily evaporable water, mm
- Param6 = 0.415 - Field capacity
- Param7 = 0.19 - Wilting point
- Param9 =  $2.3 \cdot 10^{-8}$  - Bedrock K<sub>s</sub>, cm/s



Source: Output DTN: SN0701T0502206.037, *Welcome to Massif\Massif\Validation Analyses\Lysimeter\Reynolds Creek.xmcd*.

Figure J-18. Calculated versus Measured Lysimeter Storage Plot Displayed by Reynolds Creek Interface



Source: Output DTN: SN0701T0502206.037, *Welcome to Massif\Massif\Validation Analyses\Lysimeter\Reynolds Creek.xmcd*.

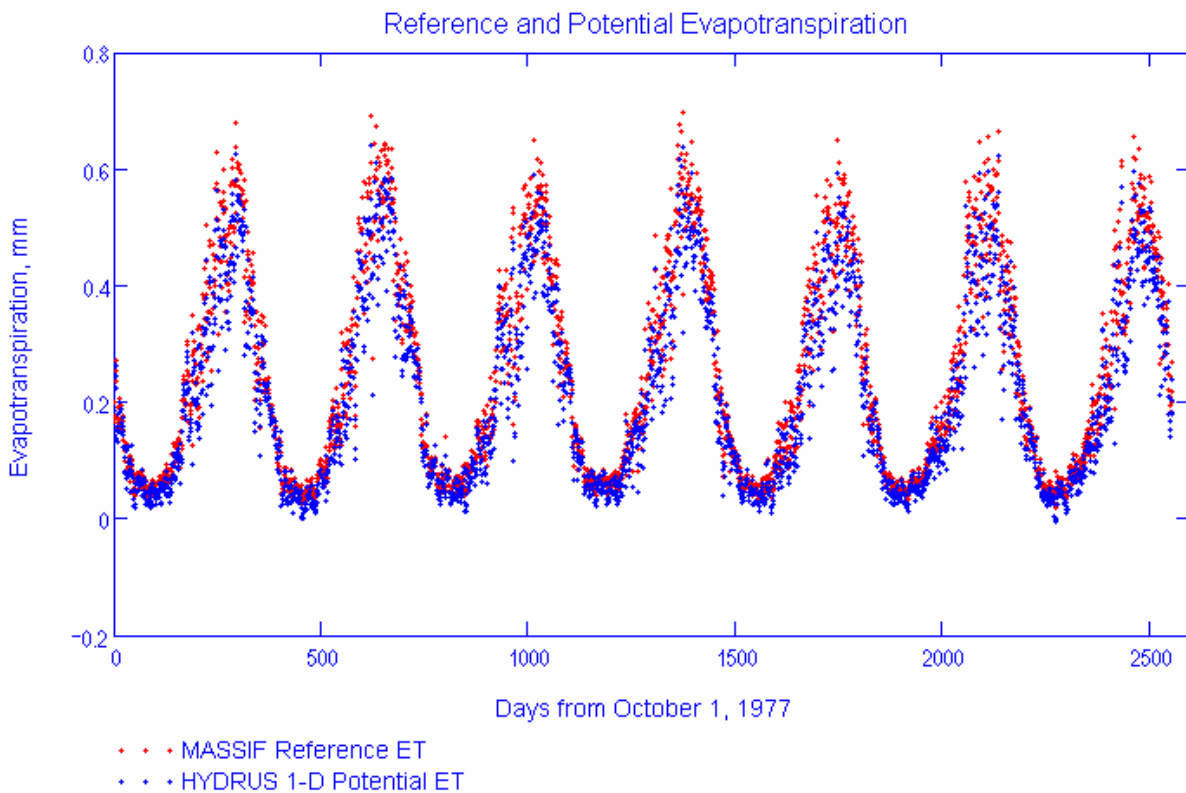
Figure J-19. Daily Mass Balance Displayed by Reynolds Creek Interface

The interface defines the optimization scheme in accordance with Equation 7.1.2-4. This includes the definition of the objective function and initial values and ranges for the parameters to be estimated. The optimization parameters are (see Section 7.1.2): diffusive evaporation parameter  $K_{c\_min}$ , canopy fraction  $f_c$ , vegetation parameter  $C_{kcb}$ , and field capacity  $\theta_f$ .

The interface runs the conjugate gradient minimization procedure, which is a built-in MathCAD function. The minimization procedure returns the values of the optimization scheme parameters that result in the minimum value of the objective function.

The interface reads an external Excel file *Hydrus1D Data&Results* that contains the HYDRUS-1D input data (including potential evapotranspiration) and modeling results (daily storage and infiltration). These data are in worksheet *RCEW*.

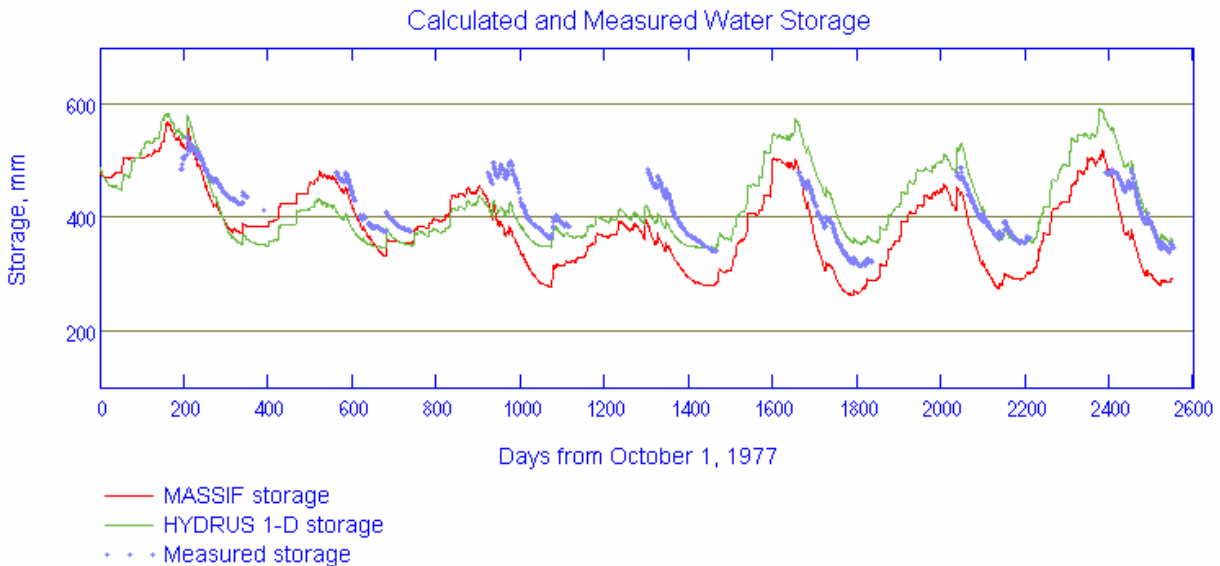
The interface displays the reference evapotranspiration calculated by MASSIF and the potential evapotranspiration that is HYDRUS-1D input (boundary condition). An example is shown in Figure J-20.



Source: Output DTN: SN0701T0502206.037, *Welcome to Massif\Massif\Validation Analyses\Lysimeter\Reynolds Creek.xmcd*.

Figure J-20. Reference Evapotranspiration and Potential Evapotranspiration Displayed by Reynolds Creek Interface

The interface displays the observed lysimeter storage and lysimeter storage calculated with MASSIF and HYDRUS-1D as shown in Figure J-21.



Source: Output DTN: SN0701T0502206.037, \Welcome to Massif\Massif\Validation Analyses\Lysimeter\Reynolds Creek.xmcd.

Figure J-21. Calculated and Measured Lysimeter Storage Displayed by Reynolds Creek Interface

The interface outputs the MASSIF daily storage and infiltration and the HYDRUS-1D daily storage and infiltration into an embedded Excel file to assist in further data processing and display. This file is used to generate Figure 7.1.2.2-2. The lysimeter storage measured in neutron probe 127707 is copied in this file from *NP127707* of *RCEWLysimeter.xls* (*RCEW* folder in Validation Output DTN: SN0607T0502206.016) to allow for comparison between the different measurements (lysimeter versus neutron probe).

The interface outputs the MASSIF daily actual evapotranspiration values into a built-in Excel file. These data are used within this file to calculate the average monthly rates of actual evapotranspiration for years 1978 and 1979 and to generate Figures 7.1.2.2-3 and 7.1.2.2-4 presented in Section 7.1.2. The file also contains the actual evapotranspiration data taken from Wight and Hanson (1990 [DIRS 177113]) needed to generate these figures. The spreadsheet *RCEW Kcb* in this built-in file contains calculations of daily  $K_{cb}$  values for the year 1978 through 1984, average annual  $K_{cb}$  values for the growing season (day 120 through 240), and average growing season  $K_{cb}$  value over the seven years of observations. The average growing season  $K_{cb}$  is compared to the data by Wight and Hanson (1990 [DIRS 177113]) in Section 7.1.2. These calculations use  $C_{kcb}$  value specified within the interface.



## J2.4 HYDRUS-1D MODELING SETUP

All the input and output HYDRUS-1D files are in subdirectory ***RCEW\_Homo*** in the ***HYDRUS\_Model*** directory in ***RCEW*** folder in Validation Output DTN: SN0607T0502206.016. The input and output files in this subdirectory were created by running HYDRUS-1D file ***RCEW\_homo.h1d*** located in the ***HYDRUS\_Model*** directory. The HYDRUS-1D modeling setup is described below.

The simulated processes are water flow (including snow hydrology), heat transport, and root uptake. The depth of the soil profile is 122 cm. It is represented with 62 nodes. The first node is at the land surface ( $z=0$  cm) and the last node is at the lysimeter bottom (122 cm). The nodes are 2 cm apart. The soil profile is homogeneous. The initial moisture content is 0.4 (see discussion above). The initial temperature is 6.1°C. The van Genuchten model in HYDRUS-1D is used to represent relationships between the saturation and pressure head and between the saturation and hydraulic conductivity. The soil parameters are (see Table J-1):

- saturated hydraulic conductivity is 18 cm/d
- van Genuchten parameter  $\alpha$  is 0.014 1/cm
- pore connectivity parameter  $l$  is 0.5 Šimunek et al. (2005 [DIRS 178140]) suggest leaving this parameter at its default value of 0.5.

The van Genuchten parameter  $n$ , saturated porosity, and residual porosity are adjusted during the simulations. These three parameters are found to have greatest impacts on the calculations. Note that the actual soil profile is heterogeneous, and the effective soil properties of the equivalent homogeneous profile are not known. Also, the saturated porosity, residual moisture content, and van Genuchten parameters  $\alpha$  and  $n$  are not measured; they were estimated using HYDRUS-1D soil property database (see the discussion above). Consequently, the appropriate parameter values may be different from the corresponding weighted average values. Some small deviation from the parameter ranges defined in Table J-1 may be expected as well.

The upper boundary is an atmospheric boundary with specified potential evaporation, potential transpiration, precipitation, and temperature. The daily values of these parameters are defined for all the period of simulation (2557 days), which is from 10/01/77 to 09/30/84. The calculation of potential evapotranspiration is discussed above. The input data used in these calculations and the resulting potential evapotranspiration values are in worksheet ***Potential ET*** of ***RCEW\_Lysimeter.xls*** (***RCEW*** folder in Validation Output DTN: SN0607T0502206.016). The potential transpiration is assumed to be equal to 0.5 of the potential evapotranspiration, based on the vegetation cover of 0.5. The potential evaporation and transpiration values are copied into the built-in HYDRUS-1D time-dependent boundary condition spreadsheet. The daily precipitation, mean daily temperature, and daily temperature amplitude values were copied from ***Climate Data*** worksheet of ***RCEW\_Lysimeter.xls*** (***RCEW*** folder in Validation Output DTN: SN0607T0502206.016).

The lower boundary is defined as a seepage boundary for flow and as a zero gradient boundary for the heat transport. See the modeling setup for the NTS lysimeter for details concerning this boundary.

The root water uptake is considered throughout 122 cm of the soil profile. The roots are uniformly distributed within this depth. The Feddes model in HYDRUS-1D is used for the stress response function. The details concerning this function are provided above (see HYDRUS-1D modeling setup for the NTS lysimeters).

The parameters describing this function are taken from HYDRUS-1D database. The values for grass in this database are used. Grass is the closest equivalent to the vegetation at the lysimeter site found in HYDRUS-1D database. Also, the sensitivity analysis showed that the Feddes model parameters have little impact on the calculations. The parameter values are provided below.

- $P_0$  is -10 cm
- $P_1$  is -25 cm
- $P_{2h}$  (under potential transpiration of 0.5 cm/day) is -300 cm (this value is not used in calculations since the maximum potential transpiration during the period of simulation was 0.32 cm/d)
- $P_{2l}$  is -1,000 cm (under potential transpiration of 0.2 cm/day)
- $P_3$  is -15,000 cm.

The resulting water stress function is similar to one shown in Figure J-12.

A number of HYDRUS-1D simulations are performed to investigate the model sensitivity and to adjust three modeling parameters. The best fit (42.3 mm) was obtained using the saturated porosity of 0.5 m<sup>3</sup>/m<sup>3</sup>, residual moisture of 0.11 m<sup>3</sup>/m<sup>3</sup>, and van Genuchten  $n=1.15$ . These values are close to the corresponding values describing clay and clay loam layers (with saturated porosity 0.506 m<sup>3</sup>/m<sup>3</sup>, residual moisture content 0.081 m<sup>3</sup>/m<sup>3</sup>, and van Genuchten  $n=1.24$ ). This means that the amount of water that can be stored in the clay and clay loam layers controls the lysimeter storage. The results of this simulation are presented in Section 7.1.2.

HYDRUS-1D input and output files (all these files are text files) for the final run are located in the subdirectory **RCEW\_Homo** in the **HYDRUS\_Model** directory in the **RCEW** folder in Validation Output DTN: SN0607T0502206.016. The input files have the extension *in* or *dat*. The output files have the extension *out*. The results presented in Section 7.1.2 are from the output file **T\_LEVEL.OUT**. This file provides the daily values of all the water balance components, including storage (column “*volume*”) and infiltration (column “*vBot*”) in cm. The storage and infiltration values are copied from this file into the **HYDRUS1D Data&Results** Excel file that is an external file read by the interface as explained above. The comparison of the HYDRUS-1D results and MASSIF results is performed within the interface.

**APPENDIX K**  
**SUPPORTING INFORMATION ON CORROBORATION OF INFILTRATION USING**  
**AN ALTERNATIVE MODEL APPROACH**



Four net infiltration scenarios were implemented with both MASSIF and HYDRUS-1D models as a part of model corroboration of the MASSIF model. The intent of this corroboration exercise is to compare net infiltration predicted by MASSIF against that predicted by the alternative model, HYDRUS-1D using a representative set of input parameter values. The summary of this study is provided in Section 7.2.2. The details on the modeling setup and supporting calculations are described below.

The four scenarios (Models) represent one-dimensional homogeneous soil columns each with a different soil depth: 50 cm for Model 1, 100 cm for Model 2, 150 cm for Model 3, and 200 cm for Model 4. The soil parameters and the boundary and initial conditions considered are identical among the models. The plant rooting depth was assumed to be equal to the soil depth in each scenario. The simulations were performed for one water year (365 days).

### **K1. MASSIF INTERFACE *ALTERNATIVE* MODEL**

An interface to MASSIF *Alternative Model* was designed specifically to implement the four conceptual models in consideration and to compare MASSIF and HYDRUS-1D results. The interface is supplied with the MASSIF package (Output DTN: SN0701T0502206.037). The interface performs the following functions described below.

The interface defines the following parameters:

- Site latitude is set equal to 36.8
- Site elevation is set equal to 1,000 m
- Soil saturated hydraulic conductivity is set equal to  $6.82 \times 10^{-5}$  cm/s
- Soil residual moisture content is set equal to  $0.022 \text{ m}^3/\text{m}^3$
- Soil saturated porosity is set equal to  $0.19 \text{ m}^3/\text{m}^3$
- Soil van Genuchten parameter *alpha* is set equal to  $0.002 \text{ cm}^{-1}$
- Soil van Genuchten parameter *n* is set equal to 1.21.

The alternative model latitude is arbitrarily selected. The only condition considered is that it should be within the latitude range of the Yucca Mountain site. The elevation for each of the scenarios is set equal to reference elevation (1,000 m) to avoid needing to correct temperature and precipitation.

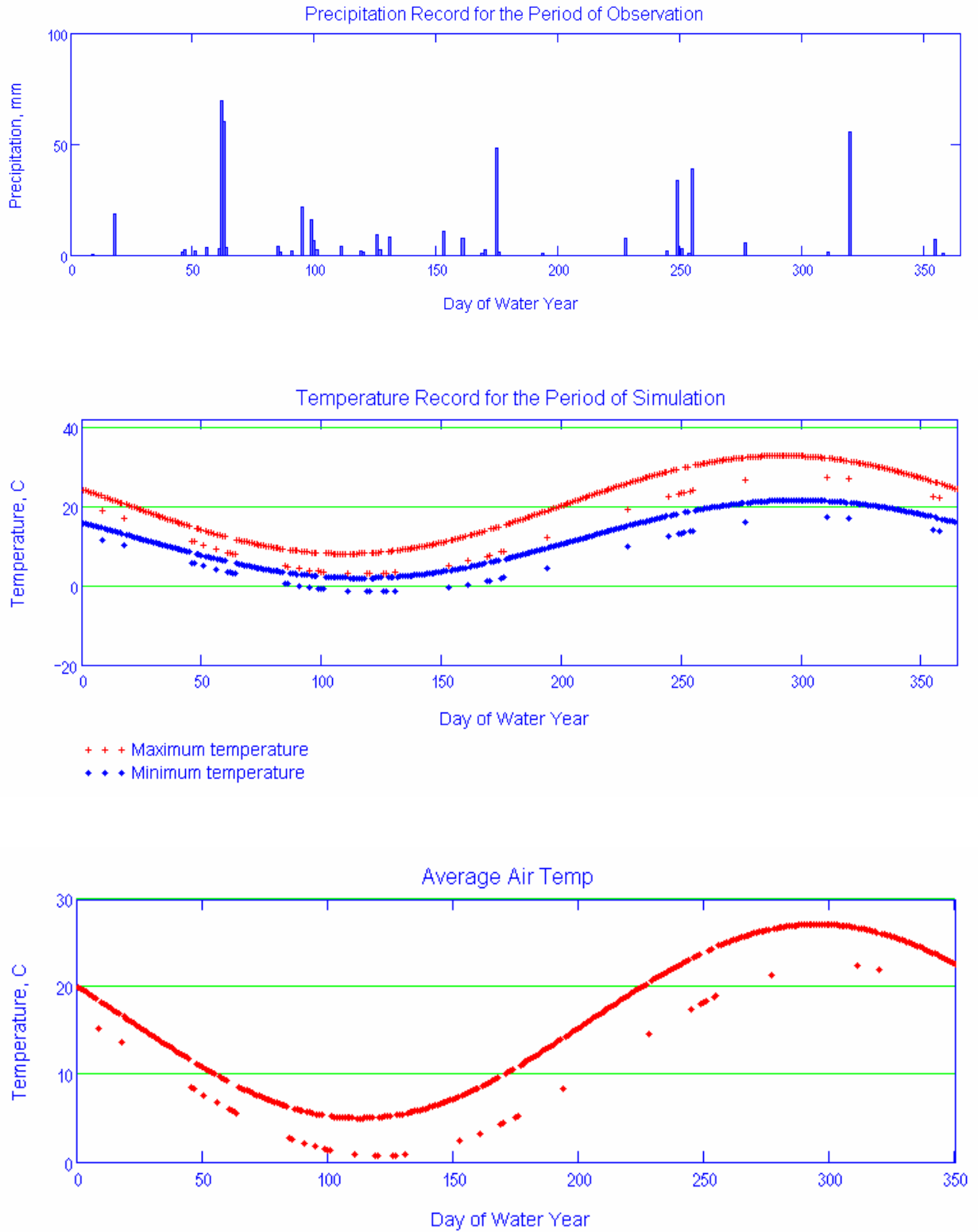
The residual moisture content and van Genuchten parameters *alpha* and *n* are not directly used in MASSIF calculations. They are used in the interface to calculate water contents at  $-1/3$ ,  $-1/10$ , and  $-60$  bars. These water contents are then used to define the field capacity and the wilting point as described below.

The interface calculates water content at  $-1/3$ ,  $-1/10$ , and  $-60$  bars using Equation J-1. The calculated field capacity at  $-1/3$  bars is  $0.173 \text{ m}^3/\text{m}^3$ , at  $-1/10$  bars is  $0.184 \text{ m}^3/\text{m}^3$ , and the wilting point at  $-60$  bars is  $0.083 \text{ m}^3/\text{m}^3$ .

The interface reads the climate data from the built-in Excel file. The climate data includes precipitation, temperature, and wind speed. These data were copied from *Weather Summary v2.1 for nominal of PD parameters.xls* located in *Present-Day Precipitation* directory within

Validation Output DTN: SN0606T0502206.014. The climate data are for Set 4 (representative year 952) with the probability of occurrence equal to 0.02. Only one water year (365 days) is considered. Note that the actual source of this particular weather data is not important as long as the same weather data are used by both MASSIF and HYDRUS. Any one-year, representative set of weather data could have been used for this corroboration activity.

The interface displays the climate data for the period of observation as shown in Figure K-1.



Source: Output DTN: SN0701T0502206.037, *Welcome to Massif\Massif\Validation Analyses\Alternative Model\Alternative\_Model.xmlcd.*

Figure K-1. Climate Data Plots for the Alternative Model Site Displayed by Alternative Model Interface

The interface calculates the number of days with mean daily temperatures below freezing during this period of simulation. The number of these days is zero.

The interface reads the geospatial parameters from the external Excel file *AM\_location.csv*. The drainage basin defined for this simulation in this file consists of four cells. Cell 1 represents Model 1, Cell 2 represents Model 2, Cell 3 represents Model 3, and Cell 4 represents Model 4. All the parameters for these cells are the same, except for the soil depth class. The Soil Depth Class is set to Class 1 for cell 1, Class 2 for cell 2, Class 3 for cell 3, and Class 4 for cell 4. The soil type is set to Type 5, and the bedrock ID is set to 406. The corresponding properties are defined below in accordance with the properties of the alternative models. The slope angle is set to 0. The reference elevation is specified to be equal to the alternative model site elevation to avoid the correction of precipitation and temperatures by MASSIF. The downstream cell ID is set to -3 to exclude run-on to these cells. The potential vegetation response (PVR) is set equal to 1.

The following parameters are MASSIF default parameters for the Present-Day climate and are not redefined by the interface:

- Site albedo (0.22)
- Dew point and storm duration parameters
- Evaporation depth  $Z_e = 0.15$  m
- Diffusive evaporation parameter  $K_{c\_min} = 0$
- Readily evaporable water parameter  $rew_1 = 6$  mm
- Depletion factor parameter  $p = 0.65$
- Plant height  $h_{plant} = 0.4$  m
- $K_{cb1} = -0.05$  and  $K_{cb2} = 9.7$ .

The vegetation canopy fraction is set equal to 0.25.

The interface sets the initial moisture content in all layers equal to  $0.08 \text{ m}^3/\text{m}^3$ . This is an arbitrary value. The only condition used was that the moisture content at the beginning of the water year should be relatively low.

Soil porosity and hydraulic conductivity for Soil Type 5 are set equal to the values defined above. This redefines the values that MASSIF reads from the built-in look-up table with the soil properties for Soil Type 5, although the exact values for these parameters are not really important as long as the values used are identical to those used by HYDRUS-1D.

Hydraulic conductivity of bedrock was set equal to  $1.13 \times 10^{-6}$  m/s. This value is slightly different from the default value read by MASSIF ( $1.3 \times 10^{-6}$  m/s); however it was set to be equal to what was used in the HYDRUS-1D runs.

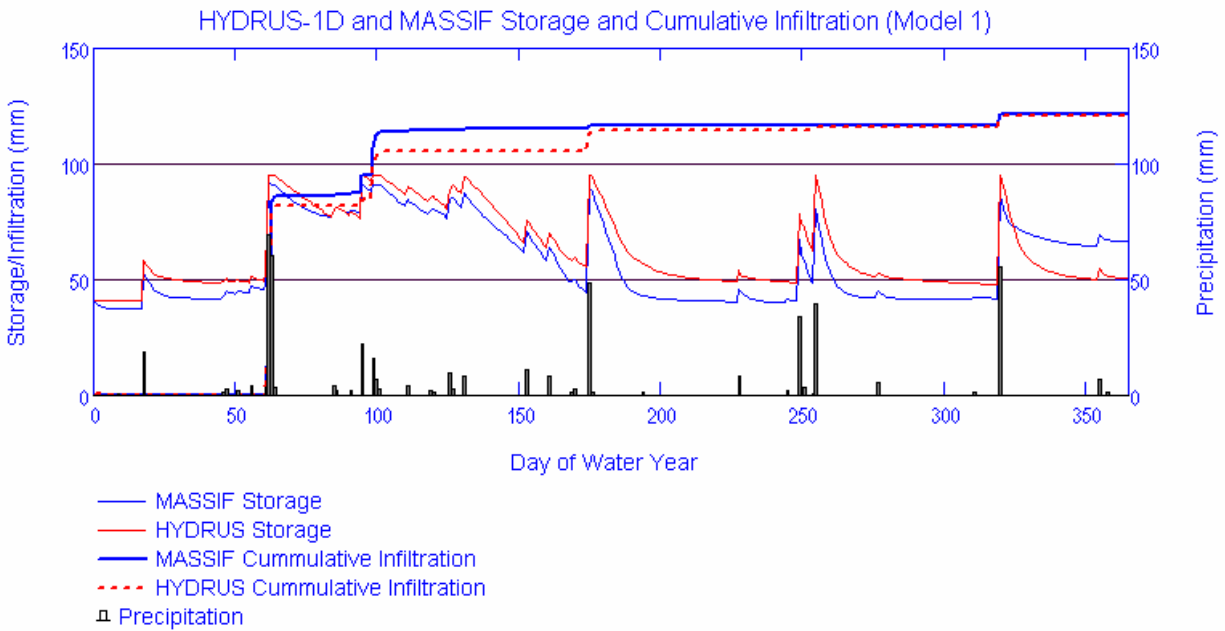
Field capacity is set to the value defined at -1/10 bar above. Wilting point of Soil Type 5 is set equal to the value defined above. This redefines the values that MASSIF reads from the built-in look-up table with the soil properties for Soil Type 5, although the exact values for these parameters are not really important as long as the values used are identical to those used by HYDRUS-1D.



The interface reads the HYDRUS-1D results (daily storage and cumulative infiltration values in mm) for the four models. These results were copied to the built-in Excel file from *Alternative\_Model\_Outputs.xls* in Validation Output DTN: SN0609T0502206.022.

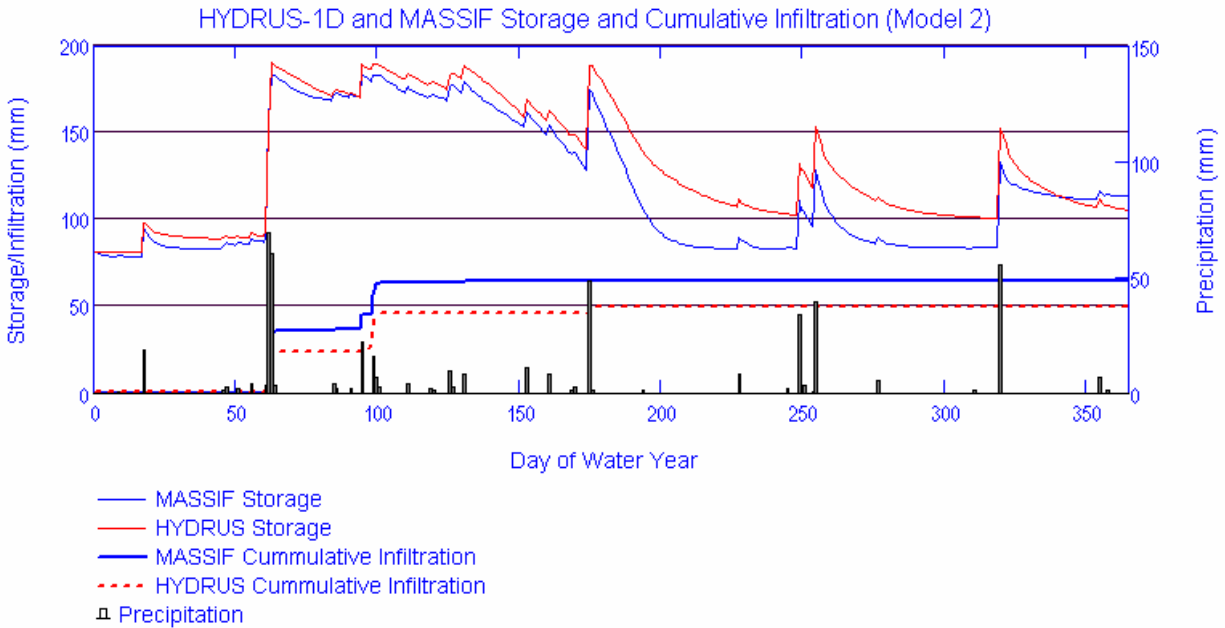
The interface defines the soil depth for each conceptual model and specifies the maximum rooting depth of 200 cm. Soil Depth Class 1 is redefined to be 50 cm, Soil Depth Class 2 is redefined to be 100 cm, Soil Depth Class 3 is redefined to be 150 cm, and the Soil Depth Class 4 is redefined to be 200 cm.

The interface runs MASSIF and stores the results of calculations for four alternative model cells. The interface calculates daily storage and daily cumulative infiltration values for each conceptual model, total annual values of the actual evapotranspiration, infiltration, and runoff, and change in storage over the one-year period. The interface calculates the mean root squared error between the daily storage calculated by MASSIF and HYDRUS-1D. The interface displays the results (daily storage and cumulative infiltration) as shown in Figures K-2 to K-5.



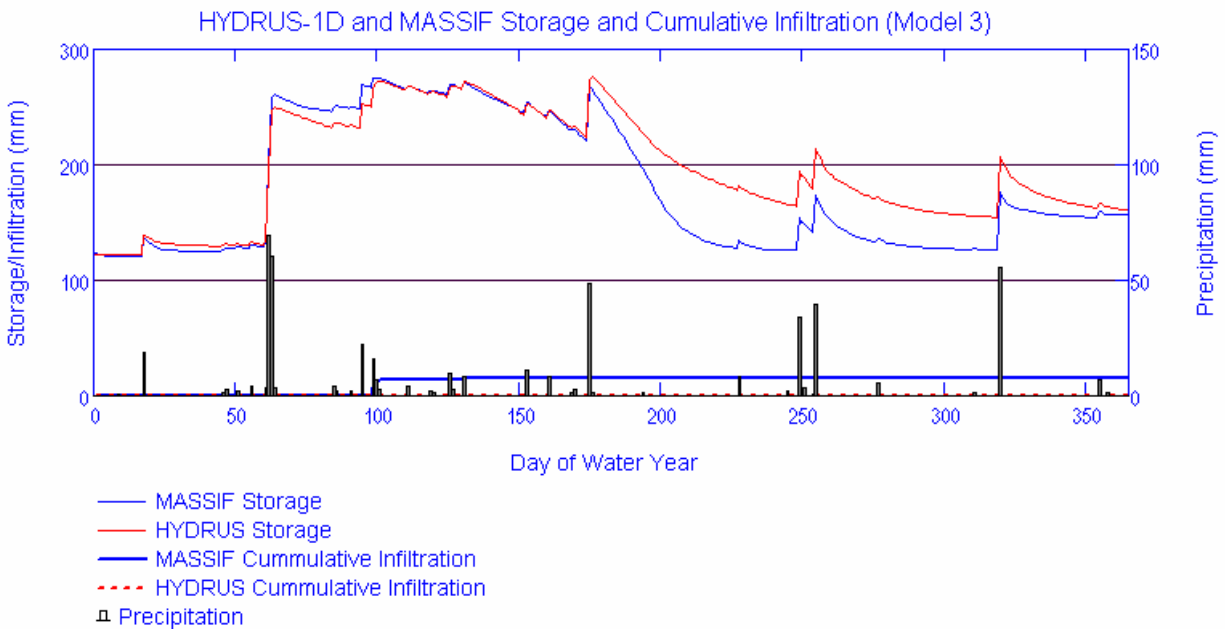
Source: Output DTN: SN0701T0502206.037, *Welcome to Massif\Massif\Validation Analyses\Alternative Model\Alternative\_Model.xmcd*.

Figure K-2. Results for Model 1 Displayed by the Alternative Model Interface



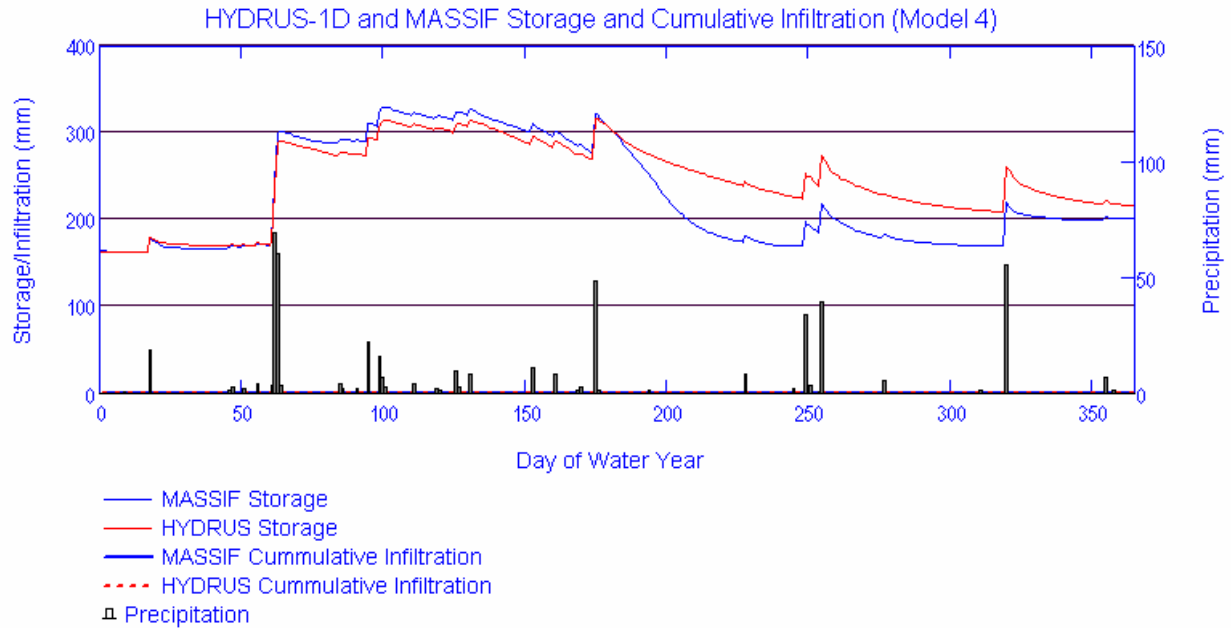
Source: Output DTN: SN0701T0502206.037, \Welcome to Massif\Massif\Validation Analyses\Alternative Model\Alternative\_Model.xmlcd.

Figure K-3. Results for Model 2 Displayed by the Interface *Alternative Model*



Source: Output DTN: SN0701T0502206.037, \Welcome to Massif\Massif\Validation Analyses\Alternative Model\Alternative\_Model.xmlcd.

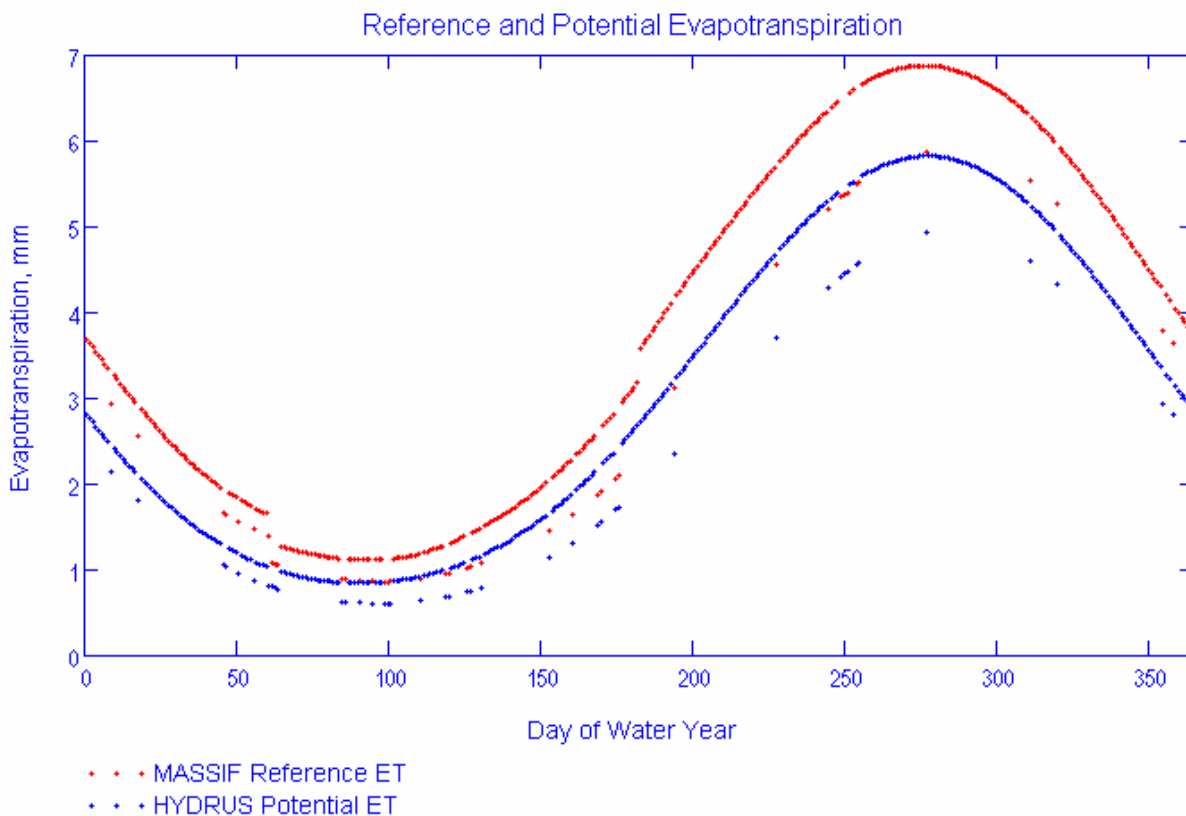
Figure K-4. Results for Model 3 Displayed by the Alternative Model Interface



Source: Output DTN: SN0701T0502206.037, *Welcome to Massif\MassifValidation Analyses\Alternative Model\Alternative\_Model.xmlcd*.

Figure K-5. Results for Model 4 Displayed by the Alternative Model Interface

The interface outputs the daily storage and daily cumulative infiltration values for each conceptual model into the built-in Excel file. The interface outputs the total annual values of the actual evapotranspiration (MASSIF), infiltration (MASSIF and HYDRUS-1D), runoff (MASSIF), change in storage over the one-year period (MASSIF), and mean root square errors into the built-in Excel file. The interface displays the reference evapotranspiration calculated by MASSIF and potential evapotranspiration specified in HYDRUS-1D (see the HYDRUS-1D modeling setup below) as shown in Figure K-6.



Source: Output DTN: SN0701T0502206.037, \Welcome to Massif\Massif\Validation Analyses\Alternative Model\Alternative\_Model.xmlcd.

Figure K-6. Limiting Evapotranspiration Displayed by the Alternative Model Interface

## K2. HYDRUS-1D MODELING SETUP

The MASSIF simulations were compared to the simulations performed using HYDRUS-1D code (Simunek et al. 2005 [DIRS 178140]). The HYDRUS-1D program numerically solves the Richards' equation for one-dimensional variably saturated water flow and heat and solute transport. A short description of HYDRUS-1D is provided in Section 6.2.4.1.

HYDRUS-1D was obtained from the Yucca Mountain Project Software Configuration Manager. The related communication and installation record are in the directory: /Alternative\_Model\_Inputs/HYDRUS\_Gen (Validation Output DTN: SN0609T0502206.021).

All the input HYDRUS-1D files are provided in Validation Output DTN: SN0609T0502206.021. There are four subdirectories in this DTN in the main directory: "Alternative\_Model\_Inputs". Directory *Alt\_Model1* contains all the input files for Model 1. These input files were created by running the HYDRUS-1D file *Alt\_Model1.h1d* located in the main directory. Directory *Alt\_Model2* contains all the input files for Model 2. These input files were created by running the HYDRUS-1D file *Alt\_Model2.h1d* located in the main directory. Directory *Alt\_Model3* contains all the input files for Model 3. These input files were created by running the HYDRUS-1D file *Alt\_Model3.h1d* located in the main directory. Directory

*Alt\_Model4* contains all the input files for Model 4. These input files were created by running the HYDRUS-1D file *Alt\_Model4.h1d* located in the main directory.

All the output HYDRUS-1D files are provided in Validation Output DTN: SN0609T0502206.022. There are four subdirectories in this DTN under the main directory: “Alternative\_Model\_Outputs”. Directory *Alt\_Model1* contains all the output files for Model 1. These output files were created by running the HYDRUS-1D file *Alt\_Model1.h1d* located in the main directory. Directory *Alt\_Model2* contains all the output files for Model 2. These output files were created by running the HYDRUS-1D file *Alt\_Model2.h1d* located in the main directory. Directory *Alt\_Model3* contains all the output files for Model 3. These output files were created by running the HYDRUS-1D file *Alt\_Model3.h1d* located in the main directory. Directory *Alt\_Model4* contains all the output files for Model 4. These output files were created by running the HYDRUS-1D file *Alt\_Model4.h1d* located in the main directory.

The HYDRUS-1D modeling setup is described as follows and is the same in all four model scenarios.

The simulated process is water flow. The heat transport is not included since the mean daily temperature is above freezing during all the periods of simulation. The root uptake is simulated through the whole model depth. The roots are uniformly distributed within this depth. The Feddes model in HYDRUS-1D is used for the stress response function. The soil profile is homogeneous. The initial moisture content is  $0.08 \text{ m}^3/\text{m}^3$ . The van Genuchten model in HYDRUS-1D is used to represent relationships between the saturation and pressure head and between the saturation and hydraulic conductivity. The soil parameters are:

- Saturated hydraulic conductivity is  $5.89 \text{ cm/d}$  ( $6.82 \times 10^{-5} \text{ cm/s}$ )
- Saturated porosity is  $0.19 \text{ m}^3/\text{m}^3$
- Residual moisture content is  $0.022 \text{ m}^3/\text{m}^3$
- van Genuchten parameter *alpha* is  $0.002 \text{ cm}^{-1}$
- van Genuchten parameter *n* is 1.21
- Pore connectivity parameter *l* is 0.5, Simunek et al. (2005 [DIRS 178140]) suggest leaving this parameter at its default value of 0.5.

The upper boundary is an atmospheric boundary with specified potential evaporation, potential transpiration, precipitation, and temperature. The daily values of these parameters are defined for all the period of simulation (365 days). The calculation of potential evapotranspiration is discussed in Appendix J. The input data used in these calculations and the resulting potential evapotranspiration values are in worksheet *Potential ET* of *Alternative\_Model\_Inputs.xls* in Validation Output DTN: SN0609T0502206.021. The potential transpiration is assumed to be equal to 0.25 of the potential evapotranspiration, based on the vegetation cover of 0.25. The potential evaporation and transpiration values are copied into the built-in HYDRUS-1D time-dependent boundary condition spreadsheet. The daily precipitation, mean daily

temperature, and daily temperature amplitude values were copied from *Weather Summary v2.1 for nominal of PD parameters.xls* located in directory *Present-Day Precipitation*. The climate data are for Set 4 (representative year 952) with the probability of occurrence equal to 0.02. These are the same data that were used in MASSIF runs. The lower boundary is defined as a seepage boundary.

The depth of the soil profile in Model 1 is 50 cm. It is represented with 51 nodes. The first node is at the land surface ( $z = 0$  cm) and the last node is at the bottom of the soil column (50 cm). The nodes are 1 cm apart. The depth of the soil profile in Model 2 is 100 cm. It is represented with 101 nodes. The first node is at the land surface ( $z = 0$  cm) and the last node is at the bottom of the soil column (100 cm). The nodes are 1 cm apart. The depth of the soil profile in Model 3 is 150 cm. It is represented with 151 nodes. The first node is at the land surface ( $z = 0$  cm) and the last node is at the bottom of the soil column (150 cm). The nodes are 1 cm apart. The depth of the soil profile in Model 4 is 200 cm. It is represented with 101 nodes. The first node is at the land surface ( $z = 0$  cm) and the last node is at the bottom of the soil column (200 cm). The nodes are 2-cm apart.

HYDRUS-1D output files (all these files are text files) in Validation Output DTN: SN0609T0502206.022 have the extension *out*. The results presented in Section 7.2.2 are from the output file *T\_LEVEL.OUT*. Each of four directories has a file with this name. This file provides the daily values of all the water balance components, including storage (column “*volume*”) and infiltration (column “*vBot*”) in cm. The storage and infiltration values were copied from these files into *Alternative\_Model\_Outputs.xls* located in the main directory of Validation Output DTN: SN0609T0502206.022 and into the built-in Excel file in *Alternative Model* interface. The comparison of the HYDRUS-1D results and MASSIF results is performed within the interface.

**APPENDIX L**  
**PRELIMINARY RESULTS AND OUTPUTS**





## L.1 PRELIMINARY OUTPUT DATA TRACKING

This appendix documents a number of preliminary unqualified DTNs that contain preliminary model results. Several minor problems were identified with the inputs used to generate these results (documented in CR 9580); therefore, these results are not considered the qualified technical product output of this report. These preliminary results remain in TDMS because an effort is being made to qualify these results in a separate data qualification report per SCI-PRO-001. This report will include an impact assessment between the final technical output and the preliminary output. Initial evaluations have shown minimal impact to the downstream users of the preliminary infiltration results.

Table L-1. List of Preliminary Output DTNs Not Qualified by This Report

<b>DTN Title</b>	<b>Preliminary DTN (NOT Qualified in this Report)</b>	<b>Qualified Output DTN (FINAL)</b>
Calculated Weather Summary for Monsoon Climate	SN0609T0502206.025	SN0701T0502206.041
Calculated Weather Summary for Present-Day Climate	SN0609T0502206.026	SN0701T0502206.040
Calculated Weather Summary for Glacial Transition Climate	SN0609T0502206.027	SN0701T0502206.042
Latin Hypercube Sample (LHS) Input and Output Files for MASSIF Calculation of Net Infiltration at Yucca Mountain	SN0610T0502206.033	SN0701T0502206.043
Monsoon Net Infiltration Results	SN0609T0502206.024	SN0701T0502206.036
Present-Day Net Infiltration Results	SN0609T0502206.028	SN0701T0502206.034
Glacial Transition Net Infiltration Results	SN0609T0502206.029	SN0701T0502206.035
MASSIF Calculation of Net Infiltration at Yucca Mountain	SN0610T0502206.032	SN0701T0502206.037

INTENTIONALLY LEFT BLANK